# Design, Preparation and Characterization of Stationary Phases for High Performance Liquid Chromatography and their Application in Pharmaceutical and Bioanalytical Analysis

**Dissertation**

der Mathematisch-Naturwissenschaftlichen Fakultät

der Eberhard Karls Universität Tübingen

zur Erlangung des Grades eines

Doktors der Naturwissenschaften

(Dr. rer. nat.)

vorgelegt von

Marc Jens Friedrich Wolter

aus Heidenheim an der Brenz

Tübingen

2025

Gedruckt mit Genehmigung der Mathematisch-Naturwissenschaftlichen Fakultät der Eberhard Karls Universität Tübingen.

| | |
|---|---|
| Tag der mündlichen Qualifikation: | 14.10.2025 |
| Dekan: | Prof. Dr. Thilo Stehle |
| 1. Berichterstatter: | Prof. Dr. Michael Lämmerhofer |
| 2. Berichterstatter: | Prof. Dr. Harald Groß |

# Design, Preparation and Characterization of Stationary Phases for High Performance Liquid Chromatography and their Application in Pharmaceutical and Bioanalytical Analysis

Marc Wolter | Pharmacist

*“Wann immer einen die Dinge erschreckten, sei es eine*

*gute Idee, sie zu messen.“*

*Daniel Kehlmann, Die Vermessung der Welt*

*To my family and friends*

*“… nullum enim officium referenda gratia magis necessarium est.”*

*Cicero, De officiis, Liber 1, 47*

# TABLE OF CONTENTS

# I. SUMMARY

## I.1 Summary (English)

Over the past few decades, new analytical challenges have driven advances in chromatographic methods and techniques. In the field of liquid chromatography, this has led to improved hardware, automated sample pretreatment, and novel stationary phases. For stationary phases, new demands have merged on efficiency, chemical stability, and new or combined separation mechanisms, leading to the development of monolithic phases, advanced spherical silica supports (core-shell particles, sub-2µm particles), microfluidic pillar-array columns, silica-based hybrid materials, organic polymeric spheres, inorganic non-silica supports, novel stationary phase surface chemistries, and mixed-mode stationary phases. However, spherical silica has remained the predominant support material for stationary phases in liquid chromatography due to its high mechanical strength and ease of functionalization.

However, there are some limitations to silica-based stationary phases. Typically, only 50% of the surface silanols can be functionalized, resulting in unwanted additional interactions between the remaining silanols and the analytes. This can lead to recovery issues, poorly shaped peaks and low efficiency. In addition, silica and its embedded functional ligands are typically prone to hydrolysis. As a result, unfavorable background noise in mass spectrometric detection accompanied by high limits of detection and quantification, limited robustness of analytical runs, and short column lifetimes can be observed. Moreover, although a wide range of columns with different surface chemistries and selectivities are commercially available, many analytical separation problems cannot be adequately solved with these available columns alone due to lack of separation selectivity. To this end, the use of orthogonal stationary phases within multidimensional chromatography setups and mixed-mode phases can provide a remedy and has led to increased research activity in this area.

In order to better understand the background of some of these drawbacks

and to ultimately overcome them, the presented studies were carried out to design and carefully investigate surface chemistries of stationary phases and to develop advanced synthesis strategies for surface modification of silica.

In the first study, the influence of the individual structural components of the chromatographic zwitterionic mixed-mode ligands of the commercial chiral columns Chiralpak ZWIX(+) and ZWIX(-) was investigated to improve the understanding of the chromatographic behavior of these phases. To this end, a series of new stationary phases were synthesized by a fragment-based design through incremental fragmentation of the chromatographic ligands. The removal of certain structural elements of these zwitterionic selectors resulted in mixed-mode phases of the type RP/ZWIX, RP/WAX and RP/SCX with modulated surface charge and hydrophilicity and therefore distinct selectivities. The phases were subjected to chromatographic tests under RP and HILIC conditions and compared with a large number of commercial columns by principal component analysis, illustrating the orthogonality of the new phases to each other and to other commercial RP, HILIC and MMC SPs. In addition, the contributions of the building blocks to the surface charge of the SPs were investigated in detail by determining ζ-potentials of the modified silica particles and electrophoretic mobilities of the free ligands in the pH range of pH 3.5 to 9.5. The combination of the ζ-potential measurements of the modified particles and the obtained electrophoretic mobilities of the individual ligands also enabled the influence of the remaining silanols of the silica support to be estimated. This is a valuable information, since the free silanols on the silica surface can contribute significantly to the chromatographic process through ionic interactions, especially at higher pH values, and other secondary interactions.

The second study addressed the proof-of-principle of thiol-ene photo-click immobilization of a chiral vinyl ligand onto silica particles for the preparation of chiral stationary phases. Several different chemical approaches were evaluated, including brush-type attachment of the ligand to thiol silica and attachment to vinyl silica via a polythiol crosslinker. A number of different

HILIC: hydrophilic interaction liquid chromatography, MMC: mixed-mode chromatography, RP: reversed-phase (chromatography), SCX: strong cation exchange, SP: stationary phase, WAX: weak anion exchange, ZWIX: zwitterionic ion exchange

synthetic approaches were compared in terms of selector coverage and chromatographic performance. Synthesis conditions were systematically optimized with respect to reaction time, educt concentrations in the reaction mixture, and type of initiation. Brush-type immobilization resulted in lower selector coverage compared to polythiol-mediated immobilization. Photo-click immobilization of the selector via coated polythiol film resulted in approximately the same surface coverage as the approach in which all reactants, including polythiol, were suspended in the vinyl silica slurry. In conclusion, thiol-ene photo-click immobilization of vinyl ligands on silica proved to be an alternative strategy to the standard thermally initiated immobilization reaction.

The third study focused on the synthesis of polythiol-silica, which is an extremely stable and easily modifiable platform for the preparation of stationary phases. The hydrolytic stability of such polymer-coated phases is attributed mainly to the multi-point attachment of the polymer film to the silica support, resulting in less column bleeding than their brush-type counterparts. The thiol groups of such polythiol-silica, which can be easily modified, for instance via thiol-ene click reactions, also facilitate the attachment of specifically designed chromatographic ligands and therefore the simple preparation of stationary phases with novel selectivies. Against this backdrop, the reproducible preparation of polythiol-silica with controlled sulfhydryl content was developed in this study and photo-induced and thermally induced synthesis strategies compared. To this end, the reaction conditions were optimized for both approaches by means of a design of experiments strategy. The thickness of the grafted polythiol layer on the modified silica particles was evaluated by determining the sulfur content by elemental analysis. The number of remaining sulfhydryl groups available for further reactions was determined using a thiol-disulfide exchange reaction specifically designed for this purpose. By combining the elemental analysis results with the number of free sulfhydryl groups, it was also possible to calculate the number of crosslinks of the polymer film to the support, which determines the hydrolytic stability of the surface coating. It was found that the photo-induced reaction had significantly higher kinetics than the thermally induced one and therefore required shorter reaction times. However, this gain in time was accompanied by poorer control of

the reaction. Thus, the thermal reaction was ultimately used to produce the optimized polythiol-silica. Finally, the polythiolated silica particles were further modified for argentation chromatography and chiral separations, which clearly demonstrated its versatility and usefulness as stable-bonded platform for the creation of stationary phases with distinct selectivities.

In the fourth study, a novel approach for thiol functionalization of silica was implemented by using (3-mercaptopropyl)silatrane for silanization and compared with the classical silanization reaction using the corresponding alkoxysilane. It was found that functionalization with the silatrane leads to a significant elevation in the proportion of triple-bound ligands as well as to a significantly increased ligand loading density, which was close to the theoretical maximum. Furthermore, the determination of C-terms by van-Deemter-analysis indicated a reduced thickness of the ligand film on the silica surface for the silatrane-based stationary phase. This can be explained by the cage-like structure and the transannular N→Si bond, which leads to a severe hydrolytic stability of the silatrane and thus prevents oligomer formation in the reaction solution. In contrast, this oligomerization can occur for the corresponding alkoxysilane in the presence of even small traces of water in the reaction solution during the silanization procedure. As a result, oligomers instead of monomers are immobilized on the silica surface, which leads to thicker layers and eventually negatively affects the mass transfer resistance. For applications where fast separations are required but the flow rate of the mobile phase is often limited by the mass transfer resistance, this improvement in chromatographic efficiency through the use of silatranes is of particular interest.

The fifth study was devoted to the hydrolytic stability of amino phases. Amino-functionalized silica particles are widely used in many analytical fields and chromatographic modes, but typically suffer extensively from hydrolytic cleavage of the embedded functional ligands due to the catalytic effect of the amino group itself, resulting in short column lifetimes, limited robustness of analytical runs, and unfavorable background noise in mass spectrometric detection. To overcome this problem, amino groups of aminopropyl-modified silica were cross-linked with triglycidyl isocyanurate, forming an extensive cycloamido-amino network on the silica surface. In addition, the initial amino functionalization was carried out by silanization using a

silatrane, yielding a high percentage of trifunctionally bound aminopropyl ligands. Subsequently, the obtained amido-amino phase was compared to a set of in-house prepared amino phases with different surface chemistries and to two commercial amino columns in terms of hydrolytic stability and chromatographic properties. As a result, the novel phase exhibited significantly higher hydrolytic stability than the precursor aminopropyl silica and achieved column stability characteristics comparable to a commercial highly stable polymeric amino column. In addition, the classical chromatographic properties were largely retained after crosslinking, making the novel amido-amino silica an excellent stable-bonded alternative to classical amino phases.

In the sixth study, a wide pore RP/WAX-type mixed-mode stationary phase with pH-dependent charge reversal was designed and synthesized for particularly hydrophobic charge-induction chromatography of proteins. HCIC is a promising alternative technique for purification and analysis of proteins and other biomolecules, since mild elution conditions can be applied and orthogonal retention profiles achieved. Therefore, silatranes were used to simultaneously immobilize octyl and pyridylethyl ligands on the same silica support. The obtained material exhibited a surface charge reversal at about pH 5.5, enabling its application in HCIC. Typically, in HCIC, analytes are first adsorbed on the stationary phase due to hydrophobic interactions and then eluted from the column in a second step due to electrostatic repulsion. This repulsion is usually induced by reversing the charge of the stationary phase by changing the pH of the mobile phase. Subsequently, a number of distinct proteins with different hydrophobicities and isoelectric points were applied to the stationary phase under HCIC and additionally under gradient-RP chromatography conditions. The elution order of the proteins obtained under these conditions was reversed, clearly demonstrating the orthogonality of the two chromatographic modes applied and the applicability of the stationary phase to both modes. Therefore, the octyl/pyridyl stationary phase demonstrated to be a promising new material for the analysis of biomolecules (such as proteins) by exploiting their hydrophobic and charge properties.

HCIC: hydrophobic charge-induction chromatography, RP: reversed-phase (chromatography), WAX: weak anion exchange, SAX: strong anion exchange

The seventh study involved the preparation of a new set of three triphenyl-modified stationary phases with and without embedded ion-exchange sites, yielding RP-, RP/SAX-, and RP-ZWIX-phases. The introduction of the bulky triphenyl ligands was intended to shield free silanols on the surface of the silica support, as well as to facilitate hydrophobic and other classical phenyl-typical interactions with analytes. The additional introduction of sulfonate and phosphonium groups, which are permanently charged under chromatographic conditions, was intended to allow electrostatic interactions and, in sum, to lead to unique new selectivities. Thiol silica was employed as the platform for the introduction of the triphenyl ligands. The latter was prepared by an innovative silatrane functionalization approach using pre-wetted silica as starting material. This approach represents an improvement over the approach presented in the fourth study and, in particular, led to a higher accessibility of the embedded thiol groups. The introduction of bulky triphenyl moieties and the formation of a dense polysiloxane layer (due to silanization with silatranes) resulted in increased shielding of silanols, as indicated by chromatographic tests. The developed triphenyl columns were finally applied to liquid chromatographic analysis of the biomolecules teicoplanin and patisiran, which demonstrated the orthogonality of the three phases and indicated the promising fit of the concept for biomolecule analysis.

RP: reversed-phase (chromatography), SAX: strong anion exchange, ZWIX: zwitterionic ion exchange

## I.2 Summary (German)

In den vergangenen Jahrzehnten kam es aufgrund stets neuer analytischer Herausforderungen zu zahlreichen Fortschritten im Bereich chromatographischer Methoden und Techniken. In der Flüssigkeitschromatographie hat dies insbesondere zur Entwicklung verbesserter Hardware, automatisierter Probenvorbereitungen und neuartigen stationären Phasen geführt. An stationäre Phasen wurden insbesondere gesteigerte Anforderungen an deren Effizienz und chemische Stabilität gestellt, sowie neue oder kombinierte Trennmechanismen gefordert. Dies führte zur Entwicklung monolithischer stationärer Phasen, verbesserter sphärischer Silikageler (Kern-Hülle-Partikel, sub-2µm Partikel), mikrofluidischer Säulenarray-Säulen, silikabasierter Hybridmaterialien, organischer Polymerphasen und anorganischer, nicht silikabasierter Materialien, sowie neuartiger Oberflächenchemien und stationärer Mixed-Mode-Phasen. Silikagel stellt jedoch aufgrund seiner hohen mechanischen Stabilität und seiner einfachen Funktionalisierbarkeit weiterhin das vorherrschende und am häufigsten verwendete Trägermaterial zur Herstellung stationärer Phasen in der Flüssigkeitschromatographie dar.

Stationäre Phasen auf Silikagelbasis weisen jedoch neben ihren vorteilhaften Eigenschaften auch einige Nachteile auf. So können nur maximal 50 % der Oberflächensilanole funktionalisiert werden, wodurch es zu unerwünschten zusätzlichen Wechselwirkungen zwischen den verbleibenden, nicht modifizierten Silanolen und den Analyten kommen kann. Diese Wechselwirkungen führen typischerweise zu Wiederfindungs- und Rückgewinnungssproblemen bestimmter Analyte, ungleichförmigen Peaks und geringer chromatographischer Effizienz der stationären Phasen. Des Weiteren sind silikabasierte Phasen in der Regel hydrolytisch instabil. Hierbei kann es sowohl zur Auflösung des Trägermaterials, als auch zur Ablösung der verankerten chromatographischen Liganden und somit zu Säulenbluten kommen. Dies kann insbesondere zu hohem Hintergrundrauschen bei der massenspektrometrischen Detektion mit einhergehenden erhöhten Nachweis- und Quantifizierungsgrenzen, sowie zu einer eingeschränkten Robustheit und Reproduzierbarkeit der Analysen führen. Ebenfalls wird die Laufzeit der chromatographischen Säulen durch die hydrolytische Instabilität solcher Phasen negativ beeinflusst. Hinzu kommt, dass

zwar bereits eine große Bandbreite an stationären Phasen mit unterschiedlichen Oberflächenchemien und Selektivitäten kommerziell verfügbar ist, viele analytische Trennprobleme jedoch aufgrund mangelnder Trennselektivität mit diesen kommerziell verfügbaren Säulen alleine nicht ausreichend gelöst werden können. Der Einsatz von orthogonalen stationären Phasen in mehrdimensionalen chromatographischen Gerätekonfigurationen, sowie die Verwendung von Mixed-Mode-Phasen ist hierfür ein möglicher Lösungsansatz und führte folglich zuletzt zu verstärkten Forschungsaktivitäten auf diesem Gebiet.

Um den Hintergrund einiger dieser nachteiligen Eigenschaften besser zu verstehen und deren Effekt schlussendlich zu verringern oder gänzlich zu überwinden, wurden die in dieser Thesis präsentierten Forschungsarbeiten durchgeführt. Diese behandelten insbesondere das Design und die Charakterisierung der Oberflächenchemie stationärer Phasen, sowie die Entwicklung alternativer Synthesestrategien für die Oberflächenmodifikation von Silikagelen.

In der ersten der präsentierten Forschungsarbeiten wurde der Einfluss der einzelnen Strukturkomponenten der chromatographischen, zwitterionischen Mixed-Mode-Liganden der kommerziellen chiralen Säulen Chiralpak ZWIX(+) und ZWIX(-) untersucht, um das Verständnis des chromatographischen Verhaltens dieser Phasen zu verbessern. Zu diesem Zweck wurde eine Reihe neuer stationärer Phasen durch schrittweise Fragmentierung der chromatographischen Liganden synthetisiert. Die Entfernung bestimmter Strukturelemente dieser zwitterionischen Selektoren führte zu Mixed-Mode-Phasen vom Typ RP/ZWIX, RP/WAX und RP/SCX mit modulierter Oberflächenladung und Hydrophilie und folglich unterschiedlichen Selektivitäten. Die Phasen wurden chromatographischen Tests unter RP- und HILIC-Bedingungen unterzogen und mittels Hauptkomponentenanalyse mit einer großen Anzahl kommerzieller Säulen verglichen, wodurch die Orthogonalität der neuen Phasen untereinander, aber auch zu anderen RP-,

HILIC: Hyrophile Interaktionschromatographie, RP: Umkehrphasenchromatographie, SCX: Starke Kationenaustauschchromatographie, WAX: Schwache Anionenaustausch-chromatographie, ZWIX: Zwitterionische Ionenaustauschchromatographie

HILIC- und MMC-SPs verdeutlicht wurde. Darüber hinaus wurden die Beiträge der einzelnen Strukturbestandteile zur Oberflächenladung der stationären Phasen eingehend untersucht, indem die Zetapotentiale der modifizierten Silikapartikel und die elektrophoretischen Mobilitäten der freien Liganden im pH-Bereich von pH 3,5 bis 9,5 bestimmt wurden. Die Kombination der Zetapotentialmessungen der modifizierten Partikel und die erhaltenen elektrophoretischen Mobilitäten der einzelnen Liganden ermöglichte des Weiteren die Abschätzung des Einflusses der verbleibenden Silanole des Trägermaterials. Dies ist eine wertvolle Information, da die freien Silanole auf der Silikaoberfläche durch ionische Wechselwirkungen, insbesondere bei höheren pH-Werten, und andere sekundäre Wechselwirkungen erhebliche Auswirkungen auf den chromatographischen Prozess haben können.

Die zweite Forschungsarbeit befasste sich mit der Eignung der photoinduzierten Thiol-En-Click-Reaktion zur Immobilisierung eines chiralen Vinylliganden auf Silikapartikeln zum Zweck der Herstellung chiraler stationärer Phasen. Es wurden verschiedene Syntheseansätze evaluiert, die sowohl die bürstenartige Immobilisierung des Liganden an Thiol-Silika als auch die Immobilisierung des Liganden über ein Polythiolnetzwerk auf Vinylsilika umfassten. Die Ansätze wurden hinsichtlich der Selektordichte und der chromatographischen Leistung verglichen. Die Synthesebedingungen wurden hinsichtlich Reaktionszeit, Eduktkonzentrationen im Reaktionsgemisch und Initiierungsart systematisch optimiert. Die Bürstenimmobilisierung führte zu einer geringeren Selektordichte im Vergleich zur Thiolpolymerimmobilisierung. Die Photoklick-Immobilisierung des Selektors über einen zuvor immobilisierten Polythiolfilm führte zu einer annähernd gleichen Selektordichte wie der Ansatz, bei dem alle Reaktanden einschließlich des Polythiols gleichzeitig im Reaktionsgemisch suspendiert wurden. Diese Forschungsarbeit hat gezeigt, dass die Thiol-En-Photoclick-Immobilisierung von Vinylliganden eine alternative Strategie zur üblichen thermisch initiierten Reaktion darstellt.

Die dritte Forschungsarbeit konzentrierte sich auf die Synthese von polythiol-modifiziertem Silikagel, welches eine äußerst stabile und leicht modifizierbare

HILIC: Hyrophile Interaktionschromatographie, MMC: Mixed-Mode-Chromatographie, SP: Stationäre Phase

Plattform für die Herstellung stationärer Phasen darstellt. Die hohe hydrolytische Stabilität solcher polymerbeschichteten Phasen beruht hauptsächlich auf der hohen Anzahl an kovalenten Verbindungen des Polymerfilms zum Trägermaterial, wodurch das Säulenbluten im Vergleich zu den entsprechenden Bürstenphasen sehr stark vermindert wird. Die Thiolgruppen solcher Polythiolphasen, die beispielsweise über einfache Thiol-Ene-Klick-Reaktionen modifiziert werden können, ermöglichen unkompliziert die Anbindung speziell entwickelter chromatographischer Liganden und somit die Herstellung stationärer Phasen mit neuen Selektivitäten. Vor diesem Hintergrund wurde in dieser Studie die reproduzierbare Synthese von polythiol-modifizierten Silikagelen mit kontrollierter Anzahl and Thiolgruppen entwickelt und diesbezüglich lichtinduzierte und thermisch induzierte Synthesestrategien verglichen. Hierzu wurden die Reaktionsbedingungen für beide Ansätze mittels einer Design-of-Experiments-Strategie optimiert. Zu diesem Zweck wurde die Dicke der aufgebrachten Polythiolschicht durch Bestimmung des Schwefelgehalts mittels Elementaranalyse abgeschätzt. Die Anzahl der verbliebenen, nicht abreagierten Thiolgruppen, die somit für weitere Reaktionen zur Verfügung stehen, wurde mithilfe einer speziell für diesen Zweck entwickelten Thiol-Disulfid-Austauschreaktion ermittelt. Durch die Kombination der Ergebnisse dieser beiden Bestimmungsmethoden konnte auch die Anzahl der Verbindungen des Polymerfilms zum Trägermaterial berechnet werden. Diese Vernetzung zur Silikaoberfläche bestimmt maßgeblich die hydrolytische Stabilität der Oberflächenbeschichtung. Es zeigte sich, dass die lichtinduzierte Reaktion eine deutlich höhere Kinetik aufwies als die thermisch induzierte und daher kürzere Reaktionszeiten erforderte. Die geringere benötigte Reaktionszeit ging jedoch mit einer schlechteren Kontrolle der Reaktion einher. Somit wurde die thermische Reaktion letztendlich zur Herstellung des optimierten polythiol-modifizierten Silikagels verwendet. Schließlich wurde das optimierte polymerbeschichtete Thiolsilikagel modifiziert und die resultierenden Phasen in der Silberionenchromatographie und chirale Chromatographie eingesetzt, wodurch die Vielseitigkeit und Nützlichkeit des hergestellten Materials als stabile Plattform für die Herstellung stationärer Phasen mit unterschiedlichen Selektivitäten eindrücklich demonstriert wurde.

In der vierten Forschungsarbeit wurde ein neuartiger Ansatz zur Thiolfunktionalisierung von Silikagelen unter Verwendung von (3-Mercaptopropyl)silatran zur Silanisierung etabliert und mit der klassischen Silanisierungsreaktion durch das entsprechende Alkoxysilan verglichen. Es zeigte sich, dass die Funktionalisierung unter Verwendung des Silatrans zu einer deutlichen Erhöhung des Anteils dreifach gebundener Liganden sowie zu einer deutlich erhöhten Ligandenbeladungsdichte, die nahe am theoretischen Maximum lag, führte. Darüber hinaus implizierte die Bestimmung der C-Terme mittels Van-Deemter-Analyse eine verringerte Dicke des Ligandenfilms auf der Silica-Oberfläche für die stationäre Phase auf Silatranbasis. Dies kann durch die käfigartige Struktur und die transannulare N→Si-Bindung erklärt werden, die zu einer hohen Hydrolysestabilität des Silatrans führt und somit die Oligomerbildung in der Reaktionslösung während der Silanisierungsreaktion verhindert. Im Gegensatz dazu kann diese Oligomerisierung bei dem entsprechenden Alkoxysilan bereits in Gegenwart geringer Spuren von Wasser in der Reaktionslösung auftreten. Dadurch können Oligomere statt Monomere auf der Silikaoberfläche immobilisiert werden, wodurch es zur Bildung dicker Ligandenfilme und letztendlich schlechten Massentransfereigenschaften kommen kann. Für Anwendungen, bei denen schnelle Trennungen und daher meist hohe Flussraten erforderlich sind, ist diese Verbesserung der Massen-transfereigenschaften durch die Funktionalisierung mittels Silatranen von besonderem Interesse.

Die fünfte Forschungsarbeit widmete sich der Hydrolysestabilität von Aminophasen, welche in vielen analytischen Bereichen und unterschiedlichen Chromatographiearten verwendet werden. Diese sind jedoch aufgrund der katalytischen Wirkung der Aminogruppe in der Regel hydrolytisch instabil. Dies führt zu einer meist kurzen Haltbarkeit der Säulen und einer geringen Robustheit der durchgeführten Analysen. Außerdem kann die Abspaltung der Liganden von der Partikeloberfläche ein ausgeprägtes Hintergrundrauschen bei der massenspektrometrischen Detektion hervorrufen. Um die hydrolytische Stabilität solcher Phasen zu erhöhen, wurde in dieser Studie ein Versuch unternommen, die Aminogruppen von aminopropyl-modifiziertem Silikagel mit Triglycidyl-isocyanurat zu vernetzen, wodurch ein ausgedehntes Cycloamido-Amino-

Netzwerk auf der Silica-Oberfläche entstand. Des Weiteren wurde die initiale Aminofunktionalisierung durch Silanisierung mit einem Silatran durchgeführt, wodurch ein großer Anteil der Aminoliganden mittels drei Bindungen an der Silikaoberfläche verankert wurde. Anschließend wurde die erhaltene quervernetzte Aminophase hinsichtlich ihrer Hydrolysestabilität und chromatographischen Eigenschaften mit einer Vielzahl selbst hergestellter Amino-Phasen mit unterschiedlicher Oberflächenchemie und mit zwei kommerziellen Amino-Säulen verglichen. Infolgedessen zeigte die neue Phase eine deutlich höhere Hydrolysestabilität als deren nicht quervernetzte Vorläuferphase und wies Stabilitätseigenschaften auf, die mit einer kommerziellen hochstabilen Polymerphase vergleichbar sind. Darüber hinaus blieben die klassischen chromatographischen Eigenschaften der Vorläuferphase nach der Vernetzung weitgehend erhalten. Die neuartige quervernetzte Aminophase stellt folglich eine hervorragende, chemisch stabile Alternative zu klassischen Aminophasen dar.

Im Zuge der sechsten Forschungsarbeit wurde eine weitporige stationäre Mixed-Mode-Phase vom RP/WAX-Typ mit pH-abhängiger Umkehr der Oberflächenladung für die hydrophe Ladungsinduktionschromatographie (HCIC) von Proteinen konzipiert und synthetisiert. HCIC ist eine vielversprechende alternative Technik zur Aufreinigung und Analyse von Proteinen und anderen Biomolekülen, da milde Elutionsbedingungen angewendet und orthogonale Retentionsprofile erzielt werden können. Für die Synthese der Phase wurden Silatrane zur Silanisierung verwendet und gleichzeitig Octyl- und Pyridylethylliganden auf demselben Silikagel immobilisiert. Das erhaltene Material zeigte schließlich eine Oberflächenladungsumkehr bei etwa pH 5,5, wodurch eine Anwendung in HCIC möglich wurde. Typischerweise werden die Analyten hierbei zunächst aufgrund hydrophober Wechsel-wirkungen an der stationären Phase adsorbiert und dann in einem zweiten Schritt aufgrund elektrostatischer Abstoßung von der Säule eluiert. Diese Abstoßung wird normalerweise durch Umkehrung der Ladung der stationären Phase induziert. Diese erfolgt durch eine Änderung des pH-Werts der mobilen Phase. Anschließend wurde eine Reihe unterschiedlicher Proteine

HCIC: Ladungsinduktionschroatographie, RP: Umkehrphasenchromatographie, WAX: Schwache Anionenaustauschchromatographie

mit unterschiedlichen Hydrophobizitäten und isoelektrischen Punkten mittels HCIC und Gradientenumkehrphasenchromatographie auf der neuen Mixed-Mode-Phase erfolgreich aufgetrennt. Hierbei wurde die Retentionsfolge der Proteine jeweils umgekehrt, wodurch die Orthogonalität der beiden angewendeten Chromatographiearten und die Anwendbarkeit der neuen stationären Phase in beiden Elutionsmodi demonstriert wurde. Die stationäre Octyl/Pyridyl-Phase erwies sich somit als vielversprechendes neues Material für die Analyse von Biomolekülen (z. B. Proteinen) aufgrund ihrer Hydrophobizität und Ladung.

Die siebte Forschungsarbeit befasste sich mit der Herstellung eines neuen Säulensets bestehend aus drei Triphenyl-modifizierten stationären Phasen mit und ohne integrierte ionische Funktionalitäten. Die drei entstanden stationären Phasen wiesen infolgedessen RP-, RP/SAX- und RP-ZWIX- (Mixed-Mode-) Eigenschaften auf. Mittels der Einführung der sperrigen Triphenyl-Liganden sollten freie Silanole auf der Oberfläche der Silikapartikel abgeschirmt werden sowie hydrophobe und andere klassische phenyl-typische Wechselwirkungen mit Analyten ermöglicht werden. Die zusätzliche Einführung der Sulfonat- und Phosphoniumgruppen, die unter chromatographischen Bedingungen permanent geladen sind, sollte elektrostatische Wechselwirkungen ermöglichen und in der Summe zu einzigartigen neuen Selektivitäten führen. Als Plattform für die Einführung der Triphenyl-Liganden wurde Thiolsilikagel eingesetzt. Dieses wurde durch ein innovatives Silanisierungskonzept unter Verwendung von befeuchtetem Silikagel hergestellt. Dieser Ansatz stellt eine Verbesserung gegenüber dem in der vierten Studie vorgestellten Ansatz dar und führte insbesondere zu einer besseren Verfügbarkeit der immobilisierten Thiolgruppen. Chromatographische Tests implizierten eine erhöhte Abschirmung freier Silanole aufgrund der sperrigen Triphenylreste und der dichten Polysiloxanschicht (die im Zuge der Silanisierung mit Silatranen entstanden ist). Die Triphenylsäulen wurden schließlich zur Analyse der Biomoleküle Teicoplanin und Patisiran eingesetzt, wobei die Orthogonalität der drei Phasen, sowie die Eignung des Konzepts für die Analyse von Biomolekülen demonstriert wurde.

HCIC: Ladungsinduktionschroatographie, RP: Umkehrphasenchromatographie, SAX: Starke Anionenaustauschchromatographie, ZWIX: Zwitterionische Ionenaustauschchromatographie

# II. LIST OF PUBLICATIONS

## II.1 Publications

**Publication I**[1] Martina Ferri, Stefanie Bäurer, Andrea Carotti, **Marc Wolter**, Belal Alshaar, Johannes Theiner, Tohru Ikegami, Caroline West, Michael Lämmerhofer, Fragment-based Design of Zwitterionic, Strong Cation- and Weak Anion-Exchange Type Mixed-mode Liquid Chromatography Ligands and their Chromatographic Exploration. *J. Chromatogr. A*, 1621 (2020) 461075.

**Publication II**[1] Christian Geibel, Kristina Dittrich, **Marc Wolter**, Michael Lämmerhofer, Thiol-ene photo-click immobilization of chiral chromatographic ligand on silica particles. *J. Chromatogr. A*, 1622 (2020) 461133.

**Publication III**[1] **Marc Wolter**, Xingyu Chen, Ulrich Woiwode, Christian Geibel, Michael Lämmerhofer, Preparation and characterization of poly(3-mercaptopropyl)methylsiloxane functionalized silica particles and their further modification for silver ion chromatography and enantioselective high-performance liquid chromatography. *J. Chromatogr. A*, 1643 (2021) 462069.

**Publication IV**[1] Christian Geibel, Johannes Theiner, **Marc Wolter**, Markus Kramer, Wolfgang Lindner, Michael Lämmerhofer, Controllable organosilane monolayer density of surface bonding using silatranes for thiol functionalization of silica particles for liquid chromatography and validation of microanalytical method for elemental composition determination. *J. Chromatogr. A*, 1653 (2021) 462418.

[1] Elsevier journal authors have the right to include their articles in a thesis or dissertation. No written permission from Elsevier is necessary.

**Publication V**[1] **Marc Wolter**, Christian Geibel, Matthias Olfert, Min Su, Wolfgang Bicker, Markus Kramer, Wolfgang Lindner, Michael Lämmerhofer, Development and chromatographic exploration of stable-bonded cross-linked amino silica against classical amino phases. *J. Sep. Sci.*, 45 (2022) 3286–3300.

**Publication VI**[2] **Marc Wolter**, Christoph Barth, Mirna Maalouf, Markus Kramer, Adrian Sievers-Engler, Michael Lämmerhofer, Wide-pore fully porous mixed-mode octyl/pyridyl-bonded silica material with pH-dependent surface charge reversal for high-performance hydrophobic charge-induction chromatography of proteins. *J. Chromatogr. A*, 1737 (2024) 465429.

**Publication VII**[1] **Marc Wolter**, Mirna Maalouf, Mateusz Janek, Cornelius Knappe, Markus Kramer, Michael Lämmerhofer, Triphenyl-modified mixed-mode stationary phases with and without embedded ion-exchange sites for high performance liquid chromatography. *J. Sep. Sci.*, 47 (2024) e70058.

[1] Authors of published Wiley articles have the right to reuse the full text of the published articles as part of their thesis or dissertation. There is no need to request permission from Wiley for this use.

[2] Elsevier journal authors have the right to include their articles in a thesis or dissertation. No written permission from Elsevier is necessary.

## II.2 Author Contributions

**Publication I** Martina Ferri: Stationary phase synthesis, zeta-potential determination, HPLC experiments, data evaluation and interpretation, visualization, writing of the manuscript, review and editing of the manuscript. Stefanie Bäurer: Data evaluation and interpretation, HPLC experiments, supervision of experiments, partial writing of the manuscript, review and editing of the manuscript. Andrea Carotti: Molecular modelling studies, visualization, review and editing of the manuscript. **Marc Wolter:** Capillary electrophoresis experiments, zeta-potential determination, stationary phase synthesis, column packing, partial writing of the manuscript. Belal Alshaar: Stationary phase synthesis, HPLC experiments. Johannes Theiner: Elemental analysis. Tohru Ikegami: General scientific concept, methodology, supervision, review and editing of the manuscript. Caroline West: General scientific concept, methodology, review and editing of the manuscript. Michael Lämmerhofer: General scientific concept, methodology, supervision, discussion of the results, review and editing of the manuscript, resources.

**Publication II** Christian Geibel: Methodology, design of experiments, stationary phase synthesis, column packing, HPLC experiments, data evaluation and interpretation, visualization, writing of the manuscript, review and editing of the manuscript. Kristina Dittrich: Synthesis of the chiral ligand, discussion and interpretation of experiments and obtained data, review and editing of the manuscript. **Marc Wolter:** Stationary phase synthesis, discussion and interpretation of experiments and obtained data, review and editing of the manuscript. Michael Lämmerhofer: General scientific concept, methodology, supervision, discussion of the results, review and editing of the manuscript, resources.

**Publication III** **Marc Wolter:** Methodology, design of experiments, supervision, preparation and characterization of modified silica particles, column packing, HPLC experiments, data evaluation and interpretation, visualization, writing of the manuscript, review and editing of the manuscript. Xingyu Chen:

Preparation and characterization of modified silica particles, HPLC experiments. Ulrich Woiwode: Preparation of modified silica particles. Christian Geibel: Preparation of modified silica particles, review and editing of the manuscript. Michael Lämmerhofer: General scientific concept, methodology, supervision, discussion of the results, review and editing of the manuscript, resources.

**Publication IV** Christian Geibel: Methodology, silatrane synthesis, stationary phase synthesis, HPLC experiments, data evaluation and interpretation, visualization, writing of the manuscript, review and editing of the manuscript. Johannes Theiner: Methodology, elemental analysis, review and editing of the manuscript. **Marc Wolter:** Silatrane synthesis, synthesis of the chiral ligand, determination of reactive sulfhydryl groups, data evaluation, discussion and interpretation of experiments and obtained data, review and editing of the manuscript. Markus Kramer: Nuclear magnetic resonance experiments, review and editing of the manuscript. Wolfgang Lindner: Methodology, review and editing the manuscript. Michael Lämmerhofer: General scientific concept, methodology, supervision, discussion of the results, review and editing of the manuscript, resources.

**Publication V** **Marc Wolter**: Conceptualization, methodology, silatrane synthesis, preparation and characterization of modified silica particles, column packing, HPLC experiments, data evaluation and interpretation, visualization, supervision, writing of the manuscript, review and editing of the manuscript. Christian Geibel: Discussion and interpretation of experiments and obtained data, review and editing of the manuscript. Matthias Olfert: HPLC experiments, discussion and interpretation of experiments and obtained data, review and editing of the manuscript. Min Su: Silatrane synthesis, review and editing of the manuscript. Wolfgang Bicker: HPLC experiments. Markus Kramer: Nuclear magnetic resonance spectroscopy experiments. Wolfgang Lindner: Methodology, review and editing of the manuscript. Michael Lämmerhofer, General scientific concept, methodology, supervision, discussion of the results, review and editing of the manuscript, resources.

**Publication VI** **Marc Wolter**: Conceptualization, methodology, silatrane synthesis, preparation and characterization of modified silica particles, column packing, HPLC experiments, data evaluation and interpretation, visualization, supervision, writing of the manuscript, review and editing of the manuscript. Christoph Barth: Preparation and characterization of modified silica particles, HPLC experiments. Mirna Maalouf: HPLC experiments. Markus Kramer: Nuclear magnetic resonance spectroscopy experiments. Adrian Sievers-Engler: Supervision, review and editing of the manuscript. Michael Lämmerhofer: General scientific concept, methodology, supervision, discussion of the results, review and editing of the manuscript, resources.

**Publication VII** **Marc Wolter**: Conceptualization, methodology, silatrane synthesis, preparation and characterization of modified silica particles, column packing, HPLC experiments, data evaluation and interpretation, visualization, supervision, writing of the manuscript, review and editing of the manuscript. Mirna Maalouf: HPLC experiments. Mateusz Janek: Preparation and characterization of modified silica particles, column packing, HPLC experiments. Cornelius Knappe: Supervision. Markus Kramer: Nuclear magnetic resonance spectroscopy experiments. Michael Lämmerhofer: General scientific concept, methodology, supervision, discussion of the results, review and editing of the manuscript, resources.

# III. LIST OF CONFERENCE CONTRIBUTIONS

**Poster presentation I** **Marc Wolter***, Ulrich Woiwode, Michael Lämmerhofer, Development of stable bond thiol modified silica with high loading density. *Jahrestagung der Deutschen Pharmazeutischen Gesellschaft e.V. (DPhG) 2019*, Heidelberg, Germany, September 1st to 4th; *presenting author.

**Poster presentation II** **Marc Wolter***, Ulrich Woiwode, Michael Lämmerhofer, Synthesis and evaluation of stable bond thiol functionalized silica by using PMPMS. *12th Balaton Symposium of High-Performance Separation Methods 2019*, Siofok, Hungary, September 11th to 13th; *presenting author.

**Poster presentation III** **Marc Wolter***, Michael Lämmerhofer, Preparation of polythiol-functionalized silica particles with adjustable sulfhydryl content and their subsequent modification for silver ion chromatography and enantioselective high-performance liquid chromatography. *Recent Developments in Pharmaceutical Analysis (RDPA) 2021*, Modena, Italy, September 6th to 8th *(virtual edition)*; *presenting author.

**Poster presentation IV** **Marc Wolter***, Michael Lämmerhofer, Characterization of PMPMS-derived stable bond polythiol-silica with adjustable thiol content and its application as precursor silica for preparation of stationary phases for argentation chromatography and enantioselective HPLC. *Jahrestagung der Deutschen Pharmazeutischen Gesellschaft (DPhG) 2021*, Leipzig, Germany, September 28th to October 1st *(virtual edition);* *presenting author.

**Poster presentation V** **Marc Wolter***, Michael Lämmerhofer, Chromatographic exploration and stability evaluation of stable bonded cross-linked amino silica. *26th International Symposium on Separation Sciences (ISSS) 2022*, Ljubljana, Slovenia, June 28th to July 1st; *presenting author.

**CHROM-artwork I** **Marc Wolter**, Ece Aydin, Matthias Olfert, The true secret behind interconversion peaks. *26th International Symposium on Separation Sciences (ISSS) 2022*, Ljubljana, Slovenia, June 28th to July 1st.

**CHROM-artwork II** **Marc Wolter**, Ece Aydin, Matthias Olfert, The real reason for column bleeding. *26th International Symposium on Separation Sciences (ISSS) 2022*, Ljubljana, Slovenia, June 28th to July 1st.

✪ **Poster presentation VI**[1] **Marc Wolter***, Michael Lämmerhofer, Preparation and chromatographic exploration of cross-linked amido-amino silica with improved hydrolytic stability and its evaluation against benchmark amino phases. *Jahrestagung der Deutschen Pharmazeutischen Gesellschaft e.V. (DPhG) 2022*, Marburg, Germany, September 13th to 16th; *presenting author.

**Oral presentation I** **Marc Wolter*,** Michael Lämmerhofer, Strategies for silica modification in stationary phase development for high performance liquid chromatography, *33. Doktorandenseminar des Arbeitskreises Separation Science der GDCh-Fachgruppe Analytische Chemie 2023*, Hohenroda, January 8th to 10th; *presenting author.

[1] awarded with the Best Poster Award sponsored by *ArchPharm* and *ChemMedChem* ✪

✪ **Poster presentation VII**[1] **Marc Wolter***, Michael Lämmerhofer, Development and investigation of a mixed-mode RP/WAX phase with pH-dependent surface charge reversal for hydrophobic charge-induction chromatography of proteins. *51st International Symposium on High Performance Liquid Phase Separations and Related Techniques (HPLC) 2023*, Düsseldorf, Germany, June 18th to 22nd; *presenting author.

**Poster presentation VIII** **Marc Wolter***, Michael Lämmerhofer, Design and chromatographic elucidation of a mixed-mode RP/WAX stationary phase for hydrophobic charge-induction chromatography of proteins. *Jahrestagung der Deutschen Pharmazeutischen Gesellschaft e.V. (DPhG) 2023*, Tübingen, Germany, October 7th to 10th; *presenting author.

[1] awarded with the Best Poster Award (2nd place) sponsored by *Agilent Technologies* ✪

# V. OBJECTIVE OF THE THESIS

New analytical challenges, driven in large part by advances in pharmacy and medicine, have propelled advances in chromatography methods and instrumentation over the past several decades. In liquid chromatography in specific, this has led to improved hardware such as ultra-high pressure systems and bio-compatible hardware, automated sample pretreatment, and novel stationary phases with new support architectures and selectivities. However, current and emerging challenges require further improvements in most fields. In the area of stationary phases for high performance liquid chromatography, new or combined selectivities are of particular interest due to the increasing complexity of analytes such as pharmaceuticals. In addition, the chemical stability and efficiency of the stationary phases must be improved to meet contemporary requirements as well. Both efficiency and selectivity influence the chromatographic resolution and thus the quality of a chromatographic separation (Figure V.1). The chemical stability of the phase determines the compatibility of the mobile phase, influences the robustness of the analytical runs, and can affect the quality of the detection as degradation products can lead to unwanted background noise. Although a number of new materials have been developed and introduced, silica remains the most important support material for stationary phases in high performance liquid chromatography due to its beneficial properties. In particular, it offers high mechanical strength and an easily modifiable surface, as well as broad solvent compatibility.

Against this backdrop, the aim of this thesis was to design, prepare and investigate new silica-based stationary phases with emphasis on surface modification to improve the efficiency and chemical stability of the phases and to establish and investigate new selectivities.

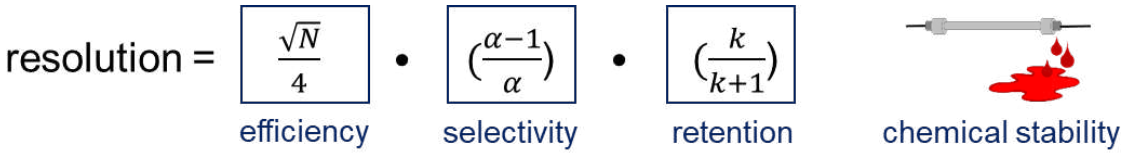


**Figure V.1** Parameters that were the subject of investigation in the course of this thesis for the improvement of stationary phases.

In particular the following goals, concepts and strategies were pursued in the studies presented in this thesis:

- Analysis of chromatographic properties of ligands: Assessing the chromatographic characteristics of the zwitterionic chiral ligands of Chiralpak ZWIX(+) and ZWIX(-) through a fragment-based approach
- Deconvolution of influence on the stationary phase surface charge: Disentangling the effects of chromatographic ligands and silica support on the overall charge of stationary phases by employing ζ-potential and electrophoretic mobility measurements
- Evaluation of alternative thiol silica modification method: Exploring thiol-ene photo-initiated radical addition as an alternative to thermal initiation for stationary phase modification reactions
- Optimization of polythiol silica synthesis: Improving the synthesis of stable-bond polythiol silica as a platform for further modification by thiol-ene click reactions or oxidation
- Assessment of an alternative approach to silanization: Investigation of silatranes as effective silanization agents for silica particles and examination of the surface chemistry properties of silatrane-modified silica
- Improvement of the stability of amino phases: Development of an amino phase with improved chemical stability via a cross-linking approach
- Exploration of innovative chromatographic selectivities for protein analysis: Development of a wide-pore mixed-mode stationary phase capable of pH-dependent charge reversal for applications in hydrophobic charge induction chromatography, providing complementary selectivity and enabling greener liquid chromatography
- Design of stationary phase surface chemistry for biomolecule analysis: Developing a series of phenyl-modified mixed-mode stationary phases with improved silica silanol shielding, opposite charge characteristics, and orthogonal chromatographic properties

# V. CHAPTER ONE

# INTRODUCTION TO HIGH-PERFORMANCE LIQUID CHROMATOGRAPHY AND STATIONARY PHASES

## V.1 Principle of high-performance liquid chromatography and instrumentation

High-performance liquid chromatography (HPLC) is a highly refined form of classical column chromatography and is a key analytical method for separating, purifying, identifying, and quantifying components within a mixture. It is used in various fields such as pharmaceutical research and quality control, food technology, and forensic and environmental analysis, and typically provides analyses with high reliability and precision. [1-3]

The principle of HPLC is based on the distribution of analytes between two phases, the stationary phase and the mobile phase. The stationary phase is typically packed into a column (or prepared in-situ within the column) and remains stationary. The mobile phase, a solvent, is forced to flow through the column by the application of pressure. The analytes are separated within the column according to their affinity for these two phases (or their size in size exclusion chromatography). The higher the affinity of an analyte for the stationary phase, the longer it will remain on the column and the greater the elution time will become. The result of a chromatographic separation is a chromatogram that represents the separation of the components of the mixture and provides parameters to describe the quality of the separation and the chromatographic system (see Figure IV.1). [4-6]

HPLC systems are typically modular in design, consisting of a solvent reservoir, degasser, pump, sample injector, temperature-controlled column oven (including column), and detector. The compartments are interconnected by valves and capillaries (see Figure 2). [7-9]

The solvent reservoir contains the mobile phase, which is degassed as it flows through the degasser upstream of the pump. Degassing removes air bubbles from the solvent, which, due to the compressibility of air, can cause pressure fluctuations in the system, reduced or prevented flow, and ghost peaks. Therefore, the removal of gas from the solvent is of great importance to increase the reproducibility of analytical runs. Typically, vacuum degassers are used in modern HPLC systems. [10]

The pump is a crucial and the most characteristic component of the HPLC system and provides a constant and continuous flow of mobile phase (from the solvent reservoir) through the column and is therefore referred to as the solvent delivery system. Generally, constant-flow pumps are employed. Constant pressure pumps are not suitable for HPLC systems because the flow rate depends on the flow resistance of the column. If the pressure drop changes, the flow rate would be

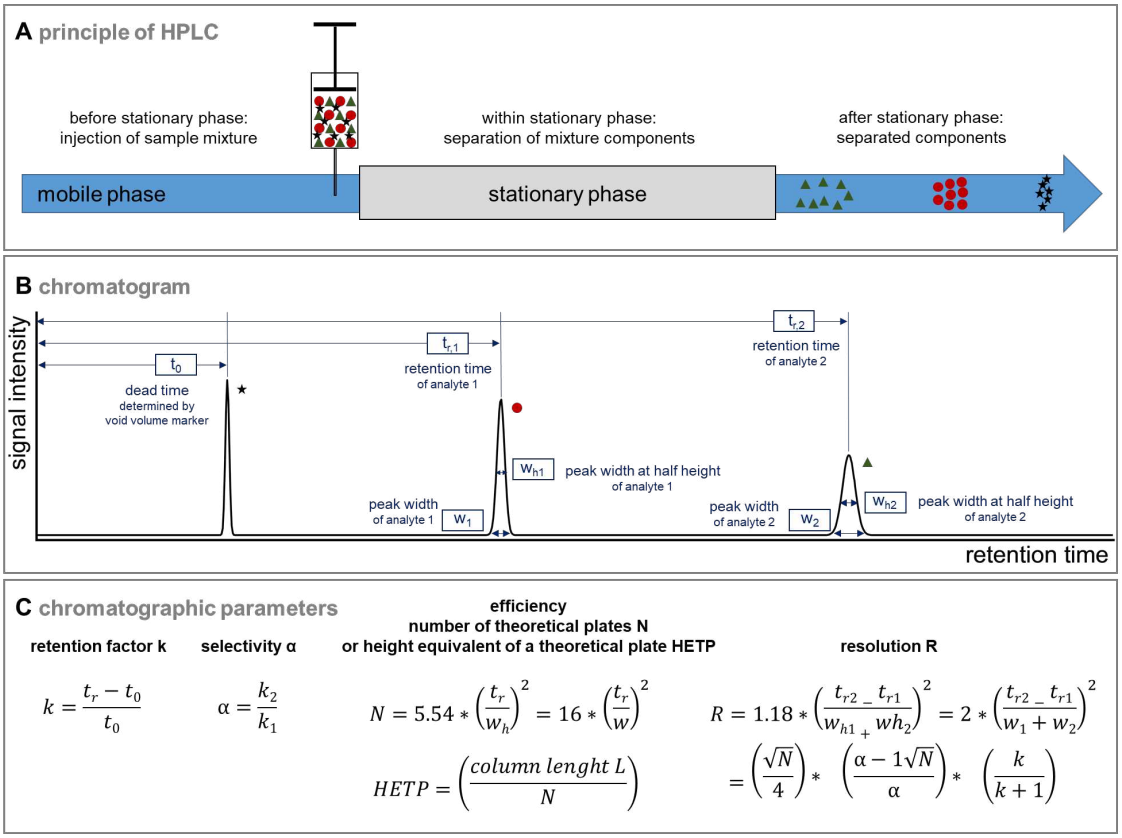


**Figure IV.1.** Principle of separation in HPLC, resulting chromatogram and chromatographic parameters. **A:** In HPLC, the mobile phase transports the sample mixture (under high pressure) through the stationary phase (column), where the separation of the components takes place. **B and C**: After the chromatographic separation, a chromatogram is obtained that provides characteristic parameters. The dead time (or void time) is the time required for a solute to pass through the column without interacting with the stationary phase and is determined by an appropriate void volume marker. Retention time is the time taken for a retained analyte to elute from the column; peak width (at the base of the peak and at half its height) represents the width of the eluted analyte band (and therefore peak broadening/dispersion). The retention factor is a measure of the distribution of an analyte between the mobile phase and the stationary phase. A higher retention factor indicates a longer retention time and thus a greater interaction with the stationary phase. Selectivity is the ratio of the retention factors of two analytes and is a measure of the ability of the chromatographic system to discriminate between two analytes (but does not provide information on peak width and therefore peak overlap and separation quality). Efficiency measures the performance of the chromatographic system and can be expressed as the number of theoretical plates or as the height equivalent to one theoretical plate (HETP or H), which can be calculated by dividing the column length by the number of plates. Resolution is probably the most important chromatographic parameter because it combines efficiency, selectivity and retention time. It measures the degree of separation between two peaks and therefore the quality of the separation. [11, 12]

difficult to control, resulting in unpredictable retention times. There are two solvent delivery modes in which the pump can operate and drive the mobile phase(s) through the system, isocratic solvent delivery (isocratic elution mode) and gradient solvent delivery (gradient elution mode). In isocratic elution mode, the composition of the mobile phase is kept constant throughout the chromatographic run, whereas in gradient elution, the composition of the mobile phase is modified. Gradient elution provides an ability to increase the elution strength of the mobile phase during the run, thereby improving peak shapes and reducing analysis time. However, unlike isocratic elution, gradient elution requires specific pumps and solvent mixers or proportioning valves. The pumps employed can be categorized as quaternary and binary pumps. For quaternary pumps (called “quaternary” because they can mix four solvents), mixing occurs before the pump; for binary pumps (called "binary" because they can mix two solvents), mixing occurs after the pump. Thus, systems where mixing takes place before the pump are classified as low pressure gradient systems, and systems where mixing takes place after the pump are classified as high pressure gradient pumps (see Figure IV.2 and IV.3). [11, 13]

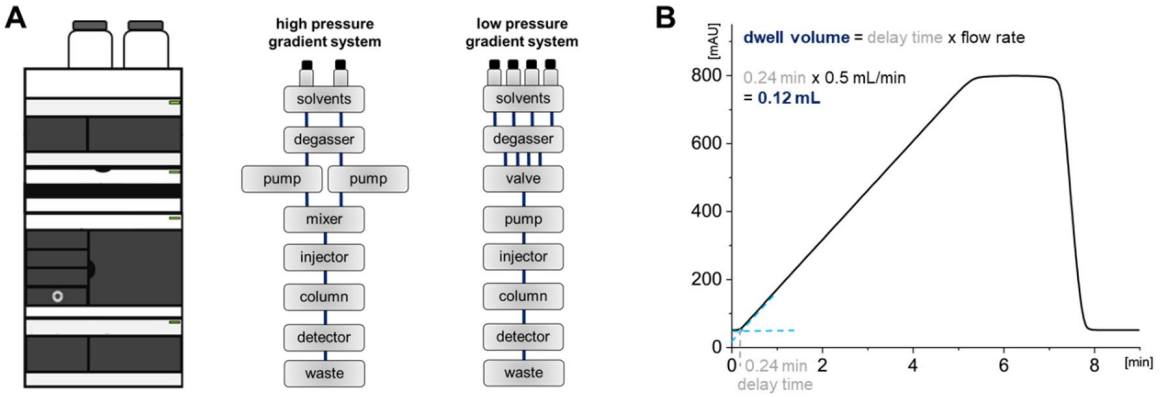


**Figure IV.2.** Modular design of gradient-HPLC systems. **A:** Arrangement of the modules in high pressure gradient and low pressure gradient systems. In general, system components are arranged to keep capillary lengths after the pump (because of dwell volume) and especially after the injector (because of void volume and peak dispersion) as short as possible. **B:** Determination of dwell volume. Dwell volume is the volume of the system from the point of solvent mixing to the column head. The dwell volume results in gradient delay times and therefore needs to be determined especially in high throughput analysis and low-flow gradient applications. The determination is generally carried out experimentally by running a gradient (e.g. 0% B to 100% B) of mobile phase A (e.g. water) and mobile phase B (e.g. water + 0.1% acetone), where the mobile phases must differ in absorbance (e.g. by adding a UV-absorbing additive, here acetone). For measurement, the column must be removed and the capillaries connected via a zero dead volume connector. The arrival of the gradient mixture is indicated by the increase in absorbance in the chromatogram. The dwell volume can then be calculated from the delay time and flow rate.

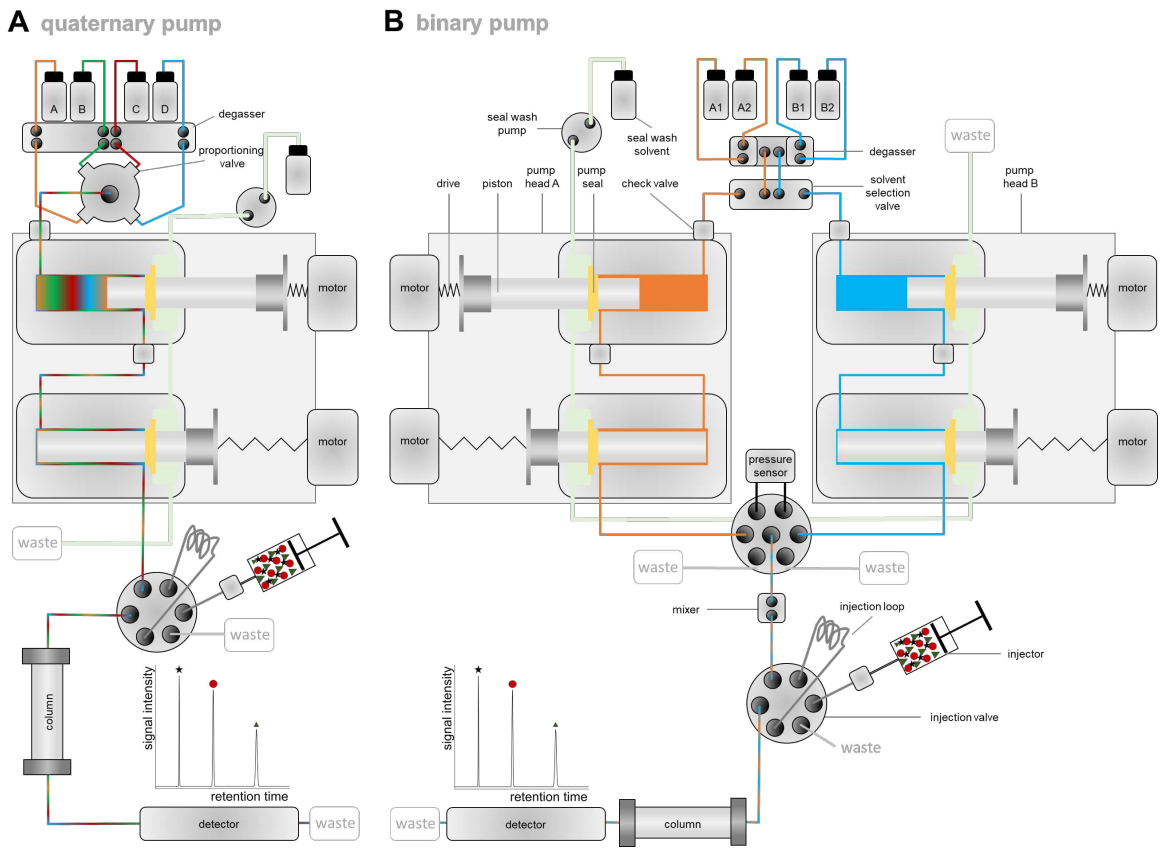


**Figure IV.3.** Schematic illustration of a quaternary (**A**) and a binary pump (**B**) employed in gradient-HPLC systems. Illustration is based on [13]. Both pumps exhibit a dual-piston in series design. In these pumps, the primary piston provides the flow to fill the secondary cylinder with a retracting secondary piston. During this process the system is in flow. Quaternary pumps consist of a pump and the gradient is created by a proportioning valve. Typically, quaternary pumps can mix up to four solvents. Therefore, the proportioning valve creates the gradient by opening a dosage valve to adjust the percentage of solvents. Inside the pump, the plunger creates a turbulent environment during suction, mixing the solvents together. Of note, some systems add mixing chambers after the pump to further homogenize the mobile phase before delivering the gradient mixture to the column. Binary pumps consist of two independent pumps (pump head A and B) and can mix two solvents together. The mixing of the mobile phase is controlled by the relative flow rate of the two pumps and the total flow rate is determined by the combined flow rates of the two pumps. Binary pumps are generally considered to provide more accurate and reproducible solvent mixtures and gradients than quaternary pumps. **Proportioning valve**: It generally consists of four solenoid valves, which are connected to the solvent bottles (via the degasser). The solvent mixing ratio is determined by the timing of the opening of the solenoid valves. **Solvent selection valve**: It allows the selection of the attached solvents. This permits more than two solvents to be connected to a binary pump system. However, only two mobile phases can be selected to build the gradient (channel A and channel B). **Pump head**: The pump head contains one or two chambers to accommodate the piston(s). In binary pumps there are two pump heads combined. **Check valve**: The valve ensures that the mobile phase can only flow in one direction. This prevents backflow and pressure drops, such as those that occur during the piston replenishment cycle. **Piston**: A rod of inert material (e.g. sapphire). It moves back and forth in a piston chamber inside the pump head, delivering the solvent. **Piston seal**: It serves to seal the piston to the rear. **Drive**: It controls the reciprocating motion of a piston. The drive train is usually powered by a motor and includes a mechanism such as a rotary or spindle drive to convert rotary motion into linear motion. **Seal wash solvent and pump**: The seal wash is used to clean the piston and plays a particularly important role when salts are dissolved in the mobile phase. it prevents them from crystallizing in the piston chamber and damaging the piston and the piston seal. **Injection valve**: It is usually a rotary valve, that allows a sample to be introduced into the column. An injection valve can be a single manual valve or part of an autosampler. The system generally consists of a needle port, a rotor/stator assembly and a replaceable sample holder.

The injector introduces the sample into the flow path of the mobile phase, usually directly in front of the column (to keep the void volume to a minimum). The injection valve provides the link between the injector and the flow path. Classic manual injection valves are rarely used in modern systems. Instead, automated sampling systems are commonly used, typically consisting of an injection module and a (temperature-controlled) sampling chamber. This allows programmed, unattended sample introduction. In addition, injection systems are now available that enable mixing (and thus on-time derivatization) of multiple samples within the autosampler prior to injection. The injector modules of autosamplers are usually of split-loop design, but push-loop and pulled-loop designs are also employed (see Figure IV.4).

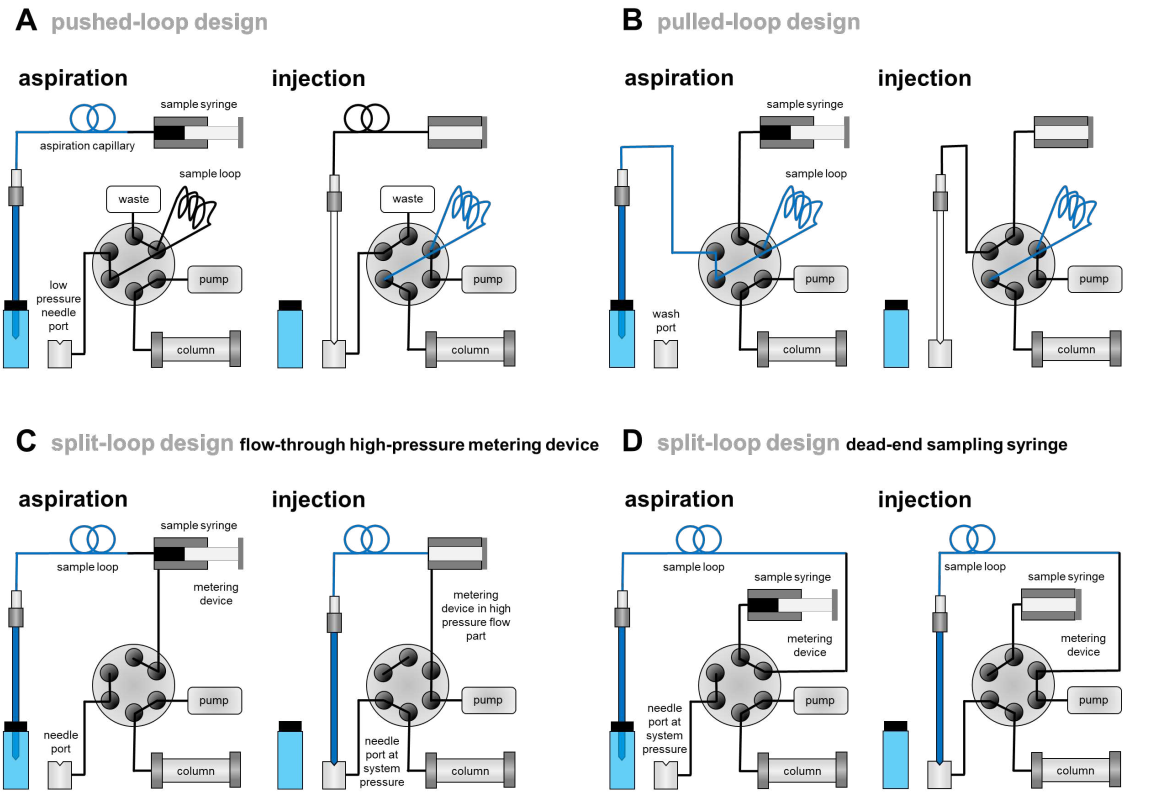


**Figure IV.4.** The figure shows the three most common operating principles of autosampler injectors: pushed-loop (**A**), pulled-loop (**B**), and split-loop designs (**C**, **D**). The figure is based on [14]. The pushed-loop design is likely to the manual injection. In contrast, the pulled-loop design does not include a needle port, which makes it more robust and reduces the contribution of injection to pre-column dispersion and dwell volume. However, there are some drawbacks, most notably higher sample consumption (as not all of the aspirated sample is typically transferred to the column) and increased carryover, which can be reduced by multiple wash cycles (which is time consuming and therefore negatively affects cycle time). The split-loop design is the most commonly used operating principle in modern autosamplers. When using a high-pressure flow-through syringe, this operating principle has the advantage of very high injection precision and constant purging of the instrument so that no air bubbles accumulate. When using a dead-end syringe, on the other hand, air can accumulate inside the syringe, which can negatively affect injection volume accuracy. However, this design has the advantage of a reduced dwell volume.

In general, a maximum injection volume of 10% of the effective column volume is considered appropriate to keep band broadening caused by the injection plug to an acceptable level. [14]

The column used in HPLC is the key component of the system, since it contains the stationary phase and is therefore where the separation of the mixture takes place. It is typically housed in a column oven compartment with adjustable temperature control. The stationary phase must be chosen with respect to the analytical problem and can be considered one of the most decisive factors in method development. Fortunately, there is now a wide variety of chromatography columns (commercially) available, which are based on different architectures and offer various selectivities (discussed in more detail in chapters IV.2 and IV.4). The development of ultra-high performance liquid chromatography (UHPLC) systems (with up to more than 1200 bar applicable pressure range) has also made it possible to use smaller particles in stationary phases, leading to a significant improvement in chromatographic performance. Previously, the backpressure associated with smaller particles could not be withstood by conventional HPLC systems (maximum of approximately 400 bar). [15-17] In addition, recent improvements in the manufacture of high-precision valves have also enabled the increasing use of multidimensional setups, in which two or more columns can be connected in series and their orthogonal selectivities combined directly in a single setup (see Fig. IV.5). [18]

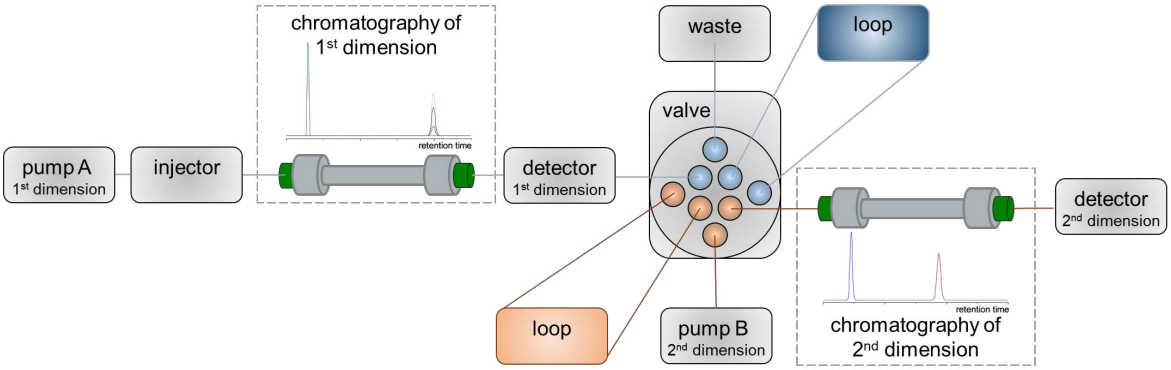


**Figure IV.5.** Simplified illustration of a (multidimensional) 2-dimenional (2D)-HPLC setup combining two orthogonal columns in the first and second dimension for sufficient separation of an analytical mixture. In the first dimension, the three components were not successfully separated as components 2 and 3 (blue and red traces) were not resolved. However, both were separated from component 1 (green trace). After transferring the co-eluted components 2 and 3 to the second dimension, the components were sufficiently discriminated by the column in the second dimension. This combination of different separation mechanisms using two orthogonal stationary phases in series is being used more and more frequently, especially in research and development departments, due to the increasing complexity of biomolecules of interest to the pharmaceutical industry (e.g. therapeutic monoclonal antibodies). [19-22]

At the end, a detector has always to be attached to the system, since HPLC by itself is only a separation method (see Table IV.1). The most common detection method hyphenated with HPLC is ultraviolet/visible light (UV/VIS) absorption detection (UVD) (see Fig. IV.6). However, fluorescence detection (FLD), mass spectrometry (MS) detection (which can be performed using a variety of mass analyzers such as quadrupole-, time-of-flight-, ion trap- or orbitrap-MS), refractive index detection (RID), charged aerosol detection (CAD), evaporative light scattering detection (ELSD) and electrochemical detection (ECD) are also commonly used. All of these detection methods are based on different principles and can therefore be used for different analytical challenges. In particular, the detectability of the analytes, the analyte concentration and the accuracy and sensitivity of the (quantifying) detector are the most important considerations when selecting a detection method, but other considerations such as the need for (complex) sample preparation (e.g. adding of a fluorescent tag) and system cost may also influence the choice of detection method. [23, 24] Moreover, the combination of several detection methods can be a viable approach to obtain a more comprehensive picture of the components of a mixture, especially in the context of structure elucidation and characterization of complex biological samples or quality control of therapeutics (see Figure IV.7). [25]

**Table IV.1.** Detectors hyphenated to HPLC. [26]

| detection method | requirements for analyte | detection limit | destructive analysis |
|---|---|---|---|
| UVD | chromophor, UV/VIS radiation between 190 and 800 nm | nanogram | non destructive |
| FLD | fluorophor or derivatization with fluoroscence tag | femtogram | non destructive |
| MS | volatile and semi-volatile ionizable analytes | picogram | destructive |
| RID | no requirements | microgram | non destructive |
| CAD | non-volatile and semi-volatile analytes | picogram | destructive |
| ELSD | non-volatile and semi-volatile analytes | nanogram | destructive |
| ECD | redox reaction occures in the presence of an electrical potential | femtogram | destructive |

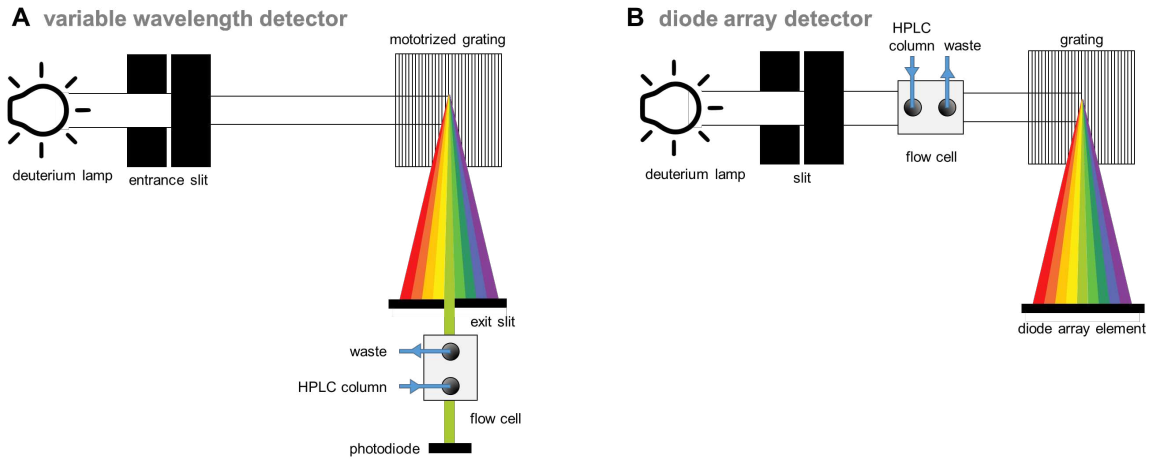


**Figure IV.6.** There are two types of UV/VIS absorption detectors usually hyphenated to HPLC systems, the variable wavelength detector (VWD) and the diode array detector (DAD). The schematic arrangement of a VWD is shown in **A**, that of a DAD in **B**. Both use a deuterium lamp (190-600 nm) as the radiation source. In a VWD the polychromatic light spectrum is directed into a monochromator. The monochromator consists of an entrance slit, a diffraction grating (or prism), and an exit slit. The motor-driven grating scatters the light spectrum and can be turned to select a particular wavelength through the exit slit to the flow cell. The transmitted light from the flow cell then strikes a single photodiode, which converts the light energy into electrical signals. Compared to VWD, DAD offers much more flexibility and capability (but is more expensive). DAD provides UV spectra of eluting peaks while operating as a multi-wavelength UV/VIS detector. In a DAD detector, the full spectrum of the deuterium lamp passes through the flow cell. The transmitted light is dispersed by a fixed grating onto a diode array element that monitors the intensity of the light at each wavelength. Most DADs use a charge-coupled diode array of 512 to 1024 diodes (or pixels) with a spectral resolution of about 1 nm. Today, the DAD is the preferred UV/VIS detector in most applications. [27]

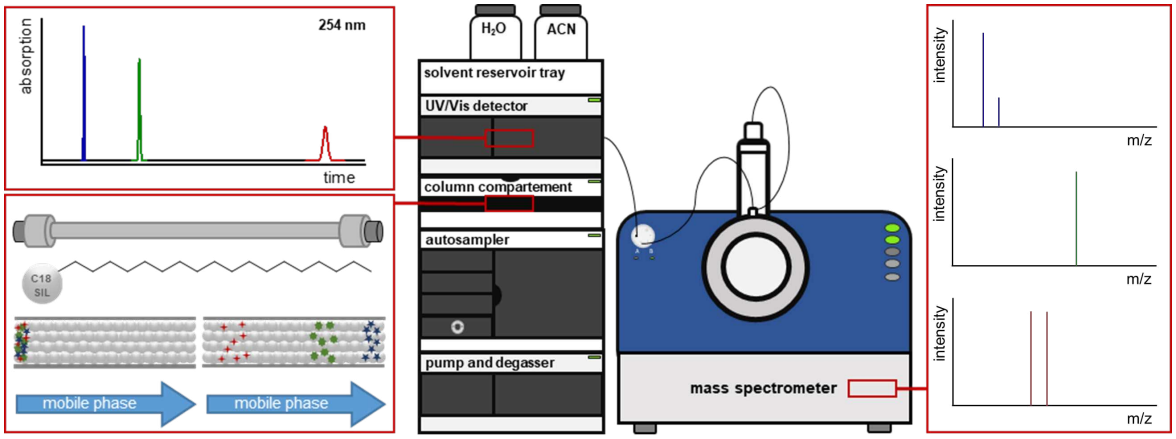


**Figure IV.7.** Experimental setup combining the two different detection methods, UV/VIS absorbance detection (UVD) and mass spectrometry (MS). After chromatographic separation (in this example on a C18 column), the analytes need to be detected. Since a single detection method may not detect all components or provide sufficient information about (unknown) analytes, it may be advantageous to combine several orthogonal detection methods. This provides a more complete picture of the components in the mixture. With UVD, analytes with a chromophore can be detected regardless of their ionizability, whereas MS detection is only possible for analytes that are ionizable. However, in contrast to UV/VIS detection, a chromophore is not required. UVD can simultaneously record the UV/VIS spectra of the molecules, while MS provides valuable information about the mass-to-charge ratio of the analytes. Therefore, the combination of these two orthogonal detection methods is a valuable and common combination, allowing analytes with a chromophore and ionizable analytes without a chromophore to be detected and mass and UV/VIS spectra to be obtained in a single run. An impressive example of this combination can be found in reference [25].

## V.2 Stationary phase architectures and column packing

In HPLC, the stationary phase is where the separation of the components of the mixture takes place and is therefore the most critical feature of the system. For this reason, stationary phases have been the subject of intensive research and development over the last few decades. As a result, a large number of different stationary phases are available today, which differ in terms of support chemistry and architecture, as well as surface (modification) chemistry (surface chemistry will be discussed in more detail in chapter IV.4). All of these properties affect the efficiency, selectivity, and chemical and mechanical stability of the stationary phases. The choice of architecture and support chemistry (as well as surface chemistry) depends on the analytical problem to be solved and the equipment available. The different types have different advantages and disadvantages, and require different technical equipment. The ideal support consists of a high surface area onto which a broad variety of chemical entities can be easily irreversibly and unalterably attached to provide useful selectivity for a range of separation challenges. In addition, physical and chemical stability over a wide range of pressures, pH, temperatures, and solvents is desirable. Availability of a variety of particle sizes with narrow particle size distribution, pore sizes, and volumes is also required. Another point to consider in this context is column packing, as most stationary phases are packed into a column (but note that monolithic phases are usually be prepared in-situ within the column). This makes the process a critical step, as the homogeneity and the density of particle-packed beds have a major impact on chromatographic performance. [28-33]

Silica-based and organic polymer-based materials are the most commonly used stationary phase supports. Other inorganic materials such as zirconium oxide, titanium oxide, alumina and porous graphitized carbon are also used, as well as silica hybrid materials. The non-silica inorganic materials are therefore of minor importance, are not widely used and are rarely commercially available. [31, 34, 35] Hybrid silica materials with coated metal oxides (such as zirconia or titania) or graphitic carbon have also been developed, but have received little attention and interest in research and commercial supply. [36-42] On the other hand, silica-organic hybrid materials, such as bridged ethylene hybrid (BEH) silica have become

very important and are increasingly used as starting material for commercial stationary phases. [15, 43-46]

There are generally two basic stationary phase architecture concepts used within HPLC columns, spherical particles and monoliths. These can also be further subdivided, mainly according to differing porosity characteristics. For particles, fully porous particles (FPP), superficially porous particles (SPP, or core-shell particles) and non-porous particles (NPP) can be distinguished. For monoliths, architectures can be divided into non-porous and porous skeletons with a usually bimodal pore size distribution (see Fig. IV.8). [28, 40, 47-49]

Silica particles for HPLC stationary phases are commonly prepared by sol-gel methods, such as the procedure described by Stöber et al. (using tetraethylorthosilicate (TEOS) as monomer, alcohol as solvent, water as reactant and ammonia as catalyst) or by aggregation of silica sols in air (to reduce metal contamination and produce high-purity silica). [50, 51] These techniques can produce silica particles with adjustable particle diameter, pore size, and pore volume with high precision and reproducibility, making customizable particles easily achievable. In addition, standard silica is available from a variety of suppliers in a

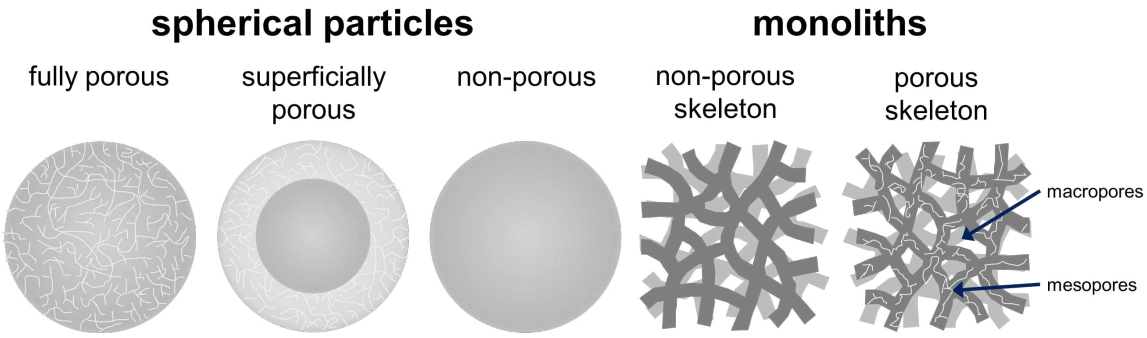


**Figure IV.8.** Overview of stationary phase architectures. There are two basic concepts used in HPLC stationary phases, particles and monoliths, which can be further divided into subcategories. Spherical particles are typically packed into columns to form a dense chromatographic bed. The porosity characteristics mainly influence the available surface area (and therefore the interaction area and loading capacity of the phase) and the mass transfer resistance, which is governed by diffusion. The mass transfer resistance decreases in the order FPP > SPP > NPP. Monoliths are prepared in-situ within the column (typically by a polymerization process using monomers, cross-linkers and porogenic solvents). Mass transfer resistance is generally even more reduced for monolithic stationary phases than for particle packed beds, as the mass transfer process is dominated by convection due to the large macropores. Monolithic columns based on silica and organic polymers are commercially available. However, the interest in monolithic columns is declining after they gained fame and interest more than twenty years ago due to the promising expectations of high efficiency/backpressure ratio and suitability for the analysis of especially large biomolecules (due to better mass transfer properties for large molecules). [28, 47-49, 52, 53]. Impressive scanning electron microscopy (SEM) images of the distinct morphologies can be found in references [54], [55], [56], [57], and [58].

wide range of qualities, sizes, and other characteristics (see Table IV.2). There are three categories of silica available today, type A (or I), type B (or II), and type C (or III) silica. Type A silica is no longer used for analytical purposes (but for preparative ones) because of its high metal impurity content, which activates surface silanols, leading to increased acidity and chelation with complexing analytes. This can lead to excessive retention, peak broadening and asymmetric peaks. Type B silica, on the other hand, is of higher quality than type A silica and contains significantly less metal impurities. Therefore, phases derived from type B silica as starting material typically offer higher efficiencies and better peak shapes. Both type A and type B silica contain a large number of acidic surface silanols, which are assumed to be responsible for one of the major drawbacks of silica supports, the additional secondary interactions of analytes with (unmodified) silanols (which, however, in some cases can also be considered as favorable). Consequently, the silanols have a significant effect on the chromatographic process. In particular, silanols can cause adverse adsorption-desorption kinetics of basic components, resulting in broad peaks and low column efficiencies for these analytes, or even complete adsorption of, for instance, large biomolecules, making bioanalysis on silica-based columns extremely challenging. [51, 59-61] The accountable surface silanols on type A and type B silica can be classified into three types, single silanols, vicinal silanols, and geminal silanols, which differ mainly in their acidity due to the formation of hydrogen bonds (see Figure IV.9A). At elevated pH, these silanols become progressively deprotonated, leading to increased secondary interactions of the analytes with the

**Table IV.2.** Quality control results of silica obtained from various suppliers according to the supplier certificates of analysis.

| | Kromasil 100-5-SIL[1] | Halo-Sil 2.7 µm 160 Å[2] | Halo-Sil 3.4 µm 400 Å[2] | Halo-Sil 2.7 µm 1000 Å[2] | EP-DF-5-100A[3] | EP-DF-5-120A[3] | EP-DF-1.8-120A[3] |
|---|---|---|---|---|---|---|---|
| **particle size [µm]** | - | 2.69 | 3.47 | 2.80 | 4.39 | 4.34 | 1.78 |
| **pore size [Å]** | - | 156.5 | 312 | 818 | 99 | 124 | 98 |
| **pore volume [ml/g]** | - | - | - | - | 0.97 | 0.95 | 0.86 |
| **surface area [$m^2$/g]** | 299 | 79.5 | 17.4 | 20.9 | 391 | 306 | 351 |
| **particle size $d_v$50 [µm]** | 6.18 | - | - | - | - | - | - |
| **particle size $d_v$90/10** | 1.44 | 1.12 | 1.11 | 1.14 | 1.41 | 1.39 | 1.35 |
| **metal content: Al [ppm]** | <1 | - | - | - | 0.3 | 1.4 | 0.5 |
| **metal content: Fe [ppm]** | 5 | - | - | - | 2.7 | 9.5 | 1.3 |
| **metal content: Na [ppm]** | 7 | - | - | - | 1.2 | 1.2 | 1 |
| **metal conent: Ti [ppm]** | - | - | - | - | 0.1 | 0.3 | 0.1 |
| **metal conent: Mg [ppm]** | - | - | - | - | 0.2 | 0.1 | 0.1 |
| **metal conent: Ca [ppm]** | - | - | - | - | 1.2 | 0.1 | 1 |

[1]Akzo Nobel [2]Advanced Materials Technolog, Inc. [3]AGC Si-Tech Co., Ltd.

silanols due to electrostatic interactions (which can be adsorptive or repulsive in nature). [62-64] Type C silica, on the other hand, does not carry a significant number of silanols on the surface. The silanols were converted to less polar hydrides (see Figure IV.9B). Thus, basic pharmaceuticals can be analyzed with good peak shape on silica-hydride stationary phases as a consequence. However, type C hydride-silica requires different surface modification strategies than type A and B silica (see chapter IV.3) and is not yet a standard material for columns in stationary phase development or commercial use (but may be in the future), mainly due to the lack of small particle sizes and missing core-shell variants on the market. [65-69] Besides the secondary silanol interactions, another disadvantage of silica supports is the narrow pH range in which such phases can be used (pH 2-8). At pH values below 2, the siloxane bonds to the immobilized ligands are cleaved (also called column bleeding), while at pH values above 8, the support itself dissolves rapidly. These effects accelerate dramatically with rising temperature and increasing water content in the mobile phase. [70-73]

In order to overcome the pH instability of silica (especially at high temperatures and high water content) and to eliminate the adverse silanol interactions, attempts have been made to use other metal oxides such as zirconium oxide or titanium oxide. These materials typically provide high chemical stability and mechanical strength (as does silica). Zirconia is one of the materials that has received the most effort. However, zirconium has acidic and basic, oxidizing and reducing properties on its

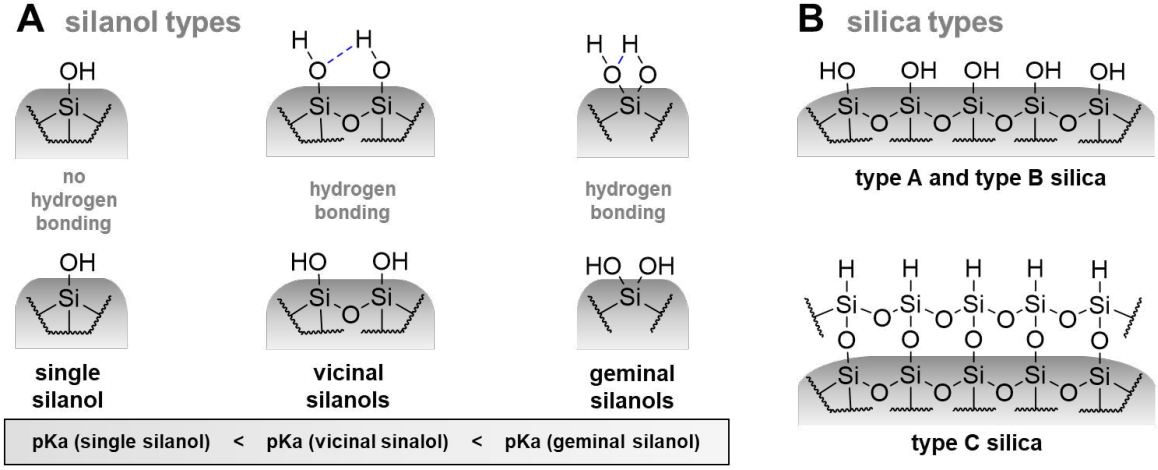


**Figure IV.9. A**: Types of silanols present on type A and B silica. Due to the different types of silanols present, the $pk_a$ values for the silica surface range from approximately 3.5 to 7.0. Hydrogen bonding stabilizes the silanol and reduces silanol acidity. [62, 63, 74] **B**: Comparison of surface chemistry of type A, B and C silica. In type C silica, approximately 95% of the silanols have been replaced by hydrides. [65, 67]

surface, which greatly complicates its use in chromatographic applications. Furthermore, the lack of experience in the synthesis (and the availability) of particles with adjustable particle size, pore volume, as well as in surface modification (in contrast to the vast experience in silica modification), has ultimately led to the relative irrelevance of such non-silica inorganic supports in today's stationary phase landscape. [31, 34, 35, 65, 70, 75, 76]

Porous graphitic carbon (PGC) particles have also been proposed as an alternative material with advantageous properties, especially due to high pH stability (pH 1-14) and temperature stability (higher than 200°C). PGC behaves relatively like alkyl silica for non-polar analytes, but offers completely different behaviour for polar compounds. However, such columns are highly susceptible to contamination, resulting in high variability, loss of capacity and poor peak shapes. Few PGC columns are commercially available today. However, there have been some recent advances in the manufacture of PGCs in terms of resistance to contamination and particle size distribution that may lead to increased use of these materials. [41, 42, 77, 78]

Another approach to overcome the pH stability issues and secondary silanol interactions of silica supports has been the implementation of polymer-based particles. Thus, organic polymer beads were developed and investigated, and as a result, (modified) polyacrylate, polymethacrylate, polystyrene and polydivinylbenzene beads and other polymer spheres, were prepared and used for HPLC applications. Such particles have mainly been synthesized by thermally or photo-initiated polymerization reactions, including suspension, emulsion, dispersion, precipitation and multi-stage seed swelling polymerization. The prepared phases offer high pH stability and can be operated over the entire pH range in many cases (making them indispensible in ion exchange chromatography). In addition, organic polymers lack unwanted secondary interactions (such as silanol interactions in silica phases) and can provide inert surfaces (making them useful for size exclusion chromatography and highly biocompatible). However, there are some drawbacks to polymeric phases, particularly in terms of mechanical stability (especially for highly porous beads) and solvent compatibility. Polymeric phases can suffer from swelling when certain solvents are used as mobile phases, which can affect particle and pore size and therefore the separation efficiency of the

chromatographic material. However, swelling problems have been greatly reduced in the materials that are commercially available today and organic polymer beads have found wide application in many fields of research and routine analysis. [79-86]

In recognition of this, silica-organic hybrid materials have been developed to combine the benefits of silica particles with those of organic polymer beads. The most common hybrid material is ethylene-bridged hybrid (BEH) silica, on the basis of which stationary phases are now commercially available (see Figure IV.10). Hybrid-silica materials can be operated in a pH range between 1 and 12 without degradation of the support and therefore represent a tremendous improvement without changing the beneficial properties of silica such as physical stability and easily modifiable surface (since the surface chemistry does not change as the surface silanols are maintained). Furthermore, the incorporation of the ethylene bridges allows fine tuning of the surface silanol content, thereby adjusting undesired silanol activity. [87-89]

In addition to these chemical and physical properties of the support materials (which particularly affect pH and pressure stability), the architecture of the materials is also a key factor for stationary phases and plays a decisive role in their chromatographic performance. The categories of phase morphology can be divided into particles and monoliths. Monoliths received a lot of attention more than twenty years ago and were considered a promising concept for future HPLC columns because they offered good efficiency-to-backpressure ratios and were particularly interesting for high throughput analysis and biomolecule analysis due to favorable mass transfer properties. In spite of these promising properties, they have not been widely

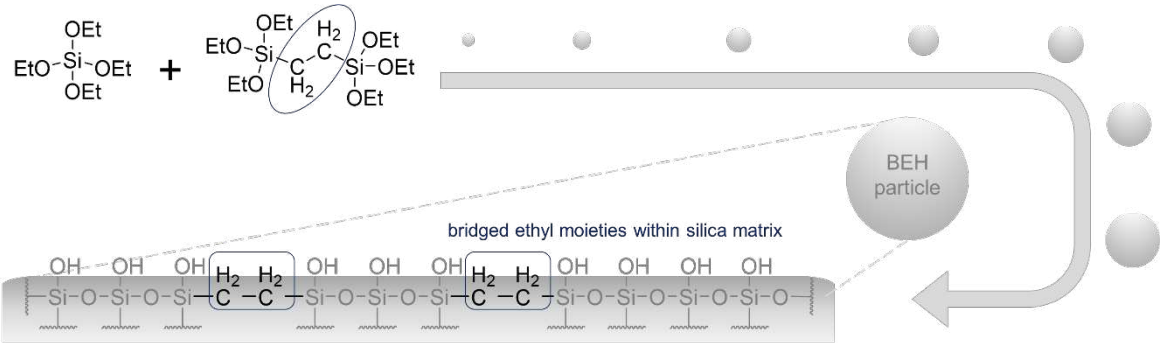


**Figure IV.10.** The ethylene-bridged hybrid silica particles are made from two monomers, tetraethoxysilane (TEOS) and bis(triethoxysilyl)ethane (BTEE), resulting in highly pH-resistant and high mechanical strength particles. [87-89]

adopted in routine applications, and there appears to be only a small amount of interest and development left in this area. On the other hand, there are some highlight developments in particle architecture that have occurred in the last decades, making research on particle-based stationary phases of paramount interest. The two milestones of the last decades have been the introduction of sub-2µm particles and core-shell technology. Both have led to tremendous improvements in column efficiency. In addition, there are still classic parameters that can be adjusted to tune the chromatographic properties of particle-based stationary phases. [28, 47-49, 52-54, 90]

Parameters that can be adjusted for particle-based stationary phases include particle size (and size distribution), pore size (and total porosity), and surface area. These parameters can be used to influence chromatographic efficiency and retention. Particle size (and size distribution) and total porosity (to account for core-shell technology) affect the efficiency of the chromatographic material, while pore size and surface area affect the retention of analytes within the column. The particle surface is the site of interaction of the analyte with the stationary phase and therefore the site of retention (or, in rare cases, repulsion). The surface area is directly related to pore size and pore volume (noteworthy, within the column, particle size also impacts the total surface area due to the corresponding density of the packing). Thus, small pore sizes are often preferred to obtain high surface areas and thus higher resolution and loading capacity. Nevertheless, the pore diameter should be at least four times larger than the hydrodynamic diameter of the analytes to ensure adequate pore penetration and therefore sufficient interaction with the stationary phase surface. Therefore, the pore size needs to be chosen appropriately for the size of the analytes to be targeted. For example, particles with pore sizes of 60-120 Å are generally used for small molecules, 100-300 Å for medium-sized analytes such as oligonucleotides, and 300-1000 Å for large biomolecules such as proteins. In addition, it should be noted that an increase in porosity is always associated with a decrease in mechanical strength and therefore a decline in the pressure limits of the stationary phases. [48, 91-93]

Particle size reduction has always been a straightforward approach to improving the performance of particle packed columns, since chromatographic efficiency is inversely proportional to particle size according to the van Deemter equation (see

Equation IV.1). Particle sizes of 10 µm and above have been progressively reduced over the years, resulting in the sub-2µm particles available today for high resolution chromatography. Sub-2µm particles provide approximately four times less plate height than conventional 5 µm particles. [49, 94, 95]

$$H = 2\lambda d_p + \frac{2\gamma D_m}{u} + f(k)\frac{d_p^2}{D_m} = A + \frac{B}{u} + Cu$$

**Equation IV.1.** Van Deemter equation. The van Deemter equation describes the dependence of the chromatographic efficiency (plate height H) on the linear velocity u. λ: packing constant, $d_p$: particle diameter, γ: obstruction factor for diffusion in a packed bed, $D_m$: diffusion coefficient of the analyte in the mobile phase, f(k): a function of the retention factor k. [95] More information about the van Deemter theory and the A-, B- and C-term can be found in Figure IV.12. It should be noted that in addition to the van Deemter equation, there are other important models that deal with chromatographic dispersion, such as the Giddings model, the Horvath-Lin model, the Knox model, and the kinetic plot model. [96-100]

On the other hand, the permeability of sub-2µm particles is about 10-30 times lower than that of 5 µm particles. Moreover, according to Equation IV.2, the pressure drop is inversely proportional to the square of the particle diameter. [95] Therefore, higher back pressures must be overcome when using sub-2µm particles. As a consequence, the introduction of ultra-high pressure systems, which enable operating pressures of more than 1200 bar, made the use of sub-2 µm particles possible for the first time and paved the way for the widespread use of these particles. Previously, conventional instruments could only handle 400 bar and could not withstand the high pressures generated by sub-2µm particle columns. [49, 94, 95]

$$\Delta P = \frac{\Phi \eta L u}{d_p^2}$$

**Equation IV.2.** The equation describes the dependence between pressure drop ΔP and linear velocity u. $d_p$: particle diameter, Φ: flow resistance factor, η: viscosity of solvent (mobile phase), L: length of packed bed (stationary phase). [95]

Another challenge to overcome when working with sub-2µm particles is frictional (or viscous) heating, which leads to non-uniform temperature gradients within the

column (see Figure IV.11). The longer the column, the more the radial temperature gradient can develop and occur along a significant part of the column length. Therefore, peak dispersion (and loss of efficiency) by frictional heating increases consequently with column length. In shorter columns, the radial temperature

gradients are only partially developed and therefore less peak broadening occurs. Thus, the detrimental effects of frictional heating can be reduced by downsizing sub-2µm particle columns. However, downsizing is limited by the contribution of the extra column volume of the chromatographic instrument and the associated peak broadening effects. A further option to overcome these drawbacks is to carry out the separations at high temperatures, as the backpressure of the column (and therefore the fractional heating) could be reduced due to the lower viscosity of the mobile phase. The drawback of this strategy is the need for an eluent preheater (and the necessary temperature stability of the column and the analytes), which adds void volume and reduces the efficiency of weakly retained analytes under isocratic conditions (since they are not refocused at the column head). [49, 94, 95, 101-104]

Superficially porous particles (or core-shell or pellicular particles) can be considered even more advantageous and show better chromatographic performance than fully porous particles of the same size. More specifically, fully porous particles need to

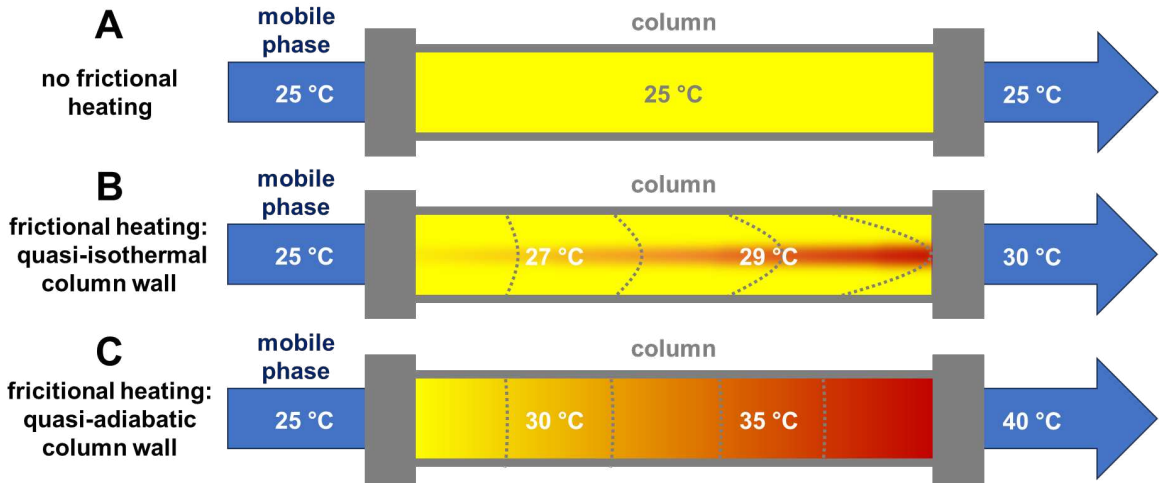


**Figure IV.11.** Schematic illustration of frictional heating effects to the column temperature profiles based on [104]. Frictional heat is generated by the resistance encountered by the mobile phase as it moves through the column. When smaller particles are used, frictional heating can increase significantly because smaller particles create a higher column backpressure. Quasi-isothermal column wall conditions (which can be created using a forced air stream inside the column oven with a high speed fan) result in axial and radial temperature gradients. Quasi-adiabatic column wall conditions, on the other hand, result in only an axial temperature gradient. Frictional heating can significantly affect chromatographic performance, in particular causing band broadening (due to the temperature-dependent increase in the diffusion coefficients of the analytes and the formed temperature gradient within the column), changes in mobile phase viscosity and therefore flow rates, and changes in retention times (due to the temperature-dependent change in the partition coefficient of the analyte between the mobile and stationary phases). [102-104]

be approximately one third smaller in diameter than core-shell particles to achieve comparable plate numbers. Thus, 3 µm core-shell particles can provide the same plate numbers as 2 µm fully porous particles. Moreover, core-shell particles have higher permeability (and therefore lower back pressures) and significantly lower frictional heating, which also contribute to their outstanding chromatographic properties. The core-shell design of such particles consists of a solid inner core surrounded by a porous outer layer. The drawback of this design is a reduction in surface area due to the non-porous core and therefore a reduction in loading capacity. On the other hand, the design has the advantage of shorter diffusion paths compared to fully porous particles of similar diameter. The shorter diffusion paths reduce the effect of mass transfer resistance on peak broadening (see C-term of the van Deemter equation; Fig. IV.12) and therefore improve efficiency. In addition, core-shell particles typically have an exceptionally narrow particle size distribution and a certain surface roughness, both leading to a better homogeneity and quality of packed column beds compared to fully porous particles. The better packing quality ultimately leads to a reduced contribution of eddy diffusion to peak broadening (see A term of the van Deemter equation; Fig. IV.12) and therefore to

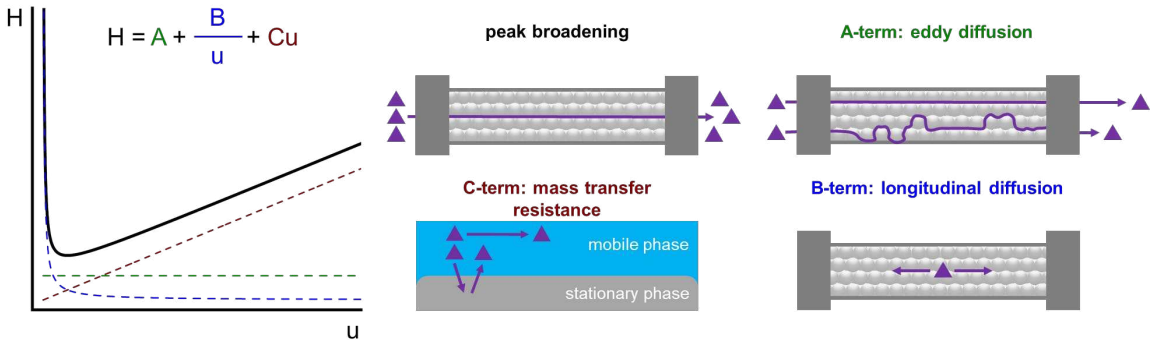


**Figure IV.12.** The van Deemter equation describes peak broadening within the chromatographic process (see also Equation 1). Accordingly, three terms contribute to peak broadening, the A-term [cm], the B-term [$cm^2/s$] and the C-term [s]. [105] The **A-term** describes the peak broadening due to different paths of the analytes through the column. It is strongly related to the homogeneity of the packed bed (and is therefore considered the packing term) and to the particle size and size distribution. The **B-term** describes the contribution of the longitudinal dispersion and depends on the diffusion coefficient of the analyte in the mobile phase, the viscosity of the mobile phase and the column temperature. The higher the flow rate, the smaller the contribution of the B term to the peak dispersion. The **C-term** describes the contribution of mass transfer resistance to peak broadening. Mass transfer is the interaction of the analytes with the surface of the stationary phase and the movement of the analytes into and out of the pores. Since there is usually no mobile phase flow in the pores of the stationary phase, mass transfer depends on the diffusion coefficient of the analytes and the viscosity of the mobile phase. Furthermore, the C-term increases especially with increasing diffusion path length and is therefore lower for small particles and core-shell particles. [106-108]

high chromatographic efficiency of core-shell particles. The outstanding properties of core-shell particles have led to considerable interest in research, industry and commerce, with many suppliers now offering core-shell particles in a wide range of sizes (mostly 1.3 µm to 3 µm) and silica qualities. [28, 58, 95, 109-115]

In order to use particles as stationary phases in high performance liquid chromatography instruments, the particles need to be packed into columns, mainly made of stainless steel (or in some cases polyether ether ketone (PEEK)). The particles are usually packed as a slurry (but dry packing is also possible) into the empty columns by applying pressure. To retain the particles, the columns are usually sealed with metal and glass frits. Stainless steel columns and frits have high mechanical strength and durability, which is essential for use in (ultra)high pressure instruments. [48, 116] However, they tend to interact with analytes via non-specific adsorptive interactions caused by charged metal surfaces or leached metal ions, which is particularly detrimental in the analysis of large biomolecules and can lead to low recovery rates and peak dispersion. This phenomenon has been studied extensively and the need for bio-compatible columns and filters has been clearly formulated. [74, 117-119] In addition to existing bio-compatible HPLC systems, some suppliers now offer bio-compatible columns (e.g. MaxPeak Premier columns from Waters Corporation). However, this is far from being standard column hardware. In-house passivation strategies (e.g. with nitric acid), which have been used in the past to make HPLC systems and empty column hardware more suitable for the analysis of biomolecules, are rarely used today and have been heavily debated in the past because they often lead to instrument damage. Sample passivation is probably the most commonly used method today. This involves multiple injections of the sample to saturate the metal surfaces with the analyte. A constant area under the curve is obtained at the end of the sample passivation process. Table IV.3 summarizes passivation techniques. [120, 121]

The slurry packing method is the most commonly used method for producing particle-packed HPLC columns. In this method, particles are dispersed in a slurry solvent and then packed into a column by applying high pressure by pumping a pushing solvent through the column (high pressure filtration). The packing pressure should be considerably higher (at least 50%) than the later operating pressure to avoid compression of the analytical bed during operation (and thus the formation of

void volumes and channels). [48, 122, 123] During the filtration process, the bed is formed when the particles come into contact with each other and become densely associated. Once this is done, particle movement is extremely limited. The structure and quality of the resulting bed depends on the shear forces between the particles, the friction between the particles and the column wall, and the axial and radial stress distributions during the packing process. The stress distribution is strongly related to the viscosity of the suspension. As (concentrated) particle suspensions are non-Newtonian fluids, the viscosity changes as a function of shear rate (shear thickening or thinning effect) and is therefore dependent on the pressure and flow rate applied in addition to the particle concentration. [29] Packing inhomogeneities can particularly affect the A-term of the van Deemter equation and therefore lead to poor column efficiencies. In general, the use of spherical and small particles, particles with narrow particle size distributions and core-shell particles results in beds with favorable packing properties and low A-terms. [48, 114, 122]

The design of column packing equipment is rarely described in the literature and there is little information available from commercial column manufacturers on the column packing process. However, the design should at least result in a sufficient introduction of the suspension from the slurry reservoir into the empty column. Therefore, the slurry reservoir outlet should have the same outlet diameter as the internal diameter of the column. In addition, the slurry reservoir should be sized to allow appropriate slurry concentrations, which have been reported to be around 7-15 %, but in fact need to be determined in packing studies to find the ideal

**Table IV.3.** Passivation strategies applied for HPLC equipment according to [121].

| procedure | mechanism | outcome and concerns |
|---|---|---|
| acid passivation | removal of free ion from surface | ▪ time consuming<br>▪ temporary<br>▪ signal suppression |
| sample passivation | temporary coating of surface | ▪ time consuming<br>▪ not stable |
| mobile phase additives | metal chelation | ▪ ion suppression<br>▪ solubility issues |
| PEEK or PEEK/metal cladding | non-interactive polymer | ▪ pressure limits of up to 400 bar for pure PEEK<br>▪ metal cladding can provide limits up to 1200 bar<br>▪ physical variability<br>▪ solvent compatibility |
| alternate metal or alloy (e.g. titanium) | iron-free metal | ▪ prone to ion leaching<br>▪ methanol pitting |
| industrial coatings | coating of surface | ▪ conformal coating<br>▪ more prolonged passivation effect |

concentrations for each case. [30, 122]

The choice of the appropriate slurry solvent (and to some extent the pushing solvent) has a major impact on the quality of the packing. In particular, the slurry solvent must be capable of forming a stable colloidal suspension of the particles and preventing them from agglomerating. The slurry solvent must be able to wet the particles sufficiently to prevent floatation (surface energy matching) and the viscosity should be such that rapid sedimentation is prevented but high column packing velocities are still possible due to acceptable backpressure (see Equation IV.3). [30, 122] Column packing with particles smaller than 3 µm requires special care in the choice of slurry solvent, because the adhesion forces between the particles are much higher than for 5 µm particles. Therefore, for particles smaller than 3 µm, highly stable suspensions must be prepared prior to slurry packing. [48]

$$v = \frac{2}{9} \cdot \frac{[\rho_K - \rho_D] \cdot r^2 \cdot g]}{\eta}$$

**Equation IV.3.** Stoke equation. The equation describes the sedimentation rate v of spherical particles in a liquid medium. The sedimentation rate decreases with increasing viscosity of the liquid phase η, decreasing particle radius r and decreasing density differences between the two phases. $\rho_K$: density of the particle, $\rho_D$: density of the liquid, g: gravitational acceleration. An examination of the influence of gas in the pores of the silica particles on the settling properties can be found in reference [124].

Another approach is to adjust the pH of the slurry solvent to create charged surfaces on the dispersed particles to induce repulsion and thus prevent agglomeration (see Table IV.4). [125] Microscopic studies and sedimentation tests can be carried out to assess the suitability of the solvent system prior to column packing studies. A good guideline for solvent selection and evaluation can be found in reference [30].

At the end of the packing procedure, the open end of the column must be closed quickly to prevent the bed from expanding. [122] Special care must be taken to avoid damaging the chromatographic bed and creating voids (by removing excess silica from the end of the column). The quality of the column packing can be assessed by determining the A-term via van Deemter analysis. The procedure is described step-by-step in reference [126]. An example can be found in reference [127]. A schematic illustration of a column packing procedure employed in research can be found in Fig. IV.13.

**Table IV.4.** Effect of the slurry medium on the performance of the prepared chromatographic columns. Here, *O-tert*-butylcarbamoyl quinine functionalized silica particles (5 µm, 100 Å, fully porous) were in-house slurry packed into empty stainless steel columns (50 x 3 mm) utilizing four different slurry media. The slurry concentration was always 250 mg/5mL and the packing pressure adjusted to 800 bar. Methanol was used as packing solvent. The plate number refers to the S-enantiomer of *N*-[(9H-fluoren-9-ylmethoxy)carbonyl]-phenylalanine. The mobile phase used for the chromatographic runs consisted of methanol, acetic acid and ammonium acetate (98/2/0.5, v/v/m). The plate numbers were determined at the optimum flow rate determined by van Deemter analysis. The best efficiency was determined by using 2-propanol + 2% acetic acid as slurry solvent, which combined highest viscosity (slow sedimentation) and acidity (repulsion of charged particles, since the functional ligand offers basic moieties).

| **slurry medium** | methanol | 2-propanol | methanol + 2% acetic acid | 2-propanol + 2% acetic acid |
|---|---|---|---|---|
| **N [$m^{-1}$]** | 57587 | 71682 | 88519 | 105860 |

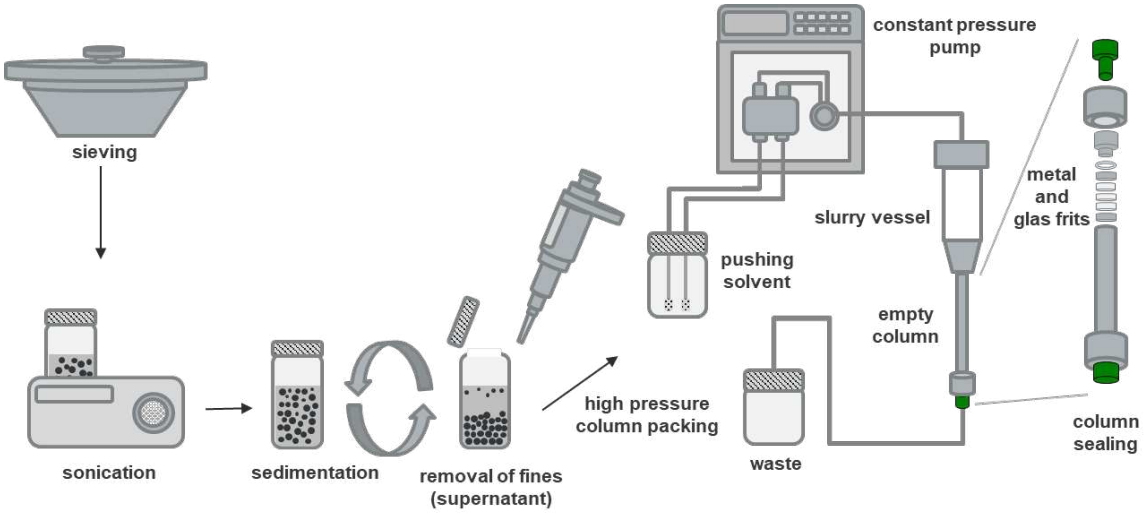


**Figure IV.13.** Schematic illustration of in-house column packing procedure. First, the dried silica is sieved through a 25 µm mesh sieve to remove lint and break up or remove large agglomerates. The silica is then weighed into a glass bottle and dispersed in the slurry solvent. Typically, 220-250 mg of silica (for 50 x 3 mm columns) was weighed into the container and 5 mL of slurry solvent was added. The dispersion was then sonicated 3 times for 10 min each. After each sonication step, the dispersion was allowed to sediment and the fines were carefully removed by discarding the supernatant. The volume removed was always replenished. The slurry was then transferred to the slurry vessel (with the empty column attached and sealed at one end) and all air was removed from the system. A constant pressure pump was then used to push the solvent through the column at 800 bar (for 100-200 Å pore size particles) or 500 bar (for 300 Å pore size particles) for at least 1 h. The column was usually sealed at both ends with 2 metal and 3 glass frits.

## V.3 Surface modification strategies for silica particles

Silica particles are rarely used unmodified as stationary phases in high performance liquid chromatography applications. Typically, the surface is chemically modified to alter the selectivity of the material, reduce silanol effects or increase hydrolytic stability. Another motivation for surface modification is the introduction of reactive functional groups that can be used to incorporate other chemical entities that would otherwise be difficult to attach to the surface. These chemical entities can add further selectivity to the stationary phase. Surface modification is typically accomplished by silanization reactions using small silanes. In addition to small silanes, another strategy is to attach polymers to the surface by adsorptive or covalent binding. Both strategies have different advantages and disadvantages and can be further subdivided in terms of immobilization chemistry. [66, 128-130]

Classical silanization is carried out using chlorosilanes or alkoxysilanes, which can undergo condensation reactions with the surface silanols of the silica support (in type A and B silica), forming Si-O-Si bonds and releasing small, volatile molecules such as hydrochloride gas, methanol or ethanol (see Fig. IV.14). These silanes are available in a great variety of side chains. [66, 131] A novel approach to surface modification is silanization with silatranes (which is also a major topic of the studies presented in this thesis). In contrast to chlorosilanes and alkoxysilanes, silatranes offer advantageous properties, mainly due to their high hydrolytic stability, which prevents the formation of oligomers in solution in the presence of (traces of) water. On the surface of the silica, however, an immobilization reaction is possible due to the catalytic effect of the silanols. In particular, thinner ligand films and high ligand densities with large amounts of trifunctional linkages were observed, indicating the formation of a dense polysiloxane layer on the surface. The formation of the polysiloxane layer is highly favorable in terms of hydrolytic stability, and the formation of a thin layer leads to beneficial mass transfer properties that improve the efficiency of phases prepared with silatranes. Unfortunately, silatranes are only available in a small variety of side chains, so they usually have to be prepared in-house in order to obtain the desired silatrane (see Fig. IV.15-19). [132-135] For type C silica, the traditional modification agents are not applicable and surface modification is typically

achieved by alkene and alkyne hydrosilylation (see Fig. IV.14). A major drawback is the requirement of a metal catalyst in these reactions and the consequent need to remove the catalyst after the reaction. [66, 136, 137]

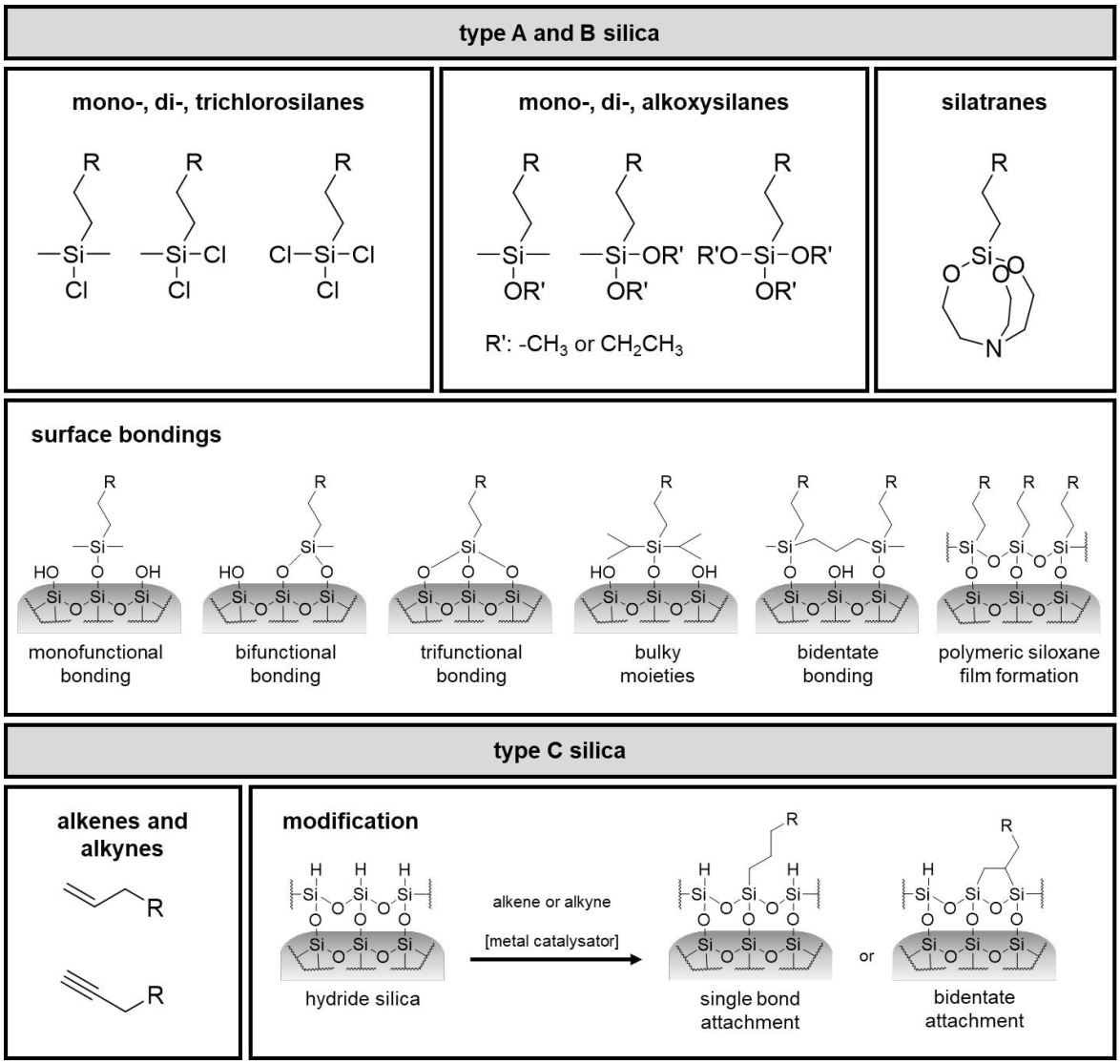


**Figure IV.14.** Surface modification agents for type A, B, and C silica and resulting bonding chemistries. Type A and B silica are silanized using chlorsilanes or alkoxysilanes. Depending on the amount of leaving groups present, mono-, bi- or trifunctional bonding can be expected. However, typical trifunctional bonding is rarely achieved with these chemistries, and bifunctional bonding typically predominates even with trichloro- and trialkoxysilanes. The higher the degree of linkage to the support, the higher the hydrolytic stability of the phases should be, which is associated with longer column life times, more robust analysis runs and less background noise in detection. By using monofunctional silanes, ligand densities of 3-4 µmol/m$^2$ can be achieved under optimal conditions, which corresponds to a reaction with about half of all silanols present on the surface (8 µmol/m$^2$). Bulky side chains (such as isopropyl or isobutyl moieties) of silanes can be utilized to increase hydrolytic stability by steric shielding in order to prevent ligand bleeding as well as to reduce silanol-analyte interactions. Bridged silanes can also be used to increase chemical stability and partially shield silanols by bidentate bonding of the bridged ligands. Polymeric siloxane monolayer formation is assumed to be beneficial in terms of surface smoothness and chemical stability. For type C silica, alkenes and alkynes must be used for modification. For alkynes, bidentate bonding can theoretically be achieved, which would also lead to increased stability of the surface grafting. [66, 132, 133, 136, 137]

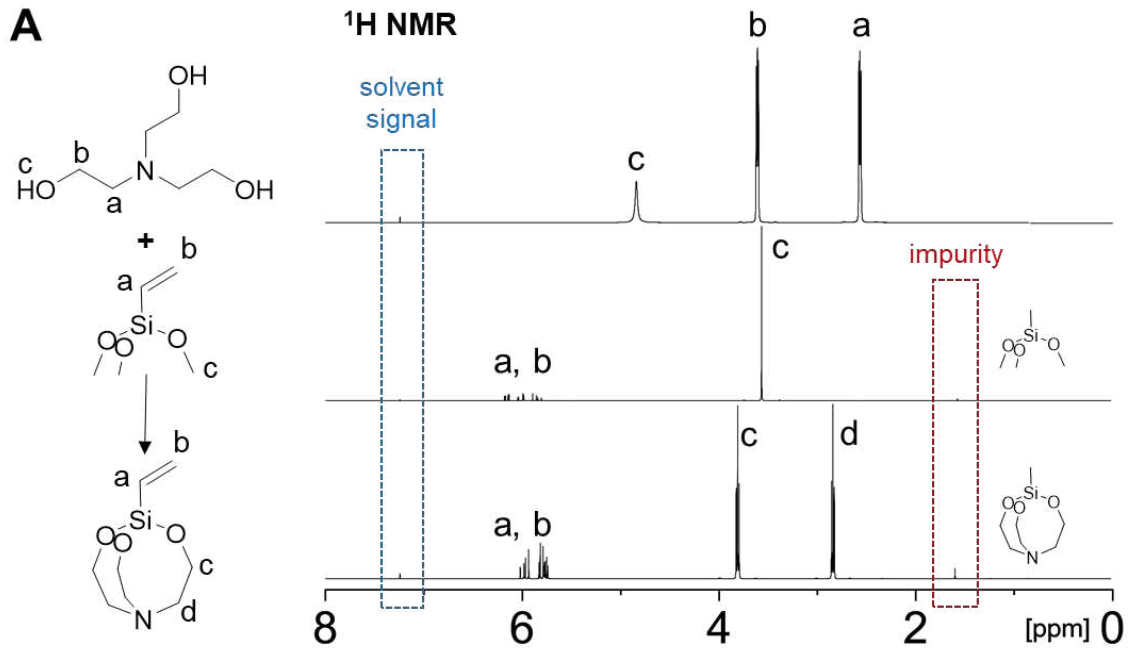


**¹H-NMR** (($J_t$ [Hz]), $CDCl_3$, 400 MHz): δ [ppm] 2.83 (t, $J_t$ = 5.86 Hz, 6H), 3.80 (t, $J_t$ = 5.86 Hz, 6H), 5.76 (dd, $J_t$ = 13.89, 5.17, 1H), 5.79 (dd, $J_t$ = 20.49, 5.17, 1H), 5.97 (dd, $J_t$ = 20.49, 13.89, 1H)

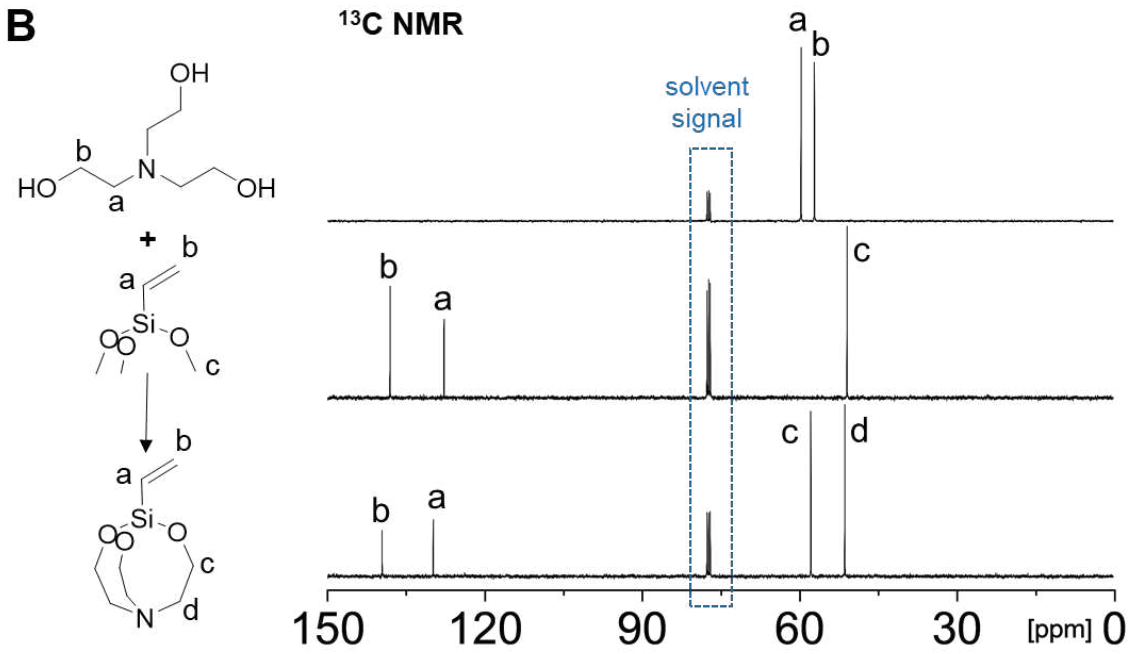


**¹³C-NMR** ($CDCl_3$, 100.6 MHz): δ [ppm] 51.22 ppm (2C), 57.71 ppm (2C), 129.81 ppm (1C), 139.5 ppm (1C)

**Figure IV.15.** Synthesis scheme for preparation of vinyl silatrane and corresponding $^1$H NMR (**A**) and $^{13}$C NMR (**B**) spectra of educts. For the in-house synthesis of vinyl silatrane, 40 mmol vinyltrimethoxysilane, 40 mmol triethanolamine, 30 mL toluene and 10 mg NaOH were initially placed in a 100 mL round bottom flask. A reflux apparatus was attached and the system was purged with nitrogen. The reaction mixture was then heated to 110°C in an oil bath. The reaction was kept under continuous stirring with a magnetic stirrer for 72 hours. The system was then cooled, and the reaction product was transferred to a glass funnel, crushed with a spatula, and washed three times with isopropanol and toluene, respectively, under slight vacuum. The reaction product was then dissolved in 50 mL of methylene chloride and slowly dropped into 75 mL of hexane using a dropping apparatus. The precipitate was then washed three more times with toluene. Finally, the reaction product was transferred to a 250 ml round-bottomed flask, dissolved again in methylene chloride and attached to a rotary evaporator. The solvent was completely evaporated and the reaction product was dried in a vacuum chamber at 60 °C for 24 h.

**A**

**(3-mercaptopropyl) silatrane**

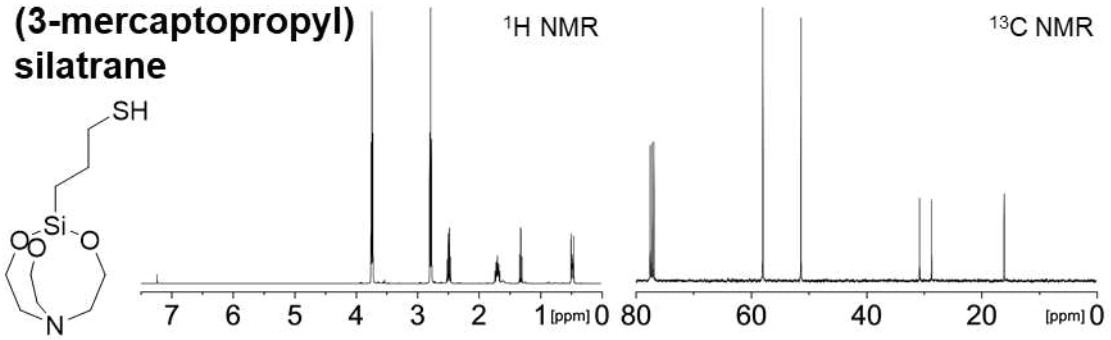


**$^{1}$H-NMR** (($J_t$ [Hz]), $CDCl_3$, 400 MHz): δ [ppm] 0.44-0.48 (m, 2H), 1.31 (t, $J_t$ = 7.90 Hz, 1H), 1.69 (q, $J_t$ = 7.88 Hz, 2H), 2.78 (t, $J_t$ = 5.82 Hz, 6H) , 3.74 (t, $J_t$ = 5.82 Hz, 6H)
**$^{13}$C-NMR** ($CDCl_3$, 100.6 MHz): δ [ppm] 15.95 (1 C), 28.58 (1 C), 30.68 (1 C), 51.32 (3 C), 57.95 (3 C)

**B**

**(3-aminopropyl) silatrane**

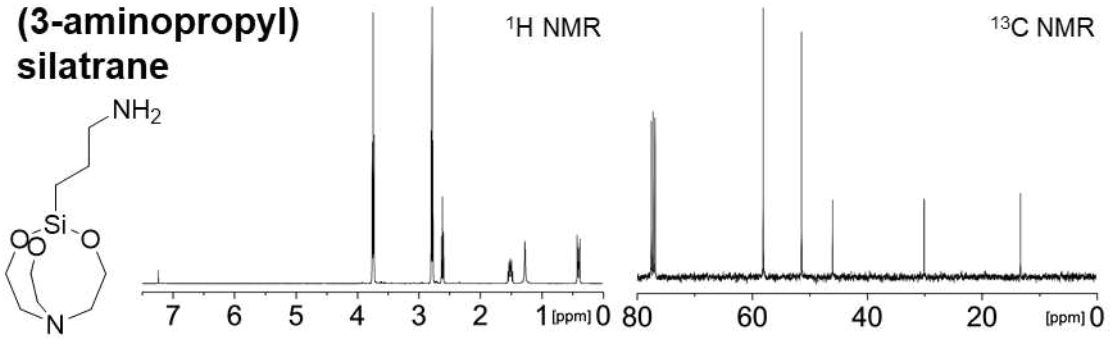


**$^{1}$H-NMR** (($J_t$ [Hz]), $CDCl_3$, 400 MHz): δ [ppm] 0.36-0.41 (m, 2H), 1.26 (br s, 2H), 1.46-1.53 (m, 2H), 2.60 (t, $J_t$ = 6.92, 2H), 2.77 (t, $J_t$ = 5.82, 6H), 3.73 (t, $J_t$ = 5.82, 6H)
**$^{13}$C-NMR** ($CDCl_3$, 100.6 MHz): δ [ppm] 13.12 (1C), 29.96 (1C), 45.93 (1C), 51.35 (3C), 58.0 (3C)

**C**

**2-(2-pyridyl)ethyl silatrane**

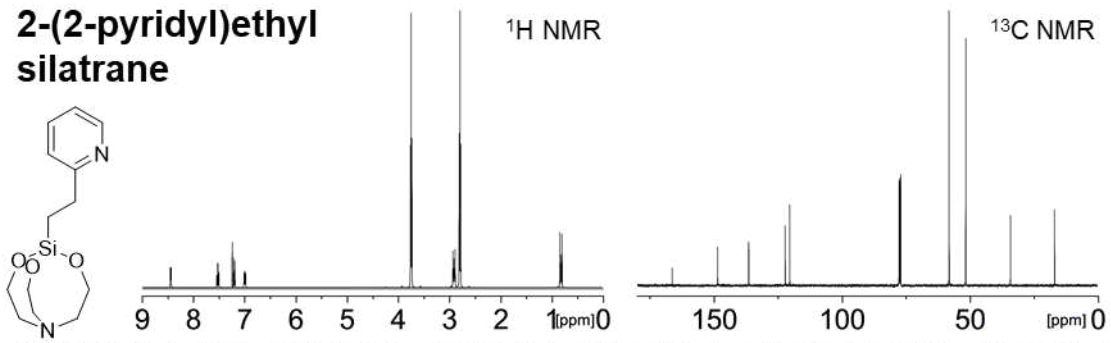


**$^{1}$H-NMR** (($J_t$ [Hz]), $CDCl_3$, 400 MHz): δ [ppm] 0.78-0.83 (m, 2H), 2.77 (t, $J_t$ = 5.82, 6H), 2.87-2.92 (m, 2H), 3.73 (t, $J_t$ = 5.82, 6H), 6.97-7.01 (m, 1H), 7.18-7.21 (m, 1H), 7.49-7.54 (m, 1H), 8.43-8.46 (m, 1H)
**$^{13}$C-NMR** ($CDCl_3$, 100.6 MHz): δ [ppm] 16.61 (1C), 33.89 (1C), 51.43 (3C), 57.96 (3C), 120.36 (1C), 122.11 (1C), 136.42 (1C), 148.59 (1C), 166.36 (1C)

**Figure IV.16.** In-house synthesized silatranes and corresponding $^{1}$H and $^{13}$C NMR spectra. Synthesis procedures for A, B and C can be found in references [138], [139] and [140].

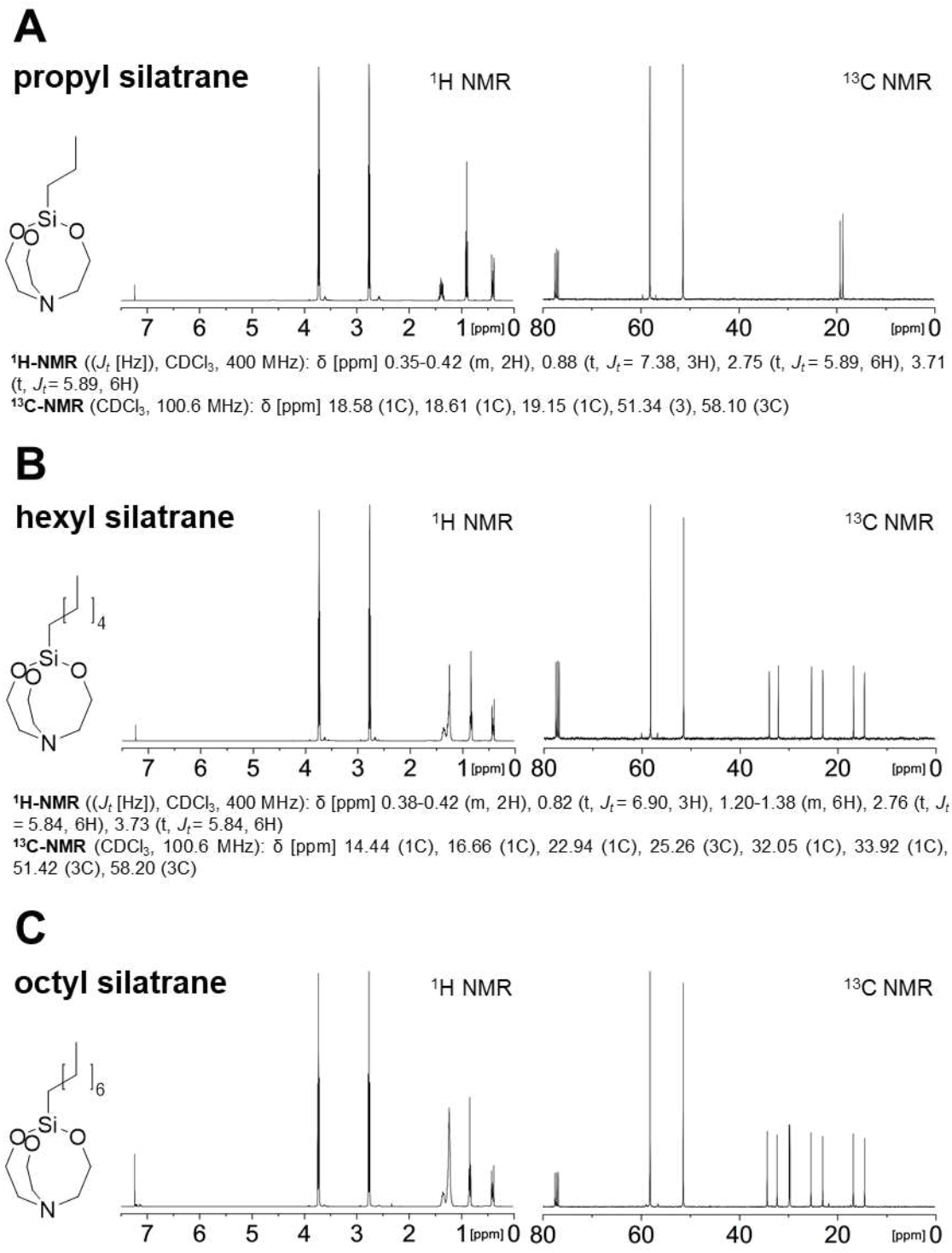


**$^1$H-NMR** (($J_t$ [Hz]), $CDCl_3$, 400 MHz): δ [ppm] 0.35-0.42 (m, 2H), 0.88 (t, $J_t$ = 7.38, 3H), 2.75 (t, $J_t$ = 5.89, 6H), 3.71 (t, $J_t$ = 5.89, 6H)
**$^{13}$C-NMR** ($CDCl_3$, 100.6 MHz): δ [ppm] 18.58 (1C), 18.61 (1C), 19.15 (1C), 51.34 (3), 58.10 (3C)

**$^1$H-NMR** (($J_t$ [Hz]), $CDCl_3$, 400 MHz): δ [ppm] 0.38-0.42 (m, 2H), 0.82 (t, $J_t$ = 6.90, 3H), 1.20-1.38 (m, 6H), 2.76 (t, $J_t$ = 5.84, 6H), 3.73 (t, $J_t$ = 5.84, 6H)
**$^{13}$C-NMR** ($CDCl_3$, 100.6 MHz): δ [ppm] 14.44 (1C), 16.66 (1C), 22.94 (1C), 25.26 (3C), 32.05 (1C), 33.92 (1C), 51.42 (3C), 58.20 (3C)

**$^1$H-NMR** (($J_t$ [Hz]), $CDCl_3$, 400 MHz): δ [ppm] 0.38-0.42 (m, 2H), 0.83 (m, $J_t$ = 6.98, 3H), 1.17-1.29 (m, 10H), 1.29-1.39 (m, 2H), 2.77 (t, $J_t$ = 5.82, 6H), 3.73 (t, $J_t$ = 5.82, 6H)
**$^{13}$C-NMR** ($CDCl_3$, 100.6 MHz): δ [ppm] 14.34ppm (1C), 16.64 ppm (1C), 22.91 ppm (1C), 25.73 ppm (1C), 29.61 ppm (1C), 29.74 ppm (1C), 32.21 ppm (1C), 34.24 ppm (1C), 51.41 ppm (3C), 58.18 ppm (3C)

**Figure IV.17.** In-house synthesized silatranes and corresponding $^1$H and $^{13}$C NMR spectra. The same procedure was used for the synthesis of A, B and C. Alkyl silatranes were synthesized from a mixture of 0.1 mol of the respective alkyltrimethoxysilane, 0.1 mol triethanolamine, 10 mL toluene and 4 mL of methanolic sodium hydroxide solution (2 %, m/v) within a round bottom flask. The flask was attached to a reflux condenser equipped with a nitrogen supply and heated up to 110 °C using an oil bath. The reaction was allowed to proceed for 96 h under continuous magnetic stirring and gentle nitrogen rinsing. Thereafter, the reaction mixture was cooled down to ambient temperature and a solid reaction product precipitated.

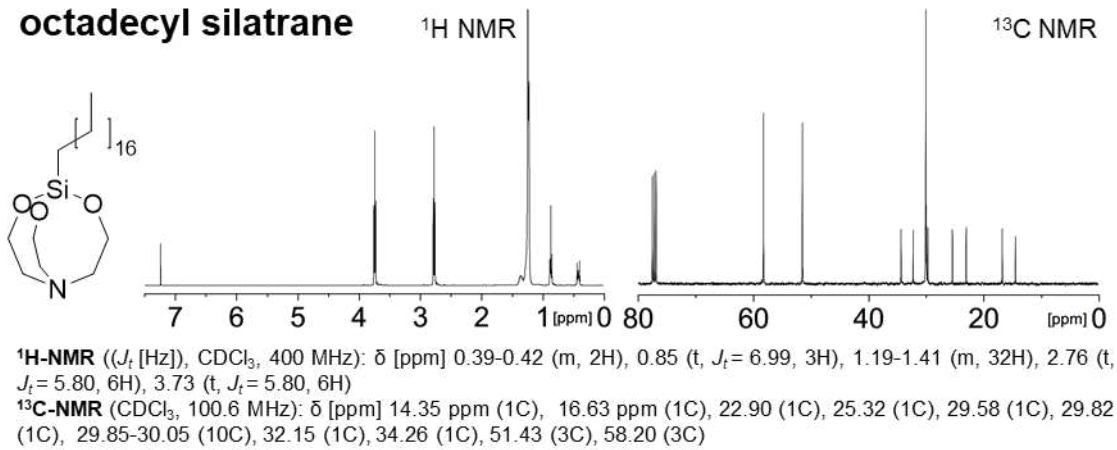


**$^1$H-NMR** (($J_t$ [Hz]), $CDCl_3$, 400 MHz): δ [ppm] 0.39-0.42 (m, 2H), 0.85 (t, $J_t$ = 6.99, 3H), 1.19-1.41 (m, 32H), 2.76 (t, $J_t$ = 5.80, 6H), 3.73 (t, $J_t$ = 5.80, 6H)
**$^{13}$C-NMR** ($CDCl_3$, 100.6 MHz): δ [ppm] 14.35 ppm (1C), 16.63 ppm (1C), 22.90 (1C), 25.32 (1C), 29.58 (1C), 29.82 (1C), 29.85-30.05 (10C), 32.15 (1C), 34.26 (1C), 51.43 (3C), 58.20 (3C)

**Figure IV.18.** In-house synthesized octadecyl silatrane and corresponding $^1$H and $^{13}$C NMR spectra. Synthesis procedure was the same as described for the other alkyl silatranes in Fig. IV.17.

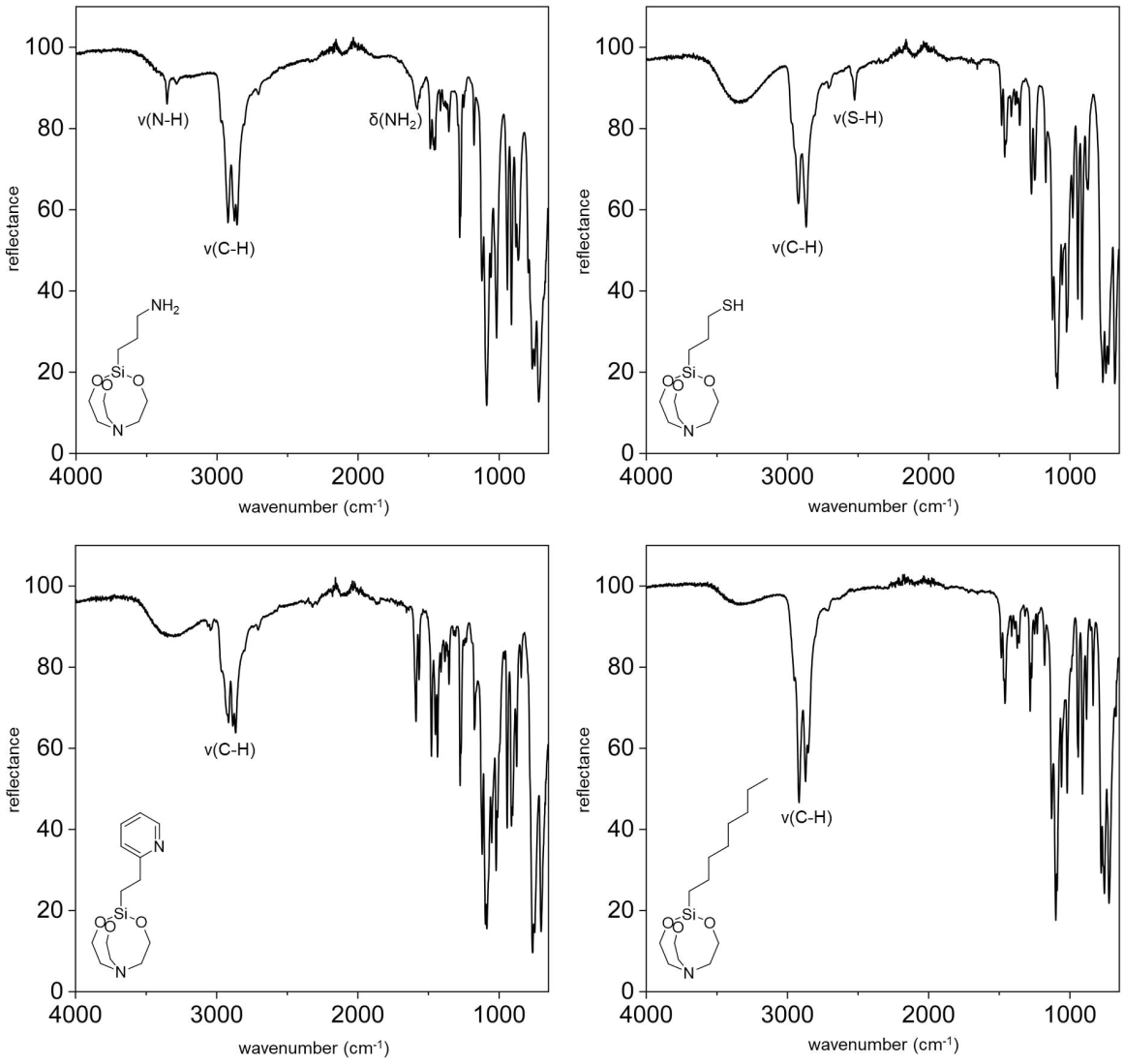


**Figure IV.19.** Infrared spectra recorded in-house from diverse silatranes utilizing an ATR-FTIR 630 Cary spectrometer from Agilent Technologies (Waldbronn, Germany).

After silanization, a large amount of silanols typically remains unreacted on the silica surface (of type A and B silica) and can lead to unwanted secondary interactions. These analyte-silanol interactions are most often considered in the context of stationary phases for reversed-phase (RP) chromatography, where several approaches were implemented to reduce silanol effects, including apolar and polar endcapping, shielding by bulky moieties (see Fig. IV.14), polar embedding and the creation of charged surfaces. [141-143] Polar endcapping and polar embedding are also considered to prevent RP phases from dewetting when using highly aqueous mobile phases (up to 100% water). [144] Charged surface columns typically have positive charges on the surface of the stationary phase, but the chemistry is kept proprietary by all manufacturers of such charged surface columns, so the exact chemistry is unknown. However, it can be assumed that the term charged surface most often refers to the use of bonded, (permanently) ionized, polar endcapping reagents. [145-147]

Apolar endcapping with small apolar silanes is the most common approach for reducing silanol activity and has become a routine procedure for RP stationary phase synthesis. In most cases, trimethylchlorosilane is used for endcapping, but other trimethylsilyl donors such as hexamethyldisilazane or bis(trimethylsilyl)trifluoroacetamide can also be used. The small endcapping agents are able to reach silanols that are sterically difficult to access and cannot be reached by larger molecules. However, even with this endcapping procedure, not all silanols can be deactivated (see Fig. IV.20A). It is assumed that a maximum of 50 % of the total silanols (8 µmol/$m^2$) can be derivatized. [142, 148-151]

In addition to apolar endcapping, polar endcapping has been reported in a few cases and is proclaimed for some commercial columns. However, the term does not seem to be well defined and information on commercially applied polar endcapping strategies is difficult to find and therefore the nature of the surface chemistry of polar endcapped columns is often unclear. Polar endcapping should be aimed at reducing silanol effects and increasing surface hydrophilicity. There are some strategies that can be referred to polar endcapping This includes the introduction of new less acidic silanols on the surface (which is in some kind contrary to the classical apolar endcapping principle, which is based on the reduction of free silanols) as well as the incorporation of polar groups bearing

ligands (neutral or basic) in close proximity to the support surface via silanization with the purpose of steric and electrostatic shielding of silanols. The latter better fits the term polar endcapping. In some cases, polar embedding is also referred to as polar endcapping. However, the concepts should be clearly distinguished. Overall, polar endcapping is more versatile and more complex than apolar endcapping, and therefore quite different. Polar endcapping reduces the silanol activity and alters the chromatographic selectivity of RP phases. [141, 152]

Since the polar endcapping chemistry of commercial stationary phases is largely unknown, it has been speculated that short-chain trialkoxysilanes may act as small polar endcapping agents for the incorporation of less acidic silanols on the surface. [152] These small molecules could reach unreacted silanols on the surface that are difficult to reach by larger molecules, similar to concept using trimethylchlorosilane in apolar endcapping. Trialkoxysilanes are able to generate silanol groups after binding to the surface by hydrolysis of the unreacted alkoxy moieties. This introduces new silanols adjacent to the support surface and increases surface hydrophilicity. The new silanols, however, offer less acidity than the silica surface silanols and therefore provoke reduced silanol activity. Additional silanols can also be created using trialkoxysilanes for initial functionalization, as one or two alkoxy groups remain after mono- or bifunctional attachment. These can also be hydrolysed to form silanol groups on the surface. Nevertheless, this second approach reduces not the number of more acidic surface silanols, but increases surface hydrophilicity. [152] Overall, these considerations should be viewed critically and were not further found in the literature.

The incorporation of polar ligands by silanization could be considered true polar endcapping. In general, however, this is not usually done with molecules as small as trimethylchlorosilane (cf. apolar endcapping) and is often done simultaneously with the introduction of other larger RP ligands (such as octadecyl residues) or is achieved by unreacted functional ligands that have been partially further modified, such as amino groups remaining after amidation with carboxylic acids in a subsequent surface modification step. The polar groups used can vary, but hydroxyl (neutral) and amino (basic) groups are the most prevalent for polar endcapping. RP phases polar endcapped usually offer similar hydrophobicities as non-endcapped or apolar endcapped phases, but higher hydrogen bonding capacities. In the case

of amino endcapping, additional electrostatic interactions can be obtained under classical pH conditions for silica stationary phases as well. Thus, on the one hand, strong interactions can also occur with acidic analytes, which can lead to worse peak shapes for such analytes. On the other hand, better peak shapes for basic analytes due to reduced silanol activity and repulsion effects can be usually observed. [141, 152, 153] Examples for polar encapped stationary phases are given in Fig. IV.20A.

Polar embedding is another strategy to reduce silanol activity and increase surface hydrophilicity of RP phases (see Fig. IV.20B). There are two approaches to implement polar embedded alkyl strands on the silica surface, a two-step surface modification and a one-step surface modification approach. In the two-step surface

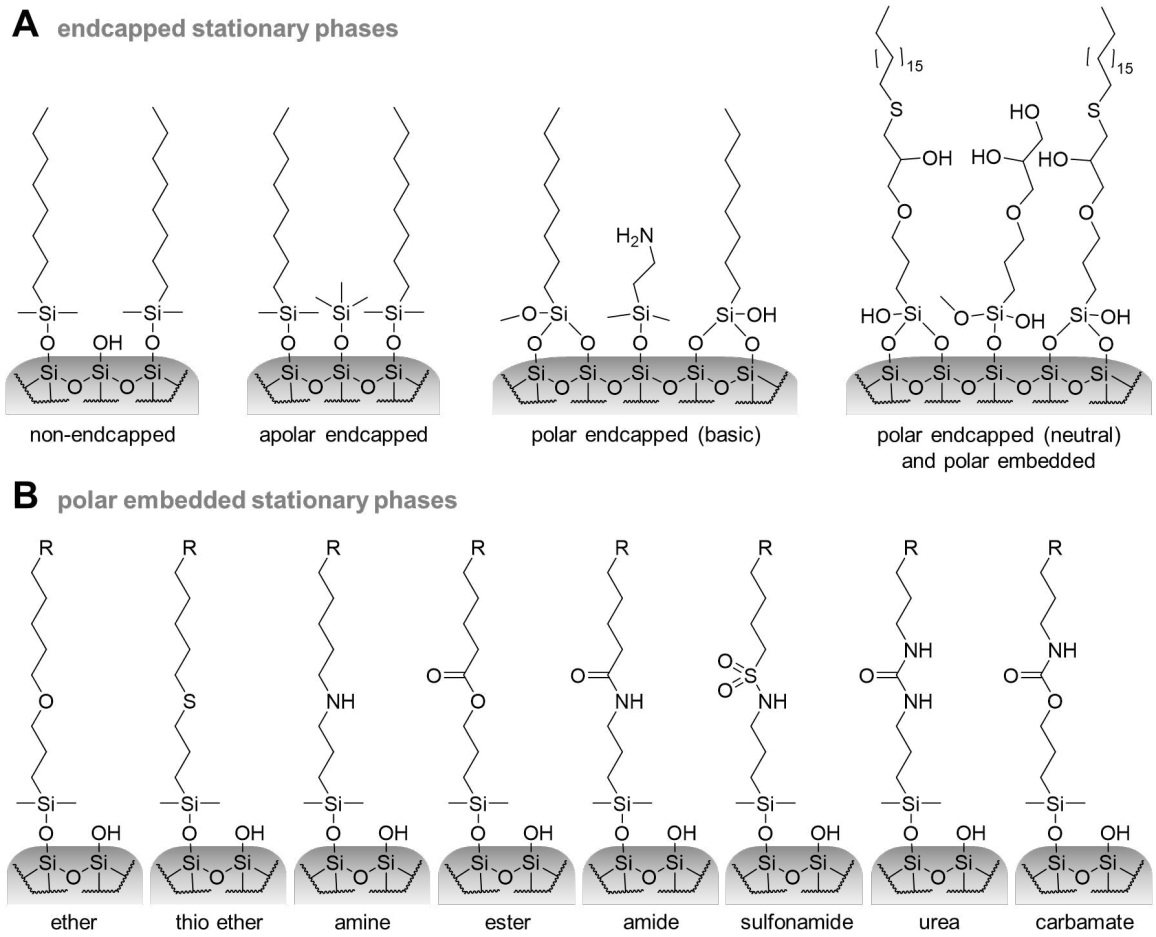


**Figure IV.20.** Examples for endcapped (**A**) and polar embedded (**B**) silica-based RP stationary phases. The polar endcapped structures are based on references [141] and [153]. Polar embedded phases contain polar groups in close proximity to the silica surface. [141]

modification approach, the silica is first modified with a functional ligand (e.g. aminopropyl) and then in a second step the functional group is modified by chemical reaction with a second agent (e.g. long chain fatty acid) to form a long alkyl ligand with a polar embedded group (e.g. amide). During the second step, typically not all firstly immobilized ligands are converted, and typically a mixed ligand surface with mixed retention mechanisms (e.g. hydrophobic and ion-exchange) is formed, which can mostly be referred to as mixed polar embedded and polar endcapped. In the one-step approach, purely polar embedded ligand surfaces can be created since the incorporation of the polar group into the apolar chain is performed prior to immobilization on the silica. Thus, functional silanes with polar embedded alkyl chains are synthesized and then immobilized on the silica surface. Phases prepared by this approach do not provide additional interaction sites due to unreacted precursor ligands on the silica surface. [143, 154-159]

To tune chemical selectivity, it is common to immobilize (specially designed) ligands on the silica surface. Such ligands are often difficult to immobilize directly on bare silica. Therefore, precursor silica with modified surfaces bearing reactive functional groups (e.g. amino groups) are prepared. These reactive groups can be easily incorporated by classical silanization reactions. The functional groups can then be used to attach secondary ligands. Reactions used for this second step of surface modification should be able to be carried out under mild conditions, with fast kinetics and high yields, and should be highly selective to avoid side reactions. The bond formed between the precursor silica and the attached ligand should also be chemically stable under the later chromatographic conditions. Common reactions include esterification, amidation, carbamate formation, epoxy reactions, radical thiol-ene/yne click reactions and azide-alkyne Huisgen cycloaddition (see Fig. IV. 21). [131, 160-171] In addition, reactive functional groups allow crosslinking of the ligands present on the surface by reaction with (small or polymeric) multifunctional crosslinking agents. Crosslinking can significantly increase the chemical stability of the surface modification. However, crosslinking can also change the chromatographic behavior of the separation material, especially in terms of selectivity and efficiency. [139, 172]

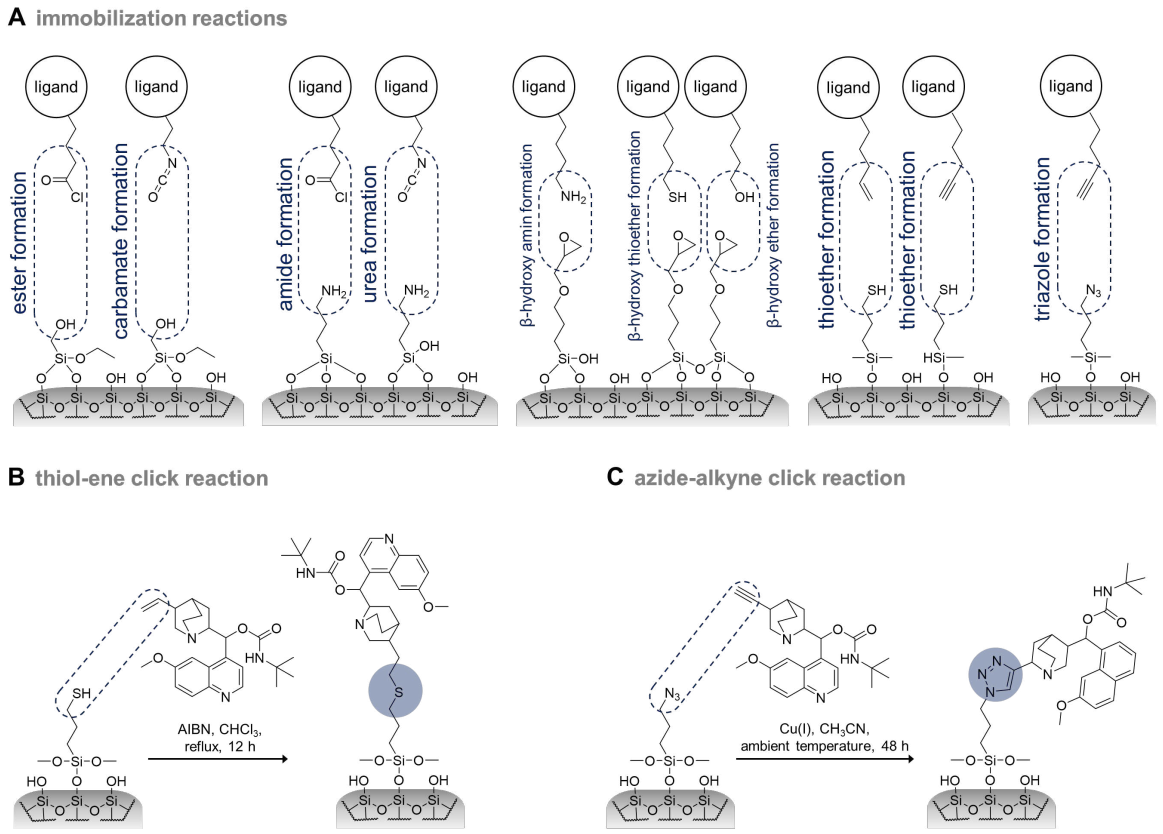


**Figure IV.21.** Immobilization reactions for chromatographic ligands on precursor silicas. In **A**, an overview is given of possible reactions that can be used to immobilize ligands on precursor silica particles. However, this overview is by no means complete. The functional groups for the ligand and the precursor silica can also be reversed. **B** shows the immobilization of a chiral ligand by thiol-ene click reaction on thiol-modified silica, based on reference [173]; AIBN: azobisisobutyronitrile. **C** shows the immobilization of the same chiral ligand by azide-alkyne click reaction (Huisgen reaction), based on reference [174].

Besides functionalization with small silanes, surface modification with polymers is also a common approach. Typically, such polymers can be immobilized on the silica particle by various chemistries and strategies, including immobilization by surface adsorption and immobilization by covalent bonding to the support via multiple interaction sites. In both approaches, cross-linking between the coated polymers can also be performed to increase the stability of the coating by forming a highly interconnected network (see Fig. IV.22). Multiple polymer layers of the same or different polymers can also be applied to the silica in order to increase the shielding of the silica surface or to create layers with different chromatographic properties. [128, 130, 175-181] An in-house strategy for sequentially coating two different polymers is shown in Figure IV.23. In general, covalently bonded polymeric phases exhibit higher chemical stability than their brush-type counterparts. However, this

higher stability is typically accompanied by lower efficiency due to the poorer mass transfer properties of these phases, caused by thick and often inhomogeneous polymer films. [182, 183] Polymers attached only by adsorption can be leached from the particles by application of mobile phases capable of dissolving the polymers. Therefore, the solubility of the polymer must be taken into account when selecting the mobile phase for such phases in order to prevent damaging the stationary phase. [139] A good illustrative example of the different solvent compatibility of adsorptively or covalently immobilized polymeric stationary phases give polysaccharide-based chiral stationary phases, which are available in both forms. [184]

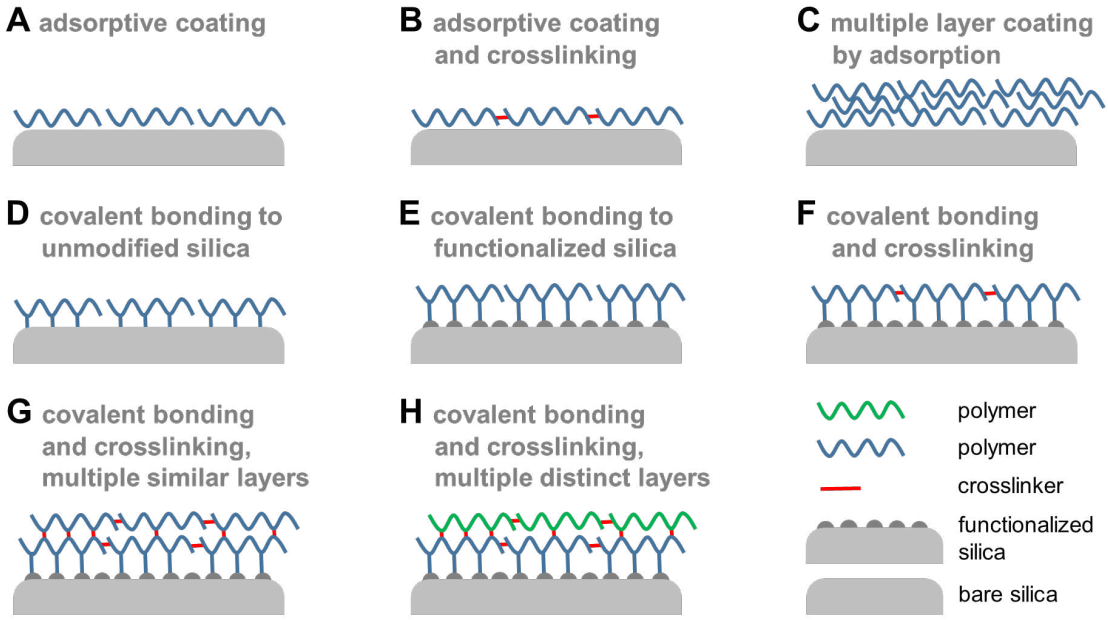


**Figure IV.22.** Strategies for the immobilization of polymers on the silica surface. **A**: Immobilization by adsorption is typically achieved by dispersing silica particles in a solution of the polymer of interest. The polymer should be efficiently dissolved in the solution. In the next step, the solvent is typically removed by evaporation and the polymer precipitates on the silica surface due to its decreasing solubility. Strong adsorption of the polymer is then achieved by attractive interactions such as electrostatic, dipole-dipole or hydrogen bonding. **B**: To achieve more stable coatings after immobilization of polymers by adsorption, a crosslinking agent can be added to the initial polymer solution and also deposited on the silica surface by solvent evaporation. Interconnection of the polymers with the crosslinking agent can then be initiated, depending on the reaction, by raising the temperature (thermally initiated reactions) or by exposure to UV radiation (photo-initiated reactions). **C**: Multiple layers of polymers can be applied to the silica. This can result in more efficient shielding of the silica surface, reduced silanol-analyte interactions and increased chemical stability of the stationary phase. **D**: Polymers containing functional groups that can react with the surface silanols (such as alkoxysilanes) can be covalently bonded to the unmodified silica support during the coating process and form a stable layer due to multiple bonds. **E**: Polymers can also be covalently bonded to pre-functionalized silica. The functionalization of the silica allows covalent bonding of polymers that could not react with bare silica. **F**: Crosslinking of the polymer chains can further increase the chemical stability by forming a highly crosslinked network. **G**: Additional similar polymer layers can be deposited on the surface to increase surface shielding. **H**: Additional distinct polymer layers can be attached in order to introduce different chemical and chromatographic properties.

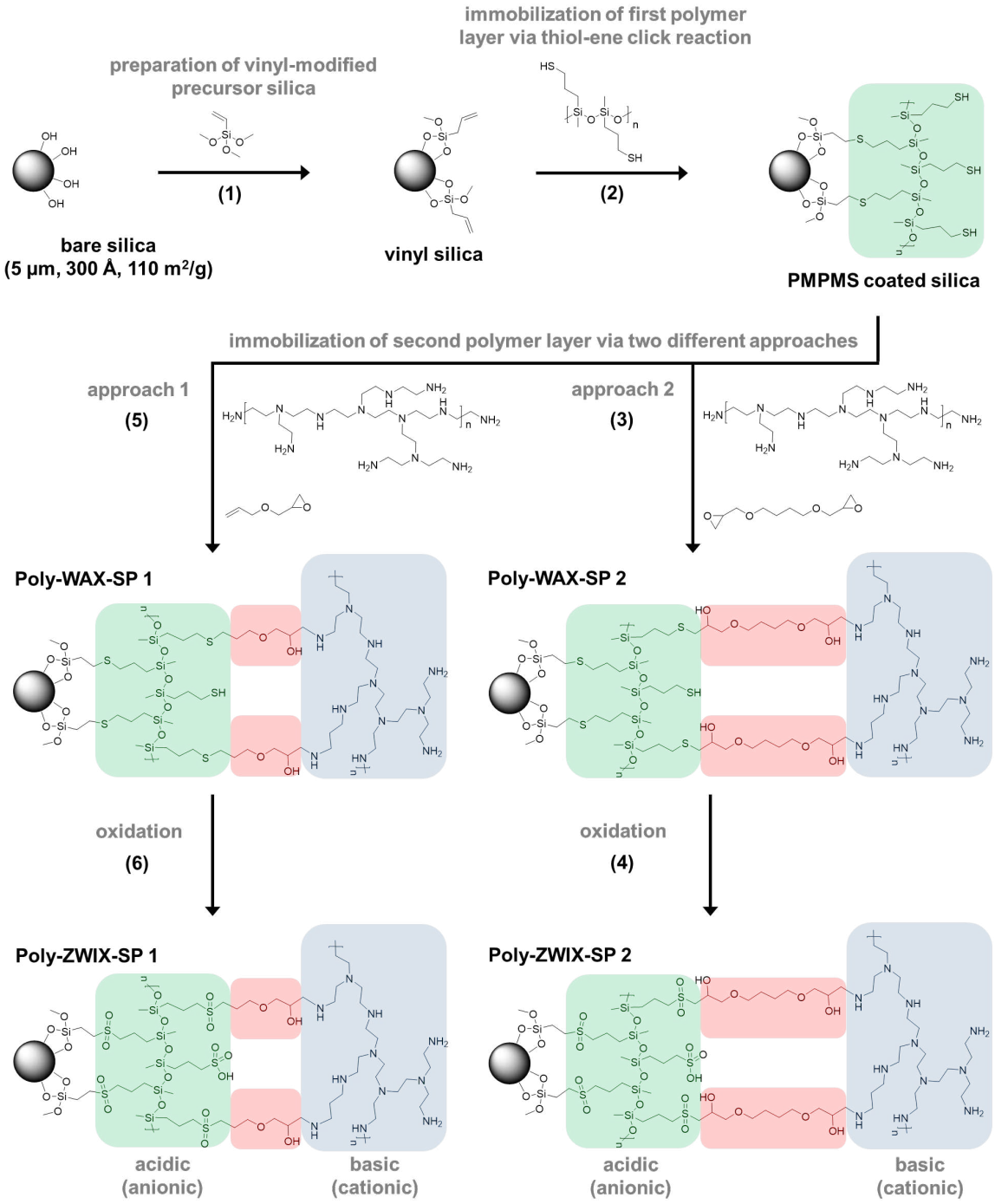


**Figure IV.23.** In-house preparation of polymeric coated zwitterionic ion-exchangers via two different immobilization approaches for the immobilization of the second polymer layer. Under chromatographic conditions the sulfonic acid groups and the amine groups of Poly-ZWIX-SP 1 and Poly-ZWIX-SP 2 are charged and therefore create a zwitterionic surface; PMPMS: poly(3-mercaptopropyl)methylsiloxane, SP: stationary phase, ZWIX: zwitterionic ion exchanger, WAX: weak anion exchanger. Reaction conditions: **(1)**: 10 g bare silica, vinyltrimethoxysilane (6 µmol/m$^2$), 4-dimethylaminopyridine (5 % n/n of vinyltrimethoxysilane), 150 mL dry toluene, reflux, 24 h, **(2)**: 3 g vinyl silica, PMPMS (10 µmol/m$^2$), AIBN (10 % n/n to vinyl groups), 25 mL methanol, solvent evaporation and subsequent heating at 60 °C for 45 min, **(3)**: 1.3 g PMPMS coated silica, polyethylenimine (PEI, Mw ~ 8000) (250 µmol/g), butanediol diglycidyl ether (50 % n/n to primary amines; 500 µmol/g), 25 mL methylene chloride, solvent evaporation and subsequent heating at 60 °C for 4h, **(5)**: preparation of coating solution: polyethylenimine (PEI, Mw ~ 8000) (250 µmol/g), allyl glycidyl ether (800 µmol/g), 25 mL 1,4-dioxan, reflux, 2 h, coating procedure: 1.3 g PMPMS coated silica, coating solution, azobisisobutyronitril (10 % n/n to vinyl to allyl glycidyl ether), solvent

evaporation and subsequent heating at 60 °C for 1 h, **(4)+(6)**: 1 g Poly-SAX-SP 1 or Poly-SAX-SP 2 silica, 40 mL methanol, 2.1 mL formic acid, dropwise adding of a mixture containing 9.5 mL formic acid and 0.5 mL hydrogen peroxide (30 % v/v), ice cooling, 4h. **Elemental analysis results**: vinyl silica: C [%]: 1.38 ± 0.01, H [%]: 0.37 ± 0.01, N [%]: < 0.03, S [%]: < 0.02, PMPMS coated silica: C [%]: 2.94 ± 0.02, H [%]: 0.69 ± 0.01, N [%]: < 0.03, S [%]: 1.10 ± 0.00, Poly-WAX-SP 1: C [%]: 3.46 ± 0.02, H [%]: 0.76 ± 0.01, N [%]: 0.32 ± 0.00, S [%]: 1.04 ± 0.00, Poly-WAX-SP 2: C [%]: 12.07 ± 0.04, H [%]: 2.37 ± 0.02, N [%]: 2.84 ± 0.01, S [%]: 0.86 ± 0.01, Poly-ZWIX-SP 1: C [%]: 3.22 ± 0.01, H [%]: 0.76 ± 0.01, N [%]: 0.31 ± 0.00, S [%]: 1.00 ± 0.01, Poly-ZWIX-SP 2: C [%]: 11.04 ± 0.03, H [%]: 2.17 ± 0.01, N [%]: 2.41 ± 0.00, S [%]: 0.76 ± 0.00.

## V.4 Surface chemistries and chromatographic modes

A wide variety of chromatographic stationary phases with different surface chemistries is available on the market nowadays (see Fig. IV.25). Depending on the surface chemistry, the columns are suitable for different chromatographic modes, which can be based on pore exclusion, partitioning and adsorption effects for separation. In addition, mixed-mode chromatography (MMC), which combines several techniques, has become popular. Three concepts can be distinguished in mixed-mode chromatography for the preparation of mixed-mode columns, the preparation of mixed beds, the generation of mixed ligand surfaces, and the immobilization of mixed-mode ligands (see Fig. IV.24). [185-187] The best-known chromatographic modes are size-exclusion chromatography (SEC), normal-phase chromatography (NPC), reversed-phase chromatography (RPC), hydrophobic-induction chromatography (HIC), hydrophilic-interaction chromatography (HILIC), ion-exchange chromatography (IEX), ion-pair reversed-phase chromatography (IP-RPC), affinity chromatography, and chiral chromatography. However, there are also many less prominent chromatographic modes, such as ion exclusion chromatography (IEC), hydrophobic charge induction chromatography (HCIC), silver ion chromatography, and many others that are not listed here.

Size exclusion chromatography is most commonly used for the purification of macromolecules such as proteins. In size exclusion chromatography, analytes are separated according to their hydrodynamic radius. Depending on their size, the analytes can enter or be excluded from the pores of the stationary phase. Larger

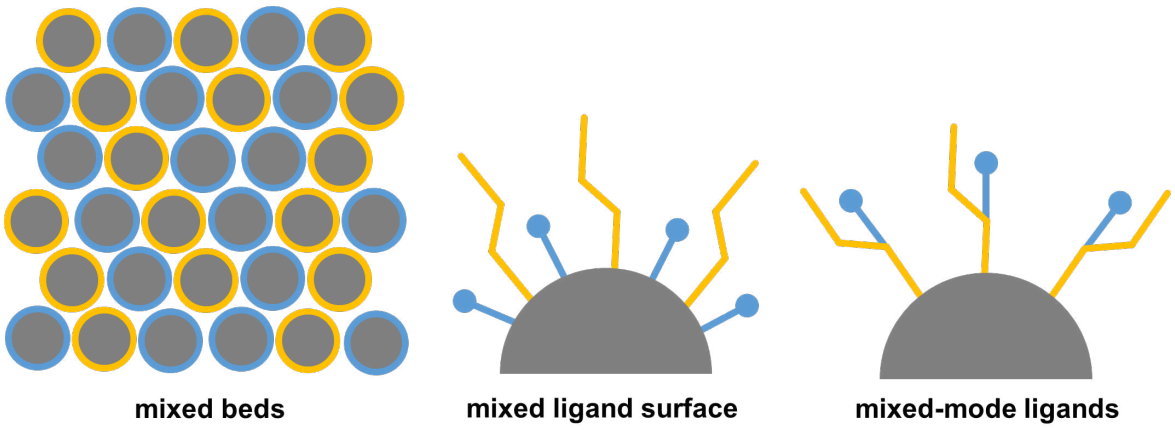


**Figure IV.24.** Concepts for creation of mixed-mode stationary phases; based on reference [185].

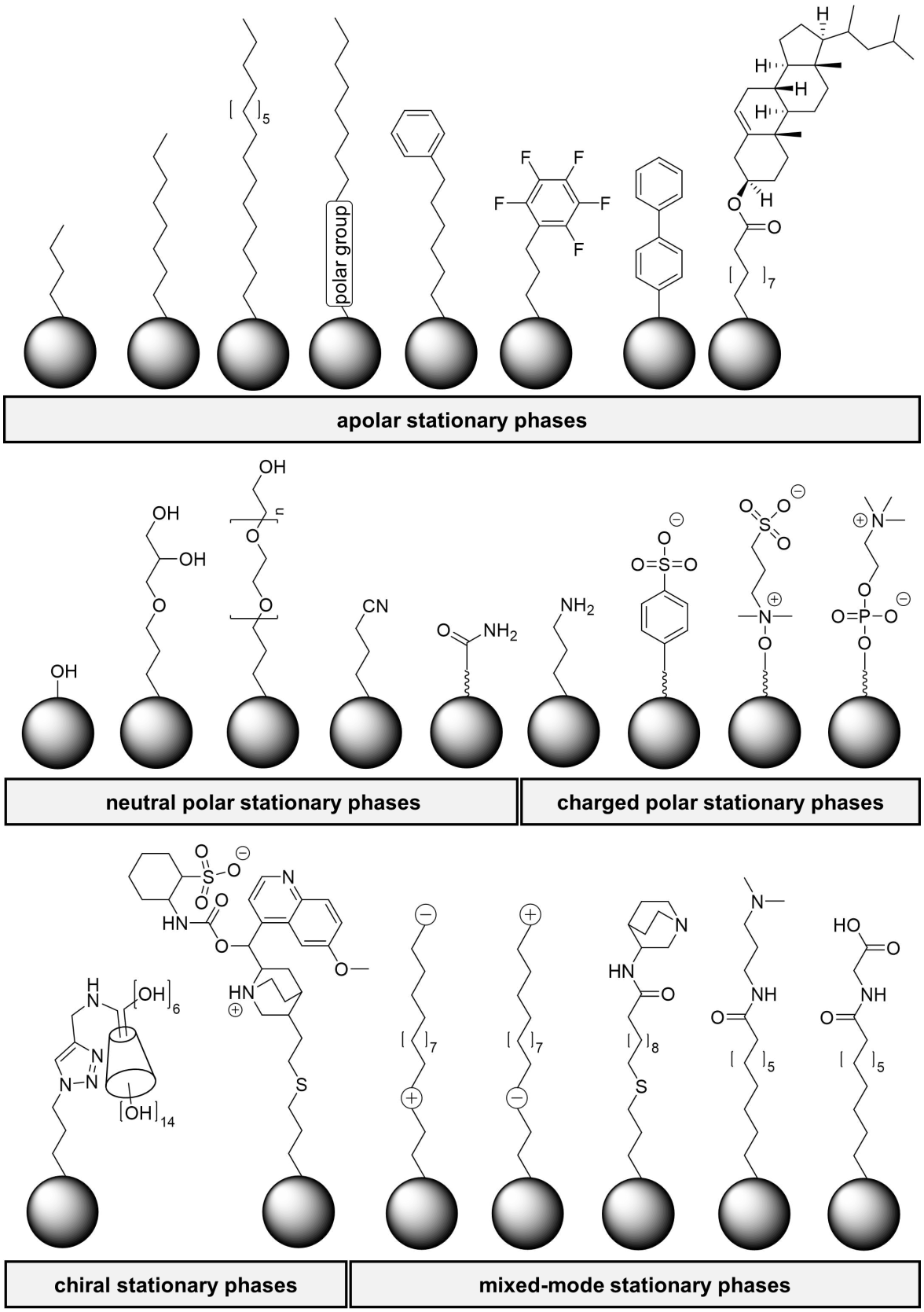


**Figure IV.25.** Overview of stationary phases to illustrate the variety of available stationary phase surface chemistries. However, this is by no means a complete picture and there are many other stationary phase surface chemistries available. Further overviews can be found in references [188], [189] and [190].

molecules cannot enter the pores and therefore migrate faster through the column. Smaller molecules can enter the pores and travel a longer distance, eluting more slowly. This results in the separation of molecules based on size (Fig. IV.26). The separation material used must have a controlled pore size and must not interfere with the analytes in order to enable this separation based on size. For this reason, organic polymer beads are most commonly employed, which typically offer fewer undesirable interactions than silica-based stationary phases. However, bare silica or modified silica particles can also be applied. For example, diol-modified silica particles or silica modified with polyethylene oxide are commonly deployed. A thorough overview of size exclusion chromatography, especially for proteins, is given in the review article presented in reference [191].

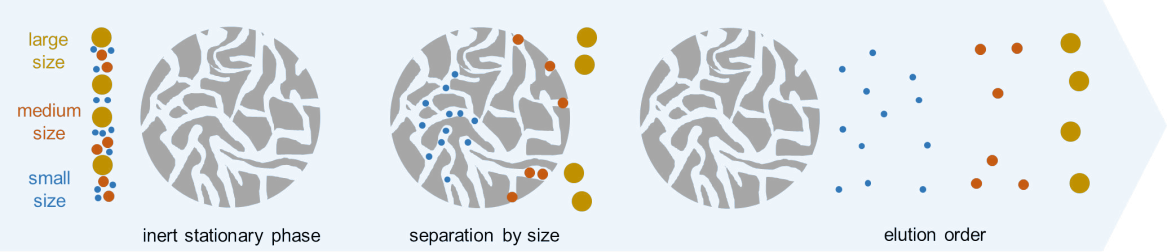


**Figure IV.26.** Illustration of the separation of analytes by size exclusion chromatography.

Normal phase chromatography (NPC) is a widely used technique for the analysis and purification of compounds, particularly for separating mixtures based on polarity differences. In NPC, the stationary phase is usually polar. The mobile phase is a non-polar solvent such as hexane or chloroform, which contrasts to the stationary phase. Commonly used stationary phases include amino, cyano, or diol phases. Bare silica can also be used. Separation occurs because compounds of different polarities interact differently with the stationary phase by polar interactions such as hydrogen-bonding or dipole-dipole interactions. More polar compounds interact more strongly with the stationary phase, leading to retention within the column, while less polar compounds elute more rapidly (Fig. IV.27). An overview of NPC can be found in the review article in the reference [192].

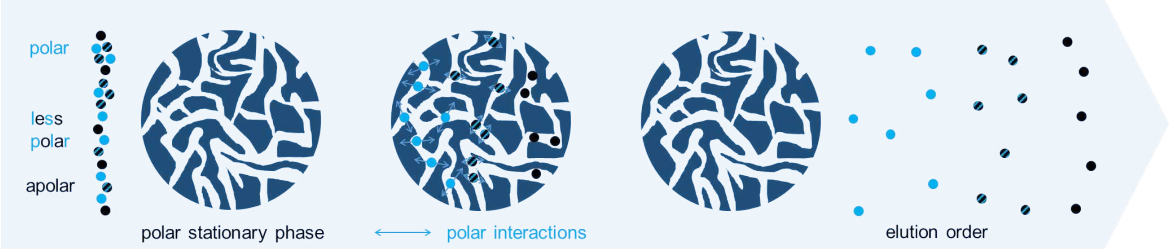


**Figure IV.27.** Illustration of the separation of analytes by normal phase chromatography.

Hydrophilic interaction chromatography (HILIC) is a widely used technique for the separation of polar analytes. For this reason, polar stationary phases are used in HILIC. These include inter alia bare silica, amide, amino and sulfobetaine phases. The mobile phase generally consists of a large proportion of organic solvent, such as acetonitrile or methanol, and a small proportion of water. The water in the mobile phase typically forms a stagnant aqueous layer on the surface of the stationary phase. Consequently, the separation of analytes occurs by partitioning between this immobilized aqueous layer and the moving water-deficient bulk mobile phase (Fig. IV.28). In addition to separation by partitioning, polar interactions between the analytes and the stationary phase, such as hydrogen bonding, dipole-dipole interactions or electrostatic interactions, have also been reported to contribute to the separation mechanisms in HILIC. As a consequence, mixed-mode techniques have been described that combine the classical separation principle of HILIC by distribution with the additional polar interactions such as hydrophilic interaction electrostatic repulsion chromatography (ERLIC). A good overview of HILIC and in particular of the stationary phases used in this technique can be found in reference [188].

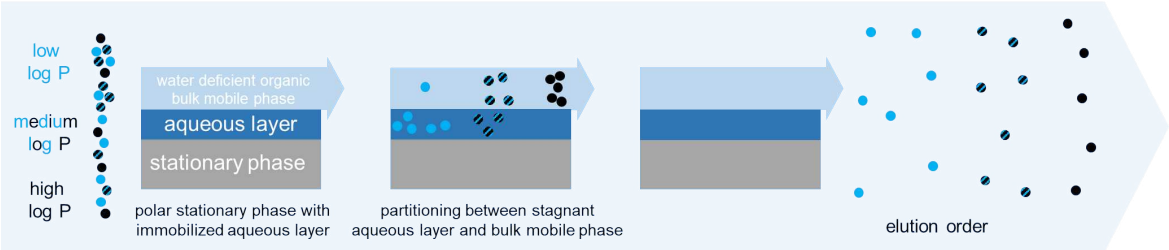


**Figure IV.28.** Illustration of the separation of analytes by hydrophilic interaction chromatography. The log P value is the logarithm of the octanol-water coefficient and is therefore a measure of the relative solubility of a compound in organic and aqueous solvents.

Reversed phase chromatography (RPC) is the most commonly used chromatographic mode in high performance liquid chromatography. As opposed to NPC, RPC separates compounds on the basis of their hydrophobicity. The stationary phase is non-polar and typically contains C4, C8, C18, phenyl groups or other hydrophobic moieties. In some cases, these phases are additionally non-polar or polar end-capped or contain polar groups embedded within their hydrophobic ligands. The mobile phases used in RPC are typically mixtures of polar solvents such as water, methanol and acetonitrile. The analytes are retained by hydrophobic interactions with the stationary phase. Compounds with higher hydrophobicity have stronger interactions, resulting in longer retention times (Fig. IV.29). The retention times of compounds can be tuned by adjusting the elution strength of the mobile phase in accordance to the eluotropic series of solvents for RPC. Hydrophobic compounds that are extensively retained in RPC and have low solubility in aqueous mobile phases can be separated by normal phase chromatography. Reference [193] provides a very good overview of reversed-phase chromatography, especially for peptides and proteins.

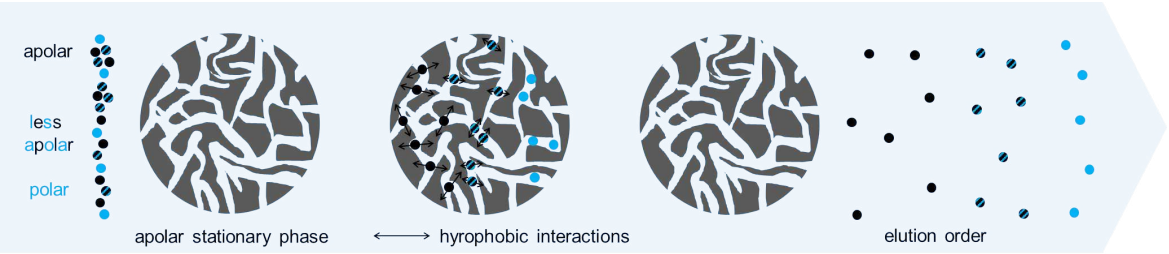


**Figure IV.29.** Illustration of the separation of analytes by reversed phase chromatography.

Ion-pair reversed phase chromatography (IP-RP) is typically used for the analysis of charged or ionizable compounds and involves the formation of ion pairs between the analytes and oppositely charged ion pairing reagents in the mobile phase. The formed apolar ion pairs interact with the stationary phase and lead to the retention of charged analytes on classical reversed-phase chromatography stationary phases (Fig. IV.30). Classic ion-pairing reagents are long-chain alkyl sulfonates or alkyl ammonium salts. The elution strength of the mobile phase can be adjusted by the amount of organic solvent contained in the mobile phase. In reference [194], the

analysis of oligonucleotides by means of ion-pair reversed-phase chromatography is described and discussed.

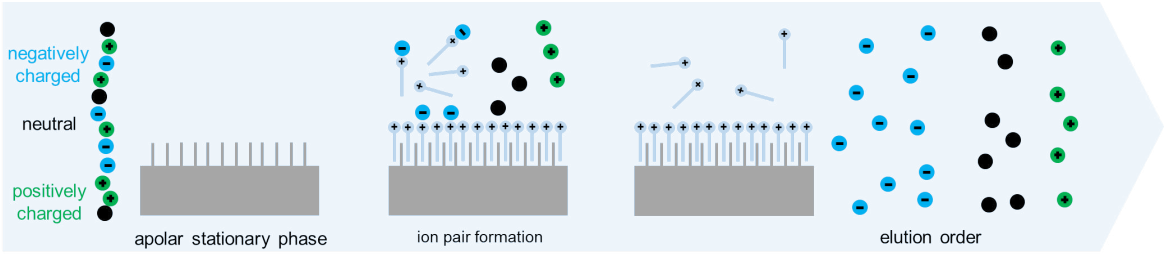


**Figure IV.30.** Illustration of the separation of analytes by ion-pair reversed phase chromatography.

Ion-exchange chromatography (IEX) is used to separate and purify a wide variety of compounds, including proteins, peptides, nucleic acids, and small molecules. It is based on the principle of reversible adsorption of analytes to the stationary phase by electrostatic attraction (Fig. IV.31). For this purpose, the stationary phase generally provides sites for ionic interactions. The stationary phase can provide either anionic (e.g. sulfonate groups) or cationic (e.g. ammonium groups) interaction sites or both. Thus, cation-, anion-, and zwitterionic ion-exchange chromatography are distinguished. The mobile phase is typically a buffer solution. The buffer salts compete with the analytes for interaction sites on the stationary phase, causing elution of the analytes. Therefore, the elution strength of the mobile phase can be adjusted by the concentration of the buffer. Reference [195] provides an in-depth look at the theory of ion exchange chromatography and its application to biopharmaceuticals.

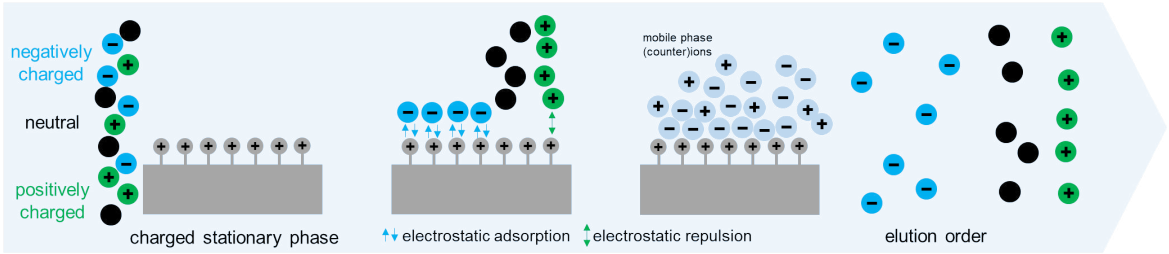


**Figure IV.31.** Illustration of the separation of analytes by ion-exchange chromatography.

Ion exclusion chromatography (IEC) is usually used for the separation of hydrophilic acids and bases. Therefore, strong anion or strong cation exchange resins are commonly used as stationary phases. Negatively charged components, such as ionized carboxylic acids, are separated on cation exchange resins. Positively charged components are separated on anion exchange resins. In IEC, strongly charged molecules with the same charge as the stationary phase are excluded from the pores of the stationary phase (Fig. IV.32). Weakly charged or neutral components can enter the pores and are retained. In particular, weak electrolytes are retained according to their degree of dissociation: the greater their dissociation, the less they are retained. As a result, analytes can be separated based on their dissociation constants. Analytes with an opposite charge to the stationary phase are retained the most, as they adsorb to the stationary phase by electrostatic interactions. The exclusion effect is typically explained by the Donnan theory, which assumes the formation of a Donnan membrane on the surface of the stationary phase that repels molecules with the same charge as the stationary phase, thus excluding them from the pores. A model for ion exclusion chromatography according to the Donnan theory is described in the reference [196].

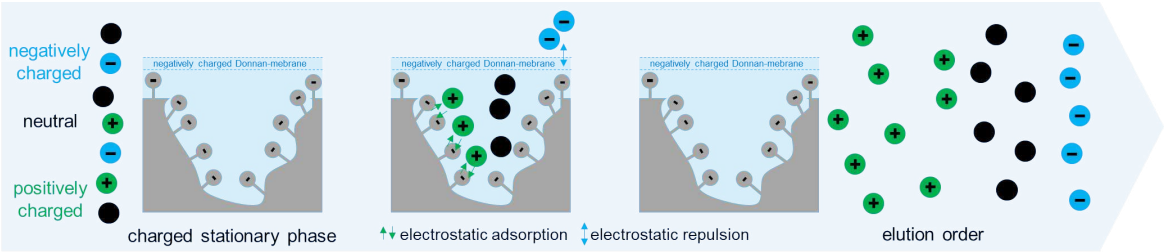


**Figure IV.32.** Illustration of the pore exclusion of charged analytes in ion-exclusion chromatography.

Hydrophobic charge induction chromatography (HCIC) is a mixed-mode chromatography technique that combines hydrophobic adsorption and electrostatic repulsion for the purification of biomolecules such as proteins. Stationary phases used in HCIC typically contain ligands that provide hydrophobic interaction sites and pH-dependent ionizable moieties, such as pyridine groups. In the first step, the target molecules are adsorbed to the stationary phase by hydrophobic binding. In the subsequent elution step, electrostatic repulsion of the bound compounds from the stationary phase is usually induced by changing the pH of the mobile phase,

leading to ionization of the stationary phase ligand and usually also of the bound compounds (Fig. IV.33). Typical HCIC stationary phase ligands are presented in reference [197].

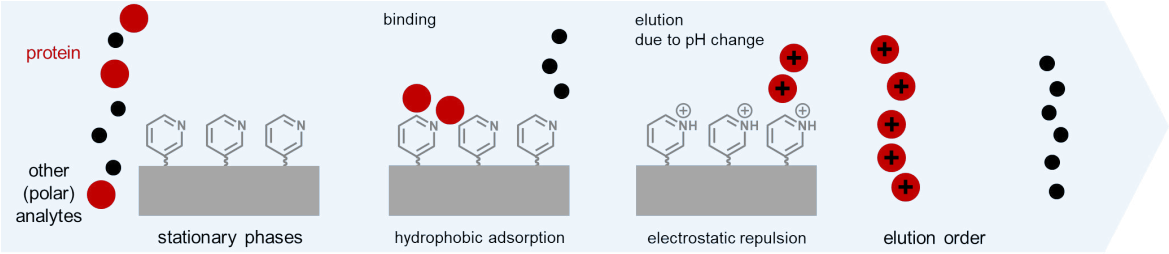


**Figure IV.33.** Illustration of retention and elution mechanism of target molecules in hydrophobic charge induction chromatography.

Silver ion chromatography is a technique mainly used for the analysis of lipids and is based on the interaction of immobilized silver ions of the stationary phase with the double bonds of the analytes. According to the Dewar-Chatt-Duncanson model, a transient charge transfer complex is formed between the silver ions and the double bonds, resulting in the retention of unsaturated compounds (Fig. IV.34). Thus, the analytes are separated according to the number of double bonds. However, the configuration of the double bonds also influences the retention behaviour. Immobilization of the silver ions on the stationary phase is usually achieved by electrostatic adsorption to strong cation exchangers on the stationary phase surface, such as sulfonate groups. The chromatographic conditions used are typical classical normal phase conditions, which prevent the detachment of the silver ions from the stationary phase. A comprehensive review of common silver ion chromatographic separation techniques is provided in reference [198].

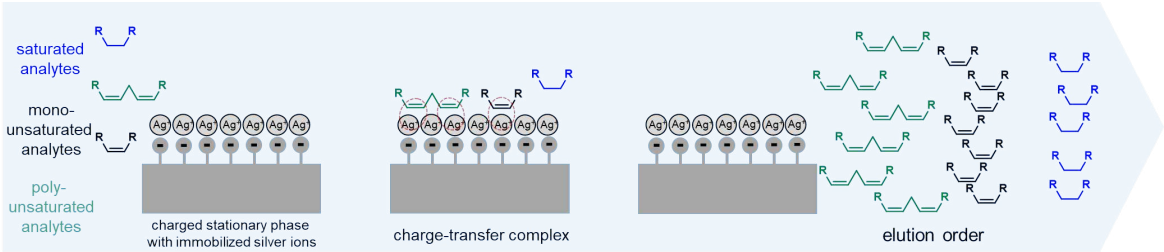


**Figure IV.34.** Illustration of separation mechanism in silver ion chromatography.

Affinity chromatography is a powerful technique for isolation and purification of specific target molecules such as proteins, antibodies or nucleic acids. Its specificity and high affinity enable the separation and purification of target molecules even in complex samples. Typically, affinity chromatography involves an initial purification step in which the target molecule is strongly retained on the column, followed by an elution step in which the target molecule is eluted from the column. The chemistry of the stationary phase affinity ligand is determined by the nature of the target molecule, as a highly specific interaction must be achieved. For example, protein A is used as affinity ligand for purification of antibodies, and nickel-nitrilotriacetic acid (Ni-NTA) is used for histidine-tagged proteins (Fig. IV.35). The specific binding prevents elution of the target molecule during the purification step and separates the target molecule from the residual sample. The subsequent elution step usually requires a change in mobile phase composition. For example, in protein A chromatography, a pH change provokes the elution of bound antibodies from the stationary phase. In Ni-NTA affinity chromatography, elution is usually induced by adding imidazole to the mobile phase in the elution step. References [199] and [200] provide an overview of the various techniques of affinity chromatography and the stationary phases used.

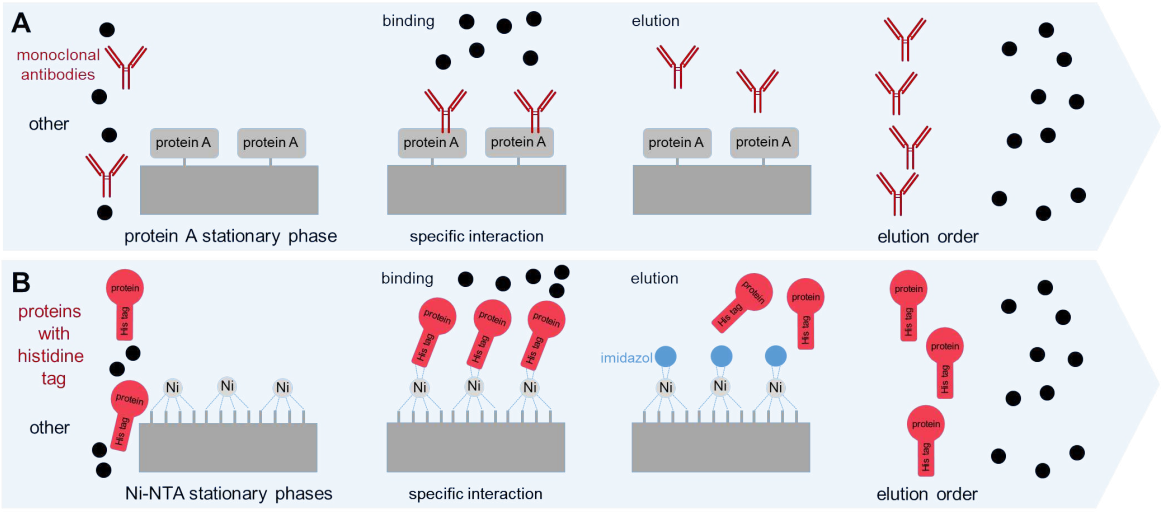


**Figure IV.35.** Illustration of protein A affintiy chromatography (A) and Ni-NTA affintiy chromatography (B).

Chiral chromatography is used to separate enantiomers and can be performed using various chromatographic modes such as normal phase, reversed phase or ion exchange chromatography. There are several different stationary phases used in chiral chromatography, such as polysaccharide-based, cyclodextrin-based, protein-based, macrocyclic or quinine alkaloid-based chiral stationary phases (CSPs). The mechanism of enantiomer discrimination on stationary phases can be explained by differences in enthalpic, entropic and steric interactions of the enantiomers with the stationary phase (Fig. IV.36). Reference [201] reviews the progress in the development of chiral stationary phases and reference [202] details the chiral recognition mechanism of the stationary phase.

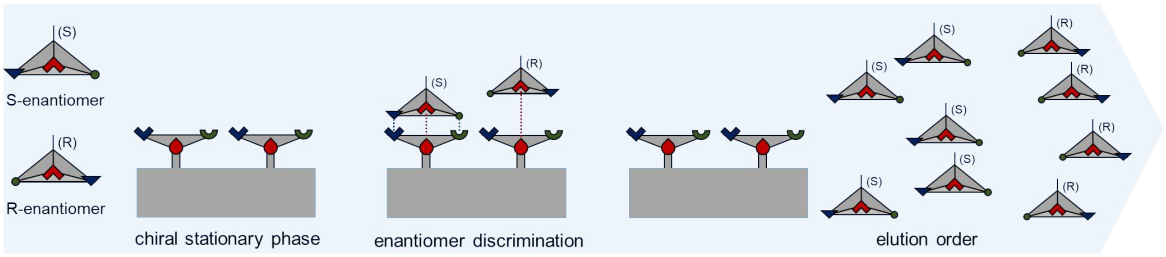


**Figure IV.36.** Illustration of the chiral recognition mechanism on a chiral stationary phase.

## V.5 Stationary phase characterization techniques

The characterization of stationary phases is of great importance for quality control of established stationary phases as well as for the evaluation of newly developed stationary phases. In routine stationary phase production, stationary phase characterization allows verification of synthesis and performance reproducibility. In stationary phase development, stationary phase characterization provides valuable information about synthesis success, stationary phase chemistry, estimation of chromatographic properties, separation mechanisms, material stability, orthogonality to other stationary phases, and possible application fields.

Figure IV. 37 gives an overview of commonly used methods for stationary phase characterization. In general, chemometric, thermal, gravimetric, porosity determination, microscopic, electromigration, spectroscopic and chromatographic methods can be distinguished. In principle, however, other methods can also be used to characterize stationary phases. [203-207]

Chemometric methods can be utilized to predict and understand stationary phase interactions with analytes via molecular modeling and are therefore a useful tool in design and method development. In addition, chemometrics can be applied to analyze and compare chromatographic data from novel and established stationary phases, thus revealing orthogonality between columns (Fig. IV.38). [208]

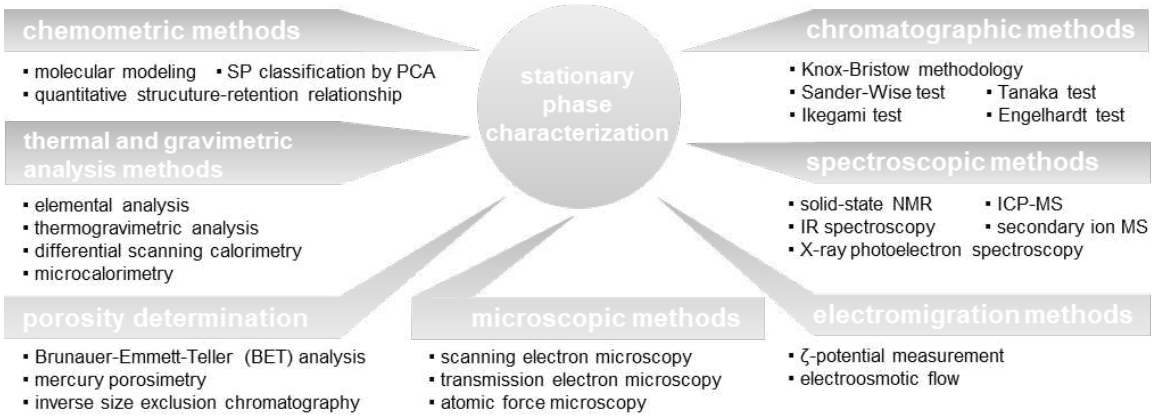


**Figure IV.37.** Overview of commonly used methods for stationary phase characterization based on [203], [204], [205], [206] and [207]; ICP: inductively coupled plasma, IR: infrared spectroscopy, MS: mass spectrometry, NMR: nuclear magnetic resonance spectroscopy, PCA: principal component analysis, SP: stationary phase.

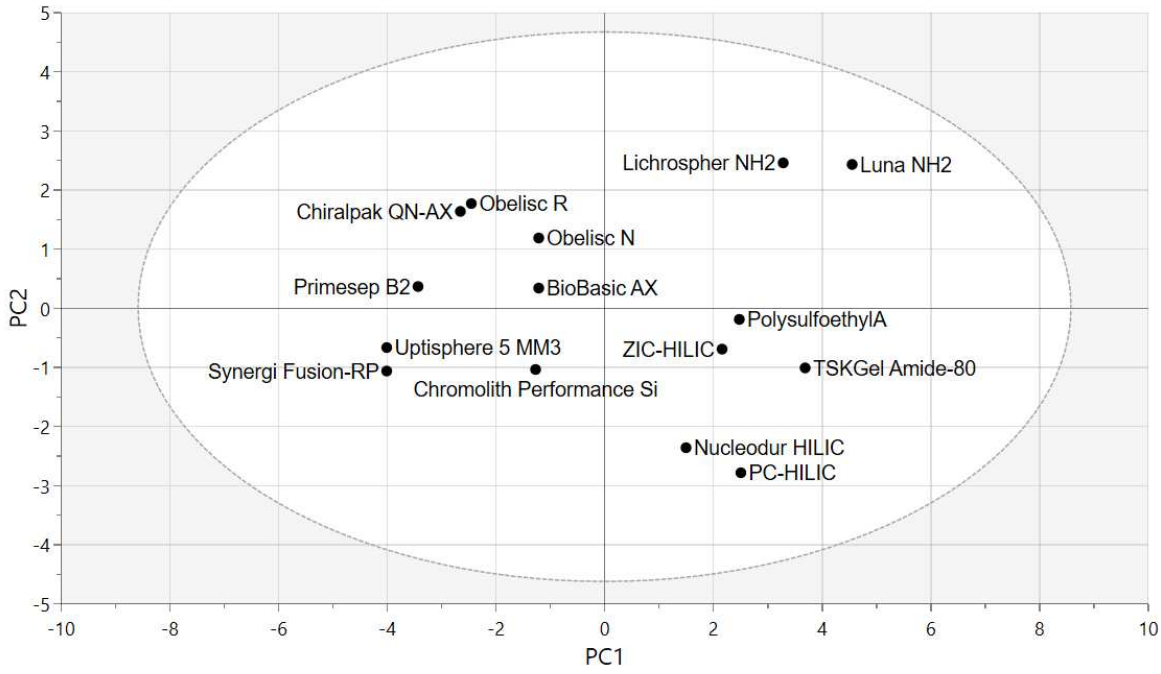


**Figure IV.38.** Stationary phase classification of commercial columns. The score plot was generated by principal component analysis of chromatographic data obtained under reversed-phase and hydrophilic interaction chromatography conditions. The chromatographic data and the surface chemistry of the stationary phases can be found in [140]. PC1 encodes the hydrophobicity of the stationary phase, while PC2 encodes the surface charge. Columns with similar chromatographic behavior are clustered next to each other, and those with different chromatographic characteristics are far apart. Thus, the orthogonality of columns can be revealed. Principal component analysis was carried out by using the multivariate data analysis software SIMCA (17.0.2) from Sartorius Stedim Data Analytics AB (Umeå, Sweden).

The surface chemistry of stationary phases can be investigated and elucidated by a variety of techniques, including thermal, gravimetric, spectroscopic, and electromigration methods. Elemental analysis, for example, can provide information on the elemental composition of the material and thus allow the calculation of ligand densities immobilized on silica supports. [132] Solid-state nuclear magnetic resonance (NMR) spectroscopy and infrared spectroscopy (Fig. IV.39) can both provide additional information about the chemical structure of the surface ligands and their successful immobilization on the support. [209-213] $^{29}$Si solid-state NMR (Fig. IV.40) can also provide information about the binding characteristics of the ligands to the support in silica-based stationary phases. [132, 209] ζ-potential measurements (Fig. IV.41) can reveal the charge properties of the stationary phase surfaces. Charge properties typically play a crucial role in chromatographic processes and are therefore of great interest. [214-216]

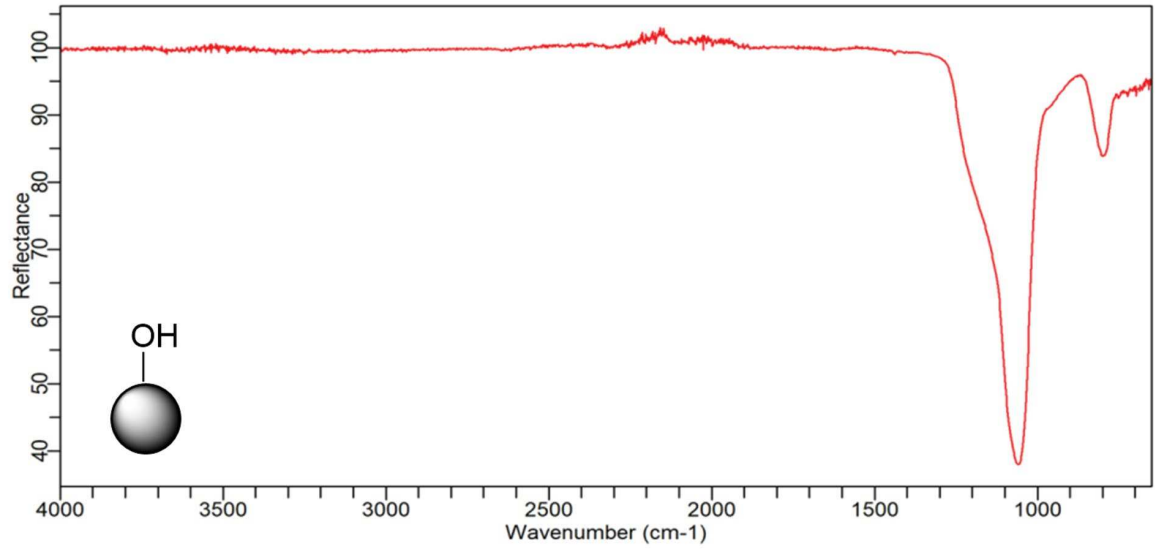


**Figure IV.39.** Infrared spectrum recorded in-house from bare silica utilizing an ATR-FTIR 630 Cary spectrometer from Agilent Technologies (Waldbronn, Germany). Spectra of modified silica particles can be found, for example, in reference [215] and [217].

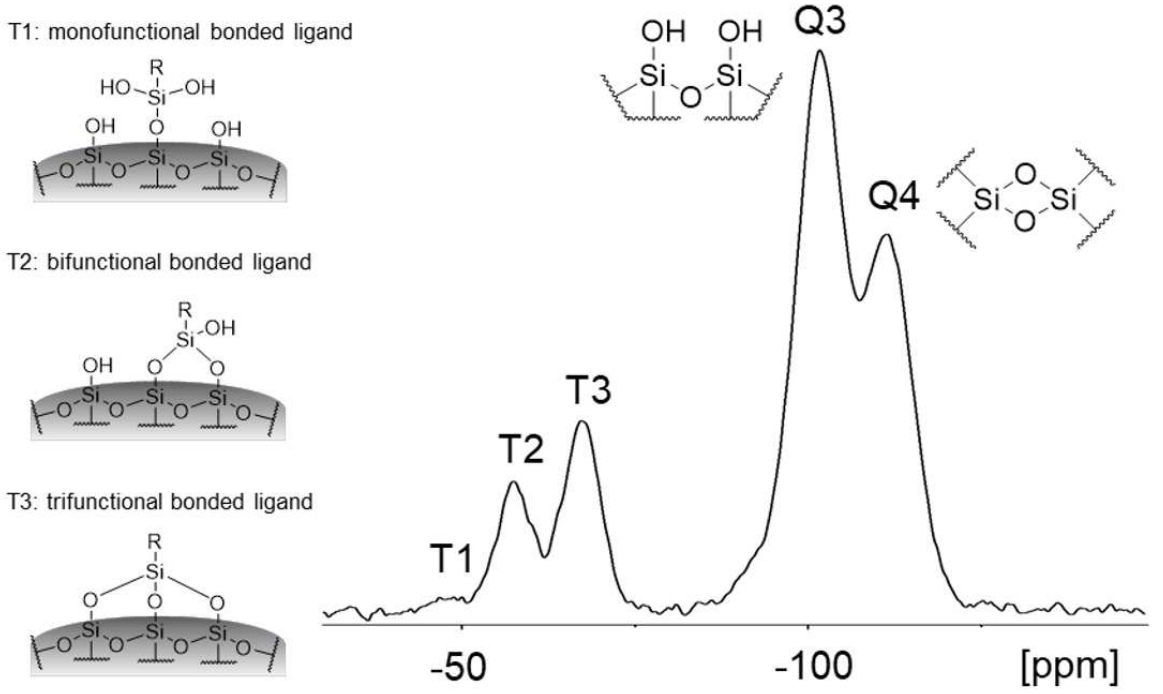


**Figure IV.40.** $^{29}$Si CP/MAS spectrum of modified silica particles. The spectrum exhibits the typical signals for the silica support (Q3: free single and vicinal silanol groups, Q4: siloxane groups) and three signals that can be assigned to the silicon atoms of the ligands immobilized to the silica support via mono-, bi- or trifunctional bonding. Other characteristic signals in $^{29}$Si CP/MAS spectra are described in [203] and [209].

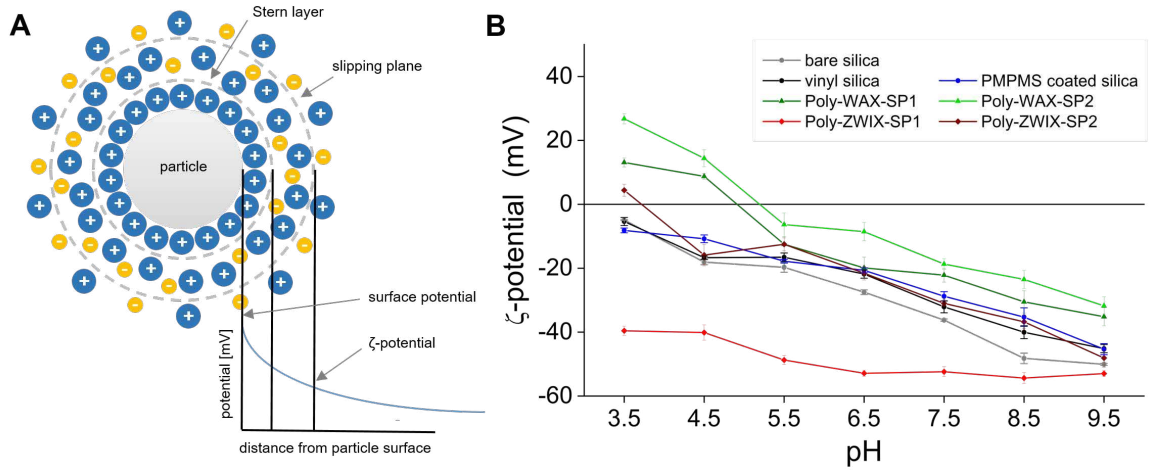


**Figure IV.41.** The ζ-potential corresponds to the surface charge of the particles and represents the charge at the shear surface (A). pH-Dependent ζ-potentials of modified and bare silica particles can be obtained by electrophoretic light scattering (B). [214, 215, 218] For determination of ζ-potentials of the modified silica particles (for synthesis procedure see Fig. IV.23), the particles were suspended in buffer solution at constant ionic strength (1mM buffer in 10 mM potassium chloride solution) yielding a concentration of 0.2 mg silica particles per mL buffer solution. The following buffers were used: buffer 1 (formic acid; pH adjusted to 3.5 with sodium hydroxide), buffer 2 (formic acid; pH adjusted to 4.5 with sodium hydroxide), buffer 3 (acetic acid; pH adjusted to 5.5 with sodium hydroxide), buffer 4 (histidine; pH adjusted to 6.5 with hydrochloric acid), buffer 5 (tris(hydroxymethyl)aminomethane; pH adjusted to 7.5 with hydrochloric acid), buffer 6 (tris(hydroxymethyl)aminomethane; pH adjusted to 8.5 with hydrochloric acid), buffer 7 (boric acid; pH adjusted to 9.5 with sodium hydroxide). Measurements were conducted using a Zetasizer NanoZS particle analyzer from Malvern Instruments (Herrenberg, Germany). The silica suspensions were analyzed 3 times at 25 °C and the equilibration time was set to 5 min. Finally, the corresponding ζ-potentials were calculated according to the Smoluchowski approximation.

The (micro-)structure of the stationary phase support material can be characterized inter alia by microscopy and by porosity determination methods. Scanning electron microscopy (SEM) and transmission electron microscopy (TEM) can be utilized to get insight into particle shape, size, pore structure, location and uniformity of pores, surface topography and roughness. [213, 219] SEM and TEM can both produce high-resolution images of samples, but their imaging approaches are different. In SEM, the sample is scanned with a focused beam and the emitted electrons are collected to produce an image of the surface (Fig. IV.42). In contrast, in TEM, the electrons are sent through the material and the electrons that pass through the material are collected. Both approaches can require sputtering of the material, which can affect the images obtained. [220, 221] This is a particular concern with SEM, where sputtering is used to reduce the surface charge of the material. Sputtering involves depositing an ultrathin film of an electrically conductive metal (e.g., gold, palladium, platinum) on a non-conductive or poorly conductive specimen. The sputtered films are typically around 10 nm thick and can smooth the surface, making the original topography

unrecognizable. As a result, other attempts now use atomic force microscopy (AFM) to characterize the surface topography. [213] Reference [222] shows both SEM and TEM images of the same modified silica particles, clearly illustrating the different characteristics of the images obtained by each technique.

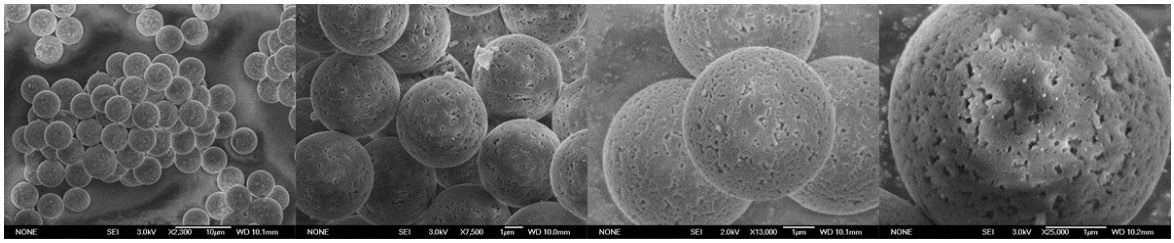

**Figure IV.42.** Scanning electron microscopy images of polystyrene-divinylbenzene spheres synthesized according to [84]. The images were in-house recorded using an JEOL JSM-6500F scanning electron microscope (no sputter coating).

In addition to microscopic methods, nitrogen adsorption (BET analysis), mercury porosimetry and inverse size exclusion chromatography (ISEC) can provide valuable information about the porosity of the material. Typically, the porosity of silica materials is determined by nitrogen adsorption via BET analysis. However, it should be taken into account that nitrogen, as a small probe molecule, can also penetrate into pores that are not available for chromatographic processes under liquid chromatography conditions. As a result, the effective surface area obtained may be much larger than the actual surface area available under chromatographic conditions. The same applies to the pore volume distribution of the stationary phases. Thus, especially ISEC can be a useful alternative, which is performed under liquid chromatographic conditions with polymeric standards and thus represents rather applicative conditions. As a result, ISEC may provide more relevant specific surface areas and pore volume distribution values than those obtained by gas adsorption (Fig. IV.43). [48]

Evaluating and exploring the chromatographic behavior of columns using chromatographic test mixtures and conditions is also an essential part of stationary phase characterization. For this purpose, numerous chromatographic tests have been developed to investigate column properties under different conditions and chromatographic modes, such as reversed-phase, normal-phase and hydrophilic interaction chromatography. Reference [207] provides a comprehensive review of prominent chromatographic tests. One of the best known

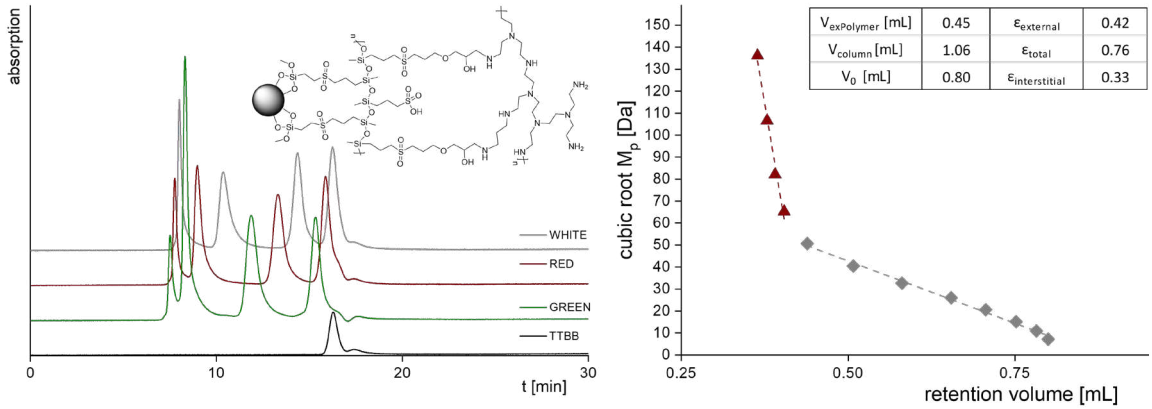


**Figure IV.43.** Porosity estimation via inverse size exclusion chromatography for double polymer-modified silica particles according to reference [127]. Modified silica (Poly-ZWIX-SP1) was prepared as described in Fig. IV.23. Molecular weights of the polymers were 370, 1,306, 3,470, 8,680, 17,600, 34,800, 66,000, 130,000, 277,000, 552,000, 1,210,000 and 2,520,000 Da. Polymers were divided into three samples (WHITE, RED, GREEN). Tri-tert-butylbenzene (TTBB) served as void volume marker.

is probably the Tanaka test, which has been used to characterize classic reversed-phase stationary phases. This test determines the number of alkyl chains, hydrophobicity, steric selectivity, hydrogen bonding capacity, ion exchange capacity at pH >7 and ion exchange capacity at pH <3 using the chromatographic conditions and test compounds shown in Table IV.5. [203, 223, 224]

In addition to the methods described, it is also beneficial to consider other suitable techniques for investigating specific properties of stationary phases. These may include (innovative) techniques from other scientific disciplines that are not commonly associated with the characterization of stationary phases.

**Table IV.5.** Conditions of the Tanaka test. [223, 224]

| test | property tested | associated stationary phase characteristics | isocratic mobile phase conditions | chromatographic measurement |
|---|---|---|---|---|
| A | amount of alkyl chains | silica surface area, surface coverage | 80% methanol and 20% water | k (amylbenzene) |
| B | hydrophobicity | surface coverage | 80% methanol and 20% water | k (amylbenzene)/ k (butylbenzene) |
| C | shape/steric selectivity | functionality of the silane, surface coverage | 80% methanol and 20% water | k (triphenylene)/ k (o-terphenyl) |
| D | hydrogen bonding capacity | amount of silanols, endcapping, surface coverage | 30% methanol and 70% water | k (caffeine)/ k (phenol) |
| E | ion exchange capacity (pH>7) | amount of silanols and ion exchange sites | 30% methanol and 70% water (aqueous portion: 0.02 M phosphate buffer, pH 7.6) | k (benzylamine)/ k (phenol) |
| F | ion exchange capacity (pH<3) | amount of silanols and ion exchange sites at pH 3, silica pretreatment | 30% methanol and 70% water (aqueous portion: 0.02 M phosphate buffer, pH 2.7) | k (amylbenzene)/ k (butylbenzene) |

## V.6 References

[1] L.R. Snyder, J.W. Dolan, Milestones in the development of liquid chromatography, Liquid chromatography: Fundamentals and instrumentation, (2013) 1-17.

[2] I. Siddique, High-performance liquid chromatography: Comprehensive techniques and cutting-edge innovations, Euro J Adv Engg Tech., 10 (2023) 66-70.

[3] M.K. Gupta, A. Ghuge, M. Parab, Y. Al-Refaei, A. Khandare, N. Dand, N. Waghmare, A comparative review on high-performance liquid chromatography (HPLC), ultra performance liquid chromatography (UPLC) & high-performance thin layer chromatography (HPTLC) with current updates, Curr Iss Pharm Med S, 35 (2022) 224-228.

[4] M.J. den Uijl, P.J. Schoenmakers, B.W.J. Pirok, M.R. van Bommel, Recent applications of retention modelling in liquid chromatography, J Sep Sci, 44 (2021) 88-114.

[5] S.C. Moldoveanu, V. David, Essentials in modern HPLC separations, Essentials in modern HPLC separations, (2013) 1-532.

[6] K. Ballschmiter, M. Wossner, Recent developments in adsorption liquid chromatography (NP-HPLC) - A review, Fresen J Anal Chem, 361 (1998) 743-755.

[7] W.R. LaCourse, M.E. LaCourse, Chapter 4 - General instrumentation in HPLC, in: S. Fanali, B. Chankvetadze, P.R. Haddad, C.F. Poole, M.-L. Riekkola (Eds.) Liquid chromatography (third edition), Elsevier (2023) 61-73.

[8] S. Fekete, I. Kohler, S. Rudaz, D. Guillarme, Importance of instrumentation for fast liquid chromatography in pharmaceutical analysis, J Pharmaceut Biomed, 87 (2014) 105-119.

[9] A. Zotou, An overview of recent advances in HPLC instrumentation, Cent Eur J Chem, 10 (2012) 554-569.

[10] J.W. Dolan, Mobile-phase degassing: What, why, and how, LCGC North America, 32 (2014) 482-487.

[11] S. Kromidas, Aspects of gradient optimization, in: Gradient HPLC for practitioners, (2019) 1-40.

[12] G. Guiochon, The limits of the separation power of unidimensional column liquid chromatography, J Chromatogr A, 1126 (2006) 6-49.

[13] K. Shoykhet, K. Broeckhoven, M.W. Dong, Modern HPLC pumps: Perspectives, principles, and practices, LCGC Eur, 32 (2019) 410-419.

[14] C. Paul, F. Steiner, M.W. Dong, HPLC autosamplers: Perspectives, principles, and practices, LCGC North America, 37 (2019) 514-529.

[15] R.E. Majors, Historical developments in HPLC and UHPLC column technology: The past 25 years, LCGC North America, 33 (2015) 818-840.

[16] D. Guillarme, J. Ruta, S. Rudaz, J.L. Veuthey, New trends in fast and high-resolution liquid chromatography: A critical comparison of existing approaches, Anal Bioanal Chem, 397 (2010) 1069-1082.

[17] M.E. Swartz, UPLC: An introduction and review, J Liq Chromatogr R T, 28 (2005) 1253-1263.

[18] R.S. van den Hurk, M. Pursch, D.R. Stoll, B.W.J. Pirok, Recent trends in two-dimensional liquid chromatography, TrAC-Trend Anal Chem, 166 (2023).

[19] I. Francois, K. Sandra, P. Sandra, Comprehensive liquid chromatography: Fundamental aspects and practical considerations - A review, Anal Chim Acta, 641 (2009) 14-31.

[20] G. Guiochon, N. Marchetti, K. Mriziq, R.A. Shalliker, Implementations of two-dimensional liquid chromatography, J Chromatogr A, 1189 (2008) 109-168.

[21] M. Gilar, P. Olivova, A.E. Daly, J.C. Gebler, Orthogonality of separation in two-dimensional liquid chromatography, Anal Chem, 77 (2005) 6426-6434.

[22] P.J. Schoenmakers, G. Vivó-Truyols, W.M.C. Decrop, A protocol for designing comprehensive two-dimensional liquid chromatography separation systems, J Chromatogr A, 1120 (2006) 282-290.

[23] M. Swartz, HPLC Detectors: A brief review, J Liq Chromatogr R T, 33 (2010) 1130-1150.

[24] M. Swartz, Seeing is believing: Detectors for HPLC, LCGC North America, 28 (2010) 880-889.

[25] M. Olfert, S. Bäurer, M. Wolter, S. Buckenmaier, E. Brito-de la Fuente, M. Lämmerhofer, Comprehensive profiling of conjugated fatty acid isomers and their lipid oxidation products by two-dimensional chiral RPxRP liquid chromatography hyphenated to UV- and SWATH-MS-detection, Anal Chim Acta, 1202 (2022).

[26] T.F. Scientific, So funktionieren HPLC-Detektoren, https://www.thermofisher.com/de/de/home/industrial/chromatography/chromatography-learning-center/liquid-chromatography-information/hplc-system-components/how-hplc-detectors-work.html, (2024).

[27] M.W. Dong, J. Wysocki, Ultraviolet detectors: Perspectives, principles, and practices, LCGC North America, 37 (2019) 750-759.

[28] T.L. Chester, Recent developments in high-performance liquid chromatography stationary phases, Anal Chem, 85 (2013) 579-589.

[29] F. Gritti, M.F. Wahab, Understanding the science behind packing high-efficiency columns and capillaries: Facts, fundamentals, challenges, and future directions, LCGC Europe, 31 (2018) 90-101.

[30] M.F. Wahab, D.C. Patel, R.M. Wimalasinghe, D.W. Armstrong, Fundamental and practical insights on the packing of modern high efficiency analytical and capillary columns, Anal Chem, 89 (2017) 8177-8191.

[31] J. Nawrocki, M.P. Rigney, A. McCormick, P.W. Carr, Chemistry of zirconia and its use in chromatography, J Chromatogr A, 657 (1993) 229-282.

[32] T. Kubo, M. Ichikawa, T. Adachi, Y. Watabe, T. Naito, K. Otuka, Development of a particle packed bed model for homogeneity evaluation of liquid chromatography column, J Chromatogr A, 1705 (2023).

[33] R.E. Majors, Developments in HPLC column packing Design, LCGC LC Column Technology Supplement, 24 (2006) 8-15.

[34] J. Nawrocki, C. Dunlap, J. Li, J. Zhao, C.V. McNeff, A. McCormick, P.W. Carr, Part II. Chromatography using ultra-stable metal oxide-based stationary phases for HPLC, J Chromatogr A, 1028 (2004) 31-62.

[35] U.R. Silva, C. Airoldi, K.E. Collins, C.H. Collins, A new generation of more pH stable reversed phases prepared by silanization of zirconized silica, J Chromatogr A, 1191 (2008) 90-98.

[36] J. Ge, L. Zhao, L.R. Chen, Y.P. Shi, Titanium-coated silica spheres prepared by self-assembly technique for use as HPLC packing, J Chromatogr Sci, 48 (2010) 29-34.

[37] H.J. Dun, W.Q. Zhang, Y. Wei, X.Q. Song, Y.M. Li, L.R. Chen, Layer-by-layer self-assembly of multilayer zirconia nanoparticles on silica spheres for HPLC packings, Anal Chem, 76 (2004) 5016-5023.

[38] A.M. Faria, D.R. Magalhaes, K.E. Collins, C.H. Collins, Characterization of zirconized silica supports for HPLC, Anal Chim Acta, 550 (2005) 137-143.

[39] H. Qian, W.Y. Li, X. Wang, F.Z. Xie, W.H. Li, Q.S. Qu, Simultaneous growth of graphene/mesoporous silica composites using liquid precursor for HPLC separations, Appl Surf Sci, 537 (2021).

[40] H.D. Qiu, X.J. Liang, M. Sun, S.X. Jiang, Development of silica-based stationary phases for high-performance liquid chromatography, Anal Bioanal Chem, 399 (2011) 3307-3322.

[41] L. Pereira, Porous graphitic carbon as a stationary phase in HPLC: Theory and applications, J Liq Chromatogr R T, 31 (2008) 1687-1731.

[42] M. Russo, M.R.T. Camillo, R. La Tella, F. Rigano, P. Donato, L. Mondello, P. Dugo, Principles and applications of porous graphitic carbon stationary phase in liquid chromatography: An update, J Chromatogr A, 1719 (2024).

[43] K.D. Wyndham, J.E. O'Gara, T.H. Walter, K.H. Glose, N.L. Lawrence, B.A. Alden, G.S. Izzo, C.J. Hudalla, P.C. Iraneta, Characterization and evaluation of C18 HPLC stationary phases based on ethyl-bridged hybrid organic/inorganic particles, Anal Chem, 75 (2003) 6781-6788.

[44] N.L. Lawrence, K.D. Wyndham, K.H. Glose, J.T. Cook, D.W. Brousmiche, P.C. Iraneta, B.A. Alden, C.A. Boissel, T.H. Walter, Comparison of different reversed-phase packing materials based on higher organic hybrid particles, MRS Online Proceedings Library, 1007 (2007) 404.

[45] K. Wyndham, T. Walter, P. Iraneta, B. Alden, E. Bouvier, C. Hudalla, N. Lawrence, D. Walsh, Synthesis and applications of BEH particles in liquid chromatography, LCGC Europe, (2012) 15-20.

[46] H. Yu, C.Y. Jia, H.B. Wu, G.J. Song, Y. Jin, Y.X. Ke, X.M. Liang, Highly stable high performance liquid chromatography stationary phase based on direct chemical modification of organic bridges in hybrid silica, J Chromatogr A, 1247 (2012) 63-70.

[47] M. Hefnawy, M. El-Gendy, H. Al-Salem, H. Marenga, A. El-Azab, A. Abdel-Aziz, A. El Gamal, M. Alanazi, A. Obaidullah, A. Al-Hossaini, A. Hefnawy, Trends in monoliths: Packings, stationary phases and nanoparticles, J Chromatogr A, 1691 (2023).

[48] K.K. Unger, R. Skudas, M.M. Schulte, Particle packed columns and monolithic columns in high-performance liquid chromatography-comparison and critical appraisal, J Chromatogr A, 1184 (2008) 393-415.

[49] F. Gritti, G. Guiochon, The current revolution in column technology: How it began, where is it going?, J Chromatogr A, 1228 (2012) 2-19.

[50] W. Stöber, A. Fink, E. Bohn, Controlled growth of monodisperse silica spheres in micron size range, J Colloid Interf Sci, 26 (1968) 62-69.

[51] B. Buszewski, S. Noga, Hydrophilic interaction liquid chromatography (HILIC) - a powerful separation technique, Anal Bioanal Chem, 402 (2012) 231-247.

[52] F. Svec, L. Geiser, Monolithic stationary phases for HPLC and sample preparation, LCGC North America, 24 (2006) 22-27.

[53] R.E. Majors, Advances in HPLC column packing design, LCGC LC Column Technology Supplement, (2004) 8-11.

[54] G. Guiochon, F. Gritti, Shell particles, trials, tribulations and triumphs, J Chromatogr A, 1218 (2011) 1915-1938.

[55] W. Zhang, S. Li, J. Zhang, Preparation and chromatographic features of fibrous core-shell HPLC packing material, Chromatographia, 81 (2018) 1249-1256.

[56] K. Nakanishi, Monolithic porous silica for high-speed HPLC, in: L. Klein, M. Aparicio, A. Jitianu (Eds.) Handbook of sol-gel science and technology: Processing, characterization and applications, Springer International Publishing, Cham, (2018) 1939-1948.

[57] M. Wolter, M. Lämmerhofer, In-situ functionalized monolithic polysiloxane-polymethacrylate composite materials from polythiol-ene double click reaction in capillary column format for enantioselective nano-high-performance liquid chromatography, J Chromatogr A, 1497 (2017) 172-179.

[58] K. Broeckhoven, G. Desmet, Advances and innovations in liquid chromatography stationary phase supports, Anal Chem, 93 (2021) 257-272.

[59] D.V. McCalley, Is hydrophilic interaction chromatography with silica columns a viable alternative to reversed-phase liquid chromatography for the analysis of ionisable compounds?, J Chromatogr A, 1171 (2007) 46-55.

[60] B.A. Olsen, Hydrophilic interaction chromatography using amino and silica columns for the determination of polar pharmaceuticals and impurities, J Chromatogr A, 913 (2001) 113-122.

[61] S. Bocian, B. Buszewski, Residual silanols at reversed-phase silica in HPLC - a contribution for a better understanding, J Sep Sci, 35 (2012) 1191-1200.

[62] A. Méndez, E. Bosch, M. Rosés, U.D. Neue, Comparison of the acidity of residual silanol groups in several liquid chromatography columns, J Chromatogr A, 986 (2003) 33-44.

[63] J. Nawrocki, The silanol group and its role in liquid chromatography, J Chromatogr A, 779 (1997) 29-71.

[64] A. Berthod, Silica - backbone material of liquid-chromatographic column packings, J Chromatogr, 549 (1991) 1-28.

[65] E.M. Borges, D.A. Volmer, Silica, hybrid silica, hydride silica and non-silica stationary phases for liquid chromatography. part II: Chemical and thermal stability, J Chromatogr Sci, 53 (2015) 1107-1122.

[66] D.A. Lopez, A.I. Green, D.S. Bell, What is on your HPLC particle? A look at stationary phase chemistry synthesis, LCGC Europe, 33 (2020) 460-465.

[67] J.J. Pesek, M.T. Matyska, R.I. Boysen, Y. Yang, M.T.W. Hearn, Aqueous normal-phase chromatography using silica-hydride-based stationary phases, TrAC-Trend Anal Chem, 42 (2013) 64-73.

[68] J.J. Pesek, R.I. Boysen, M.T.W. Hearn, M.T. Matyska, Hydride-based HPLC stationary phases: A rapidly evolving technology for the development of new bio-analytical methods, Anal Methods-UK, 6 (2014) 4496-4503.

[69] J.J. Pesek, M.T. Matyska, Hydride-based silica stationary phases for HPLC: Fundamental properties and applications, J Sep Sci, 28 (2005) 1845-1854.

[70] D.J. Anderson, High-performance liquid-chromatography (advances in packing materials), Anal Chem, 67 (1995) 475-486.

[71] H.A. Claessens, M.A. van Straten, J.J. Kirkland, Effect of buffers on silica-based column stability in reversed-phase high-performance liquid chromatography, J Chromatogr A, 728 (1996) 259-270.

[72] E.M. Borges, M.R. Euerby, An appraisal of the chemical and thermal stability of silica based reversed-phase liquid chromatographic stationary phases employed within the pharmaceutical environment, J Pharmaceut Biomed, 77 (2013) 100-115.

[73] U.D. Neue, T.H. Walter, B.A. Alden, Z.P. Jiang, R.P. Fisk, J.T. Cook, K.H. Glose, J.L. Carmody, J.M. Grassi, Y.F. Cheng, Z.L. Lu, R.J. Crowley, Use of high-performance LC packings from pH 1 to pH 12, Am Lab, 31 (1999) 36-39.

[74] A. Rimola, D. Costa, M. Sodupe, J.F. Lambert, P. Ugliengo, Silica surface features and their role in the adsorption of biomolecules: Computational modeling and experiments, Chem Rev, 113 (2013) 4216-4313.

[75] J. Nawrocki, C. Dunlap, A. McCormick, P.W. Carr, Part I. Chromatography using ultra-stable metal oxide-based stationary phases for HPLC, J Chromatogr A, 1028 (2004) 1-30.

[76] M. Grun, A.A. Kurganov, S. Schacht, F. Schuth, K.K. Unger, Comparison of an ordered mesoporous aluminosilicate, silica, alumina, titania and zirconia in normal-phase high-performance liquid chromatography, J Chromatogr A, 740 (1996) 1-9.

[77] T.E. Bapiro, F.M. Richards, D.I. Jodrell, Understanding the complexity of porous graphitic carbon (PGC) chromatography: modulation of mobile-stationary phase interactions overcomes loss of retention and reduces variability, Anal Chem, 88 (2016) 6190-6194.

[78] M.J.K. W.R. Betz, C.W. Frantz, J.M. Jones, W. Maule, K.G. Espenschied, C.E., Muraco, C. Corman, M. Ye, United States patent (US 11,806,693B2) HPLC carbon with narrow particle size distribution, (2021).

[79] M.T. Gokmen, F.E. Du Prez, Porous polymer particles - a comprehensive guide to synthesis, characterization, functionalization and applications, Prog Polym Sci, 37 (2012) 365-405.

[80] H.L. Zeng, J.D. Peng, H.J. Peng, X. Wang, Z.L. Zhang, H.Q. Yang, J.Y. Yu, J.J. Wu, Preparation of polymer-based amino acid stationary phase and its application for mixed-mode chromatography, Chromatographia, 87 (2024) 147-157.

[81] S. Zhang, R.Z. Tang, D.Y. Wang, S.J. Ma, S.C. Jia, Z. Gao, B.L. Gong, J.J. Ou, Fabrication of highly crosslinked and monodispersed silicon-containing polymeric microspheres via photo-initiated polymerization and their application in capillary liquid chromatography, J Chromatogr A, 1659 (2021).

[82] M. Yang, Y.G. Guo, Q. Wu, Y. Luan, G. Wang, Synthesis and properties of amphiphilic nonspherical SPS/PS composite particles by multi-step seeded swelling polymerization, Polymer, 55 (2014) 1948-1954.

[83] X. Sun, J. Li, L. Xu, Synthesis of penetrable poly(methacrylic acid-co-ethylene glycol dimethacrylate) microsphere and its HPLC application in protein separation, Talanta, 185 (2018) 182-190.

[84] A.V. Zatirakha, A.D. Smolenkov, A.V. Pirogov, P.N. Nesterenko, O.A. Shpigun, Preparation and characterisation of anion exchangers with dihydroxy-containing alkyl substitutes in the quaternary ammonium functional groups, J Chromatogr A, 1323 (2014) 104-114.

[85] E. Unsal, B. Elmas, S.T. Çamli, M. Tuncel, S. Senel, A. Tuncel, Monodisperse-porous poly(styrene-co-divinylbenzene) beads providing high column efficiency in reversed phase HPLC, J Appl Polym Sci, 95 (2005) 1430-1438.

[86] X.Y. Liu, Y. Wang, H.L. Cong, Y.Q. Shen, B. Yu, A review of the design of packing materials for ion chromatography, J Chromatogr A, 1653 (2021).

[87] T.H. Walter, B.A. Alden, K. Berthelette, Evaluation of the base stability of hydrophilic interaction chromatography columns packed with silica or ethylene-bridged hybrid particles, Separations, 9 (2022).

[88] T.H. Walter, C. Boissel, J.A. Field, N.L. Lawrence, Further evaluation of the base stability of hydrophilic interaction chromatography columns cacked with silica or ethylene-bridged hybrid particles, Separations, 10 (2023).

[89] C.J.H. Bonnie Alden, Kevin Wyndham, Thomas Walter, Nicole Lawrence, Edouard Bouvier, Daniel Walsh, Pamela Iraneta, Synthesis and applications of BEH particles in liquid chromatography, LCGC Supplements, 30 (2012) 20-29.

[90] A.M. Siouffi, About the term in the van Deemter's equation of plate height in monoliths, J Chromatogr A, 1126 (2006) 86-94.

[91] B.M. Wagner, S.A. Schuster, B.E. Boyes, T.J. Shields, W.L. Miles, M.J. Haynes, R.E. Moran, J.J. Kirkland, M.R. Schure, Superficially porous particles with 1000 Å pores for large biomolecule high performance liquid chromatography and polymer size exclusion chromatography, J Chromatogr A, 1489 (2017) 75-85.

[92] J. Bagge, M. Enmark, M. Lesko, F. Limé, T. Fornstedt, J. Samuelsson, Impact of stationary-phase pore size on chromatographic performance using oligonucleotide separation as a model, J Chromatogr A, 1634 (2020).

[93] B.W. Sands, Y.S. Kim, J.L. Bass, Characterization of bonded-phase silica-gels with different pore diameters, J Chromatogr, 360 (1986) 353-369.

[94] P.W. Carr, X.L. Wang, D.R. Stoll, Effect of pressure, particle size, and time on optimizing performance in liquid chromatography, Anal Chem, 81 (2009) 5342-5353.

[95] E.M. Borges, M.A. Rostagno, M.A.A. Meireles, Sub-2 μm fully porous and partially porous (core-shell) stationary phases for reversed phase liquid chromatography, Rsc Adv, 4 (2014) 22875-22887.

[96] K.M. Usher, C.R. Simmons, J.G. Dorsey, Modeling chromatographic dispersion: A comparison of popular equations, J Chromatogr A, 1200 (2008) 122-128.

[97] K. Broeckhoven, D. Cabooter, S. Eeltink, G. Desmet, Kinetic plot based comparison of the efficiency and peak capacity of high-performance liquid chromatography columns: Theoretical background and selected examples, J Chromatogr A, 1228 (2012) 20-30.

[98] J.C. Giddings, Dynamics of mass transfer and generalized nonequilibrium theory of chromatography, Berichte der Bunsengesellschaft für physikalische Chemie, 69 (1965) 773-782.

[99] C. Horvath, H.J. Lin, Movement and band spreading of unsorbed solutes in liquid-Chromatography, J Chromatogr, 126 (1976) 401-420.

[100] J.H. Knox, Practical aspects of LC theory, J Chromatogr Sci, 15 (1977) 352-364.

[101] F. Gritti, M. Martin, G. Guiochon, Influence of viscous friction heating on the efficiency of columns operated under very high pressures, Anal Chem, 81 (2009) 3365-3384.

[102] A. de Villiers, H. Lauer, R. Szucs, S. Goodall, P. Sandra, Influence of frictional heating on temperature gradients in ultra-high-pressure liquid chromatography on 2.1 mm ID columns, J Chromatogr A, 1113 (2006) 84-91.

[103] D.V. McCalley, The impact of pressure and frictional heating on retention, selectivity and efficiency in ultra-high-pressure liquid chromatography, TrAC-Trend Anal Chem, 63 (2014) 31-43.

[104] M. Heidorn, The role of temperature and column thermostatting in liquid chromatography, Thermo Fischer Scientific, White Paper 71499.

[105] J.J. Hsiao, G.O. Staples, D.R. Stoll, Troubleshooting LC separations of biomolecules, part 1: Background, and the meaning of inertness, LCGC Europe, 33 (2020) 122-126.

[106] J.P. Grinias, J.M. Godinho, Liquid chromatography column design and dimensional analysis of the van Deemter equation, LCGC North America, 40 (2022) 367-370.

[107] J.H. Knox, H.P. Scott, B-term and C-term in the van Deemter equation for liquid-chromatography, J Chromatogr, 282 (1983) 297-313.

[108] F. Gritti, G. Guiochon, The van Deemter equation: Assumptions, limits, and adjustment to modern high performance liquid chromatography, J Chromatogr A, 1302 (2013) 1-13.

[109] R. Hayes, A. Ahmed, T. Edge, H.F. Zhang, Core-shell particles: Preparation, fundamentals and applications in high performance liquid chromatography, J Chromatogr A, 1357 (2014) 36-52.

[110] S. Fekete, J. Fekete, K. Ganzler, Shell and small particles; Evaluation of new column technology, J Pharmaceut Biomed, 49 (2009) 64-71.

[111] S. Fekete, D. Guillarme, Kinetic evaluation of new generation of column packed with 1.3 μm core-shell particles, J Chromatogr A, 1308 (2013) 104-113.

[112] D. Cabooter, A. Fanigliulo, G. Bellazzi, B. Allieri, A. Rottigni, G. Desmet, Relationship between the particle size distribution of commercial fully porous and superficially porous high-performance liquid chromatography column packings and their chromatographic performance, J Chromatogr A, 1217 (2010) 7074-7081.

[113] N. Tanaka, D.V. McCalley, Core-shell, ultrasmall particles, monoliths, and other support Materials in High-Performance Liquid Chromatography, Anal Chem, 88 (2016) 279-298.

[114] F. Gritti, D.S. Bell, G. Guiochon, Particle size distribution and column efficiency. An ongoing debate revived with 1.9 µm Titan-C

particles, J Chromatogr A, 1355 (2014) 179-192.

[115] F. Gritti, I. Leonardis, J. Abia, G. Guiochon, Physical properties and structure of fine core-shell particles used as packing materials for chromatography Relationships between particle characteristics and column performance, J Chromatogr A, 1217 (2010) 3819-3843.

[116] K.K. Unger, S. Lamotte, E. Machtejevas, Column technology in liquid chromatography, Liquid Chromatography: Fundamentals and Instrumentation, (2013) 41-86.

[117] M. Gilar, M. DeLano, F. Gritti, Mitigation of analyte loss on metal surfaces in liquid chromatography, J Chromatogr A, 1650 (2021).

[118] G.J. Guimaraes, M.G. Bartlett, Managing nonspecific adsorption to liquid chromatography hardware: A review, Anal Chim Acta, 1250 (2023).

[119] H. Lardeux, A. Goyon, K. Zhang, J.M. Nguyen, M.A. Lauber, D. Guillarme, V. D'Atri, The impact of low adsorption surfaces for the analysis of DNA and RNA oligonucleotides, J Chromatogr A, 1677 (2022).

[120] K. Collins, C. Collins, C. Bertran, Stainless steel surfaces in LC systems, part II - passivation and practical recommendations, LCGC North America, 18 (2000) 688–692.

[121] D.A. Lopez, J. Bischof, Methods for the passivation of HPLC instruments and columns, LCGC Europe, 36 (2023) 218-224.

[122] J.J. Kirkland, J.J. DeStefano, The art and science of forming packed analytical high-performance liquid chromatography columns, J Chromatogr A, 1126 (2006) 50-57.

[123] J. Dingenen, Columns and packing methods, Analusis, 26 (1998) 18-32.

[124] J.P.C. Vissers, J. Laven, H.A. Claessens, C.A. Cramers, W.G.M. Agterof, Sedimentation behaviour and colloidal properties of porous, chemically modified silicas in non-aqueous solvents, Colloid Surface A, 126 (1997) 33-44.

[125] M. Verzele, C. Dewaele, D. Duquet, Observations and ideas on slurry packing of liquid-chromatography columns, J Chromatogr, 391 (1987) 111-118.

[126] A. Andrés, K. Broeckhoven, G. Desmet, Methods for the experimental characterization and analysis of the efficiency and speed of chromatographic columns: A step-by-step tutorial, Anal Chim Acta, 894 (2015) 20-34.

[127] C. Geibel, K. Dittrich, U. Woiwode, M. Kohout, T. Zhang, W. Lindner, M. Lammerhofer, Evaluation of superficially porous particle based zwitterionic chiral ion exchangers against fully porous particle benchmarks for enantioselective ultra-high performance liquid chromatography, J Chromatogr A, 1603 (2019) 130-140.

[128] M. Petro, D. Berek, Polymers immobilized on silica-gels as stationary phases for liquid-chromatography, Chromatographia, 37 (1993) 549-561.

[129] D.F. Horgan, J.N. Little, Comparison of conventionally-coated and chemically-bonded stationary phases in liquid chromatography, J Chromatogr Sci, 10 (1972) 76-&.

[130] C. Fernandes, J. Teixeira, M.M.M. Pinto, M.E. Tiritan, strategies for preparation of chiral stationary phases: Progress on coating and immobilization methods, Molecules, 26 (2021).

[131] D.C. Locke, Chemically bonded stationary phases for liquid chromatography, J Chromatogr Sci, 11 (1973) 120-128.

[132] C. Geibel, J. Theiner, M. Wolter, M. Kramer, W. Lindner, M. Lämmerhofer, Controllable organosilane monolayer density of surface bonding using silatranes for thiol functionalization of silica particles for liquid chromatography and validation of microanalytical method for elemental composition determination, J Chromatogr A, 1653 (2021).

[133] T.J. Lee, L.K. Chau, C.J. Huang, Controlled silanization: High molecular regularity of functional thiol groups on siloxane coatings, Langmuir, 36 (2020) 5935-5943.

[134] I.H. Imrich Sebestian, Chemically bonded phases in chromatography, Advances in Chromatography, 14 (1976) 75-83.

[135] A.A. Issa, A.S. Luyt, Kinetics of alkoxysilanes and organoalkoxysilanes polymerization: A review, Polymers-Basel, 11 (2019).

[136] M. Matyska, J. Pesek, The development of silica hydride stationary phases for high-performance liquid chromatography from conception to commercialization, Separations, 6 (2019).

[137] J.E. Sandoval, J.J. Pesek, Synthesis and characterization of a hydride-modified porous silica material as an intermediate in the preparation of chemically bonded chromatographic stationary phases, Anal Chem, 61 (1989) 2067-2075.

[138] M. Wolter, C. Barth, M. Maalouf, M. Kramer, A. Sievers-Engler, M. Lämmerhofer, Wide-pore fully porous mixed-mode octyl/pyridyl-bonded silica material with pH-dependent surface charge reversal for high-performance hydrophobic charge-induction chromatography of proteins, J Chromatogr A, 1737 (2024).

[139] M. Wolter, C. Geibel, M. Olfert, M. Su, W. Bicker, M. Kramer, W. Lindner, M. Lämmerhofer, Development and chromatographic exploration of stable-bonded cross-linked amino silica against classical amino phases, J Sep Sci, 45 (2022) 3286-3300.

[140] M. Wolter, M. Maalouf, M. Janek, C. Knappe, M. Kramer, M. Lämmerhofer, Triphenyl-modified mixed-mode stationary phases with and without embedded ion-exchange sites for high-performance liquid chromatography, J Sep Sci, 47 (2024).

[141] G.P. O'Sullivan, N.M. Scully, J.D. Glennon, Polar-embedded and Polar-endcapped stationary phases for LC, Anal Lett, 43 (2010) 1609-1629.

[142] C. Dewaele, P. Mussche, M. Verzele, Endcapping of high-performance liquid-chromatography packings derived from silica-gel, J High Res Chromatog, 5 (1982) 616-620.

[143] M.R. Euerby, P. Petersson, Chromatographic classification and comparison of commercially available reversed-phase liquid chromatographic columns containing polar embedded groups/amino endcappings using principal component analysis, J Chromatogr A, 1088 (2005) 1-15.

[144] T.H. Walter, Iraneta, P., Capparella, M., Mechanism of retention loss when C8 and C18 HPLC columns are used with highly aqueous mobile phases, J Chromatogr A, 1075 (2005) 177-183.

[145] T. Taylor, Charged stationary phases in reversed phase HPLC, Columns - The LCGC Blog, (2024).

[146] U. Neue, P. Iraneta, F. Gritti, G. Guiochon, Adsorption of cations onto positively charged surface mesopores, J Chromatogr A, 1318 (2013) 72-83.

[147] T.H. Walter, R.W. Andrews, Recent innovations in UHPLC columns and instrumentation, TrAC-Trend Anal Chem, 63 (2014) 14-20.

[148] W.H. Pirkle, R.S. Readnour, The influence of end-capping on the enantioselectivity of a chiral phase, Chromatographia, 31 (1991) 129-132.

[149] K.D. Mcmurtrey, Reaction of silica-gel with trimethylsilyl donors under conditions useful for end-capping HPLC bonded phase packings, J Liq Chromatogr, 11 (1988) 3375-3384.

[150] C. Yang, T. Ikegami, T. Hara, N. Tanaka, Improved endcapping method of monolithic silica columns, J Chromatogr A, 1130 (2006) 175-181.

[151] B. Buszewski, K. Krupczynska, R.M. Gadzala-Kopciuch, G. Rychlicki, R. Kaliszan, Evaluation of HPLC columns: A study on surface homogeneity of chemically bonded stationary phases, J Sep Sci, 26 (2003) 313-321.

[152] R.E. Majors, M. Przybyciel, Columns for reversed-phase LC separations in highly aqueous mobile phases, LCGC North America, 7 (2002).

[153] H.Y. Liu, Z.Y. Li, D. Liu, Y.W. Xue, Z.G. Shi, A simple method for the synthesis of a polar-embedded and polar-endcapped reversed-phase chromatographic packing with low activity of residue silanols, J Chromatogr A, 1443 (2016) 175-180.

[154] J.E. O'Gara, D.P. Walsh, C.H. Phoebe, B.A. Alden, I.S.P. Bouvier, P.C. Iraneta, M. Capparella, T.H. Walter, Embedded-polar-group bonded phases for high performance liquid chromatography, LCGC North America, 19 (2001) 632-642.

[155] B. Buszewski, J. Schmid, K. Albert, E. Bayer, Chemically bonded phases for the reversed-phase high-performance liquid-chromatographic separation of basic substances, J Chromatogr, 552 (1991) 415-427.

[156] T.L. Ascah, B. Feibush, Novel, Highly deactivated reversed-phase for basic compounds, J Chromatogr, 506 (1990) 357-369.

[157] N.S. Wilson, J. Gilroy, J.W. Dolan, L.R. Snyder, Column selectivity in reversed-phase liquid chromatography - VI. Columns with embedded or end-capping polar groups, J Chromatogr A, 1026 (2004) 91-100.

[158] X.D. Liu, A. Bordunov, M. Tracy, R. Slingsby, N. Avdalovic, C. Pohl, Development of a polar-embedded stationary phase with unique properties, J Chromatogr A, 1119 (2006) 120-127.

[159] B. Buszewski, T. Welerowicz, Stationary phases with special structural properties for high-throughput separation techniques: Preparation, characterization and applications, Comb Chem High T Scr, 7 (2004) 291-312.

[160] S. Bocian, A. Nowaczyk, B. Buszewski, Synthesis and characterization of ester-bonded stationary phases for liquid chromatography, Talanta, 131 (2015) 684-692.

[161] C.V. Bui, T. Rosenau, H. Hettegger, Immobilization of a cellulose carbamate-type chiral selector onto silica gel by alkyne-azide click chemistry for the preparation of chiral stationary chromatography phases, Cellulose, 30 (2023) 915-932.

[162] Z.M. Guo, Y.F. Liu, J.Y. Xu, Q. Xu, X.Y. Xue, F.F. Zhang, Y.X. Ke, X.M. Liang, A.W. Lei, Novel reversed-phase high-performance liquid chromatography stationary phase with oligo(ethylene glycol) "click" to silica, J Chromatogr A, 1191 (2008) 78-82.

[163] J. Nakazawa, T.D.P. Stack, Controlled loadings in a mesoporous material: Click-on silica, J Am Chem Soc, 130 (2008) 14360-14361.

[164] Z.M. Guo, A.W. Lei, X.M. Liang, Q. Xu, Click chemistry: a new facile and efficient strategy for preparation of functionalized HPLC packings, Chem Commun, (2006) 4512-4514.

[165] K.M. Kacprzak, N.M. Maier, W. Lindner, Triazolo-linked cinchona alkaloid carbamate anion exchange-type chiral stationary phases: Synthesis by click chemistry and evaluation, J Chromatogr A, 1218 (2011) 1452-1460.

[166] K.M. Kacprzak, W. Lindner, Novel pirkle-type quinine 3,5-dinitrophenylcarbamate chiral stationary phase implementing click chemistry, J Sep Sci, 34 (2011) 2391-2396.

[167] D. Wolrab, P. Frühauf, M. Kohout, W. Lindner, Click chemistry immobilization strategies in the development of strong cation exchanger chiral stationary phases for HPLC, J Sep Sci, 36 (2013) 2826-2837.

[168] A. Marechal, R. El-Debs, V. Dugas, C. Demesmay, Is click chemistry attractive for separation sciences?, J Sep Sci, 36 (2013) 2049-2062.

[169] L.S. Li, Y.L. Gao, J.L. Sun, L. Chen, J. Li, Preparation of thioglycerol-modified silica through thiol-epoxy click reaction and its application in HILIC for detection of oligosaccharide in beverages, Food Chem, 402 (2023).

[170] L. Wang, Z. Li, Y. Wang, N. Li, D. Hu, W. Wu, J.x. Hu, D. Pei, M. Lv, A singular chromatographic column breakthrough: Achieving full polarity range separations with the epoxy propanol molecular cage bonded silica stationary phase, J Chromatogr A, 1730 (2024).

[171] Y.J. Liu, Q. Du, B.C. Yang, F.F. Zhang, C.H. Chu, X.M. Liang, Silica based click amino stationary phase for ion chromatography and hydrophilic interaction liquid chromatography, Analyst, 137 (2012) 1624-1628.

[172] E.P. Shields, S.G. Weber, A pH-stable, crosslinked stationary phase based on the thiol-yne reaction, J Chromatogr A, 1598 (2019) 132-140.

[173] A. Mandl, L. Nicoletti, M. Lämmerhofer, W. Lindner, Quinine versus carbamoylated quinine-based chiral anion exchangers: A comparison regarding enantioselectivity for N-protected amino acids and other chiral acids, J Chromatogr A, 858 (1999) 1-11.

[174] K.M. Kacprzak, N.M. Maier, W. Lindner, Highly efficient immobilization of Cinchona alkaloid derivatives to silica gel via click chemistry, Tetrahedron Lett, 47 (2006) 8721-8726.

[175] G. Schomburg, Polymer coating of surfaces in column liquid-chromatography and capillary electrophoresis, TrAC-Trend Anal Chem, 10 (1991) 163-169.

[176] A.M. Faria, C.R. Silva, C.H. Collins, I.C.S.F. Jardim, Development of a polymer-coated stationary phase with improved chemical stability in alkaline mobile phases, J Sep Sci, 31 (2008) 953-960.

[177] S.L. Ji, F.F. Zhang, S.J. Wu, B.C. Yang, X.M. Liang, Facile preparation of polyvinyl alcohol coated SiO2 stationary phases for high performance liquid chromatography, Analyst, 139 (2014) 5594-5599.

[178] S.L. Ji, Y. Zheng, F.F. Zhang, X.M. Liang, B.C. Yang, A polyvinyl alcohol-coated silica gel stationary phase for hydrophilic interaction chromatography, Analyst, 140 (2015) 6250-6253.

[179] C.B.G. Bottoli, Z.F. Chaudhry, D.A. Fonseca, K.E. Collins, C.H. Collins, Poly(alkylmethylsiloxanes) thermally immobilized on silica as stationary phases for high-performance liquid chromatography, J Chromatogr A, 948 (2002) 121-128.

[180] A.M. Faria, C.H. Collins, I.C.S.F. Jardim, State-of-the-art in immobilized polymer stationary phases for high-performance liquid chromatography, J Brazil Chem Soc, 20 (2009) 1385-1398.

[181] M. Guillaume, B. Sebille, Study of a polymer immobilized on silica gel as stationary phase for chiral liquid chromatography, Eur Polym J, 32 (1996) 19-26.

[182] A. Zimmermann, J. Horak, A. Sievers-Engler, C. Sanwald, W. Lindner, M. Kramer, M. Lämmerhofer, Surface-crosslinked poly(3-mercaptopropyl)- methylsiloxane-coatings on silica as new platform for low-bleed mass spectrometry-compatible functionalized stationary phases synthesized via thiol-ene click reaction, J Chromatogr A, 1436 (2016) 73-83.

[183] M. Wolter, X.Y. Chen, U. Woiwode, C. Geibel, M. Lämmerhofer, Preparation and characterization of poly(3-mercaptopropyl)methylsiloxane functionalized silica particles and their further modification for silver ion chromatography and enantioselective high-performance liquid chromatography, J Chromatogr A, 1643 (2021).

[184] B. Chankvetadze, Recent trends in preparation, investigation and application of polysaccharide-based chiral stationary phases for separation of enantiomers in high-performance liquid chromatography, TrAC-Trend Anal Chem, 122 (2020).

[185] K. Zhang, X.D. Liu, Mixed-mode chromatography in pharmaceutical and biopharmaceutical applications, J Pharmaceut Biomed, 128 (2016) 73-88.

[186] D. Sykora, P. Rezanka, K. Záruba, V. Král, Recent advances in mixed-mode chromatographic stationary phases, J Sep Sci, 42 (2019) 89-129.

[187] L.J. Wang, W.L. Wei, Z.N. Xia, X. Jie, Z.Z.L. Xia, Recent advances in materials for stationary phases of mixed-mode high-performance liquid chromatography, TrAC-Trend Anal Chem, 80 (2016) 495-506.

[188] P. Jandera, Stationary and mobile phases in hydrophilic interaction chromatography: A review, Anal Chim Acta, 692 (2011) 1-25.

[189] P. Zuvela, M. Skoczylas, J.J. Liu, T. Baczek, R. Kaliszan, M.W. Wong, B. Buszewski, K. Héberger, Column characterization and selection systems in reversed-phase high-performance liquid chromatography, Chem Rev, 119 (2019) 4818-4818.

[190] J. Teixeira, M.E. Tiritan, M.M.M. Pinto, C. Fernandes, Chiral stationary phases for liquid chromatography: Recent developments, Molecules, 24 (2019).

[191] S. Fekete, A. Beck, J.L. Veuthey, D. Guillarme, Theory and practice of size exclusion chromatography for the analysis of protein aggregates, J Pharmaceut Biomed, 101 (2014) 161-173.

[192] S.R. Abbott, Practical aspects of normal-phase chromatography, J Chromatogr Sci, 18 (1980) 540-550.

[193] S. Fekete, J.L. Veuthey, D. Guillarme, New trends in reversed-phase liquid chromatographic separations of therapeutic peptides and proteins: Theory and applications, J Pharmaceut Biomed, 69 (2012) 9-27.

[194] T. Fornstedt, M. Enmark, Separation of therapeutic oligonucleotides using ion-pair reversed-phase chromatography based on fundamental separation science, J Chromatogr Open, 3 (2023).

[195] S. Fekete, A. Beck, J.L. Veuthey, D. Guillarme, Ion-exchange chromatography for the characterization of biopharmaceuticals, J Pharmaceut Biomed, 113 (2015) 43-55.

[196] G. Lodi, G. Storti, L.A. Pellegrini, M. Morbidelli, Ion exclusion chromatography: Model development and experimental evaluation, Ind Eng Chem Res, 56 (2017) 1621-1632.

[197] M.T. Li, Q.L. Zhang, D.Q. Lin, S.J. Yao, Development and application of hydrophobic charge-induction chromatography for bioseparation, J Chromatogr B, 1134 (2019).

[198] N. Tryon-Tasson, D. Ryoo, P. Eor, J.L. Anderson, Silver-mediated separations: A comprehensive review on advancements of argentation chromatography, facilitated transport membranes, and solid-phase extraction techniques and their applications, J Chromatogr A, 1705 (2023).

[199] D.S. Hage, J.A. Anguizola, C. Bi, R. Li, R. Matsuda, E. Papastavros, E. Pfaunmiller, J. Vargas, X.W. Zheng, Pharmaceutical and biomedical applications of affinity chromatography: Recent trends and developments, J Pharmaceut Biomed, 69 (2012) 93-105.

[200] E.L. Rodriguez, S. Poddar, S. Iftekhar, K. Suh, A.G. Woolfork, S. Ovbude, A. Pekarek, M. Walters, S. Lott, D.S. Hage, Affinity chromatography: A review of trends and developments over the past 50 years, J Chromatogr B, 1157 (2020).

[201] J.H. Zhang, S.M. Xie, L.M. Yuan, Recent progress in the development of chiral stationary phases for high-performance liquid chromatography, J Sep Sci, 45 (2022) 51-77.

[202] G.K.E. Scriba, Update on chiral recognition mechanisms in separation science, J Sep Sci, 47 (2024).

[203] K. Krupczynska, B. Buszewski, Characterizing HPLC stationary phases, Anal Chem, 76 (2004) 226a-234a.

[204] S. Kowalska, K. Krupczynska, B. Buszewski, Some remarks on characterization and application of stationary phases for RP-HPLC determination of biologically important compounds, Biomed Chromatogr, 20 (2006) 4-22.

[205] E. Lesellier, C. West, Description and comparison of chromatographic tests and chemometric methods for packed column classification, J Chromatogr A, 1158 (2007) 329-360.

[206] C. Galea, D. Mangelings, Y.V. Heyden, Characterization and classification of stationary phases in HPLC and SFC - a review, Anal Chim Acta, 886 (2015) 1-15.

[207] U.D. Neue, Stationary phase characterization and method development, J Sep Sci, 30 (2007) 1611-1627.

[208] S. Bäurer, M. Ferri, A. Carotti, S. Neubauer, R. Sardella, M. Lämmerhofer, Mixed-mode chromatography characteristics of chiralpak ZWIX(+) and ZWIX(-) and elucidation of their chromatographic orthogonality for LC x LC application, Anal Chim Acta, 1093 (2020) 168-179.

[209] K. Albert, NMR investigations of stationary phases, J Sep Sci, 26 (2003) 215-224.

[210] C. Hellriegel, U. Skogsberg, K. Albert, M. Lämmerhofer, N.M. Maier, W. Lindner, Characterization of a chiral stationary phase by HR/MAS NMR spectroscopy and investigation of enantioselective interaction with chiral ligates by transferred NOE, J Am Chem Soc, 126 (2004) 3809-3816.

[211] C.W. Huck, L. Bittner, Infrared spectroscopy: A novel tool for the physicochemical characterization of particulate, monolithic and coated stationary phases, Chromatographia, 73 (2011) 29-34.

[212] L.C. Sander, J.B. Callis, L.R. Field, Fourier-transform infrared spectrometric determination of alkyl chain conformation on chemically bonded reversed-phase liquid-chromatography packings, Anal Chem, 55 (1983) 1068-1075.

[213] M.A. Legg, M.J. Wirth, Probing topography and tailing for commercial stationary phases using AFM, FT-IR, and HPLC, Anal Chem, 78 (2006) 6457-6464.

[214] O.L.S. Muñoz, E.P. Hernández, M. Lämmerhofer, W. Lindner, E. Kenndler, Estimation and comparison of ζ-potentials of silica-based anion-exchange type porous particles for capillary electrochromatography from electrophoretic and electroosmotic mobility, Electrophoresis, 24 (2003) 390-398.

[215] M. Ferri, S. Bäurer, A. Carotti, M. Wolter, B. Alshaar, J. Theiner, T. Ikegami, C. West, M. Lämmerhofer, Fragment-based design of zwitterionic, strong cation- and weak anion-exchange type mixed-mode liquid chromatography ligands and their chromatographic exploration, J Chromatogr A, 1621 (2020).

[216] B. Buszewski, M. Jackowska, S. Bocian, E. Dziubakiewicz, Application of the zeta potential for stationary phase characterization in ion chromatography, J Sep Sci, 36 (2013) 156-163.

[217] J.Y. Yu, J.D. Peng, H.J. Peng, Z.L. Zhang, K. Fan, P. Luo, J.J. Wu, H.Q. Yang, H.L. Zeng, X. Wang, Preparation of three structurally similar stationary phases with different ionizable terminal groups and evaluation of their retention performances under multiple modes in high performance liquid chromatography, J Chromatogr A, 1708 (2023).

[218] C.N. Lunardi, A.J. Gomes, F.S. Rocha, J. De Tommaso, G.S. Patience, Experimental methods in chemical engineering: Zeta potential, The Canadian Journal of Chemical Engineering, 99 (2021) 627-639.

[219] N. Aissaoui, L. Bergaoui, J. Landoulsi, J.F. Lambert, S. Boujday, Silane layers on silicon surfaces: Mechanism of interaction, stability, and influence on protein adsorption, Langmuir, 28 (2012) 656-665.

[220] B.J. Inkson, 2 - Scanning electron microscopy (SEM) and transmission electron microscopy (TEM) for materials characterization, in: G. Hübschen, I. Altpeter, R. Tschuncky, H.-G. Herrmann (Eds.) Materials Characterization Using Nondestructive Evaluation (NDE) Methods, Woodhead Publishing, (2016) 17-43.

[221] R.F. Egerton, R. McLeod, F. Wang, M. Malac, Basic questions related to electron-induced sputtering in the TEM, Ultramicroscopy, 110 (2010) 991-997.

[222] T. Chen, L. Zhu, H. Lu, G. Song, Y. Li, H. Zhou, P. Li, W. Zhu, H. Xu, L. Shao, Preparation and application of covalently bonded polysaccharide-modified stationary phase for per aqueous liquid chromatography, Anal Chim Acta, 964 (2017) 195-202.

[223] K. Kimata, K. Iwaguchi, S. Onishi, K. Jinno, R. Eksteen, K. Hosoya, M. Araki, N. Tanaka, Chromatographic characterization of silica C18 packing materials. Correlation between a preparation method and retention behavior of stationary phase, J Chromatogr Sci, 27 (1989) 721-728.

[224] C. McHale, A. Soliven, S. Schuster, A simple approach for reversed phase column comparisons via the Tanaka test, Microchem J, 162 (2021).

*“In theory, theory and practice are the same. In practice, they are not.”*

*Albert Einstein*

# VI. CHAPTER TWO

## Fragment-based Design of Zwitterionic, Strong Cation- and Weak Anion-Exchange Type Mixed-mode Liquid Chromatography Ligands and their Chromatographic Exploration

## VI.1 Publication I – Main Document

Journal of Chromatography A 1621 (2020) 461075

Contents lists available at ScienceDirect

Journal of Chromatography A

journal homepage: www.elsevier.com/locate/chroma

# Fragment-based Design of Zwitterionic, Strong Cation- and Weak Anion-Exchange Type Mixed-mode Liquid Chromatography Ligands and their Chromatographic Exploration

Martina Ferri[a,b,1], Stefanie Bäurer[a,1], Andrea Carotti[b], Marc Wolter[a], Belal Alshaar[a], Johannes Theiner[c], Tohru Ikegami[a,d], Caroline West[e], Michael Lämmerhofer[a,*]

[a] Institute of Pharmaceutical Sciences, Pharmaceutical (Bio-)Analysis, University of Tübingen, Auf der Morgenstelle 8, 72076 Tübingen, Germany
[b] Department of Pharmaceutical Sciences, University of Perugia, Via del Liceo 1, 06123 Perugia, Italy
[c] "Mikroanalytisches Laboratorium", University of Vienna, Währinger Strasse 42, 1090, Vienna, Austria
[d] Department of Materials Synthesis, Faculty of Molecular Chemistry and Engineering, Kyoto Institute of Technology, Matsugasaki, Sakyo-ku, Kyoto 606-8585, Japan
[e] University of Orléans, Institute of Organic and Analytical Chemistry, CNRS UMR 7311, Rue de Chartres BP 6759, 45067 Orléans, France

ARTICLE INFO

*Article history:*
Received 9 November 2019
Revised 20 March 2020
Accepted 23 March 2020
Available online 20 April 2020

*Keywords:*
Mixed-mode chromatography
molecular dynamics simulation
zwitterionic mixed-mode ion-exchangers
mixed-mode cation-exchangers
mixed-mode anion-exchangers
hydrophilic interaction chromatography (HILIC)

ABSTRACT

The role of individual functional groups has been assessed with regard to surface charge and chromatographic retention. Coatings were prepared from various fragments of the chiral zwitterionic materials Chiralpak ZWIX(+) and ZWIX(-). The different chromatographic ligands allowed fine tuning of the surface charge. Chiralpak ZWIX phases showed strongly negative $\zeta$-potentials over the entire pH-range. Zwitterionic congeners with quinuclidine and sulfonic acid moieties but lacking the quinolone ring in the ligand structure exhibited shifted $\zeta$-potentials of around + 5 to 20 mV depending on the surrounding residues. Capillary electrophoretic mobilitiy measurements with the chromatographic ligands and molecular dynamics simulations were carried out to offer some explanation of these surface charge differences of the distinct zwitterionic stationary phases. The new mixed-mode phases were also chromatographically characterized by simple RP and HILIC tests. The results allowed their positioning within a large variety of different commercially available RP, HILIC and mixed-mode phases, which were evaluated as well, by multivariate data processing using principal component analysis. The new mixed-mode phases overall exhibit reasonable hydrophilicity-lipophilicity balance and enable retention of ionic compounds by additional ionic interactions through weak anion-exchange (WAX-type), strong cation-exchange (SCX-type) or both (RP/ZWIX-type). Hence, the new RP/ZWIX phases can be flexible tools for selectivity tuning in RP and HILIC separations.



## 1. Introduction

Mixed-mode chromatography (MMC) [1–7] has raised interest as an alternative LC separation mode to reversed-phase (RP) LC [8,9] and hydrophilic interaction chromatography (HILIC) [10–12]. It combines distinct retention and separation principles, respectively, in one column. This can be accomplished by i) blending of distinct particles, e.g. RP particles and ion-exchangers (mixed bed), ii) mixing of chromatographic ligands with different retention principles on the same support (mixed-ligand), iii) distinct retention principles on one chromatographic ligand (mixed-mode ligand) [4]. Multimodality (e.g. applicability in RP, HILIC, cation exchange (CX), anion exchange (AX), ion-exclusion (IEC), hydrophobic interaction chromatography (HIC) [13]), orthogonality/complementarity to RP and HILIC, wider scope of application [2], enhanced flexibility in method development and optimization [13], and higher sample loading capacity compared to RP in preparative applications [14] are features of MMC phases. They have found applications for analysis of oligonucleotides [1,15,16], peptides [13,14,17–19], proteins [20], metabolites [2] and simultaneous analysis of pharmaceuticals and their counterions [4,21], as well as for comprehensive analysis of natural products by multidimensional separations [22], and many more.

* Corresponding author: Prof. Dr. Michael Lämmerhofer, Pharmaceutical (Bio-)Analysis, Institute of Pharmaceutical Sciences, University of Tübingen, Auf der Morgenstelle 8, 72076 Tübingen, Germany
*E-mail address:* michael.laemmerhofer@uni-tuebingen.de (M. Lämmerhofer).
[1] Shared first authorship

https://doi.org/10.1016/j.chroma.2020.461075
0021-9673/

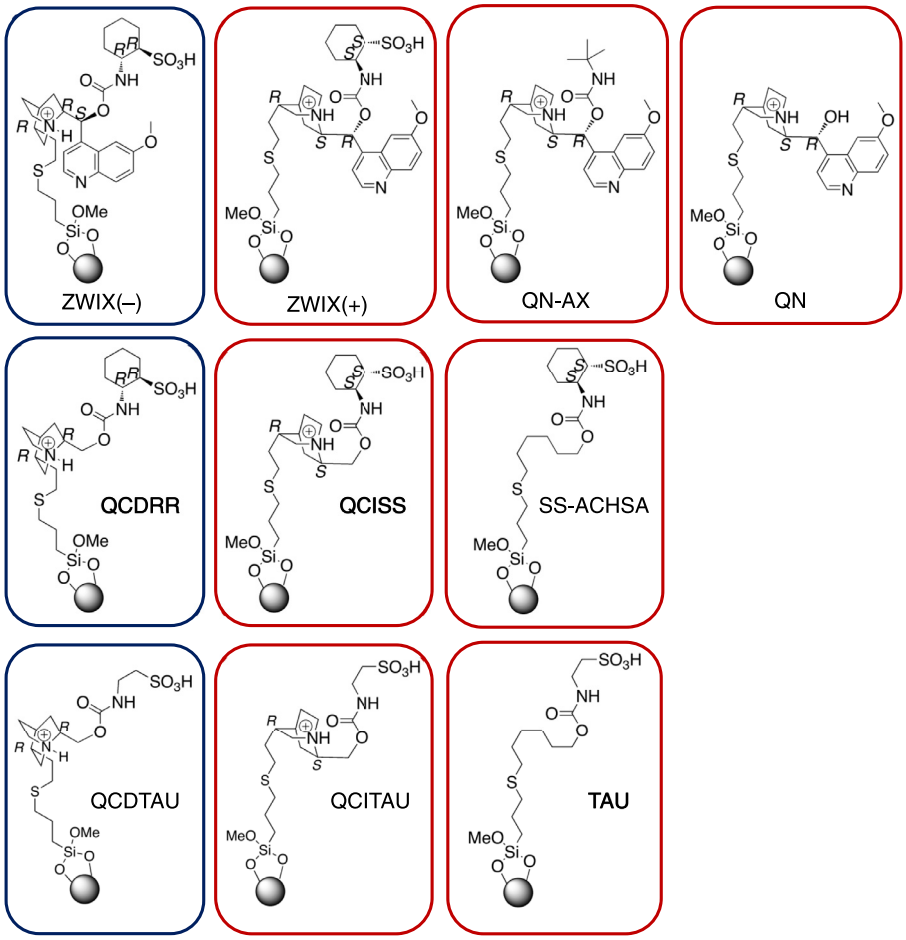


**Fig. 1.** Surface chemistries of the investigated zwitterionic, strong cation- and weak anion-exchange type mixed-mode stationary phases.

A number of distinct chromatographic modalities (i.e. retention principles) have been combined in MMC. For example, combination of size-exclusion with RP has been realized by so-called internal surface RP phases [23], HILIC with RP e.g. [24] or by the commercial column Acclaim Mixed-Mode HILIC-1 (from Thermo Fisher Scientific) [4]. Most commonly, however, ion-exchange is combined with RP or HILIC to yield RP/AX [1,14,16,25–27], RP/CX [28], RP/ZWIX [29], HILIC/AX [30,31], HILIC/CX [32], HILIC/ZWIX [33] phases (all available as either weak or strong ion-exchanger modalities). Trimodal phases combining e.g. cation-exchange, anion-exchange and RP have been proposed as well [4,34,35]. The combination of electrostatic repulsion with HILIC elution was termed ERLIC [36]. Many of the ionic liquid-derived LC phases [37] as well as several zwitterionic stationary phases [38] reported in the literature can also be classified as MMC phases. Further, more advanced mixed-mode phases have been proposed such as those combining chiral stationary phases with size exclusion principles (internal surface chiral stationary phase) [39,40].

In general, chiral stationary phases can act per se as mixed-mode phases owing to their plurality of functional groups. Therefore, it is not surprising that they have been examined for challenging achiral applications [41–43]. In this work we explore the mixed-mode chromatography behavior of Chiralpak ZWIX(+) and ZWIX(-), i.e. cinchonan carbamate based chiral stationary phases decorated with cyclohexylsulfonic acid carbamate residues [44]. This chiral selector contains both anion (WAX) and cation exchanger (SCX) functionalities as well as hydrophobic moieties and can be classified as a RP/SCX/WAX trimodal mixed-mode phase (RP/ZWIX for short). To better understand the incremental contributions of the various interaction sites to the mixed-mode chromatography behavior, a fragment-based design was adopted to devise a series of structural analogs of this ZWIX-type MMC phase (Fig. 1). Thus, new RP/WAX, RP/SCX and RP/ZWIX type MMC phases were obtained which are characterized herein regarding their surface charge (pH-dependent $\zeta$-potentials), multimodal applicability in RPLC and HILIC, hydrophilicity/lipophilicity balance (HLB) and anion- and cation-exchange capability. A benchmarking study was performed which allowed the classification of these phases among groups of commercial RP, HILIC and MMC phases. In addition, a molecular dynamics simulation was carried out to explain surface charge differences of the distinct zwitterionic stationary phases by conformational preferences of the different selectors.

## 2. Experimental

### 2.1. Materials

Chiralpak ZWIX(+) (150 × 3 mm ID, 3 µm) and ZWIX(-) (150 × 4 mm ID, 3 µm) were purchased from Chiral Technologies Europe (Ilkirch, France). The weak anion-exchange stationary phases QN-AX and QN were prepared as described elsewhere [45,46]. Quinine, quincorine ((*2S,4S,5R*)-2-hydroxymethyl-5-vinylquinuclidine, QCI) and quincoridine ((*2R,4S,5R*)-2-hydroxymethyl-5-vinylquinuclidine, QCD) (all as free bases) were from Buchler (Braunschweig, Ger-

many) (note, configurational descriptors are inconsistently used in the literature which may be confusing. The above terminology is identical to the CA index terminology (*1S,2S,4S,5R*)-5-ethenyl-1-azabicyclo[2.2.2]octane-2-methanol for quincorine, CAS registry number (RN) 207129-35-9, and (*1S,2R,4S,5R*)-5-ethenyl-1-azabicyclo[2.2.2]octane-2-methanol for quincoridine, CAS RN 207129-36-0).

The silica used for immobilization of the new chromatographic ligands was Daisogel 3 µm, 120 Å (DAISO Fine Chem GmbH, Düsseldorf, Germany). 3-Mercaptopropyl-modified silica was utilized for the immobilization of the chromatographic ligands and was synthesized as described previously [45]. 4-Nitrophenyl chloroformate, *N,O*-bis(trimethylsilyl)acetamide (BSA), calcium hydride ($CaH_2$), taurine, 5-hexen-1-ol, 4-dimethylaminopyridine, and 3-mercaptopropyltrimethoxysilane were purchased from Sigma Aldrich (Munich, Germany). (*1R,2R*)- and (*1S,2S*)-*trans*-2-aminocyclohexanesulfonic acid (ACHSA) were kindly donated by Chiral Technologies Europe. Methanol (MeOH), hexane, diethyl ether, toluene and dichloromethane (DCM) used for the synthesis were technical grade and purchased from Brenntag (Essen, Germany). Acetonitrile (ACN) and methanol HPLC grade were used for HPLC analysis and ultrapure water was obtained by purification of demineralized water using Elga PureLab Ultra Purification System (Celle, Germany). Mobile-phase additives acetic acid, formic acid (FA), ammonium acetate ($NH_4Ac$) and trifluoroacetic acid (TFA) were of analytical grade (Sigma-Aldrich).

The analytes of the RP test, butylbenzene (BuB), pentylbenzene (PeB), *N-tert*-butoxycarbonyl-prolyl-phenylalanine (BocProPhe) and the reagents *O,O*-diethylthiochlorophosphate (DETCP) and triethylamine for the synthesis of *O,O*-diethylthiophosphate (DETP), and of the HILIC tests (theophylline (Tp), theobromine (Tb), uridine (U) and 2'-deoxyuridine (2dU), adenosine, cytidine, guanosine, thymidine, ascorbic acid, nicotinic acid, pyridoxine, riboflavin, thiamine), as well as the void volume markers 1,3,5-tri-*tert*-butylbenzene (TTBB) and toluene (for HILIC) were purchased from Sigma Aldrich (Munich, Germany).

### 2.2. Instrumentation and software

The chromatographic tests were performed on an 1100 series HPLC instrument from Agilent Technologies (Waldbronn, Germany) equipped with a degasser, binary pump, column compartment with temperature control, a variable wavelength detector (VWD) and a charged aerosol detector (CAD, Thermo Scientific, Munich, Germany) or an Agilent Technologies LC MSD-SL ion-trap mass-spectrometer. Mobile phases for the chromatographic tests and other conditions are specified in respective figure captions.

Nuclear magnetic resonance (NMR) spectroscopy experiments were done on a Bruker Avance 400 MHz with methanol-$d_4$, DMSO-$d_6$, or $CDCl_3$ as solvents. The chemical shifts are described in ppm. The software MestReNova (Mestrelab Research, Santiago de Compostela, Spain) was used for data processing.

For chiroptical analysis, optical rotation (OR) was measured with an instrument from Anton Paar MCP 200 (Graz, Austria) at 589 nm ($Na_{589}$) using a 1 dm quartz cuvette with 1 mL volume.

Electrophoretic light scattering measurements for determination of the $\zeta$-potentials were performed on a Zetasizer NanoZS particle analyzer equipped with a Universal Dip Cell (Malvern Instruments, Herrenberg, Germany). pKa values were calculated with Marvin Sketch (14.12.15.0). The software by SIMCA Multivariate Data Analysis Solution (Version 15.0.2.5959, Sartorius Stedim Data Analytics AB, Umeå, Sweden) was used for the principal component analysis with the following parameters: level of significance: 95 %, normalized in units of standard deviation, no weighting, autoscaled, centered.

### 2.3. Synthesis of the chromatographic ligands

The synthesis of the chromatographic ligands followed procedures as described for the ZWIX phases [44].

*General Procedure (A) for the synthesis of carbonate derivatives **1**, **2** and **3**:*

To a solution of the appropriate alcohol, quincoridine, quincorine or 5-hexen-1-ol, (8.97 mmol) in dry toluene (56 mL) 4-nitrophenyl chloroformate (1.8 g, 9.06 mmol) was added portionwise. A precipitate was quickly formed after addition of the chloroformate. To complete the reaction, it was stirred at room temperature for 16 hours. The precipitate was collected by filtration and washed with *n*-hexane (3 × 20 mL). The solid residue was dried under vacuum at room temperature for 16 hours. The desired product was used directly for the next step without further purification because of limited stability.

*(2R,4S,5R)-2-[(4-Nitrophenyloxycarbonyl)oxy]methyl)-5-vinylquinuclidin-1-ium chloride (**1**)*

Starting from quincoridine (1.5 g, 8.97 mmol) and 4-nitrophenyl chloroformate (1.8 g, 9.06 mmol) following the general procedure **A**, the desired product **1** was obtained as white solid (3.02 g, yield 91 %).

*(2S,4S,5R)-2-([(4-Nitrophenoxycarbonyl)oxy]methyl)-5-vinylquinuclidin-1-ium chloride (**2**)*

Starting from quincorine (1.5 g, 8.97 mmol) and 4-nitrophenyl chloroformate (1.8 g, 9.06 mmol) following the general procedure **A**, the desired product **2** was obtained as white solid (3.74 g, yield 100 %).

*Hex-5-en-1-yl (4-nitrophenyl) carbonate (**3**)*

Triethylamine ($Et_3N$) (5.4 mL, 38.85 mmol) was added to a solution of hex-5-en-1-ol (1.3 g, 12.95 mmol) in dry DCM (45 mL). Afterwards, the mixture was cooled to 0°C and 4-nitrophenyl chloroformate (2.9 g, 14.24 mmol) was added in one portion. The reaction was stirred at room temperature for 16 hours. Then, the reaction mixture was directly used for the next step without any purification step. An aliquot, however, was purified for characterization. For this purpose, the reaction was diluted with DCM and it was washed with aqueous 10% citric acid (3 × 20 mL) and aqueous saturated $NaHCO_3$ (3 × 20 mL). The organic phase was dried over $Na_2SO_4$, filtered and concentrated under reduced pressure. The desired product **3** was obtained as yellowish oil (3.46 g, 40% yield) and it was used directly for the next step. $^1$H-NMR ($CDCl_3$, 400 MHz) $\delta$ 1.46-1.62 (m, 3H), 1.76-1.84 (m, 2H), 2.06-2.17 (m, 2H), 4.32 (t, $J_t$ = 6.8 Hz, 1H), 4.96-5.08 (m, 2H), 5.78-5.88 (m, 1H), 7.40 (d, $J_d$ = 9.2 Hz, 2H), 8.30 (d, $J_d$ = 9.2 Hz, 2H).

*General Procedure (B) for the synthesis of carbamate derivatives **4**-**9** (selectors of QCDRR (**4**), QCISS (**5**), QCDTAU (**6**), QCITAU (**7**), SS-ACHSA (**8**) and TAU (**9**))*:

To a finely ground suspension of the appropriate 2-amino-1-sulfonic acid (5.96 mmol) in dry DCM (100 mL), BSA (4.4 mL, 17.88 mmol) was added dropwise. Then the mixture was stirred and heated to reflux (42°C) for 48 hours. After this time, the reaction was cooled to room temperature and the appropriate carbonate derivative (**1**-**3**) (2.20 g, 5.96 mmol) was added portionwise. Stirring of the reaction was continued for 16 hours at room temperature. Then the mixture was cooled to room temperature, quenched with MeOH (3 mL) and stirred for a few more minutes. The reaction was filtered in order to eliminate unreacted free amino sulfonic acid. The organic phase was concentrated under vacuum and the crude product was purified through further work up.

In detail, for compounds **4**-**7**, the main impurity, 4-nitrophenol, was removed by liquid-liquid extraction with basified water (saturated solution of $NaHCO_3$, pH 8) and ethyl acetate. Then, the aqueous phase, which was produced after extraction with ethyl acetate, was firstly acidified with HCl (3 mol/L) (pH adjusted to approx. 5/6), concentrated under vacuum and co-evaporated several times

**Table 1**
Elemental analysis data and selector coverages of the new mixed-mode stationary phases.

| Chromatographic ligand (selector) | Class | C(%) | H(%) | N(%) | S(%) | Coverage (μmol/g) |
|---|---|---|---|---|---|---|
| QN | WAX | 8.85 | 1.34 | 0.69 | 2.07 | 236 |
| QCITAU | ZWIX | 8.35 | 1.73 | 0.68 | 2.37 | 236 |
| QCDTAU | ZWIX | 8.03 | 1.69 | 0.61 | 2.35 | 211 |
| QCISS | ZWIX | 8.61 | 1.77 | 0.55 | 2.36 | 190 |
| QCDRR | ZWIX | 8.96 | 1.80 | 0.6 | 2.41 | 208 |
| SS-ACHSA | SCX | 5.81 | 1.32 | 0.32 | 2.50 | 199 |
| TAU | SCX | 5.63 | 1.41 | 0.23 | 2.71 | 146 |
| Mean (of all SPs) | | | | | | 204 |
| Standard deviation | | | | | | 31 |

with ethanol (note, the product turned out to be too polar to be extracted from water with organic solvents; possibly salting out with ammonium or sodium sulfate could improve extraction yields but was not tested in this work). The product was then solubilized in DCM/MeOH. After that, it was filtered in order to eliminate inorganic salts and concentrated under vacuum. Finally, the product was dried under vacuum at room temperature over the weekend.

For compounds **8** and **9**, flash chromatography on RP phase (C18-modified silica, mobile phase methanol/water) was employed for further purification and removal of 4-nitrophenol.

### 2.4. Immobilization of the ligands on thiol-modified silica particles

Typically 2.0 g of the thiol-modified silica gel were suspended in MeOH (8 mL), degassed and added to a solution of the chiral selector (0.3 mmol/g of silica, except for WAX-type QN phase 0.25 mmol/g) in MeOH (4 mL) under nitrogen. Then, azobis(isobutyronitrile) (AIBN 4 mM, 8 mg) was added to the mixture and it was heated to reflux (66°C) for 7 hours under nitrogen with mechanical stirring. The modified silica was isolated by filtration (glass filter funnel porosity 4) and washed with hot methanol (4 × 3 mL). It was dried in the vacuum oven at 65°C for 24 hours. The modified silica gels were subjected to elemental analysis and the results are given in Table 1.

The modified silica gels were finally slurry packed into stainless steel columns (150 × 3 mm ID).

### 2.5. ζ-Potentials

pH-Dependent ζ-potential determinations were carried out with a suspension of 0.2 mg/mL particles in 10 mM KCl solutions containing 1 mM of the following buffers: formic acid/sodium formate, acetic acid/sodium acetate, histidine (titrated with HCl to pH), tris/tris-HCl, boric acid/sodium borate. The dip cell was thermostated to 25°C. All measurements were performed in triplicates. The Von Smoluchowski equation (Supplementary, Equ. S1) was used for the calculation of the ζ-potentials.

### 2.6. Determination of effective electrophoretic mobilities by CE

The effective mobility of the analytes was determined by capillary electrophoresis using a Hewlett Packard 3D Capillary Electrophoresis system (Agilent, Waldbronn, Germany) at different pH values. The background electrolytes were the same as described above for the ζ-potential measurements (10 mM KCl in 1 mM buffer solutions). Thiourea was used as EOF marker. Experiments were carried out in positive mode, applying a voltage of 15 kV, or in negative mode, applying a voltage of -10kV, respectively, using a bare fused-silica capillary (ID 50 μm) of 50.5 cm total length and 42.0 effective length. The temperature was adjusted to 20°C and detection was carried out at 210 nm for all analytes except for SS-ACHSA. For experiments with SS-ACHSA 0.5 mM sodium *p*-toluenesulfonate was added to the buffer systems and SS-ACHSA was detected by indirect UV detection at 200 nm (Ref. 235 nm). Hydrodynamic injection was performed by applying 50 mbar for 5 s. Preconditioning was done by flushing the capillary with 0.1 M NaOH for 2 min, followed by MilliQ water for 2 min and finally with the respective buffer for 3 min prior to each run. Postconditioning was done by flushing the capillary for 3 min with MilliQ water at the end of each run.

### 2.7. Molecular modelling methods

The Maestro 12.1 graphical interface of the Schrödinger Suite 2019-3 (Schrödinger, LLC, New York, NY) was used. As reported in the previous work [47] a cubic box was built with a 30 Å side length. For a realistic reproduction of the stationary phase environment, four 3-mercaptopropyl-functionalized silanols (~1.97 mol $m^{-2}$), eight free silanols (~8.0 mol $m^{-2}$) and forty-five silicon atoms were considered for each grafted selector (SO) unit (~0.5 mol $m^{-2}$), at the base of the box. All the silicon atoms and their bonded hydrogen atoms in the base layer were set frozen during the molecular dynamics. The box was solvated with water. The three simulations with the three CSP systems were performed in the canonical ensemble at 298 K. The temperature in the simulation cell was maintained constant through use of a Nosé-Hoover thermostat [48,49]. All the other parameters in the simulation study were left to default values in the Desmond Molecular Dynamics System (version 5.9, Schrödinger, LLC, New York, NY) present in the Schrödinger Suite 2019-3 [50]. A production run produced 3000 frames during the 1 μs dynamics, with an integration time of 2 fs. All the conformations of the three simulated SOs, namely ZWIX(+), QCISS and QCITAU, were extracted by each frame and used to calculate different molecular properties. In particular, intramolecular salt-bridges (SB) and H-bonds (HB) were counted for each conformation analyzed, together with the relative conformational energy of the SO (SELF-SO, obtained subtracting the energy minima recorded along the trajectory by the energy of the frame, in kcal $mol^{-1}$), and the Polar Surface Area (PSA, in $Å^2$). The latter surface descriptor was calculated by the QikProp package (version 6.1, Schrödinger, LLC, New York, NY, 2019). A *k-mean* clustering protocol using KNIME 4.0 software (KNIME, Konstanz, Germany) was used on three numeric matrices containing the frame number, the SELF-SO and the distance measured between the sulfur atom of the sulfonic acid group and the nitrogen of the quinuclidinium moiety of each frame. Five clusters were set and plotted as a bubble graph.

## 3. Results and discussion

### 3.1. Design, synthesis of ligands and immobilization by thiol-ene click reaction

The design of the new WAX-type, SCX-type and ZWIX-type MMC ligands is outlined in Fig. 1. It was based on the fragmentation of the Chiralpak ZWIX(+) (quinine-derived; *1S,3R,4S,8S,9R*) and ZWIX(-) (quinidine-derived; *1S,3R,4S,8R,9S*) selectors [44]. Leaving out the 2-sulfocyclohexyl residue of ZWIX(+) along with

its carbamate moiety yielded a WAX-type ligand and quinine-based stationary phase, respectively. Its chiral separation capability was already described previously [45,46,51]. Replacement of the 2-sulfocyclohexyl moiety of ZWIX(+) by a *tert*-butyl carbamate residue gave the WAX-type ligand which is part of the commercial chiral stationary phase Chiralpak QN-AX and served as reference material in some of the following studies. ZWIX(+) and ZWIX(-) have a bulky, hydrophobic methoxyquinoline ring. Upon its removal, ligands retaining their zwitterionic nature, thus termed RP/ZWIX-type, were obtained. They have been synthesized from either quincorine (QCI) or quincoridine (QCD) (with configurations as in quinine and quinidine, respectively, but one stereogenic center less; see experimental section for specification of absolute configurations). WAX-type quincorine-derived ligands have been proposed as chemoaffinity type stationary phases for plasmid DNA isoform and topoisomer separations [52]. Through this structural change the resultant RP/ZWIX selectors, QCISS and QCDRR, lose their $\pi$-$\pi$-interaction capabilities and further a steric barrier which may significantly influence their conformational flexibility. By replacement of the 2-sulfocyclohexyl residue by a 2-sulfoethyl residue, taurine-derived zwitterionic RP/ZWIX-type MMC materials, termed QCITAU and QCDTAU, were obtained having four carbons less. Taurine-analogs of Chiralpak ZWIX have been reported by Lindner and coworkers as zwitterionic chiral stationary phases [44]. Taurine-derivatized polyaspartamide-modified silica is a commercial SCX-type stationary phase (Polysulfoethyl A) [53] frequently used as first dimension separation material in 2-dimensional peptide separations. In order to further explore the influence of the quinuclidine moiety of the QCI/QCD-derived RP/ZWIX phases on retention profiles and MMC behavior, respectively, it was replaced by 5-hexen-1-ol as *O*-carbamate residue resulting in SCX-type MMC ligands (SS-ACHSA and TAU) (Fig. 1). The synthesis of these RP/ZWIX and RP/SCX MMC ligands followed the procedures reported by Hoffmann et al. for ZWIX(+) and ZWIX(-) [44]. Reaction schemes can be found in the suppl. material and detailed protocols for ligand synthesis in the experimental part.

All new MMC selectors were immobilized on 3-mercaptopropyl-modified silica (Fig. 1) following a well-established procedure which allows adjustment of dedicated selector coverages, whereby herein a ligand coverage of 200 µmol/g was targeted. Thiol-ene click reaction using thermal initiation and azobis(isobutyronitrile) (AIBN) as radical initiator was employed (see Experimental for details). In general, 68±16% of the ligand added to the reaction mixture was bonded to the thiol silica, as confirmed through elemental analysis. The detailed results of the elemental analysis and the calculated selector coverages are given in Table 1. It can be seen that all ligand coverages are in a comparable range (204±31 µmol/g; mean and standard deviation over all distinct phases listed in Table 1).

### 3.2. $\zeta$-Potentials

In mixed-mode chromatography, the surface charge of the chromatographic particles under employed conditions plays a decisive role for the separation of charged compounds. It can be conveniently characterized by pH-dependent $\zeta$-potential determinations using electrophoretic light scattering measurements as recently proposed [16,26,54–57]. Particles with charged surface suspended in electrolyte solutions (e.g. buffered mobile phases) build up an electrical double layer which consists of a uniform layer of counterions (Stern layer) followed by a heterogeneous layer of mixed ionic species at the surface. In this diffusive layer counterions are enriched as compared to the solution surrounding the solvated particle in which the ions are in equilibrium like in the employed background electrolyte solution. If an electric field is applied, the charged particles will start moving in the solution and a shear plane is formed on the solvated particle. The potential at this slipping plane is defined as the $\zeta$-potential [58–60] and can be used to characterize the surface charge of the particles in presence of the given electrolyte solution. The particle radius of the investigated MMC materials is large compared to the thickness of the double layer, which can be characterized by the Debye length ($1/\kappa$), i.e. $\kappa r >> 1$. For such cases, the Smoluchowski model for calculation of the $\zeta$-potentials (see Suppl. Material chapter 2 for more details) is considered valid under the assumption that complications arising from particle porosity, surface conductance and surface roughness are negligible under the employed conditions. Since ionizable groups on the surface can change their dissociation state under different chromatographic conditions, determination of $\zeta$-potentials over a wide pH-range typically employed in LC is most meaningful and was performed between pH 3.5 and 9.5 with 1 mM buffers in 10 mM KCl to keep ionic strength constant during all measurements. The results are depicted in Fig. 2.

The WAX-type QN and QN-AX phases behave quite similarly in terms of their $\zeta$-potentials (Fig. 2a). They showed positive $\zeta$-potentials at low pH values due to the presence of the tertiary amine of the quinuclidine ring ($pK_a$ (QN/QN-AX) = 8.91/8.43, $pK_a$ (QN/QN-AX) of quinoline = 4.06/4.08 as calculated with Marvin Sketch 14.12.15.0). In general, $\zeta$-potentials of these WAX-type materials remained positive up to pH 7.5 and turned negative due to the dominating influence of residual silanols at pH above 8.

The introduction of the sulfonic acid moiety ($pK_a$ = -0.97, calculated with Marvin Sketch) of the 2-sulfocyclohexyl residue in ZWIX(+) and ZWIX(-) resulted in a significant negative offset of the $\zeta$-potentials of around -30 to -50 mV thus adopting negative values over the entire pH range. It indicates a negative surface charge and demonstrates that it is mainly dominated by the fully dissociated sulfonic acid moiety. This is in line with former publications on zwitterionic stationary phases for HILIC, such as ZIC-HILIC [61], which have shown that these materials are cation-exchangers under low ionic strength conditions, i.e. at salt levels below 20 mM [62]. This observation has been often ascribed to the proximity of the anionic group (the sulfonate) of the ligand on the surface while the cationic moiety is shielded in the interior on these stationary phases. However, inversion of the cationic and anionic groups of the ligand, e.g. in ZIC-cHILIC did not lead to surface charge reversal; ZIC-cHILIC still exhibits negative $\zeta$ potential, albeit not as extreme as that of ZIC-HILIC [63,64]. Fragmentation of the ZWIX selector was supposed to give additional insight.

Thus, Fig. 2b compares all the QCI/QCD-derived RP/ZWIX phases with Chiralpak ZWIX(+) and ZWIX(-). By eliminating the quinoline ring of ZWIX(+) and ZWIX(-), respectively, furnishing quincorine- (QCI) and quincoridine-derived (QCD) MMC phases with 2-sulfocyclohexyl residue (QCISS and QCDRR) a significant positive shift in $\zeta$-potentials of around +15 to +20 mM was observed yielding positive values in the pH range < 5. Above pH 5 the surface charge changed its sign and was still negative indicating that there is a pH-dependent charge reversal at mild conditions easily possible in these materials. Upon replacement of the 2-sulfocyclohexyl residue by a 2-sulfoethyl group furnishing QCITAU and QCDTAU a further but smaller positive shift of the $\zeta$-potentials of around 5 to 15 mV was found. For the quincorine-derived taurine-based QCITAU, relatively stable $\zeta$-potentials of around +20 mV were obtained in the pH range between 3.5 and 6.5. The $\zeta$-potential of this material turned negative only above pH 7. Overall, it appears that group contributions are largely additive but there are some interesting delicate group effects which are not simple to explain. For instance, the absence or presence of the quinoline ring does not explain the large shift between ZWIX(+)/ZWIX(-) and QCI/QCD phases. It is hypothesized that due to the quinoline ring conformational freedom of the ZWIX selectors is constrained which presents this selector in an extended open conformation ex-

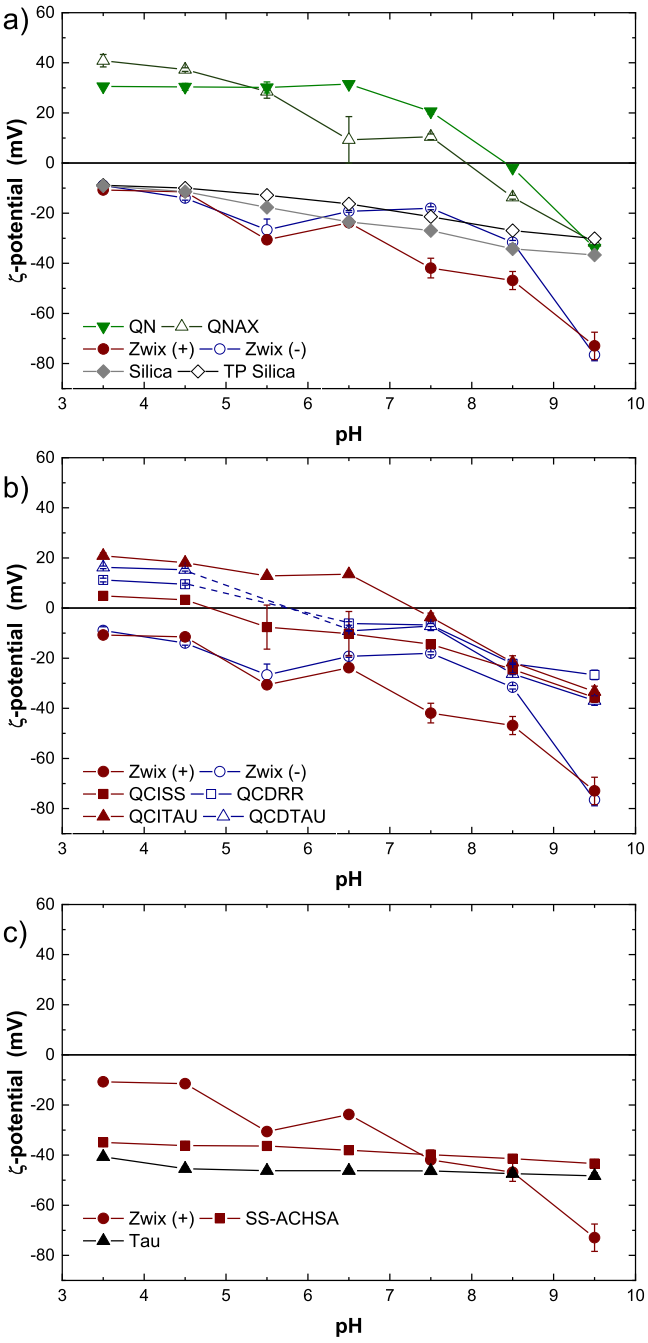


**Fig. 2.** ζ-Potentials determined in dependence of pH. (a) Cationic selectors (QN, QN-AX) in comparison to ZWIX(+), ZWIX (-) and supporting silica as well as thiol-modified silica, (b) all zwitterionic selectors in comparison, (c) anionic ligands in comparison to ZWIX(+).

posing the sulfonate moiety towards the outer surface of the particles and the positively charged quinuclidinium ring closer to the interior i.e. silica surface. Since 1:1 intramolecular ion-pair formation is not easily possible in this ligand due to constrained conformations, the surface is net negatively charged from the dominating effect of the surface sulfonate (SCX). On the other hand, absence of the quinoline ring gives the QCI- and QCD-derivative much larger conformational flexibility. This should enable much better intramolecular charge saturation by intramolecular ion-pair formation. Consequently, the sulfonate moiety gets less exposed to the surface leading to less negative or even positive ζ-potentials. The effect seems to be more pronounced in the corresponding QCI/QCD-TAU ligands in which the sulfonic acid side chain is less constrained compared to the sulfocyclohexyl side chain, thus favorable for intramolecular ion-pair formation and charge compensation.

Fig. 2c depicts the ζ-potentials of SCX-type MMC materials in comparison to ZWIX(+). The SCX-type MMC phases SS-ACHSA and TAU have a stable negative ζ-potential of around -40 mV over the entire pH range. On the contrary, the weak anion exchange moiety of ZWIX(+) has a modulating effect which depends on the pH owing to its weakly basic quinuclidine group that changes its dissociation state over the investigated pH range.

Notably, the ζ-potentials (around pH 5) agree relatively well with the LSER d- terms recently measured by SFC on the same set of columns [65] which validates that the above presented ζ-potential measurements are representative also for the employed chromatographic situations. In general, the currently investigated MMC stationary phases differ not only in surface hydrophilicity/hydrophobicity but also in surface charge. Thus, a set of new mixed-mode ion-exchangers becomes available which will allow a fine tuning of separations due to their slightly distinct surface charge character.

### 3.3. Net charge of zwitterionic selectors as measured by electrophoresis

To deconvolute the contribution of silica and of surface effects (selective ion accumulation effects on the surface) from the net charge of the chromatographic ligands, electrophoretic measurements of the ligands attached to thiol silica were performed in free solution by CE using the same background electrolyte (BGE) as for ζ-potential determinations. Fig. 3a shows the results of the determination of effective electrophoretic mobilities of the ligands in dependence on the pH of the BGE. The cationic ligands QN and QN-AX exhibit positive mobilities over the entire pH range (except for QN-AX at pH 9.5). The lower mobilities of QN-AX (with its *tert*-butylcarbamoyl residue) can be explained by a larger hydrodynamic radius. On the other hand, the anionic ligand *SS*-ACHSA has stable negative mobilities over the entire investigated pH-range, as expected. The ZWIX ligands possess positive mobilities in the pH range 3.5 to 4.5, negative mobilities in the pH range 7.5 to 9.5 and migrate with the electroosmotic flow (EOF) between pH 5.5 and 6.5. QCISS and QCITAU migrate with the EOF over the entire pH-range (Fig. 3a). These results seem to disprove that the excess negative charge of the ZWIX phases revealed by above ζ-potential measurements is due to excess negative charge on the zwitterionic selectors.

The question then arises why differences in the ζ-potentials are observed between ZWIX(+), QCISS and QCITAU in spite of their same number and type of ionizable groups (always quinuclidinium and sulfonate) in the same bonding distance (always same 7 atom spacer between $N^+$ and sulfonate), respectively. A concept worth considering is the chaotropic effect. It is known that the elution order in ion chromatography is from least to most chaotropic, i.e. chaotropes give stronger electrostatic interactions than kosmotropes [30]. Alpert has pointed out [66] that chaotropic ions are less well hydrated than are kosmotropic ions. This correlates with the strength of ionic interactions. This phenomenon also accounts for the worse retention of chaotropes in HILIC [30]. Chaotropic and kosmotropic effects are well described for inorganic ions but unfortunately our understanding of such lyotropic and solvation effects is not very well developed for organic molecules. It is therefore difficult to apply to the current situation but may play a role. Another effect, however, may be invoked as well. Materials with zwitterionic functional groups lose their ion-exchange capacity when the mobile phase contains a sufficiently high concentration of salt. The mechanism is that the concentration of po-

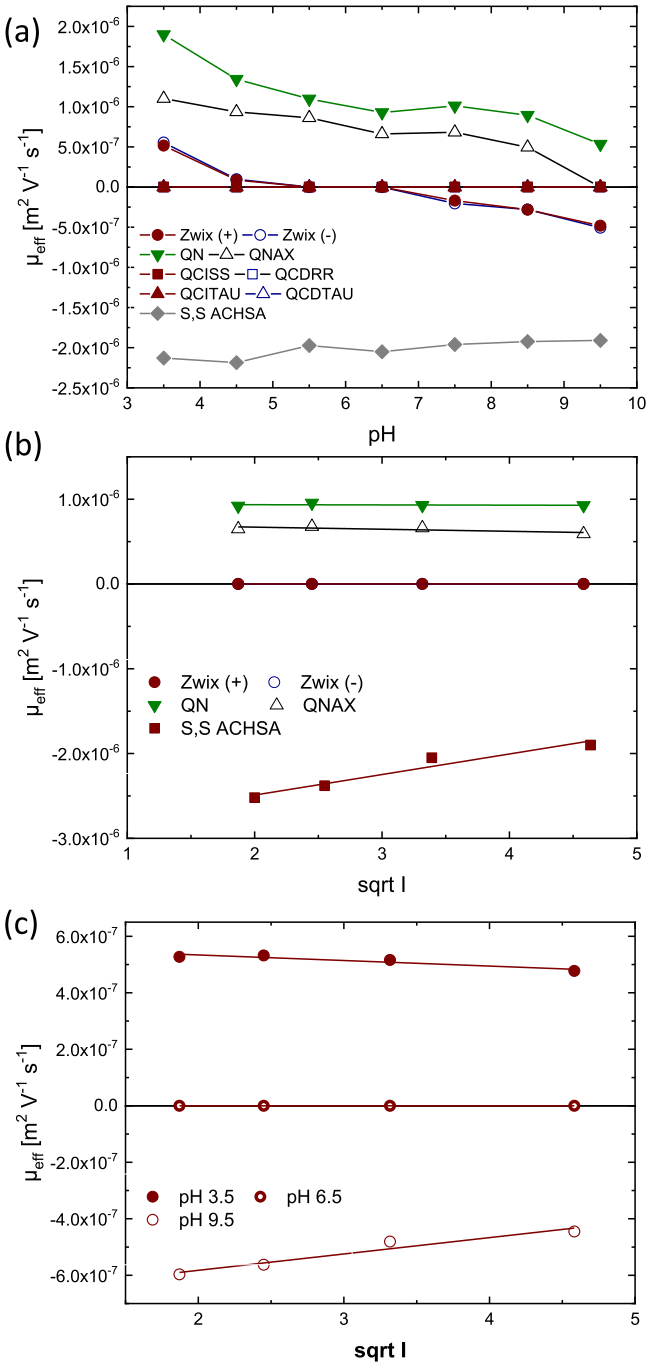


**Fig. 3.** Effective electrophoretic mobilities of ligands in free solution by CE using the same electrolytes as for $\zeta$–potential measurements in Fig. 2. (a) Effective mobilities at 10 mM KCl in 1 mM buffer, (b) selected ligands and their change in effective mobilities with ionic strength at pH 6.5, (c) effect of ionic strength on effective mobilities of ZWIX(+) at three different pH-values (3.5, 6.5 and 9.5).

tential counterions is high enough to titrate the charged groups of the bonding. Distinct ionic functionalities may be differently solvated and may have different affinities for counterions [30]. Pavel Nesterenko claimed in his work on ion chromatography media that cationic groups (amines) are titrated at significantly lower concentrations of salt than are anionic groups [38]. In fact, this would account for the net negative potential exhibited at low salt concentrations by both ZIC-HILIC, ZIC-cHILIC and related media such as current ZWIX materials; the amine groups (here quinuclidinium) are titrated by their counterions at lower salt concentrations than are the acidic groups (here, sulfonates). The low salt concentrations that is used herein for $\zeta$-potential measurements would tend to accentuate this disparity. It is conceivable that the difference between ZWIX, QCISS and QCITAU can be explained in these terms notwithstanding the structural elements (quinuclidinium and sulfonate) being the same, just due to distinct solvation effects originating from different neighbor moieties. A disparity in polarity (and hydration) between the taurine ligand in QCITAU and the cyclohexylsulfonate ligand in QCISS could lead to the effect that they are titrated at different concentrations of counterions. Therefore, their charge potentials would differ at low concentrations of salt. However, it may be argued that if this is the case it should be visible by electrophoretic mobilities as well which were performed under the same conditions. Obviously, this is not the case, as can be seen from Fig 3a, i.e. the curve for ZWIX selectors; unlike $\zeta$-potentials of the modified particles, effective mobilities of the mere ligands do not exhibit a negative sign over the entire pH range.

In order to have a deeper look into the ion titration effect, electrophoretic mobilities were measured at distinct ionic strengths (Fig. 3b and 3c). A convenient way to test for the ion titration effect, i.e. the change in effective charge with ionic strength, is to apply the Debye-Hückel-Onsager (DHO) limiting law of conductance and its transformation into mobilities [67]. In a simplified form it is written as a function of the ionic strength according to (Eq. 1)

$$\mu_{act,i} = \mu_{0,i} - A\sqrt{I} \tag{1}$$

wherein $A$ is the Onsager slope, $I$ the ionic strength, $\mu_{act,i}$ and $\mu_{0,i}$ are the actual and absolute electrophoretic mobilities at actual and zero ionic strength. For sake of simplicity, we report ionic strength effects for effective mobilities $\mu_{eff}$ which are related to $\mu_{act,i}$ by Eq. 2

$$\mu_{eff} = \frac{\sum_{k=1}^{n} c_k \cdot \mu_{act,i} \cdot z_k}{c} \tag{2}$$

Wherein, for a compound with $n$ ionic forms, $c_k$, $z_i$ and $c$ are the concentration and charge number of the kth ionic species and $c$ the total concentration of the compound. Mobilities depend on the ion-solvent interactions which determine the size of the solvated ions and thus the Stokes radii for frictional resistance. They further depend, amongst other things, on ion-ion interactions between analyte ion and ionic species of the BGE which reduce the mobility in solutions with finite ionic strength relative to the limiting case at infinite dilution. These ion–ion interactions were initially described by the theory of Debye, Hückel and Onsager, based on the model of the ion cloud with the introduction of electrophoretic and relaxation effects (see Eq. 1). It was recently reported that the Onsager slope A of mobility vs $\sqrt{I}$ is linearly correlated with the solute charge. Herein, we use this relationship to get an idea whether the cationic site (quinuclidine) and anionic site (sulfonate) are titrated to different extents. The absolute values of effective mobilities at zero ionic strength depend on solvation effects and hydrodynamic radius and are not suitable parameters for such a comparison. However, the slope of the simplified Onsager Eq. 1 at pH 6.5 for individual selector moieties (QN and SS-ACHSA) might give some indication for this effect (note, in the zwitterionic ZWIX(+) selector the two contributions cancel out each other completely, giving 0 effective mobilities). $K^+$ and $Cl^-$ have about the same hydrodynamic radius ($K^+$ 1.25 Å and $Cl^-$ 1.20 Å, [68]) and same charge number; they should therefore be equivalent in strength for titrating respective counterions. The graphical results are given in Fig. 3b for pH 6.5. It can be seen that the ion-ion titration effect as revealed by the Onsager slope is stronger for the sulfonate compound (*SS*-ACHSA) than the quinuclidinium compound (QN), which does not support the idea that ammonium ions are titrated at lower concentrations than anions. The same trend is seen for the ZWIX(+) selector in Fig. 3c for different pH values (pH

3.5 and 9.5) which again shows that the ZWIX selector in its anionic form is stronger affected by titration with counterions than in its cationic form at pH 3.5. Unfortunately, the relevant zwitterionic selectors (ZWIX, QCISS, QCITAU) do not show any mobility at pH 6.5 (i.e. the opposite charges fully compensate each other) and therefore a direct proof of the counterion tirtration effect in zwitterionic selectors is not possible by this method. However, it can be concluded that other factors could play a role as well.

### 3.4. Molecular modeling

The distinct surface charges of the zwitterionic phases under investigation, as measured by $\zeta$-potentials, cannot be sufficiently explained by the immobilized functional groups alone and above considerations. Molecular modeling was therefore selected to support the hypothesis raised above that conformational differences and intramolecular ion-pairing are responsible for distinct surface net charges. In particular, molecular dynamics (MD) calculations were performed for three selectors: ZWIX(+), QCISS, QCITAU.

From the MDs, 3000 frames were extracted for each selector and individually analyzed counting the intramolecular salt-bridges (SB) and H-bonds (HB) present in that specific conformation, together with its PSA (polar surface area). The HB and SB measurement results are reported in a bar graph in Suppl. Material. From Suppl. Fig S19 it is possible to note that the sum of the intramolecular interactions (HB+SB) is larger for QCITAU (793) than ZWIX(+) (733), which in turn is larger than for QCISS (713). Comparing the exposed polar surface area of the selectors may give some idea about the compactness of the chromatographic ligand. Indeed, the mean polar surface area (PSA) is 142 (±2.9) Å$^2$ for ZWIX(+), 125.3 (±3.7) Å$^2$ for QCISS and 130.4 (±3.4) Å$^2$ for QCITAU. In general, QCITAU displays a high number of intramolecular interactions (HB+SB) and a quite low PSA exposed. On the other hand, QCISS has similar HB+SB value compared to ZWIX(+), but a lower PSA exposed. However, these data do not fully explain the trends in surface charge shown in Fig. 2.

For this reason, a different analysis was performed. Each of the three series of 3000 molecules, one for each SO trajectory, were clustered (k-mean) into 5 groups according to the frame relative conformational energies (SELF-SO) and the distance measured between the sulfur atom of the sulfonic acid group and the nitrogen of the quinuclidinium moiety. The results are shown in Fig. 4.

Fig. 4a shows a scatter plot of the measured distance versus the relative conformational energies (calculated with Schrödinger Suite) in the form of a bubble graph (note, in particular, we used a utility aiming at the analysis of MD trajectories called Simulation Event Analysis that can monitor energies and interactions along time. Relative values were created by subtracting the minimum energy recorded for the examined selector from the values of all the frames). The size of the bubbles represents the cluster population. It can be seen that QCITAU and QCISS behave similarly, while ZWIX(+) shows significantly different profile. ZWIX(+) reveals exclusively conformers embedded by a long sulphur-nitrogen distance (>6.0 Å), indicating the presence of a

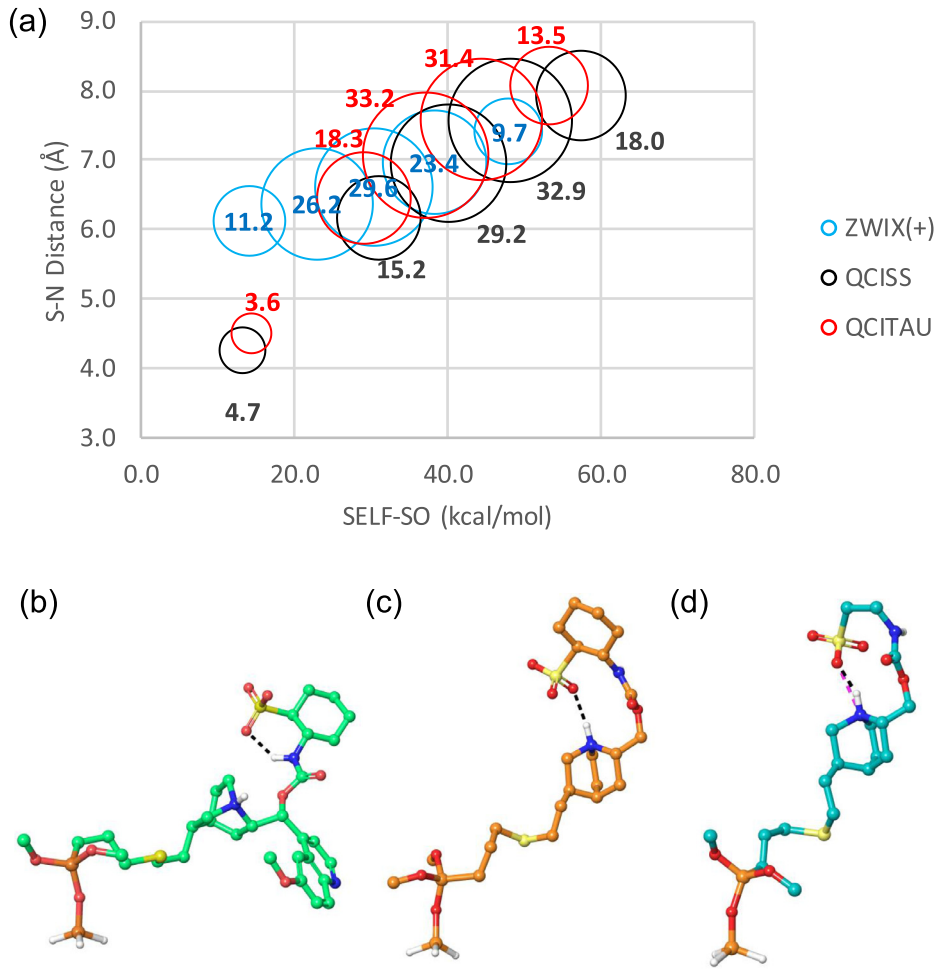


**Fig. 4.** Results of MD calculations of ZWIX(+), QCISS and QCITAU selectors: (a) Intramolecular distances between S of sulfonic acid and N of quinuclidinium moiety measured for the 3000 frames and grouped into 5 clusters, (b) exemplary conformer of the lowest energy cluster of ZWIX(+), (c) of QCISS and (d) of QCITAU.

very weak intramolecular electrostatic interaction. On the other hand, both QCITAU and QCISS exhibit favorable low energy clusters with short distance conformers (~4 Å between S and N) which is indicative for a strong intramolecular ion-pairing. The main difference that can be seen between QCITAU and QCISS clusters is that QCITAU displays barycenters characterized by 3-4 kcal/mol lower conformational energy distribution compared to that of QCISS. This outcome could indicate that, on average, conformers displaying short sulphur-nitrogen distances are energetically more stable (see Fig. 4a). Figures 4b-d illustrate the energy minima conformer for each selector, ZWIX(+) (Fig. 4b), QCISS (Fig. 4c) and QCITAU (Fig. 4d). Overall, these results support to some extent the above raised hypothesis that more favorable intramolecular ion-pairing may lead to less negative surface charge of the zwitterionic selectors by shielding the sulfonic acid group intramolecularly.

While this remains an unproven hypothesis, it may be worth to be considered as hypothesis for explanation of the $\zeta$–potential differences of the distinct zwitterionic phases. In general, the set of data presented herein always explains some but not all effects observed.

Overall, three possible explanations have been presented: i) differential solvation and titration of cations and anions by respective counterions, ii) surface effects such as specific ion gradients due to more complex double layers, and iii) intramolecular charge neutralization by intramolecular ion-pairing to a characteristic extent when the conformational flexibility and solvation is altered by different structural elements due to other neighboring effects. Yet, finally it remains open which one is responsible for the observed $\zeta$-potential shifts within the series of congeneric zwitterionic materials or whether all partially contribute to it.

### 3.5. Chromatographic characterization

Simple test mixtures were injected in RP and HILIC elution mode to examine the multimodal applicability of the new MMC phases for i) RP-type separations, ii) HILIC utility, and iii) ion-exchange properties. The results will be mainly discussed in the form of chromatographic parameters of binary analyte combinations.

The surface lipophilicity and capability of the MMC phases to serve for LC separations based on lipophilicity differences of analytes in RP elution mode can be well expressed by the separation factors of an analyte pair differing by a methylene increment. Thus, butylbenzene (BuB) and pentylbenzene (PeB) were part of an RP test mixture along with two acids with different lipophilicity (DETP and BocProPhe). In general, $\alpha(CH_2)$ values of the new MMC phases ranged between 1.33 for the TAU RP/SCX phase and 1.47 for the QN RP/WAX phase. Thus, it can be concluded that the current MMC phases have moderate hydrophobicities and methylene selectivities as compared to RP phases (e.g. $\alpha(CH_2)$ of the polar RP phase Synergi Fusion RP is 1.79 [25]). On the other hand, this is characteristic for mixed-mode phases, being indicative of their hydrophilicity-lipophilicity balance, which makes them applicable in both RP and HILIC elution modes (*vide infra*). Exemplary chromatograms are given for QCITAU, QCISS and QN in Fig. 5 which documents that separations of analytes that differ just by a methylene increment are still feasible on these MMC phases. Peaks 3 and 4 are butyl- and pentylbenzenes; their retention and methylene selectivities increase in the order QCITAU < QCISS < QN. Also, the two acids elute in the order of their lipophilicity (DETP 1 < BocProPhe 2). However, as far as the anion-exchange capacity of the distinct MMC phases is concerned, there are significant differences. The general retentivity of the acids and anion-exchange capacity follows the same order as described for the $\zeta$-potentials (*vide supra*): QN > QCITAU > QCISS (Fig. 5). The significantly higher anion-exchange retention increment of the QCITAU vs QCISS is remarkable as these two MMC phases differ just in a tetramethylene bridge which gives the former more conformational flexibility, obviously with some significant effect on net surface charge.

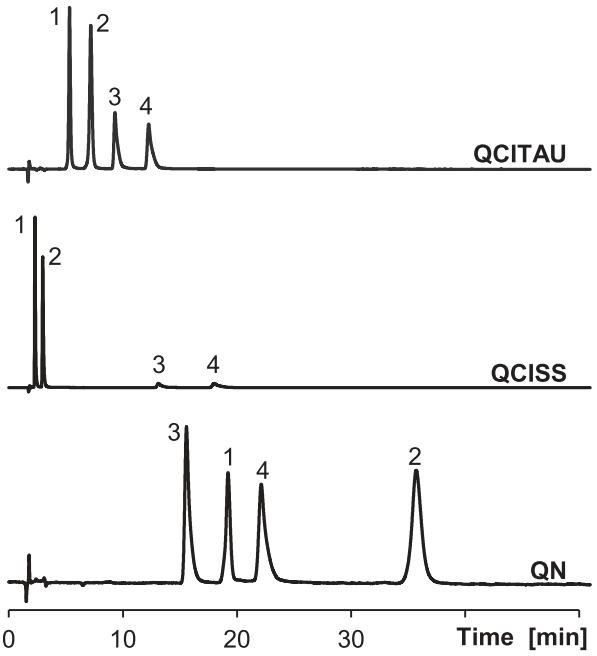


**Fig. 5.** Chromatographic characterization: Reversed-phase elution mode. Mobile Phase: a mixture of ACN and $H_2O$ (40:60, v/v), containing 50 mmol acetic acid in 1 L mobile phase, apparent pH 6, adjusted with ammonia in the polar organic mixture; Flow rate: 0.5 mL/min, 25°C, 0.8 mg/mL of each analyte (1. DETP, 2. BocProPhe, 3. BuB, 4.PeB), injection volume: 5 µL, 220 nm

The HILIC applicability was characterized by a test mixture consisting of toluene (1), caffeine (2), theobromine (3), theophylline (4), 2-deoxyuridine (5), 5-methyluridine (6) and uridine (7) [69] (Fig. 6). In the chromatograms of Fig. 6 it can be seen that all of the tested new MMC phases can well baseline-resolve the peak pair uridine (7) and 2-deoxyuridine (5) indicating a good hydroxy group selectivity for all of them. The methyl group selectivity in HILIC significantly varied between the distinct phases. It was for instance better on QCDTAU than on QCDRR (both ZWIX-type MMC), TAU (SCX-type) and QN (WAX-type). Overall, QCDTAU showed the best separation in HILIC for this test mixture with a baseline separation of all seven peaks.

These results confirm the multimodal applicability of the current MMC phases in RP and HILIC elution modes. The chromatographic efficiencies of these mixed-mode ion-exchangers are, however, slightly lower than those of corresponding RP particles due to a slow adsorption-desorption kinetics (significant C-term from slow adsorption-desorption rate constants), in particular for ionic analytes. This is in line with the general characteristics in terms of chromatographic efficiencies of ion-exchange processes.

### 3.6. Benchmarking study

The final question that was addressed in our study was related to the relative chromatographic characteristics compared to formerly described commercial and non-commercial mixed-mode phases as well as in comparison to popular HILIC phases.

The results are first discussed based on simple binary plots of chromatographic parameters [70]. Fig. 7 depicts a plot of surface acidity (as probed by the separation factor between theobromine, Tb, and theophylline, Tp) *versus* surface hydrophilicity as measured by the retention factor of uridine (both measured under HILIC conditions). Theophylline is weakly acidic while both

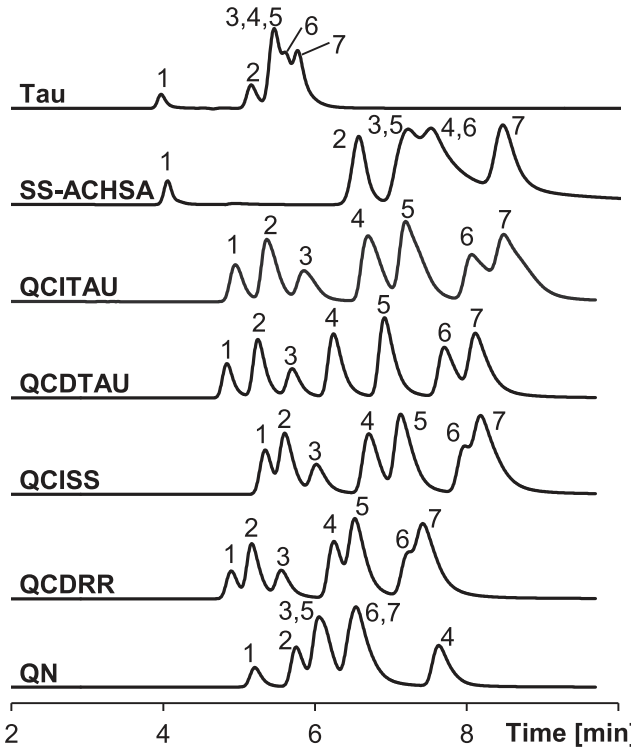


**Fig. 6.** Chromatographic characterization: HILIC elution mode. Mobile Phase: 90 % (v) ACN / 10% (v) aqueous 20 mM $NH_4Ac$ (pH 4.7) solution, flow rate: 0.21 mL/min (linear flow velocity: 0.66 mm/s*), T ==30°C, injection volume: 2 µL, λ = 254 nm, 1. Toluene (1 µL/mL), 2. Caffeine, 3. Theobromine, 4. Theophylline, 5. 2'-Deoxyuridine, 6. 5-Methyluridine, 7. Uridine (0.1 µg/mL), dissolved in ACN:$H_2O$ (90:10; v/v).*[69]

theophylline and theobromine are dimethylxanthines with comparable hydrophilicity. If the surface is acidic, then Tp is less retained due to electrostatic repulsion effects. Again here it becomes evident that the quincorine- and quincoridine-based zwitterionic mixed-mode phases are less acidic than ZWIX(+) and ZWIX(-), as the points for QCITAU (16), QCDRR (17), QCISS (18) and QCDTAU (20) are placed lower on the y-scale of this acidity vs. hydrophilicity plot than ZWIX(-) (33) and ZWIX(+) (34) (see Fig. 7). On the other hand, it is worthwhile mentioning that the latter are still less acidic than the popular zwitterionic sulfobetaine based ZIC-HILIC phase (1 and 2 in Figure 7).

Fig. 8 shows a plot of the methylene selectivity (from RP elution mode) indicating phase hydrophobicity against the retention factor of uridine (from HILIC) denoting the hydrophilicity of the stationary phase surface. Four clusters can be assigned: i) Cluster I: The commercial HILIC phases ZIC-HILIC, TSKgel Amide-80, Polysulfoethyl A and the amino phase Luna $NH_2$ show strong retention of uridine but low methylene selectivity in RP due to their high hydrophilicity. ii) Cluster II: Chromolith Si and Biobasic AX are both hydrophilic as indicated by their low methylene selectivity. However, they show at the same time modest retention for uridine in HILIC mode. iii) Cluster III: A series of WAX-type mixed-mode phases all exhibit relatively high methylene increments (around 1.5 to 1.6) but are widely spread on the *k*(uridine) scale (hydrophilicity scale) in HILIC. The Acclaim Mixed-mode WAX-1 phase and a non-commercial *N*-undecenyl-3-aminoquinuclidine based RP/WAX phase (WAX AQ360) [25] also reveal reasonable retention for uridine and thus good HILIC behavior. They were even outperformed in terms of HILIC behavior by a similar *N*-undecenyl-2-dimethylaminoethylamide-bonded RP/WAX phase (WAX DMAE) [25]. iv) Cluster IV: The current zwitterionic MMC phases cluster together at low *k*(uridine) and intermediate levels of methylene selectivity. It demonstrates that these phases are not the best choice for HILIC separations of neutral compounds

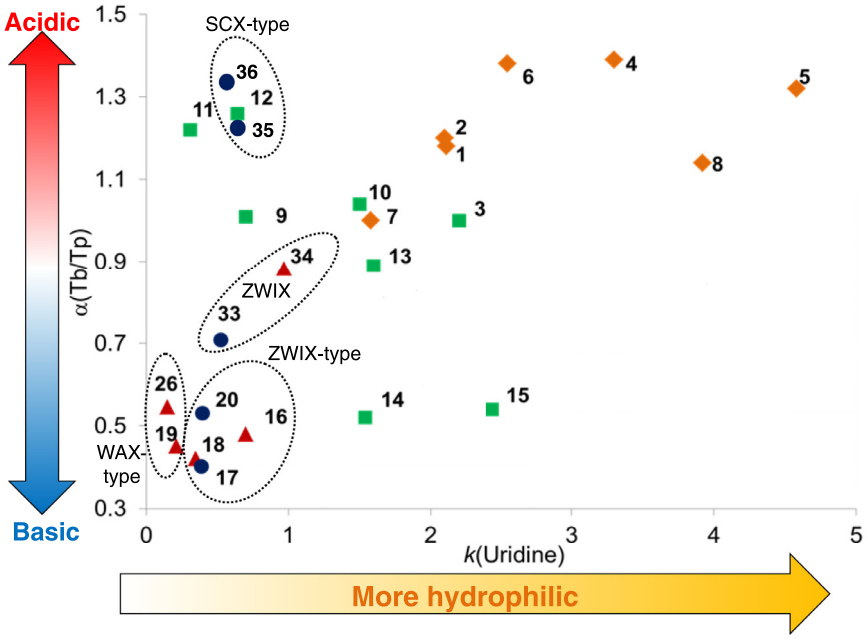


**Fig. 7.** Comparative visualization of acidic and basic surface properties of the tested stationary phases using the example of the selectivity of theobromine and theophylline (α(Tb/Tp) against their surface hydrophilicity measured on the retention of uridine (*k*(uridine). Chromatographic test conditions can be found in Supplemental Material (3.1) in accordance to ref. [25]. 1. ZIC-HILIC (5µm); 2. ZIC-HILIC (3.5 µm); 3. Nucleodur HILIC (3 µm); 4 TSKgel Amide-80 (5 µm); 5. TSKgel Amide-80 (3 µm); 6. XBridge Amide (3.5 µm); 7. PolySULFOETHYL A (3 µm); 8. PolyHYDROXYETHYL A (3 µm); 9. CYCLOBOND I (5 µm); 10. LiChrospher Diol (5 µm); 11. Chromolith Si; 12. HALO HILIC (2.7 µm); 13. COSMOSIL HILIC (5 µm); 14. Sugar-D (5 µm); 15. NH2-MS (5 µm); 16. QCITAU (3 µm), 17. QCDRR (3 µm); 18. QCISS (3 µm), 19. QN (3 µm), 20. QCDTAU (3 µm), 26. Chiralpak QN-AX, 33. ZWIX(-) (3 µm), 34. ZWIX(+) (3 µm); 35. TAU (3 µm); 36. SS-ACHSA (3 µm) Surface chemistries of other stationary phases are depicted in Suppl. Fig. S17 and S18.

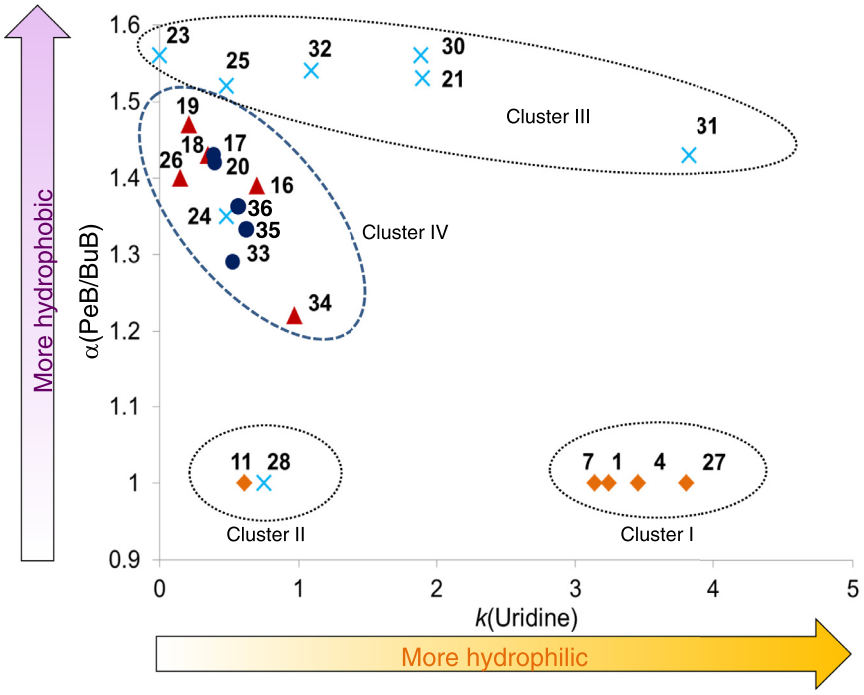


**Fig. 8.** Characterization of hydrophilic and hydrophobic surface properties (hydrophilic-lipophilic balance, HLB) based on the retention factor of uridine (*k*(uridine) and the methylene selectivity (α(PeB/BuB) of selected stationary phases. Chromatographic test conditions were as stated in Figure 5 for methylene selectivity (α(PeB/BuB)) and Figure 6 (*k*(uridine) in accordance to ref. [25] and can be found in the Supplemental Material sub-chapter 3.1. 1. ZIC-HILIC (5µm); 4 TSKgel Amide-80 (5 µm); 7. Poly-SULFOETHYL (3 µm); 11. Chromolith Si; 16. QCITAU (3 µm), 17. QCDRR (3 µm); 18. QCISS (3µm), 19. QN (3µm), 20. QCDTAU (3 µm), 21. Acclaim Mixed Mode WAX-1; 23. Primesep B2; 24. Obelisc R; 25. Obelisc N; 26. Chiralpak QN-AX, 27. Luna NH2; 28. BioBasic AX; 30. WAX AQ360; 31. WAX DMAE; 32. WAX BAMQO 33. ZWIX (-) (3µm), 34. ZWIX (+) (3 µm); 35. TAU (3µm); 36. SS-ACHSA (3 µm). Surface chemistries of stationary phases can be found in the Supplemental Material Suppl. Fig. S17 and S18.

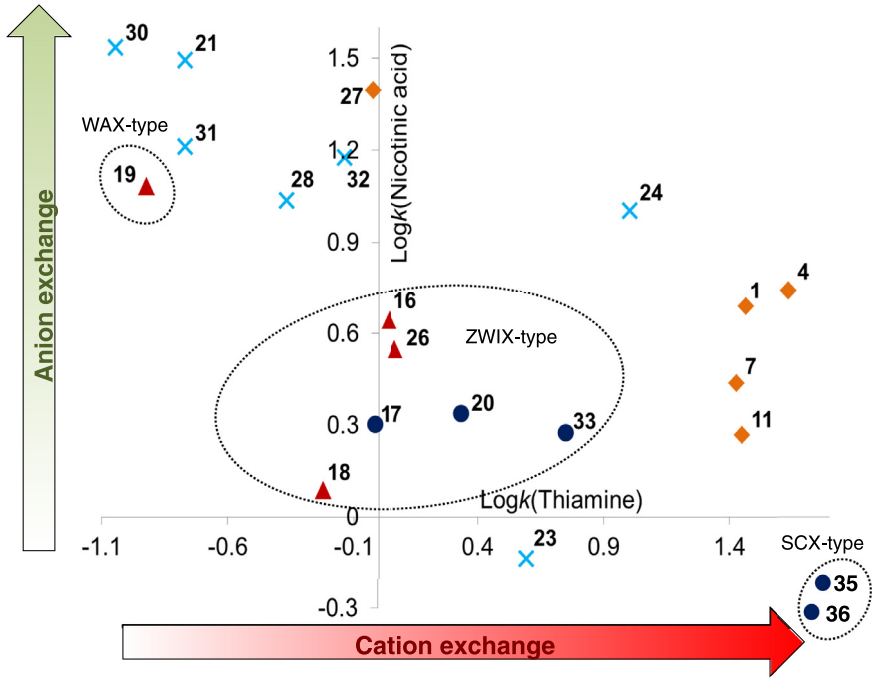


**Fig. 9.** Chromatographic categorization of the surface charge properties of the investigated mixed-mode columns: Anion-exchange as measured by log *k* for nicotinic acid and cation-exchange as determined by log *k* of thiamine. Conditions and stationary phase chemistries can be found in the Supplemental Material Chapter 3.1 (analysis of vitamins). Labels (numbers) as defined in Fig. 6 and 7.

but may be quite useful for HILIC separations of charged (anionic, cationic and zwitterionic) analytes. They still show potential for RP-type separations of both neutral and ionic analytes.

This is underpinned by Fig. 9 which shows a plot of log *k* of nicotinic acid (mostly retained due to anion exchange retention) *vs* log *k* of thiamine (mainly due to cation exchange) under HILIC conditions. WAX-type QN phase has pronounced anion-exchange capacity while SCX-type TAU and ACHSA are classified as cation-exchangers as expected. The zwitterionic mixed-mode phases of this work are in the middle of a diagonal line between the SCX-type and WAX-type phases. They have moderate anion and moderate cation exchange capacity. The ZWIX(-) phase is shifted on the

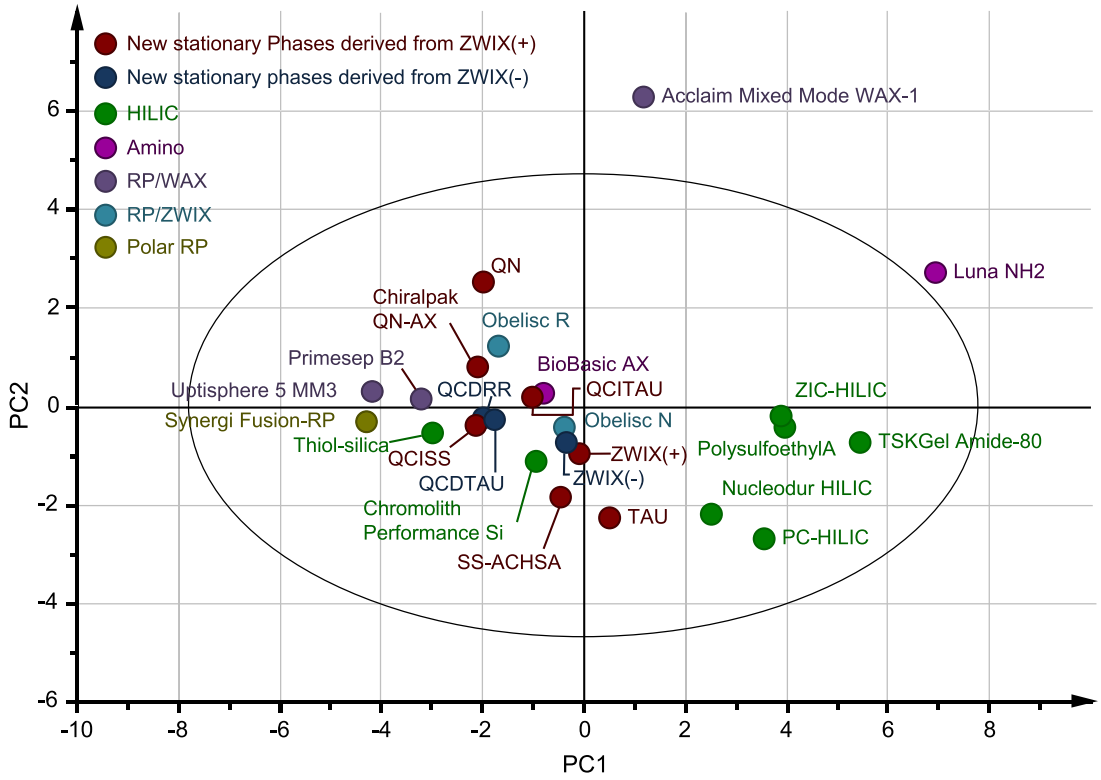


**Fig. 10.** Benchmarking study by principal component analysis (PCA): Score plot of first two principal components. Chromatographic conditions and evaluated stationary phases can be found in the Supplementary Material.

cation exchange scale to larger values, indicating again its stronger acidic character as compared to the quincorine- and quincoridine-derived zwitterionic MMC phases. Furthermore, it is striking that there is a slight shift to higher cation-exchange character when the quincorine (QCI) moiety in the zwitterionic MMC phases is exchanged for the quincoridine moiety (QCD) (Fig 9).

Last but not least, a principal component analysis (PCA) was performed to classify the columns along with commercial RP, HILIC and mixed-mode phases. Retention factors of the chromatographic test mixture of the RP test (Fig 5), of nucleosides from a HILIC test, purines in HILIC mode, and vitamins in HILIC mode as factors (variables) were subjected to PCA. The score plot of the first two principal components PC1 and PC2 is shown in Fig. 10. PC1 and PC2 explain 51.1% and 18.3 % of the variance in the data, both together 69.4%. Columns with similar retention behavior are located on this score plot in close proximity. The more different the retention behavior, the greater is the distance from each other. In this particular case, the PC1 axis is a descriptor of the hydrophilicity, the PC2 axis represents the effective charge of the modified silica particles. Stationary phases with polar surfaces can be found at high PC1 values (e.g. HILIC phases like Luna $NH_2$, ZIC-HILIC, Polysulfoethyl A, PC-HILIC and TSKGel Amide-80). On the opposite end of the PC1 axis, stationary phases with a predominantly apolar surface are found, like the polar RP phase Synergi Fusion-RP or the mixed-mode phase Uptisphere 5 MM3 which is an RP phase with quaternary ammonium endcapping. Mixed-mode phases such as Primesep B2, Obelisc R and N, including the current zwitterionic MMC phases, are located in the middle of the PC1 axis, indicative of their hydrophilicity-lipophilicity balance (see Fig. 10). The PC2 axis, in contrast, primarily quantifies the effective charge state of the surface of the stationary phases. Mixed-mode anion exchange columns like Acclaim Mixed Mode WAX-1 are found at high PC2 values and net negatively charged phases like PC-HILIC at low (i.e. negative) PC2 values. The current mixed-mode phases are aligned on PC2 in accordance to the $\zeta$-potentials measured at around pH 7.5. The WAX-type QN phase has the highest score, then the WAX-type QN-AX, followed by the zwitterionic quincorine and quincoridine MMC phases (QCITAU, QCDTAU, QCDRR, QCISS). ZWIX(+) and ZWIX(-) are already on the negative scale i.e. they have acidic excess on the surface. SCX-type SS-ACHSA and TAU have the lowest score on PC2 and thus the most acidic character, as expected.

It can be concluded that PCA is a useful tool to characterize and classify stationary phases. It confirms what was discussed before by $\zeta$-potentials and binary chromatographic plots. The new set of MMC stationary phases span a reasonably wide surface character and represent a useful supplement to the toolbox of stationary phases. To document their utility in practical applications will be the topic of future works.

## 4. Conclusions

A series of new silica-based stationary phases for mixed mode chromatography have been synthesized in this study. They were obtained by a fragment-based design through incremental fragmentation of the chromatographic ligand of the commercial chiral columns Chiralpak ZWIX(+) and ZWIX(-). These chiral stationary phases consist of a zwitterionic chromatographic ligand and show MMC behaviour. They exhibit utility for achiral separations with selectivity orthogonal to that of RP and HILIC phases. The removal of certain structural elements of these zwitterionic selectors has led to RP/ZWIX, RP/WAX and RP/SCX-type MMC phases with modulated surface charge and hydrophilicity/lipophilicity. They showed sufficient methylene selectivity under RP elution conditions for RP-type separations as well as enough retention for neutral polar compounds under HILIC conditions to allow for multimodal applicability. Besides, the RP/ZWIX phases possess both moderate anion- and cation-exchange capacity with low retentivity which could be advantageous in practical applications especially under mild elu-

tion conditions such as those required for ESI-MS detection. Their practical utility is currently being elucidated and will be reported elsewhere.

## Declaration of Competing Interest

The authors declare that they have no known competing financial interests or personal relationships that could have appeared to influence the work reported in this paper.

## CRediT authorship contribution statement

**Martina Ferri:** Investigation, Formal analysis, Visualization, Writing - original draft, Writing - review & editing. **Stefanie Bäurer:** Data curation, Formal analysis, Investigation, Supervision, Writing - original draft, Writing - review & editing. **Andrea Carotti:** Methodology, Visualization, Writing - review & editing. **Marc Wolter:** Investigation, Writing - original draft. **Belal Alshaar:** Investigation. **Johannes Theiner:** Investigation. **Tohru Ikegami:** Conceptualization, Methodology, Supervision, Writing - review & editing, Funding acquisition. **Caroline West:** Conceptualization, Methodology, Writing - review & editing. **Michael Lämmerhofer:** Conceptualization, Methodology, Supervision, Writing - review & editing, Resources.

## Acknowledgements

We are grateful to Pilar Franco from Chiral Technologies Europe for providing the Chiralpak ZWIX columns and the trans-ACHSA enantiomers. This research was partially supported by the Ministry of Education, Science, Sports and Culture, Grant-in Aid for Scientific Research (C), Japan, 2017-2019 (17K05900, Tohru Ikegami)

## Supplementary materials

Supplementary material associated with this article can be found, in the online version, at doi:10.1016/j.chroma.2020.461075.

## References

[1] L.W. McLaughlin, Mixed-mode chromatography of nucleic acids, Chem. Rev. 89 (1989) 309–319.
[2] W. Bicker, M. Laemmerhofer, W. Lindner, Mixed-mode stationary phases as a complementary selectivity concept in liquid chromatography-tandem mass spectrometry-based bioanalytical assays, Anal. Bioanal. Chem. 390 (2008) 263–266.
[3] L. Zhang, Q. Dai, X. Qiao, C. Yu, X. Qin, H. Yan, Mixed-mode chromatographic stationary phases: Recent advancements and its applications for high-performance liquid chromatography, TrAC Trends in Analytical Chemistry 82 (2016) 143–163.
[4] K. Zhang, X. Liu, Mixed-mode chromatography in pharmaceutical and biopharmaceutical applications, J Pharm Biomed Anal 128 (2016) 73–88.
[5] L. Wang, W. Wei, Z. Xia, X. Jie, Z.Z. Xia, Recent advances in materials for stationary phases of mixed-mode high-performance liquid chromatography, TrAC, Trends Anal. Chem. 80 (2016) 495–506.
[6] E. Lemasson, S. Bertin, P. Henning, E. Lesellier, C. West, Mixed Mode Chromatography - A Review, Supplement to LCGC Europe / LCGC North America 30 (2017) 22–33.
[7] D. Sykora, P. Rezanka, K. Zaruba, V. Kral, Recent advances in mixed-mode chromatographic stationary phases, J Sep Sci 42 (2019) 89–129.
[8] L.R. Snyder, J.W. Dolan, D.H. Marchand, P.W. Carr, The hydrophobic-subtraction model of reversed-phase column selectivity, Adv. Chromatogr. (Boca Raton, FL, U. S.) 50 (2012) 297–376.
[9] B. Bidlingmeyer, C.C. Chan, P. Fastino, R. Henry, P. Koerner, A.T. Maule, M.R.C. Marques, U. Neue, L. Ng, H. Pappa, L. Sander, C. Santasania, L. Snyder, T. Wozniak, HPLC Column Classification, Pharmacopeial Forum 31 (2005) 637–645.
[10] A.J. Alpert, Hydrophilic-interaction chromatography for the separation of peptides, nucleic acids and other polar compounds, J Chromatogr 499 (1990) 177–196.
[11] P. Hemstroem, K. Irgum, Hydrophilic interaction chromatography, J. Sep. Sci. 29 (2006) 1784–1821.
[12] P. Jandera, P. Janas, Recent advances in stationary phases and understanding of retention in hydrophilic interaction chromatography, A review, Anal. Chim. Acta 967 (2017) 12–32.
[13] M. Laemmerhofer, R. Nogueira, W. Lindner, Multi-modal applicability of a reversed-phase/weak-anion exchange material in reversed-phase, anion-exchange, ion-exclusion, hydrophilic interaction and hydrophobic interaction chromatography modes, Anal. Bioanal. Chem. 400 (2011) 2517–2530.
[14] R. Nogueira, M. Laemmerhofer, W. Lindner, Alternative high-performance liquid chromatographic peptide separation and purification concept using a new mixed-mode reversed-phase/weak anion-exchange type stationary phase, J. Chromatogr. A 1089 (2005) 158–169.
[15] R. Bischoff, L.W. McLaughlin, Mixed-mode chromatographic matrices for the resolution of transfer ribonucleic acids, J Chromatogr 317 (1984) 251–261.
[16] S. Baeurer, A. Zimmermann, U. Woiwode, O.L. Sanchez Munoz, M. Kramer, J. Horak, W. Lindner, W. Bicker, M. Laemmerhofer, Stable-bond polymeric reversed-phase/weak anion-exchange mixed-mode stationary phases obtained by simultaneous functionalization and crosslinking of a poly(3-mercaptopropyl)methylsiloxane-film on vinyl silica via thiol-ene double click reaction, J Chromatogr A (2019).
[17] B.Y. Zhu, C.T. Mant, R.S. Hodges, Mixed-mode hydrophilic and ionic interaction chromatography rivals reversed-phase liquid chromatography for the separation of peptides, J. Chromatogr. 594 (1992) 75–86.
[18] C.T. Mant, R.S. Hodges, Mixed-mode hydrophilic interaction/cation-exchange chromatography (HILIC/CEX) of peptides and proteins, J. Sep. Sci. 31 (2008) 2754–2773.
[19] C. Liu, P. Bults, R. Bischoff, J. Crommen, Q. Wang, Z. Jiang, Separation of deamidated peptides with mixed-mode chromatography using phospholipid-functionalized monolithic stationary phases, J, Chromatogr. A 1603 (2019) 417–421.
[20] L. Ding, Z. Guo, X. Liang, Z. Hu, Mixed-mode reversed phase/positively charged repulsion chromatography for intact protein separation, J Pharm Biomed Anal 138 (2017) 63–69.
[21] K. Zhang, L. Dai, N.P. Chetwyn, Simultaneous determination of positive and negative pharmaceutical counterions using mixed-mode chromatography coupled with charged aerosol detector, J. Chromatogr. A 1217 (2010) 5776–5784.
[22] J. Xu, X. Zhang, Z. Guo, J. Yan, L. Yu, X. Li, X. Xue, X. Liang, Orthogonal separation and identification of long-chain peptides from scorpion Buthus martensi Karsch venom by using two-dimensional mixed-mode reversed phase-reversed phase chromatography coupled to tandem mass spectrometry, Analyst (Cambridge, U. K.) 138 (2013) 1835–1843.
[23] I.H. Hagestam, T.C. Pinkerton, Internal surface reversed-phase silica supports for liquid chromatography, Anal. Chem. 57 (1985) 1757–1763.
[24] Z. Guo, Y. Jin, T. Liang, Y. Liu, Q. Xu, X. Liang, A. Lei, Synthesis, chromatographic evaluation and hydrophilic interaction/reversed-phase mixed-mode behavior of a "Click beta-cyclodextrin" stationary phase, J Chromatogr A 1216 (2009) 257–263.
[25] M. Laemmerhofer, M. Richter, J. Wu, R. Nogueira, W. Bicker, W. Lindner, Mixed-mode ion-exchangers and their comparative chromatographic characterization in reversed-phase and hydrophilic interaction chromatography elution modes, J Sep Sci 31 (2008) 2572–2588.
[26] A. Zimmermann, J. Horak, O.L. Sánchez Muñoz, M. Laemmerhofer, Surface charge fine tuning of reversed-phase/weak anion-exchange type mixed-mode stationary phases for milder elution conditions, J Chromatogr A 1409 (2015) 189–200.
[27] J. Wei, Z. Guo, P. Zhang, F. Zhang, B. Yang, X. Liang, A new reversed-phase/strong anion-exchange mixed-mode stationary phase based on polar-copolymerized approach and its application in the enrichment of aristolochic acids, Journal of Chromatography A 1246 (2012) 129–136.
[28] X. Cai, Z. Guo, X. Xue, J. Xu, X. Zhang, X. Liang, Two-dimensional liquid chromatography separation of peptides using reversed-phase/weak cation-exchange mixed-mode column in first dimension, J Chromatogr A 1228 (2012) 242–249.
[29] A.F. Gargano, T. Leek, W. Lindner, M. Laemmerhofer, Mixed-mode chromatography with zwitterionic phosphopeptidomimetic selectors from Ugi multicomponent reaction, J Chromatogr A 1317 (2013) 12–21.
[30] M.E.A. Ibrahim, C.A. Lucy, Mixed mode HILIC/anion exchange separations on latex coated silica monoliths, Talanta 100 (2012) 313–319.
[31] M.-X. Chen, Z.-Y. Cao, Y. Jiang, Z.-W. Zhu, Direct determination of glyphosate and its major metabolite, aminomethylphosphonic acid, in fruits and vegetables by mixed-mode hydrophilic interaction/weak anion-exchange liquid chromatography coupled with electrospray tandem mass spectrometry, J. Chromatogr. A 1272 (2013) 90–99.
[32] X. Dong, A. Shen, Z. Gou, D. Chen, X. Liang, Hydrophilic interaction/weak cation-exchange mixed-mode chromatography for chitooligosaccharides separation, Carbohydr Res 361 (2012) 195–199.
[33] A. Shen, X. Li, X. Dong, J. Wei, Z. Guo, X. Liang, Glutathione-based zwitterionic stationary phase for hydrophilic interaction/cation-exchange mixed-mode chromatography, J Chromatogr A 1314 (2013) 63–69.
[34] X. Liu, C.A. Pohl, HILIC behavior of a reversed-phase/cation-exchange/anion-exchange trimode column, J. Sep. Sci. 33 (2010) 779–786.
[35] A.A. Kazarian, M.R. Taylor, P.R. Haddad, P.N. Nesterenko, B. Paull, Single column comprehensive analysis of pharmaceutical preparations using dual-injection mixed-mode (ion-exchange and reversed-phase) and hydrophilic interaction liquid chromatography, J. Pharm. Biomed. Anal. 86 (2013) 174–181.
[36] A.J. Alpert, Electrostatic repulsion hydrophilic interaction chromatography for isocratic separation of charged solutes and selective isolation of phosphopeptides, Anal Chem 80 (2008) 62–76.
[37] X. Shi, L. Qiao, G. Xu, Recent development of ionic liquid stationary phases for liquid chromatography, J. Chromatogr. A 1420 (2015) 1–15.

[38] E.P. Nesterenko, P.N. Nesterenko, B. Paull, Zwitterionic ion-exchangers in ion chromatography: A review of recent developments, Anal Chim Acta 652 (2009) 3–21.
[39] F. Gasparrini, G. Cancelliere, A. Ciogli, I. D'Acquarica, D. Misiti, C. Villani, New chiral and restricted-access materials containing glycopeptides as selectors for the high-performance liquid chromatographic determination of chiral drugs in biological matrices, J. Chromatogr. A 1191 (2008) 205–213.
[40] H. Wang, D. Xu, P. Jiang, M. Zhang, X. Dong, Novel restricted access chiral stationary phase synthesized via atom transfer radical polymerization for the analysis of chiral drugs in biological matrices, Analyst (Cambridge, U. K.) 135 (2010) 1785–1792.
[41] B. Zhang, R. Soukup, D.W. Armstrong, Selective separations of peptides with sequence deletions, single amino acid polymorphisms, and/or epimeric centers using macrocyclic glycopeptide liquid chromatography stationary phases, Journal of Chromatography A 1053 (2004) 89–99.
[42] E.L. Regalado, C.J. Welch, Separation of achiral analytes using supercritical fluid chromatography with chiral stationary phases, TrAC Trends in Analytical Chemistry 67 (2015) 74–81.
[43] F. Ianni, F. Blasi, D. Giusepponi, A. Coletti, F. Galli, B. Chankvetadze, R. Galarini, R. Sardella, Liquid chromatography separation of $\alpha$- and $\gamma$-linolenic acid positional isomers with a stationary phase based on covalently immobilized cellulose tris(3,5-dichlorophenylcarbamate), Journal of Chromatography A (2019) 460461.
[44] C.V. Hoffmann, R. Pell, M. Laemmerhofer, W. Lindner, Synergistic Effects on Enantioselectivity of Zwitterionic Chiral Stationary Phases for Separations of Chiral Acids, Bases, and Amino Acids by HPLC, Analytical Chemistry 80 (2008) 8780–8789.
[45] A. Mandl, L. Nicoletti, M. Laemmerhofer, W. Lindner, Quinine- versus carbamoylated quinine-based chiral anion exchangers: A comparison regarding enantioselectivity for *N*-protected amino acids and other chiral acids, Journal of Chromatography A 858 (1999) 1–11.
[46] U. Woiwode, M. Ferri, N.M. Maier, W. Lindner, M. Laemmerhofer, Complementary enantioselectivity profiles of chiral cinchonan carbamate selectors with distinct carbamate residues and their implementation in enantioselective two-dimensional high-performance liquid chromatography of amino acids, Journal of Chromatography A 1558 (2018) 29–36.
[47] R. Sardella, A. Macchiarulo, F. Urbinati, F. Ianni, A. Carotti, M. Kohout, W. Lindner, A. Peter, I. Ilisz, Exploring the enantiorecognition mechanism of Cinchona alkaloid-based zwitterionic chiral stationary phases and the basic trans-paroxetine enantiomers, J Sep Sci 41 (2018) 1199–1207.
[48] W.G. Hoover, Canonical dynamics: Equilibrium phase-space distributions, Physical Review A 31 (1985) 1695–1697.
[49] S. Nose, A unified formulation of the constant temperature molecular dynamics methods, The Journal of Chemical Physics 81 (1984) 511–519.
[50] D.E. Shaw, A fast, scalable method for the parallel evaluation of distance-limited pairwise particle interactions, J Comput Chem 26 (2005) 1318–1328.
[51] C. Rosini, C. Bertucci, D. Pini, P. Altemura, P. Salvadori, Cinchona alkaloids for preparing new, easily accessible chiral stationary phases. I. 11-(10,11-Dihydro-6′-methoxycinchonan-9-ol)-thiopropylsilanized silica, Tetrahedron Lett. 26 (1985) 3361–3364.
[52] M. Mahut, W. Lindner, M. Laemmerhofer, Molecular Recognition Principles and Stationary-Phase Characteristics of Topoisomer-Selective Chemoaffinity Materials for Chromatographic Separation of Circular Plasmid DNA Topoisomers, J. Am. Chem. Soc. 134 (2012) 859–862.
[53] A.J. Alpert, P.C. Andrews, Cation-exchange chromatography of peptides on poly(2-sulfoethyl aspartamide)-silica, J. Chromatogr 443 (1988) 85–96.
[54] O.L. Sanchez Munoz, E. Perez Hernandez, M. Laemmerhofer, W. Lindner, E. Kenndler, Estimation and comparison of $\zeta$-potentials of silica-based anion-exchange type porous particles for capillary electrochromatography from electrophoretic and electroosmotic mobility, Electrophoresis 24 (2003) 390–398.
[55] B. Buszewski, S. Bocian, E. Dziubakiewicz, Zeta potential determination as a new way of stationary phases characterization for liquid chromatography, J. Sep. Sci. 33 (2010) 1529–1537.
[56] U. Woiwode, A. Sievers-Engler, A. Zimmermann, W. Lindner, O.L. Sanchez Munoz, M. Laemmerhofer, Surface-anchored counterions on weak chiral anion-exchangers accelerate separations and improve their compatibility for mass-spectrometry-hyphenation, J Chromatogr A 1503 (2017) 21–31.
[57] S. Baeurer, S. Polnick, O.L. Sanchez Munoz, M. Kramer, M. Laemmerhofer, *N*-Propyl-*N*'-2-pyridylurea-modified silica as mixed-mode stationary phase with moderate weak anion exchange capacity and pH-dependent surface charge reversal, J Chromatogr A 1560 (2018) 45–54.
[58] J. Stahlberg, Retention models for ions in chromatography, J. Chromatogr. A 855 (1999) 3–55.
[59] A.V. Delgado, F. Gonzalez-Caballero, R.J. Hunter, L.K. Koopal, J. Lyklema, Measurement and interpretation of electrokinetic phenomena, J. Colloid Interface Sci. 309 (2007) 194–224.
[60] A.V. Delgado, F. Gonzalez-Caballero, R.J. Hunter, L.K. Koopal, J. Lyklema, S. Alkafeef, E. Chibowski, C. Grosse, A.S. Dukhin, S.S. Dukhin, K. Furusawa, R. Jack, N. Kallay, M. Kaszuba, M. Kosmulski, R. Noremberg, R.W. O'Brien, V. Ribitsch, V.N. Shilov, F. Simon, C. Werner, A. Zhukov, R. Zimmermann, Measurement and interpretation of electrokinetic phenomena: (IUPAC technical report), Pure Appl. Chem. 77 (2005) 1753–1805.
[61] W. Jiang, K. Irgum, Covalently Bonded Polymeric Zwitterionic Stationary Phase for Simultaneous Separation of Inorganic Cations and Anions, Analytical Chemistry 71 (1999) 333–344.
[62] C. West, E. Auroux, Deconvoluting the effects of buffer salt concentration in hydrophilic interaction chromatography on a zwitterionic stationary phase, Journal of Chromatography A 1461 (2016) 92–97.
[63] W. Jiang, G. Fischer, Y. Girmay, K. Irgum, Zwitterionic stationary phase with covalently bonded phosphorylcholine type polymer grafts and its applicability to separation of peptides in the hydrophilic interaction liquid chromatography mode, Journal of Chromatography A 1127 (2006) 82–91.
[64] Z.-Y. Wu, J. Liu, H. Shi, P.J. Marriott, The retention behaviour of amino acids in hydrophilic interaction liquid chromatography on zwitterionic stationary phases, Journal of Separation Science 36 (2013) 2217–2222.
[65] A. Raimbault, C.M.A. Ma, M. Ferri, S. Bäurer, P. Bonnet, S. Bourg, M. Laemmerhofer, C. West, Cinchona-based zwitterionic stationary phases: Exploring retention and enantioseparation mechanisms in supercritical fluid chromatography with a fragmentation approach, J Chromatogr A, accepted (2019).
[66] A.J. Alpert, Effect of salts on retention in hydrophilic interaction chromatography, Journal of Chromatography A 1538 (2018) 45–53.
[67] A. Jouyban, E. Kenndler, Theoretical and empirical approaches to express the mobility of small ions in capillary electrophoresis, ELECTROPHORESIS 27 (2006) 992–1005.
[68] F. Foret, L. Krivankova, P. Bocek, Capillary Zone Electrophoresis (Electrophoresis Library) Hardcover, Second Edition ed., VCH Publishing, 1993 October.
[69] Y. Kawachi, T. Ikegami, H. Takubo, Y. Ikegami, M. Miyamoto, N. Tanaka, Chromatographic characterization of hydrophilic interaction liquid chromatography stationary phases: Hydrophilicity, charge effects, structural selectivity, and separation efficiency, J. Chromatogr. A 1218 (2011) 5903–5919.
[70] T. Ikegami, Manuscript will be submitted soon.

## VI.2 Publication I – Supplementary Material

# Fragment-based design of zwitterionic, strong cation- and weak anion-exchange type mixed-mode liquid chromatography ligands and their chromatographic exploration

Martina Ferri [a,b #], Stefanie Bäurer [a #], Andrea Carotti [b], **Marc Wolter** [a], Belal Alshaar [a], Johannes Theiner [c], Tohru Ikegami [a,d], Caroline West [e], Michael Lämmerhofer [a,*]

[a] Institute of Pharmaceutical Sciences, Pharmaceutical (Bio-)Analysis, University of Tübingen, Auf der Morgenstelle 8, 72076 Tübingen, Germany
[b] Department of Pharmaceutical Sciences, University of Perugia, Via del Liceo 1, 06123 Perugia, Italy
[c] Institute of Physical Chemistry, University of Vienna, Währinger Strasse 42, 1090, Vienna, Austria
[d] Department of Materials Synthesis, Faculty of Molecular Chemistry and Engineering, Kyoto Institute of Technology, Matsugasaki, Sakyo-ku, Kyoto 606-8585, Japan
[e] University of Orleans, Institute of Organic and Analytical Chemistry, CNRS UMR 7311, Rue de Chartres BP 6759, 45067 Orleans, France

[#] shared first authorship  * corresponding author

# Table of contents

**PART V: Characterization of modified silica gels by FTIR-spectroscopy**

- Figure S15 FTIR spectra of the two RP/ZWIX MMC phases QCISS and QCDRR.
- Figure S16 FTIR spectra of the two RP/ZWIX MMC phases QCITAU and QCDTAU as well as of the WAX-type QN phase.

**PART VI: ζ-Potential determination**

- Equation S1 Helmholtz-Smoluchowski equation.

**PART VII: Chromatographic characterization under HILIC and RP conditions for column classification**

- Figure S17 Surface structure of commercial columns.
- Figure S18 Surface structures of investigated non-commercial RP/WAX mixed mode phases.

## PART I: Overview of prepared stationary phases

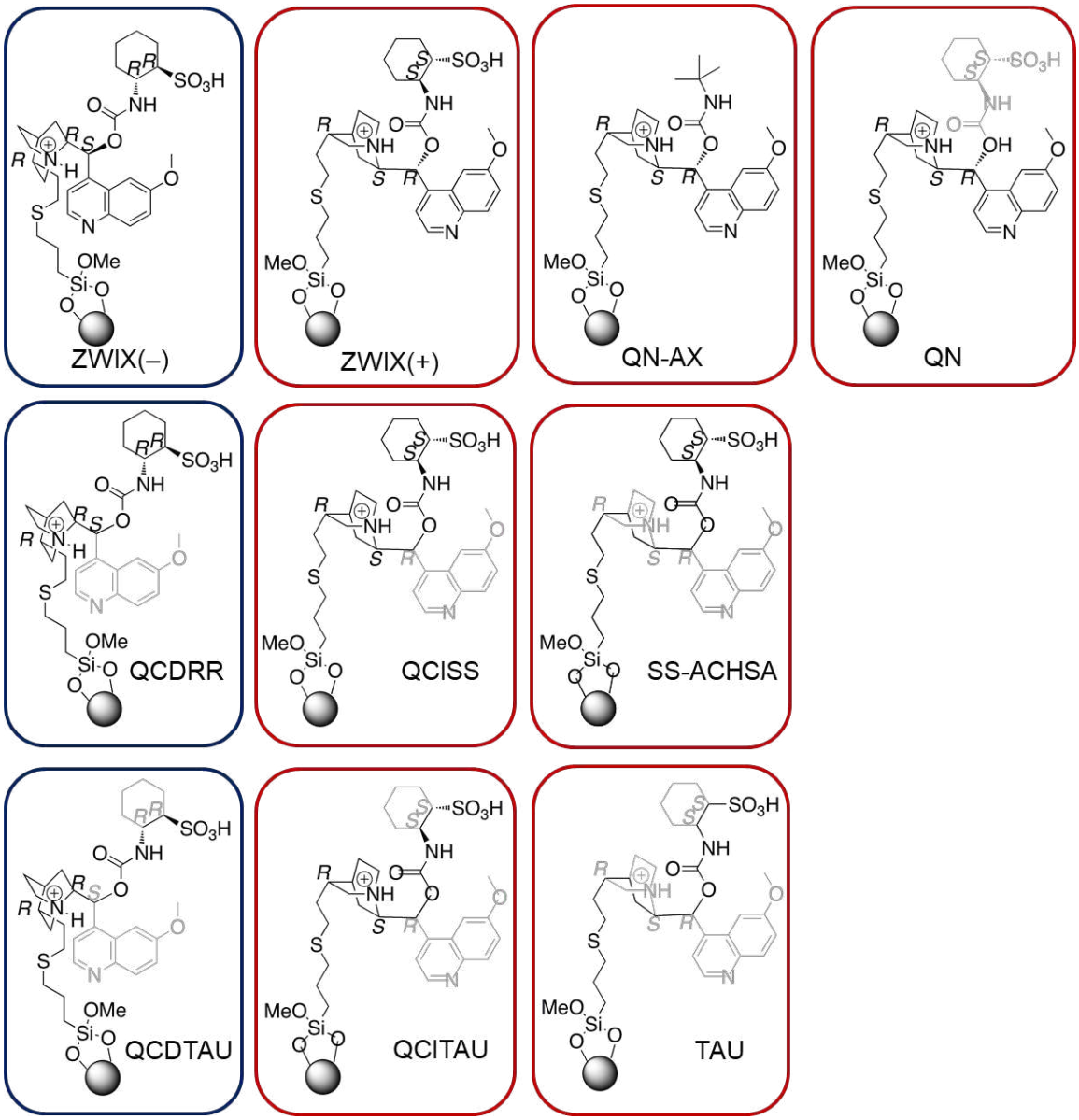


**Scheme S1.** Selector structures of this work with removed parts indicated in light grey. Blue frame means configurations derived from quinidine and red frame configurations derived from quinine.

## PART II: Synthesis of mixed-mode stationary phases and their characterization

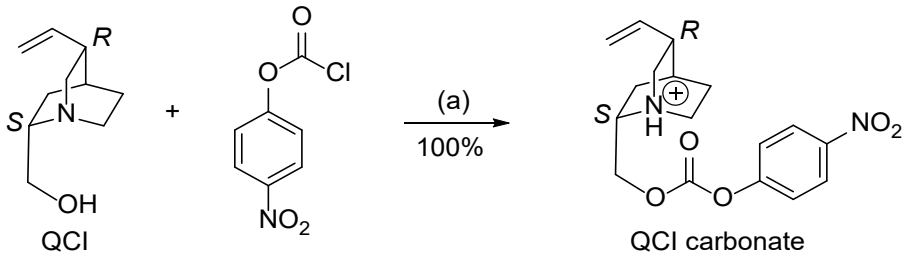


**Fig. S1.** Synthesis of (*2S,4S,5R*)-2-((((4-nitrophenoxy)carbonyl)oxy)methyl)-5-vinylquinuclidin-1-ium chloride QCI carbonate. Reagents and conditions: (a) Toluene, r.t., 16h.

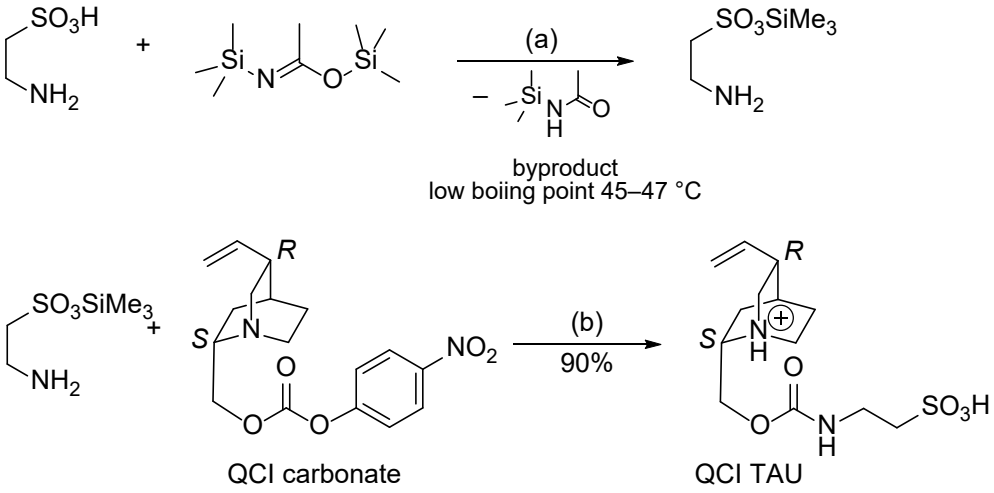


**Fig. S2.** Synthesis of (*2S,4S,5R*)-2-((((2-sulfoethyl)carbamoyl)oxy)methyl)-5-vinylquinuclidin-1-ium (QCITAU). Reagents and conditions: (a) $CH_2Cl_2$, BSA, reflux 48h. then (b) $CH_2Cl_2$, r.t., 16h.

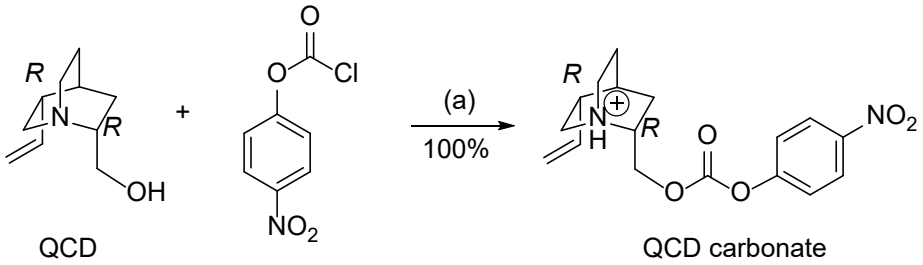


**Fig. S3.** Synthesis of (*2R,4S,5R*)-2-((((4-nitrophenyl)carbamoyl)oxy)methyl)-5-vinylquinuclidin-1-ium chloride QCD carbonate. Reagents and conditions: (a) Toluene, r.t., 16h.

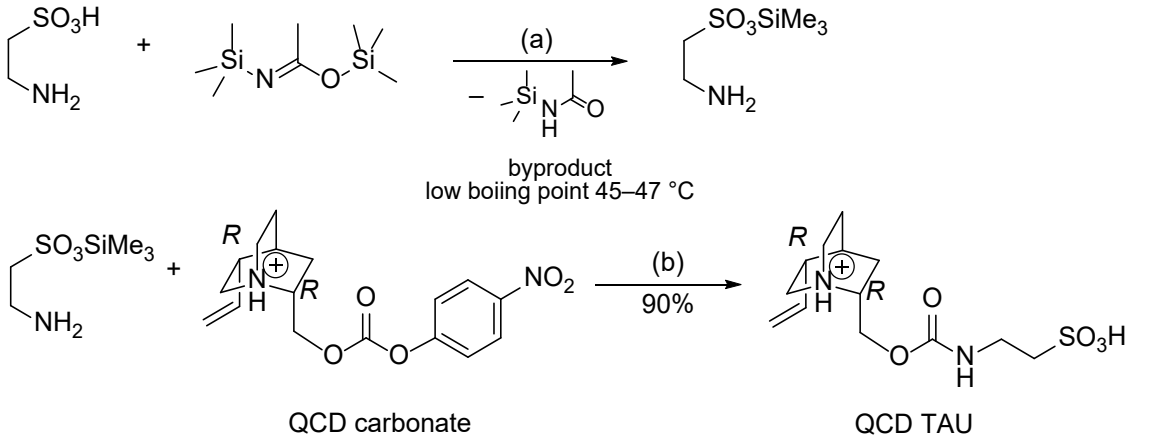


**Fig. S4.** Synthesis of (*2R,4S,5R*)-2-((((2-sulfoethyl)carbamoyl)oxy)methyl)-5-vinylquinuclidin-1-ium chloride (QCDTAU). Reagents and conditions: (a) $CH_2Cl_2$, BSA, reflux 48h. then (b) $CH_2Cl_2$, r.t., 16h.

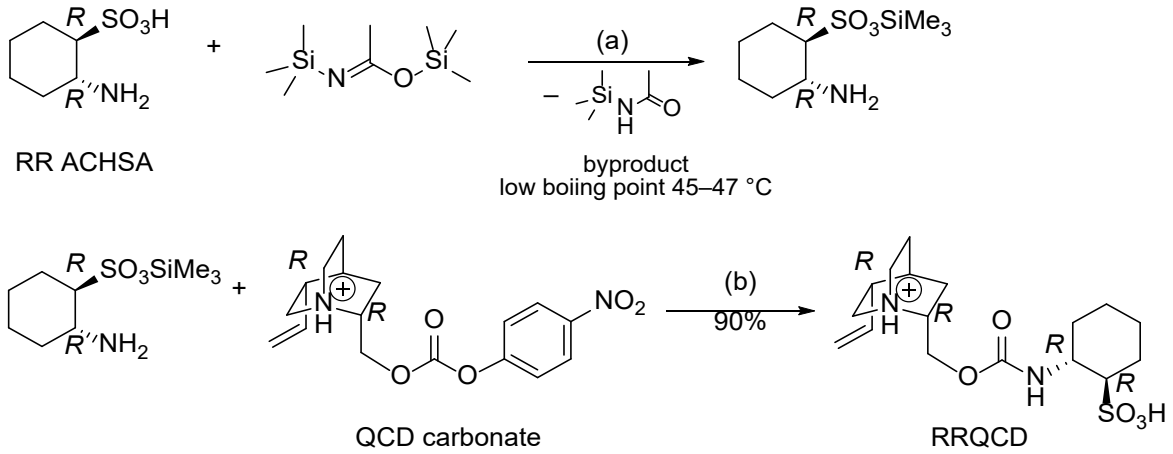


**Fig. S5.** Synthesis of (*2R,4S,5R*)-2-(((((1R,2R)-2-sulfocyclohexyl)carbamoyl)-oxy)methyl)-5-vinylquinuclidin-1-ium chloride (RRQCD). Reagents and conditions: (a) $CH_2Cl_2$, BSA, reflux 48h, then (b) $CH_2Cl_2$, r.t., 16h.

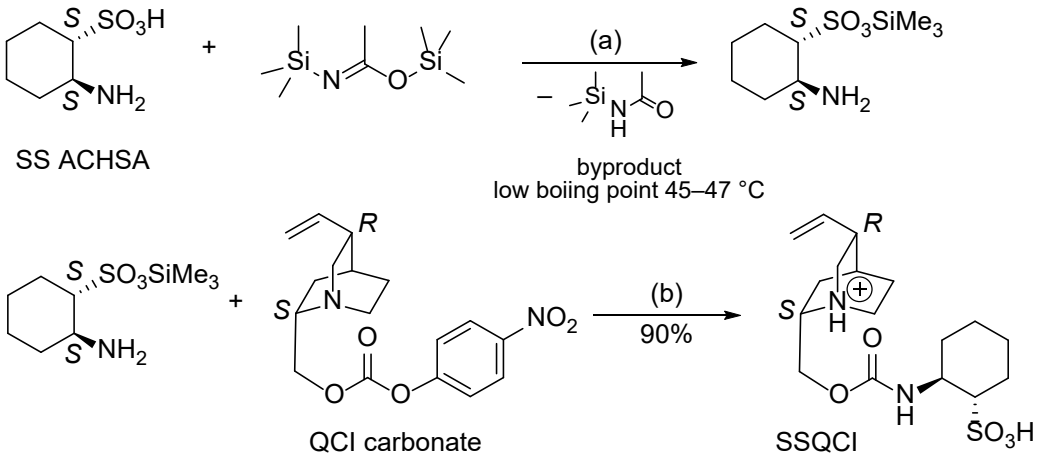


**Fig. S6.** Synthesis of (*2S,4S,5R*)-2-(((((1S,2S)-2-sulfocyclohexyl)carbamoyl)-oxy)methyl)-5-vinylquinuclidin-1-ium (SSQCl). Reagents and conditions: (a) $CH_2Cl_2$, BSA, reflux 48h, then (b) $CH_2Cl_2$, r.t., 16h.

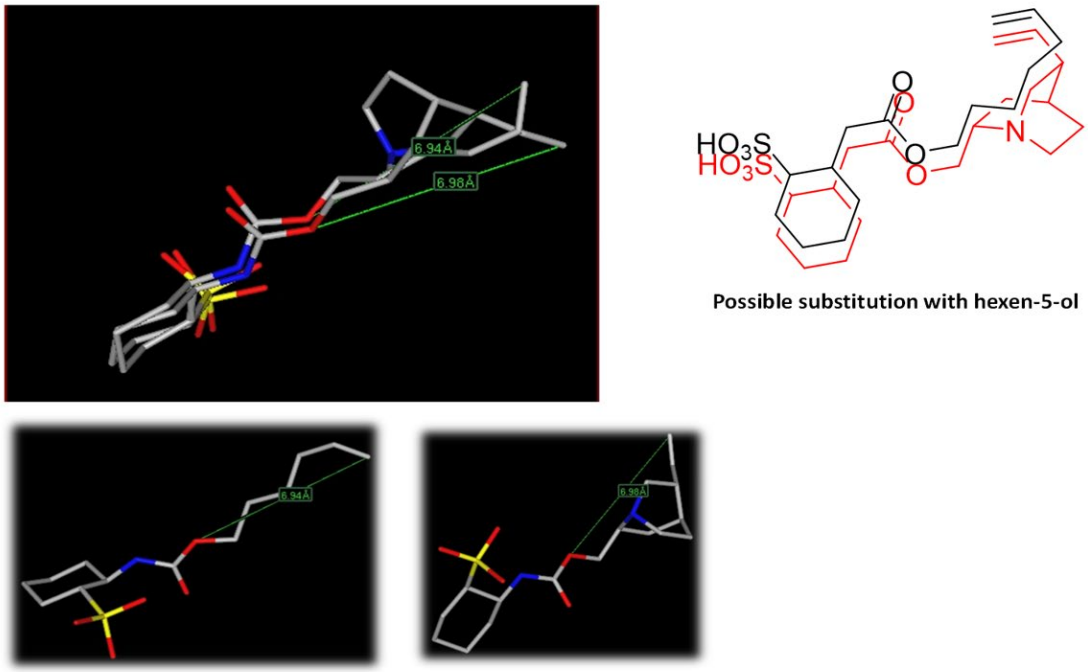


**Fig. S7.** 3D-alignment using MarvinSketch 14.12.15.0 of new derivative with hexen-5-ol chain and the quinuclidine precursor.

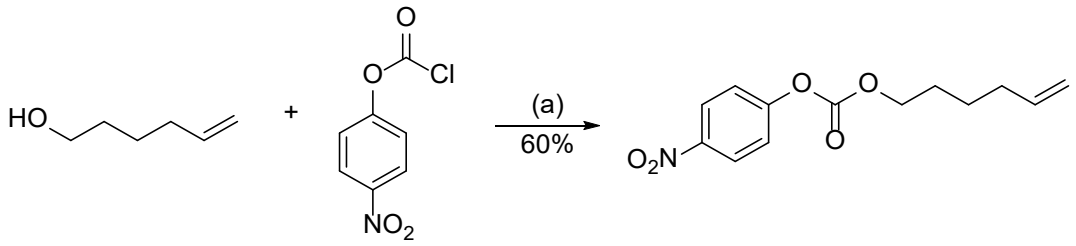


**Fig. S8.** Synthesis of hex-5-en-1-yl (4-nitrophenyl) carbonate. Reagents and conditions: (a) $CH_2Cl_2$, $Et_3N$, 0°C then r.t., 16h.

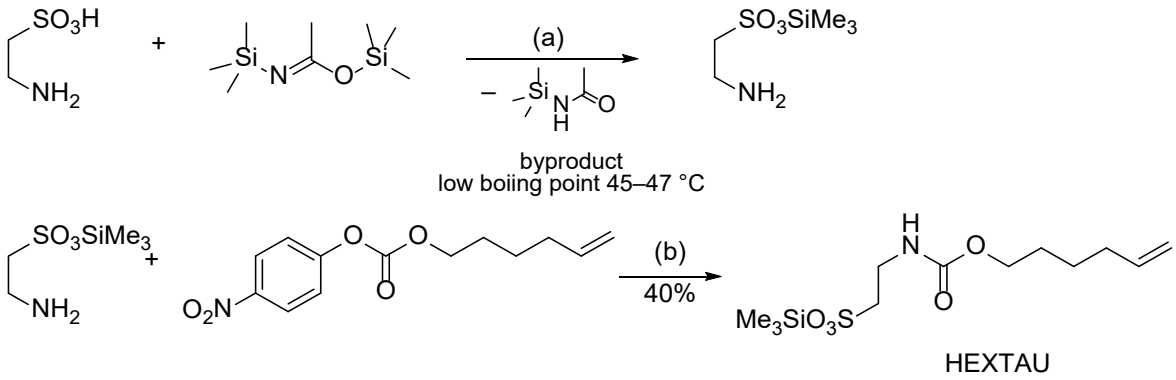


**Fig. S9.** Synthesis of 2-(((hex-5-en-1-yloxy) carbonyl) amino)ethane-1-sulfonic acid (HEXTAU) , Reagent and conditions: (a) $CH_2Cl_2$, BSA, reflux 48h, then (b) $CH_2Cl_2$, r.t., 16h.

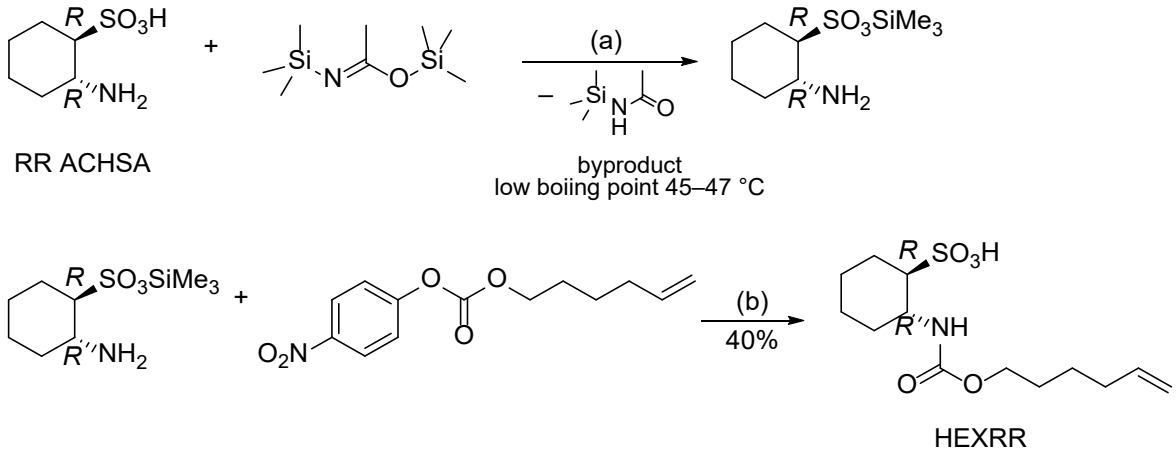


**Fig. S10.** Synthesis of (*1R,2R*)-2-(((hex-5-en-1-yloxy)carbonyl)amino)cyclo-hexane-1-sulfonic acid (HEXRR). Reagents and conditions: (a) $CH_2Cl_2$, BSA, reflux 48h, then (b)$CH_2Cl_2$, r.t., 16h.

## PART III: Detailed characterization of the synthesized selectors

### Synthesis control by MS analysis

The chromatographic separation for the structure elucidation was performed on a Kinetex C18, 50 x 2.1 mm, 2.7 µm column (Phenomenex, Torrance, CA, USA). The measurement was carried out with 0.1% FA in acetonitrile and water with the following gradient profiles. The gradient, which was used for structure elucidation via UHPLC-QTOF-MS/MS (Agilent 1290 UHPLC instrument coupled to Triple TOF 5600+ from Sciex with CTC Pal autosampler), started at 5% B and increased to 95% B in 4.0 min and to 99% B in additional 0.5 min, followed by re-equilibration with 5% B for 1.5 min. The electrospray (ESI) settings were chosen as follows: curtain gas (CUR): 30, Ion Source Gas 1 (GS 1): 50 and Ion Source Gas 2 (GS 2): 40, IonSpray Voltage Floating (ISVF) 4500 and temperature was 500 °C. The QTOF was operated in negative mode and the m/z range 30 to 2000 was scanned. The TOF experiment had an accumulation time of 100 ms and was combined with 20 TOF MS2 experiments using information dependent acquisition (IDA) leading to a period cycle time of 551 ms.

**Data S1.** *(2R,4S,5R)-2-{[(((1R,2R)-1-Sulfocyclohexyl)carbamoyl)oxy]methyl}-5-vinylquinuclidin-1-ium chloride (QCDRR, 4)*

Starting from RR-ACHSA (1.07 g, 5.96 mmol) and **1** (2.20 g, 5.96 mmol) following the general procedure **B**, the title compound **4** was obtained as yellowish oil (2.7 g, yield 90%).

Specific rotation: + 15.77 (10 mg/mL in MeOH)

$^{1}$H-NMR ($CD_3OD$, 400 MHz): δ 1.24-1.37 (m, 3H), 1.49-1.64 (m, 3H), 1.78-1.80 (m, 2H), 1.89-1.92 (m, 2H), 2.03-2.11 (m, 4H), 2.35 (d, $J_d$ = 13.6 Hz, 1H), 2.56 (td, $J_t$ = 12.4 Hz, $J_d$ = 4.0 Hz, 1H) 2.82 (q, $J_q$ = 8 Hz, 1H), 3.36-3.39 (m, 3H), 3.50-3.54 (m, 1H), 3.81.3.85 (m, 2H), 5.23-5.29 (m, 2H), 5.91-6.00 (m, 1H) ppm.

$^{13}$C-NMR ($CD_3OD$, 100.6 MHz): δ 20.94, 22.90, 24.41, 24.91, 26.28, 27.41, 33.49, 36.56, 45.03, 50.50, 56.71, 59.31, 60.64, 63.14, 116.16, 136.71, 155.43 ppm.

HRMS (ESI-QTOF, negative mode): m/z calcd for $C_{17}H_{27}N_2O_5S$ $[M-H]^-$, 371.1641; found, 371.1630; HRMS (ESI-QTOF, positive mode): m/z calcd for $C_{17}H_{29}N_2O_5S$ $[M+H]^+$, 373.1797; found, 373.1814

**Data S2.** *(2S,4S,5R)-2-{[(((1S,2S)-1-Sulfocyclohexyl)carbamoyl)oxy]methyl}-5-vinylquinuclidin-1-ium (QCISS, 5)*

Starting from SS-ACHSA (1.07 g, 5.96 mmol) and **2** (2.20 g, 5.96 mmol) following the general procedure **B**, the title compound **5** was obtained as yellowish oil (2.3 g, yield 90%).

Specific rotation: + 20.00 (10 mg/mL in MeOH)

$^1$H-NMR ($CD_3OD$, 400 MHz): δ 1.28-1.41 (m, 4H), 1.45-1.57 (m, 1H), 1.78-1.80 (m, 2H), 1.89-1.91 (m, 2H), 1.97-1.99 (m, 2H), 2.08-2.11 (m, 1H), 2.15-2.24 (m, 1H), 2.33-2.37 (m, 1H), 2.56 (td, $J_t$ = 10.8 Hz, $J_d$ = 4 Hz, 1H), 2.80-2.87 (m, 1H), 3.14-3.22 (m, 1H), 3.28-3.30 (m, 1H), 3.58-3.65 (m, 3H), 3.81-3.92 (m, 2H), 5.24-5.31 (m, 2H), 5.93-6.00 (m, 1H) ppm.

$^{13}$C-NMR ($CD_3OD$, 100.6 MHz): δ 21.17, 23.45, 24.42, 24.92, 26.16, 27.42, 33.53, 36.70, 40.72, 50.53, 52.67, 56.75, 61.27, 63.13, 115.94, 137.70, 155.15 ppm.

HRMS (ESI-QTOF, negative mode): m/z calcd for $C_{17}H_{27}N_2O_5S$ $[M-H]^-$, 371.1641; found, 371.1619; HRMS (ESI-QTOF, positive mode): m/z calcd for $C_{17}H_{29}N_2O_5S$ $[M+H]^+$, 373.1797; found, 373.1795

**Data S3.** *(2R,4S,5R)-2-{[((2-Sulfoethyl)carbamoyl)oxy]methyl}-5-vinylquinuclidin-1-ium chloride (QCDTAU, 6)*

Starting from taurine (0.746 g, 5.96 mmol) and **1** (2.20 g, 5.96 mmol) following the general procedure **B**, the desired product **6** was obtained as yellowish oil (2.25 g, yield 90%).

Specific rotation: + 29.7 (10 mg/mL in MeOH)

$^1$H-NMR ($CD_3OD$, 400 MHz): δ 1.60-1.67 (m, 1H), 2.01-2.11 (m, 4H), 2.81-2.84 (m, 1H), 2.91 (t, $J_t$ = 5.20 Hz, 1H), 2.97-3.01 (m, 1H), 3.36-3.54 (m, 4H), 3.65-3.85 (m, 2H), 4.16-4.47 (m, 2H), 5.22-5.29 (m, 3H), 5.91-6.00 (m, 1H) ppm.

$^{13}$C-NMR ($CD_3OD$, 100.6 MHz): δ 21.03, 22.89, 26.31, 36.64, 36.92, 51.13, 56.73, 59.32, 60.76,´61.12, 116.49, 136.64 ppm.

HRMS (ESI-QTOF, negative mode): m/z calcd for $C_{13}H_{21}N_2O_5S$ $[M-H]^-$, 317.1171; found, 317.1165; HRMS (ESI-QTOF, positive mode): m/z calcd for $C_{13}H_{23}N_2O_5S$ $[M+H]^+$, 319.1328; found, 319.1321

**Data S4.** *(2S,4S,5R)-2-{[((2-Sulfoethyl)carbamoyl)oxy]methyl}-5-vinylquinuclidin-1-ium (QCITAU, 7)*

Starting from taurine (0.746 g, 5.96 mmol) and **2** (2.20 g, 5.96 mmol) following the general procedure **B**, the desired product **7** was obtained as a yellowish oil (1.73 g, yield 90%).

Specific rotation: + 6.77 (10 mg/mL in MeOH)

$^1$H-NMR ($CD_3OD$, 400 MHz): δ 1.31-1.44 (m, 1H), 2.00 (m, 2H) 2.06-2.25 (m, 2H), 2.88 (m, 1H), 2.92 (t, $J_t$ = 4 Hz, 1H), 3.00 (t, $J_t$ = 8 Hz, 1H), 3.22-3.28 (m, 2H) 3.54-3.69 (m, 4H), 3.74-3.85 (m, 1H), 4.22-4.39 (m, 2H), 5.26 (t, $J_t$ = 12 Hz, 2H), 5.94-6.03 (m, 1H) ppm.

$^{13}$C-NMR ($CD_3OD$, 100.6 MHz): δ 21.26, 23.44, 26.10, 36.71, 36.91, 49.85, 51.12, 52.71, 56.61, 61.46, 116.05, 137.60 ppm.

HRMS (ESI-QTOF, negative mode): m/z calcd for $C_{13}H_{21}N_2O_5S$ $[M-H]^-$, 317.1171; found, 317.1169; HRMS (ESI-QTOF, positive mode): m/z calcd for $C_{13}H_{23}N_2O_5S$ $[M+H]^+$, 319.1328; found, 319.1309

**Data S5.** *(1S,2S)-2-{[(Hex-5-en-1-yloxy)carbonyl]amino}cyclohexane-1-sulfonic acid (SS-ACHSA, 8)*

Starting from SS-ACHSA (1.00 g, 5.58 mmol) and **3** (2.05 g, 7.76 mmol) following the general procedure **B**, the title compound **8** was obtained as yellowish oil (0.4 g, yield 40%).

$^1$H-NMR ($CD_3OD$, 400,MHz): δ=8.24 (bp,OH), 5.81 (m,5H), 4.95 (dd,2H), 3.99 (d,2H), 3.32 (m,1H), 2.36 (m,1H), 2.10 (m,2H), 1.83 (m,2H), 1.65 (m,2H), 1.51 (m,2H), 1.51 (m,2H), 1.51 (m,2H), 1.35 (m,2H) ppm

$^{13}$C-NMR ($CD_3OD$, 400,MHz):δ=164.39, 140.11, 115.35, 63.98, 51.25, 49.25, 46.51, 36.62, 33.19, 28.60, 25.12, 25.09, 22.87 ppm

HRMS (ESI-QTOF, negative mode): m/z calcd for $C_{13}H_{22}NO_5S$ $[M-H]^-$, 304.1219; found, 304.1225

**Data S6.** *2-{[(Hex-5-en-1-yloxy)carbonyl]amino}ethane-1-sulfonic acid (TAU, 9)*

Starting from taurine (1.30 g, 10.10 mmol) and **3** (2.05 g, 7.76 mmol) following the general procedure **B**, the title compound **9** was obtained as yellowish oil (0.25 g, yield 20 %).

$^1$H-NMR (DMSO-d6, 400 MHz): δ 9.24 (bp, OH), 6.56 (bp, NH), 5.78 (m, 5H), 4.90 (dd, 2H), 3.90 (t, 3H), 3.25 (m, 2H), 2.58 (m, 2H), 2.047 (m, 2H), 1.53 (m, 2H), 1.37 (m, 2H) ppm.

$^{13}$C-NMR (DMSO-d6, 100MHz): δ 164.43, 138.94, 115.37, 63.79, 51.08, 46.22, 37.62, 28.60, 25.09 ppm.

HRMS (ESI-QTOF, negative mode): m/z calcd for $C_9H_{16}NO_5S$ $[M-H]^-$, 250.0749; found, 250.0742

## PART IV: Synthesis of modified silica

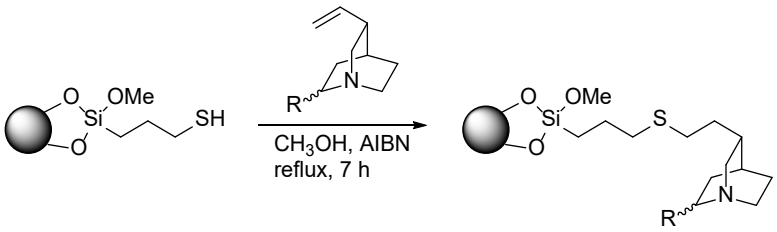


**Fig. S11.** Synthesis scheme for the immobilization of the selectors.

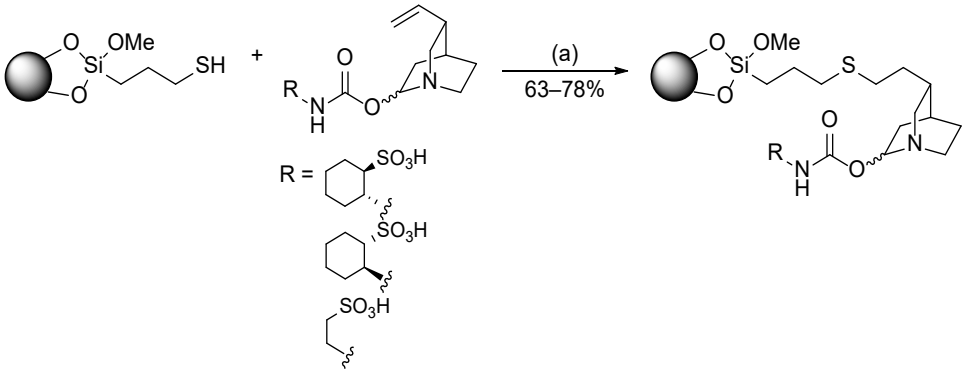


**Fig. S12.** Thiol-ene-click reaction to obtain immobilized derivatives. Reagents and conditions: a) MeOH, AIBN, reflux, 7h.

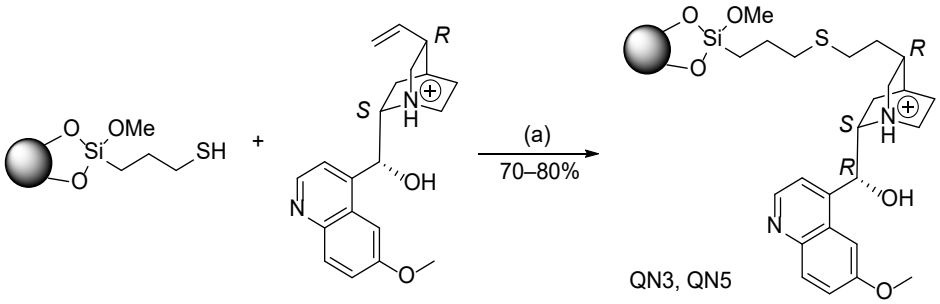


**Fig. S13.** Thiol-ene-click reaction to obtain immobilized derivative (QN3, QN5). Reagents and conditions: a) MeOH, AIBN, reflux, 7h.

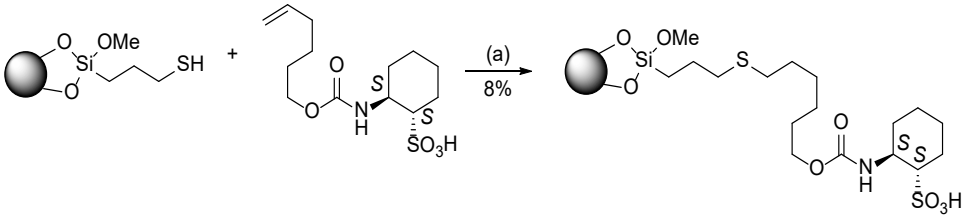


**Fig. S14.** Thiol-ene-click reaction to obtain immobilized derivative. Reagents and conditions: a) MeOH, AIBN, reflux, 7h.

## PART V: Characterization of modified silica gels by FTIR-spectroscopy

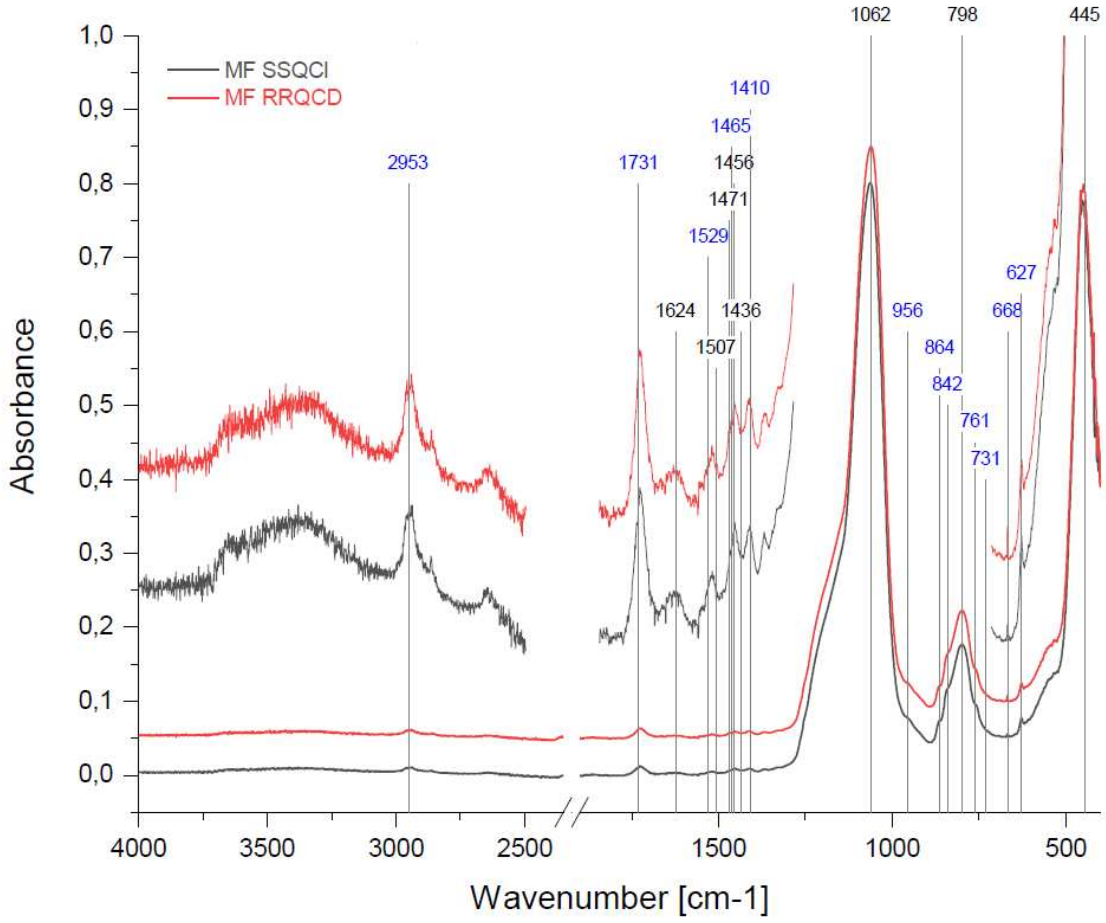


**Fig. S15.** FTIR spectra of the two RP/ZWIX MMC phases QCISS (black) and QCDRR (red). The IR-band at 1731 cm-1 is the C=O stretching vibration of the carbamate group and indicates successful immobilization of the corresponding zwitterionic ligands.

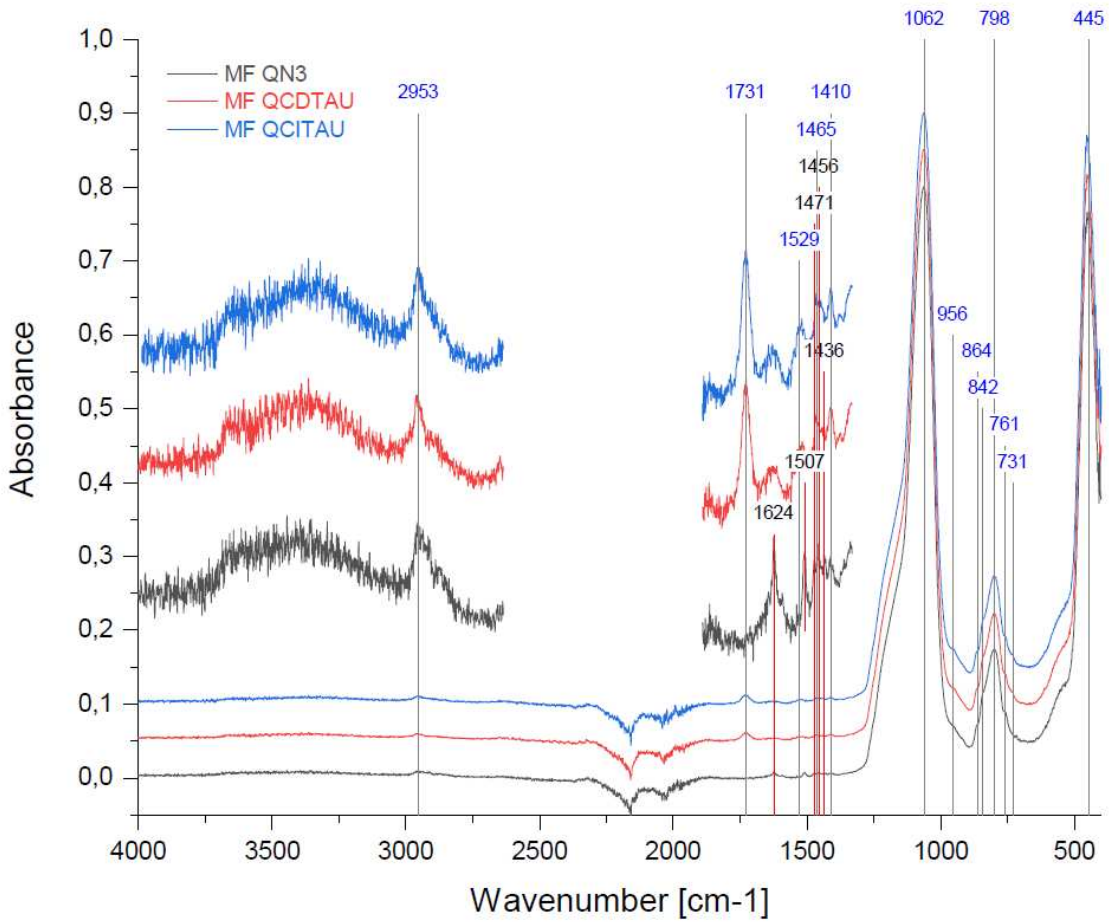


**Fig. S16.** FTIR spectra of the two RP/ZWIX MMC phases QCITAU (blue) and QCDTAU (red) as well as of the WAX-type QN phase (black). The IR-band at 1731 cm-1 is the C=O stretching vibration of the carbamate group and indicates successful immobilization of the corresponding zwitterionic ligands while this band is absent for QN which has no carbamate group. The band at 1624 cm-1 of the QN material indicates the C=C stretching vibration of the quinoline ring which is absent in the zwitterionic QCITAU and QCDTAU.

# PART VI: ζ-Potential determination

**Equation 1.** Helmholtz-Smoluchowski equation.

$$\mu_E = C\frac{\varepsilon_0 \cdot \varepsilon_r \cdot \zeta}{\eta}$$

$\mu_E$: mobility of a particle $\varepsilon_R$: relative permittivity $\varepsilon_0$: permittivity of vacuum

$C$: The constant C becomes 2/3 for $\kappa r<0.1$ ($\kappa$, Debye parameter; $\kappa^{-1}$, Debye length) (Hückel approximation) and 1 for $\kappa r>100$ (Smoluchowski approximation).

$\eta$: viscosity

# PART VII: Chromatographic characterization under HILIC and RP conditions for column classification

## Material and methods

The stationary phases which were included in the test set for the evaluation of the chromatographic properties comprised all stationary phases depicted in Fig S2. The RP-HPLC separations were carried out using a mobile phase consisting of ACN/$H_2O$ (2:3, v/v) and 0.29 % acetic acid ($C_{tot}$ = 50 mM). The apparent pH value was adjusted to 6 with ammonia in the polar organic mixture. The mobile phases of the HILIC measurements consisted as follows: The organic modifier ACN was mixed with water in the ratio 95:5 (v/v) for the analysis of xanthines and 90:10 (v/v) for the nucleosides and vitamins, containing ammonium acetate (5 mM referred to the total volume) as buffer. The pH was not adjusted and remained at approximately 8 in the polar organic mixture. The mobile phase was used for dissolving the analytes. For the RP test the concentration was 0.8 mg $mL^{-1}$ (injection volume 5 µL) and for the HILIC tests 1.0 mg $mL^{-1}$ (injection volume 2 µL). The flow rate was 1.7 mm $s^{-1}$ at 25°C. The detection wavelength was 220 nm. The void volume was determined with uracil (RP) and toluene (HILIC).

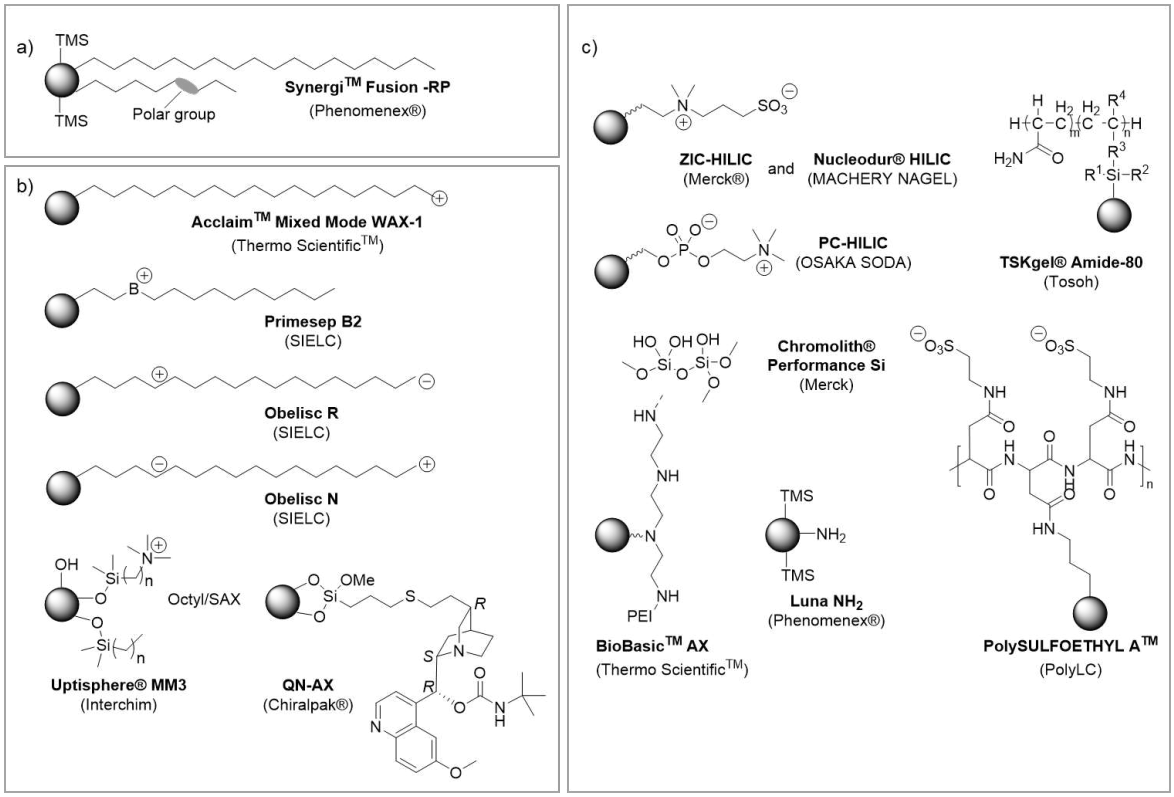


**Fig. S17.** Surface structure of investigated a) RP, b) mixed mode and c) HILIC stationary phases which were chromatographically evaluated for the principal component analysis.

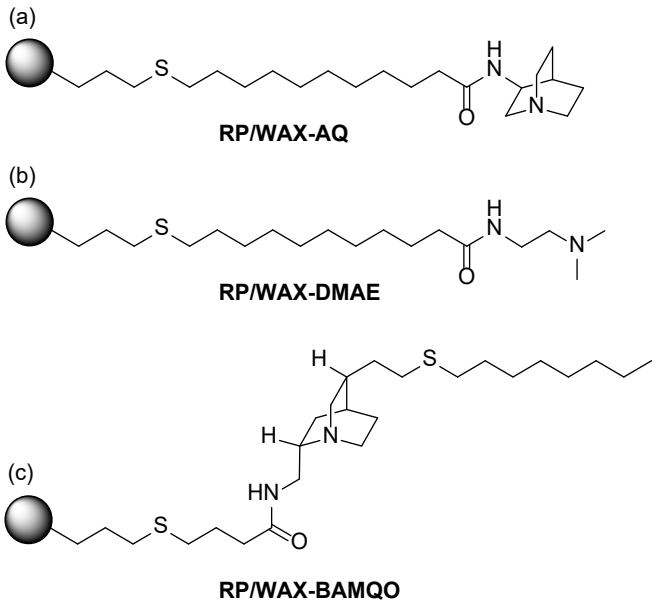


**Fig. S18.** Surface structures of investigated non-commercial RP/WAX mixed mode phases.

# VII. CHAPTER THREE

# Thiol-ene photo-click immobilization of a chiral chromatographic ligand on silica particles

## VII.1 Publication II – Main Document

Journal of Chromatography A 1622 (2020) 461133

Contents lists available at ScienceDirect

Journal of Chromatography A

journal homepage: www.elsevier.com/locate/chroma

# Thiol-ene photo-click immobilization of a chiral chromatographic ligand on silica particles

Christian Geibel, Kristina Dittrich, Marc Wolter, Michael Lämmerhofer*

*Institute of Pharmaceutical Sciences, Pharmaceutical (Bio-)Analysis, University of Tübingen, Auf der Morgenstelle 8, 72076 Tübingen, Germany*

ARTICLE INFO

*Article history:*
Received 7 March 2020
Revised 9 April 2020
Accepted 14 April 2020
Available online 19 April 2020

*Keywords:*
Chiral stationary phase
Chiral separation
Chiral ion-exchanger
Thiol-ene click reaction
Photoreaction
Photoinitiator

ABSTRACT

This work reports procedures for the immobilization of vinyl ligands on silica particles by UV-initiated thiol-ene radical addition reaction (photo-click immobilization). *tert*–Butylcarbamoyl quinine was the functional ligand (ene component) for the synthesis of chiral stationary phases. Two distinct surface chemistries were evaluated. In one approach, the ligand was directly attached to 3-mercaptopropyl-silica triggered by radicals generated by UV irradiation from a photoinitiator. In another approach, the ligand was immobilized onto vinyl silica via poly(3-mercaptopropyl-methylsiloxane) (PMPMS) as crosslinker by a photoinitiated double click reaction in which functionalization with chiral ligand and crosslinking to vinylsilica occurred simultaneously in one synthesis step. PMPMS-bonded CSPs were prepared from suspension (slurry method) or solventless after coating of the polythiol onto the vinylsilica surface (film method). Optimization by a design of experiment approach showed that the reaction time is the prime variable to optimize the surface coverage of chiral selector which also increased with PMPMS concentration. When the film formation of the latter approach was assisted by a minute volume of toluene during photo-click immobilization, selector coverage could be significantly increased to 0.73 μmol/m$^2$ in a 2 h synthesis compared to 0.44 μmol/m$^2$ by the solventless film method and 0.47 μmol/m$^2$ by the slurry method under otherwise comparable conditions. The solvent assistance improved the chromatographic efficiency of the film method and resulted equal minimal reduced plate height of 2.6 as the slurry method for a chiral probe (Fmoc-Phe). The mass transfer resistance was around factor 2 smaller with the solvent-assisted film method as compared to the film approach without toluene, presumably due to a more homogenous distribution of the thin polymer film owing to lower dynamic viscosity in presence of toluene.



## 1. Introduction

Immobilization of chromatographic ligands on silica surfaces allows flexible tailoring of the selectivity of stationary phases for various HPLC applications. Simple, well controllable and quantitative reactions are favourable for this purpose. Thiol-ene and thiol–yne click chemistries raised significant interest for this purpose [1,2]. The gain in popularity of thiol click reactions in the past decade was somehow stimulated by the enormous popularity of Huisgen azide–yne 1,3-dipolar cycloaddition. What its application for the immobilization of chromatographic ligands is concerned, thiol click reactions are not a new chemistry. It has already been utilized in the late 1980s and beginning of 1990s for the immobilization of chiral selectors with vinyl groups to thiol-modified silica gels [3–6]. Known as radical addition reaction they were typically performed by using 2,2′-azobis(2-methylpropionitrile) (AIBN) as radical initiator and thermal initiation of the addition reaction. It has been widely exploited for the synthesis of stationary phases for chiral separation, reversed-phase type, ion-exchange type, mixed-mode stationary phases, hydrophilic interaction liquid chromatography (HILIC) and ionic-liquid stationary phases [7–19]. This immobilization strategy was also extended to thiol–yne addition reaction [1,20,21].

Instead of thermal initiation of the addition reaction, UV initiated thiol-ene and thiol–yne reactions have attracted some attention. These photo-initiated variants have been exploited for instance in sensor sciences to modify surfaces because it allows convenient, spatially controlled micropatterning [22–24]. Thiol-ene photopolymerization has become quite popular for preparation of polysilsesquioxane (POSS)-based monolithic capillary columns in UV-transparent fused-silica capillaries [25–30]. It is a straightforward approach to obtain a functionalized monolithic capillary column in a single step within a few minutes with dedicated

* Corresponding author.
*E-mail address:* michael.laemmerhofer@uni-tuebingen.de (M. Lämmerhofer).

https://doi.org/10.1016/j.chroma.2020.461133
0021-9673/

surface chemistry through incorporation of a functional monomer and tailored macropore structure via porogenic solvents. Besides these straightforward and simple single step approaches, functionalized monolithic capillary columns have also been prepared via two-step photo-initiated reactions in which a reactive POSS-based monolith was formed in the first step which was functionalized e.g. by photo-initiated thiol–yne click reaction e.g. for reversed-phase (RP) and strong cation-exchange (SCX) [31] or for boronate affinity chromatography [32]. While photo-initiated click addition or polymerization reaction were quite popular for the preparation of monolithic capillary columns, this reaction type was rarely used for particle functionalization. Yet, a recent study used photo-click reaction for the synthesis of functional silanes which were subsequently immobilized to silica particles by a conventional silanization reaction [33]. A direct photo-initiated thiol-ene or thiol–yne immobilization of chromatographic ligands on silica has not been reported.

In this study, we present the results of such a direct photo-click immobilization of a chromatographic ligand. The chiral selector *tert*–butylcarbamoylquinine (tBuCQN) which carries a vinyl group serves as a model ene component for immobilizing ligands on thiol-silica via photoinitiated click addition reaction. Thiol-ene and thiol–yne addition reactions were classified as click reactions because these chemical transformations proceed with high yields under mild reaction conditions, can tolerate water and oxygen (although oxygen may consume some radicals and oxidize the thiol component to disulfide), are adoptable for a wide range of starting materials, selectively react with each other (almost) without side reactions, and reactions can be performed in water or various organic solvents [34]. 3-Mercaptopropyl-modified silica (brush-type) and poly(3-mercaptopropyl-methylsiloxane) (PMPMS), respectively, represented the thiol component whereby the latter was crosslinked to vinyl-modified silica during the photoclick reaction. A number of distinct synthesis approaches (Fig. 1) were compared to each other with regard to selector coverages and chromatographic performances. Synthesis conditions were systematically optimized with regard to reaction time, educt concentrations in the reaction mixture and type of initiation.

## 2. Experimental

### 2.1. Materials

Spherical silica particles Kromasil 5 µm, 200 Å (200 $m^2$/g) and 100 Å (300 $m^2$/g), were supplied by Eka Chemicals (Bohus, Sweden). The chiral selector *tert*–butylcarbamoylquinine (tBuCQN) was synthesized as described elsewhere [35,36]. 2,2-Dimethoxy-2-phenylacetophenone (DMPA) and 4-dimethylaminopyridine (DMAP) were obtained from Sigma Aldrich (Munich, Germany). Vinyltrimethoxysilane, 3-mercaptopropylmethyldimethoxysilane and poly(3-mercaptopropyl)methylsiloxane (PMPMS, homopolymer, [102783-03-9], viscosity 75–150 cSt.) were supplied by ABCR Chemicals (Karlsruhe, Germany). Test compounds *N*-[(9H-*fluoren*-9-*ylmethoxy*)*carbonyl*]-phenylalanine (Fmoc-Phe), *N*-acetyl-phenylalanine (Ac-Phe), *N*-carbobenzoxy-phenylalanine (Z-Phe) and 2-(2,4-dichlorphenoxy)propanoic acid (dichlorprop) were obtained by Sigma Aldrich or synthesized in-house according to ref. [37,38]. Empty stainless steel columns (all with a dimension of 50 × 3 mm) were supplied by Bischoff Chromatography (Leonberg, Germany).

### 2.2. Instrumentation

The chromatographic experiments were conducted on an Agilent 1290 Infinity series liquid chromatographic system from Agilent Technologies (Waldbronn, Germany). The system consisted of a binary pump, a thermostatted column compartment (TCC), a diode array detector (DAD) and an autosampler. To obtain a minimal extra-column volume and minimize extra-column peak dispersion, the system was equipped with an ultralow dispersion kit. This included a Max-Light ultralow dispersion cartridge flow cell (inner volume 0.6 µL) and an ultralow dispersion needle seat assembly (1 µL injected). MarvelX capillaries from Idex Corporation (Lake Forest, Illinois, USA) were installed from autosampler to TCC (350 mm length x 0.075 mm inner diameter) and from TCC to DAD (250 mm x 0.075 mm). Subsequent to packing, columns were washed overnight with methanol at a flow rate of 0.5 mL/min. The

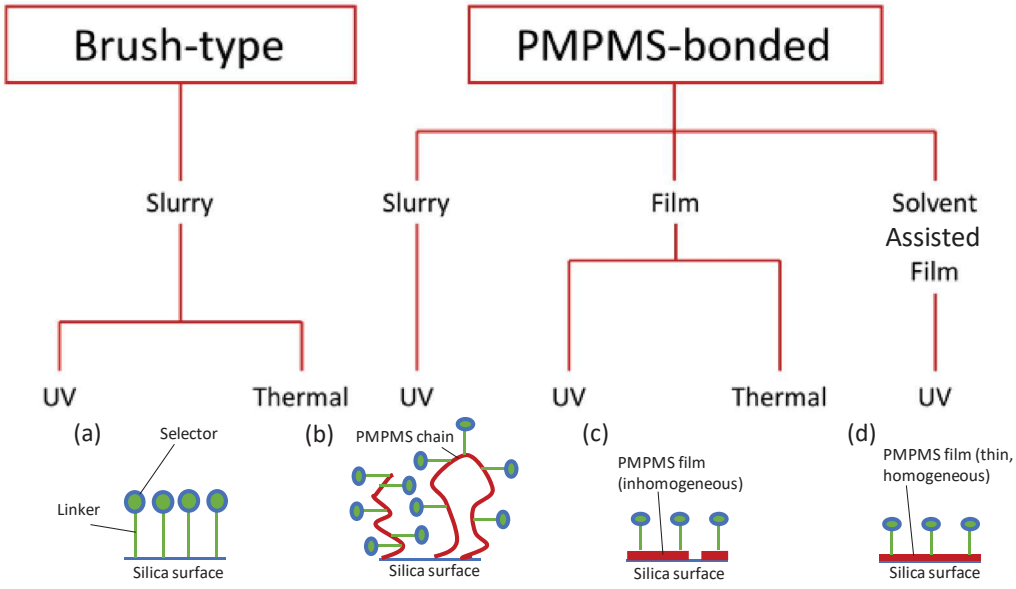


**Fig. 1.** Schematic overview of the employed synthesis strategies. CSP morphology on top, reaction method in the middle panel, and type of initiation of the radical addition reaction at the bottom. Schemes of resulting tentative surface morphologies: (a) Brush-type, (b) PMPMS-bonded slurry method, (c) PMPMS-bonded film method, and (d) PMPMS-bonded solvent-assisted film method.

flow rate was varied between 0.015 and 2.5 mL/min for generation of Van Deemter curves, always taking care that the maximum pressure of 800 bar was not exceeded. The column temperature was kept constant at 25 °C. With isocratic conditions, extra column volume was determined to be 13 µL with an extra-column peak variance of 7 $\mu L^2$ (determination was carried out by second moment method with Fmoc-phenylalanine as sample, flow rate of 0.5 mL/min, and a column temperature of 25 °C). Columns were slurry packed with a smartline pneumatic pump, model 1950, from Knauer (Berlin, Germany). Data analysis was performed by using ChemStation Offline Software (Rev. B.04.03 [16], 2010) from Agilent Technologies. For data acquisition OpenLab CDS ChemStation Online Software (Rev. C.01.03 [37], 2011) from Agilent Technologies was utilized. For systematic optimization by design of experiments (DoE) approach, MODDE Pro-Ver. 12.1.0.5491 from Sartorius Stedim (Umeå, Sweden) was used.

### 2.3. Chiral stationary phase (CSP) synthesis

#### 2.3.1. Synthesis of vinylsilica

18.26 g of silica particles (5 µm, pore size 200 Å) were dispersed in 200 mL toluene and heated to reflux while stirring with a mechanical stirrer. The first 50 mL of toluene were distilled off to remove traces of water. Vinyltrimethoxysilane (6 µmol per $m^2$; 3.36 mL) and 5 mol% of the catalyst 4-dimethylaminopyridine were added. Before the reaction was started, the reaction flask was flushed with nitrogen for 10 min. Reaction took place by refluxing under nitrogen atmosphere for 16 h. The product was repeatedly washed with boiling toluene and boiling methanol, three times each. After drying of the vinylated silica gel, it was subjected to elemental analysis. Results were as follows: C: 2.19 ± 0.02 wt%, H: 0.52 ± 0.00 wt%, N: 0.02 ± 0.00 wt%, S: 0.00 ± 0.00 wt%, corresponding to 1.82 µmol/$m^2$ immobilized vinyl groups (for sake of simplicity the initial specific surface area of the unmodified silica as specified by the supplier was used in all calculations).

#### 2.3.2. Synthesis of thiol-modified silica

10.01 g of silica particles (5 µm, pore size 100 Å) were dispersed in toluene. After distilling off the water-containing azeotrope of toluene and water, 3-mercaptopropylmethyldimethoxysilane (5.5 µmol per $m^2$; 2.98 mL) and 10 mol% of 4-dimethylaminopyridine were added. After flushing the system with nitrogen for 10 min, the reaction was held under reflux and under nitrogen atmosphere. Reaction time was 7 h. Subsequently, the product was washed with boiling methanol and boiling toluene, three times each. After drying the modified silica gel was subjected to elemental analysis. Results were as follows: C: 3.85 ± 0.02 wt%, H: 0.92 ± 0.01 wt%, N: 0.00 ± 0.00 wt%, S: 2.15 ± 0.03 wt%, corresponding to 2.23 µmol/$m^2$ immobilized thiol (related to the initial specific surface area).

#### 2.3.3. Photoreactions

Film-type reactions as well as solvent assisted film-type reactions were carried out in a round bottom flask (Duran Glastechnik, Wertheim/Main, Germany) consisting of borosilicate glass, the volume of the vessel was 250 mL. The reactions following the slurry method were carried out in a three neck flask, volume, material and supplier were likewise (Duran Glastechnik, Wertheim/Main, Germany) equipped with a mechanical stirrer and reflux condenser. The glass has a negligible UV-absorption in the range from 310 nm upwards. The UV lamp (Ultra Vitalux, 300 W, from Osram, Munich, Germany) has a radiant power of 13.6 W in the UV-A spectrum (315 – 400 nm) and 3.0 W in the UV-B spectrum (280 – 315 nm). PMPMS was only partly soluble in methanol and formed a homogenous emulsion in methanol. The average molecular weight of PMPMS is 4000 – 7000 g/mol, containing 1 active thiol group per monomer and a monomeric molecular weight of roughly 343 g/mol, resulting in 12 – 20 active thiol groups per mol.

For the film method, a solid, thin layer on the inside of the round bottom flask was irradiated with UV-light. No co-solvent or diluent (non-solvent) was added.

#### 2.3.4. Photo-click immobilization of chromatographic ligand

The distinct synthesis procedures are schematically outlined in Fig. 1 and can be generally divided into (PMPMS) polymer-bonded and brush-type phases. The thermally initiated immobilization reactions were described previously, for the PMPMS-bonded stationary phase in ref. [39] and for the brush-type phase in ref. [35]. Amongst the photo-click immobilization reactions via polythiol (PMPMS) polymer layer three distinct variants were evaluated: i) a slurry method, ii) a film method, and iii) a solvent-assisted film method.

For the slurry method, 0.136 mmol tBuCQN were dissolved in 10 mL of degassed methanol. 0.5 g of vinylated silica were added and the suspension was stirred with a mechanical stirrer. The system was flushed with nitrogen and 0.226 mmol PMPMS were added. After 10 min, DMPA (0.0136 mmol) was added to the reaction mixture and the thiol-ene click reaction was initiated by UV irradiation with a UV lamp (Ultra Vitalux, 300 W, from Osram, Munich, Germany). The UV lamp was positioned in a distance of 15 cm to the reaction flask (angle to upright flask: 180°). A Dimroth cooler prevented loss of methanol by evaporation due to the heat generated by the UV lamp. The reaction mixture was exposed to UV light for certain reaction times as specified in Table 1. Afterwards, the UV lamp was switched off and the product was washed with boiling toluene and boiling methanol three times each. Finally, it was dried at 60 °C overnight.

For the (solvent-less) film method, the same quantities of reactants were added to 20 mL of methanol. After dispersing the vinylsilica in methanol, methanol was completely removed by slow evaporation, resulting in a thin film of PMPMS and other reactants on the silica surface. Irradiation with UV light as well as washing was carried out the same way as described above for the slurry method.

For the solvent assisted film method the synthesis procedure was the same as for the solvent-less film method. However, the reaction was performed in presence of a small amount of less volatile toluene. Instead of dispersing vinylsilica in methanol, it was dispersed in a mixture of 20 mL methanol and the amount of toluene as stated in Table 1 (CSPs # 21 and 22). Afterwards, methanol was completely removed while taking care that the toluene was not evaporated but remained in the reaction mixture. Apart from this, the synthesis protocol was the same as described above.

For comparison, the tBuCQN selector was also immobilized on 3-mercaptopropyl-modified silica yielding typical brush-type CSPs. For this sake, the slurry method as described above was chosen for comparison with some slight modifications. Most importantly, vinylsilica was replaced by 3-mercaptopropylsilica and PMPMS was omitted from the reaction mixture. Five batches were synthesized with identical quantities of educts (tBuCQN, DMPA) in the reaction mixture as described above for the slurry method. Reaction times of 30, 60, 120 and 420 min were examined. The fifth synthesis batch was carried out by thermal initiation with AIBN as radical starter as described previously [35].

All methods have been carried out with distinct quantities of reactants as specified in Table 1 along with the results of the surface coverages.

#### 2.3.5. Oxidation of CSP # 22

An aliquot of CSP # 22 (1 g) was suspended in 10 mL methanol and 0.9 mL formic acid 99%. To this suspension, 3.4 mL performic

**Table 1**
Summary of the starting conditions and results for CSP synthesis.

| | Reaction conditions | | | | | | Results[a] | | | | |
|---|---|---|---|---|---|---|---|---|---|---|---|
| CSP # | Reaction type | Initiation | Reaction time [min] | Initial weight [µmol/m$^2$] tBuCQN | Amount of added toluene Sulfur (PMPMS) | Coverage [µmol/m$^2$][b] added toluene | Coverage [µmol/m$^2$][b] tBuCQN | Sulfur | Ratio S/SO[c] | Yield [%] tBuCQN | Sulfur |
| 1 | Brush-type[d] | T | 420 | – | – | – | 1.14 | – | – | – | – |
| 2 | Brush-type[e] | UV | 30 | 1.36 | – | – | 0.19 ± 0.001 | 2.14 ± 0.010 | 11.16 | 14.0 | – |
| 3 | Brush-type[e] | UV | 60 | 1.36 | – | – | 0.21 ± 0.002 | 2.12 ± 0.039 | 10.05 | 15.4 | – |
| 4 | Brush-type[e] | UV | 120 | 1.36 | – | – | 0.20 ± 0.002 | 2.15 ± 0.018 | 10.68 | 14.7 | – |
| 5 | Brush-type[e] | UV | 420 | 1.36 | – | – | 0.41 ± 0.007 | 1.90 ± 0.065 | 4.64 | 30.1 | – |
| 6 | film | UV | 120 | 1.36 | 2.26 | – | 0.44 ± 0.001 | 1.20 ± 0.018 | 2.73 | 32.4 | 53.2 |
| 7 | slurry | UV | 120 | 1.36 | 2.26 | – | 0.47 ± 0.002 | 1.18 ± 0.030 | 2.51 | 34.6 | 52.2 |
| 8 | film | UV | 60 | 1.36 | 2.26 | – | 0.35 ± 0.010 | 1.15 ± 0.055 | 3.31 | 25.6 | 51.1 |
| 9 | slurry | UV | 60 | 1.36 | 2.26 | – | 0.29 ± 0.014 | 0.55 ± 0.011 | 1.91 | 21.0 | 24.2 |
| 10 | film | UV | 30 | 1.36 | 2.26 | – | 0.34 ± 0.008 | 1.13 ± 0.056 | 3.31 | 25.0 | 50.0 |
| 11 | slurry | UV | 30 | 1.36 | 2.26 | – | 0.14 ± 0.010 | 0.48 ± 0.008 | 3.33 | 10.6 | 21.3 |
| 12 | film | UV | 60 | 2.72 | 2.26 | – | 0.21 ± 0.003 | 0.52 ± 0.058 | 2.48 | 7.7 | 22.9 |
| 13 | film | UV | 60 | 1.36 | 1.70 | – | 0.34 ± 0.004 | 0.88 ± 0.047 | 2.59 | 24.9 | 51.6 |
| 14 | film | UV | 60 | 2.72 | 1.70 | – | 0.22 ± 0.010 | 0.45 ± 0.009 | 2.10 | 8.1 | 26.5 |
| 15 | film | UV | 60 | 1.36 | 3.40 | – | 0.42 ± 0.002 | 1.48 ± 0.055 | 3.55 | 30.6 | 43.5 |
| 16 | film | UV | 60 | 2.72 | 3.40 | – | 0.36 ± 0.000 | 0.84 ± 0.014 | 2.34 | 13.1 | 24.6 |
| 17 | slurry | UV | 231 | 1.36 | 2.26 | – | 0.20 ± 0.003 | 1.02 ± 0.011 | 5.20 | 14.7 | 45.1 |
| 18 | slurry | UV | 388 | 1.36 | 2.26 | – | 0.25 ± 0.000 | 1.23 ± 0.021 | 4.93 | 18.4 | 54.4 |
| 19 | film | UV | 376 | 1.36 | 2.26 | – | 0.62 ± 0.007 | 1.97 ± 0.078 | 3.18 | 45.6 | 87.2 |
| 20 | film | UV | 706 | 1.36 | 2.26 | – | 0.66 ± 0.007 | 2.05 ± 0.020 | 3.11 | 48.5 | 90.7 |
| 21 | solvent assisted film[f] | UV | 120 | 1.36 | 2.26 | 2 mL | 0.61 ± 0.005 | 1.89 ± 0.042 | 3.10 | 44.9 | 83.6 |
| 22 | solvent assisted film[f] | UV | 120 | 1.36 | 2.26 | 1 mL | 0.73 ± 0.007 | 2.11 ± 0.192 | 2.89 | 53.7 | 93.4 |
| 23 | film, thermal[g] | T | 120 | 1.36 | 2.26 | – | 0.50 | 1.23 | 2.46 | 36.8 | 54.4 |
| 24 | film, thermal[g] | T | 240 | 1.36 | 2.26 | – | 0.55 | 1.39 | 2.53 | 40.4 | 61.5 |
| 25 | film, thermal[g] | T | 480 | 1.36 | 2.26 | – | 0.57 | 1.75 | 3.07 | 41.9 | 77.4 |

[a] results based on elemental analysis.
[b] specific surface area (as stated by the manufacturer): 200 Å FPP = 200 m$^2$/g, 100 Å = 300 m$^2$/g.
[c] S = sulfur, SO = selector = tBuCQN.
[d] thermally initiated brush-type material on 5 µm, 120 Å FPP was used as benchmark.
[e] brushtype phases were synthesized on 5 µm 100 Å particles.
[f] solvent assisted film was carried out with additional toluene on particles.
[g] no standard deviation available, as the thermal CSPs were only determined once.

acid (obtained by incubation of formic acid 99% with hydrogen peroxide solution 30%, 95:5 (v/v) in an ice bath for 30 min) were dropwise added under ice cooling and mechanical stirring. After 6 h reaction at room temperature, the modified oxidized silica gel was washed with a mixture of water/methanol (50:50, v/v) until a neutral pH was obtained. After multiple washing steps with hot methanol the material was dried at 60 °C under vacuum.

*2.3.6. Column packing*

All CSPs were slurry packed with the same slurry medium and transport (push) solvent. As transport solvent, HPLC-grade methanol was used. Slurry medium for all CSPs was isopropanol with 10% acetic acid. Concentration was 300 mg CSP in 10 mL slurry medium. The pressure was kept constant at 800 bars and packing was performed for 1 h.

## 3. Results and discussion

### *3.1. Synthesis procedures*

Vinyl ligands are commonly immobilized on thiol-silica by thermally initiated thiol-ene click chemistry using AIBN as radical initiator. The reaction of tBuCQN with 3-mercaptopropyl-silica by this thiol-ene click immobilization leads to a brush-type CSP (CSP # 1) and serves as reference in this work [35,36]. The surface coverage with tBuCQN is typically around 1 µmol/m$^2$ but can be adjusted by the relative concentration of tBuCQN in the reaction mixture resulting in a controlled selector coverage [40].

The above reaction involves the refluxing of a suspension of silica particles (slurry) i.e. the boiling of organic solvent over several hours. From this viewpoint, photoinitiation appeared attractive as it can be performed at ambient temperature i.e. no boiling of organic solvents is needed which may be a safety argument in larger synthesis batches. The idea of using photo-click immobilization was partly also driven by reports that UV-initiated radical addition reactions may occur with short reaction times [41]. Another driving force to use photoreactions may be thermal instability of reaction components which was, however, not the case in this work. For the current photoclick immobilization reaction, the photoinitiator represents a key component. A popular photoinitiator is DMPA (Fig. 2a). DMPA breaks down upon UV light irradiation at its absorption maximum at roughly 330 nm [42] and forms two radicals (namely a benzaldehyde and a (dimethoxy)methylbenzene radical) that can start the reaction by transferring the radical either to the double bond (of the functional ligand; ene component), or to the thiol group of the thiol reactant. Both radical products from the UV-triggered decomposition of DMPA can act as starting agents for the radical addition reaction. After photochemical formation of a thiyl radical, the subsequent hydrothiolation reaction on the C=C bond yields an intermediate carbon-centered radical with following chain transfer to another molecule of thiol [41]. This thiol-ene click reaction gives a product with an anti-Markovnikov configuration (Fig. 2a). Thermal and photoinitiated reactions lead to the same products, yet radical initiators are typically different (azo initiators in case of thermal initiation).

Two generally distinct chemical approaches were pursued. In one approach (PMPMS-bonded), the functional ligand tBuCQN was immobilized via a polythiol film of PMPMS on vinylsilica (Fig. 2b), similar to a procedure introduced by Zimmermann et al. with ther-

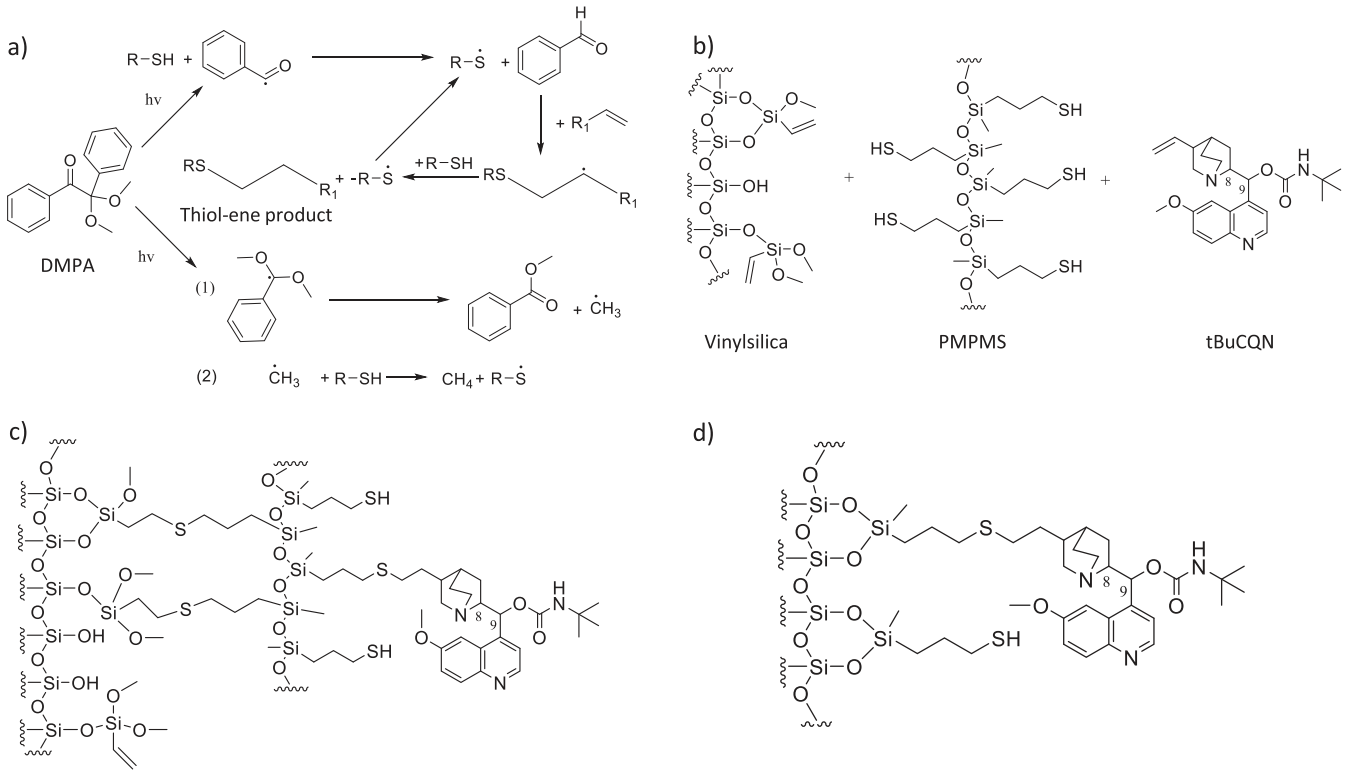


**Fig. 2.** Reaction scheme of the thiol-ene photo-click immobilization. a) UV irradiation-triggered decomposition of the radical photoinitiator 2,2-dimethoxy-2-phenylacetophenone (DMPA) and the propagation to the target molecule. b) Reactants of the PMPMS-bonded approach (vinylized silica particles, crosslinker poly(3-mercaptopropyl)methylsiloxane, PMPMS, functional ligand *tert*–butylcarbamoylquinine, tBuCQN, i.e. the chiral selector). c) Surface chemistry of the resultant PMPMS-bonded CSPs. d) Surface structure of the brush-type CSPs.

mal initiation [43]. Evidently, the two ene components, chiral selector and vinyl groups on the silica surface, are competing for the thiyl radicals formed by UV irradiation from PMPMS. The reaction product is shown in Fig. 2c. In the second approach a brush-type bonding is obtained by immobilization of the ligand tBuCQN on thiol-silica in a methanolic slurry. Fig. 2d shows the structure of the brush-type CSP as resulting from photoinitiated thiol-ene click reaction (CSPs # 2 – 5) as well as in the benchmark obtained by thermal initiated reaction (CSP # 1).

### 3.2. Brush-type CSP by photoclick immobilization

First, brush-type photo-clicked CSPs were prepared by an approach resembling the common synthesis procedure of thermally initiated brush-type CSP. Thus, a slurry of thiol-silica in methanol containing 1.36 µmol/m$^2$ tBuCQN and DMPA was treated with UV light. The reaction time was investigated as experimental variable and the reaction was carried out at ambient temperature in a vented fume hood under stirring. It can be seen in Table 1 that after 30 min a selector coverage of 0.19 µmol/m$^2$ resulted (CSP # 2) corresponding to a 14% yield only. As reaction time was extended, the selector coverage increased (*cf*. CSPs # 2 - 5) reaching 0.41 µmol/m$^2$ (30% yield) after 7 h, corresponding to an equal reaction time used for the synthesis of the thermally initiated brush-type reference CSP. It is evident that under chosen conditions the surface coverage is lower by UV irradiation. The lower reaction temperature can be one of the contributing factors for the lower surface coverage with photo-click reaction. There are certainly several ways to optimize this type of reaction, however, a different approach was then pursued, viz. photo-click immobilization via PMPMS.

### 3.3. Optimization of polythiol-bonded photo-click CSP synthesis

A fractional factorial design has been chosen to find optimal reaction conditions for the optimization of the PMPMS-bonded CSP synthesis. Three distinct approaches were evaluated: i) A slurry method: the vinylsilica was suspended in methanol in which the PMPMS was finely dispersed. tBuCQN and DMPA were dissolved in this reaction mixture and the radical addition reaction initiated by UV irradiation of the suspension. ii) A (solvent-less) film method: the same reaction mixture as in i) was prepared, but before reaction the solvent (MeOH) was completely evaporated. Thereby, the liquid PMPMS formed a thin film on the vinylsilica surface and the photo-reaction proceeded in this thin film that contained the selector and radical initiator. iii) A solvent-assisted film method: In this approach, a small amount of toluene was added to the reaction mixture prepared like in approach i). The methanol in the slurry was completely evaporated while the toluene remained in the reaction mixture. It should support the formation of a more homogenous film of the reaction mixture as well as accelerate reaction kinetics due to lower dynamic viscosity and higher diffusivity of the thiyl radicals in the solvent film.

In the course of the optimization of the reaction conditions, different synthesis batches were prepared, varying in synthesis method (slurry method, film method and solvent-assisted film method), reaction time, and initial concentration of educts as well as initiation type (UV irradiation vs temperature) (see Table 1). The optimization was assisted by DoE software MODDE to find the best compromise in terms of selector coverage, yield and chromatographic performance. Tentative surface morphologies are depicted in Fig. 1a-d. The brush-type phase has relatively regularly ordered and oriented homogeneously distributed selector moieties attached to the silica surface (Fig. 1a). In the PMPMS-bonded slurry method

the polythiol may be attached to the surface as a chain or loop on which the selector moieties are attached (Fig. 1b). In the film methods the PMPMS is bonded horizontally and selector moieties are attached to this polymer film. Since the PMPMS is poorly soluble in methanol it may form an inhomogeneous film or patches on the surface which might be less favorable (Fig. 1c). PMPMS on the other hand is well soluble in toluene. The resultant polymer film is thus deemed to be more homogeneous (Fig. 1d).

*3.3.1. Comparison of synthesis procedures*

Three different synthesis strategies have been tested for the PMPMS-bonded reaction procedure, slurry and film method as well as solvent-assisted film method. Only the general procedure was varied, while other variables were kept identical. For the following comparison of the different synthesis methods, CSP # 6, 7, 21 and 22 are taken into account. Selector coverages (in µmol/m$^2$) were calculated from the nitrogen content of elemental analysis assuming a specific surface area of 200 m$^2$/g (as stated by the silica manufacturer i.e. for sake of simplicity the calculations were based on the initial surface area of the silica). One has to consider that as an inevitable consequence of ligand immobilization, the pore space and consequently specific surface area of the parent silica particles may change significantly, especially when polymeric ligands and cross-linkers are employed like herein, and hence the reported values have to be regarded as approximations of the true surface coverage. However, they should adequately reflect the relative trends which are of interest here. Reaction mixtures were charged with the same initial amount of selector (1.36 µmol/m$^2$) and PMPMS (2.26 µmol/m$^2$). As can be seen from Table 1, for a 120 min reaction time film and slurry methods afforded essentially the same selector coverages (0.44 vs 0.47 µmol/m$^2$) as well as sulfur loadings (1.20 vs 1.18 µmol/m$^2$) which corresponds to around 34% yields for selector bonding and around 53% yields for PMPMS immobilization (*cf.* CSP # 6 and 7). At identical reaction times, the surface coverages of selector and sulfur could be increased to 0.61 and 0.73 µmol/m$^2$ (tBuCQN) as well as 1.89 and 2.11 µmol/m$^2$ (sulfur) (corresponding to yields in the order of 45–54% and 84–93% for tBuCQN and PMPMS, respectively) in presence of 2 and 1 mL toluene, respectively, by the solvent-assisted film method (*cf.* CSP # 21 and 22). The thermally initiated film method provided coverages of 0.50 and 1.23 µmol/m$^2$ for selector and sulfur, respectively, at the same reaction time (120 min) corresponding to 34 and 54% yields (CSP # 23). This is quite comparable to the UV-initiated film method (CSP # 1). On contrary, the UV-initiated brush-type CSP # 4 showed by a factor of ~2 lower immobilization yields.

For evaluation of the chromatographic performance of these newly synthesized CSPs, Fmoc-Phe served as test compound. The *S*-enantiomer was always stronger retained than the *R*-enantiomer. The results of the chromatographic parameters on the different CSPs are summarized in Table 2 along with test conditions. For a deeper insight into peak dispersion contributions in dependence of synthesis parameters, we recorded for each column a Van Deemter (H/u) curve and the coefficients for Eddy diffusion (A-term), longitudinal diffusion (B-term) and mass transfer resistance (C-term) derived by curve fitting using the Van Deemter equation are given in Table 2. It is quite interesting to note that retention factors were systematically lower with the slurry method compared to the film method in spite of similar selector and thiol coverages (*cf.* CSP # 6 - 11 in Tables 1 and 2). Separation factors are comparable (~1.5). The slurry method gives on average slightly better chromatographic efficiency as can be seen from higher theoretical plate numbers ($N_{1,opt}/m$) and lower reduced plate height at optimal flow rate $h_{min}$. The coefficients of the Van Deemter equation clearly reveal a significantly lower mass transfer resistance (C-term) for the slurry method, most probably due to the lower selector coverage, while the A-terms are relatively similar (*cf.* CSP 6 and 7 in Table 2). On the other hand, it is worthwhile to note that the higher selector coverage of the CSPs # 21 and 22 prepared with the solvent-assisted film method is not associated with higher C-term. It seems that the solvent added during the photo-click reaction reduces the dynamic viscosity of the PMPMS film and enhances the diffusivity of the reactants (PMPMS, selector and UV irradiation-triggered radicals) during reaction. The solvent appears to improve both the reaction rates and morphology of the surface coating, possibly leading to a more homogenous, thinner film compared to thick irregular patches without solvent. The results in terms of C-term are comparable to the ones of the thermally initiated film approach (CSP # 23 - 25) although the latter have a lower selector coverage.

*3.3.2. Effect of reaction time*

The solvent-assisted film approach gave the best results in the above described initial tests. However, further optimization experiments with regard to surface coverage, enantioselectivity and chromatographic efficiency focused on film and slurry methods to keep the reaction process simple and avoid the additional influence of the reaction solvent. To figure out the influence of the reaction time on the selector coverages, film and slurry synthesis strategies have been tested with different reaction times between 30 min and 2 h. Results regarding selector and sulfur coverages can be found in Table 1 and corresponding chromatographic performance data in Table 2. Fig. 3 visualizes the major trends in graphical form. Here, it can be seen that the increase in selector and sulfur coverage with reaction time is steeper for the slurry method than the film approach (Fig. 3a and 3b). It mainly tells us that in case of the slurry method the faster bonding rate of PMPMS onto the surface limits the overall selector immobilization efficiency. At 30 min and 1 h reaction time, selector coverages are significantly higher for the film method due to more reactive sulfhydryls on the silica surface (Fig. 3a and 3b). After 3 h of reaction, the selector coverage was, however, comparable as stated above. Also, the ratio of sulfur-to-selector is very similar (Fig. 3c). Fig. 3d shows that the retention factors are plateauing at two distinct levels for film (higher $k$ of around 2.4) and slurry method (lower $k$ at around 1) with little variation in dependence on reaction time. Since plate numbers drop with reaction time, also resolution is smaller with 3 h reaction in case of the film method (Fig. 3e and 3f). Fig. 3f again confirms that chromatographic efficiencies are significantly higher for the slurry method which might have something to do with the specific morphology of the PMPMS film or chains.

*3.3.3. Effect of reactants' concentration*

The initial quantities of reactants and their ratio to each other represent crucial factors for the optimization of the photo-click immobilization process with regard to surface coverage, enantioselectivity and chromatographic efficiency. Consequently, initial amounts of tBuCQN as well as PMPMS in the starting reaction mixture were systematically altered along with reaction time. In order to understand the change of the response (viz. here the tBuCQN surface coverage) in dependence on the investigated factors, a DoE approach using a screening design was utilized. tBuCQN and PMPMS in the reaction mixture and reaction time were continuous variables in the design and the synthesis method (slurry and film approach) were considered as discrete variables. A fractional factorial design Resolution IV was employed. Due to a limited number of experiments a model with linear terms only was evaluated and the coefficients as well as statistical parameters are given in Suppl. Material. The resultant model gives useful trends of the different factors, however, does not have predictive quality which was not the goal of this screening design (note, the inclusion of quadratic terms and model derivation by PLS rather than MLR improved the predictive quality but statistical parameters could

**Table 2**
Summary of the chromatographic results.

| | Reaction conditions | Coverage | | | Chromatographic results[a] | | | | | | | |
|---|---|---|---|---|---|---|---|---|---|---|---|---|
| CSP # | Reaction type | Initiation | Reaction time [min] | tBuCQN [µmol/m²] | $k_1$ | $\alpha_{opt}$[b] | R[c] | $N_{1,opt}/m^2$ | $h_{min}$ | A [$10^{-3}$ mm] | B [$10^{-3}$ mm² $s^{-1}$] | C [$10^{-3}$ s] |
| 1 | Brush-type[d, e] | T | 420 | 1.14 | 3.40 | 1.54 | 4.47 | 61,753 | 3.24 | 8.66 ± 1.64 | 0.76 ± 0.17 | 7.84 ± 0.29 |
| 2 | Brush-type | UV | 30 | 0.19 ± 0.001 | 0.56 | 1.52 | 1.65 | 86,640 | 2.31 | 7.22 ± 0.74 | 2.21 ± 0.13 | 3.88 ± 0.08 |
| 3 | Brush-type | UV | 60 | 0.21 ± 0.002 | 0.49 | 1.52 | 1.22 | 81,900 | 2.44 | 3.39 ± 1.10 | 3.29 ± 0.20 | 6.87 ± 0.13 |
| 4 | Brush-type | UV | 120 | 0.20 ± 0.002 | 0.33 | 1.52 | 1.05 | 75,500 | 2.65 | 4.64 ± 1.72 | 2.68 ± 0.45 | 5.38 ± 0.26 |
| 5 | Brush-type | UV | 420 | 0.41 ± 0.007 | 1.61 | 1.32 | 1.46 | 73,880 | 2.71 | 7.30 ± 0.61 | 2.48 ± 0.11 | 5.95 ± 0.07 |
| 6 | film | UV | 120 | 0.44 ± 0.001 | 0.73 | 1.46 | 1.22 | 61,375 | 3.26 | 7.64 ± 0.65 | 2.32 ± 0.11 | 7.65 ± 0.09 |
| 7 | slurry | UV | 120 | 0.47 ± 0.002 | 0.14 | 1.52 | 0.75 | 76,546 | 2.61 | 9.30 ± 2.12 | 1.87 ± 0.31 | 3.33 ± 0.56 |
| 8 | film | UV | 60 | 0.35 ± 0.010 | 0.62 | 1.48 | 1.24 | 64,055 | 3.12 | 9.1 ± 0.96 | 2.09 ± 0.17 | 6.60 ± 0.11 |
| 9 | slurry | UV | 60 | 0.29 ± 0.014 | 0.18 | 1.51 | 0.80 | 74,087 | 2.70 | 9.00 ± 1.64 | 2.60 ± 0.39 | 3.40 ± 0.34 |
| 10 | film | UV | 30 | 0.34 ± 0.008 | 0.58 | 1.52 | 1.51 | 69,909 | 2.86 | 7.28 ± 2.69 | 6.51 ± 0.48 | 4.36 ± 0.31 |
| 11 | slurry | UV | 30 | 0.14 ± 0.010 | 0.14 | 1.47 | 0.45 | 92,374 | 2.17 | 4.59 ± 2.61 | 3.76 ± 0.98 | 3.54 ± 0.76 |
| 12 | film | UV | 60 | 0.21 ± 0.003 | 0.19 | 1.52 | 0.58 | 54,656 | 3.66 | 9.04 ± 2.71 | 4.07 ± 0.58 | 7.73 ± 0.89 |
| 13 | film | UV | 60 | 0.34 ± 0.004 | 0.50 | 1.50 | 1.32 | 75,227 | 2.66 | 7.66 ± 0.48 | 1.72 ± 0.08 | 4.60 ± 0.07 |
| 14 | film | UV | 60 | 0.22 ± 0.010 | 0.17 | 1.48 | 0.60 | 80,758 | 2.48 | 8.03 ± 2.78 | 2.20 ± 0.41 | 3.89 ± 0.74 |
| 15 | film | UV | 60 | 0.42 ± 0.002 | 0.62 | 1.50 | 1.17 | 55,398 | 3.61 | 9.00 ± 0.85 | 2.72 ± 0.14 | 7.90 ± 0.12 |
| 16 | film | UV | 60 | 0.36 ± 0.000 | 0.41 | 1.55 | 1.12 | 61,975 | 3.23 | 7.00 ± 1.07 | 2.74 ± 0.19 | 6.02 ± 0.12 |
| 17 | slurry | UV | 231 | 0.20 ± 0.003 | 0.33 | 1.38 | 1.00 | 60,320 | 2.82 | 7.72 ± 4.89 | 3.13 ± 1.27 | 5.89 ± 0.62 |
| 18 | slurry | UV | 388 | 0.25 ± 0.000 | 0.52 | 1.32 | 0.80 | 82,040 | 2.44 | 4.89 ± 2.00 | 2.49 ± 0.37 | 6.19 ± 0.28 |
| 19 | film | UV | 376 | 0.62 ± 0.007 | 1.08 | 1.40 | 0.59 | 32,240 | 6.20 | 15.49 ± 1.53 | 1.78 ± 0.20 | 36.41 ± 0.78 |
| 20 | film | UV | 706 | 0.66 ± 0.007 | 0.90 | 1.42 | 0.47 | 24,620 | 8.12 | 23.1 ± 4.40 | 1.33 ± 0.50 | 65.96 ± 3.72 |
| 21 | solvent assisted film[f] | UV | 120 | 0.61 ± 0.005 | 0.70 | 1.44 | 1.95 | 76,500 | 2.61 | 8.85 ± 0.86 | 3.50 ± 0.12 | 3.56 ± 0.10 |
| 22 | solvent assisted film[g] | UV | 120 | 0.73 ± 0.007 | 0.92 | 1.41 | 1.81 | 57,780 | 3.46 | 12.26 ± 1.03 | 2.94 ± 0.18 | 4.55 ± 0.12 |
| 23 | film, thermal[d, g] | T | 120 | 0.50 | 0.74 | 1.51 | 3.00 | 37,620 | 5.32 | 21.59 ± 1.04 | 1.96 ± 0.52 | 4.61 ± 0.13 |
| 24 | film, thermal[d, g] | T | 240 | 0.55 | 0.75 | 1.52 | 3.92 | 66,340 | 3.01 | 9.38 ± 0.72 | 2.87 ± 0.13 | 4.00 ± 0.10 |
| 25 | film, thermal[d, g] | T | 480 | 0.57 | 1.07 | 1.50 | 4.68 | 67,560 | 2.96 | 8.01 ± 0.26 | 2.86 ± 0.45 | 4.14 ± 0.36 |

[a] mob. ph. MeOH/Ac/NH4Ac (98/2/0.5, v/v/w).
[b] index "opt" stands for results at optimum flow rate.
[c] R at a linear flow rate of 5.89 mm/s.
[d] column length for CSPs 1 and 23 - 25: 150 mm.
[e] commercial brush-type material on 5 µm, 120 Å FPP was used as benchmark.
[f] solvent assisted film was carried out with additional toluene on particles.
[g] results for coverages of CSP 23 - 25 taken from Schmitt et al. [39].

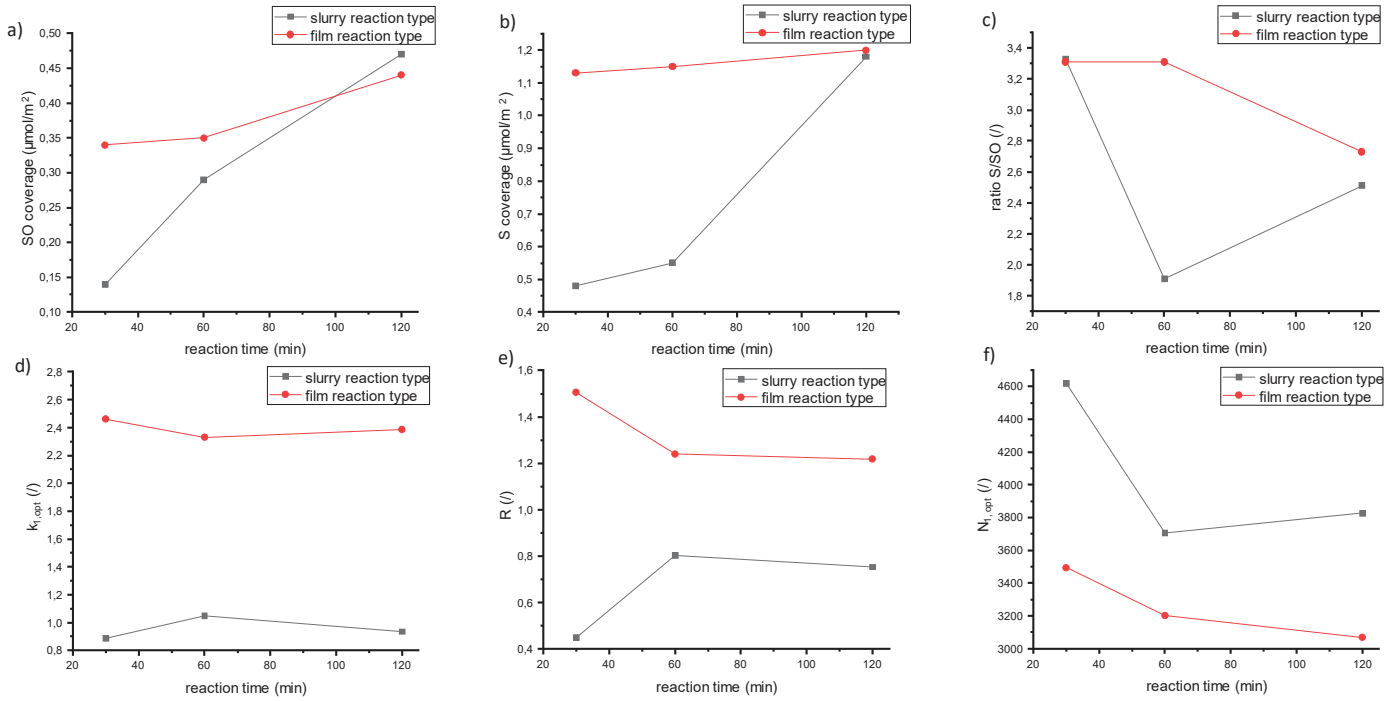


**Fig. 3.** Effect of reaction time on surface coverages of tBuCQN selector (SO) (a), sulfur (S) coverage (b), sulfur (S)/selector (SO) ratio (c), retention factor $k_1$ at optimal flow velocity (d), resolution (e), column plate number (at optimal flow velocity) ($L$ = 5 cm) (f) for slurry and film method. The data correspond to CSPs # 6 – 11.

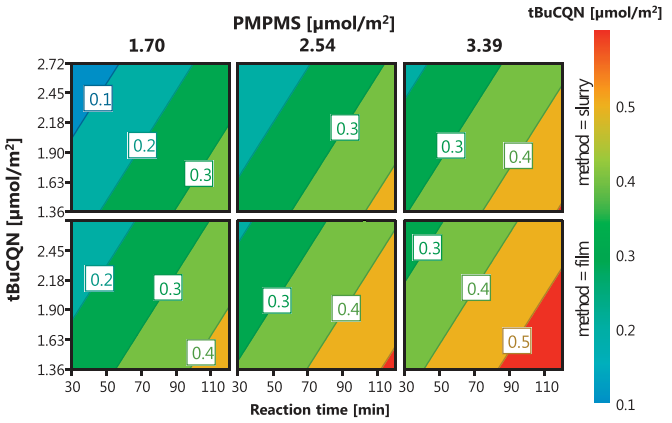


**Fig. 4.** DoE optimization for the synthesis of the chiral stationary phase considering 4 factors, tBuCQN and PMPMS concentrations, reaction time and synthesis approach (film as well as slurry method). The top panels show the response surfaces (tBuCQN coverage) for the slurry method, the bottom panels for the film method.

not be comprehensively evaluated). Response surfaces for the linear model are depicted in Fig. 4. They show that the surface coverage increases with reaction time and PMPMS amount in the reaction mixture. On contrary, the model also reveals that a higher selector concentration in the reaction mixture leads to lower surface coverage, which is a bit counterintuitive at first glance. It may, however, be explained by increasing modification of the thiols of PMPMS by the selector so that these thiols are not available for surface grafting anymore. From this viewpoint this result also makes sense because of the competitive nature of reactions taking place. An initial weight ratio of 2.5 of sulfur (PMPMS) and selector seems to be most promising with the chosen conditions.

### 3.4. Chromatographic performance

A summary of the chromatographic performance of the synthesized CSPs is given in Table 2. In general, the main goal of the development of a useful CSP is to obtain sufficient enantioselectivity and good chromatographic performance, i.e. low plate height. This does not necessitate a high selector coverage. However, a certain concentration of chiral selector is needed. As can be seen from Table 2, the average separation factor of all synthesized columns is 1.47 (± 0.06) which corresponds to an RSD of 4.4% while selector coverages and retention factors show variances of 43.7% and 93.5% RSD, respectively. Even the CSP with the lowest selector coverage (CSP # 11) having grafted 0.14 µmol/m$^2$ of tBuCQN only gives a separation factor of 1.47. The chromatographic efficiency seems to depend on several factors, amongst others on the method of immobilization but to some extent also on the surface coverage. It is interesting to note that the C-term is smaller for the slurry method as compared to the film method in the experiments of direct comparison (CSP # 6 vs 7, 8 vs 9, and 10 vs 11). Overall, reduced plate heights in the order of 2 to 4 are decent but can be certainly further improved. In particular, column packing may need systematic optimization, as can be deduced from the A-terms (see Table 2).

Fig. 5 depicts a comparison of test chromatograms of Fmoc-Phe-obtained with CSPs prepared by distinct approaches. Note that Fig. 5a) as well as Fig. 5c) were recorded with a 150 mm long column while all other chromatograms were recorded with 50 mm long columns. All columns were based on 5 µm particles. The mobile phase for all chromatograms was methanol/acetic acid/ammonium acetate (98/2/0.5, v/v/w), and all chromatograms were recorded at the optimal linear velocity of 0.88 mm/s. It can be seen that the brush-type phase synthesized by thermally initiated click reaction (CSP # 1) gives symmetrical peaks with reduced minimal plate height $h_{min}$ of 3.24 and 61,753 plates/m (Fig. 5a). The corresponding photo-clicked brush-type CSP with the same 7 h reaction time (CSP # 5) produced 73,890 plates/m and provided a $h_{min}$ of 2.71. The peak width at half height looks better which may be related to the significantly lower selector coverage (0.40 and 1.14 µmol/m$^2$ for CSP # 5 and 1, respectively). Peak widths at the basis are, unfortunately, a bit unfavorable for the photo-initiated brush phase and may indicate a sub-optimal column packing. Optimization of column packing may overcome this problem but was not performed in this work because CSPs were synthesized in small quantities only. Another option for improving the peak shape is to oxidize residual thiols and thioethers (vide infra). Figs. 5c) to 5e) show test chromatograms of the thermally initiated (CSP # 23) and UV-initiated film synthesis method (CSP # 6) as well as UV-initiated slurry approach (CSP # 7). In spite of comparable selector coverages of 0.47 (± 0.03) µmol/m$^2$, chromatographic parameters are significantly different. For example, the slurry method furnished columns with much less retention (as mentioned above). The chromatographic efficiency increased from 37,620/m ($h_{min}$ 5.32) for CSP # 23 (thermal initiation, film), to 61,375/m ($h_{min}$ 3.26) for CSP # 6 (UV initiation, film) to 76,546/m ($h_{min}$ 2.61) for CSP # 7 (UV initiation, slurry). The UV-initiated solvent-assisted film method (Fig. 5f, CSP # 21) gave slightly better performance in terms of peak width at half height compared to the approach without toluene (Fig. 5d, CSP # 6) (76,500 plates/m; $h_{min}$ 2.61).

The lower selector coverages of the CSPs synthesized by photo-click immobilization in combination with the employed standard mobile phase (methanol/acetic acid/ammonium acetate, 98/2/0.5, v/v/w) led to small retention factors. However, simple dilution of this mobile phase with MeOH to reduce the ionic strength and counterion concentration of the mobile phase afforded a significantly weaker eluent and appropriate retention factors (Fig. 6). A 1:20 and 1:40 (v/v) diluted mobile phase provided baseline separations of Fmoc-Phe-on CSP # 7 prepared by UV-initiated slurry method (Fig. 6b and c) and allowed to adjust largely equivalent separations to the brush-type benchmark on CSP # 6 prepared by UV-initiated film method (Fig. 6d–f). The diluted mobile phases render elution conditions better compatible with mass spectrometry and electrospray ionization, respectively.

The chromatographic data in Table 2 were derived from experiments with the same mobile phase. Due to distinct retention factors perfect comparability may be compromised. Thus, CSPs prepared by UV- and thermally initiated click immobilization by film approach (CSP # 10 and 24, respectively) were compared using isoeluotropic conditions, i.e. equal retention factor adjusted by mobile phase dilution, with regard to their Van Deemter curves (Fig. 7). It can be seen that CSP # 24 (thermally initiated film method) shows slight superiority in terms of chromatographic efficiency. The mass transfer resistance term (C-term) is slightly smaller for the thermally initiated method. This might be caused by the inability of the UV light rays to penetrate deeply into the pores of the silica to start the immobilization process. Especially when applying the film method, diffusion of the radicals and the photoinitiator's decomposition products that are formed on the better accessible outer surface of the silica into the pores is limited due to poor diffusivity in the viscous polymer film. Hence, at ambient temperature the selector bonding to the vinyl silica surface inside the pores is inefficient and the surface might be chemically more heterogeneous as compared to reaction at higher temperature of the thermally initiated process. However, both columns show a comparable minimum in reduced plate height (3.83 for CSP # 10, 3.01 for CSP # 24 (both for isoelutropic conditions, values for reduced plate height with undiluted mobile phase: 2.86 for CSP # 10, 3.01 for CSP # 24)).

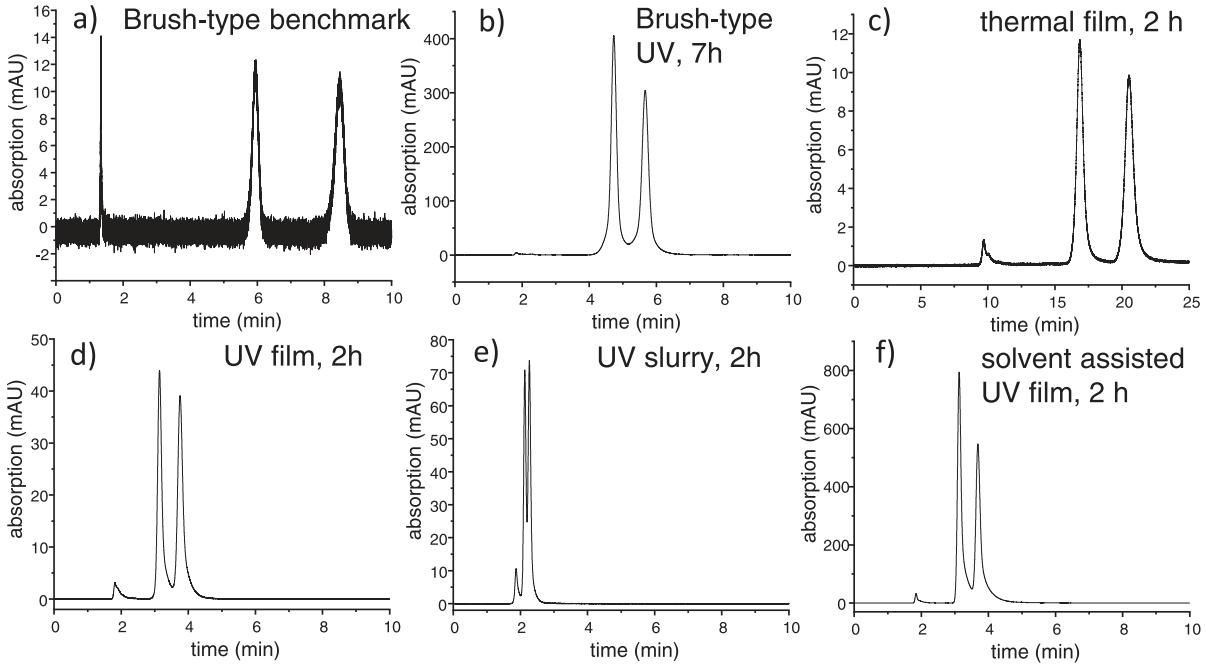


**Fig. 5.** Representative chromatograms for the distinct synthesis approaches. (a) Brush-type benchmark obtained by thermally initiated thiol-ene click immobilization (CSP # 1). (b) UV-initiated brush-type CSP (CSP # 5), (c) thermally initiated PMPMS-bonded film method (2 h reaction time) (CSP # 23), (d) UV-initiated PMPMS-bonded film method (2 h reaction) (CSP # 6), (e) UV-initiated PMPMS-bonded slurry method (2 h) (CSP # 7), (f) solvent-assisted UV-initiated PMPMS-bonded film method with 2 mL toluene (CSP # 21). All chromatograms were recorded with methanol/acetic acid/ammonium acetate (98/2/0.5, v/v/w) as mobile phase and Fmoc-Phe-as analyte. Flow rate for all chromatograms is 0.15 ml/min. Column length 150 mm (a,c) and 50 mm (b,d,e,f), respectively.

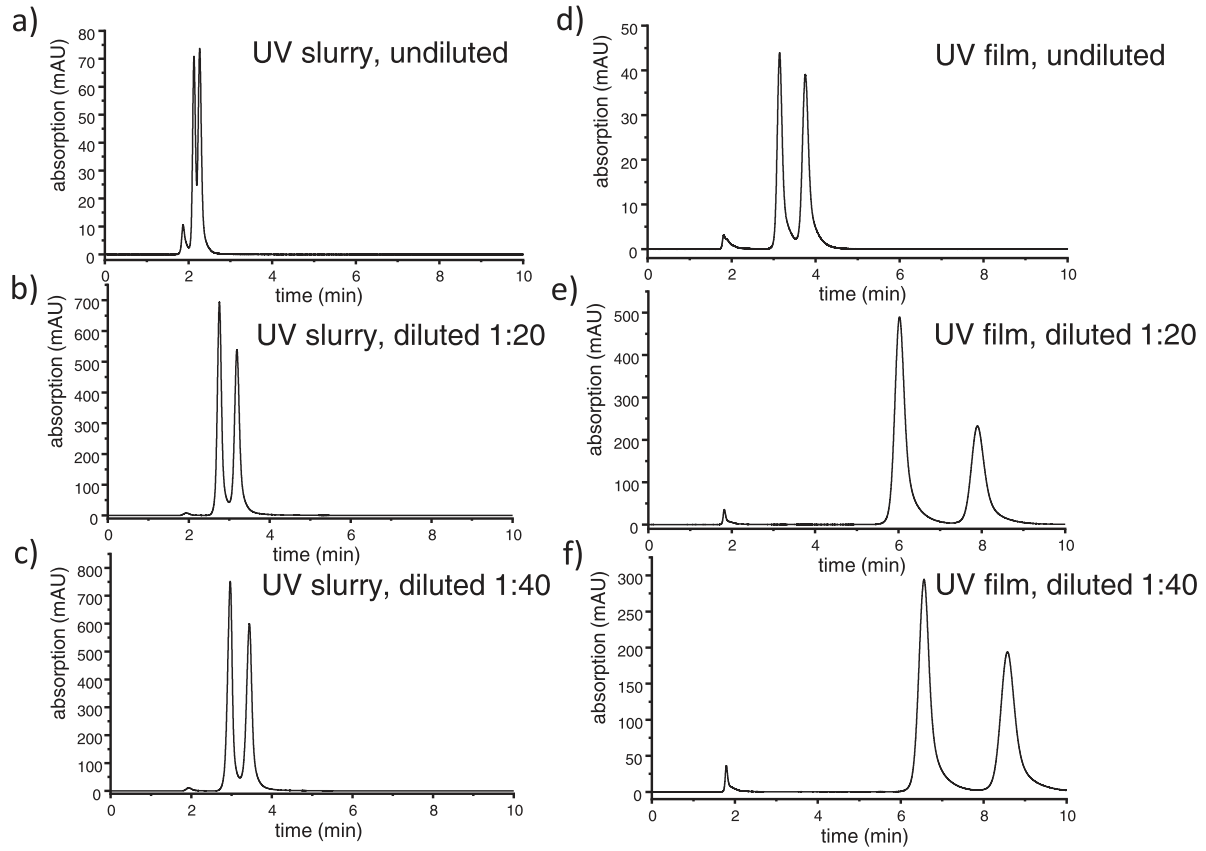


**Fig. 6.** Effect of ionic strength (mobile phase dilution) on separation of Fmoc-Phe-on PMPMS-bonded CSP synthesized by UV-initiated slurry method (CSP # 7) (a,b,c) and by UV-initiated film method (CSP # 6) (d,e,f) (reaction time 120 min for both). Eluents, methanol/acetic acid/ammonium acetate (98/2/0.5, v/v/w) (a,d), 1:20 diluted (b,e) and 1:40 diluted mobile phase (c,f). Flow rate for all chromatograms was 0.15 ml/min, detection at 254 nm.

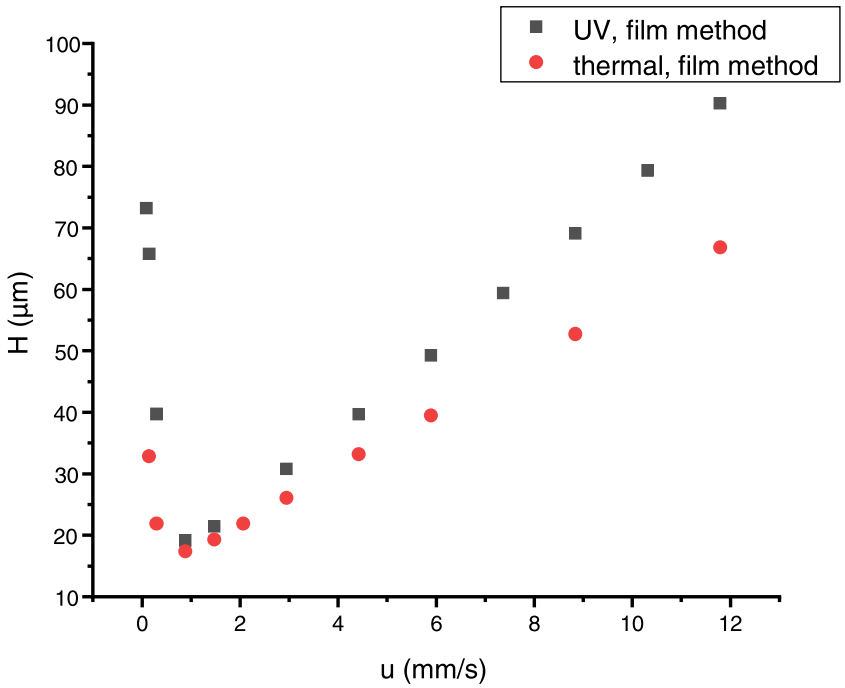


**Fig. 7.** Comparison of efficiencies (Van Deemter curves) of PMPMS-bonded CSPs prepared by UV-initiated (CSP # 10) and thermally initiated film method (CSP # 24) at isoeluotropic conditions. Mobile phase was methanol/acetic acid/ammonium acetate (98/2/0.5, v/v/w) for thermally initiated CSP, and (99.74/0.26/0.065, v/v/w) for UV-initiated CSP.

As indicated above, oxidation of the surface to modify residual thiols into sulfonic acid groups and thioethers into sulfons is a simple strategy to improve peak shapes. It seems that the presence of sulfonate groups minimizes secondary interactions which translates into more symmetrical peaks as is documented by a comparison of non-oxidized and oxidized CSP # 22 (see Fig. 8). The solvent-assisted photoclick synthesized non-oxidized CSP # 22 shows an ugly peak asymmetry as the material is a bit sticky during column packing (Fig. 8a). In contrast, the oxidized CSP # 22 obtained by treatment with performic acid shows perfect peak symmetry (Fig. 8b).

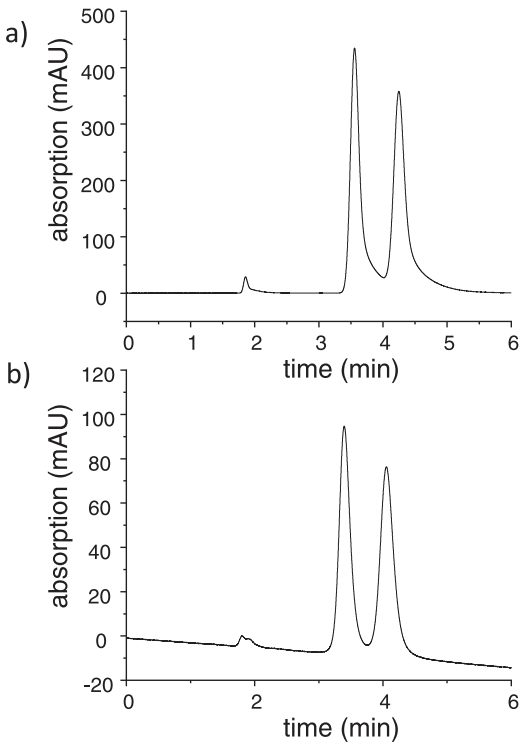


**Fig. 8.** Comparison of peak symmetry obtained with (a) non-oxidized CSP # 22, and (b) oxidized CSP # 22. Conditions: (a) Mobile phase, methanol/acetic acid/ammonium acetate (98/2/0.5, v/v/w), and (b) with isoelutropic conditions, i.e. mobile phase of (a) diluted with methanol (50:50; v/v); flow rate, 0.15 mL/min (a and b).

Overall, the thermal immobilization methods seem to be superior than photo-click immobilization in the current version. However, photochemical methods might become an interesting alternative to the thermal methods, if some specific limitations as outlined in the Conclusions (vide infra) can be addressed successfully.

## 4. Conclusions

In this work, we presented the proof-of-principle of thiol-ene photo-click immobilization of a chiral vinyl ligand on silica particles. Distinct approaches of linking chemistries were evaluated comprising brush-type bonding of the ligand to thiol silica and its bonding to vinylsilica via a polythiol crosslinker. Brush-type photo-click immobilization yielded lower selector coverages as compared to polythiol-mediated photo-click immobilization. Photoclick immobilization of the selector via coated polythiol film yielded about the same surface coverage as compared to the approach in which all reactants including polythiol were suspended in the slurry of vinyl-silica. In spite of similar selector coverages, the former showed stronger retention for a chiral acidic probe. A solvent-assisted film approach with toluene allowed to enhance yields of the immobilization reaction to ~90% for thiol and ~50% for selector. Separation factors achieved with the distinct approaches were relatively constant (1.47 ± 0.6), but retention factors differed significantly when identical mobile phases were applied. Resultant phases with low coverage and low retention, respectively, required adjustment of the ionic strength in the mobile phase. Overall, useful CSPs were obtained but the procedure has certainly some room for further improvements. For example, the photoinitiator should be fine-tuned. Its absorbance maximum should not overlap with

absorbance bands of the selector, so that the UV light is more efficiently exploited for generation of radicals. It is expected that reaction rates can then be accelerated. The light source might be another factor for optimization and the transmittance of the reaction vessel should also be considered. To what extent the UV light permeates the silica particles is unclear. However, it is known that toluene and xylene make porous silica translucent which could be beneficial in terms of local radical concentrations inside the pores. The solvent-assisted film approach has some potential for further optimization in this regard. While the application of temperature may be favourable in terms of homogeneity of the coated film, the UV-initiated process at ambient temperature is regarded a mild and safe process, worth to be considered as alternative.

## Declaration of Competing Interest

The authors declare that they have no known competing financial interests or personal relationships that could have appeared to influence the work reported in this paper.

## Supplementary materials

Supplementary material associated with this article can be found, in the online version, at doi:10.1016/j.chroma.2020.461133.

## CRediT authorship contribution statement

**Christian Geibel:** Investigation, Methodology, Formal analysis, Data curation, Visualization, Writing - original draft, Writing - review & editing. **Kristina Dittrich:** Investigation, Data curation, Writing - review & editing. **Marc Wolter:** Investigation, Writing - review & editing. **Michael Lämmerhofer:** Conceptualization, Methodology, Supervision, Writing - review & editing, Resources.

## References

[1] X. Liang, A. Shen, Z. Guo, The application of thiol-ene/yne radical click chemistry in surface modification and functionalization, in: A. Lowe, C. Bowman (Eds.), Thiol-X Chemistries in Polymer and Materials Science, Royal Society of Chemistry, 2013, pp. 286–308.
[2] L.F. Ribeiro, J.C. Masini, F. Svec, Use of thiol functionalities for the preparation of porous monolithic structures and modulation of their surface chemistry: a review, Trends Anal. Chem. 118 (2019) 606–624.
[3] C. Rosini, C. Bertucci, D. Pini, P. Altemura, P. Salvadori, Cinchona alkaloids for preparing new, easily accessible chiral stationary phases. I. 11-(10,11-Dihydro-6′-methoxycinchonan-9-ol)-thiopropylsilanized silica, Tetrahedron Lett. 26 (1985) 3361–3364.
[4] E. Veigl, B. Böhs, A. Mandl, D. Krametter, W. Lindner, Evaluation of silica gel-based brush type chiral cation exchangers with (S)-N-(3,5-dinitrobenzoyl)tyrosine as chiral selector: attempt to interpret the discouraging results, J. Chromatogr. A 694 (1995) 151–161.
[5] A. Tambute, L. Siret, A. Begos, M. Caude, Improvement of the enantiorecognition ability of tyrosine-derived chiral stationary phases: direct resolution of 1,2-amino-alcohols ($\beta$-blockers), Chirality 4 (1992) 36–42.
[6] M. Lämmerhofer, W. Lindner, Quinine and quinidine derivatives as chiral selectors. I. Brush type chiral stationary phases for high-performance liquid chromatography based on cinchonan carbamates and their application as chiral anion exchangers, J. Chromatogr. A 741 (1996) 33–48.
[7] J. Horak, W. Lindner, Investigations on the chromatographic behavior of hybrid reversed-phase materials containing electron donor–acceptor systems: I. Contribution of sulfur–aromatic interactions, J. Chromatogr. A 1043 (2004) 177–194.
[8] R. Nogueira, M. Lämmerhofer, W. Lindner, Alternative high-performance liquid chromatographic peptide separation and purification concept using a new mixed-mode reversed-phase/weak anion-exchange type stationary phase, J. Chromatogr. A 1089 (2005) 158–169.
[9] B. Preinerstorfer, W. Bicker, W. Lindner, M. Lämmerhofer, Development of reactive thiol-modified monolithic capillaries and in-column surface functionalization by radical addition of a chromatographic ligand for capillary electrochromatography, J. Chromatogr. A 1044 (2004) 187–199.
[10] A. Shen, Z. Guo, L. Yu, L. Cao, X. Liang, A novel zwitterionic hilic stationary phase based on "thiol-ene" click chemistry between cysteine and vinyl silica, Chem. Commun. 47 (2011) 4550–4552.
[11] E.J. Carrasco-Correa, M. Ferri, U. Woiwode, Y. Ma, J.M. Herrero-Martinez, G. Ramis-Ramos, W. Lindner, M. Lämmerhofer, Zwitterionic codeine-derived methacrylate monoliths for enantioselective capillary electrochromatography of chiral acids and chiral bases, Electrophoresis 39 (2018) 2558–2565.
[12] M. Kohout, S. Wernisch, J. Tuma, H. Hettegger, J. Picha, W. Lindner, Effect of different immobilization strategies on chiral recognition properties of cinchona-based anion exchangers, J. Sep. Sci. 41 (2018) 1355–1364.
[13] M. De Martino, G. Bencivenni, A. Mazzanti, S. Menta, O.H. Ismail, R. Sabia, A. Ciogli, 3,5-Dinitrobenzoyl-9-amino-9-deoxy-9-epiquinine as pirkle-anion exchange hybrid-type chiral selector in high-performance liquid chromatography, Chromatographia 80 (2017) 751–762.
[14] L. Qiao, H. Li, Y. Shan, S. Wang, X. Shi, X. Lu, G. Xu, Study of surface-bonded dicationic ionic liquids as stationary phases for hydrophilic interaction chromatography, J. Chromatogr. A 1330 (2014) 40–50.
[15] A.F.G. Gargano, T. Leek, W. Lindner, M. Lämmerhofer, Mixed-mode chromatography with zwitterionic phosphopeptidomimetic selectors from UGI multicomponent reaction, J. Chromatogr. A 1317 (2013) 12–21.
[16] L. Qiao, A. Dou, X. Shi, H. Li, Y. Shan, X. Lu, G. Xu, Development and evaluation of new imidazolium-based zwitterionic stationary phases for hydrophilic interaction chromatography, J. Chromatogr. A 1286 (2013) 137–145.
[17] A. Shen, X. Li, X. Dong, J. Wei, Z. Guo, X. Liang, Glutathione-based zwitterionic stationary phase for hydrophilic interaction/cation-exchange mixed-mode chromatography, J. Chromatogr. A 1314 (2013) 63–69.
[18] Q. Wang, Y. Long, L. Yao, L. Xu, Z.-.G. Shi, L. Xu, Preparation, characterization and application of a reversed phase liquid chromatography/hydrophilic interaction chromatography mixed-mode C18-DTT stationary phase, Talanta 146 (2016) 442–451.
[19] C. Xiong, J. Yuan, Z. Wang, S. Wang, C. Yuan, L. Wang, Preparation and evaluation of a hydrophilic interaction and cation-exchange chromatography stationary phase modified with 2-methacryloyloxyethyl phosphorylcholine, J. Chromatogr. A 1546 (2018) 56–65.
[20] T.T.H. Dao, M. Guerrouache, B. Carbonnier, Thiol-yne click adamantane monolithic stationary phase for capillary electrochromatography, Chin. J. Chem. 30 (2012) 2281–2284.
[21] E.P. Shields, S.G. Weber, A liquid chromatographic charge transfer stationary phase based on the thiol-yne reaction, J. Chromatogr. A 1591 (2019) 1–6.
[22] P. Jonkheijm, D. Weinrich, M. Köhn, H. Engelkamp, P.C.M. Christianen, J. Kuhlmann, J.C. Maan, D. Nüsse, H. Schroeder, R. Wacker, R. Breinbauer, C.M. Niemeyer, H. Waldmann, Photochemical surface patterning by the thiol-ene reaction, Angew. Chem. Int. Ed. 47 (2008) 4421–4424.
[23] C. Wendeln, S. Rinnen, C. Schulz, H.F. Arlinghaus, B.J. Ravoo, Photochemical microcontact printing by thiol-ene and thiol-yne click chemistry, Langmuir 26 (2010) 15966–15971.
[24] E. Melnik, P. Muellner, O. Bethge, E. Bertagnolli, R. Hainberger, M. Lämmerhofer, Streptavidin binding as a model to characterize thiol-ene chemistry-based polyamine surfaces for reversible photonic protein biosensing, Chem. Commun. 50 (2014) 2424–2427.
[25] H. Zhang, J. Ou, Z. Liu, H. Wang, Y. Wei, H. Zou, Preparation of hybrid monolithic columns via “One-Pot” photoinitiated thiol–acrylate polymerization for retention-independent performance in capillary liquid chromatography, Anal. Chem. 87 (2015) 8789–8797.
[26] C. Kip, C. Demir, A. Tuncel, One pot synthesis of carboxyl functionalized-polyhedral oligomeric siloxane based monolith via photoinitiated thiol-methacrylate polymerization for nano-hydrophilic interaction chromatography, J. Chromatogr. A 1502 (2017) 14–23.
[27] Y. Wang, S. Ma, Y. Chen, L. Zhang, J. Ou, Y. Shen, M. Ye, Thiol-radical-mediated polymerization for preparation of POSS-containing polyacrylate monoliths in capillary liquid chromatography, Talanta 190 (2018) 62–69.
[28] C. Kip, S. Liu, X. Fu, A. Tuncel, M. Lämmerhofer, In-situ photopolymerized C4-functionalized organosilicon monoliths for reversed-phase protein separation in nano-liquid chromatography, Talanta 198 (2019) 330–336.
[29] Y. Wang, S. Ma, L. Zhang, N. Zhang, Y. Li, J. Ou, Y. Shen, M. Ye, Fast fabrication of a hybrid monolithic column containing cyclic and aliphatic hydrophobic ligands via photo-initiated thiol-ene polymerization, J. Sep. Sci. 42 (2019) 1332–1340.
[30] M. Li, X. Lei, Y. Huang, Y. Guo, B. Zhang, F. Tang, X. Wu, Ternary thiol-ene photopolymerization for facile preparation of ionic liquid-functionalized hybrid monolithic columns based on polyhedral oligomeric silsesquioxanes, J. Chromatogr. A 1597 (2019) 167–178.
[31] H. Zhang, S. Ma, Y. Yao, Y. Li, Y. Li, J. Ou, M. Ye, Y. Wei, Facile preparation of multi-functionalized hybrid monoliths via two-step photo-initiated reactions for two-dimensional liquid chromatography-mass spectrometry, J. Chromatogr. A 1524 (2017) 135–142.
[32] M.B. Espina-Benitez, J. Randon, C. Demesmay, V. Dugas, Development of a new in-line coupling of a miniaturized boronate affinity monolithic column with reversed-phase silica monolithic capillary column for analysis of cis-diol-containing nucleoside compounds, J. Chromatogr. A 1597 (2019) 209–213.
[33] X. Wang, J. Peng, H. Peng, J. Chen, H. Xian, R. Ni, S. Li, D. Long, Z. Zhang, Preparation of two ionic liquid bonded stationary phases and comparative evaluation under mixed-mode of reversed phase/ hydrophilic interaction/ ion exchange chromatography, J. Chromatogr. A 1605 (2019) 460372.
[34] A.V. Bordoni, M.V. Lombardo, A. Wolosiuk, Photochemical radical thiol–ene click-based methodologies for silica and transition metal oxides materials chemical modification: a mini-review, RSC Adv. 6 (2016) 77410–77426.
[35] A. Mandl, L. Nicoletti, M. Lämmerhofer, W. Lindner, Quinine- versus carbamoylated quinine-based chiral anion exchangers: a comparison regarding enantioselectivity for N-protected amino acids and other chiral acids, J. Chromatogr. A 858 (1999) 1–11.

[36] N. Maier, L. Nicoletti, M. Lämmerhofer, W. Lindner, Enantioselective anion exchangers based on cinchona alkaloid-derived carbamates: influence of C8/C9 stereochemistry on chiral recognition, Chirality 11 (1999) 522–528.
[37] T. Teerlink, Derivatization of posttranslationally modified amino acids, J. Chromatogr. B Biomed. Sci. Appl. 659 (1994) 185–207.
[38] I.S. Krull, Z. Deyl, H. Lingemann, General strategies and selection of derivatization reactions for liquid chromatography and capillary electrophoresis, J. Chromatogr. B Biomed. Sci. Appl. 659 (1994) 1–17.
[39] K. Schmitt, M. Lämmerhofer, Optimization of the surface modification process of cross-linked polythiol-coated chiral stationary phases synthesized by a two-step thiol-ene click reaction, J. Sep. Sci. 41 (2018) 1338–1345.
[40] P. Levkin, N. Maier, W. Lindner, V. Schurig, A practical method for the quantitative assessment of non-enantioselective versus enantioselective interactions encountered in liquid chromatography on brush-type chiral stationary phase, J. Chromatogr. A 1269 (2012) 270–278.
[41] A.B. Lowe, Thiol-ene “click” reactions and recent applications in polymer and materials synthesis, Polym. Chem. 1 (2010) 17–36.
[42] N.F. Ayub, S. Hashim, J. Jamaluddin, N. Adrus, New UV LED curing approach for polyacrylamide and poly(N-isopropylacrylamide) hydrogels, New J. Chem. 41 (2017) 5613–5619.
[43] A. Zimmermann, J. Horak, A. Sievers-Engler, C. Sanwald, W. Lindner, M. Kramer, M. Lämmerhofer, Surface-crosslinked poly(3-mercaptopropyl)methylsiloxane-coatings on silica as new platform for low-bleed mass spectrometry-compatible functionalized stationary phases synthesized via thiol-ene click reaction, J. Chromatogr. A 1436 (2016) 73–83.

## VII.2 Publication II – Supplementary Material

# Thiol-ene photo-click immobilization of a chiral chromatographic ligand on silica particles

Christian Geibel [a], Kristina Dittrich [a], **Marc Wolter** [a], Michael Lämmerhofer [a,*]

[a] Institute of Pharmaceutical Sciences, Pharmaceutical (Bio-)Analysis, University of Tübingen, Auf der Morgenstelle 8, 72076 Tübingen, Germany

* corresponding author

# Table of contents

# PART I: Chromatographic evaluation

**Table S1a**. Summary of the chromatographic results with diluted mobile phase.

| | | starting conditions | | | | | |
|---|---|---|---|---|---|---|---|
| CSP # | reaction type | reaction time [min] | initial weight [mmol][1] | | initial weight [µmol/m$^2$] | | dilution factor of mob. phase[2] |
| | | | tBuCQN | PMPMS | tBuCQN | PMPMS | |
| 1 | Film | 120 | 0.136 | 0.226 | 1.36 | 2.26 | no dilution |
| | | | | | | | 01:20 |
| | | | | | | | 01:40 |
| 2 | Slurry | | | | | | no dilution |
| | | | | | | | 01:20 |
| | | | | | | | 01:40 |

[1] all initial weights based on 0.5 g vinylated silica

[2] dilution was performed with methanol to obtain lower amounts of additives

**Table S1b**. Summary of the chromatographic results with diluted mobile phase.

| | | chromatographic results[3] | | | | | | | | | |
|---|---|---|---|---|---|---|---|---|---|---|---|
| CSP # | dilution factor of mob. phase[2] | $k_1$ | $\alpha_{opt}$[4] | $R_{opt}$[4] | $R_{5.89mm/s}$[5] | $N_{1,\,opt}$[4] | $N_{1,\,opt}/m$[4] | $h_{min}$ | A [$10^{-3}$mm] | B [$10^{-3}$mm$^2$ s$^{-1}$] | C [$10^{-3}$s] |
| 1 | no dilution | 0.73 | 1.46 | 2.39 | 1.22 | 3069 | 61375 | 3.26 | 7.64 ± 0.65 | 2.32 ± 0.11 | 7.65 ± 0.09 |
| | 01:20 | 2.31 | 1.45 | 3.51 | 1.97 | 2810 | 56200 | 3.56 | 12.14 ± 1.39 | 2.43 ± 0.25 | 6.68 ± 0.16 |
| | 01:40 | 2.66 | 1.42 | 3.53 | 2.02 | 2865 | 57300 | 3.49 | 11.71 ± 1.12 | 2.62 ± 0.20 | 6.18 ± 0.13 |
| 2 | no dilution | 0.14 | 1.52 | 0.94 | 0.75 | 3827 | 76546 | 2.61 | 9.30 ± 2.12 | 1.87 ± 0.31 | 3.33 ± 0.56 |
| | 01:20 | 0.42 | 1.53 | 2.05 | 1.30 | 3278 | 65560 | 3.05 | 7.50 ± 0.73 | 2.90 ± 0.13 | 5.02 ± 0.85 |
| | 01:40 | 0.53 | 1.46 | 2.01 | 1.28 | 2920 | 58400 | 3.43 | 10.95 ± 0.43 | 3.29 ± 0.77 | 4.53 ± 0.49 |

[3] mob. ph. MeOH/Ac/$NH_4$Ac (98/2/0.5, v/v/w) or diluted as stated

[4] index "opt" stands for results at optimum flow rate

[5] R at a linear flow rate of 5.89 mm/s

## PART II: Design of experiment

**Table S2.** Summary of the statistic parameters of the selector coverage prediction versus the observed results.

| SO coverage | Coeff. SC | Standard Error | P | Conf. Int. (±) |
|---|---|---|---|---|
| Constant | 619,202 | 480,811 | 1.35E-01 | 117,651 |
| time | 210,695 | 536,969 | 0,00776799 | 131,392 |
| initial weight SO | -128,383 | 404,345 | 0,0191948 | 989,405 |
| initial weight linker | 131,014 | 536,968 | 0,0504793 | 131,392 |
| method (DF = 1) | | | | |
| film | 794,366 | 404,345 | 0,0970777 | 989,405 |
| slurry | -794,366 | 404,345 | 0,0970777 | 989,405 |

N = 11, DF = 6, R2 = 0.846, RSD = 11.01

red = values higher than p = 0.05

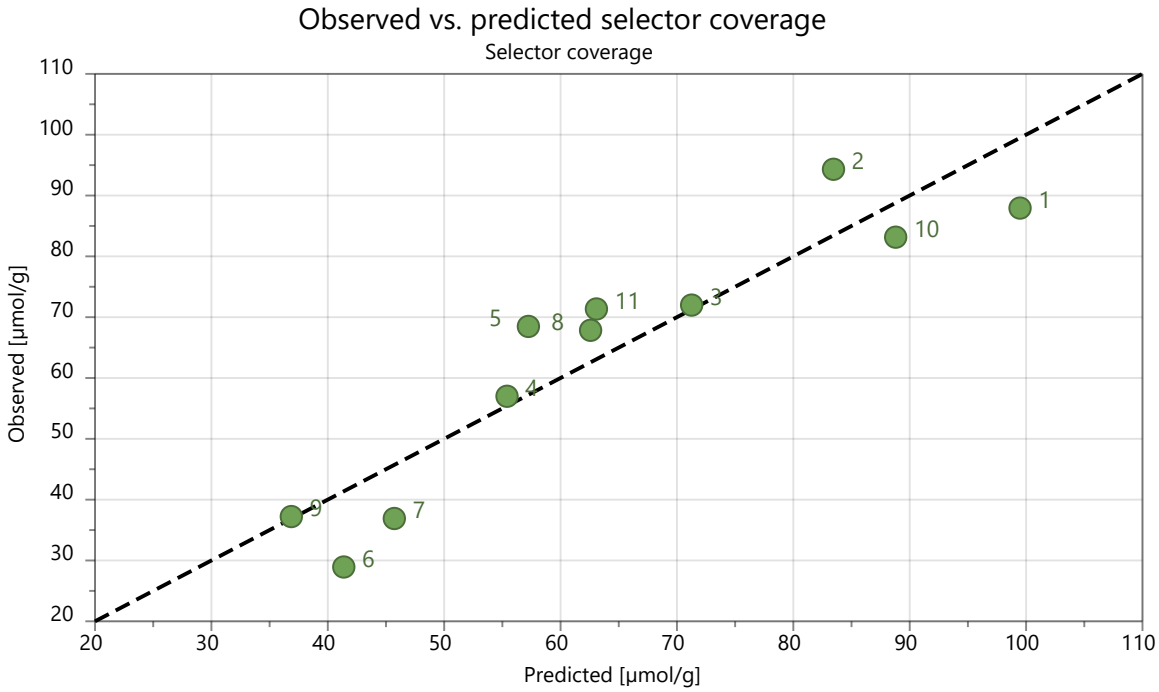


**Fig. S1.** Observed vs predicted selector coverage as calculated by MODDE Pro Ver. 12.1.0.5491 from Sartorius Stedim (Umeå, Sweden). Note that the numbers refer to the CSPs 6 - 16 from table 1 and 2.

# VIII. CHAPTER FOUR

## Preparation and characterization of poly(3-mercaptopropyl)methylsiloxane functionalized silica particles and their further modification for silver ion chromatography and enantioselective high-performance liquid chromatography

## VIII.1 Publication III – Main Document

Journal of Chromatography A 1643 (2021) 462069

Contents lists available at ScienceDirect

Journal of Chromatography A

journal homepage: www.elsevier.com/locate/chroma

# Preparation and characterization of poly(3-mercaptopropyl)methylsiloxane functionalized silica particles and their further modification for silver ion chromatography and enantioselective high-performance liquid chromatography

Marc Wolter[a], Xingyu Chen[a], Ulrich Woiwode[a,b], Christian Geibel[a], Michael Lämmerhofer[a,*]

[a] Institute of Pharmaceutical Sciences, Pharmaceutical (Bio-)Analysis, University of Tübingen, Auf der Morgenstelle 8, 72076 Tübingen, Germany
[b] TECHPharm GmbH, Draisstraße 14, 76646 Bruchsal, Germany

ARTICLE INFO

*Article history:*
Received 6 February 2021
Revised 10 March 2021
Accepted 11 March 2021
Available online 15 March 2021

*Keywords:*
Polythiol-functionalized silica
Polysiloxane-coated silica particles
Thiol-ene click reaction
Thiol-disulfide exchange reaction
Silver ion (argentation) chromatography
Chiral separation

ABSTRACT

The present work reports on the preparation of polythiol-functionalized silica particles by thermally and photo-initiated radical addition reactions using poly(3-mercaptopropyl)methylsiloxane (PMPMS) as sulfhydryl group-rich surface modification reagent. Prior to surface modification with PMPMS, the silica was vinylized with vinyl trimethoxysilane. Finally, the usefulness of the thiolated silica particles was demonstrated by their further modification for various HPLC applications such as argentation chromatography and chiral separations. Aiming at a sulfhydryl group-rich, thin PMPMS layer on the surface of the silica several factors such as quantity of PMPMS, radical starter and reaction time were investigated by a design of experiment (DoE) approach. In thermally induced polymerization reactions 2,2'-azobis(isobutyronitrile) (AIBN) was used as radical starter, in photo-induced reactions 2,2-dimethoxy-2-phenylacetophenone (DMPA) was used instead. The incorporation of PMPMS was evaluated by elemental analysis and reactive and accessible sulfhydryl groups were determined by performing a thiol-disulfide exchange reaction with 2,2'-dipyridyl disulfide (DPDS). Consequently, thiol-functionalized silica particles (200 Å, 5 µm) with 1.81 ± 0.07 µmol sulfhydryl groups per $m^2$ were prepared and further functionalized for silver ion chromatography and chiral separation chromatography clearly proving its utility as platform for further silica functionalization. The fabricated stationary phase for silver ion chromatography showed promising separation abilities for fatty acid methyl esters (FAME) according to the amount of double bonds within the fatty acid residue and cis- and trans-stilbene as model molecule for cis-trans isomerism. After the successful incorporation of *O-tert*-butylcarbamoyl quinine (tBuCQN) as chiral selector via thiol-ene click chemistry onto the PMPMS layer, the obtained chiral stationary phases (CSP) showed good separation of derivatized amino acids in polar organic elution mode comparable with a column based on commercially available CHIRALPAK QN-AX silica particles (120 Å, 5 µm).



## 1. Introduction

Thiol-functionalized silica is a popular material in a wide range of areas such as heavy metal capture, catalysis and chromatography (e.g. for protein separation by thiol-disulfide exchange of sulfhydryl groups containing proteins in covalent chromatography and for the development of stationary phases). Hence, the preparation of stable thiol-functionalized silica particles with adjustable sulfhydryl content is of high interest [1]. Typically, thiol-functionalization of silica particles is carried out by silanization reactions using alkoxysilanes or chlorosilanes obtaining a mono- or bifunctional siloxane bonding to the silica resulting in so called brush type phases [2-8]. Such bondings are susceptible to hydrolytic cleavage of the resultant Si-O-Si bonds, especially under aqueous mobile phase conditions in reversed-phase and hydrophilic interaction liquid chromatography (HILIC) elution modes. Therefore, alternative bonding chemistries are desirable to obtain more stable ligand attachment, minimize column bleeding and reduce back-

* Author for correspondence: Prof. Dr. Michael Lämmerhofer, Pharmaceutical (Bio-)Analysis, Institute of Pharmaceutical Sciences, University of Tübingen, Auf der Morgenstelle 8, 72076 Tübingen, Germany. T +49 7071 29 78793; F +49 7071 29 4565.
*E-mail address:* michael.laemmerhofer@uni-tuebingen.de (M. Lämmerhofer).

https://doi.org/10.1016/j.chroma.2021.462069
0021-9673/

ground signals from detached chromatographic ligands in particular in mass spectrometry (MS) detection. Polymeric coating strategies proved to reduce this phenomenon and consequently PMPMS coated functionalized stationary phases containing enantioselective ligands were prepared in one-pot synthesis procedures showing less column bleeding than the respective brush-type phases [2,9-11]. In these former studies, crosslinking of the PMPMS film and its functionalization took place simultaneously in one reaction in a thiol-ene double click reaction. Thereby, the two click reactions occur in competitive manner which makes it more difficult to adjust ligand coverages. For this and other reasons, it may be desirable to generate a general polymer bonded PMPMS-based thiol-functionalized silica platform with adjustable sulfhydryl group content which may serve as flexible reactive intermediate for further functionalization with controlled ligand coverage.

The aim of this work was to develop a strategy for the synthesis of PMPMS-based silica with controlled reactive sulfhydryl surface concentration by use of a design of experiment strategy. As model systems for further modification on the polymeric thiol-silica platform, a chiral stationary phase and a silver-ion chromatography material were selected to demonstrate the utility of the approach. First, enantioselective ligands based on cinchona alkaloids were linked to sulfhydryl groups of the PMPMS modified silica particles by thiol-ene click reaction yielding a stable bonding. Second, thiol-functionalized silica particles can represent the base material for the separation of lipids by silver ion chromatography. The free thiol groups can easily be oxidized and loaded with silver ions which are strongly adsorbed under normal phase conditions. As silver ion chromatography provides the possibility to separate lipids according to their number of double bonds and configuration, this technique is preferably used in food industry, lipid chemistry, clinical and pharmaceutical analysis, plant and animal physiology [12,13]. There are only a few HPLC columns dealing with this concept commercially available (e.g. ChromSpher Lipids, Silver Column KANTO) and silver ion chromatography columns are mainly prepared in house using commercially available cation exchange columns by adding adsorbed silver ions on the surface of the silica particles [14,15].

## 2. Experimental

### 2.1. Materials

Spherical silica particles ProntoSil 200-5-Si (200 Å, 5 µm, 200 $m^2/g$) and empty stainless steel columns (50 × 3 mm) were purchased from Bischoff Chromatography (Leonberg, Germany). *O-tert*-Butylcarbamoyl quinine (tBuCQN) was synthesized as described elsewhere [16]. Radical starters 2,2-dimethoxy-2-phenylacetophenone (DMPA), 2,2'-azobis(isobutyronitrile) (AIBN) and 2,2'-dipyridyl disulfide (DPDS), 2-mercaptoethanol, methyl oleate, methyl linoleate, methyl linolenate, 4-dimethylaminopyridine (DMAP), tris(2-carboxyethyl)phosphine (TCEP), 2-(2,4-dichlorophenoxy)propanoic acid (dichlorprop), histidine, boric acid, nitric acid ($HNO_3$), tris(hydroxymethyl)aminomethane (Tris), sodium hydroxide (NaOH), sodium dihydrogen phosphate monohydrate ($NaH_2PO_4$ x $H_2O$), potassium chloride (KCl), ammonium iron (III) sulfate dodecahydrate ($NH_4Fe(SO_4)_2$ x 12 $H_2O$), ammonium thiocyanate ($NH_4SCN$), potassium iodide, silver nitrate, hydrogen peroxide (30 %) and *N,O*-bis(trimethylsilyl)acetamide (BSA) were obtained from Sigma Aldrich (Munich, Germany). The derivatized amino acids *N*-[(9H-fluoren-9-ylmethoxy)carbonyl]-phenylalanine (Fmoc-Phe), *N*-acetyl-phenylalanine (Ac-Phe), *N*-carbobenzoxy-phenylalanine (Z-Phe), *N*-(3,5-dinitrobenzoyl)-leucine (DNB-Leu) and the respective enantiomers were supplied by Sigma Aldrich or synthesized in-house according to ref. [17,18]. Vinyl trimethoxysilane and poly(3-mercaptopropyl)methylsiloxane (viscosity: 75-150 cSt., molecular weight: 4000-7000 g/mol) (PMPMS) were both received from ABCR Chemicals (Karlsruhe, Germany). Sulfanilamide was supplied from Elemental Microanalysis (Okehampton, Devon, UK). The solvents toluene, methanol, acetonitrile (ACN) and n-hexane were of technical grade or HPLC grade and purchased from Brenntag (Essen, Germany) and Sigma Aldrich, respectively. MilliQ water was purified by using an Elga PureLab Ultra Purification System (Celle, Germany). Acetic acid, formic acid (FA) and ammonium acetate ($NH_4Ac$) were all of analytical grade and obtained from Sigma Aldrich.

### 2.2. Instrumentation and software

Chromatographic tests were performed on an Agilent 1100 series HPLC system (Agilent, Waldbronn, Germany) equipped with a degasser, binary pump, column compartment with temperature control and a variable wavelength detector (VWD) or an Agilent LC MSD-SL ion-trap mass-spectrometer. Mobile phases for the chromatographic tests and other conditions are specified in respective figure captions or subchapters. $\zeta$-Potentials were determined by electrophoretic light scattering measurements using a Zetasizer NanoZS particle analyzer equipped with folded capillary cells (Malvern Instruments, Herrenberg, Germany). Elemental analyses were carried out using an EA 3000 CHNS-O elemental analyser from EuroVector SpA (Milan, Italy). The stationary phases were slurry packed into stainless steel columns by using a Smartline Pneumatic Pump 1950 from Knauer (Berlin, Germany). The design of experiments (DoE) approach was software-supported by using MODDE Pro Ver. 12.1.0.54.91 from Sartorius Stedim (Umeå, Sweden). MarvinSketch 20.19 (ChemAxon, www.chemaxon.de) was used for estimation of $pK_a$ values.

### 2.3. Preparation of modified silica particles

#### 2.3.1. Synthesis of vinylized silica

15 g bare silica particles (200 Å, 5 µm) were dried in a vacuum oven at 60 °C for 24 h and then suspended in 200 mL toluene within a triple neck flask equipped with a distillation bridge and a stirrer. During continuous stirring the suspension was heated up to reflux and 50 mL toluene were distilled off and discarded subsequently in order to remove traces of water from the system. Thereafter, the system was cooled down to room temperature and the distillation bridge was exchanged by a reflux condenser. Vinyl trimethoxysilane (6 µmol per $m^2$ silica) or a mixture of vinyl trimethoxysilane and BSA were along with DMAP (5 % n/n related to vinyl trimethoxysilane and BSA) added to the mixture and a nitrogen supply was attached. The system was flushed with nitrogen for 15 min and after that the suspension was heated up to reflux and the reaction was allowed to proceed for 24 h under continuous gentle nitrogen rinsing and stirring. Finally, the silica was washed 3 times with boiling toluene and methanol each using a glass funnel of porosity 4 and dried in a vacuum oven at 60 °C for 24 h.

#### 2.3.2. Synthesis of PMPMS thiol-functionalized silica

Typically, 0.6 g dried vinylized silica, PMPMS and radical initiator were suspended in 25 mL methanol within a 100 mL round bottom flask (Duran Glastechnik, Wertheim/Main, Germany, negligible UV absorption in the range above 310 nm). Hereafter, the solvent was evaporated by using a rotary evaporator resulting in a thin PMPMS film on the silica surface. After flushing the flask with nitrogen for 10 min, it was placed in a heating chamber tempered at 60 °C for thermally induced reactions with AIBN. For the UV-initiated reaction with DMPA as radical initiator, it was continuously rotated using a rotor attached to the flaskś head with 60

**Table 1**
Experimental conditions and results of the photochemical and the thermochemical approach for the preparation of PMPMS thiol-functionalized silica particles

| Photochemical Approach | | | | | | | Thermochemical Approach | | | | | | |
|---|---|---|---|---|---|---|---|---|---|---|---|---|---|
| | Experimental conditions | | | Outcome | | | | Experimental conditions | | | Outcome | | |
| # | DMPA [%][1] | PMPMS [mmol/g] | time [min] | S[2] [µmol/g] | SH[3] [µmol/g] | SH/S [%] | # | AIBN [%][1] | PMPMS [mmol/g] | time [min] | S[2] [µmol/g] | SH[3] [µmol/g] | SH/S [%] |
| P1 | 10 | 0.25 | 5 | 206.1 | 36.3 | 17.6 | T1 | 10 | 0.25 | 60 | 199.0 | 22.9 | 11.5 |
| P2 | 10 | 0.25 | 15 | 214.3 | 34.6 | 16.1 | T2 | 10 | 0.25 | 120 | 191.5 | 47.8 | 25.0 |
| P3 | 10 | 0.25 | 30 | 218.3 | 28.6 | 13.1 | T3 | 10 | 0.25 | 180 | 199.8 | 33.8 | 16.9 |
| P4 | 10 | 0.5 | 5 | 331.1 | 53.0 | 16.0 | T4 | 10 | 0.5 | 60 | 408.5 | 155.5 | 38.1 |
| P5 | 10 | 0.5 | 15 | 359.5 | 47.8 | 13.3 | T5 | 10 | 0.5 | 120 | 426.2 | 108.7 | 25.5 |
| P6 | 10 | 0.5 | 30 | 348.6 | 32.4 | 9.3 | T6 | 10 | 0.5 | 180 | 431.6 | 43.1 | 10.0 |
| P7 | 10 | 1 | 5 | 671.7 | 126.7 | 18.9 | T7 | 10 | 1 | 60 | 711.2 | 329.0 | 46.3 |
| P8 | 10 | 1 | 15 | 716.4 | 65.4 | 9.1 | T8 | 10 | 1 | 120 | 748.6 | 260.4 | 34.8 |
| P9 | 10 | 1 | 30 | 862.5 | 59.7 | 6.9 | T9 | 10 | 1 | 180 | 733.6 | 195.7 | 26.7 |
| P10 | 10 | 0.5 | 15 | 336.6 | 40.7 | 12.1 | T10 | 10 | 0.5 | 120 | 438.4 | 120.7 | 27.5 |
| P11 | 10 | 1 | 2 | 555.2 | 277.4 | 50.0 | **T11** | **10** | **1** | **45** | **644.1 ± 16.6[4]** | **361.5 ± 13.8[4]** | **56.2 ± 2.8[4]** |
| P12 | 5 | 1 | 2 | 541.0 | 271.2 | 50.1 | T12 | 10 | 1 | 30 | 355.4 | 163.2 | 45.9 |
| P13 | 2.5 | 1 | 2 | 513.3 | 240.5 | 46.9 | T13 | 5 | 1 | 30 | 306.8 | 188.7 | 61.5 |

[1] mol% related to the total amount of vinyl groups in the reaction mixture
[2] calculated by elemental analysis data based on %S
[3] determined by a thiol-disulfid exchange reaction with DPDS[4] based on reproducing the synthesis procedure for four times

rpm at ambient temperature in a well-vented hood with the Ultra-Vitalux UV lamp (Osram, Munich, Germany). Here, the UV lamp (300 W, radiant power of 13.6 W in the UV-A (315-400 nm) and 3.0 W in the UV-B (280-315 nm) spectral range) was positioned in a distance of 10 cm to the flaskś outer wall and an angle of 135 ° relative to the flaskś rotation axis (for scheme of reaction setup see Suppl. Fig. S5). Detailed reaction conditions are given in Table 1. In the end, the silica was washed 3 times with boiling toluene and methanol each using a glass funnel of porosity 4 and dried in a vacuum oven at 60 °C for 12 h.

*2.3.3. Oxidation of PMPMS thiol-functionalized silica*

Free reactive sulfhydryl groups available on the PMPMS thiol-functionalized silica particles were oxidized by using performic acid resulting in sulfonic acid groups. For this purpose, 0.5 g of PMPMS-functionalized silica were suspended in a mixture of 40 mL methanol and 2.1 mL formic acid and a mixture of 0.5 mL hydrogen peroxide (30 % v/v) and 9.5 mL formic acid was added dropwise to the suspension. The reaction was allowed to proceed for 4 h under continuous stirring and ice bath cooling. Lastly, the silica was washed 3 times with hot methanol using a glass funnel of porosity 4 and dried in a vacuum oven at 60 °C for 24 h.

*2.3.4. Immobilization of silver ions onto oxidized silica*

In order to adsorb silver ions onto the surface of the modified silica particles, 0.4 g of the silica were dispersed in 20 mL 0.1 M silver nitrate solution (water/methanol, 50/50; v/v) for 2 h under continuous stirring. Afterwards, the silica was washed several times with a mixture of methanol and water (50/50; v/v) until there was no more precipitation of silver iodide observed by adding a 0.1 M potassium iodide solution. Lastly, the silica was washed 3 times with boiling methanol using a glass funnel of porosity 4 prior to drying in a vacuum oven at 60 °C for 24 h.

*2.3.5. Immobilization of* O-tert-*butyl carbamoyl quinine via thiol-ene click reaction onto PMPMS thiol-functionalized silica*

0.5 g of dried PMPMS thiol-functionalized silica particles were suspended in 80 mL methanol within a triple neck flask equipped with a distillation bridge and a stirrer. The suspension was heated up to 80 °C and 40 mL methanol (for SP5) or 60 mL methanol (for SP6), respectively, were distilled off and discarded. Afterwards, the system was cooled down and the distillation bridge was replaced by a reflux condenser. Subsequently, tBuCQN as functional ene-component (4 µmol per $m^2$ silica) and AIBN as radical initiator (10 % n/n according to vinyl groups of tBuCQN) were added to the suspension. Then, the system was flushed with nitrogen for 15 min. Afterwards, the suspension was heated up to 80 °C and the reaction allowed to proceed for 7 h under continuous gentle nitrogen rinsing and stirring. Finally, the silica was washed with boiling toluene and methanol 3 times each and dried in a vacuum oven at 60 °C for 24 h.

*2.4. Evaluation of modified silica particles*

*2.4.1. Elemental Analysis*

The elemental composition of the modified silica particles was determined by elemental analysis in order to calculate the amount of incorporated PMPMS, tBuCQN and vinyl groups. Typically, 2 mg of the silica were weighed into a tin capsule and were provided to the elemental analyzer. Helium of 5.0 quality was used as carrier gas and detection was carried out after separation of the formed $CO_2$, $H_2O$, $N_2$ and $SO_2$ by gas chromatography using a thermal conductivity detector (TCD). Here, sulfanilamide was used as reference substance.

*2.4.2. Determination of sulfhydryl group content*

For the determination of reactive and accessible sulfhydryl groups on the silica surface a thiol-disulfide exchange reaction with DPDS was performed according to ref. [19,20] and the formed 2-pyridyl thiol and its tautomerized thione form, respectively, were quantified by RP-HPLC-UV/Vis. Therefore, 10 mg of dried PMPMS thiol-functionalized silica particles were weighed into a micro centrifuge tube which was impervious to light. Subsequently, 1 mL 0.1 M DPDS solution (in ACN) was added. The centrifuge tube was intensively shaken for 3 h and then centrifuged. The supernatant was diluted with ACN in a ratio of 1 to 10. The concentration of 2-pyridyl thiol and its tautomerized thione form was finally quantified by RP-HPLC-UV/Vis. Detailed conditions are given in Suppl. Material. 2-Mercaptoethanol was used as calibrant for the preparation of the calibration function for the quantification of the reactive sulfhydryl content.

*2.4.3. Determination of immobilized silver ion content*

The silver ion loading of the silica particles was determined indirectly by titration (according to Volhard) of the silver ions not adsorbed and thus remaining in the washing solvent. Thus, 0.1 mL saturated $NH_4Fe(SO_4)_2$ solution as endpoint indicator was added

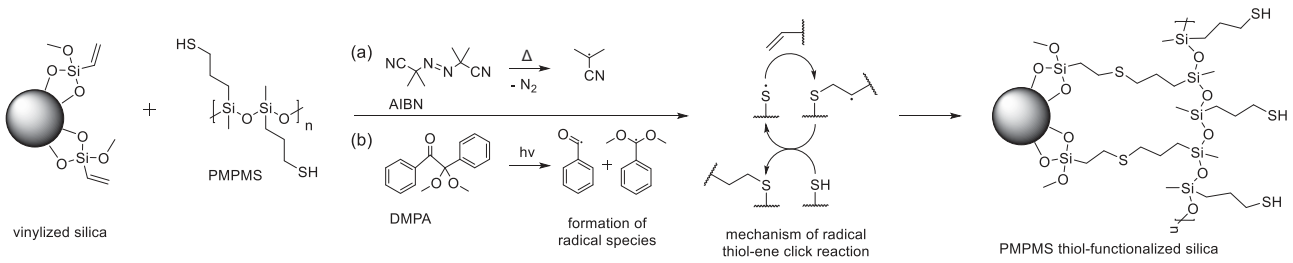


**Fig. 1.** Reaction scheme of (poly)thiol-ene click reaction of vinylized silica (ene-component) and PMPMS (thiol component) for (a) thermally or (b) photochemically induced reactions.

and the pH was adjusted with $HNO_3$ obtaining a concentration of 1 mol/L $HNO_3$. The titration was carried out by using 0.01 M $NH_4SCN$ solution as titrant to the visually determined endpoint. A reference titration of 0.1 M $AgNO_3$ solution (water/methanol, 50/50; v/v) was performed.

#### 2.4.4. ζ-Potentials

pH-dependent ζ-potential determinations were conducted in a pH range from 3.5 to 9.5 with a suspension of 0.2 mg/mL particles in 10 mM KCl solutions containing 1 mM of the following buffers: formic acid/sodium formate, acetic acid/sodium acetate, histidine, tris/tris-HCl, boric acid/sodium borate [21]. Thereby, folded capillary cells were used for the measurements and all experiments were performed in triplicates. Prior to each measurement the temperature of the suspension was equilibrated to 25 °C. ζ-potentials were calculated according to the von Smoluchowski equation.

### 2.5. Preparation of HPLC columns and chromatographic tests

#### 2.5.1. Column packing

The silica was slurry packed into empty stainless-steel columns (50 mm x 3 mm) applying a pressure of 800 bar for 1 h. Methanol was used as pushing solvent and the slurry was usually prepared by using 2-propanol reaching a concentration of 50 mg silica per mL. For the packing of tBuCQN modified silica particles 10 % (v/v) acetic acid was added to the slurry solvent. In the end, the column was rinsed for 12 h with methanol at a flow rate of 0.5 mL/min. Prior to column packing, the silica was sieved using a stainless-steel sieve of mesh size 25 µm.

#### 2.5.2. Separation of fatty acid methyl esters by silver ion chromatography

A mixture of 3 different fatty acid methyl esters (FAMEs) with same carbon number, but differing in the number of double bonds located in the fatty acid residue, was prepared. Therefore, 0.5 mg/mL methyl oleate, 0.25 mg/mL methyl linoleate and 0.125 mg/mL methyl linolenate were dissolved in hexane. The mobile phase consisted of hexane plus 0.15 % (vol%) ACN and the flow rate was adjusted to 0.5 mL/min. 2 µL of the sample were injected onto the column and the detection was carried out using a VWD at 210 nm.

#### 2.5.3. Separation of cis- and trans-stilbene by silver ion chromatography

A mixture of cis- and trans-stilbene in hexane was prepared reaching a concentration of 0.1 mg/mL of the two isomers each. The mobile phase consisted of hexane plus 0.15 % (v/v) ACN and the flow rate was adjusted to 0.2 mL/min. 2 µL of the sample were injected onto the column and the detection was carried out using a VWD at 254 nm.

#### 2.5.4. Separation of chiral compounds by enantioselective HPLC

In order to evaluate the performance of the tBuCQN containing CSPs (SP5-7) a chromatographic chiral separation test was performed using the chiral acids Ac-Phe, Fmoc-Phe, Z-Phe, DNB-Leu and dichlorprop as test substances. Therefore, a mobile phase consisting of methanol and 50 mM ammonium acetate buffer (80/20; v/v) with a pH adjusted to 6 by glacial acetic acid was used. The analytes were dissolved in the mobile phase gaining a concentration of 0.1 mg/mL. The flow rate was set to 0.5 mL/min and the temperature was adjusted to 25 °C. The detection was carried out at 254 nm and the injection volume was amounted to 2 µL.

## 3. Results and discussion

Synthesis procedures for PMPMS thiol-functionalized silica particles as well as quantification of immobilized PMPMS and unreacted sulfhydryl groups

PMPMS thiol-functionalized silica particles were prepared with the goal to achieve a thin PMPMS film and a controlled concentration of reactive sulfhydryl groups on top of the silica surface. A slurry of all reactands (vinylized silica, PMPMS and radical initiator) in methanol was prepared and after careful mixing the solvent evaporated to obtain a thin film of PMPMS on the silica surface. Two different approaches were employed to crosslink the PMPMS to the silica surface. Both were based on thiol-ene click reactions between PMPMS as thiol component and vinylized silica (5 µm, 200 Å, vinyl group content of 3.30 ± 0.03 µmol/$m^2$) as ene-component differing in the radical formation step [8,10,22]. The respective reaction schemes are illustrated in Fig. 1. In the thermochemical approach, the radicals were formed by thermally initiated decomposition of AIBN (Fig. 1a). In the photochemical approach, the radicals necessary for the initiation of the radical addition reaction were generated by disintegration of DMPA ($\lambda_{max}$ ~ 330 nm according to ref. [23]) via UV light irradiation (Fig. 1b). The final reaction product is the same for the photo-initiated and the thermally initiated reactions. After thermally or UV initiated radical formation, the radical is transferred from the initiators' decomposition products to the sulfhydryl groups of the thiol component. The formed thiyl radical leads to a hydrothiolation reaction on the double bond of the ene-component resulting in the formation of a thio ether. Thereby, an intermediate carbon-centered radical is generated, which provokes a prolonged reaction by transferring the radical to the next sulfhydryl group [24]. In practice, for both approaches a thin solid layer of vinylized silica with coated PMPMS film containing the radical starter was created at the inner wall of a round bottom flask first and the reaction was subsequently initiated by applying UV light irradiation or heat (60 °C), respectively. By using this film method, the PMPMS polymers accumulated on the silica surface and due to their liquid nature did not require any solvent during the reaction. It means the PMPMS layer was anchored to the vinylized silica through formation of thio ethers by a solvent-less thiol-ene click reaction.

Thereafter, the prepared PMPMS thiol-functionalized silica particles were characterized by the total amount of coated PMPMS and its percentage of unreacted, free sulfhydryl groups available for further modification. The total sulfur (sulfhydryl and thio ether) was determined by elemental analysis measurements. Additionally, a thiol-disulfide exchange reaction was performed for the purpose of quantifying the residual reactive sulfhydryl groups due to the loss of information regarding the chemical state of the sulfur assessed by elemental analysis. The thiol-disulfide exchange reaction, used for sulfhydryl monitoring, is depicted in the Suppl. Material. DPDS reacts with the sulfhydryls of the modified silica particles by fast reaction kinetics to 2-pyridyl thiol. 2-Pyridyl thiol is converted into its tautomeric thione form and consequently shifts the equilibrium to the product side. For this reason, it has been approved to be a very reliable method for the quantitative determination of sulfhydryl groups, also on solid surfaces. 2-Mercaptoethanol was used as reference substance for calibration and 2-pyridyl thiol and its corresponding tautomer were finally quantified by HPLC-UV/VIS [19,20]. A small number of adjoining sulfhydryl groups might be oxidized in the course of the radical addition reaction resulting in the formation of disulfide bonds. Therefore, the PMPMS thiol-functionalized silica particles were treated with TCEP (in methanol/50 mM $NaH_2PO_4$ (20/80, v/v), with 10-fold molar excess of TCEP related to the total sulfur content) for 8 h prior to the sulfhydryl group determination in order to reduce the formed disulfide bonds and achieve a higher content of free sulfhydryl groups. However, there was no significant increase concerning the sulfhydryl group content determined with and without treatment with TCEP. Hence, it can be concluded that the formation of disulfide bonds during the reaction is not of relevance and the TCEP step therefore not required.

### *3.1. Optimization of PMPMS thiol-functionalized silica by using a DoE approach*

The reaction conditions have to be tuned such that a sufficient number of crosslinks to the surface vinyl groups secures the irreversible covalent immobilization of the PMPMS film but at the same time a high concentration of surface sulfhydryls should remain available for further functionalization. For this purpose, a full factorial design with 3 levels was chosen to systematically evaluate and optimize the main factors of the reaction comprising the type of radical initiation method (photochemical or thermochemical), the reaction time and the quantity of PMPMS in the polymerization mixture. In the course of this endeavor, the goal was to find the best compromise between a thin PMPMS layer and a high sulfhydryl group loading on the silica surface. To this end, several synthesis batches were prepared differing in the investigated factors. The concentration of the radical initiators (DMPA and AIBN) were kept constant at 10 mol% (related to the vinyl groups in the reaction mixture) except for the conclusive experiments (#P11-13, #T11-13). The detailed information of the experimental reaction parameters is given in Table 1. It is striking that the photo-initiated reactions lead to higher PMPMS loadings in considerably shorter reaction times compared to the thermally initiated ones. For instance, a coverage of 716 µmol sulfur/g PMPMS-modified silica (#P8) was achieved within 15 min using the photochemical approach. In contrast, the thermochemical approach afforded only 355 µmol sulfur/g PMPMS-modified silica (#T12) after 30 min under the same conditions. A comparable loading, however, was achieved after 60 min (#T7, 711.2 µmol/g) for the thermochemical approach. This higher reaction kinetics of photo-initiated radical addition reactions was already reported for thiol-ene click reactions and was the driving force to test this approach in this work [25]. Unfortunately, this higher reaction kinetics was associated with a decreased free sulfhydryl concentration on the particle surface (*cf.* #P8-9). The highest sulfhydryl group content obtained by this synthesis approach was 277 µmol/g (#P11). This corresponds to around 50 % reactive sulfhydryl groups of the total sulfur content and was obtained with a reaction time of only 2 min. A further reduction of reaction time could lead to a further increase, but in this case also the ratio of thio ethers to free sulfhydryl groups might be changed for the worse leading to limited stability of the surface bonding. Certainly, a sufficient anchor-

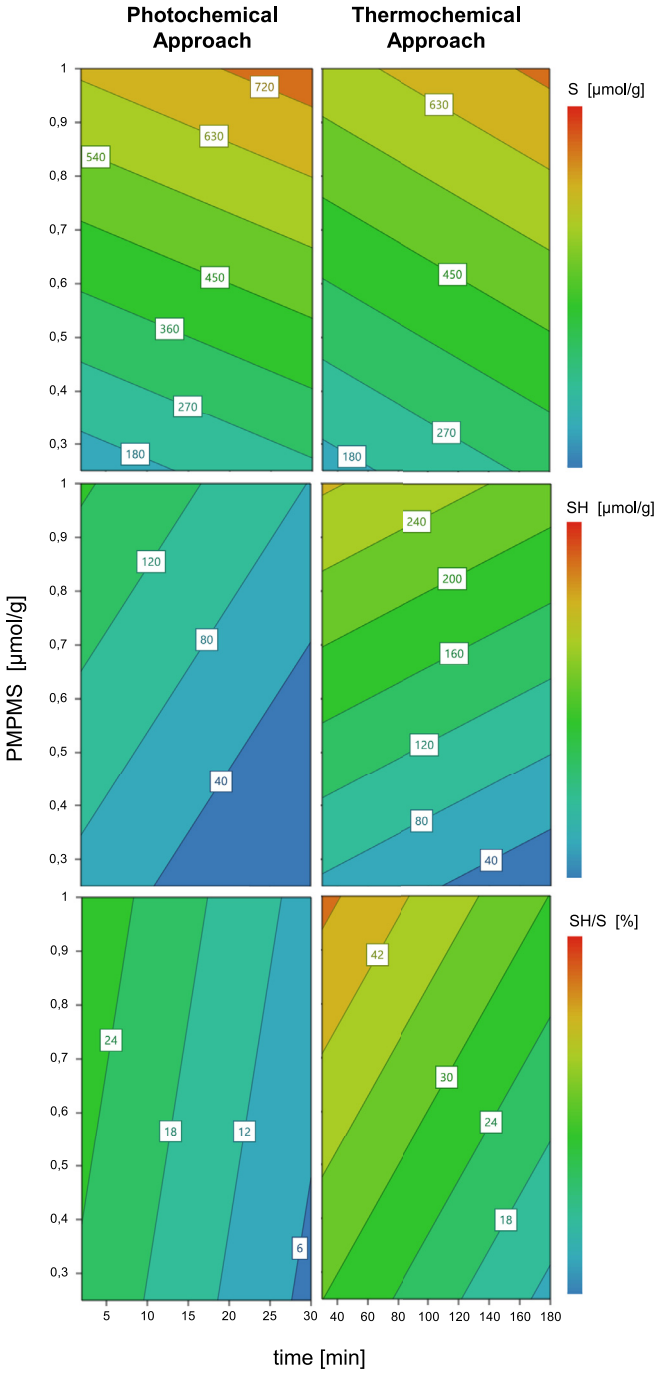


**Fig. 2.** Design of experiment optimization for the synthesis of PMPMS thiol-functionalized silica particles considering mainly 3 factors: PMPMS concentration, reaction time and radical initiation method (photochemical or thermochemical). The panels on the left side illustrate the total amount of incorporated sulfur (S), the sulfhydryl group content (SH) and the ratio of sulfhydryl groups to the total incorporated sulfur amount (SH/S) for the photochemical approach. The panels on the right side show the corresponding results for the thermochemical approach as well.

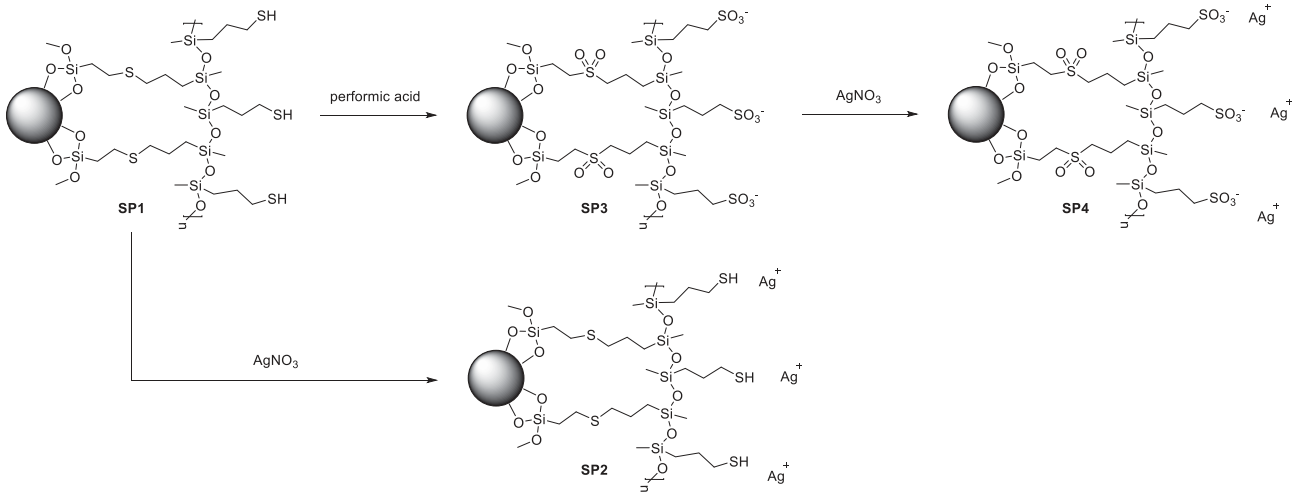


**Fig. 3.** Surface chemistries of the prepared stationary phases SP1-4. All stationary phases are based on #T11 (200 Å, 5 µm, Table 1) and were slurry packed into stainless steel columns of 50 mm x 3 mm size.

ing of the PMPMS layer to the silica via thio ethers is as necessary as a high amount of free sulfhydryl groups.

As the reaction kinetics might also be influenced by the percentage of the radical initiator, it was varied for #P11-13. However, there were no considerable differences concerning the outcome. Thus, it might be assumed that for the photochemical approach the radical initiator content was not of tremendous importance due to the high reaction kinetics and a sufficient number of radicals also at factor 4 lower initiator concentration.

For both approaches raising the PMPMS percentage in the reaction mixture leads to increasing amounts of incorporated PMPMS as well. In sharp contrast to the photochemical approach, however, the thermochemical approach resulted simultaneously in higher sulfhydryl group contents due to its lower reaction kinetics. According to #T7-9 a maximum incorporation of approximately 710-750 µmol/g PMPMS can be achieved using the thermochemical approach under the specified conditions (see Table 1). On the other hand, the ratio of free sulfhydryl groups to thio ethers decreased with higher reaction times from 46.3 % for #T7 (60 min) to 26.7 % for #T9 (180 min). Thus, the reaction time was decreased to 45 min leading to a final sulfhydryl group loading of 362 ± 14 µmol/g for #T11. Simultaneously, the percentage of the sulfhydryl groups was 56.2 ± 2.8 % of the total incorporated sulfur, which enables still a satisfying anchoring of the PMPMS layer to the silica besides the sufficient availability of unreacted sulfhydryl groups. The discussed effects are presented as response surfaces created by DoE software MODDE in Fig. 2. It becomes evident that the sulfhydryl group concentration on the surface and the percentage of crosslinks to the silica surface can be finely controlled using this model. In conclusion, #T11 was used for the preparation of the further investigated chromatographic materials (SP1-SP7).

### *3.2. Surface modification of PMPMS-bonded silica for silver ion chromatography*

Silver ion chromatography, also well known as argentation chromatography, is a technique mainly used for the analysis of lipids with normal-phase conditions. In this chromatographic mode, lipids are mainly separated according to their number of olefinic double bonds of the unsaturated fatty acid residues due to the formation of a transient charge-transfer-complex between the silver ions adsorbed on the stationary phase and the double bonds of the analytes according to the Dewar-Chatt-Duncanson model [26]. Here, the double bonds serve as electron donor from the occupied $2\pi$ bonding orbital into the empty 5s and 5p orbitals of the metal ion. Likewise, electrons from the occupied 4d orbitals of the metal ion are donated into the free antibonding $2\pi^*$ orbitals of the double bond. This combination of $\sigma$-donation and $\pi$-back-bonding interactions stabilizes the formed charge-transfer-complex leading to potent retention of unsaturated molecules in silver ion chromatography. Thereby, the complexation effect increases with the number of double bonds and is affected by the double bondsćonfiguration and position as well [26-30].

Four new stationary phases (SP1-4) have been synthesized from PMPMS thiol-functionalized silica particles (#T11, Table 1; SP1). Two stationary phases contained adsorbed silver ions, namely SP2 and SP4 (Fig. 3). SP2 was generated by directly immobilizing silver ions onto the sulfhydryl group rich surface of the PMPMS thiol-functionalized silica particles (SP1) due to the interaction between silver ions and free non-binding valence electrons of the sulfur functionality. For the generation of SP4 the sulfhydryl groups were first oxidized by using performic acid prior to the immobilization of the silver ions resulting in a sulfonic acid-rich strong cation exchange phase (SP3). It can be loaded with silver ions which are bound by strong electrostatic interactions under normal phase conditions (SP4). The successful oxidation of the sulfhydryl groups was indirectly proven by pH-dependent $\zeta$-potential measurements via electrophoretic light scattering. Sulfhydryl groups ($pK_a$ ~ 9.7 to 10.5) and sulfonic acid groups ($pK_a$ ~ -1.9 to -1.2) differ dramatically in their $pK_a$ values resulting in alteration of the surface charge upon oxidation of SP1 to SP3. As illustrated in Fig. 4, SP1 and SP3 showed both negative $\zeta$-potentials over the entire pH range. However, SP3 showed significantly lower $\zeta$-potentials than SP1 in the low pH range from 3.5 to 6.5 due to fully dissociated acidic sulfonic acid groups. For SP1 the $\zeta$-potentials are determined by less acidic functionalities (sulfhydryl and silanol groups), which are hardly deprotonated under acidic conditions. The comparable negative $\zeta$-potentials at higher pH values for SP1 and SP3 are mainly due to the contribution of free acidic silanol groups ($pK_a$ ~ 6-7), which were completely deprotonated in this pH range.

The quantity of adsorbed silver ions was determined by titration and turned out to be much higher for sulfonic acid-functionalized SP4 than for thiol-phase SP2, as can be seen in Table 2. It suggests a stronger affinity of the silver ions for SP4 because of the electrostatic interactions between sulfonate moieties and silver ions as compared to the dative (coordinative) bond between thiol and silver ion of SP2.

**Table 2**
Summary and characteristics of the prepared stationary phases

| SP | particle size[1] [µm] | pore size[1] [Å] | specific surface area[1] [m²/g] | C[2] [%] | H[2] [%] | N[2] [%] | S[2] [%] | vinyl groups[3] [µmol/m²] | S[4] [µmol/m²] | SH[5] [µmol/m²] | tBuCQN[4] [µmol/m²] | Ag+[6] [µmol/m²] |
|---|---|---|---|---|---|---|---|---|---|---|---|---|
| vinylized silica | 5 | 200 | 200 | 2.38 ± 0.02 | 0.55 ± 0.01 | < 0.02 | < 0.02 | 3.30 ± 0.03 | - | - | - | - |
| SP1 | 5 | 200 | 200 | 5.31 ± 0.03 | 1.14 ± 0.01 | 0.05 ± 0.00 | 2.10 ± 0.01 | - | 3.28 ± 0.02 | 1.81 | - | - |
| SP2 | 5 | 200 | 200 | - | - | - | - | - | 3.28 ± 0.02[7] | - | - | 0.11 |
| SP3 | 5 | 200 | 200 | 4.20 ± 0.00 | 0.94 ± 0.01 | 0.04 ± 0.00 | 1.53 ± 0.00 | - | 2.39 ± 0.00 | 0.03 | - | - |
| SP4 | 5 | 200 | 200 | - | - | - | - | - | 2.39 ± 0.00[7] | - | - | 0.66 |
| SP5 | 5 | 200 | 200 | 7.53 ± 0.03 | 1.35 ± 0.02 | 0.33 ± 0.01 | 1.94 ± 0.02 | - | 3.03 ± 0.03 | 0.12 | 0.39 ± 0.01 | - |
| SP6 | 5 | 200 | 200 | 9.22 ± 0.02 | 1.59 ± 0.00 | 0.70 ± 0.01 | 2.01 ± 0.02 | - | 3.13 ± 0.02 | 0.16 | 0.84 ± 0.01 | - |
| SP7 | 5 | 120 | 334[8] | - | - | - | - | - | - | - | 1.14[8] | - |

[1] as stated by the silica supplier
[2] determined by elemental analysis
[3] calculated based on elemental analysis data assuming a bifunctional bonding of VTMS to the silica
[4] calculated based on elemental analysis data
[5] determined by a thiol-disulfid exchange reaction with DPDS
[6] as determined by Volhard titration[7]calculated based on the elemental anaylsis data for the respective precursor silica SP1 and SP3 and the determined silver loading
[8] according to ref. [11]

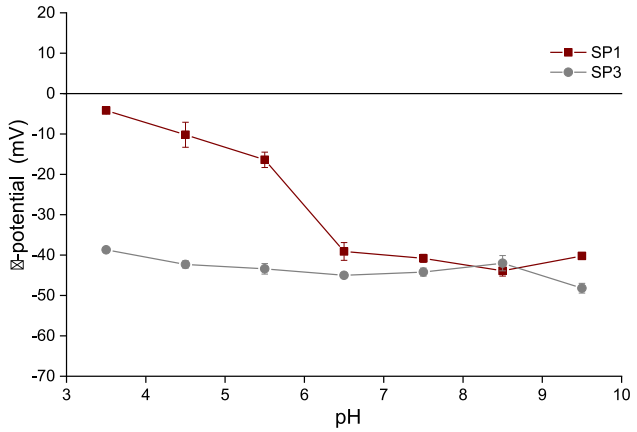


**Fig. 4.** pH dependence of $\zeta$-potentials for SP1 and SP3.

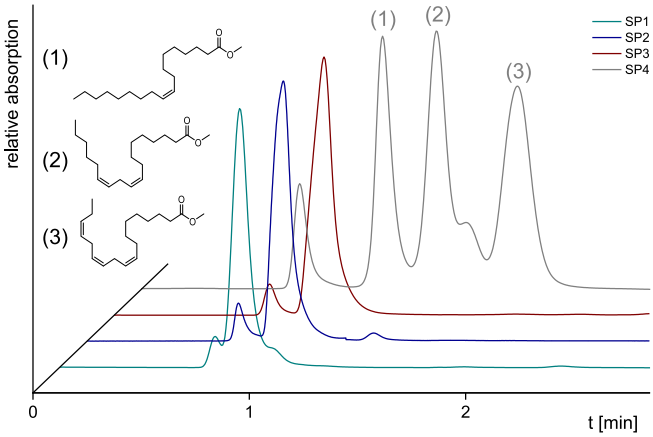


**Fig. 5.** Chromatographic results for SP1-SP4 for the separation of FAME (mobile phase: hexane plus 0.15 % ACN, flow rate: 0.5 mL/min, detection: 210 nm, injection volume: 2 µL, sample concentration: 0.5 mg/mL methyl oleate, 0.25 mg/mL methyl linoleate, 0.125 mg/mL methyl linolenate).

The chromatographic performance of the stationary phases SP1-SP4 for the separation of lipids in silver ion chromatography was evaluated with a test mixture of three C18 fatty acid methyl esters differing in the number of double bonds. Thereby, a mixture of hexane and acetonitrile as polar modifier was used as eluent. The percentage of acetonitrile in hexane was kept below 0.15 % (v/v), as hexane and acetonitrile are poorly miscible and eluents with more than 1.5 % (v/v) acetonitrile were reported to result in reproducibility issues [13]. Unlike SP1-3, SP4 was able to separate the three fatty acid methyl esters according to their double bond numbers. The respective chromatogram is depicted in Fig. 5. It is noteworthy that there was no separation observed for SP2 indicating the favorable performance of SP4. Two factors might cause this phenomenon. Firstly, the amount of immobilized silver ions on SP2 might be inadequate. Secondly, the silver ions might not be attached strongly enough to the stationary phase, as there is only a weak coordinate bonding to the sulfhydryl groups maybe leading to elution of silver ions together with the analytes. However, it is unambiguous that the separation was based on the interaction with the silver ions, as the fatty acid methyl esters were not separated by SP3. Furthermore, as illustrated in Fig. 6, SP4 afforded the separation of cis- and trans-stilbene as model molecules for cis-trans isomerism under the same conditions as well. Hence, it becomes evident that PMPMS thiol-functionalized silica after its oxidation and subsequent silver ion loading leads to a useful stationary phase for silver ion chromatography. Further improvements of

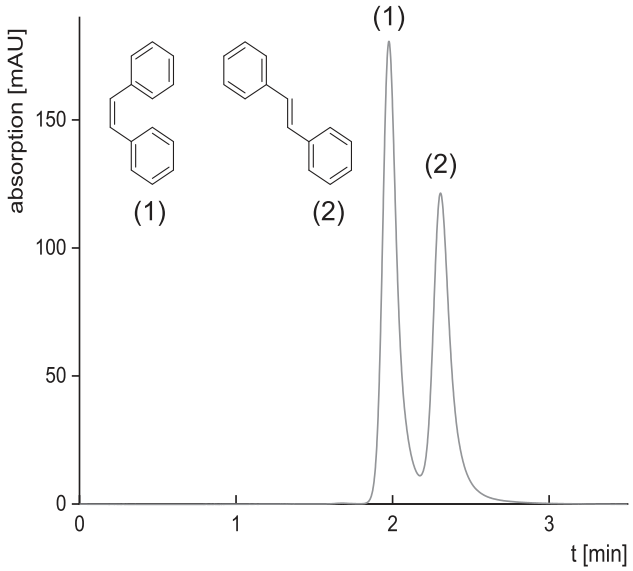


**Fig. 6.** Chromatographic results for SP4 in silver ion mode for the separation of cis- and trans stilbene (mobile phase: hexane plus 0.15 % ACN, flow rate: 0.2 mL/min, detection: 254 nm, injection volume: 2 µL, sample concentration: 0.1 mg/mL cis-stilbene, 0.1 mg/mL trans-stilbene).

resolution are enabled by longer columns, as in this case a column of 50 mm x 3 mm was used and commercially available columns for silver ion chromatography normally deal with much larger dimensions (e.g. Agilent ChromoSpher Lipids 250 mm x 4.6 mm).

### *3.3. Surface modification of PMPMS-bonded silica for enantioselective high-performance liquid chromatography*

PMPMS thiol-functionalized silica particles represent a convenient particle platform for the further introduction of functional ligands by thiol-ene click reactions. To this end, tBuCQN was selected as model ligand to document this type of surface functionalization and compare the performance of the resultant HPLC columns (SP5, SP6; Fig. 7) to a benchmark [4,7,31-35]. As benchmark, a column of 50 mm x 3 mm size corresponding to the CHIRALPAK QN-AX silica particles (120 Å, 5 µm) was synthesized and packed in-house (SP7; Fig. 7). The preparation of SP5 and SP6 was carried out as described in the experimental section by thermally initiated thiol-ene click reaction using two different slurry concentrations differing by factor 2. As can be seen from Table 2, this resulted in a roughly doubled tBuCQN coverage for SP6 (more concentrated slurry; 0.84 ± 0.01 µmol/m$^2$) in comparison to SP5 (0.39 ± 0.01 µmol/m$^2$). Moreover, another series of stationary phases were prepared in which the degree of surface vinyl groups of the underlying supporting particles was varied. As shown in Table 3, silica was vinylized by using a mixture of varying amounts of vinyl trimethoxysilane (VTMS) and BSA to keep the total silane content and the degree of surface silanol modification constant. In the following steps, the prepared vinylized silica particles were functionalized with PMPMS and tBuCQN under the same conditions as for SP6. The results of PMPMS and tBuCQN incorporation are summarized in Table 3 and illustrated in Fig. 8. It can be seen that raising the vinyl group content entailed a rising PMPMS coverage and consequently an increased amount of immobilized tBuCQN. The linear increase of PMPMS coating, sulfhydryl and ligand coverage with increase of VTMS on the supporting particles provides a framework to control surface coverage with functional moieties and chromatographic ligand, respectively. It allows to tune the stationary phase for maximal coverage, as favorable for preparative chromatography,

**Table 3**
Influence of the vinyl group content on the amount of incorporated PMPMS and tBuCQN

| | SP | particle size[1] [µm] | pore size[1] [Å] | specific surface area[1] [m$^2$/g] | VTMS/BSA[2] [n/n] | C[3] [%] | S[4] [µmol/m$^2$] | SH[5] [µmol/m$^2$] | S[6] [µmol/m$^2$] | tBuCQN[7] [µmol/m$^2$] |
|---|---|---|---|---|---|---|---|---|---|---|
| #1 | tBuCQN-PMPMS thiol-functionalized vinylized silica (SP6) | 5 | 200 | 200 | 100/0 | 2.38 ± 0.02 | 3.28 ± 0.02 | 1.81 | 3.13 ± 0.02 | 0.84 ± 0.01 |
| #2 | tBuCQN-PMPMS thiol-functionalized vinylized silica | 5 | 200 | 200 | 75/25 | 2.66 ± 0.06 | 2.18 ± 0.02 | 1.09 | 1.88 ± 0.01 | 0.71 ± 0.00 |
| #3 | tBuCQN-PMPMS thiol-functionalized vinylized silica | 5 | 200 | 200 | 50/50 | 2.39 ± 0.05 | 1.63 ± 0.01 | 0.90 | 1.34 ± 0.01 | 0.49 ± 0.01 |
| #4 | tBuCQN-PMPMS thiol-functionalized vinylized silica | 5 | 200 | 200 | 25/75 | 2.41 ± 0.04 | 1.32 ± 0.01 | 0.72 | 1.22 ± 0.01 | 0.35 ± 0.01 |

[1] as stated by the silica supplier
[2] ratio of VTMS and BSA in the vinylization mixture for the synthesis of vinylized silica
[3] carbon content of the vinylized silica, determined by elemental analysis
[4] amount of incorporated sulfur (PMPMS) of the PMPMS thiol-functionalized vinylized silica determined by elemental analysis data
[5] amount of free sulfhydryl groups of the PMPMS thiol-functionalized vinylized silica determined by a thiol-disulfid exchange reaction with DPDS
[6] amount of incorporated sulfur (PMPMS) of the tBuCQN-PMPMS thiol-functionalized silica determined by elemental analysis data
[7] amount of incorporated chiral selector (tBuCQN) of the tBuCQN-PMPMS thiol-functionalized silica determined by elemental analysis data

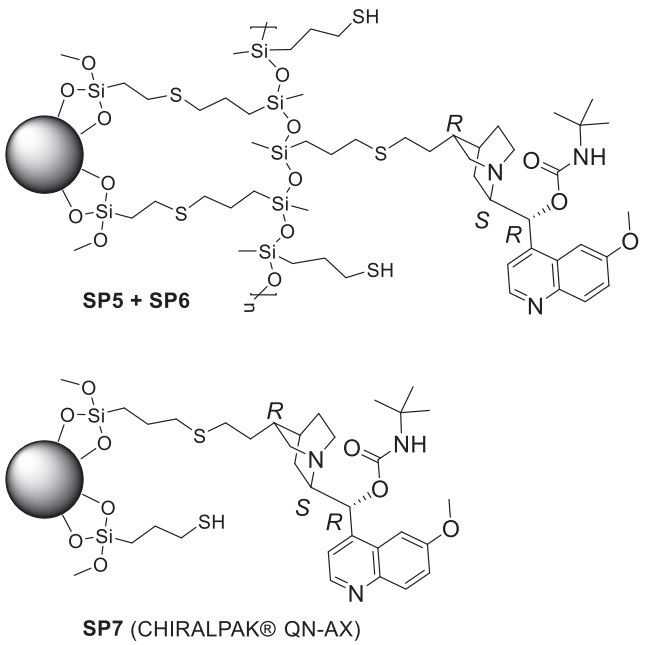


**Fig. 7.** Surface chemistries of the prepared stationary phases SP5-7. SP5 and SP6 are based on #T11 (200 Å, 5 µm, Table 1), whereas SP7 from silica of 120 Å pore size and 5 µm particle size. All stationary phases were slurry packed into stainless steel columns of 50 mm x 3 mm size.

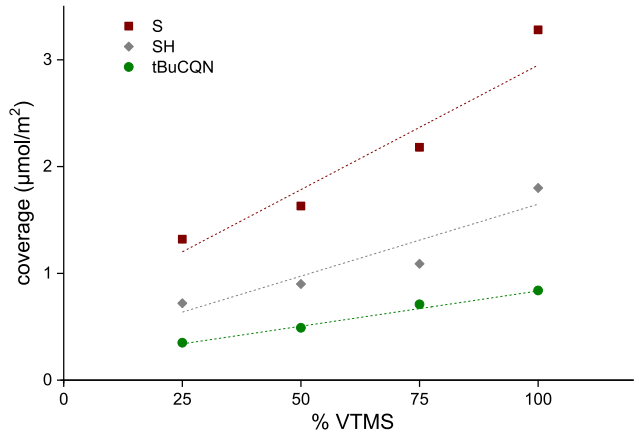


**Fig. 8.** Incorporation of PMPMS and tBuCQN in dependence of the initial vinyl group content of precursor vinylized silica. The x-axis represents the percentage of vinylization agent VTMS in the vinylization mixture for the preparation of vinylized silica. The y-axis shows the ensuing achieved PMPMS coverage plus its sulfhydryl content and the finally immobilized amount of tBuCQN.

or thin film and low coverage, which gives better chromatographic efficiencies.

SP5 and SP6 were finally chromatographically tested and compared to SP7 regarding their performance by separating several chiral acids in polar organic elution mode (Table 4,Fig. 9). Enantioselectivities of all three chiral stationary phases are in the same range for all analytes, while retention factors increased significantly with rising selector coverages. This indicates that the retention of the chiral acids applied in these tests are mainly based on the interaction with the chiral ligand, whereas the interaction with the siloxane backbone is of minor relevance. However, in comparison to the benchmark CSP SP7, the plate numbers for the PMPMS coated CSPs SP5 and SP6 are significantly lower resulting in slightly lower resolution. It seems that there is still room for further improvement in this regard and thinner PMPMS coatings should be examined for optimal chromatographic efficiencies.

**Table 4**
Chromatographic results and column performance of tBuCQN based stationary phases SP5-7

| | SP5 | | | | | SP6 | | | | | SP7 | | | | |
|---|---|---|---|---|---|---|---|---|---|---|---|---|---|---|---|
| | $k_1$ | $k_2$ | $\alpha$ | R | $N_1$ | $N_2$ | $k_1$ | $k_2$ | $\alpha$ | R | $N_1$ | $N_2$ | $k_1$ | $k_2$ | $\alpha$ | R | $N_1$ | $N_2$ |
| Dichlorprop | 1.87 | 2.29 | 1.23 | 1.31 | 1548 | 1409 | 5.62 | 6.76 | 1.20 | 1.37 | 1214 | 1155 | 8.55 | 10.38 | 1.21 | 2.32 | 2836 | 2795 |
| Ac-Phe | 0.30 | 0.50 | 1.67 | 1.36 | 1485 | 1390 | 0.90 | 1.29 | 1.44 | 1.63 | 1268 | 1125 | 2.71 | 3.75 | 1.38 | 2.78 | 2321 | 1892 |
| Z-Phe | 1.82 | 2.14 | 1.18 | 1.03 | 1469 | 1287 | 4.77 | 5.48 | 1.15 | 0.93 | 1101 | 982 | 8.34 | 10.00 | 1.20 | 1.99 | 2375 | 2361 |
| Fmoc-Phe | 5.34 | 7.35 | 1.38 | 2.32 | 1137 | 1142 | 14.00 | 18.80 | 1.34 | 2.21 | 1002 | 1033 | 18.34 | 27.42 | 1.50 | 4.53 | 2280 | 2241 |
| DNB-Leu | 1.84 | 24.26 | 13.16 | 14.79 | 1367 | 1369 | 6.00 | 64.34 | 10.73 | 13.70 | 1010 | 1165 | 8.36 | 126.45 | 15.13 | 26.49 | 2388 | 3890 |

mobile phase: methanol/50 mM ammonium acetate buffer (80/20 v/v), pH adjusted to 6, flow rate: 0.5 mL/min, detection: 254 nm, temperature: 25°C, injection volume: 2 µL, sample concentration: 0.1 mg/mL

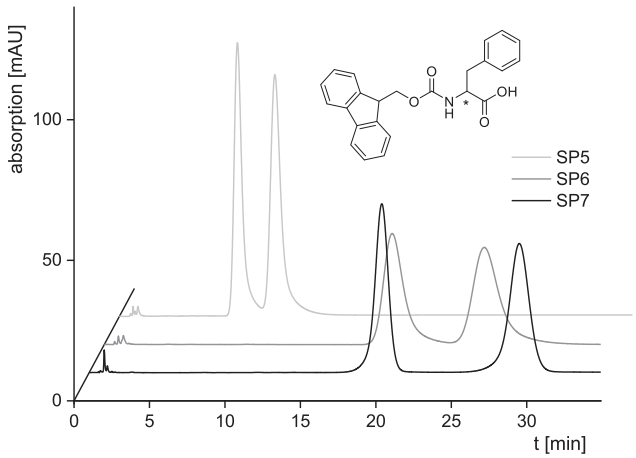


**Fig. 9.** Chromatographic results for the chiral separation of Fmoc-Phe for SP5-7. The chiral centre of the amino acid residue is marked by *. The elution order was always R<S.

Nevertheless, the polymer based chiral stationary phases showed a solid performance and proved the excellent aptitude of PMPMS thiol-functionalized silica as platform for the attachment of functional ligands.

## 4. Conclusions

In this work, the preparation of polythiol-functionalized silica particles by immobilization of PMPMS via thiol-ene click reaction and its further modification for silver ion chromatography and enantioselective high-performance liquid chromatography was presented and discussed. Thereby, two different approaches of initiation of the radical addition reaction used for the anchoring of PMPMS to vinylized silica were evaluated. Subsequently, elemental analysis and a thiol-disulfide exchange reaction with DPDS were utilized to determine the amount of embedded PMPMS and the percentage of unreacted sulfhydryl groups. In doing so, it turned out that the thermochemical initiation led to more adequate PMPMS coatings and consequently the optimized polythiol-functionalized silica particles were used for further studies. Hence, stationary phases for silver ion chromatography and enantioselective HPLC were prepared. Thus, after the oxidation of the sulfhydryl groups of the polythiol-functionalized silica particles and its ensuing loading with silver ions, the evolved stationary phase showed fine performance with regard to the separation of fatty acid methyl esters according to their number of double bonds and the separation of cis- and trans-stilbene. The bonding of tBuCQN on the PMPMS layer led to stationary phases that worked well for the enantioseparation of chiral acids. Conclusively, PMPMS thiol-functionalized silica particles were successfully synthesized and its suitability for further modification was proven.

## Declaration of Competing Interest

The authors declare that they have no known competing financial interests or personal relationships that could have appeared to influence the work reported in this paper.

## Supplementary materials

Supplementary material associated with this article can be found, in the online version, at doi:10.1016/j.chroma.2021.462069.

## References

[1] M. Najafi, R. Rostamian, A.A. Rafati, Chemically modified silica gel with thiol group as an adsorbent for retention of some toxic soft metal ions from water and industrial effluent, Chem. Eng. J. 168 (2011) 426–432.
[2] A. Zimmermann, J. Horak, A. Sievers-Engler, C. Sanwald, W. Lindner, M. Kramer, M. Lämmerhofer, Surface-crosslinked poly(3-mercaptopropyl)methylsiloxane-coatings on silica as new platform for low-bleed mass spectrometry-compatible functionalized stationary phases synthesized via thiol-ene click reaction, J. Chromatogr. A 1436 (2016) 73–83.
[3] A. Mandl, L. Nicoletti, M. Lämmerhofer, W. Lindner, Quinine- versus carbamoylated quinine-based chiral anion exchangers: A comparison regarding enantioselectivity for N-protected amino acids and other chiral acids, J. Chromatogr. A 858 (1999) 1–11.
[4] C. Czerwenka, M. Lämmerhofer, N.M. Maier, K. Rissanen, W. Lindner, Direct high-performance liquid chromatographic separation of peptide enantiomers: Study on chiral recognition by systematic evaluation of the influence of structural features of the chiral selectors on enantioselectivity, Anal. Chem. 74 (2002) 5658–5666.
[5] A.F.G. Gargano, M. Kohout, P. Macikova, M. Lämmerhofer, W. Lindner, Direct high-performance liquid chromatographic enantioseparation of free alpha-, beta- and gamma-aminophosphonic acids employing cinchona-based chiral zwitterionic ion exchangers, Anal. Bioanal. Chem. 405 (2013) 8027–8038.
[6] F. Ianni, R. Sardella, A. Carotti, B. Natalini, W. Lindner, M. Lämmerhofer, Quinine-Based Zwitterionic Chiral Stationary Phase as a Complementary Tool for Peptide Analysis: Mobile Phase Effects on Enantio- and Stereoselectivity of Underivatized Oligopeptides, Chirality 28 (2016) 5–16.
[7] Q.Q. Wang, P.J. Zhu, M. Ruan, H.H. Wu, K. Peng, H. Han, G.W. Somsen, J. Crommen, Z.J. Jiang, Chiral separation of acidic compounds using an O-9-(tert-butylcarbamoyl)quinidine functionalized monolith in micro-liquid chromatography, J. Chromatogr. A 1444 (2016) 64–73.
[8] M. Lämmerhofer, W. Lindner, Quinine and quinidine derivatives as chiral selectors I. Brush type chiral stationary phases for high-performance liquid chromatography based on cinchonan carbamates and their application as chiral anion exchangers, J. Chromatogr. A 741 (1996) 33–48.
[9] S. Bäurer, A. Zimmermann, U. Woiwode, O.L. Sánchez Muñoz, M. Kramer, J. Horak, W. Lindner, W. Bicker, M. Lämmerhofer, Stable-bond polymeric reversed-phase/weak anion-exchange mixed-mode stationary phases obtained by simultaneous functionalization and crosslinking of a poly(3-mercaptopropyl)methylsiloxane-film on vinyl silica via thiol-ene double click reaction, J. Chromatogr. A 1593 (2019) 110–118.
[10] C. Geibel, K. Dittrich, M. Wolter, M. Lämmerhofer, Thiol-ene photo-click immobilization of a chiral chromatographic ligand on silica particles, J. Chromatogr. A 1622 (2020) 461133.
[11] K. Schmitt, M. Lämmerhofer, Optimization of the surface modification process of cross-linked polythiol-coated chiral stationary phases synthesized by a two-step thiol-ene click reaction, J. Sep. Sci. 41 (2018) 1338–1345.
[12] R.O. Adlof, Separation of cis and trans unsaturated fatty acid methyl esters by silver ion high-performance liquid chromatography, J. Chromatogr. A 659 (1994) 95–99.
[13] R. Adlof, G. List, Analysis of triglyceride isomers by silver-ion high-performance liquid chromatography. Effect of column temperature on retention times, J. Chromatogr. A 1046 (2004) 109–113.
[14] G. Dobson, W.W. Christie, B. Nikolova-Damyanova, Silver ion chromatography of lipids and fatty acids, J. Chromatogr. B: Biomed. Sci. Appl. 671 (1995) 197–222.
[15] S.M. Momchilova, B.M. Nikolova-Damyanova, Advances in silver ion chromatography for the analysis of fatty acids and triacylglycerols-2001 to 2011, Anal. Sci. 28 (2012) 837–844.
[16] N.M. Maier, L. Nicoletti, M. Lämmerhofer, W. Lindner, Enantioselective anion exchangers based on cinchona alkaloid-derived carbamates: influence of C8/C9 stereochemistry on chiral recognition, Chirality 11 (1999) 522–528.
[17] I.S. Krull, Z. Deyl, H. Lingeman, General strategies and selection of derivatization reactions for liquid chromatography and capillary electrophoresis, J. Chromatogr. B: Biomed. Sci. Appl. 659 (1994) 1–17.
[18] T. Teerlink, Derivatization of posttranslationally modified amino acids, J. Chromatogr. B: Biomed. Sci. Appl. 659 (1994) 185–207.
[19] B. Preinerstorfer, W. Bicker, W. Lindner, M. Lämmerhofer, Development of reactive thiol-modified monolithic capillaries and in-column surface functionalization by radical addition of a chromatographic ligand for capillary electrochromatography, J. Chromatogr. A 1044 (2004) 187–199.
[20] R. Nogueira, M. Lämmerhofer, N.M. Maier, W. Lindner, Spectrophotometric determination of sulfhydryl concentration on the surface of thiol-modified chromatographic silica particles using 2,2′-dipyridyl disulfide reagent, Anal. Chim. Acta 533 (2005) 179–183.
[21] O.L. Sánchez Muñoz, E.P. Hernandez, M. Lämmerhofer, W. Lindner, E. Kenndler, Estimation and comparison of zeta-potentials of silica-based anion-exchange type porous particles for capillary electrochromatography from electrophoretic and electroosmotic mobility, Electrophoresis 24 (2003) 390–398.
[22] L.F. Ribeiro, J.C. Masini, F. Svec, Use of thiol functionalities for the preparation of porous monolithic structures and modulation of their surface chemistry: A review, Trends Anal. Chem. 118 (2019) 606–624.
[23] N.F. Ayub, S. Hashim, J. Jamaluddin, N. Adrus, New UV LED curing approach for polyacrylamide and poly(N-isopropylacrylamide) hydrogels, New J. Chem. 41 (2017) 5613–5619.

[24] P. Levkin, N.M. Maier, W. Lindner, V. Schurig, A practical method for the quantitative assessment of non-enantioselective versus enantioselective interactions encountered in liquid chromatography on brush-type chiral stationary phase, J. Chromatogr. A 1269 (2012) 270–278.
[25] A.B. Lowe, Thiol-ene "click" reactions and recent applications in polymer and materials synthesis, Polym. Chem-Uk 1 (2010) 17–36.
[26] M. Holčapek, M. Lísa, Chapter 4 - Silver-Ion Liquid Chromatography–Mass Spectrometry, in: M. Holčapek, W.C. Byrdwell (Eds.), Handbook of Advanced Chromatography/Mass Spectrometry Techniques, AOCS Press, 2017, pp. 115–140.
[27] B. Nikolova-Damyanova, Retention of lipids in silver ion high-performance liquid chromatography: Facts and assumptions, J. Chromatogr. A 1216 (2009) 1815–1824.
[28] C.R. Scholfield, E.A. Emken, Isolation of methylcis-15-octadecenoate by chromatography on a silver-treated macroreticular exchange resin, Lipids 1 (1966) 235–236.
[29] J.D. Chatt, L.A Olefin, Co-ordination Compounds. Part III.* Infra-red Spectra and Structure: Attempted Preparation of Acetylene Complexes, J. Chem. Soc. (1953) 2939–2947.
[30] B. Nikolova-Damyanova, W.W. Christie, B. Herslof, Mechanistic aspects of fatty acid retention in silver ion chromatography, J. Chromatogr. A 749 (1996) 47–54.
[31] U. Woiwode, S. Neubauer, W. Lindner, S. Buckenmaier, M. Lämmerhofer, Enantioselective multiple heartcut two-dimensional ultra-high-performance liquid chromatography method with a coreshell chiral stationary phase in the second dimension for analysis of all proteinogenic amino acids in a single run, J. Chromatogr. A 1562 (2018) 69–77.
[32] M. Wolter, M. Lämmerhofer, In-situ functionalized monolithic polysiloxane-polymethacrylate composite materials from polythiol-ene double click reaction in capillary column format for enantioselective nano-high-performance liquid chromatography, J. Chromatogr. A 1497 (2017) 172–179.
[33] V. Piette, M. Lämmerhofer, W. Lindner, J. Crommen, Enantiomer separation of N-protected amino acids by non-aqueous capillary electrophoresis and high-performance liquid chromatography with tert.-butyl carbamoylated quinine in either the background electrolyte or the stationary phase, J. Chromatogr. A 987 (2003) 421–427.
[34] M. Lämmerhofer, D. Hebenstreit, E. Gavioli, W. Lindner, A. Mucha, P. Kafarski, P. Wieczorek, High-performance liquid chromatographic enantiomer separation and determination of absolute configurations of phosphinic acid analogues of dipeptides and their alpha-aminophosphinic acid precursors, Tetrahedron: Asymmetry 14 (2003) 2557–2565.
[35] E. Tobler, M. Lämmerhofer, G. Mancini, W. Lindner, On-column deracemization of an atropisomeric biphenyl by quinine-based stationary phase and determination of rotational energy barrier by enantioselective stopped-flow HPLC and CEC, Chirality 13 (2001) 641–647.

## VIII.2 Publication III – Supplementary Material

# Preparation and characterization of poly(3-mercaptopropyl)methyl siloxane functionalized silica particles and their further modification for silver ion chromatography and enantioselective high-performance liquid chromatography

**Marc Wolter** [a], Xingyu Chen [a], Ulrich Woiwode [a,b], Christian Geibel [a], Michael Lämmerhofer [a,*]

[a] Institute of Pharmaceutical Sciences, Pharmaceutical (Bio-)Analysis, University of Tübingen, Auf der Morgenstelle 8, 72076 Tübingen, Germany
[b] TECHPharm GmbH, Draisstraße 14, 76646 Bruchsal, Germany

* corresponding author

# Table of contents

## PART I: Synthesis of modified silica particles

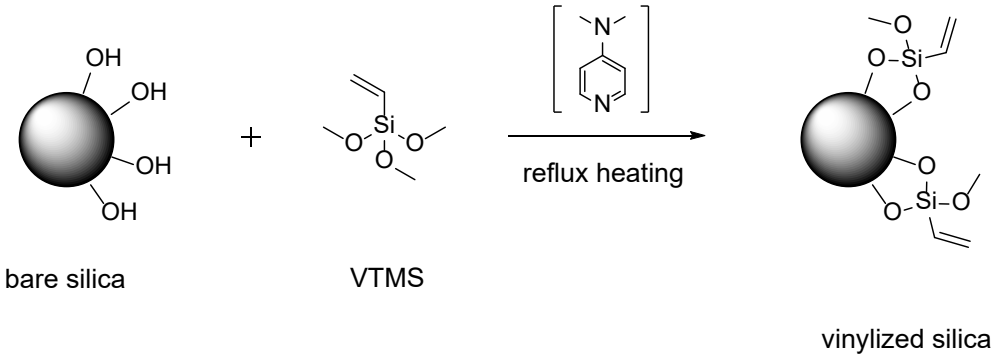


**Fig. S1.** Reaction scheme for the synthesis of vinylized silica.

## PART II: Determination of sulfhydryl groups via DPDS assay

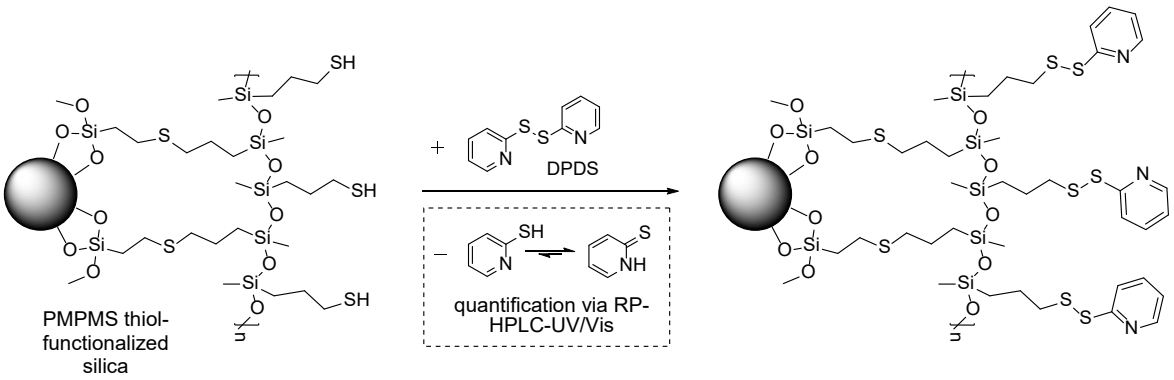


**Fig. S2.** Determination of free and accessible sulfhydryl groups via thiol-disulfide exchange reaction using DPDS: Reaction scheme for the thiol-disulfide exchange reaction.

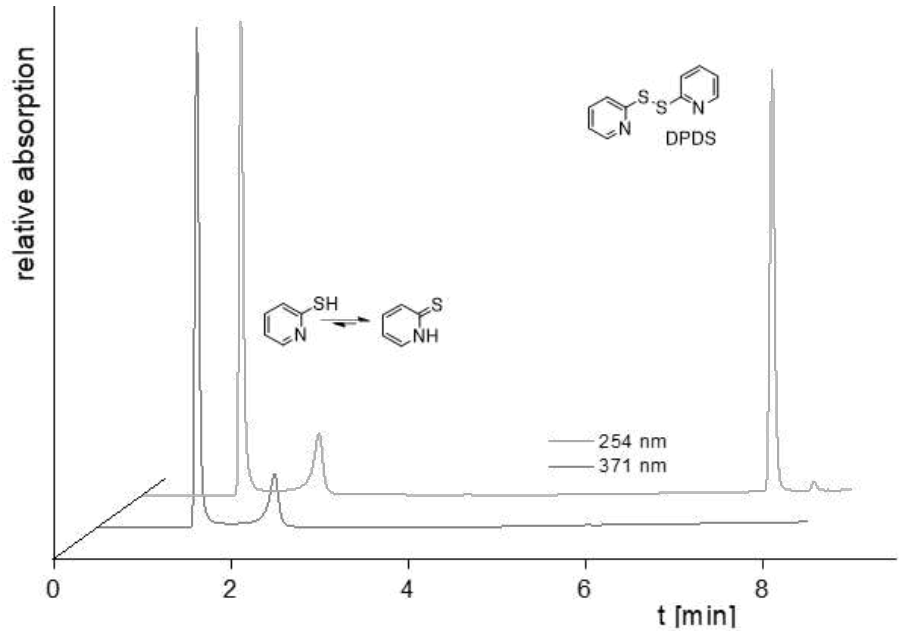


**Fig. S3.** Determination of free and accessible sulfhydryl groups via thiol-disulfide exchange reaction using DPDS: Quantification of the generated 2-pyridyl thiol and its tautomeric thione form via RP-HPLC-UV/VIS (Kinetex 2.6 µm C18 100 Å 50 x 4.6 mm, mobile phase: A: $H_2O$ + 0.1 % FA, B: ACN, gradient: 0-7 min 5-90 % B, 7-9 min 90-5 % B, 9-15 min 5% B, flow: 0.5 mL/min, detection: 371 nm and 254 nm, injection volume: 5 µL, temperature: 25 °C). The peaks were identified by hyphenation to an Agilent LC MSD-SL ion-trap mass spectrometer.

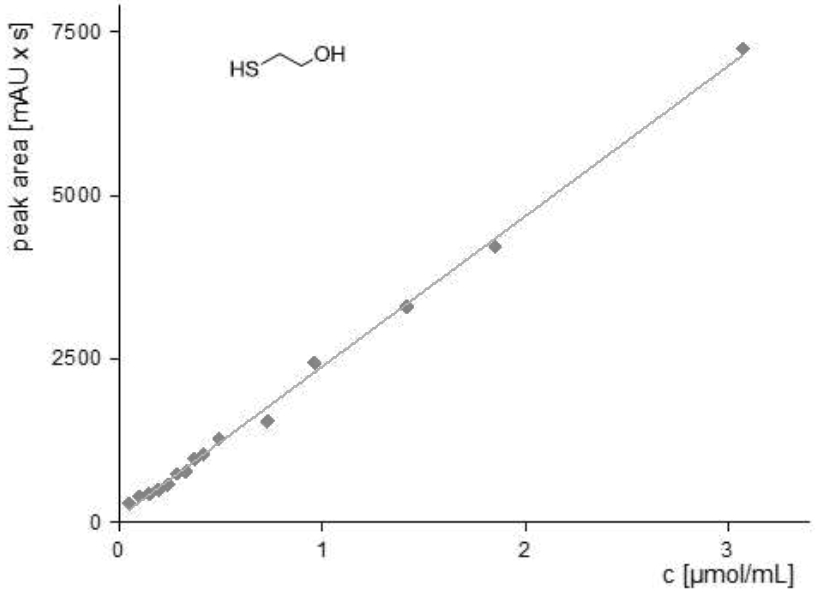


**Fig. S4.** Determination of free and accessible sulfhydryl groups via a thiol-disulfide exchange reaction using DPDS: Calibration line based on 2-mercaptoethanol as reference substance with known sulfhydryl group content. The peak area was determined by summing the areas of 2-pyridyl thiol and its tautomerized thione form.

## PART III: Design of experiment approach

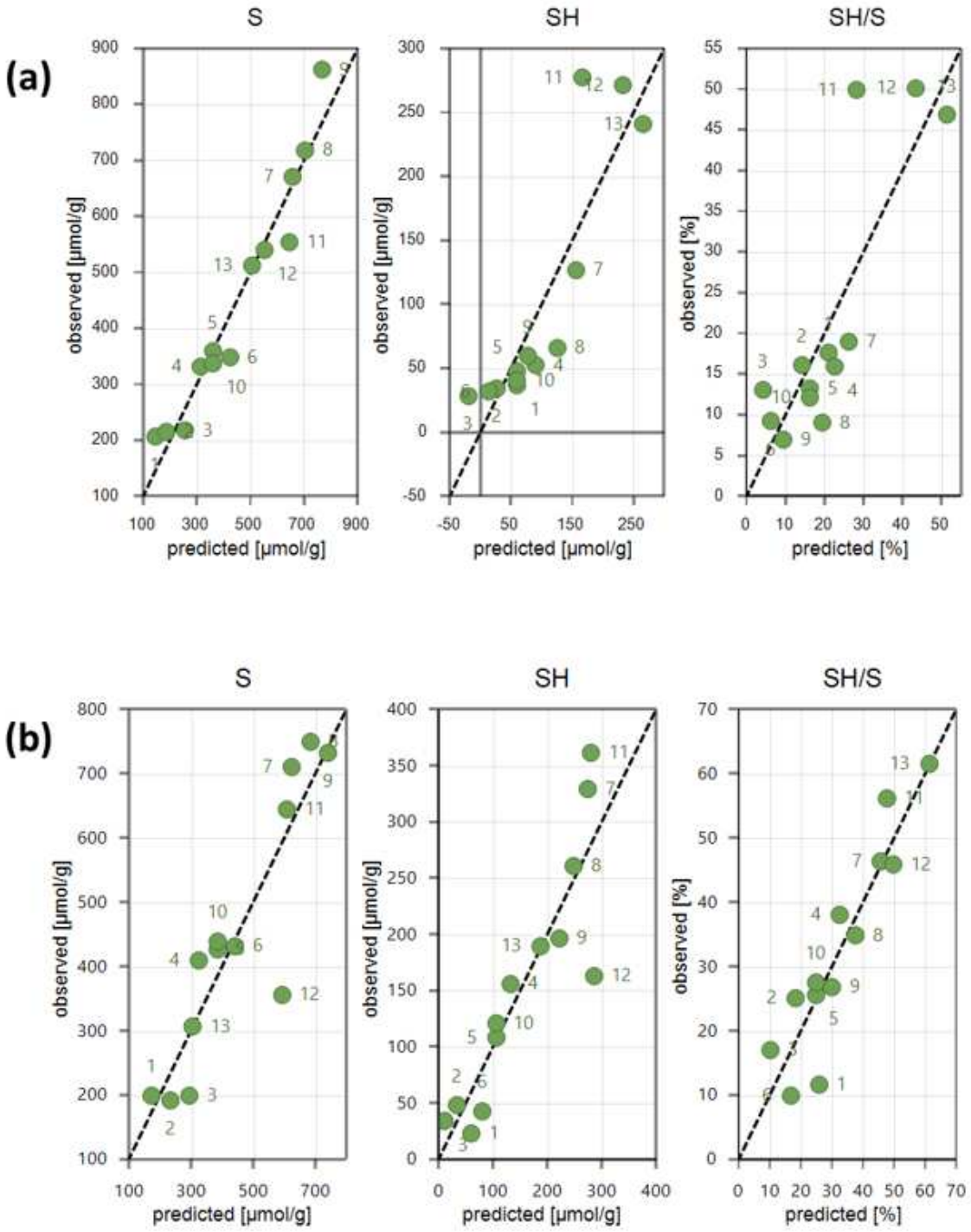


**Fig. S5.** Observed vs. predicted sulphur (S; sulphur correlates directly with PMPMS), sulfhydryl (SH) content and its respective ratio for (a) the photochemical approach and (b) the thermochemical approach as calculated by MODDE Pro Ver. 12.1.0.54.91 from Sartorius Stedim (Umeå, Sweden). Note that the numbers refer to #P1-13 for (a) and #T1-13 for (b) from Table 1.

**Table. S1.** Statistic parameters for DoE models observed vs. predicted sulphur (S), sulfhydryl content (SH) and its respective ratio. p > 0.05 was coloured red.

| Thermochemical approach | | | | | | | | | | | | |
|---|---|---|---|---|---|---|---|---|---|---|---|---|
| | S | | | | SH | | | | SH/S | | | |
| | Coeff. SC | Std. Err. | P | Conf.int (±) | Coeff. SC | Std. Err. | P | Conf.int (±) | Coeff. SC | Std. Err. | P | Conf.int (±) |
| constant | 231.838 | 84.964 | 0.023 | 192.204 | 75.577 | 48.594 | 0.154 | 109.927 | 38.824 | 6.416 | 0.002 | 14.515 |
| PMPMS | 222.121 | 36.794 | 0.000 | 83.234 | 106.001 | 21.044 | 0.001 | 47.604 | 9.827 | 2.779 | 0.006 | 6.286 |
| time | 76.778 | 44.009 | 0.115 | 99.556 | -31.609 | 25.170 | 0.241 | 56.939 | -10.008 | 3.323 | 0.015 | 7.518 |
| radical starter | 211.143 | 87.281 | 0.039 | 197.446 | 73.461 | 49.919 | 0.173 | 112.925 | -8.555 | 6.591 | 0.227 | 14.911 |
| | N=13, DF=9, Q2=0.655, R2=0.835, R2 adj.=0.779, Cond.no.=5.864, RSD=7.697, Conficence=0.95 | | | | | | | | | | | |
| | | | | | | | | | | | | |
| **Photochemical approach** | | | | | | | | | | | | |
| | S | | | | SH | | | | SH/S | | | |
| | Coeff. SC | Std. Err. | P | Conf.int (±) | Coeff. SC | Std. Err. | P | Conf.int (±) | Coeff. SC | Std. Err. | P | Conf.int (±) |
| constant | 379.781 | 30.509 | 5.63E-07 | 69.017 | 123.396 | 27.633 | 0.002 | 62.510 | 27.839 | 5.215 | 4.69E-04 | 11.797 |
| PMPMS | 257.654 | 21.365 | 7.38E-07 | 48.331 | 48.945 | 19.351 | 0.032 | 43.775 | 2.592 | 3.518 | 0.496 | 8.261 |
| time | 62.071 | 24.108 | 0.030 | 54.536 | -43.533 | 21.835 | 0.077 | 49.395 | -9.297 | 4.121 | 0.050 | 9.322 |
| radical starter | 69.524 | 30.828 | 0.051 | 69.738 | -50.326 | 27.921 | 0.105 | 63.163 | -11.524 | 5.269 | 0.057 | 11.920 |
| | N=13, DF=9, Q2=0.341, R2=0.717, R2 adj.=0.623, Cond.no.=3.575, RSD=9.869, Conficence=0.95 | | | | | | | | | | | |

## PART IV: Silver ion chromatography

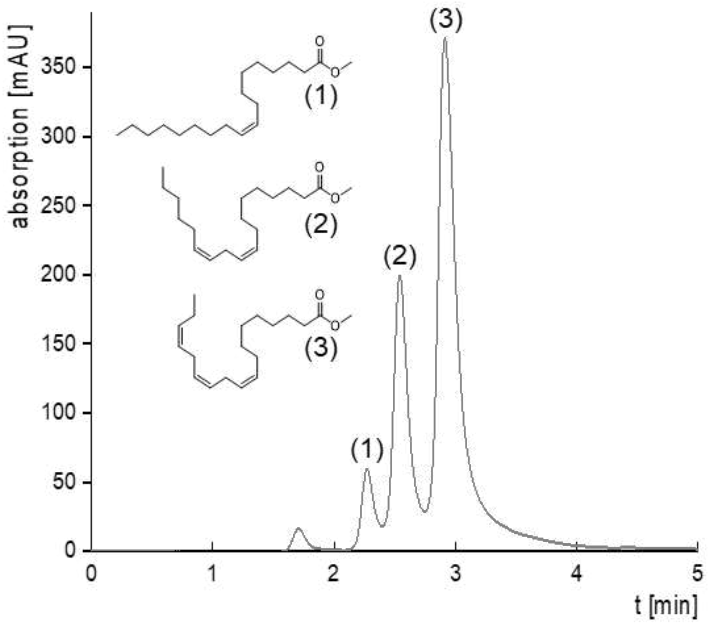


**Fig. S6.** Chromatographic results for SP4 in silver ion mode for the separation of FAME with different flow rate than in Fig. 5: (1) methyl oleate, (2) methyl linoleate, (3) methyl linolenate (mobile phase: hexane plus 0.15% (v/v) ACN, flow rate: 0.2 mL/min, detection: 210 nm, injection volume: 2 µL, sample concentration: 0.25 mg/mL for each FAME)

## PART V: Surface charge characterization

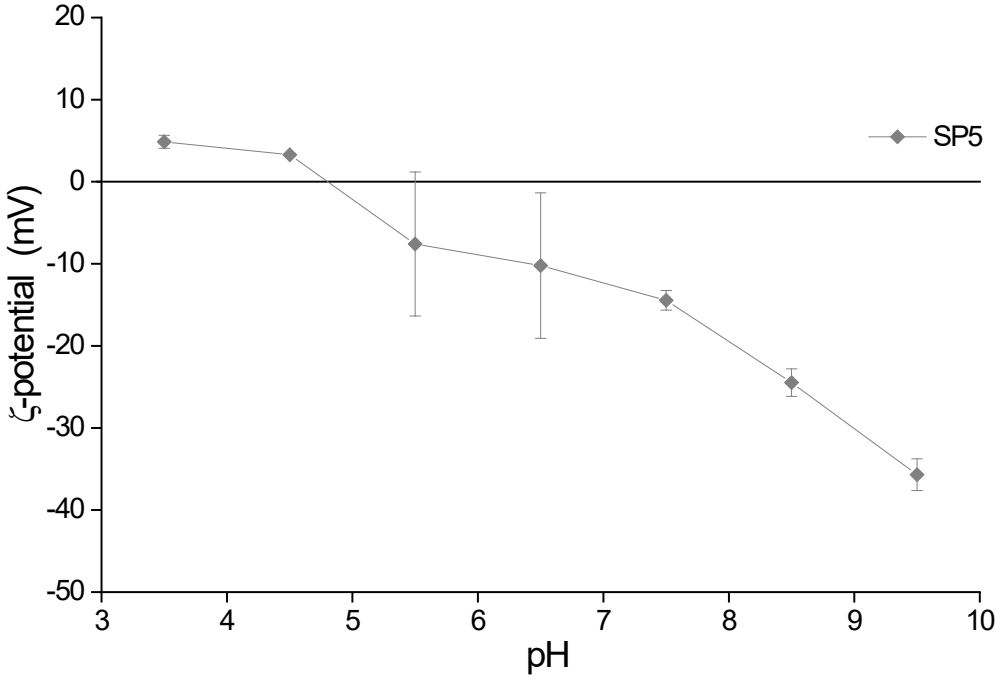


**Fig. S7.** pH dependent ζ-potentials for SP5.

$$\mu_E = C\frac{\varepsilon_0 \cdot \varepsilon_r \cdot \zeta}{\eta}$$

$\mu_E$: mobility of a particle

*C*: The constant C becomes 2/3 for $\kappa r<0.1$ ($\kappa$, Debye parameter; $\kappa^{-1}$, Debye length) (Hückel approximation) and 1 for $\kappa r>100$ (Smoluchowski approximation).

$\varepsilon_R$: relative permittivity

$\varepsilon_0$: permittivity of vacuum

$\eta$: viscosity

**Equ. S1.** Von Smoluchowski equation used for the calculation of the ζ-potentials.

## PART VI: Enantioselective HPLC

| | SP5 | | | | | SP6 | | | | | SP7 | | | | |
|---|---|---|---|---|---|---|---|---|---|---|---|---|---|---|---|
| | $k_1$ | $k_2$ | α | R | $N_1$ | $N_2$ | $k_1$ | $k_2$ | α | R | $N_1$ | $N_2$ | $k_1$ | $k_2$ | α | R | $N_1$ | $N_2$ |
| Dichlorprop | 1.86 | 2.28 | 1.22 | 1.03 | 999 | 884 | 5.61 | 6.74 | 1.20 | 1.07 | 780 | 724 | 8.53 | 10.33 | 1.21 | 1.86 | 1841 | 1850 |
| Ac-Phe | 0.30 | 0.50 | 1.64 | 1.01 | 843 | 819 | 0.92 | 1.32 | 1.43 | 1.28 | 788 | 721 | 2.72 | 3.75 | 1.38 | 2.28 | 1510 | 1290 |
| Z-Phe | 1.80 | 2.12 | 1.18 | 0.68 | 664 | 618 | 4.78 | 5.47 | 1.15 | 0.66 | 554 | 513 | 8.28 | 9.93 | 1.20 | 1.61 | 1549 | 1528 |
| Fmoc-Phe | 5.29 | 7.25 | 1.37 | 1.84 | 747 | 736 | 13.88 | 18.63 | 1.34 | 1.75 | 637 | 649 | 18.08 | 28.48 | 1.58 | 4.14 | 1418 | 1531 |
| DNB-Leu | 1.83 | 23.69 | 12.91 | 11.57 | 870 | 842 | 5.91 | 63.14 | 10.68 | 10.76 | 644 | 718 | 12.72 | 122.64 | 9.64 | 15.61 | 2322 | 1451 |

**Table S2.** Chromatographic results and column performance of tBuCQN based stationary phases SP5-7 with different flow rate than in Table 3 (methanol/50 mM ammonium acetate buffer (80/20 v/v), pH adjusted to 6, flow rate: 1.0 mL/min, detection: 254 nm, temperature: 25 °C, injection volume: 2 µL, sample concentration: 0.1 mg/mL).

# IX. CHAPTER FIVE

## Controllable organosilane monolayer density of surface bonding using silatranes for thiol functionalization of silica particles for liquid chromatography and validation of microanalytical method for elemental composition determination

## IX.1 Publication IV – Main Document

Journal of Chromatography A 1653 (2021) 462418

Contents lists available at ScienceDirect

Journal of Chromatography A

journal homepage: www.elsevier.com/locate/chroma

# Controllable organosilane monolayer density of surface bonding using silatranes for thiol functionalization of silica particles for liquid chromatography and validation of microanalytical method for elemental composition determination

Christian Geibel[a], Johannes Theiner[b], Marc Wolter[a], Markus Kramer[c], Wolfgang Lindner[d], Michael Lämmerhofer[a,*]

[a] Institute of Pharmaceutical Sciences, Pharmaceutical (Bio-)Analyses, University of Tübingen, Auf der Morgenstelle 8, Tübingen 72076, Germany
[b] Mikroanalytisches Laboratorium, University of Vienna, Währingerstrasse 42, Vienna 1090, Austria
[c] Institute of Organic Chemistry, University of Tübingen, Auf der Morgenstelle 18, Tübingen 72076, Germany
[d] Institute of Analytical Chemistry, University of Vienna, Währingerstrasse 38, Vienna 1090, Austria

ARTICLE INFO

*Article history:*
Received 7 May 2021
Revised 15 July 2021
Accepted 17 July 2021
Available online 22 July 2021

*Keywords:*
Silica gel functionalization
Chiral stationary phase
Thiol-ene click reaction
Self-assembled monolayer
Solid-state NMR
Elemental analysis validation

ABSTRACT

The present work systematically investigates a new strategy for the functionalization of silica gel using alkyl silatrane chemistry instead of alkylsilanes for synthesis of chromatographic stationary phases. In this work, silica was chemically modified for further functionalization by a thiol-ene click reaction. Thus, 3-mercaptopropylsilatrane (MPS) was used which is capable to form self-assembled monolayers (SAM) on top of silanol surfaces in a controlled manner as previously shown for silicon wafers. The utility of this chemistry for stationary phase synthesis in liquid chromatography was not evaluated yet. Hence, silica surface modifications using MPS were studied in comparison to established 3-mercaptopropyltrimethoxysilane (MPTMS) chemistry. First, the employed elemental analysis method was validated and it showed excellent intra-day and inter-day precisions (typically less than 5% RSD). It could be shown that the reaction kinetics of MPS was roughly 35-times faster than with MPTMS. After 30 min reaction time with MPS, the thiol content reached 74% of the maximal coverage. Due to controlled chemistry with MPS, which does not lead to oligomeric siloxane network at the silica surface, the ligand coverage was lower. However, multiple silanization cycles with MPS led to a dense surface coverage (around 4 µmol $m^{-2}$). $^{29}$Si cross polarization/magic angle spinning (CP/MAS) solid-state NMR revealed distinct $T^1/T^2/T^3$ ratios for MPS and MPTMS materials with up to 80% $T^3$ (indicative for trifunctional siloxane linkage) for MPS and around 20% $T^3$ for MPTMS. This indicates a more homogeneous, thinner monolayer film of MPS on the silica surface, as compared to an irregular thick oligomeric siloxane network with MPTMS. Bonding of quinine carbamate as chiral selector afforded an efficient chiral stationary phase (CSP) for chromatographic enantiomer separation. Separation factors were comparable to MPTMS-bonded CSP, however, chromatographic efficiency was much better for the MPS-bonded CSP. H/u curves indicated a reduced mass transfer resistance by roughly factor 3 for MPS- compared to MPTMS-bonded CSP. This confirms better chromatographic performance of surfaces with homogeneous monolayer compared to network structures on the silica surface which suffer from poor stationary phase mass transfer.



## 1. Introduction

Dedicated surface functionalization of silica particles is a crucial step in the development of stationary phases for the diverse retention principles in liquid chromatography [1]. In a variety of chromatographic modes, e.g. octadecylsilica, direct surface modification by a single silanization reaction of silica silanols with mono-, di- and trifunctional alkoxy- or chloro-alkylsilanes is a preferred approach [2,3]. For other separation principles, e.g. affinity and enantioselective LC, it is convenient to attach first a reactive anchor to the silica surface by a vinylization reaction and couple the affinity ligand or chiral selector in a second step to the reactive particles. Numerous publications have shown the advantage of either thiol or vinyl moieties as reactive groups for further surface

* Correspondence author.
*E-mail address:* michael.laemmerhofer@uni-tuebingen.de (M. Lämmerhofer).

https://doi.org/10.1016/j.chroma.2021.462418
0021-9673/

functionalization [4–12]. Correspondingly, the thiol-ene click reaction has gained great popularity for dedicated functionalization of stationary phases. Surface coverage and density of the ligand on the silica surface, orientation and chemical environment, accessibility of the ligand's binding site for the analytes play a major role for both thermodynamic and kinetic properties of the stationary phase. Hence, a good control over the surface functionalization steps of the porous silica particles is mandatory as it can have a major influence on the overall chromatographic performance of the resulting column. Uncontrolled functionalization may lead to non-ordered and imperfect layers on the silica surface with associated negative characteristics such as inaccessibility of thiol groups for the thiol-ene click reaction and suboptimal kinetic performance in liquid chromatography.

It is evident that the first stage of silica surface modification is a critical step in stationary phase synthesis. Considering the great importance, however, only a limited number of articles focused on the study of organo-silane monolayer formation on silica surface [3,13]. It is common understanding nowadays that di- and trifunctional silanes under anhydrous conditions lead to monomeric phases similar to monofunctional silanes [3]. With trifunctional silanes and presence of water in the reaction mixture silane polymerization may occur and these silane polymers may subsequently attach to the silica surface affording polymeric phases. If the synthesis is carried out with trifunctional silanes and humidified silica which carries a water monolayer on the surface, the silane polymerization occurs parallel to the silica surface giving a dense self-assembled monolayer of polysiloxane coating (horizontal polymerization) [3,13]. It can be distinguished from the more random vertical polymerization that results from solution polymerization and subsequent multipoint attachment with some silane groups not directly attached to the silica surface [13]. Horizontal polymerization provides higher density and due to its well-ordered regular surface structure and good accessibility of the chromatographic ligand should provide better chromatographic characteristics and higher stability.

In this work, we address a new way of functionalization of silica particles by silatrane chemistry and compare this with the well-established functionalization via trialkoxysilanes. In particular, 3-mercaptopropylsilatrane (MPS) is used as reactive component for the silanization in comparison to 3-mercaptopropyltrimethoxysilane (MPTMS) as benchmark trialkoxysilane (see Fig. 1a). Due to the transannular dative bond between silicon and nitrogen, silatranes are more stable towards hydrolysis than their respective trialkoxysilanes, at least in neutral aqueous solution [14], which makes the handling of the substance more convenient. In presence of acid, the reactivity of the silatrane will be higher due to the increased proton affinity in comparison to their trialkoxysilane analogues [14], mainly because of the pentacoordination of silicon due to the dative N→Si bond [15]. The resistance to hydrolytic degradation of the silatrane inhibits the formation of a heterogeneous siloxane network on the surface in favour for a thin, homogenous monomolecular layer [16]. This in turn might be of great advantage for the functionalization of silica particles with narrow pores (e.g. 100 Å and smaller) avoiding blockage of the pores by polysiloxane network structure. Moreover, silatrane derivatives are straightforward to synthesize from its respective silane counterparts. To our knowledge, this is the first study on the silatrane based functionalization of silica particles for application in liquid chromatography. In this work, we demonstrate the synthesis, reaction kinetics, surface chemistry as elucidated by solid-state NMR, characterization by elemental analysis and liquid chromatography of MPS functionalized silica particles in comparison to MPTMS-bonded silica after functionalization with a quinine carbamate chiral selector.

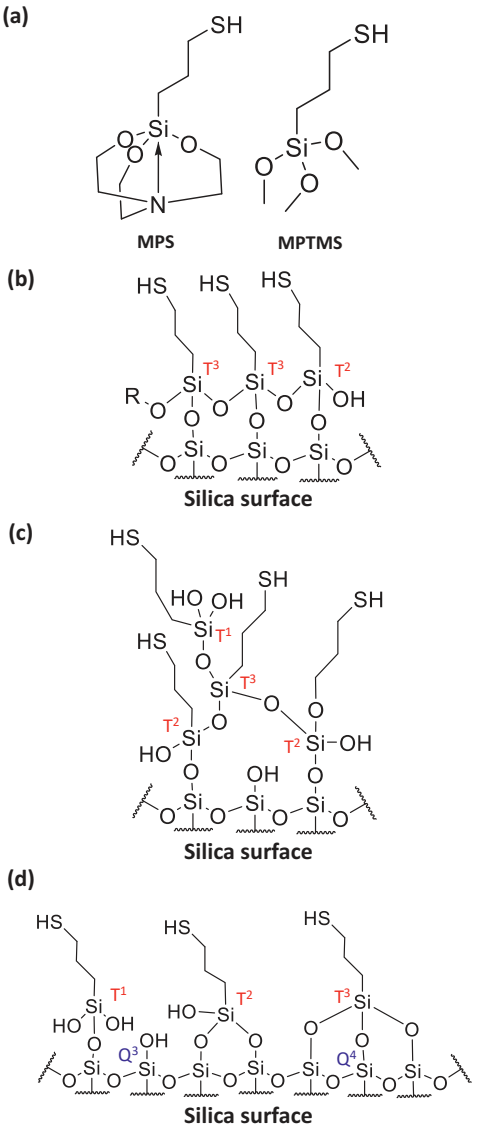


**Fig. 1.** Silanization agents for silica particles and tentative surface morphologies. (a) 3-mercaptopropylsilatrane (MPS) as new functionalization agent of silica surfaces on the left hand side and commonly used 3-mercaptopropyltrimethoxysilane (MPTMS) on the right hand side. (b) Controlled dense monolayer surface structure obtained by MPS-based silanization of silica surface, (c) uncontrolled irregular oligomeric siloxane structure postulated by silanization with MPTMS [17], and (d) possible monomeric siloxane bondings in accordance to what is typically claimed by the literature for trifunctional silanes reacted under anhydrous conditions such as expected for the present MPTMS silanization. For explanation, see text.

## 2. Experimental

### 2.1. Materials

Spherical silica particles (Kromasil, 3 µm, 100 Å, specific surface area 300 $m^2/g$) were supplied by Eka Chemicals (Bohus, Sweden), superficially porous silica particles (SPP) (Halo Sil 2.7 µm, 90 Å, specific surface area 125 $m^2/g$) were supplied by Advanced Materials Technologies (Wilmington, DE, USA). 3-Mercaptopropyltrimethoxysilane was obtained from ABCR Chemicals (Karlsruhe, Germany). *tert*-Butylcarbamoylquinine was synthesized in-house, using quinine from Buchler (Braunschweig, Germany) and *tert*-butyl isocyanate as well as dibutyltin dilaurate from Sigma Aldrich (Munich, Germany). Sodium hydroxide, anhydrous toluene, 4-dimethylaminopyridine (DMAP),

*N*-[(9H-fluoren-9-ylmethoxy)carbonyl]-phenylalanine (FMOC-Phe), azobis(isobutyronitrile) (AIBN), tri-*tert*-butylbenzene (TTBB), 2,2'-dipyridyl disulfide (DPDS), 2-mercaptoethanol, formic acid (FA, analytical grade), acetic acid (AA, analytical grade), ammonium acetate and acetonitrile (ACN, HPLC grade) were also purchased from Sigma Aldrich. MilliQ water was purified by using an Elga PureLab Ultra Purification System (Celle, Germany). All empty stainless steel columns were supplied by Bischoff Chromatography (Leonberg, Germany) and had the dimensions of 50 mm × 3 mm i.d.. Porosity determination was carried out by inverse size-exclusion chromatography (ISEC) using the "ReadyCal Kit Polystyrene" by PSS Polymer Standards Service GmbH (Mainz, Germany) with twelve distinct molecular weights (370, 1,306, 3,470, 8,680, 17,600, 34,800, 66,000, 130,000, 277,000, 552,000, 1,210,000 and 2,520,000 Da).

### 2.2. Instrumentation

All columns were packed using a Smartline pneumatic pump, model 1950, supplied by Knauer (Berlin, Germany). ISEC measurements as well as H/u-curve recordings were conducted on an Agilent 1290 Infinity series liquid chromatographic system from Agilent Technologies (Waldbronn, Germany), equipped with a binary pump, a thermostatted column compartment, a UV diode array detector and an autosampler. The detector was equipped with a MaxLight ultralow dispersion cartridge flow cell with an inner volume of 0.6 µL. Furthermore, to reduce the extra column volume an ultralow dispersion needle seat assembly and connecting capillaries with 0.075 mm inner diameter (autosampler to column compartment, 350 mm length; column compartment to detector, 250 mm length) were installed. For elemental analysis, the elemental analyser EA 3000 CHNS-O from EuroVector SpA (Milan, Italy) was used. Solid-state NMR spectra were acquired on a Bruker Avance III HD 300 XWB spectrometer and soluble samples on a Bruker Avance III HDX 400 spectrometer (Bruker, Rheinstetten, Germany). Data were processed with Bruker TopSpin 4.0.8 software.

### 2.3. Solid-state NMR

Double bearing zirconia rotors were used for $^{13}C$ as well as for $^{29}Si$ cross polarization (CP)/magic angle spinning (MAS) NMR analysis. Thereby, the spinning rate was set to 8000 Hz for $^{13}C$-NMR and 4000 Hz for $^{29}Si$-NMR experiments. The 90° proton pulse was set to 2.5 µs for $^{13}C$ and 3.3 µs for $^{29}Si$, the CP contact time was 2 ms for $^{13}C$ and 5 ms for $^{29}Si$ and the relaxation delay 2 s for both nuclei.

### 2.4. Elemental analysis

For the determination of the C/H/N/S content of the modified silica gel, 3 to 4 mg of the particles were filled into a tin capsule and left to be oxidized by the elemental analyser. Standard parameters for C/H/N/S-analysis were applied. Analytes $CO_2$, $H_2O$, $N_2$ and $SO_2$ were generated by flash combustion and micro-Dumas-reduction and online separated by gas chromatography using helium (quality 5.0) as carrier gas. The products were detected using a thermal conductivity detector (TCD).

Quantification was done using peak areas and calibrating relative to sulphanilamide and 2,5-bis(5-*tert*-butyl-2-benzo-oxazol-2-yl) thiophene (BBOT) standards analysed repeatedly during the same analysis run. Only NIST-certified reference material was used. Blank values for C, H and N were registered for empty tin vials. A zero blank for S was defined as qualification proof. The linearity of sensitivity was verified as replicates at 2 to 10 mg sample weight did not show any mass correlation in the analysis results.

#### 2.4.1. Preparation of quality control (QC) sample

For the preparation of the QC sample by adsorptive bonding of a thiolated quinine carbamate selector with a targeted selector coverage of 100 µmol/g, 300 mg bare silica and 47.2 mg 10,11-dihydro-11-[(2-hydroxyethyl)thio]-9-[*N*-(*tert*-butyl-)carbamoyl]-cinchonan-9-ol were added to a 10 mL round bottom flask together with 2 mL of toluene and 3 mL of methanol. The mixture was sonicated for 30 min, after which it was gently stirred overnight (~ 18 h). Afterwards, the solvent was removed by rotary evaporation. The product was then dried in a vacuum oven (-700 mbar, 60 °C) for two days before it was subjected to elemental analysis. Bare silica as negative control was dried in a vacuum oven (-700 mbar, 60 °C) for two days and subjected to elemental analysis as well.

### 2.5. Silanization (synthesis of thiol silicas)

#### 2.5.1. Synthesis of 3-mercaptopropyl-modified SPP silica for validation of EA

Halo Sil 2.7 µm, 90 Å (1.5 g) was dried at 60 °C under reduced pressure and then suspended in 75 mL toluene. 30 mL of toluene were distilled off to remove water azeotropically. Afterwards, 450 µL MPTMS (1.5 mmol/g silica) and 20 mg of DMAP (0.1 mmol/g silica) were added. The reactor was flushed with nitrogen for 10 min and left stirring at 110 °C under reflux. Afterwards, the slurry was filtered using a glass funnel (porosity 5). Washing steps with boiling toluene and boiling methanol were performed 3 times each. Subsequently, the silica gel was dried in a drying oven at 60 °C under atmospheric pressure for 15 h and afterwards at 60 °C in a vacuum oven.

#### 2.5.2. Synthesis of 3-mercaptopropylsilatrane (MPS)

For the synthesis of 3-mercaptopropylsilatrane (MPS), the procedure of Ref. [17] was followed with slight modifications. Anhydrous toluene was used as solvent. Equimolar amounts of 3-mercaptopropyltrimethoxysilane (MPTMS) and triethanolamine (17.76 mmol each, corresponding to 3.3 mL MPTMS and 2.36 mL triethanolamine) were dissolved in 30 mL toluene. After adding 5 mg NaOH, the solution was heated to reflux for 30 h. Subsequently, the mixture was left cooling down to room temperature and slowly dropped into n-hexane in a beaker inducing crystallization. After complete crystallization, the white crystals were dried for three days at 60 °C in vacuum. $^1H$-NMR showed a purity of 96%. $^1H$-NMR [$CDCl_3$, 400 MHz]: $\delta$ (ppm) = 0.47 (m, 2H), 1.31 (t, $J$ = 7.99 Hz, 1H), 1.70 (m, 2H), 2.49 (q, $J$ = 7.65 Hz, 2H), 2.78 (t, $J$ = 5.82 Hz, 2H), 3.74 (t, $J$ = 5.82 Hz, 2H). $^{13}C$-NMR: $\delta$ (ppm) 57.75 ($CH_2$), 51.12 ($CH_2$), 30.47 ($CH_2$), 28.37 ($CH_2$), 15.73 ($CH_2$). $^{29}Si$-NMR: $\delta$ (ppm) -67.01 ($RSiO_3$). NMR data for MPTMS gave the following values: $^1H$-NMR [$CDCl_3$, 400 Hz]: $\delta$ (ppm) 0.73 (m, 2H), 1.31 (t, $J$ = 7.93 Hz, H), 1.70 (m, 2H), 2.52 (q, $J$ = 7.44 Hz, 2H), 3.55 (s, 9H). $^{13}C$-NMR: $\delta$ (ppm) 50.57 ($CH_3$), 27.57 ($CH_2$), 27.45 ($CH_2$), 8.23 ($CH_2$). $^{29}Si$-CP/MAS-NMR: $\delta$ (ppm) -42.52 ($RSiO_3$).

#### 2.5.3. Determination of reaction kinetics

For the determination of the reaction kinetics of MPS in comparison to MPTMS, the reaction with both silanes was carried out under comparable conditions. 5 g bare silica gel (3 µm, 100 Å) was dispersed in 15 mL anhydrous toluene. After adding of 10 mg DMAP and 8 mmol of MPS (or MPTMS, respectively), the reaction vessel was heated to reflux under mechanical stirring. The mixture was allowed to react for 7 h. After 30 min, 1, 2 and 4 h, samples (1 mL) were drawn, having a total of 5 measuring time points per reaction. All samples were washed with boiling toluene and boiling methanol three times each and dried overnight at 60 °C in a vacuum oven. The samples were subsequently subjected to elemental analysis (C/H/N/S).

**Table 1**
Validation of elememental analyses method: Intra-day and inter-day precisions.

| | coverage [µmol/m²] | intra-day precision σ [%] | | | | | | | | | | | | inter-day precision σ [%] | | | |
|---|---|---|---|---|---|---|---|---|---|---|---|---|---|---|---|---|---|
| | | day 1 | | | | day 2 | | | | day 3 | | | | | | | |
| | | C | H | N | S | C | H | N | S | C | H | N | S | C | H | N | S |
| low range (tBuCQN-TP-SPP) [3] | 0.00 ± 0.00[1] | 2.25 | 5.88 | - | 3.70 | 0.55 | 21.10 | - | 1.37 | 0.32 | 0.00 | - | 3.22 | 0.66 | 6.15 | - | 2.50 |
| | 0.11 ± 0.00[1] | 1.18 | 5.75 | 3.96 | 2.24 | 1.05 | 7.53 | 3.91 | 0.67 | 0.59 | 2.71 | 3.21 | 0.70 | 0.59 | 4.40 | 8.81 | 1.48 |
| | 0.13 ± 0.00[1] | 1.63 | 1.17 | 3.45 | 0.31 | 1.28 | 1.14 | 1.34 | 1.88 | 0.93 | 0.00 | 4.25 | 1.72 | 1.21 | 1.78 | 2.73 | 1.11 |
| | 0.16 ± 0.01[1] | 0.45 | 3.40 | 2.37 | 2.24 | 0.26 | 1.16 | 2.16 | 0.87 | 0.52 | 1.19 | 4.33 | 2.06 | 0.40 | 2.68 | 4.57 | 1.61 |
| | 0.18 ± 0.00[1] | 0.62 | 1.89 | 3.14 | 2.05 | 0.00 | 1.89 | 0.49 | 0.92 | 0.46 | 1.15 | 1.89 | 1.78 | 0.53 | 2.95 | 3.51 | 0.98 |
| | 0.22 ± 0.00[1] | 0.88 | 2.96 | 2.42 | 1.89 | 0.24 | 1.10 | 0.60 | 0.73 | 0.49 | 0.00 | 1.90 | 0.32 | 0.35 | 3.46 | 3.01 | 1.35 |
| high range (tBuCQN-TP-FPP) [3] | 0.56 ± 0.01[2] | 0.75 | 0.75 | 3.77 | 1.56 | n.a. | n.a. | n.a. | n.a. | n.a. | n.a. | n.a. | n.a. | n.a. | n.a. | n.a. | n.a. |
| | 0.67 ± 0.01[2] | 0.92 | 1.84 | 4.22 | 0.94 | n.a. | n.a. | n.a. | n.a. | n.a. | n.a. | n.a. | n.a. | n.a. | n.a. | n.a. | n.a. |
| | 0.88 ± 0.03[2] | 1.64 | 3.12 | 7.37 | 3.01 | n.a. | n.a. | n.a. | n.a. | n.a. | n.a. | n.a. | n.a. | n.a. | n.a. | n.a. | n.a. |
| | 1.85 ± 0.05[2] | 1.30 | 2.29 | 9.75 | 3.01 | n.a. | n.a. | n.a. | n.a. | n.a. | n.a. | n.a. | n.a. | n.a. | n.a. | n.a. | n.a. |
| | 2.36 ± 0.06[2] | 0.81 | 1.56 | 3.53 | 2.92 | n.a. | n.a. | n.a. | n.a. | n.a. | n.a. | n.a. | n.a. | n.a. | n.a. | n.a. | n.a. |
| | 0.95 ± 0.02[2] | 0.79 | 0.56 | 0.73 | 2.19 | n.a. | n.a. | n.a. | n.a. | n.a. | n.a. | n.a. | n.a. | n.a. | n.a. | n.a. | n.a. |
| | 1.10 ± 0.02[2] | 0.65 | 0.94 | 0.50 | 2.19 | n.a. | n.a. | n.a. | n.a. | n.a. | n.a. | n.a. | n.a. | n.a. | n.a. | n.a. | n.a. |
| | 1.21 ± 0.04[2] | 0.60 | 0.53 | 0.29 | 3.98 | n.a. | n.a. | n.a. | n.a. | n.a. | n.a. | n.a. | n.a. | n.a. | n.a. | n.a. | n.a. |
| | 1.24 ± 0.01[2] | 0.45 | 0.55 | 1.52 | 0.70 | n.a. | n.a. | n.a. | n.a. | n.a. | n.a. | n.a. | n.a. | n.a. | n.a. | n.a. | n.a. |
| | 1.33 ± 0.03[2] | 0.00 | 0.53 | 0.00 | 2.68 | n.a. | n.a. | n.a. | n.a. | n.a. | n.a. | n.a. | n.a. | n.a. | n.a. | n.a. | n.a. |
| quinidine sulfate (adsorbed to silica) | 0.07 ± 0.00[1] | 0.71 | 1.38 | 1.58 | 0.71 | 0.56 | 1.81 | 2.22 | 0.15 | 1.70 | 3.23 | 0.52 | 1.96 | 0.21 | 1.27 | - | 0.94 |
| | 0.13 ± 0.00[1] | 0.29 | 1.18 | 1.43 | 0.16 | 1.08 | 1.24 | 1.85 | 1.49 | 0.50 | 5.83 | 2.12 | 0.73 | 0.13 | 2.90 | 14.31 | 1.76 |
| | 0.40 ± 0.00[1] | 0.39 | 1.83 | 0.72 | 0.69 | 0.51 | 2.25 | 0.42 | 1.65 | 0.26 | 3.30 | 0.82 | 0.35 | 0.09 | 2.72 | 7.56 | 0.63 |
| | 0.59 ± 0.00[1] | 0.37 | 1.01 | 0.13 | 0.62 | 0.89 | 1.87 | 1.14 | 0.00 | 2.58 | 2.43 | 1.80 | 0.97 | 1.33 | 1.35 | 5.99 | 1.31 |
| | 1.18 ± 0.01[1] | 0.99 | 1.10 | 0.66 | 0.58 | 0.24 | 0.27 | 0.58 | 0.18 | 0.27 | 0.78 | 0.19 | 0.33 | 0.68 | 0.51 | 2.47 | 2.36 |

[1] selector coverage referred to nitrogen content
[2] selector coverage referred to sulfur content
[3] SPP, superficially porous particles; FPP, fully porous particles

*2.5.4. Optimization of MPS-based surface functionalization*

To further optimize the surface functionalization, different conditions for the hydrolysis step were tested. Hydrolysis was carried out with MeOH/$H_2O$ (80/20; v/v) + 0.1% (v/v) FA, MeOH/$H_2O$ (50/50; v/v) + 0.1% (v/v) FA, MeOH/$H_2O$ (20/80; v/v) + 0.1% (v/v) FA, MeOH/0.1 M HCl (50/50; v/v) and isopropanol/$H_2O$ (20/80; v/v) + 0.1% (v/v) FA, each of those experiments was conducted in reflux for four hours. Furthermore, multiple alternate hydrolysis/re-functionalization cycles with MPS were performed with up to four cycles to see if the sulfur loading can be further increased.

*2.6. Preparation of chiral stationary phases*

Further modification of the thiol functionalized silica was performed with *tert*-butylcarbamoylquinine (tBuCQN) as selector, synthesized according to the protocol published in Ref. [18]. The immobilization of the chiral selector tBuCQN on thiol silicas followed the protocol reported by Maier et al. [19,20].

*2.6.1. Stationary phase synthesis by thiol-ene click reaction for validation of EA*

Five samples of CSP with defined tBuCQN selector amount on 3-mercaptopropyl-modified SPP were synthesized. Thus, 250 mg of the MPTMS modified silica gel and 6.62, 13.24, 19.86, 26.48 and 39.72 mg tBuCQN, respectively, were suspended in 50 mL methanol. Together with 10 mol% AIBN (related to the ene component tBuCQN), the mixture was held under reflux for 8 h while being gently stirred. Washing steps with boiling toluene and boiling methanol while filtering through a glass funnel, porosity 5, were performed three times each. Subsequently, the slurry was left for drying overnight in a drying oven (60 °C, atmospheric pressure) and subsequently for 24 h at 60 °C in a vacuum oven. The results of the elemental analysis are summarized in Table 1.

*2.6.2. Thiol-ene click reaction of tBuCQN and thiol functionalized silica*

For the loading of the modified silica gel with selector, 1 g of the modified silica gel (either modified with MPTMS or MPS, respectively) was suspended in 10 mL methanol. After adding 255 mg (0.6 mmol) tBuCQN and 5 mg azobis(isobutyronitrile), the suspension was heated to reflux under mechanical stirring for 7 h. Afterwards, the mixture was left cooling down to room temperature, transferred to a glass filter funnel (porosity 5) and washed with boiling toluene and boiling methanol, three times each. To finalize the synthesis, the product was dried in a vacuum oven at 65 °C overnight.

*2.7. Inverse size exclusion chromatography (ISEC) for porosity determination*

To get a deeper insight on the particle's surface morphology, the determination of both the internal and external porosity of the stationary phase, in this case bare silica, MPS-functionalized as well as MPTMS-functionalized silica was conducted. To do so, a polymer kit with defined molecular weights of 12 different polymers was used. Those polymers were divided into three samples and diluted with THF to a concentration of 1.0 mg/mL (except for 2,520,000 Da and 1,210,000 Da: 0.5 mg/mL). Void volume marker was tri-*tert*-butylbenzene (TTBB, concentration: 1 mg/mL), mobile phase was 100% THF. The flow rate was set at 0.05 mL/min, injection volume was 0.5 µL, detection wavelength was 254 nm and the column temperature was set to 30 °C. After measuring each sample in triplicates, the cubic root of the polymer's molecular weight was plotted against the elution volume (adjusted for the extra column volume) [21]. Accordingly, two specifiable lines are visible after linear regression, which indicate the excluded (steeper line) and included polymers (flatter part). By finding the intersection between both regression lines, the interstitial (or external) volume ($V_e$) can be defined [22]. $V_0$ stands for the void volume (elution volume of TTBB), $V_{col}$ is the geometrical volume of the empty, unpacked column which can be calculated by $V_{col} = \pi r^2 L$ ($r$ = radius,

$L$ = length). From those values, the porosities can be derived. External ($\varepsilon_e$) and total porosity ($\varepsilon_t$) were determined by Eq. (1a) and (1b).

$$\varepsilon_e = \frac{V_e}{V_{col}} \quad \text{(Eq. 1a)}$$

$$\varepsilon_t = \frac{V_0}{V_{col}} \quad \text{(Eq. 1b)}$$

The internal porosity can be calculated from the difference of the total porosity and the measured external porosity by (Eq. (2)):

$$\varepsilon_i = \varepsilon_t - \varepsilon_e = \frac{V_0}{V_{col}} \frac{V_e}{V_{col}} \quad \text{(Eq. 2)}$$

### 2.8. H/u curve recording and mass transfer resistance comparison

H/u curves were recorded using *N*-[(9H-fluoren-9-ylmethoxy)carbonyl] (FMOC) protected phenylalanine as analyte. For the MPTMS-bonded CSP the mobile phase was methanol/acetic acid/ammonium acetate (98/2/0.5, v/v/w). For the MPS-bonded CSP the mobile phase was adjusted to isoelutropic conditions by diluting the above-mentioned mobile phase with methanol. Flow rates ranged from 0.015 mL/min to 2.5 mL/min. Sixteen (16) data points were recorded. The total pressure was kept under the packing pressure of 800 bar during the measurements. A-, B-, and C-term were calculated by non-linear regression using the Van Deemter model.

### 2.9. Determination of reactive thiol groups on the silica surface by DPDS-assay

Reactive and accessible sulfhydryl groups on the silica surface were determined by performing a thiol-disulfide exchange reaction with 2,2'-dipyridyl disulfide (DPDS) [10,23,24]. For this purpose, typically, 10 mg of thiol-funtionalized silica particles were suspended in 1 mL 0.1 M DPDS solution (in ACN) within a micro centrifuge tube which was impervious to light. After vigouros shaking for 3 h the tubes were centrifuged and the supernatant was diluted with ACN in a ratio of 1 to 10. Subsequently, pyridine-2-thiol and 1,2-dihydropyridine-2-thione formed in the course of the disulfide exchange reaction were quantified by RP-HPLC-UV/Vis. 2-Mercaptoethanol was used as calibrant for the preparation of the calibration function due to its known thiol group content.

## 3. Results and discussion

### 3.1. Validation of elemental analysis

Elemental analysis (EA) of the bonded silica materials was carried out for the determination of the surface coverage of sulfur. Typical measurement uncertainties of microanalytical EA of organic surface bondings on inorganic materials such as modified silica particles are scarcely reported. In this research the validity of the results is greatly relying on the validity of the EA data. In order to get an idea about the reliability of EA for this purpose, in particular in the low surface concentration range which is of relevance in the course of a kinetics study of silatrane in comparison to alkoxysilane chemistry, a series of thiol-modified silicas with distinct controlled 3-mercaptorpropyltrimethoxysilane modification was synthesized and the intra-assay and inter-day precision of EA determined. The results are summarized in Table 1.

It can be seen that the repeatability of the elemental analysis is mostly exceptional in spite of the low content of the determined elements on the inorganic silica backbone. Intra-day precisions for carbon (which was present in a range between 1.7 and 14%) were less than 2.6% RSD, for hydrogen (determined in the range between

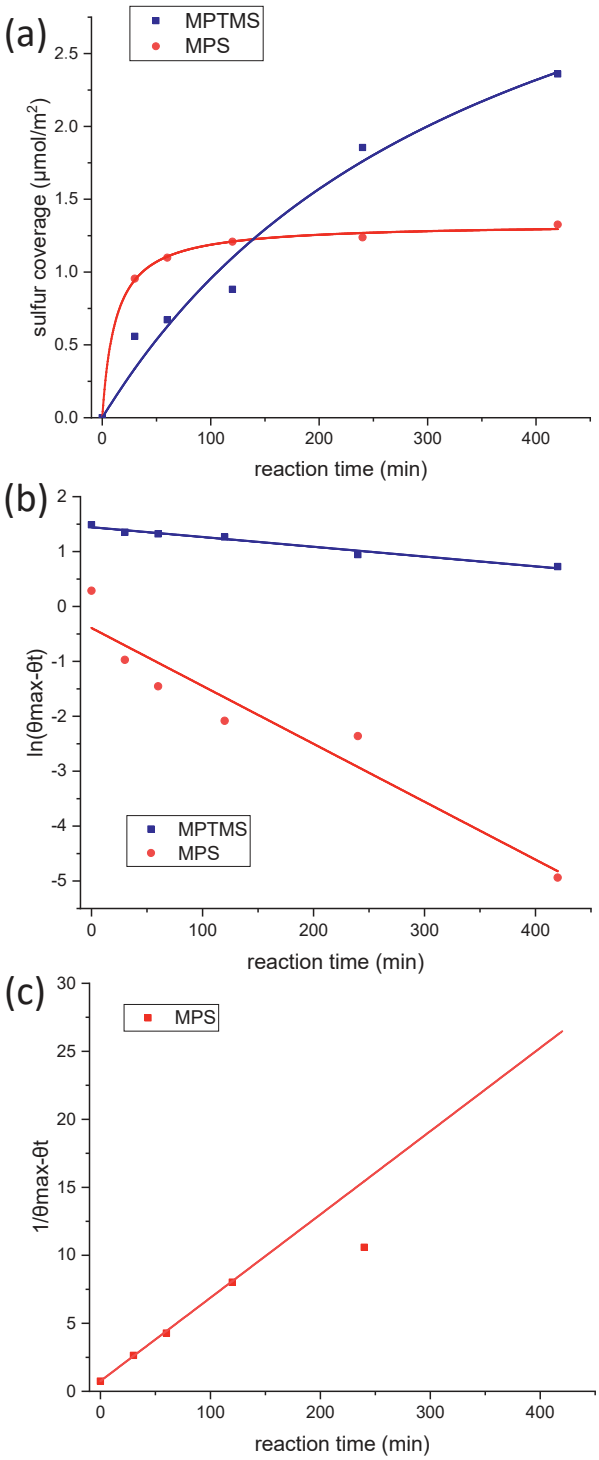


**Fig. 2.** Reaction kinetics of MPS and MPTMS silanization. (a) Sulfur coverage plotted in dependence on the reaction time. (b) Linearized form. For the determination of the rate constant $k$, a linearization of the obtained data was performed. Linearization was done by subtracting the sulfur coverage at a given reaction time t, $\theta_t$ from the maximum sulfur coverage $\theta_{max}$ followed by a logarithmic calculus. Plotting this result versus the reaction time allows to derive $k$ from the slope, which in turn gives access to the half-time. (c) Plot of $1/(\theta_{max} - \theta_t)$ against reaction time for the determination of $k$ and reaction half-time, as MPS seems to show second order kinetics.

**Table 2**
Validation of elemental analysis method: accuracy.

| | target coverage | theoretically expected [%] | | | | experimental [%] | | | | accuracy [%] | | | | precision (intra-day) RSD [%] | | | |
|---|---|---|---|---|---|---|---|---|---|---|---|---|---|---|---|---|---|
| | µmol/m² | C | H | N | S | C | H | N | S | C | H | N | S | C | H | N | S |
| QC Bare Silica | 0 | 0.00 | 0.24 | 0.00 | 0.00 | 0.76 ± 0.01 | 0.62 ± 0.01 | < 0.03 | 0.01 ± 0.00 | - | - | - | - | 1.3 | 1.6 | - | < 0.1 |
| QC | 100 | 3.12 | 0.99 [1] | 0.42 | 0.32 | 3.35 ± 0.07 | 0.82 ± 0.01 | 0.40 ± 0.01 | 0.28 ± 0.00 | 107.3 ± 2.2 | 82.8 ± 1.0 | 95.2 ± 2.4 | 87.3 ± 0.0 | 2.1 | 1.2 | 2.5 | < 0.1 |

[1] values for *H* adjusted for hydrogen values in bare silica

**Table 3**
Overview on the results of the elemental analysis of the MPTMS-derivatized silica and the first cycle of the MPS-derivatized silica.

| reaction type | time [min] | C % | H % | N % | S % | N µmol/m² | S µmol/m² | N µmol/g | S µmol/g | k min⁻¹ | $t_{1/2}$ min |
|---|---|---|---|---|---|---|---|---|---|---|---|
| MPTMS | 30 | 1.33 ± 0.004 | 0.68 ± 0.068 | 0.00 ± 0.000 | 0.54 ± 0.015 | 0.00 | 0.56 | 0 | 167 | 0.0018 ± 0.00015 | 389 ± 32 |
| | 60 | 1.58 ± 0.004 | 0.71 ± 0.073 | 0.00 ± 0.000 | 0.65 ± 0.005 | 0.00 | 0.67 | 0 | 202 | | |
| | 120 | 1.90 ± 0.011 | 0.72 ± 0.070 | 0.00 ± 0.000 | 0.85 ± 0.002 | 0.00 | 0.88 | 0 | 265 | | |
| | 240 | 3.28 ± 0.012 | 0.88 ± 0.035 | 0.00 ± 0.000 | 1.78 ± 0.010 | 0.00 | 1.85 | 0 | 556 | | |
| | 420 | 4.00 ± 0.002 | 0.94 ± 0.009 | 0.01 ± 0.001 | 2.27 ± 0.024 | 0.03 | 2.36 | 9 | 708 | | |
| MPS | 30 | 4.07 ± 0.035 | 1.0 ± 0.019 | 0.46 ± 0.005 | 0.92 ± 0.016 | 1.10 | 0.95 | 331 | 286 | 0.057 ± 0.0024 | 11 ± 1 |
| | 60 | 4.38 ± 0.081 | 1.04 ± 0.041 | 0.51 ± 0.003 | 1.06 ± 0.020 | 1.22 | 1.10 | 367 | 330 | | |
| | 120 | 4.49 ± 0.050 | 1.06 ± 0.009 | 0.52 ± 0.001 | 1.16 ± 0.043 | 1.24 | 1.21 | 371 | 362 | | |
| | 240 | 4.76 ± 0.055 | 1.10 ± 0.015 | 0.59 ± 0.001 | 1.19 ± 0.056 | 1.41 | 1.24 | 422 | 371 | | |
| | 420 | 4.98 ± 0.011 | 1.11 ± 0.004 | 0.63 ± 0.002 | 1.28 ± 0.028 | 1.49 | 1.33 | 447 | 398 | | |

0.4 and 2%) less than 8%, for nitrogen (present in a range between 0 and 1.5%) less than 10% and for sulfur (analyzed in a range of 0.5 and 3.7%) less than 4%. Corresponding inter-day precisions were < 1.3% (C), < 7% (H), < 15% (N), and < 2.5% (S).

Table 2 shows the validation results of accuracy determined as % recovery for the different elements of the prepared quality control (QC) material. Accuracies range from 95 ± 2% (for N) over 107 ± 2% (for C), to 87 ± 0% (for S) and are all in the acceptable range of up to ± 15% bias. For H, the bias is a bit larger but still within ± 20% (accuracy 82.8 ± 1.0%); however, H is anyway usually not considered in surface coverage determination. Especially for nitrogen, which is usually used to determine the selector loading (when the selector contains nitrogen) we observe high accuracy (~5% bias). The results also document that the sulfur determination is valid and reliable enough for the quantification of the functionalization yield in the present work with sulfur-containing MPS.

It can be concluded that the elemental analysis on the inorganic backbone gives, in spite of low elemental percentages, highly reliable values with satisfactory intra-day and inter-day precision as well as accuracy within common acceptance limits and is therefore suitable to determine surface bonding densities and selector coverages, respectively, reliably over a wide range.

### 3.2. Silanization

#### 3.2.1. Reaction kinetics of surface silanization

Two identical synthesis batches but once with MPTMS and once with MPS as silanization reagent were run for the study of the reaction kinetics of the two distinct silanes. A sample was taken in regular time intervals (0.5, 1, 2, 4, 7 h reaction time). The results of the EA are summarized in Table 3. MPTMS derivatization gave higher final sulfur coverages after 7 h reaction time reaching about 700 µmol sulfur per g silica. In sharp contrast, MPS derivatization reacts much faster; after 30 min a surface coverage of 286 µmol/g could be reached (vs 168 µmol/g) corresponding to a 70% higher coverage than with MPTMS. However, after 120 min of reaction time no further increase of the sulfur content was found with MPS (see Fig. 2). A maximal surface coverage of approximately 400 µmol/g resulted with MPS as compared to the 700 µmol/g with MPTMS. This is surprising but could be explained by a controlled monolayer formation with MPS (Fig. 1b), while on contrary an uncontrolled oligomeric siloxane surface structure may be formed with MPTMS (Fig. 1c). In fact, this is in agreement with findings of surface modification on silicon wafers with these two reagents under anhydrous conditions. Surface roughness was found to be 4-fold higher with MPTMS-modified samples than that of MPS [17]. However, as discussed in the introduction, in the literature it is claimed that trifunctional silanes react under nonaqueous conditions to give monomeric bondings (Fig. 1d). In our opinion, the structure shown in Fig. 1c is more likely to be formed in comparison to the one depicted in Fig. 1d. On the one hand, oligomeric structures and thicker layer were shown to occur for MPTMS on the surface of silicon wafers [17]. Traces of water in the reaction mixture may lead to the formation of complex oligomeric structures which then, due to hindered accessibility to the surface silanols, slowly attach to the surface. So the slow reaction kinetics itself may be an indication for the formation of oligomeric siloxane aggregates on the silica surface as schematically depicted in Fig. 1c. Furthermore, high sulfur loadings in combination with low $T^3$ signals in $^{29}$Si CP/MAS solid-state NMR (*vide infra*) are in support of a chaotic, oligomeric structure instead of an ordered, perforated, monomolecular layer (as shown in Fig. 1d) when using MPTMS (see Table 3 for EA and Fig. 4 for NMR results).

Next, the reaction kinetics was determined. The reaction rate follows a second order kinetics according to Eq. (3a)

$$Rate = \frac{d[AB]}{dt} = k[A][B] \quad \text{(Eq. 3a)}$$

wherein [A], [B] and [AB] are the surface silanol, MPS or MPTMS and product concentrations, respectively, and *k* the reaction rate constant. Since silanols and reactands are present in about the same concentration, which allows to simplify the situation to the integral form of the rate law according to Eq. (3b).

$$\frac{1}{[A]_t} = \frac{1}{[A]_0} + kt \quad \text{(Eq. 3b)}$$

$[A]_0$ is the silanol concentration at the start of the reaction and is, assuming a stoichiometric reactivity between silanol and MPS in accordance to Fig. 1b, equivalent to the maximal thiol surface coverage $\theta_{max}$. $[A]_t$ is the free silanol concentration at time $t$ and can thus be written as $\theta_{max} - \theta_t$ (with $\theta_t$ being the coverage of silica with MPS or MPTMS). If this is the case, a plot of $1/(\theta_{max} - \theta_t)$ versus t should give a straight line with a positive slope $k$.

On the other hand, for the determination of the reaction rate constants, a pseudo first-order kinetics could be assumed, e.g. if not all silanols are accessible and thus the reagent is in reasonably large excess, in accordance to Ref. [17]. In this case, the concentration of the reagent can be assumed as constant and the reaction rate depends on the concentration of available silanols [A]. The general differential form of the rate law for (pseudo) first order kinetics can be written as Eq. (3c)

$$Rate = -\frac{d[A]}{dt} = k[A] \quad \text{(Eq. 3c)}$$

or in its integral form

$$\ln\,[A]_t = \ln\,[A]_0 - kt \quad \text{(Eq. 3d)}$$

$[A]_0$ and $[A]_t$ can be again substituted by $\theta_{max}$ and $\theta_{max} - \theta_t$, respectively. A plot of $\ln\,(\theta_{max} - \theta_t)$ versus t will yield a straight line with the slope $-k$.

To solve this equation for the rate constant $k$, a value for the maximum sulfur coverage must be derived. This is readily possible by applying a Langmuir isotherm model which gives access to $\theta_{max}$ (Eq. 4).

$$\theta_t = \frac{\theta_{max} \cdot K \cdot C_t}{1 + K \cdot C_t} \quad \text{(Eq. 4)}$$

wherein $C_t$ refers to the equilibrium concentration of MPS or MPTMS at time $t$ for this chemisorption process (i.e. reactant not bound to silica) and $K$ to the equilibrium constant. Having determined $k$ from Eq. (3b) to (3d) the half-life of the reaction can be calculated by Eq. (5)

$$t_{1/2} = \frac{\ln(2)}{k} \quad \text{(Eq. 5)}$$

The non-linear fit afforded surface coverages $\theta_{max}$ of 4.4 ± 1.1 µmol/m$^2$ (1329 ± 318 µmol/g) for the functionalization with MPTMS and 1.33 ± 0.02 µmol/m$^2$ (340 ± 5 µmol/g) for its silatrane counterpart with satisfactory quality of fit ($R^2$ value of 0.966 for MPTMS and 0.998 for MPS). It is evident from Fig. 2a that the plateau is reached much faster with MPS. Apparently, the excess of MPS was too low to validly assume a pseudo fist order kinetics which on the other hand seems to be valid for MPTMS. The linearization, as shown in Fig. 2b, shows a poor model fit for MPS. For this reason, a linearization for a second order kinetics was assumed. Here, $1/(\theta_{max} - \theta_t)$ was plotted against time. By doing so, rate constants $k$ of 0.0018 min$^{-1}$ for MPTMS (from pseudo 1st order model) *vs* 0.061 min$^{-1}$ for MPS (from 2nd order model) have been calculated corresponding to a reaction half-life of 389 min for the former and only 11 min for the latter (Table 3). Thus, the functionalization with MPS can be performed roughly 35 times faster than with MPTMS. On the other hand, the maximal surface coverage with MPS is lower than with MPTMS, but this is not necessarily a disadvantage as separation factors do not increase linearly with selector coverages.

### *3.2.2. Thiol silica surface chemistry and phase characterization by $^{29}$Si and $^{13}$C CP/MAS solid state NMR*

If we look at the EA results of Table 3, it is striking that in case of MPS silanization approach a nitrogen coverage equivalent to the sulfur surface concentration is obtained after the reaction. This could indicate an incomplete, only mono- or bivalent bonding of the MPS to the silica particles with a residual triethanolamine residue on the silane (see Fig. 3, reaction product A). Hence, an acidic hydrolysis step of the modified silica particles with MeOH/water (80/20, v/v) containing 0.1% (v/v) FA was subsequently carried out to cleave the triethanolamine moiety (see Fig. 3, B). A second cycle of silanization and hydrolysis was then carried out with MPS (Fig. 3, C). To better understand the surface chemistry, CP/MAS solid-state NMR spectra were acquired and the modified silica gels also subjected to EA (Table 4a). It can be seen that the first hydrolysis cycle (H1 in Table 4a) did not alter the sulfur coverage while the nitrogen was largely hydrolytically cleaved. The second silanization cycle (F2) brought a significant increase in sulfur content (from 1.31 to 3.98 µmol/m$^2$) and a similar nitrogen content as in the first silanization cycle. It appears that a dense layer of 3-mercaptopropyl-functionalities is obtained on the silica surface, approximating the maximal surface coverage that, according to text books [25], can be achieved by small silanes (note, ca. 4 out of 8 µmol silanols per m$^2$ silica surface modifiable by small silanes). After hydrolytic cleavage, again the majority of the nitrogen was removed from the modified silica without loss of sulfur (see Table 4a).

In order to gain deeper insights into the surface chemistry of the silica particles, $^{29}$Si and $^{13}$C CP/MAS NMR spectra were recorded in solid state. A single spectrum of the final MPTMS-derivatized silica gel as well as of every step of the MPS derivatization was acquired to monitor the functionalization process thoroughly. The $^{29}$Si spectrum of MPTMS-derivatized silica gel shows signals for mono-, bi- and trifunctional siloxane bond (referred to as $T^1$, $T^2$ and $T^3$) [26] (see Fig. 4a). MPS-derivatized silica (after the first silanization cycle and before hydrolysis) also showed all three possible bonding forms, but with notably less intensity for the signal corresponding to monofunctional siloxane bond (see Fig. 4b). Apparently, a bivalent bonding is favored when working in the absence of water, as the triethanolamine moiety is not cleaved from the silane under these conditions. Aqueous acidic treatment with methanol/water (80/20) containing 0.1% formic acid and subsequent treatment with MPS as well as hydrolysis in a second cycle of MPS derivatization led to a total loss of the $T^1$ signal and a tremendous rise of $T^3$ signal (see Fig. 4c). It may indicate a homogenous thin polysiloxane monolayer on the silica surface as depicted in Fig. 1b. The high thiol surface coverage of this material with around 4 µmol/m$^2$ sulfur and the high $T^3/T^2$ ratio disprove a monomeric surface bonding like shown in Fig. 1d and typically expected for anhydrous reaction conditions according to literature reports [3]. Furthermore, a second set of signals corresponding to Si of the silica surface can be found. The signal at -100 ppm corresponds to Si of free (isolated, vicinal and vicinal-bridged) silanols ($Q^3$), a weak shoulder at -95 ppm indicates presence of some geminal silanols ($Q^2$), and the signal at -110 ppm is due to quaternary Si of the siloxane network ($Q^4$). Unfortunately, CP/MAS NMR spectroscopy does not allow to derive direct quantitative information from these signal intensities in a strict manner. For this reason, we considered direct MAS NMR which unfortunately requires long measurement times and is not practical for a larger set of samples. Exemplarily, we show in the Suppl. Material the comparison of $^{29}$Si solid-state MAS NMR spectra acquired with and without CP. The latter was acquired with high-power decoupling (HPDec) (see Suppl. Fig. S4). It turned out that the $T^2/T^3$ ratio, which is primarily of interest for our interpretation, was fairly the same with and without CP while the ratio between Q and Q/T signals was varied. Due to missing protons in the $Q^4$ bulk material and thus missing CP the major difference is visible for that signal. Hence, the relative T-signal intensities of the $^{29}$Si CP/MAS NMR spectra may also give a meaningful trend for the relative presence of the distinct (mono-, di- and trifunctional) siloxane bonding states at least from a semi-quantitative viewpoint and relative comparisons of the same signals in different materials.

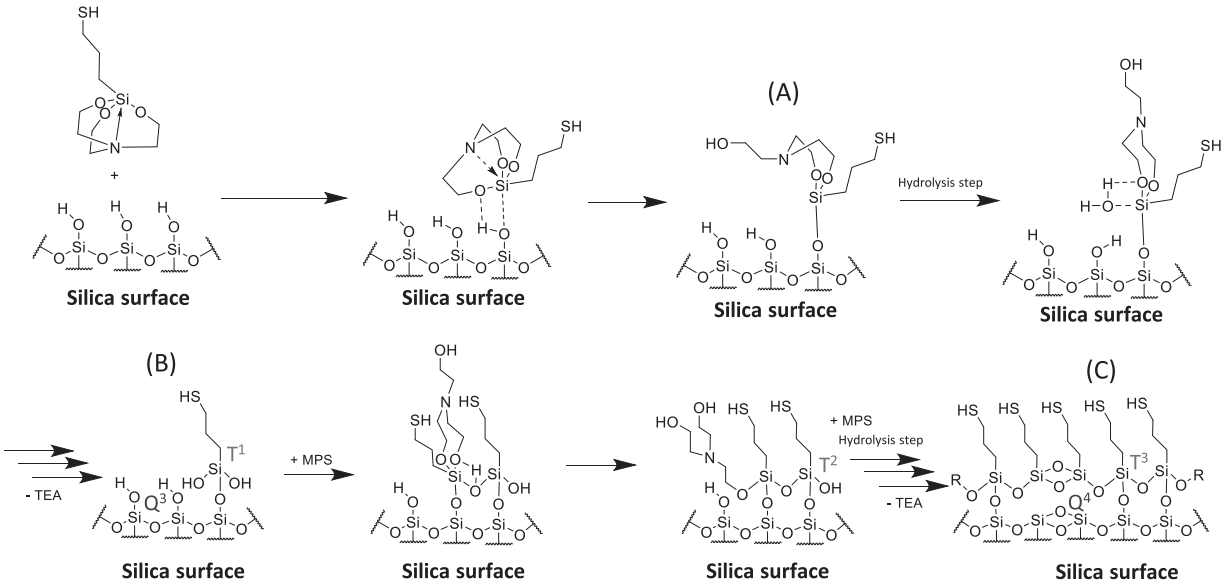


**Fig. 3.** Proposed reaction scheme of silanization of the silica surface by MPS. The proposed self-assembled monolayer (SAM) attached to vicinal silanols in the drawing represents an idealized view but may be interrupted and restarted at Si-O-Si moieties of the silica or bridged via double siloxane bonds of the organosilane layer on top of the silica surface.

**Table 4**
Overview on sulfur and nitrogen coverage (determined by elemental analysis) and percentage of $T^1$, $T^2$ and $T^3$ (determined by solid state NMR).

| reaction cycle | S % | N % | $T^1$ % | $T^2$ % | $T^3$ % | total sulfur[2] [µmol/m$^2$] | free thiol[3] [µmol/m$^2$] | free thiol % of total sulfur |
|---|---|---|---|---|---|---|---|---|
| **(a)** twofold MPS-functionalization/hydrolysis cycles (hydrolysis performed with MeOH/$H_2O$ (80/20; v/v) + 0.1% (v/v) FA) | | | | | | | | |
| F1[1] | 1.28 | 0.63 | 5 | 55 | 40 | 1.33 | n.a. | n.a. |
| H1[1] | 1.26 | 0.10 | - | 59 | 41 | 1.31 | n.a. | n.a. |
| F2 | 3.83 | 0.75 | - | 18 | 82 | 3.98 | n.a. | n.a. |
| H2 | 3.96 | 0.20 | - | 37 | 63 | 4.12 | n.a. | n.a. |
| **(b)** fourfold MPS-functionalization/hydrolysis cycles (hydrolysis performed with MeOH/$H_2O$ (20/80; v/v) + 0.1% (v/v) FA) | | | | | | | | |
| F1 | 1.34 | 0.51 | 7 | 63 | 30 | 1.39 | 0.73 | 53 |
| H1 | 1.32 | 0.03 | 1 | 43 | 56 | 1.38 | 1.05 | 76 |
| F2 | 2.26 | 0.42 | 5 | 51 | 44 | 2.35 | 0.97 | 41 |
| H2 | 2.31 | 0.06 | 4 | 42 | 54 | 2.40 | 1.13 | 47 |
| F3 | 2.94 | 0.35 | 3 | 43 | 54 | 3.06 | 1.13 | 37 |
| H3 | 2.75 | 0.07 | 5 | 46 | 49 | 2.86 | 1.43 | 50 |
| F4 | 3.61 | 0.34 | 5 | 48 | 47 | 3.75 | 1.37 | 37 |
| H4 | 3.44 | 0.08 | 2 | 41 | 57 | 3.58 | 1.85 | 52 |

[1] F stands for functionalization cycle, H for hydrolysis cycle
[2] as determined by elemental analysis
[3] as determined by DPDS assay

### 3.2.3. Proposed reaction scheme

As previously suggested for silicon wafers [27,28], the reaction is induced by the attachment of silatrane to a silanol group of the silica surface. The high-field shift for $^{29}$Si in the $^{29}$Si-CP/MAS-NMR spectrum for MPS indicates a higher electron density at the silicon, due to the dative bond from N to Si. This leads to an increased proton affinity of silatranes in comparison to the silane analogues [14,15]. This high proton affinity of the oxygen drives the protonation of the silatrane by the silanol hydrogen, thus weakening the transannular N→Si bond. This in turn weakens the electron density on the silicon, favoring the nucleophilic attack of the hydroxyl oxygen at the silicon atom which drives the attachment to the silica surface. By formation of an Si-O-Si bond on the silica surface, the intramolecular Si-O bond will be cleaved, displacing the hydroxyl proton from the silica surface. The subsequent step needs an acidic aqueous hydrolysis, following a similar mechanism as described above, leading finally to an (ideally) triethanolamine-cleaved 3-mercaptopropylsilane residue bearing two silanol moieties [29]. Those free silanols can act as active centers for cleavage of the triethanolamine moiety of the following MPS molecule, leading ideally to the final product C shown in Fig. 3.

### 3.2.4. Optimization of the surface bonding

A number of factors were considered for further optimization of the surface and bonding chemistry, respectively: (i) more repetitive cycles of silanization and hydrolysis, and (ii) hydrolysis conditions. Furthermore, rehydroxylation of the silica particles prior to surface modification was examined as well but did not bring any differences which let us assume that a rehydroxylation step was already carried out by the silica supplier (see Suppl. Material Fig. S2 and S3 as well as Suppl. Table S1 for more details).

Two cycles of MPS-modification of silica revealed high sulfur densities, higher than typically reached with MPTMS (~3 µmol/m$^2$). As mentioned above, with small silanes like trimethylsilane, usually only roughly half of the silanol groups can be functionalized [30] leading to a maximal surface coverage of around 4 µmol/m$^2$ [25,31]. To further explore the limits of surface coverage, a synthesis approach with more cycles was performed. Four cycles of alter-

**Table 5**
Evaluated hydrolysis strategies and their impact on nitrogen and sulfur content

| | before hydrolysis | | after hydrolysis | | change in % | |
|---|---|---|---|---|---|---|
| hydrolysis strategy | N [µmol/m²] | S [µmol/m²] | N [µmol/m²] | S [µmol/m²] | of N | of S |
| MeOH/$H_2O$ (20/80; v/v) + 0.1% (v/v) FA | 1.21 | 1.39 | 0.07 | 1.38 | 94.2 | -0.7 |
| MeOH/$H_2O$ (50/50; v/v) + 0.1% (v/v) FA | 1.49 | 1.33 | 0.20 | 1.42 | 86.6 | 6.8 |
| MeOH/$H_2O$ (80/20; v/v) + 0.1% (v/v) FA | 1.49 | 1.33 | 0.24 | 1.31 | 83.9 | -1.5 |
| MeOH/0.1 M HCl (50/50; v/v) | 1.49 | 1.33 | 0.21 | 1.44 | 85.9 | 8.3 |
| Isopropanol/$H_2O$ (20/80, v/v) + 0.1% (v/v) FA | 1.49 | 1.33 | 0.13 | 1.42 | 91.3 | 6.8 |

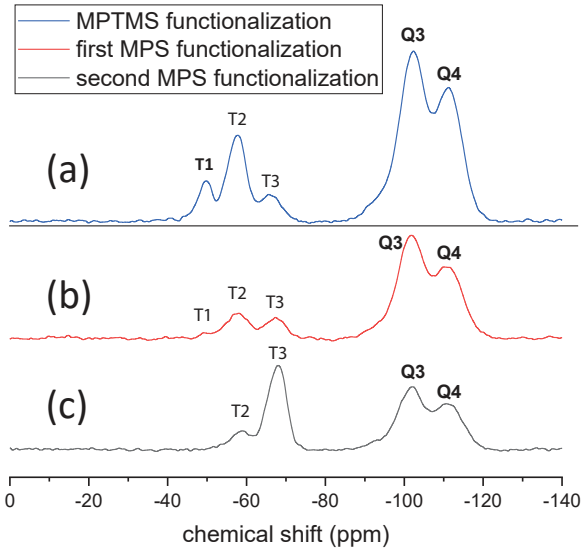


**Fig. 4.** $^{29}$Si CP/MAS solid-state NMR spectra of MPTMS and MPS functionalization. (a) MPTMS functionalization for comparison. (b) After first cycle of MPS modification before hydrolysis step. (c) After second cycle of MPS derivatization and after subsequent hydrolysis step. Noteworthy is the remarkable shift towards trivalent bond ($T^3$) and the complete loss of monovalent bond ($T^1$). Note, percentages of each signal corresponding to the different bonding states for MPS as obtained by deconvolution can be found in Table 4a.

nate MPS functionalization and hydrolysis were conducted. Since the hydrolysis of the triethanolamine residue was not fully complete with the previously used conditions (MeOH/water (80/20, v/v) + 0.1% (v/v) FA), a higher water content was employed (MeOH/water (20/80, v/v) + 0.1% (v/v) FA). Every sample was investigated by CP/MAS solid state NMR (see Fig. 5 for $^{13}$C CP/MAS NMR) as well as by EA. The results are summarized in Table 4b. It can be seen that the first silanization reaction yielded the same sulfur coverage as in the first synthesis batch described above (1.39 vs 1.33 µmol/m²). It documents excellent reproducibility of the reaction. On the other hand, the higher water content during the hydrolysis step indeed led to slightly better hydrolysis yield. However, the increase in sulfur with each cycle of silanization was lower and only after four cycles reached the levels of the two-cycle approach with lower water content during hydrolysis (Table 4a). Besides, also the relative percentage of $T^3$ signal corresponding to trifunctional siloxane bonding was slightly lower, but again approached the level of the two-step method after 4 cycles.

Finally, five different hydrolysis strategies were compared in terms of their ability to cleave the triethanolamine moiety from the surface of the functionalized silica. Results are presented in Table 5. None of the hydrolysis protocols led to a significant loss of the sulfur coverage (< 10% in all cases). The hydrolysis efficiency for the triethanolamine moiety increased with the aqueous content in the reaction mixture (94.2% with 80% water, 86.6% with 50% water, 83.9% with 20% water). Exchange of 0.1% FA by 0.1 M HCl as well as replacement of methanol by 2-propanol as wetting agent did not make a significant difference (Table 5).

In summary, the protocol with 80% MeOH and 0.1% FA was favorable both in view of a high sulfur coverage and high trifunctional siloxane bonding. As silatranes show a high proton affinity [14,15], a low amount of water in the reaction vessel might be sufficient and beneficial for the formation of the MPS monolayer.

### *3.2.5. ISEC for porosity determination*

Silanization with MPTMS can easily lead to uncontrolled oligomeric bonding layer as schematically depicted in Fig. 1c. If this occurs excessively, the narrow pores of the silica particles might become partly inaccessible. For this reason, it was tested whether ISEC has the potential to provide information on the film thickness and pore accessibility in MPTMS- and MPS-modified silica. Complete characterization of the pore structure of plain silica particle column, MPTMS- and MPS-modified silica column might give indirectly some idea about the pore structure (total, external and internal porosities) in these columns. Especially the internal porosity, which indicates the porosity inside the particles (and therefore the size of the pores), could lead to useful information. The thinner the film inside the pores, the higher the internal porosity. Bare silica shows an internal porosity of 0.323 ± 0.0075. While the functionalization with MPTMS reveals an internal porosity of 0.307 ± 0.0059, MPS provided a slightly higher value of 0.316 ± 0.0046 (see Table 6). Although the difference is minor and not really significant from a strict statistical viewpoint, there might be a slight trend recognizable from these ISEC data following the expectations.

## *3.3. Thiol functionalization*

### *3.3.1. Thiol functionalization by thiol-ene click reaction*

The thiolated silica material can be conveniently functionalized for chromatographic purposes by thiol-ene click reaction with chromatographic ligands bearing a vinyl-group. As a model system we explore here the attachment of a chiral *tert*-butylcarbamoylquinine selector which has been thoroughly described recently so that plenty of data are available for comparison. The reaction scheme is depicted in Fig. 6. This thiol-ene click reaction relies on radicals generated by a radical initiator and the availability of reactive sulfhydryls.

As elemental analysis provides no information concerning the chemical state of the determined sulfur, the proportion of free reactive thiol groups on the silica surface was analyzed by a LC-UV assay based on a thiol-disulfide exchange reaction using 2,2'-dipyridyldisulfide (DPDS). Here, the reaction of thiols with DPDS leads to the generation of equimolar amounts of pyridine-2-thiol which is quickly converted into its tautomeric thione form shifting the equilibrium to the product side [23,24]. Hence, the formed pyridine-2-thiol and its tautomer were quantified by RP-HPLC-UV/Vis using 2-mercaptoethanol as calibrant. The sulfhydryl content of the prepared silica particles determined in this manner is given in Table 4b along with EA data, total sulfur coverage, and percentage of free reactive sulfhydryls related to the total sulfur content. It can be seen that with each silanization cycle the sulfhydryl surface concentration is increased. It is furthermore

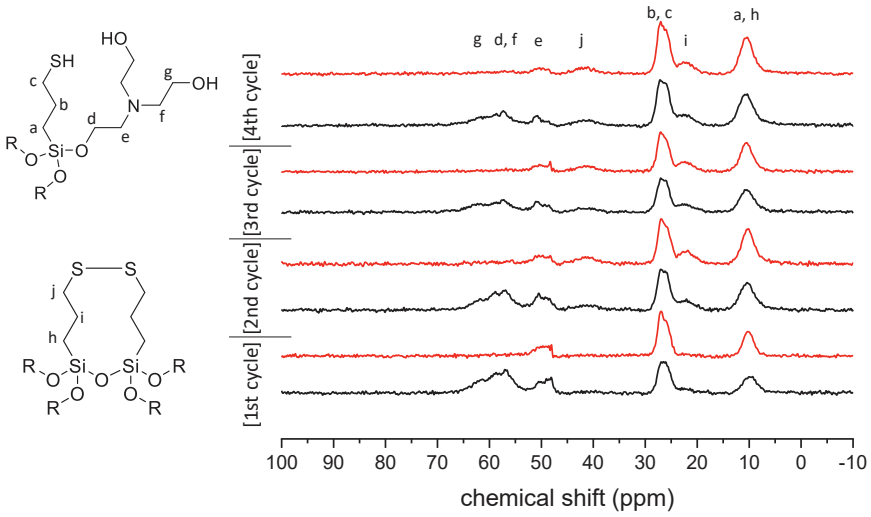


**Fig. 5.** $^{13}C$ CP/MAS solid-state NMR spectra of four cycles of MPS functionalization and hydrolysis. Functionalization is colored in black, hydrolysis in red. Note, that the triethanolamine signals (broad peak at ~57 ppm) appears at every functionalization and disappears almost completely after every hydrolysis. Further notable are the signals at roughly 23 ppm and 41 ppm. They first appear after the second functionalization cycle and then do not vanish again throughout all further steps. This might indicate disulfide bridges formed between neighboured 3-mercaptopropyl moieties.

**Table 6**
Results of ISEC and chromatographic evaluation

| | bare Silica | MPTMS-functionalized[2] | MPS-functionalized (2 cycles)[3] |
|---|---|---|---|
| $\varepsilon_e$ | 0.344 ± 0.0022 | 0.347 ± 0.0042 | 0.349 ± 0.0025 |
| $\varepsilon_i$ | 0.323 ± 0.0075 | 0.307 ± 0.0059 | 0.316 ± 0.0046 |
| $\varepsilon_t$ | 0.668 ± 0.0053 | 0.653 ± 0.0017 | 0.665 ± 0.0021 |
| selector coverage [µmol/m$^2$] | - | 1.14 | 0.25 |
| $k_1$ | - | 5.33 | 5.04 |
| $\alpha$ | - | 1.60 | 1.57 |
| *Rs* | - | 5.28 | 6.62 |
| *N* $m^{-1}$ [1] | - | 56140 | 96560 |
| $h_{red}$ | - | 6.33 | 3.45 |
| $h_{red,\ uopt}$ | - | 3.56 | 3.43 |
| *A [µm]* | - | 6.91 | 7.40 |
| *B* [$cm^2\ s^{-1}$] | - | 1.86 | 2.18 |
| *C term (peak 1) [ms]* | - | 3.06 | 1.14 |
| *C term (peak 2) [ms]* | - | 3.40 | 1.12 |

[1] determined at a linear flow rate of 2.82 mm/s (= 0.5 mL/min), as shown in Fig. 7a
[2] mobile phase for chromatographic measurements: methanol/acetic acid/ammonium acetate (98/2/0.5, v/v/w)
[3] mobile phase for chromatographic measurements: mobile phase as used for MPTMS, diluted with 97% methanol

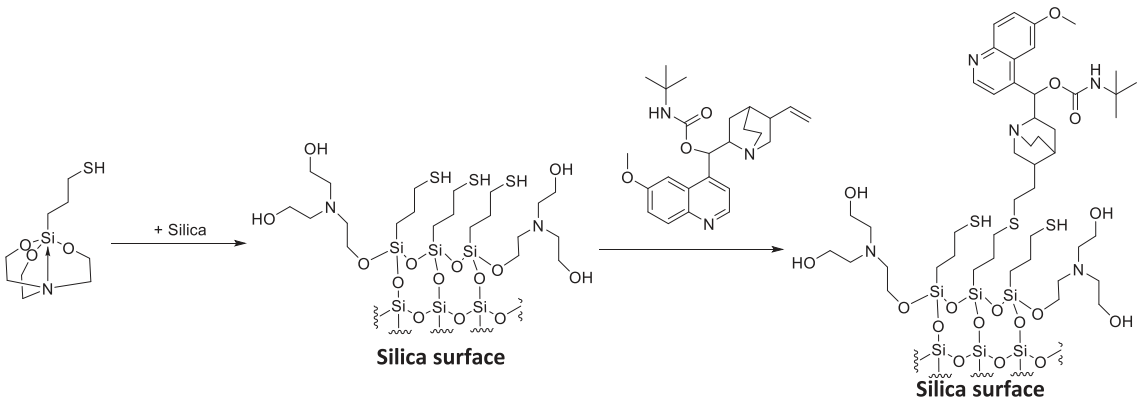


**Fig. 6.** Reaction scheme of thiol functionalization for enantioselective liquid chromatography by thiol-ene click reaction.

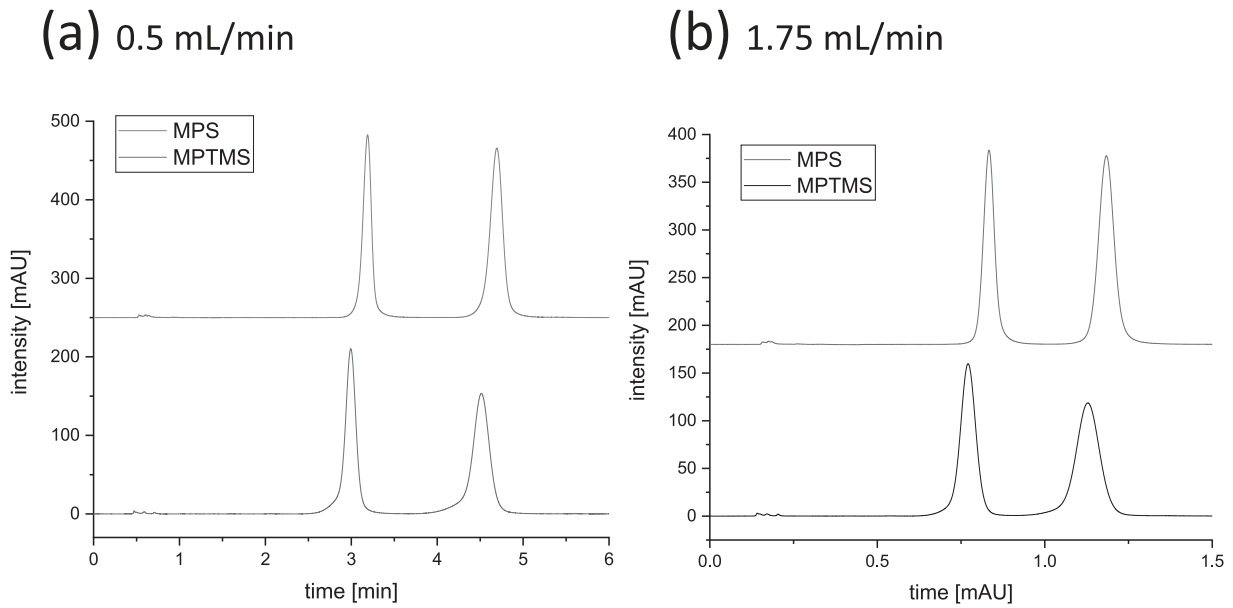


**Fig. 7.** Exemplary chromatograms for the enantiomer separation of FMOC-Phe on MPTMS-bonded tBuCQN-CSP (black traces) and MPS-bonded tBuCQN-CSP (2 silanization/hydrolysis cycles) (red traces). All columns were of the dimensions 50 × 3 mm (L x i.d.), $T$ = 25 °C, flow rate: 0.5 mL/min (a) and 1.75 mL/min (b). Mobile phase: (MPTMS-bonded tBuCQN-CSP, black trace) methanol/acetic acid/ammonium acetate (98/2/0.5, v/v/w), (MPS-bonded tBuCQN-CSP, red trace) 3% of mobile phase specified for MPTMS-bonded CSP diluted with methanol. Plate numbers are in (a) (0.5 mL/min): MPS: Peak 1: 94,900 N/m, Peak 2: 96,560 N/m; MPTMS: Peak 1: 56,150 N/m, Peak 2: 52,690 N/m and in (b) (1.75 mL/min): MPS: Peak 1: 56,300 N/m, Peak 2: 57,440 N/m; MPTMS: Peak 1: 25,320 N/m, Peak 2: 23,210 N/m

striking that the sulfhydryl concentration is significantly higher after the hydrolysis step in each cycle, although the total sulfur content is slightly decreased. At first glance this finding is surprising. However, it may be ascribed to the reducing nature of formic acid which itself can be oxidized to carbon dioxide. If we look at the percentages of sulfur which are available as sulfhydryls and therefore reactive for thiol-ene click reaction we must notice that with increasing thiol density the fraction of disulfides is increasing so that one cannot fully exploit the significant gain of thiol ligands with each silanization cycle. Only around 50% of thiol ligands are available as free thiols for thiol-ene click reaction (after the last hydrolysis step) while this percentage was still 76% after the first silanization/hydrolysis cycle (see Table 4b).

For this reason, the selector coverage for the MPS-bonded CSP approach by thiol-ene click reaction was much lower than expected. Thiols seem to get further inactivated during the radical-initiated thiol-ene click reaction of the selector due to disulfide formation of sterically favorable 3-mercaptopropyl residues which are close enough for disulfide bridge formation of adjacent surface thiols. Thus, only 0.25 µmol tBuCQN ligand per $m^2$ on an MPS-modified silica material with a sulfur content of 3.76 µmol/$m^2$ were immobilized (resp. 4.12 µmol/$m^2$ before selector immobilization, see H2 in Table 4a). Thus, the MPS based column had eminently lower selector coverage than its MPTMS counterpart while showing higher sulfur loadings (selector, 1.14 µmol/$m^2$; sulfur, 1.86 µmol/$m^2$). A reduction step of disulfides with tris(2-carboxyethyl)phosphine prior to selector bonding did not bring about a significant increase of selector coverage (0.33 instead of 0.25 µmol/$m^2$). The fact, that not all sulfur atoms and not even all reactive sulfhydryls (as determined by DPDS assay) are available for immobilization supports the hypothesis that disulfide bridges were formed during the functionalization supported by their close proximity in the polymeric surface bonding.

### 3.4. Chromatographic evaluation

Columns packed with the two types of tBuCQN silica particles, viz. MPTMS- and MPS-bonded (2 silanization/hydrolysis cycles as shown in Table 4a), were chromatographically evaluated. The results are summarized in Table 6 and representative chromatograms are depicted in Fig. 7. For the chromatographic evaluation of the MPS-derived CSPs, isoelutropic conditions (in terms of ionic strength) have been adjusted by dilution of the initial mobile phase (methanol/acetic acid/ammonium acetate; 98/2/0.5, v/v/w), used for the chromatographic test of the MPTMS-bonded CSP, with MeOH to obtain comparable conditions. MPTMS-bonded CSP (with selector coverage of 1.14 µmol/$m^2$) showed an enantioselectivity of 1.60 while the corresponding MPS-bonded CSP with 0.25 µmol/$m^2$

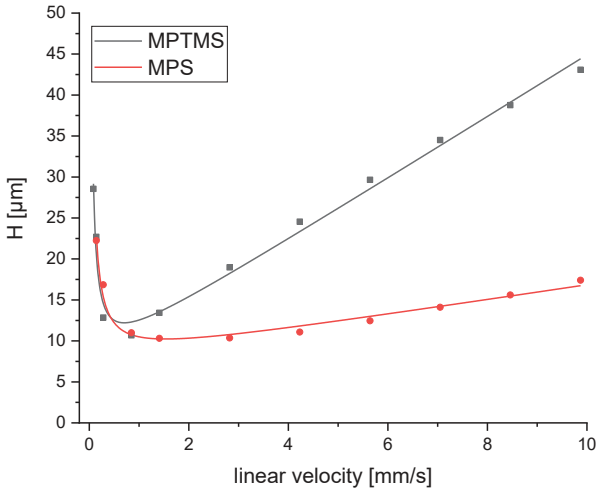


**Fig. 8.** H/u curves for the enantiomer separation of FMOC-Phe on MPTMS-bonded tBuCQN-CSP (black curve), MPS-bonded tBuCQN-CSP (2 silanization/hydrolysis cycles) (red curve). All columns were of the dimensions 50 × 3 mm (L x i.d.), $T$ = 25 °C, mobile phase: (MPTMS-bonded CSP) methanol/acetic acid/ammonium acetate (98/2/0.5, v/v/w), (MPS-bonded CSP) 3% of mobile phase used for MPTMS-bonded CSP diluted with methanol. Note, column packing was not fully optimized specifically for each type of column, however, the fact that both A-terms and $h_{red}$ at $u_{opt}$ are comparable for MPS- and MPTMS-bonded CSPs indicates that their packing quality is comparable and does not significantly bias this comparison.

selector coverage exhibited a separation factor of 1.57. It is evident that the selector coverage has only a minor effect on enantioselectivity enabling comparable results (see Table 6). At a flow rate of 0.5 mL/min (linear flow velocity of 2.82 mm/s), the resolution was superior for the MPS-bonded CSP column than the MPTMS-bonded CSP by around 25% (6.62 vs 5.28). Under optimal linear flow velocity of each CSP (0.25 mL/min for MPS- and 0.15 mL/min for MPTMS-bonded CSP), reduced plate height $h_{red}$ were virtually identical.

Furthermore, Van Deemter curves were recorded under isoeluotropic conditions for the distinct CSPs to evaluate the effect of the bonding layer structure on the mass transfer (Fig. 8). In terms of resistance to mass transfer, MPS-functionalized silica clearly outperforms its MPTMS functionalized counterpart. While the MPTMS-bonded CSP could achieve a C-term of 3.06 ms for the first eluted peak (3.40 ms for the second eluted peak), MPS-bonded CSP showed a C-term of 1.14 ms for the first eluted peak (1.12 ms for the second eluted peak). This corresponds to a reduced mass transfer term by factor of 3 for the MPS-bonded CSP compared to the MPTMS-bonded CSP which may be indicative for a more homogeneous thinner surface bonding structure for the MPS-based bonding as schematically illustrated in Fig. 1b and c. It can be explained by a more strongly hindered pore diffusion and/or slower exchange rate in the organosilane layer network to which selector moieties are attached in case of the MPTMS-bonded CSP. Unfortunately, it is difficult to measure surface roughness and bonding thickness inside silica pores to proof this hypothesis. However, it was experimentally proven for flat sensor surfaces [17] and it can be assumed that this advantage is transferable to the silica surfaces of porous silica particles. The experimental results and findings in this paper point into this direction. Consequently, it can be concluded that the new silatrane surface bondings are promising for future chromatographic materials due to their regularity, greater homogeneity and controllable film thickness.

## 4. Conclusion

Silica surface modification by silanization with functional silatranes, e.g. 3-mercaptopropylsilatrane (MPS) is a promising strategy for the development of functionalized silica materials. Although the silatrane chemistry is generally around for decades, its implementation for silica gel modification represents a new approach. Using elemental analysis, which was thoroughly validated to document its suitability for this research and proved excellent intra-day and inter-day precision, as well as solid-state NMR we could verify the surface chemistry of a dense homogenous polysiloxane monolayer on top of the silica surface by a high percentage of $T^3$ signal in $^{29}$Si CP/MAS solid-state NMR, indicative for a large fraction of trifunctional siloxane bonding. Of great interest is the fast reaction kinetics, which was roughly 35 times faster for the functional silatrane than its respective silane and can lead to faster and denser functionalization films on the silica surface. This very dense functional polymer layer approaches surface coverages commonly assumed as the theoretical maximum limit for the functionalization of silanols on silica (4 µmol/m$^2$). The price to pay for the high sulfur density and high regularity in case of 3-mercaptopropylsilatrane was the high propensity for formation of disulfide bridges, which makes a certain fraction of thiols inaccessible for further reaction and derivatization, respectively. On the other hand, multiple reaction cycles of silanization and hydrolysis (of triethanolamine residues) are required for ending up with a dense polysiloxane layer on the silica surface. Low aqueous hydroorganic mixture with formic acid was favourable in the hydrolysis step. The thinner homogeneous monomolecular film of the MPS functionalization agent in the presented strategy turned out to be superior to the non-ordered, heterogeneous MPTMS-derived thicker layer. The MPS-bonded chiral stationary phase based on quinine carbamate revealed explicitly lowered resistance to mass transfer, as indicated by a factor 3 lower C-term, compared to corresponding MPTMS-based material making this functionalization chemistry a promising strategy for the optimization of stationary phases in liquid chromatography. This may be of particular interest for fast separations, in which the C-term is often limiting the performance of a column. The present work paves the way for further research on other functional silica materials and shows the potential of using silatranes as powerful functionalization agents in liquid chromatography.

## Declaration of Competing Interest

The authors declare that they have no known competing financial interests or personal relationships that could have appeared to influence the work reported in this paper.

## Supplementary materials

Supplementary material associated with this article can be found in the online version at doi:10.1016/j.chroma.2021.462418.

## CRediT authorship contribution statement

**Christian Geibel:** Investigation, Methodology, Formal analysis, Data curation, Visualization, Writing – original draft, Writing – review & editing. **Johannes Theiner:** Investigation, Methodology, Writing – review & editing. **Marc Wolter:** Investigation, Writing – review & editing. **Markus Kramer:** Investigation, Writing – review & editing. **Wolfgang Lindner:** Methodology, Writing – review & editing. **Michael Lämmerhofer:** Conceptualization, Methodology, Supervision, Writing – review & editing, Resources.

## References

[1] P. Žuvela, M. Skoczylas, J.J. Liu, T. Bączek, R. Kaliszan, M.W. Wong, B. Buszewski, Column characterization and selection systems in reversed-phase high-performance liquid chromatography, Chem. Rev. 119 (2019) 3674–3729.
[2] B. Buszewski, S. Bocian, G. Rychlicki, M. Matyska, J. Pesek, Determination of accessible silanols groups on silica gel surfaces using microcalorimetric measurements, J. Chromatogr. A 1232 (2012) 43–46.
[3] M. Pursch, L. Sander, K. Albert, Peer reviewed: understanding reversed-phase LC with solid-state NMR, Anal. Chem. 71 (1999) 733A–741A.
[4] X. Liang, A. Shen, Z. Guo, The application of thiol-ene/yne radical click chemistry in surface modification and functionalization, in: Thiol-X Chemistries in Polymer and Materials Science, The Royal Society of Chemistry, 2013, pp. 286–308.
[5] C. Rosini, C. Bertucci, D. Pini, P. Altemura, P. Salvadori, Cinchona alkaloids for preparing new, easily accessible chiral stationary phases.I. 11-(10,11-Dihydro-6′-methoxy-cinchonan-9-OL)-tiopropylsilanized silica, Tetrahedron Lett. 26 (1985) 3361–3364.
[6] C. Geibel, K. Dittrich, M. Wolter, M. Lämmerhofer, Thiol-ene photo-click immobilization of a chiral chromatographic ligand on silica particles, J. Chromatogr. A 1622 (2020) 461133.
[7] M. Lämmerhofer, W. Lindner, Quinine and quinidine derivatives as chiral selectors I. Brush type chiral stationary phases for high-performance liquid chromatography based on cinchonan carbamates and their application as chiral anion exchangers, J. Chromatogr. A 741 (1996) 33–48.
[8] A. Shen, Z. Guo, L. Yu, L. Cao, X. Liang, A novel zwitterionic HILIC stationary phase based on “thiol-ene” click chemistry between cysteine and vinyl silica, Chem. Commun. 47 (2011) 4550–4552.
[9] M. De Martino, G. Bencivenni, A. Mazzanti, S. Menta, O.H. Ismail, R. Sabia, A. Ciogli, 3,5-Dinitrobenzoyl-9-amino-9-deoxy-9-epiquinine as pirkle-anion exchange hybrid-type chiral selector in high-performance liquid chromatography, Chromatographia 80 (2017) 751–762.
[10] M. Wolter, X. Chen, U. Woiwode, C. Geibel, M. Lämmerhofer, Preparation and characterization of poly(3-mercaptopropyl)methylsiloxane functionalized silica particles and their further modification for silver ion chromatography and enantioselective high-performance liquid chromatography, J. Chromatogr. A 1643 (2021) 462069.
[11] Q. Wang, Y. Long, L. Yao, L. Xu, Z.-G. Shi, L. Xu, Preparation, characterization and application of a reversed phase liquid chromatography/hydrophilic interaction chromatography mixed-mode C18-DTT stationary phase, Talanta 146 (2016) 442–451.

[12] X. Yao, T.T.Y. Tan, Y. Wang, Thiol–ene click chemistry derived cationic cyclodextrin chiral stationary phase and its enhanced separation performance in liquid chromatography, J. Chromatogr. A 1326 (2014) 80–88.
[13] M.J. Wirth, H.O. Fatunmbi, Horizontal polymerization of mixed trifunctional silanes on silica. 2. Application to chromatographic silica gel, Anal. Chem. 65 (1993) 822–826.
[14] J.K. Puri, R. Singh, V.K. Chahal, Silatranes: a review on their synthesis, structure, reactivity and applications, Chem. Soc. Rev. 40 (2011) 1791–1840.
[15] A. Yoshikawa, M.S. Gordon, V.F. Sidorkin, V.A. Pestunovich, Proton affinities of the silatranes and their analogues, Organometallics 20 (2001) 927–931.
[16] C.J. Huang, Y.Y. Zheng, Controlled silanization using functional silatrane for thin and homogeneous antifouling coatings, Langmuir 35 (2019) 1662–1671.
[17] T.J. Lee, L.K. Chau, C.J. Huang, Controlled silanization: high molecular regularity of functional Thiol groups on siloxane coatings, Langmuir 36 (2020) 5935–5943.
[18] A. Mandl, L. Nicoletti, M. Lämmerhofer, W. Lindner, Quinine versus carbamoylated quinine-based chiral anion exchangers. A comparison regarding enantioselectivity for N-protected amino acids and other chiral acids, J. Chromatogr. A 858 (1999) 1–11.
[19] N.M. Maier, L. Nicoletti, M. Lämmerhofer, W. Lindner, Enantioselective anion exchangers based on cinchona alkaloid-derived carbamates: influence of C8/C9 stereochemistry on chiral recognition, Chirality 11 (1999) 522–528.
[20] P. Levkin, N.M. Maier, W. Lindner, V. Schurig, A practical method for the quantitative assessment of non-enantioselective versus enantioselective interactions encountered in liquid chromatography on brush-type chiral stationary phase, J. Chromatogr. A 1269 (2012) 270–278.
[21] O.H. Ismail, L. Pasti, A. Ciogli, C. Villani, J. Kocergin, S. Anderson, F. Gasparrini, A. Cavazzini, M. Catani, Pirkle-type chiral stationary phase on core–shell and fully porous particles: are superficially porous particles always the better choice toward ultrafast high-performance enantioseparations? J. Chromatogr. A 1466 (2016) 96–104.
[22] A. Andrés, K. Broeckhoven, G. Desmet, Methods for the experimental characterization and analysis of the efficiency and speed of chromatographic columns: a step-by-step tutorial, Anal. Chim. Acta 894 (2015) 20–34.
[23] B. Preinerstorfer, W. Bicker, W. Lindner, M. Lämmerhofer, Development of reactive thiol-modified monolithic capillaries and in-column surface functionalization by radical addition of a chromatographic ligand for capillary electrochromatography, J. Chromatogr. A 1044 (2004) 187–199.
[24] R. Nogueira, M. Lämmerhofer, N. Maier, W. Lindner, Spectrophotometric determination of sulfhydryl concentration on the surface of thiol-modified chromatographic silica particles using 2,2′-dipyridyl disulfide reagent, Anal. Chim. Acta 533 (2005) 179–183.
[25] K.K. Unger, Porous Silica - its Properties and Use as Support in Column Liquid Chromatography, Elsevier, Amsterdam, 1979.
[26] C. Hellriegel, U. Skogsberg, K. Albert, M. Lämmerhofer, N.M. Maier, W. Lindner, Characterization of a chiral stationary phase by HR/MAS NMR spectroscopy and investigation of enantioselective interaction with chiral ligates by transferred NOE, J. Am. Chem. Soc. 126 (2004) 3809–3816.
[27] S. Sok, M.S. Gordon, A dash of protons: a theoretical study on the hydrolysis mechanism of 1-substituted silatranes and their protonated analogs, Comput. Theor. Chem. 987 (2012) 2–15.
[28] D. Chachkov, R. Ismagilova, Y. Vereshchagina, Mechanism of reactions of 1-substituted silatranes and germatranes, 2,2-disubstituted silocanes and germocanes, 1,1,1-trisubstituted hyposilatranes and hypogermatranes with alcohols (methanol, ethanol): DFT study, Molecules 25 (2020) 2803.
[29] Y.-T. Tseng, H.-Y. Lu, J.-R. Li, W.-J. Tung, W.-H. Chen, L.-K. Chau, Facile functionalization of polymer surfaces in aqueous and polar organic solvents *via* 3-mercaptopropylsilatrane, ACS Appl. Mater. Interface 8 (2016) 34159–34169.
[30] H. Engelhardt, C. Blay, J. Saar, Reversed phase chromatography – the mystery of surface silanols, Chromatographia 62 (2005) s19–s29.
[31] K.K. Unger, S. Lamotte, E. Machtejevas, Chapter 3, Column Technology in LC, in S. Fanali, P. Haddad, C. Pool, P. Shoemakers, and D. LLoyd (editors), Handbook of Separation Science: Liquid Chromatography, Vol.1, Chapter 3 (2013) 41–86.

## IX.2 Publication IV – Supplementary Material

# Controllable organosilane monolayer density of surface bonding using silatranes for thiol functionalization of silica particles for liquid chromatography and validation of microanalytical method for elemental composition determination

Christian Geibel [a], Johannes Theiner [b], **Marc Wolter** [a], Markus Kramer [c], Wolfgang Lindner [d], Michael Lämmerhofer [a,*]

[a] Institute of Pharmaceutical Sciences, Pharmaceutical (Bio-)Analysis, University of Tübingen, Auf der Morgenstelle 8, 72076 Tübingen, Germany

[b] Mikroanalytisches Laboratorium, University of Vienna, Währingerstrasse 42, 1090, Vienna, Austria

[c] Institute of Organic Chemistry, University of Tübingen, Auf der Morgenstelle 18, 72076 Tübingen, Germany

[d] Institute of Analytical Chemistry, University of Vienna, Währingerstrasse 38, 1090, Vienna, Austria

* corresponding author

# Table of contents

## PART I: $^{29}$Si-NMR of functionalization agents

To be able to determine the electron density on the silicon atom of the two used functionalization agents, $^{29}$Si-NMR spectra were recorded (details for synthesis: see main document). Fig. S1 shows the spectra of MPS (a) and MPTMS (b), indicating a high-field shift for MPS in comparison with MPTMS. Due to the dative bond, a higher electron density is present at the silicon in MPS.

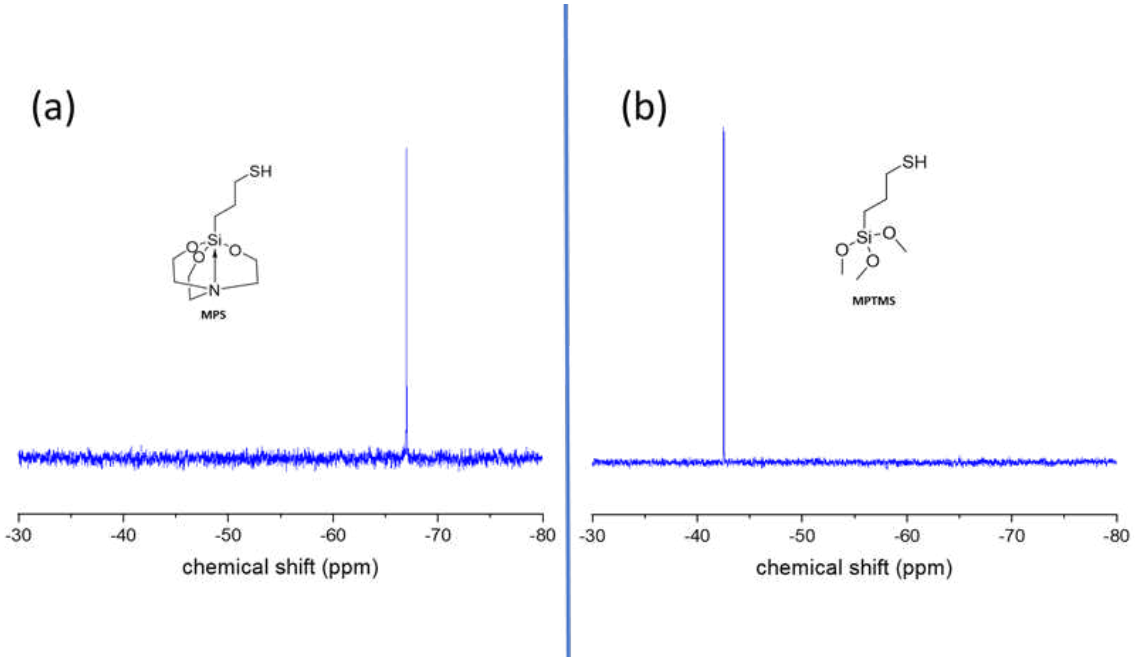


**Fig. S1**. $^{29}$Si-NMR spectra of MPS (a) and MPTMS (b).

## PART II: Rehydroxylation

The silanization with MPS requires free silanols. As the silica production process undergoes a calcination step at temperatures above ~ 400 - 500 °C, silica will not only be dehydrated i.e. desorbing its physisorbed water, but will also lose silanols due to a condensation reaction, i.e. it will be dehydroxylated leading to elevated levels of surface siloxane groups [1-4]. For this reason, a rehydroxylation step prior to silanization was evaluated for increasing the surface coverage already after the first silanization cycle. To do so, bare silica gel was heated to reflux in 0.1 M HCl for 3 hours and subsequently dried at 60 °C in vacuum overnight. Afterwards, functionalization with MPS was carried out as described in the main document. The dried material was subjected to elemental analysis and CP/MAS solid state NMR. EA showed comparable results for both nitrogen and sulfur coverage. As in this case, trivalent silane bondings were present even at a lower percentage than without hydroxylation, this strategy was abandoned.

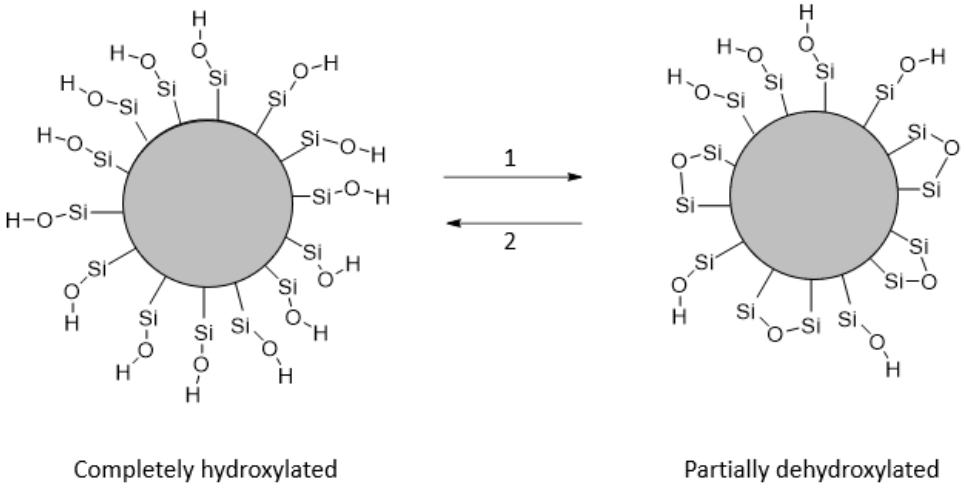


**Fig. S2.** Shown is a completely hydroxylated silica particle (left) and a partially dehydroxylated silica particle (right). The Si-O-Si groups on the right side are not available for a functionalization with MPS. 1 describes the act of dehydroxylation under the influence of heat while losing water in a condensation reaction. 2 describes the rehydroxylation with aqueous 0.1 M HCl in reflux for 3 hours.

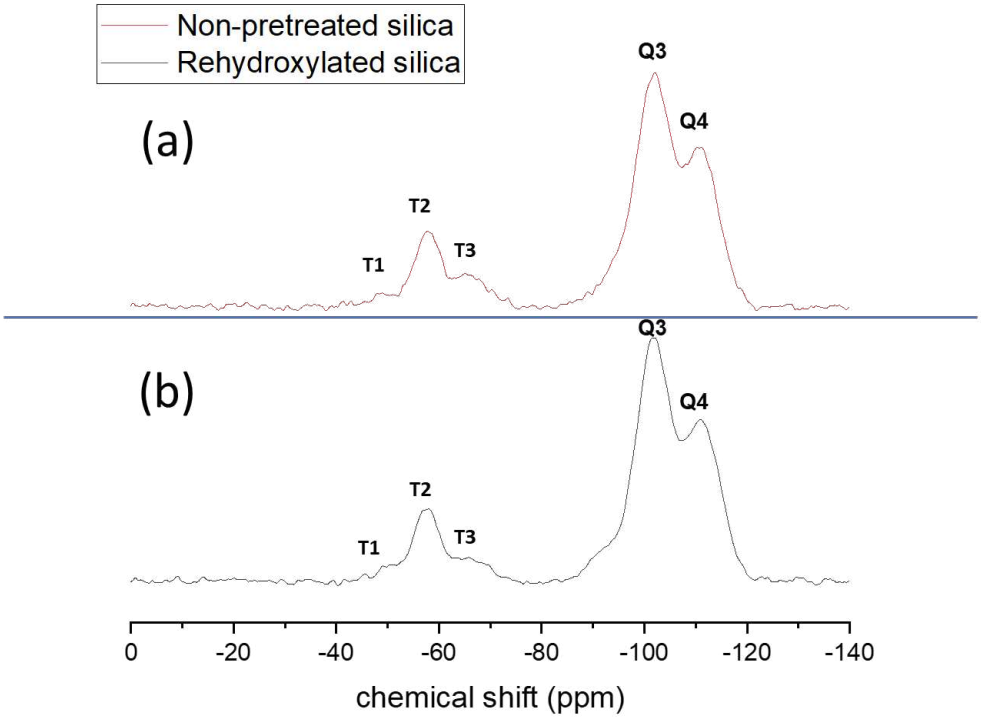


**Fig. S3.** $^{29}$Si CP/MAS solid-state NMR spectra of a) non-pretreated silica and b) rehydroxylated silica after functionalization with MPS.

**Table S1**. Elemental analysis results of non-pretreated and rehydroxylated silica after MPS functionalization.

| | C<br>% | H<br>% | N<br>% | S<br>% |
|---|---|---|---|---|
| Non-pretreated silica | 4.98 | 1.11 | 0.63 | 1.28 |
| Rehydroxylated silica | 4.34 | 1.11 | 0.53 | 1.21 |

## PART III: $^{29}$Si CP/MAS vs HPDec/MAS solid state NMR

Cross-polarization (CP) in combination with magic angle spinning (MAS) is a common technique for enhancing sensitivity in solid-state NMR spectroscopy. By transferring the proton-spin polarization to less sensitive carbon ($^{13}$C) or silicon ($^{29}$Si) nuclei (both having low abundance and lower gyromagnetic ratio) through heteronuclear dipolar coupling by adjusting Hartmann-Hahn conditions, the signal-to-noise ratio can be greatly improved and measurement times can be reduced. Unfortunately, this technique does not allow accurate quantification of the different $^{29}$Si signals by their integrals. However, we assumed that the integrals within the T signal groups allow to derive some rough trends.

To support this assumption, spectra obtained by $^{29}$Si CP/MAS NMR were compared to those of MAS NMR. In high-power decoupled (HPDec) MAS NMR, only heteronuclear dipolar coupling effects are suppressed. The resulting spectra are shown in Fig. S4. It is clearly visible that Q-signals, especially $Q^4$, are not comparable. As $Q^4$ is not bearing a proton (as hydroxyl moiety) bonded to the measured silicon, the signal-suppressing effect in cross-polarization mode is much stronger on $Q^4$ than on $Q^3$ [5]. T signals on the other hand seem to be fairly well comparable (Fig. S4). While CP/MAS gave a ratio of 4.8/46.0/49.2 ($T^1/T^2/T^3$), HPDec/MAS measurement resulted in a ratio of 0/45.5/54.5 ($T^1/T^2/T^3$). $T^1$ was not detectable in HPDec/MAS, as it disappeared in the noise in the absence of cross-polarization. Apart from that fact, the results are pretty well comparable – showing a ratio of 48.3/51.7 ($T^2/T^3$ in CP/MAS) vs. 45.5/54.5 ($T^2/T^3$ in HPDec) taking only $T^2$ and $T^3$ into account. This indicates that CP/MAS can be used for a rough estimation of the bonding state from relative T-signals which are of relevance for this work. The percentages of T units obtained by deconvolution from the spectra of solid-state NMR given in Table 4 of the main document should be regarded as an estimation rather than accurate quantification to indicate some trends.

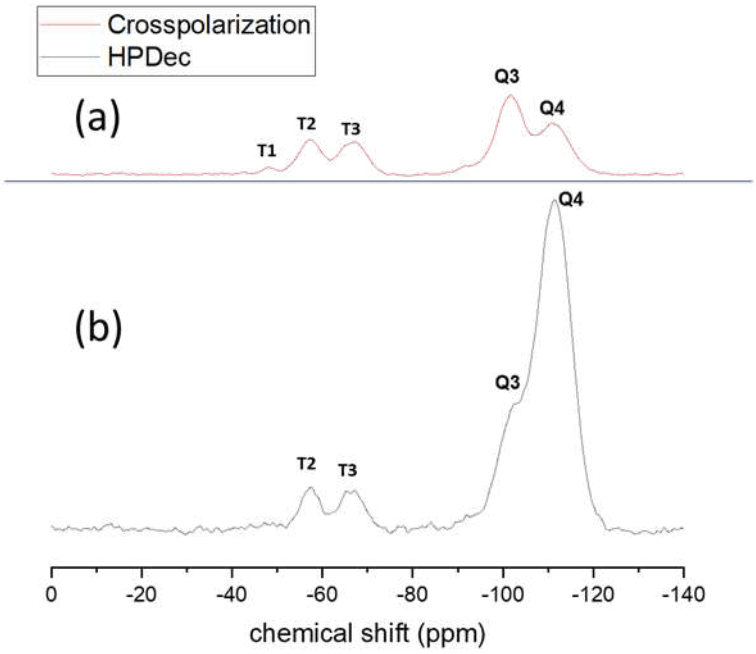


**Fig. S4.** Solid-state NMR spectra of the same MPS-functionalized silica gel, a) recorded with $^{29}$Si CP/MAS solid-state NMR, b) recorded with HPDec/MAS solid-state NMR.

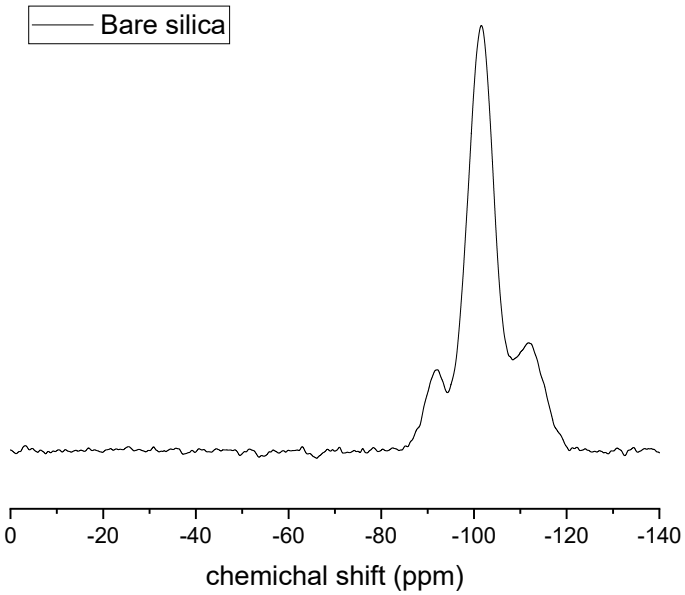


**Fig. S5.** Solid-state $^{29}$Si CP/MAS-NMR spectrum of bare silica used as starting material for all experiments.

## PART IV: Validation of elemental analysis method

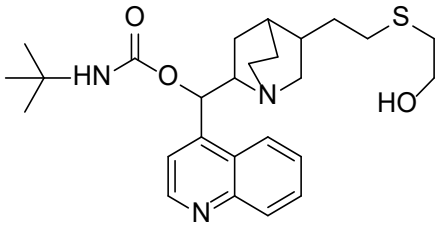


**Fig. S6.** Structure used for the synthesis of the adsorptively bound thiolated quinine carbamate silica gel which served as quality control (QC) standard.

## PART V: References

[1] E.F. Vansant, P. Van Der Voort, K.C. Vrancken, Chapter 3 The surface chemistry of silica, in: E.F. Vansant, P. Van Der Voort, K.C. Vrancken (Eds.) Studies in Surface Science and Catalysis, Elsevier, 1995, pp. 59-77.

[2] L.T. Zhuravlev, The Surface Chemistry of Amorphous Silica. Zhuravlev Model, Colloid Surface A, 173 (2000) 1-38.

[3] V. Dugas, Y. Chevalier, Surface hydroxylation and silane grafting on fumed and thermal silica, J Colloid Interface Sci, 264 (2003) 354-361.

[4] H.E. Bergna, Colloid Chemistry of Silica, in: The Colloid Chemistry of Silica, American Chemical Society, 1994, pp. 1-47.

[5] I.G. Shenderovich, D. Mauder, D. Akcakayiran, G. Buntkowsky, H.-H. Limbach, G.H. Findenegg, NMR Provides Checklist of Generic Properties for Atomic-Scale Models of Periodic Mesoporous Silicas, J. Phys. Chem. B, 111 (2007) 12088-12096.

# X. CHAPTER SIX

# Development and chromatographic exploration of stable-bonded cross-linked amino silica against classical amino phases

## X.1 Publication V – Main Document

Received: 31 March 2022 | Revised: 8 May 2022 | Accepted: 19 May 2022

DOI: 10.1002/jssc.202200268

JOURNAL OF SEPARATION SCIENCE

RESEARCH ARTICLE

# Development and chromatographic exploration of stable-bonded cross-linked amino silica against classical amino phases

**Marc Wolter**[1] | **Christian Geibel**[1] | **Matthias Olfert**[1] | **Min Su**[1] | **Wolfgang Bicker**[2,3] | **Markus Kramer**[4] | **Wolfgang Lindner**[2] | **Michael Lämmerhofer**[1]

[1]Institute of Pharmaceutical Sciences, Pharmaceutical (Bio-)Analysis, University of Tübingen, Tübingen, Germany

[2]Institute of Analytical Chemistry, University of Vienna, Vienna, Austria

[3]FTC – Forensic-Toxicological Laboratory, Vienna, Austria

[4]Institute of Organic Chemistry, University of Tübingen, Tübingen, Germany

**Correspondence**
Michael Lämmerhofer, Pharmaceutical (Bio-)Analysis, Institute of Pharmaceutical Sciences, University of Tübingen, Auf der Morgenstelle 8, 72076 Tübingen, Germany.
Email: michael.laemmerhofer@uni-tuebingen.de

The present work reports on a novel stable-bonded amino silica stationary phase obtained by crosslinking of surface aminopropyl moieties using triglycidyl isocyanurate. The obtained cross-linked amido-amino network silica material exhibited superior hydrolytic stability compared to classical 3-aminopropyl phases and showed, inter alia, excellent separation of nine therapeutically effective sulfonamides in hydrophilic interaction/weak anion exchange chromatography elution mode. Additionally, the separation of carbohydrates was investigated under classical hydrophilic interaction chromatography conditions as well proving the suitability of the novel phase for such applications. For the evaluation of the hydrolytic stability the prepared material, as well as two commercially available benchmark columns and a set of in-house synthesized amino-modified materials, were exposed to harsh aqueous mobile phase conditions for in total of 50 h at elevated temperature. In this context, the materials were examined by elemental analysis, ($^{13}$C and $^{29}$Si cross-polarization/magic angle spinning) solid-state nuclear magnetic resonance, and a chromatographic test before and subsequent to the exposure to these stress conditions. Lastly, the new stationary phase was classified in comparison to a set of commercially available stationary phases by principal component analysis of resultant retention factors gained from chromatographic standard tests.

**KEYWORDS**
(3-aminopropyl)silatrane, hydrolytic stability, silica functionalization, solid-state NMR spectroscopy, stationary phase characterization

**Article Related Abbreviations:** AcPhe, *N*-acetyl-L-phenylalanine; AcPheOEt, *N*-acetyl-phenylalanine ethyl ester; AcTrp, *N*-acetyl-Trp; AEX, anion-exchange; APS, 3-aminopropyl silica; APTES, (3-aminopropyl)triethoxysilane; BocProPhe, *N*-tert-butoxycarbonyl-prolyl-phenylalanine; BuB, butylbenzene; DETP, O,O-diethyl thiophosphate; DMAP, 4-dimethylaminopyridine; FA, formic acid; HILIC, hydrophilic interaction liquid chromatography; PeB, pentylbenzene; Phe, L-phenylalanine; PheOMe, L-phenylalanine methyl ester; RPC, reversed phase chromatography; SP, stationary phase; TCC, column compartment; THF, anhydrous tetrahydrofuran; Trp, L-tryptophan; WAXC, weak anion exchange chromatography.

## 1 | INTRODUCTION

Amino-functionalized silica is a commonly used material in a variety of analytical fields and is frequently applied, for instance, for the liquid chromatographic separation of polar analytes in pharmaceutical research and quality control [1–4]. For amino-functionalization of silica particles, (3-aminopropyl)triethoxysilane [APTES]) is the most frequently utilized reagent for silanization reaction leading to the classical 3-aminopropyl silica (APS) stationary phase (SP) [5–9]. However, other amino organosilanes such as (*N*,*N*-diethyl-3-aminopropyl)trimethoxysilane or (3-[2-aminoethylamino]propyl)trimethoxysilane, for instance, were reported as well [10–12]. Disadvantageously, amino phases usually suffer extensively from hydrolytic cleavage of the organosilane moieties provoking unfavorable background noise in mass spectrometry detection, limited robustness of analytical runs, and short column lifetimes, especially under aqueous mobile phase conditions in RPLC, hydrophilic interaction LC (HILIC) and weak anion exchange chromatography (WAX) elution modes. Thereby, the hydrolysis of the chemical Si-O-Si bonds on the silica surface is enhanced by the self-catalytic effect of the amino group in presence of water [5, 12]. Consequently, a sufficient anchoring of the amino ligand to the silica support is desirable and of tremendous importance to reduce this phenomenon to a minimum. In the case of classic APTES silanization chemistry, a mixture of mono-, di- and trifunctional siloxane bonds is obtained with a dominance of difunctional siloxane bonds. It is expected that trifunctional siloxane bonding of the aminopropyl ligand to the silica support may be beneficial for the phase stability compared to mono- or difunctional bonding. In this regard, it was reported recently for the preparation of thiol-modified silica that silatranes instead of trialkoxysilanes lead to an enhanced proportion of trifunctional bonded organosilane ligand with advantageous surface properties [13]. Besides, polymers were suggested as functionalization agents resulting in phases suffering less from ligand bleeding due to multiple covalent bonds between the polymer and the support. Unfortunately, the advantageous higher stability of those phases is accompanied by lower column efficiencies in many cases [14–18]. In terms of amino phases, polyethylenimine (PEI) was applied as a polymeric coating reagent for the preparation of amino-functionalized silica particles in some cases. Thus, for instance, Lawson et al. showed the usefulness of silica particles coated with adsorbed PEI films for analysis and purification of synthetic oligonucleotides [19]. However, the PEI film was not covalently bound to the support in this study, which might lead to the detachment of the polymer from the support under certain conditions. Moreover, Alpert et al. and Kopaciewicz et al. reported the subsequent crosslinking of the adsorbed PEI film by multifunctional oxiranes via amine-epoxy reaction to obtain SPs suitable for the separation of proteins and nucleotides [20, 21]. Nevertheless, the stability of these PEI phases under chromatographic conditions was not well reported, especially after a long time of use or exposure to harsh mobile phase conditions. Hence, it is not clear to which extent the crosslinking avoids the bleeding tendency of the functional polymer from the support. In addition, it seems to be an auspicious approach to anchor the PEI film additionally covalently to the silica support in the first step in order to decelerate the gradual detachment of the functional polymer. For this purpose, epoxy groups can be introduced firstly on the silica surface by silanization with (3-glycidyloxypropyl)trimethoxysilane making the covalent immobilization of PEI subsequently via amine-epoxy nucleophilic substitution reaction possible [22]. These cross-linked PEI phases have also significant carbon content and hence some hydrophobic interaction retention contributions when operated with aqueous mobile phases resulting in a kind of reversed-phase/mixed-mode character, not really featuring the hydrophilic properties of classical APS.

Against this background, a new cross-linked amino silica was prepared by using triglycidyl isocyanurate for crosslinking of aminopropyl moieties on the surface in this study. For this purpose, 3-aminopropyl modification of bare silica particles was carried out by silanization reaction using (3-aminopropyl)silatrane in a first step. Afterward, the generated material was compared with a set of in-house prepared amino phases stemming from several nitrogen-bearing reactants with distinct surface chemistries (see Figure 1) and two commercially available amino columns serving as benchmarks. In this regard, a classical commercial amino phase (classical APS) derived from the silanization reaction of (3-aminopropyl)trialkoxysilane with the silica support was selected as well as a commercial polymeric amino phase (polymeric APS) dealing with the concept of polymeric surface functionalization of the silica support.

## 2 | MATERIALS AND METHODS

### 2.1 | Materials

Spherical silica particles (Kromasil, 100 Å, 5 μm, 320 $m^2/g$) were purchased from Eka Chemicals (Bohus, Sweden), and empty stainless steel columns (50 × 3 mm) were supplied from Bischoff Chromatography (Leonberg, Germany). (3-Aminopropyl)silatrane was synthesized [23] (cf. S1–3). Branched PEI (average $M_w$ ~ 800; PEI), (3-glycidyloxypropyl)trimethoxysilane, 1,4-butanediol

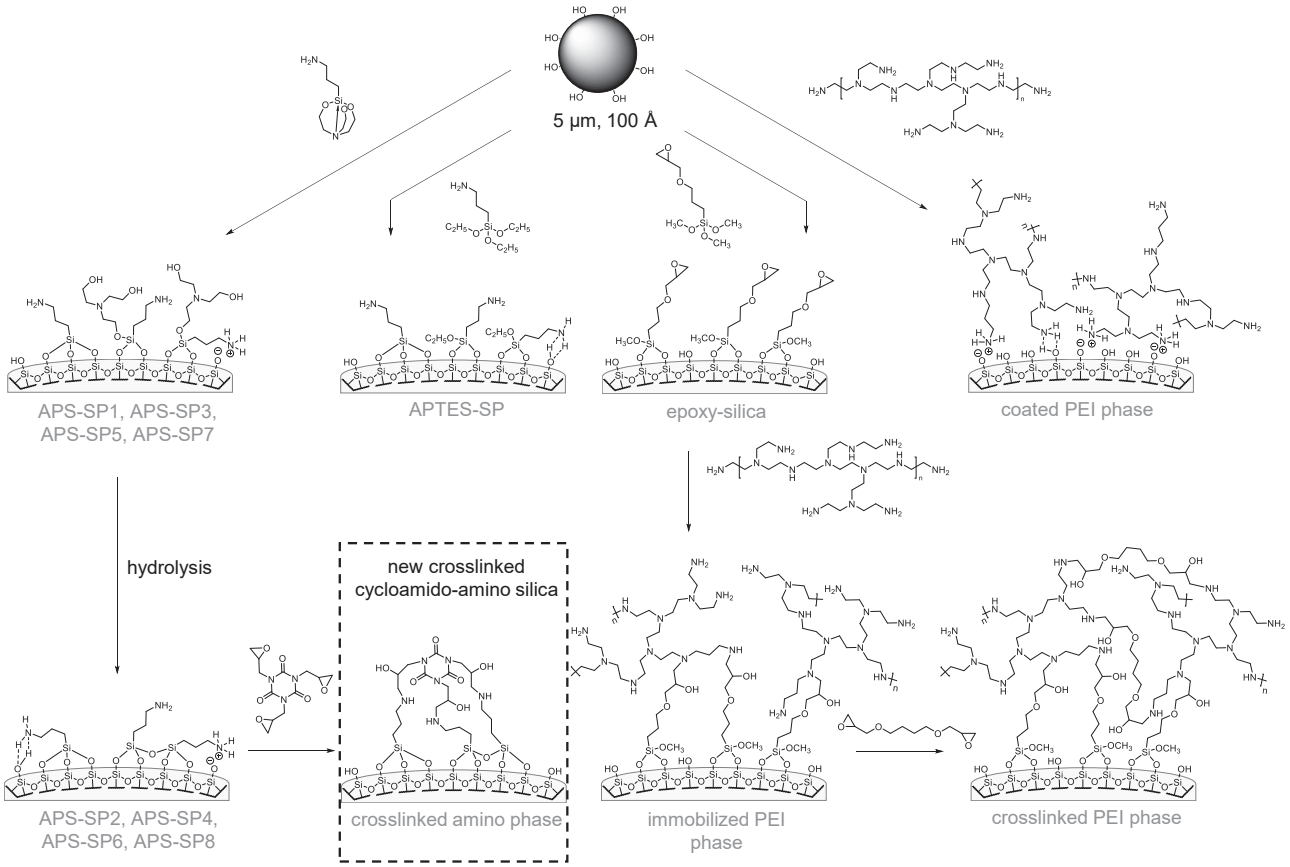


**FIGURE 1** Overview of the in-house prepared amino phases. Detailed synthesis procedures for the (3-aminopropyl)triethoxysilane (APTES)- and polyethylenimine-derived phases are reported in the supplementary material (see also Figures S4–7)

diglycidyl ether, triglycidyl isocyanurate, APTES, triethanolamine, 4-dimethylaminopyridine (DMAP), acetone, butylbenzene (BuB), pentylbenzene (PeB), adenosine, guanosine, cytidine, thymidine, uridine, nicotinic acid, pyridoxine hydrochloride, ascorbic acid, riboflavin, thiamine hydrochloride, caffeine, theophylline, theobromine, O,O-diethyl chlorothiophosphate, triethylamine, *N*-tert-butoxycarbonyl-prolyl-phenylalanine (BocProPhe), L-phenylalanine (Phe), *N*-acetyl-L-phenylalanine (AcPhe), L-tryptophan (Trp), *N*-acetyl-Trp (AcTrp), furosemide, sulphanilamide, sulfaguanidine, sulfacetamide, sulfamerazine, sulfadiazine, sulfadimethoxine, sulfamethoxazole, sulfisoxazole, D-xylose, D-fructose, D-glucose, D-galactose, sucrose, lactose monohydrate, maltose monohydrate, maltotriose hydrate, and deuterated chloroform were obtained from Sigma Aldrich (Munich, Germany). O,O-diethyl thiophosphate (DETP) was freshly synthesized from hydrolysis of O,O-diethyl chlorothiophosphate in presence of triethylamine. L-Phenylalanine methyl ester (PheOMe), Trp hydrochloride, and *N*-acetyl-phenylalanine ethyl ester (AcPheOEt) were purchased from ABCR Chemicals (Karlsruhe, Germany). Sulfanilamide (reference standard for elemental analysis) was supplied from elemental microanalysis (Okehampton, Devon, UK). The solvents (anhydrous) toluene, (anhydrous) chloroform, (anhydrous) methanol (MeOH), anhydrous 1,4-dioxane, anhydrous tetrahydrofuran (THF), methylene chloride and ACN were of technical grade or HPLC grade and purchased from Brenntag (Essen, Germany) and Sigma Aldrich, respectively. Acetonitrile of MS grade quality was obtained from Carl Roth (Karlsruhe, Germany). Ultrapure water was obtained from deionized water by purification using an Elga PureLab Ultra Purification System (Celle, Germany). Acetic acid, formic acid (FA), and ammonia were all of the analytical grades obtained from Sigma Aldrich.

## 2.2 | Instrumentation and software

Elemental analysis was conducted using an EA 3000 CHNS-O elemental analyzer from EuroVector SpA (Milan, Italy). Liquid-state NMR experiments were carried out using a Bruker Avance 400 MHz spectrometer (Bruker, Rheinstetten, Germany), whereas solid-state nuclear magnetic resonance spectroscopy (solid-state NMR) experiments were performed using a Bruker Avance III HD XWB 300 spectrometer. NMR parameters are specified

(cf. Figure S13). NMR data were processed by Topspin 4.0.8 software from Bruker. HPLC experiments were all performed on HPLC systems from Agilent Technologies (Waldbronn, Germany). Thereby, the evaluation of the hydrolytic resistance of the SPs was investigated using an Agilent 1100 series HPLC system featured with a degasser, quaternary pump, autosampler, column compartment (TCC), and a diode array detector. H/u-curves were recorded on an Agilent 1290 Infinity UHPLC system equipped with a degasser, binary pump, autosampler, TCC, and diode array detector. Here, the system was modified with a Max-Light ultralow dispersion cartridge flow cell (0.6 µl), an ultralow dispersion needle seat assembly (1 µl injected), and MarvelX capillaries (0.075 mm id) from Idex Corporation (Lake Forest, Illinois, USA) leading to a determined extra-column volume of 11 µl. Withal, OpenLab CDS ChemStation Online Software (Rev. C.01.03 (37), 2011), and ChemStation Offline Software (Rev. B.04.03 (16), 2010) from Agilent Technologies were used for data acquisition and analysis. Carbohydrate analysis was carried out using an Agilent 1290 Infinity UHPLC system apparelled with a binary pump, a degasser, and a TCC. The system was hyphenated to an HTS PAL autosampler from CTC Analytics (Zwingen, Switzerland) and an API 4000 LC/MS/MS system from Sciex (Ontario, Canada) equipped with a Turbo Spray ion source operated with an ESI probe. System control and data acquisition were done by Analyst 1.7 software from Sciex and Chronos 5.1.20 software (Axel Semrau, Sprockhövel, Germany). MS data evaluation was performed with PeakView 2.2 software from Sciex. For the studies concerning the hydrolytic stability always freshly prepared chromatographic columns were used. For chromatographic experiments, SPs were slurry packed into stainless steel columns using a Smartline Pneumatic Pump 1950 from Knauer (Berlin, Germany). SIMCA Multivariate Data Analytics Solution (Version 15.0.2.5959) software from Sartorius Stedim Data Analytics AB (Umeå, Sweden) was utilized for performing the principal component analysis (PCA; no weighting, autoscaled, and centered). Data visualization was carried out using OriginPro 2019 (OriginLab, Northampton, Massachusetts, USA). More detailed information is given in the respective figure captions or subchapters.

## 2.3 | Preparation of APS-SP1-8 by grafting (3-aminopropyl)silatrane onto bare silica

Bare silica particles (5 g; 100 Å, 5 µm, 320 $m^2$/g) were suspended in 25 ml anhydrous toluene within a 100 ml triple neck flask. After adding (3-aminopropyl)silatrane (8 µmol/$m^2$) and 4-dimethylaminopyridine (10 mol% related to [3-aminopropyl]silatrane) a reflux condenser equipped with a nitrogen supply and a mechanical stirrer was attached to the flask and the system was flushed with nitrogen for 10 min. Afterward, the reaction vessel was heated up to reflux and the reaction was allowed to proceed for 3 h under a nitrogen atmosphere. Hereafter, the reaction product was transferred to a glass funnel of porosity 4, washed with boiling MeOH and boiling toluene three times each, and dried in a vacuum chamber for 12 h at 60°C. Finally, the prepared amino-functionalized silica particles were treated with a mixture of MeOH, water, and FA (20/80/0.1; v/v/v; 50 ml) under reflux for 2 h. Thereafter, the silica was washed again with hot MeOH and hot toluene three times each and dried in a vacuum chamber at 60°C. This procedure was repeated four times withholding always aliquots (APS-SP1-7) before and after the treatment with the mixture of MeOH, water, and FA for subsequent characterization. The resultant aminopropyl-functionalized silica (APS-SP8) was packed into a stainless-steel column for further chromatographic characterization. In addition, an aliquot of APS-SP8 was used for the preparation of the cross-linked amino silica.

## 2.4 | Preparation of cross-linked amino phase from aminopropyl silica

Note that, 0.5 g of APS-SP8 were suspended in 10 ml tetrahydrofuran within a 100 ml round bottom flask. After adding triglycidyl isocyanurate (0.5 µmol/µmol N of APS-SP8 silica; dissolved in THF) the suspension was sonicated for 15 min under a nitrogen atmosphere. Then, the flask was attached to a rotary evaporator and the solvent evaporated at 30°C generating a thin silica film on the flask's inner wall. Subsequently, the flask was rinsed with nitrogen and placed in a heating chamber at 100°C for 6 h. Finally, the silica was washed three times each with boiling methylene chloride, boiling MeOH, and boiling toluene and dried in a vacuum chamber at 60°C for 24 h.

## 2.5 | Hydrolytic stability test

In order to evaluate the hydrolytic stability of the in-house prepared amino SPs and two commercially available amino phases (classical APS, polymeric APS; 100 mm × 4 mm), all columns were continuously rinsed with a mobile phase consisting of ACN, water, and acetic acid (30/70/0.1; v/v/v, pH adjusted to 5 with ammonia) at 60°C applying a linear flow velocity of 1.33 mm/s. After defined periods of time (0, 7, 20, and 50 h) the SPs were characterized chromatographically for 45 min at 25°C using BocProPhe and DETP as test analytes. Therefore, the column was equilibrated to the chromatographic test conditions for 30 min prior to

injection of the probes. For the chromatographic test, the mobile phase was composed of ACN, water, and acetic acid (20/80/0.1; v/v/v, pH adjusted to 5 with ammonia), and the linear flow velocity was set to 1.33 mm/s as well. The test analytes were dissolved in the mobile phase (0.8 mg/ml) and the injection volume was 2 µl. Acetone was used as a void marker and detection was carried out at 220 nm.

## 3 | RESULTS AND DISCUSSION

### 3.1 | Synthesis and surface elucidation of classical and silatrane-based aminopropyl-functionalized silica particles

3-Aminopropyl silica is a classical SP in liquid chromatography which is also part of all common pharmacopeias. For instance, the USP describes L8 as an essentially monomolecular layer of aminopropylsilane ($NH_2$) chemically bonded to totally porous silica gel support, 3–10 µm in diameter and finds several applications for polar analyte separations, such as sugars, under aqueous mobile phase conditions. Unfortunately, its utility is greatly reduced by limited stability originating from self-catalytic hydrolysis of the siloxane bond by a mechanism illustrated in Figure S9. The instability restricts the robustness and hence the applicability in validated assays. In a first attempt to stabilize the aminopropyl silica surface, we evaluated a new surface bonding chemistry using silatranes instead of trialkoxysilanes. Silanization of silica particles using functional silatranes was most recently reported to be superior to silanization using alkoxysilanes due to a higher trifunctional bonding percentage and reduced mass transfer resistance of the resultant materials [13]. For this purpose, (3-aminopropyl)silatrane was synthesized from APTES, and corresponding 3-aminopropyl-functionalized silica from the two reagents was evaluated against each other.

The immobilization of APTES was carried out by classical silanization reaction in toluene with DMAP as a catalyst, which increases the nucleophilicity of silanols (Figure S10), leading to APTES-SP. However, APTES was reported to catalyze the reaction by itself as well as expedite the reaction under non-aqueous conditions [9, 11, 20, 24–28]. Elemental analysis revealed the successful immobilization with ligand coverage of 3.32 µmol/$m^2$ for the APTES-SP. $^{13}$C CP/MAS NMR confirms the ligand on the silica (Figure 2A, top) and $^{29}$Si CP/MAS NMR reveals the bonding states, for example, besides difunctional (T2) and trifunctional siloxane bondings (T3) also a certain amount of monofunctional siloxane bonds (T1) which are most labile and easily hydrolytically cleaved off (Figure 2B, top).

Likewise, (3-aminopropyl)silatrane was bonded onto silica by silanization using the same conditions in toluene with DMAP. However, after the reaction, a triethanolamine residue remained still bound to the ligand's silicon atom (see Figure 1 and Figure S11) [13]. It was hydrolytically cleaved off by a second reaction step applying a successive treatment with a mixture of MeOH, water, and FA. This silanization/hydrolysis procedure was repeated sequentially a total of four times resulting in APS-SP1-8 (odd number SP after silanization step; even-numbered SP after hydrolysis). Characterization of the resulting materials by $^{13}$C CP/MAS NMR analysis revealed the same signals for the aminopropyl ligand and an additional signal corresponding to the ethylene moieties of the triethanolamine residue (see Figure 2A; APS-SP1). It can be seen in Figure 2A that this signal disappears after each hydrolysis cycle which proves the successful hydrolysis of the residual triethanolamine moieties.

Information about the ligand coverage can be conveniently derived from elemental analysis (see Table 1). It can be seen that the nitrogen content and surface coverage, respectively, increase with the first three cycles of silanization/hydrolysis from 2.95 to 3.43 µmol/$m^2$, but do not change significantly anymore in the fourth cycle (3.35 µmol/$m^2$ nitrogen of APS-SP8). According to the determined elemental composition of the prepared materials, similar aminopropyl densities for APTES-SP and APS-SP8 (APS-SP8: 3.35 µmol/$m^2$ vs. APTES-SP: 3.32 µmol/$m^2$; see Table 1) were finally obtained.

Solid-state $^{29}$Si CP/MAS NMR analysis revealed a significant difference in surface bonding for both generated amino materials (see Figure 2B) [13, 29–31]. The signal for monofunctional siloxane bond T1, observed in APTES-silica, disappears and only signals for difunctional (T2) and trifunctional (T3) siloxane bonds are found in (3-aminopropyl)silatrane derived silicas. Furthermore, with each cycle of silanization/hydrolysis, the T3 signal increases and T2 relatively decreases indicating that the quantity of trifunctional bonded siloxanes is increasing which is expected to improve the stability of the bonding. It can be seen in the $^{29}$Si CP/MAS NMR spectra (see Figure 2B) that the signal intensity of the trifunctional siloxane bond for APS-SP8 in contrast to APTES-SP is increased by a factor of about 2 (see Table S1; 33% T3 for APTES-SP vs. 70% T3 for APS-SP8). Here, a direct quantitative comparison of the signals should be meaningful and seems feasible due to the similarities in contact times [13, 30]. Furthermore, even after the first reaction cycle, a significantly greater signal proportion of trifunctional anchored ligand was achieved by the approach using APS (48% T3 for APS-SP2 vs. 33% T3 for APTES-SP). In conclusion, applying APS for amino-functionalization instead APTES leads to 3-aminopropyl-bonded silica with

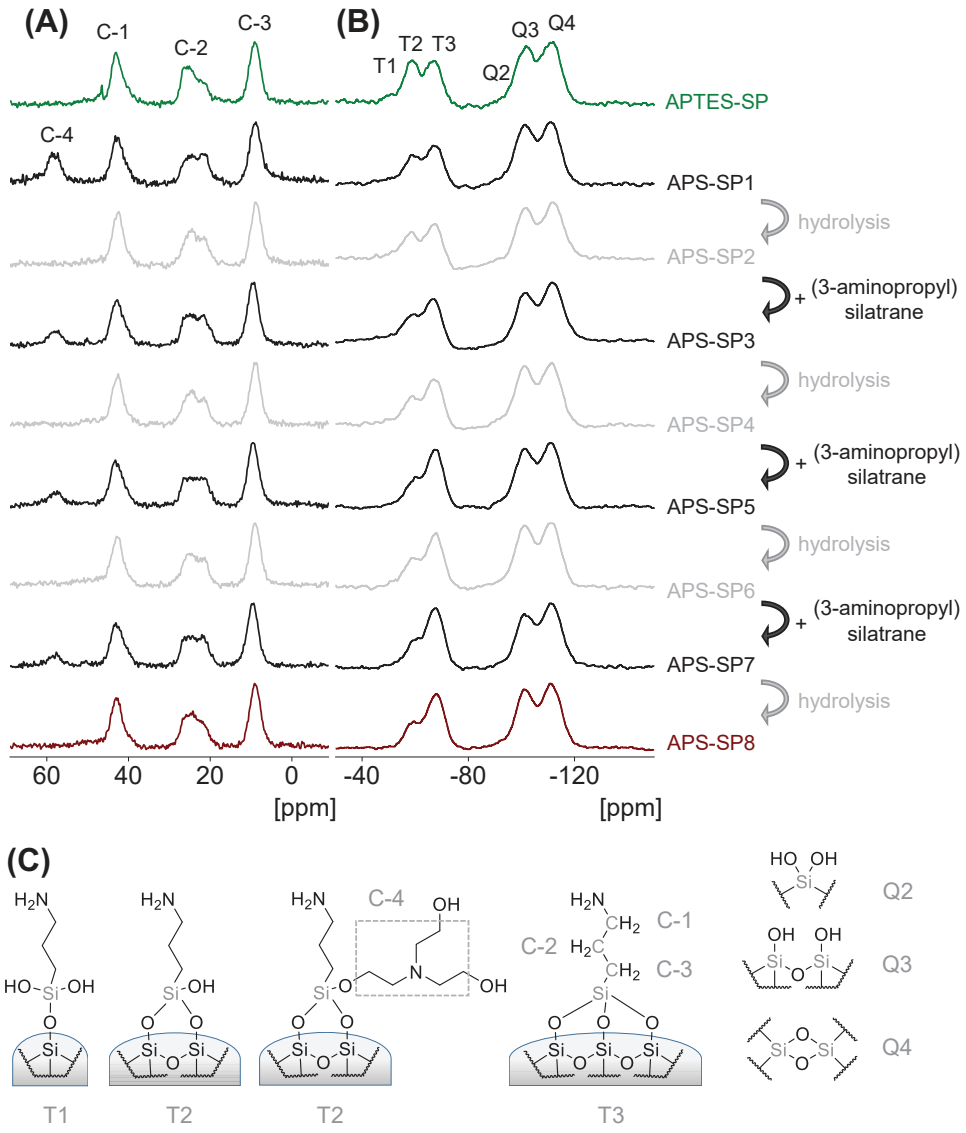


**FIGURE 2** Solid-state NMR spectra of 3-aminopropyl)triethoxysilane–stationary phase (APTES-SP) and 3-aminopropyl silica (APS)-SP1-8: (A) $^{13}$C CP/MAS NMR spectra: Signals at δ(C-1) ~ 43 ppm, δ(C-2) ~ 22–25 ppm, δ(C-3) ~ 9 ppm can be assigned to the incorporated aminopropyl moiety. Peak splitting of δ(C-2) was originated in particular from the resonance of the respective protonated and unprotonated species located at the acidic silica surface which are typically balanced in dynamical equilibrium with each other. Withal, the protonated species exhibits a resonance at δ ~ 22 ppm for C-2, whereas the unprotonated one is responsible for the downfield shift to δ ~ 25 ppm [47, 48]. The spectrum of APTES-SP lacks distinctive signals for the ethoxy groups of the embedded ligand typically located at δ ~ 56 ppm and δ ~ 16 ppm [28]. Thence, the ethoxy residues might probably be hydrolyzed by air moisture or moisture trapped in the pores of the silica particles facilitated by the catalytic effect of the amino groups, whereas the resulting volatile ethanol might be evaporated subsequently [49]. The spectra of APS-SP1+3+5+7 exhibited a broad resonance peak in the area of δ ~ 56 ppm to δ ~ 60 ppm (C-4) which can clearly be assigned to the carbon atoms of the triethanolamine residue still attached to the functional ligand after its mono- or difunctional binding to the silica. Consistently, the extinction of this signal observed after each hydrolysis step evinced unequivocally the efficacious cleavage of this undesired residue. (B) $^{29}$Si CP/MAS NMR spectra: Besides the three typical signals for silica (Q2: geminal silanol groups, Q3: free single and vicinal silanol groups, Q4: siloxane groups) peaks in the range between - 50 ppm and - 80 ppm (T1, T2, and T3) can be assigned to the silicon atoms of the various aminoalkyl siloxane moieties introduced on the surface giving information about the proportion of mono-, di- and trifunctional anchored ligands. (C) Assignment of the signals to the respective chemical structures

**TABLE 1** Summary of elemental analysis data

| SP | C[a] [wt%] | H[a] [wt%] | N[a] [wt%] | N[b] [μmol/m²] |
|---|---|---|---|---|
| APTES-SP | 4.57 ± 0.02 | 1.21 ± 0.01 | 1.49 ± 0.01 | 3.32 |
| APTES-SP[c] | 1.27 ± 0.03 | 0.79 ± 0.01 | 0.10 ± 0.00 | 0.22 |
| APS-SP1 | 5.92 ± 0.02 | 1.51 ± 0.01 | 1.87 ± 0.01 | 4.17 |
| APS-SP2 | 3.67 ± 0.01 | 1.07 ± 0.03 | 1.32 ± 0.00 | 2.95 |
| APS-SP3 | 6.81 ± 0.14 | 1.58 ± 0.02 | 1.92 ± 0.01 | 4.28 |
| APS-SP4 | 4.03 ± 0.00 | 1.10 ± 0.00 | 1.46 ± 0.02 | 3.25 |
| APS-SP5 | 6.83 ± 0.23 | 1.59 ± 0.03 | 2.03 ± 0.01 | 4.53 |
| APS-SP6 | 4.19 ± 0.02 | 1.12 ± 0.01 | 1.54 ± 0.01 | 3.43 |
| APS-SP7 | 6.72 ± 0.02 | 1.59 ± 0.01 | 2.06 ± 0.00 | 4.6 |
| APS-SP8 | 4.40 ± 0.01 | 1.14 ± 0.00 | 1.50 ± 0.00 | 3.35 |
| APS-SP8[c] | 1.43 ± 0.02 | 0.81 ± 0.02 | 0.17 ± 0.00 | 0.39 |
| cross-linked amino phase | 10.67 ± 0.02 | 1.77 ± 0.03 | 3.34 ± 0.01 | 7.45 |
| cross-linked amino phase[c] | 10.78 ± 0.07 | 1.87 ± 0.05 | 3.19 ± 0.01 | 7.12 |
| classical APS[d] | 2.18 | 0.82 | 0.67 | 1.37 |
| classical APS[c] | 1.32 | 0.77 | 0.18 | 0.37 |
| coated PEI phase | 3.90 ± 0.04 | 1.05 ± 0.00 | 1.87 ± 0.00 | 4.16 |
| coated PEI phase[c] | 1.21 ± 0.02 | 0.61 ± 0.02 | 0.09 ± 0.02 | 0.21 |
| epoxy-silica | 2.75 ± 0.00 | 0.73 ± 0.01 | < 0.02 | – |
| immobilized PEI phase | 6.08 ± 0.00 | 1.35 ± 0.01 | 2.14 ± 0.01 | 4.77 |
| immobilized PEI phase[c] | 6.04 ± 0.06 | 1.39 ± 0.02 | 1.82 ± 0.02 | 4.06 |
| cross-linked PEI phase | 8.77 ± 0.02 | 1.71 ± 0.02 | 1.96 ± 0.02 | 4.37 |
| cross-linked PEI phase[c] | 8.32 ± 0.02 | 1.60 ± 0.01 | 1.81 ± 0.01 | 4.04 |
| polymeric APS[e] | 10.09 | 2.31 | 2.84 | 5.07 |
| polymeric APS[c] | 10.04 | 2.18 | 2.36 | 4.21 |

Abbreviations: APS, 3-aminopropyl silica; APTES, 3-aminopropyl)triethoxysilane; SP, stationary phase.
[a]determined by elemental analysis.
[b]calculated based on N [wt%].
[c]after stress test.
[d]specific surface area according to manufacturer: 350 m²/g.
[e]specific surface area according to manufacturer: 400 m²/g.

significantly increased trifunctional bonding characteristics of the ligands to the support with tentative favorable stability (vide infra).

## 3.2 | Preparation of cross-linked amino silica

In order to further enhance the stability of the prepared aminopropyl modified silica, amino groups of APS-SP8 were cross-linked using triglycidyl isocyanurate resulting via amine-epoxy nucleophilic substitution reaction in a three-dimensional polar cycloamido-aminopropyl network structure as surface bonding (Figure 1). For this purpose, the APS-silica was homogeneously dispersed in THF, the crosslinker was added, and the THF subsequently mostly evaporated to obtain a thin liquid layer on the silica surface preventing precipitation of the dissolved crosslinking agent. The nucleophilic ring-opening reaction was catalyzed by the amino groups and facilitated due to the polarization of the carbon-oxygen bond and the Bayer ring strain [32, 33]. The primary amino groups can react with epoxy functionalities furnishing secondary amines and hydroxy groups, which can both react in a second step again with a crosslinker leading to an extensive network (see Figure S8). However, amine-epoxy reactions are usually favored.

The resultant amido-amino network silica was characterized by elemental analysis. By this crosslinking step, the nitrogen quantity of the material was increased from 3.35 μmol/m² to 7.45 μmol/m² according to elemental analysis measurements (see Table 1) which indicates the

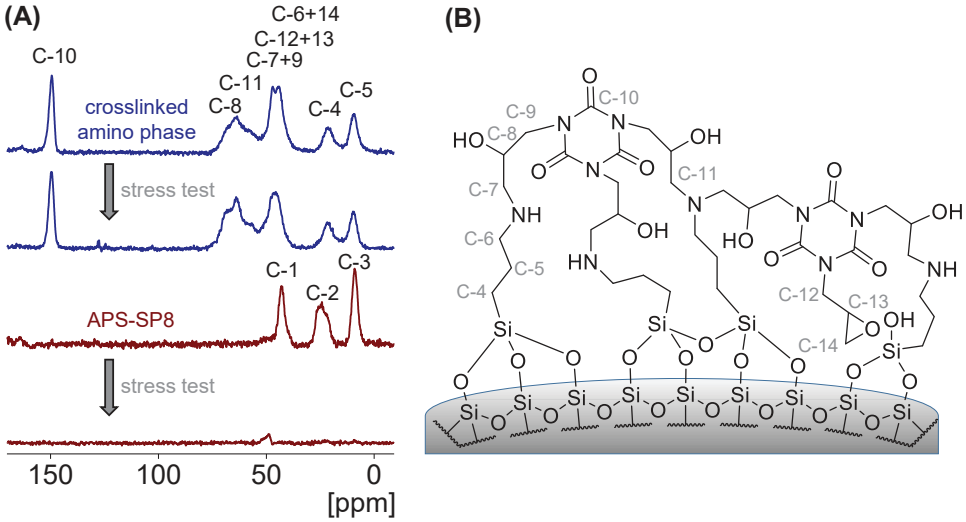


**FIGURE 3** (A) Solid-state $^{13}C$ CP/MAS NMR spectra of cross-linked amino phase and 3-aminopropyl silica (APS)-SP8 before and after the exposure to stress conditions and (B) signal assignment for cross-linked amino phase. The signal assignment for APS-SP8 is specified in Figure 2

incorporation of roughly 1.37 μmol/m$^2$ triglycidyl isocyanurate. This means that each crosslinker has, on average, reacted with 2.5 amino groups, or in other words, 50% of the crosslinkers have reacted with 2 and 50% with 3 amino groups. This leads to a thin polymeric network of (secondary and tertiary) amino, amide, and hydroxy groups on top of the silica surface. In this context, solid-state $^{13}C$ CP/MAS NMR analysis proved the successful reaction as well (see Figure 3). Here, in particular, the emerged predominant amide carbon bond (C-10) confirms the effective incorporation of the crosslinking agent. This SP should be highly stable, while the hydrophilic basic character is supposed to be largely maintained.

## 3.3 | Preparation of coated, immobilized, and cross-linked PEI silica for comparison

In order to compare the hydrolytic stability of the new cross-linked aminopropyl silica phase in comparison to polymeric amino phases, a variety of PEI-based SPs were synthesized. To this end, three distinct approaches were carried out applying branched PEI as a functional amino group-rich reagent for the functionalization of silica and three distinct procedures for SP preparation, for example, a coated PEI phase, an immobilized PEI phase, and a cross-linked PEI phase (see Figure 1). In the first approach, PEI was attached physically to the surface of silica particles by hydrogen-bonding and electrostatic interactions between the basic amino groups of PEI and the acidic silanols located on the support's surface resulting in the coated PEI phase [20]. In the second approach, the silica was first modified with (3-glycidyloxypropyl)trimethoxysilane resulting in epoxy-silica. Subsequently, PEI was coated by the same procedure on top of the epoxy-silica particles but additionally anchored chemically by nucleophilic ring-opening reaction of epoxy groups by amines under neat conditions (i.e., without solvent). Here, PEI accumulated on the silica surface and did not require any solvent due to its liquid nature. The primary and secondary amines of PEI then reacted with the terminal carbon of the oxiran moieties on the surface resulting in the formation of β-hydroxy amine bridges. Thereby, the kinetics of the epoxides' aminolysis is much faster for the primary amines than for the secondary amines, whereas tertiary amines usually do not react [34–37]. Owing to the large quantity of primary and secondary amino groups of PEI that can react, a layer of immobilized PEI anchored by multiple binding sites to the silica surface was created by this approach (immobilized PEI phase). For the third approach, the immobilized PEI units were additionally cross-linked using 1,4-butanediol diglycidyl ether resulting in an amino-rich, high molecular network on top of the silica surface (cross-linked PEI phase). For all three approaches, elemental analysis was utilized to estimate the quantity of incorporated PEI according to the assessed nitrogen content (see Table 1). It can be seen that the carbon content increases from coated to immobilized to cross-linked PEI phases while the nitrogen content was lower for the coated phase and remained essentially constant after crosslinking. These results indicate the successful formation of a network structure that is supposed to be highly stable and can serve as a reference in terms of stability.

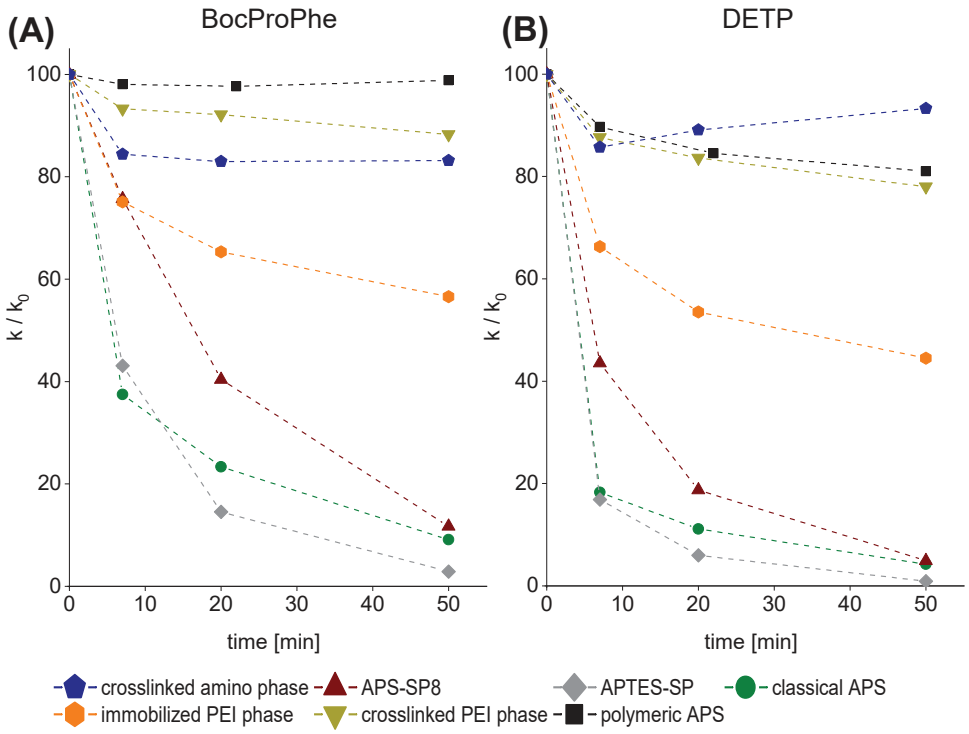


**FIGURE 4** Relative retention of *N*-tert-butoxycarbonyl-prolyl-phenylalanine (BocProPhe) (A) and O,O-diethyl thiophosphate (DETP) (B) after defined periods of time flushing the investigated columns with stress solution (ACN/$H_2O$/acetic acid, 30/70/0.1; v/v, pH 5, 60°C)

## 3.4 | Hydrolytic stability of the novel cross-linked amino silica phase in comparison to classical brush-type and polymeric amino phases

The new cross-linked amido-aminopropyl silica SP was evaluated regarding its hydrolytic stability in comparison to two commercially available amino phases (classical brush-type 3-aminopropyl-silica, briefly termed classical APS, and a polymeric amino phase (Phenomenex Luna $NH_2$), termed polymeric APS). Furthermore, an in-house prepared brush-type APTES-silica (APTES-SP) and a number of polymeric PEI phases (coated PEI, immobilized PEI, and cross-linked PEI) were tested as well to gain further insights into specific stabilities of bondings of amino phases. Due to different bonding, the latter ones lack detachment of the functional ligands due to the catalytic effect of the amino moiety under aqueous conditions [5]. For this purpose, all columns were subjected to a stress test and applied to harsh mobile phase conditions. Basically, they were flushed with a highly aqueous mixture of water, ACN, and acetic acid (adjusted to pH 5) at 60°C for in total of 50 h. After defined periods of time, the retention of two acidic test analytes (BocProPhe and DETP) was investigated, in order to estimate the loss of bonding by hydrolytic cleavage (see Figure 4). For this evaluation, retention factors *k* were normalized by the initial retention factor $k_0$ measured before applying stress conditions to the column. Additionally, the nitrogen content was assessed for all phases before and after exposure to the stress solution by elemental analysis. The results are presented in Figure 5.

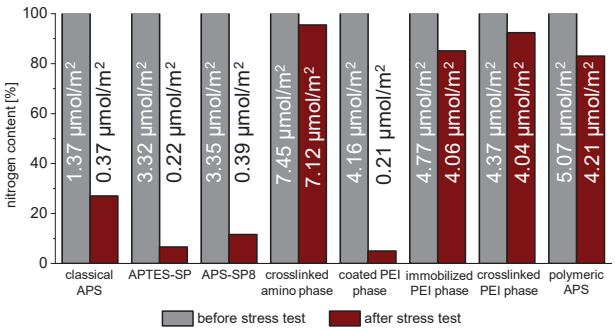


**FIGURE 5** Quantity of incorporated nitrogen of the prepared amino silica gels and two commercial amino phases before and after performing the stress test under highly aqueous conditions and elevated temperatures. The nitrogen content was determined by elemental analysis [13]

As can be seen in Figure 4, retention factors of BocProPhe and DETP drop quickly for the brush-type aminopropyl phases (classical APS, APTES-SP). After 50 h

of stress treatment, retention factors dropped by a factor of about 5 compared to the initial retention factor. The silatrane-bonded brush-type APS-SP8 is significantly more stable and the retention loss occurs less rapidly. Unfortunately, after 50 h stress conditioning, there is not much difference from the other brush-type amino phases. Hence, it becomes evident that trifunctional siloxane bonding of 3-aminopropyl ligand is not enough stable, and other concepts are required. The polymeric phase containing physically adsorbed PEI (coated PEI phase) showed almost no retention of the analytes even after the first equilibration step during the test. For this reason, it is not considered in Figure 4. The immobilized PEI phase adopts an intermediate state of stability. It is relatively stable and after 50 h stress testing still, around 60% of the retention is remaining. The cross-linked PEI phase, on the contrary, is highly stable (Figure 4). The same applies to the commercial polymeric amino phase (polymeric APS; Luna $NH_2$). On the other hand, the new cross-linked amino phase with network structure showed similar stability as the cross-linked PEI phase and Luna $NH_2$. After an initial drop, by which presumably remaining non-cross-linked aminopropyl ligands were removed, this cross-linked amino phase was very stable and pertained its retention characteristics over the tested period (see Figure 4).

These findings are confirmed by the elemental analysis of the SPs from the emptied column after stress testing. It is evident from Figure 5 that the nitrogen content is dramatically dropped for the commercial aminopropyl silica (classical APS). The same is observed for APTES-silica, while the corresponding silatrane-bonded amino phase (APS-SP8) showed slightly higher, but also low, nitrogen content, as expected from the retention characteristics of Figure 4. In contrast, the commercial polymeric amino phase Luna $NH_2$ (polymeric APS) experienced only a minor nitrogen loss, a determined by elemental analysis, in the course of column stressing (80% of N still present after the stress test) (Figure 5), which corresponded to the chromatographic test. As mentioned above, the coated PEI phase almost completely lost the nitrogen and thus retention. The immobilized and cross-linked PEI phase retained 80 and 90% of the initial nitrogen, respectively, being indicative of high stability as expected. Interestingly, the cross-linked amido-amino network silica (cross-linked amino phase) had nitrogen close to 100% of its initial value after the stress test and showed the lowest loss of nitrogen of all tested phases (Figure 5). This is promising and confirms the stable bonding.

Hence, the beneficial hydrolytic stability characteristics of the new cross-linked amino phase should enable analysis at high temperatures in aqueous chromatographic modes such as HILIC or RPLC. Furthermore, extended column lifetimes are typically associated with diminished ligand bleeding as well as reduced MS background noise.

## 3.5 | Chromatographic evaluation of cross-linked versus brush-type amino phases in three chromatographic modes (HILIC, RPC, and WAXC)

The surface of the prepared novel cross-linked amino phase offers a multitude of interaction opportunities due to its various functional groups. Amino, amide, hydroxy and residual silanol groups create an overwhelmingly polar surface in spite of its high carbon content (10.7% C vs. 4.6% C on APTES silica) with a large quantity of electron acceptor and donor sites.

The carbon content of ~11% comes close to C8 RP phases. To evaluate whether residual hydrophobic selectivity (as assessed by the methylene selectivity $\alpha_{CH2}$) is available, a simple RP test was devised [38]. For this exploration, under RPC conditions a mixture of two lipophilic alkylbenzenes differing in one methylene unit (BuB and PeB) and two acidic compounds differing in lipophilicity and acidity was utilized. The alkylbenzenes were not retained on the new cross-linked amino phase and thus exhibited a similar hydrophobic retention profile to the other amino phases that showed no or negligible retention of the neutral alkylbenzenes (cf. Figure 6A and Table S6). This confirmed the overbalancing hydrophilic character of the new amido-amino polymer network on the silica surface. In contrast, all phases showed sufficient retention and excellent separation of the two acidic compounds. Expectedly, the more lipophilic acid BocProPhe is eluted typically prior to DETP, except for classical APS due to its low amino group coverage (1.37 μmol N/$m^2$).

The strongly hydrophilic character thus classifies the novel cross-linked amido-amino phase as a tentative HILIC phase (potentially complementary to classical amide and sulfobetaine chemistries as well as to unmodified silica) [39–41]. Thus, three sets of analytes (nucleosides, xanthines, and vitamins) were selected to examine the chromatographic performance of the SPs under HILIC conditions. The resultant chromatograms for the nucleoside test mixture are depicted in Figure 6B in comparison to the amino phase APS-SP8; for chromatographic parameters (Table S6 and Figure S15). The elution patterns are very similar, yet the cross-linked amido-amino phase showed added selectivity and could resolve adenosine from uridine which co-eluted on the amino phase APS-SP8. The retention factor of uridine can be used as a probe to characterize the hydrophilicity of the surface in HILIC mode. It measured a $k_{uridine}$ of 3.03 on the cross-linked amino phase, comparable to the TSKGel Amide-80 HILIC phase

($k_{uridine}$ 3.45; cf. Table S6). The brush-type aminopropyl phase APS-SP8 gave a retention factor $k_{uridine}$ of 6.46 indicating higher hydrophilicity. The investigated xanthines differed in degree and position of *N*-methylation. Thus, the trimethyl xanthine derivative caffeine is eluted first on the cross-linked amino phase in HILIC mode, whereas the acidic dimethyl theophylline is eluted last, after theobromine, which is indicative of the basic surface character (cf. Figure S15). Finally, the separation of various water-soluble vitamins was examined as illustrated in Figure S15. Here, in particular, the negatively charged vitamins ascorbic acid and nicotinic acid are eluted subsequently to the neutral or positively charged ones due to the AEX capacity of the SP. Overall, the cross-linked amido-amino phase exhibited decreased retention in HILIC for all analytes compared to its aminopropyl precursor phase, presumably due to better silanol accessibility of the polar analytes.

Since the new phase offers weak AEX capacity properties a set of derivatized amino acids was utilized to evaluate the effect of surface charge in more detail. In this context, the ionic strength (10, 20, and 50 mM) and the pH value (3.5, 5, and 7) of the mobile phase were studied. The amino acid derivatives differed with regard to their acidity and basicity. Thus, two acidic (AcPhe, AcTrp), two basic (PheOMe and Trp hydrochloride), two zwitterionic (Phe, Trp), and one neutral analyte (AcPheOEt) were part of this test mixture. The respective chromatograms for the phenylalanine derivatives are depicted in Figure 6C for the cross-linked amino phase and its brush amino phase precursor (APS-SP8). It becomes evident that retention is strong for the acidic amino acid derivatives. Moreover, the cross-linked amino phase exhibits AEX capacity over the pH range from 3.5 to 7. Maximal retention was observed in the intermediate pH range (pH 5; see Figure 7 and Figure S17) where the product of the degree of dissociation of the acidic amino acid derivatives (AcPhe, AcTrp) and the basic groups on the SP furnished a maximum. As expected, the ionic strength of the mobile phase significantly affects the retention of the acidic derivatives which can be scrutinized in greater detail by the stoichiometric displacement model (Equation (1); a linear decrease of log *k* with log counterion concentration *c*) which offers a straightforward possibility to prove the prevalence of the anionic exchange process (Figure 7) [42, 43].

$$\log k = \log K_z - z \log c \quad (1)$$

where in, the slope *z* describes the ratio between the effective involved charges of the analyte and the counterions, log $K_z$ represents the intercept on the log *k*-axis (retention factor at 1 M counterion concentration) and is depending on the applied ion-exchange system. The largest log $K_z$ values were achieved at pH 5 for AcPhe (pH 3.5: 1.88 ± 0.01, pH 5: 2.68 ± 0.00, pH 7: 1.61 ± 0.07) and AcTrp (pH 3.5: 1.90 ± 0.01, pH 5: 2.60 ± 0.07, pH 7: 1.84 ± 0.03) illustrating the strongest electrostatic interaction between the analytes and the SP at this pH.

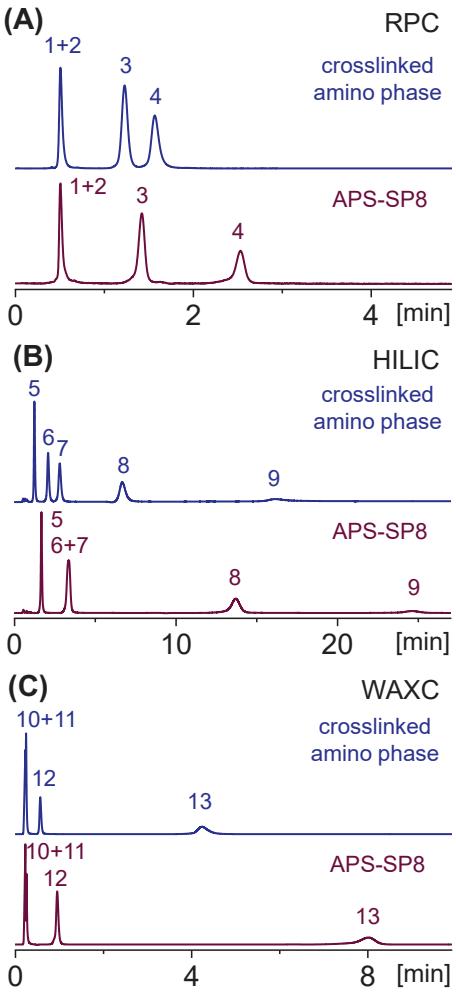


**FIGURE 6** Chromatograms obtained from the characterization of cross-linked amino phase and 3-aminopropyl silica (APS)-SP8 under RPC (A), HILIC (B), and weak anion exchange chromatography (WAXC) (pH 5, 50 mM) (C) conditions [42]. The following analytes were used for chromatographic exploration: BuB (1), PeB (2), *N*-tert-butoxycarbonyl-prolyl-phenylalanine (BocProPhe) (3), O,O-diethyl thiophosphate (DETP) (4), thymidine (5), uridine (6), adenosine (7), cytidine (8), guanosine (9), L-phenylalanine methyl ester (PheOMe) (10), *N*-acetyl-phenylalanine ethyl ester (AcPheOEt) (11), L-phenylalanine (Phe) (12), *N*-acetyl-L-phenylalanine (AcPhe) (13). Detailed chromatographic conditions and parameters can be found in the supplementary material

From these results, it can be derived that the current cross-linked amino phase has characteristic retention increments of amino phases and can be a useful SP replacing classical amino phases with a more stable material with similar retention behavior.

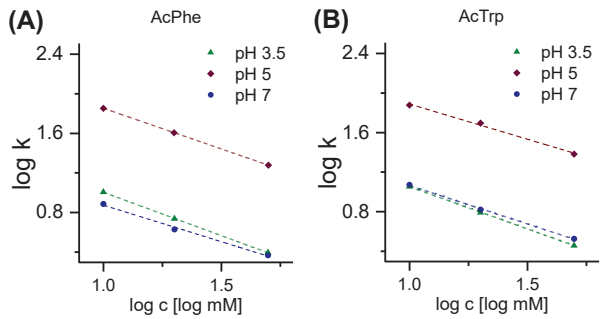


**FIGURE 7** Evaluation of the ion-exchange capacity of the cross-linked amino phase for *N*-acetyl-L-phenylalanine (AcPhe) (A) and *N*-acetyl-L-tryptophan (AcTrp) (B) under varying buffer concentrations and pH values. Detailed conditions are given in Figure S17

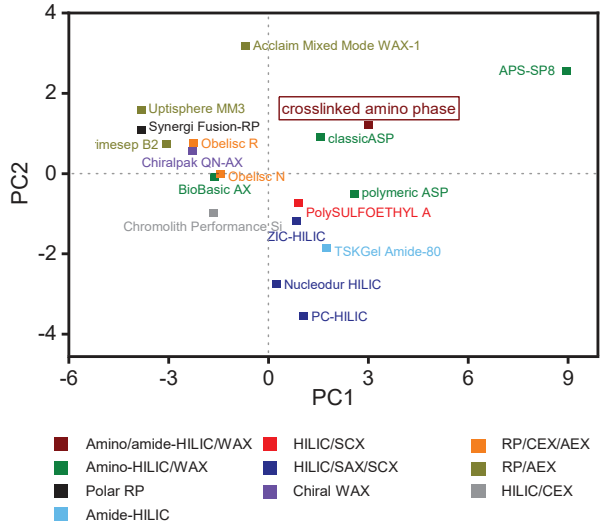


**FIGURE 8** Score plot of principal component analysis (PCA)

## 3.6 | Classification of cross-linked amino silica compared to commercial benchmarks by PCA

Finally, a benchmarking study was performed to assess the position, in terms of similarity and orthogonality of retention characteristics, of the new cross-linked amino phase amongst a number of classical HILIC, polar RP, mixed-mode, and amino phases. Thus, the resultant retention factors obtained for the test analytes examined under HILIC and RP conditions were subjected to a PCA in order to classify the various columns. Retention factors and surface chemistries of the SPs used are depicted (cf. Figure S19 and Table S6). The score plots of the PCA are shown in Figure 8, and the corresponding loadings plot in Figure S21. It becomes evident that the latent variable PC1 reflects increasing hydrophilicity of the surface of the SPs the larger the scores. On the contrary, the latent variable PC2 encodes for the charge of the SPs which varies from net negative to net positive with increasing PC2 scores. It is striking that the new cross-linked amino material was located nearby the classic APS in the score plot. Interestingly, its precursor APS-SP8 appears to have a more dissimilar character illustrating the effect of crosslinking leading to apparently decreased hydrophilicity and lower surface charge. The new cross-linked amino phase has higher hydrophilicity than the commercial polymeric PEI phase (BioBasic AX) and comparable hydrophilicity to the commercial polymeric APS (Luna $NH_2$). It turns out to be significantly more polar than the evaluated polar RP (Synergi Fusion) and mixed-mode phases (Acclaim Mixed-mode WAX1, Uptisphere MM3, Primesep B2, Obelisc R and N, and Chiralpak QN-AX). In conclusion, the new cross-linked amido-amino network silica (cross-linked amino phase) was mapped at a similar PC1-axis level as most HILIC and amino phases emphasizing its significant hydrophilicity while at the PC2-axis level, the material showed similar charge levels as the classical amino phase and significant orthogonality to common HILIC phases with amide (TSKgel Amide-80) and sulfobetaine chemistry (ZIC-HILIC, PC-HILIC, and nucleolar HILIC).

## 3.7 | Potential applications

### 3.7.1 | Carbohydrates

Carbohydrate analysis is of considerable practical importance in many fields (including food and drug analysis as well as metabolomics). Due to the hydrophilic character of carbohydrates, HILIC represents a preferred chromatographic mode for their analysis. Thus, the usability of the cross-linked amino phase was evaluated for the analysis of six carbohydrates under classical HILIC conditions. An exemplary chromatogram is depicted in Figure 9; more extensive data are provided (see Figure S22 and Table S7). As can be seen, all six carbohydrates can be separated under the given isocratic chromatographic conditions in accordance with their distribution coefficient logP (see Figure S23). It is striking that single peaks were observed for all carbohydrates, also the reducing ones, and no anomers were resolved such as by many HILIC columns [44, 45]. This avoids complications and limits isomeric overlaps. Investigations into the retention mechanism (study of temperature and ACN dependency) revealed common behaviors. Thus, retention decreases with increasing temperatures and increasing concentration *c* of water in the mobile phase. In consequence, the new cross-linked amido-amino network silica demonstrated its usefulness for the separation of polar carbohydrates in HILIC mode.

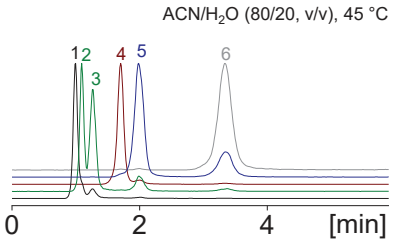


**FIGURE 9** Separation of six carbohydrates on the cross-linked amino phase by hydrophilic interaction liquid chromatography (HILIC)-MS/MS (mobile phase: ACN/$H_2O$ (80/20, v/v), flow rate: 0.5 ml/min, temperature: 45°C, detection by mass spectrometry [parameters are defined in the Supporting Information], analytes: xylose (1), fructose (2), glucose (3), sucrose (4), maltose (5), maltotriose (6))

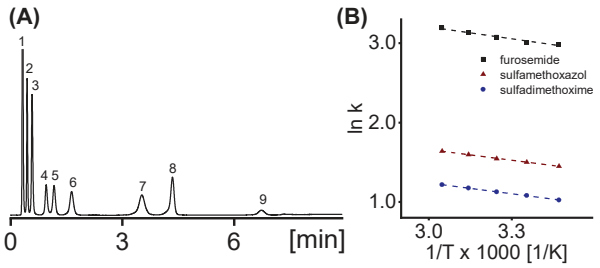


**FIGURE 10** Separation of nine sulfonamides under hydrophilic interaction liquid chromatography–weak anion exchange chromatography (HILIC-WAX) elution mode. (A) Chromatogram obtained under gradient elution at 55°C. The mobile phase consisted of ACN/$H_2O$ (90/10, v/v) and ammonium acetate (pH 7; gradient: 0 –20 mM in 10 min). Analytes: sulfanilamide (1), sulfaguanidine (2), sulfamerazine (3), sulfadiazine (4), sulfadimethoxine (5), sulfamethoxazole (6), sulfacetamide (7), sulfisoxazole (8), and furosemide (9). (B) vant't Hoff plot illustrating the effect of temperature *T* on the obtained retention factors *k*. Further chromatographic parameters are given in the Supporting Information

### 3.7.2 | Sulfonamides

Finally, the separation of sulfonamides was evaluated as another potential application of the new cross-linked amino phase. The sulfonamide structural element is present in a variety of drug classes (including antibiotics, antidiabetics, and diuretics) and is typically characterized by its amphoteric nature due to the basic aromatic amino functionality and the acidic -$SO_2$-NH- moiety. The compounds are hydrophilic and hence a HILIC-type separation appears most appropriate.

Initially, the main factors with influence on retention and selectivity, such as water content, buffer concentration, and temperature were investigated. This study revealed some unexpected behaviors. As can be seen in Figure S24 the separation of 7 sulfonamides was feasible under isocratic HILIC conditions without the addition of buffer ions to the mobile phase (cf. Figure S24H–K). Interestingly, retention increased with the water content (from 5% to 20%) (except for sulfaguanidine (2)). This is counterintuitive for a HILIC mechanism, however, may be related to increasing dissociation of the weakly acidic sulfonamide with higher water content and hence strengthened ionic interactions. However, two analytes (sulfisoxazole and furosemide) could not be eluted under these conditions, probably due to strong AEX interactions. To balance the ionic interactions required the addition of counterions (buffer anions) to the mobile phase (cf. Figure S24E–G). In doing so, the increase of buffer concentration leads to faster elution, especially for the more strongly retained analytes proving the underlying ion-exchange mechanism. Finally, the influence of temperature on the separation was examined in the range from 15 to 55°C (cf. Figure S24A–E). Unexpectedly, retention of the analytes was enhanced with rising temperatures which is illustrated in the respective vant't Hoff plot in Figure 10B. This is contrary to the common behavior that shows decreasing retention times with an increase in column temperatures (enthalpic control). One possible explanation for this behavior could be entropic control of the adsorption process, e.g. increased retention due to the release of water shells on analytes and SP associated with a gain in entropy. However, the effect might be also explained by the temperature-dependent change of acidity of the analytes and basicity of the SP, respectively. Since dissociation is typically an endothermic process for most acids, acidity usually increases along with the temperature. Thus, it was reported that $pK_a$ values of weak acids (or $pK_b$ values of weak bases) can shift up to −0.03 units/K [46]. Consequently, the rise in temperature might strengthen the ionic interactions between the SP and analytes owing to an alteration of the acido-basic properties of the system leading finally to an enhanced AEX process at elevated temperatures. The optimized isocratic separation of the complex sulfonamide mixture is shown in Figure 10A. In conclusion, the analysis of hydrophilic sulfonamides documents the applicability of the new cross-linked amino phase under HILIC-WAX mode revealing stable and robust separations even at elevated temperatures. This SP holds some promise to complement the parameter space of SP surface chemistries in HPLC.

## 4 | CONCLUDING REMARKS

In this work, the preparation of novel cross-linked amino silica was reported. The novel stable-bonded amino silica phase exhibited greater hydrolytic stability after crosslinking than the precursor aminopropyl silica and achieved

column stability characteristics comparable to a commercial highly stable polymeric amino column. The chromatographic performance of the novel phase was investigated under several chromatographic conditions including RPLC, HILIC, and WAX chromatography elution modes. It turned out that the material preserved AEX capacity after crosslinking. The retention characteristics and usefulness of the material were illustrated by the separation of nucleosides, water-soluble vitamins, sulfonamides, and carbohydrates. Overall, the novel cross-linked amido-amino phase showed interesting chromatographic performance combining typical amino phase behavior in the chromatographic space with exceptional column stability. It, therefore, represents an excellent alternative to classical amino phases appropriate for the analysis of polar or charged analytes.

## ACKNOWLEDGMENT

Open access funding enabled and organized by Projekt DEAL.

## CONFLICT OF INTEREST

The authors declare that they have no known competing financial interests or personal relationships that could have appeared to influence the work reported in this paper.

## DATA AVAILABILITY STATEMENT

Data are available in the article, Supporting Information, or upon reasonable request from the authors.

## ORCID

*Michael Lämmerhofer* https://orcid.org/0000-0002-1318-0974

## REFERENCES

1. Olsen BA. Hydrophilic interaction chromatography using amino and silica columns for the determination of polar pharmaceuticals and impurities. J Chromatogr A. 2001;913:113–22.
2. Li RP, Zhang Y, Lee CC, Liu LM, Huang YP. Hydrophilic interaction chromatography separation mechanisms of tetracyclines on amino-bonded silica column. J Sep Sci. 2011;34:1508–16.
3. Oyler AR, Armstrong BL, Cha JY, Zhou MX, Yang Q, Robinson RI, Dunphy R, Burinsky DJ. Hydrophilic interaction chromatography on amino-silica phases complements reversed-phase high-performance chromatography and capillary electrophoresis for peptide analysis. J Chromatogr A. 1996;724:378–83.
4. Sanchez-Mata MC, Penuela-Teruel MJ, Camara-Hurtado M, Diez-Marques C, Torija-Isasa ME. Determination of mono-, di-, and oligosaccharides in legumes by high-performance liquid chromatography using an amino-bonded silica column. J Agr Food Chem. 1998;46:3648–52.
5. Etienne M, Walcarius A. Analytical investigation of the chemical reactivity and stability of aminopropyl-grafted silica in aqueous medium. Talanta 2003;59:1173–88.
6. Luan ZH, Fournier JA, Wooten JB, Miser DE. Preparation and characterization of (3-aminopropyl)triethoxysilane-modified mesoporous SBA-15 silica molecular sieves. Micropor Mesopor Mat. 2005;83:150–8.
7. Palmai M, Nagy LN, Mihaly J, Varga Z, Tarkanyi G, Mizsei R, Szigyarto IC, Kiss T, Kremmer T, Bota A. Preparation, purification, and characterization of aminopropyl-functionalized silica sol. J Colloid Interf Sci. 2013;390:34–40.
8. Vrancken KC, Van Der Voort P, Possemiers K, Vansant EF. Surface and structural-properties of silica-gel in the modification with gamma-aminopropyltriethoxysilane. J Colloid Interf Sci. 1995;174:86–91.
9. Waddell TG, Leyden DE, Debello MT. The nature of organosilane to silica-surface sonding. J Am Chem Soc. 1981;103:5303–7.
10. Liu HM, Jin P, Jiang M, Duan Y, Zhu GZ, Yu H, Qiu HD. Performance evaluation of silica microspheres functionalized by different amine-ligands for hydrophilic interaction chromatography. J Chromatogr A 2021;1640:461967.
11. Vrancken KC, Possemiers K, Vandervoort P, Vansant EF. Surface modification of silica-gels with aminoorganosilanes. Colloid Surface A. 1995;98:235–41.
12. Gimpel M, Unger K. Hydrolytically stable chemically bonded silica supports with metal complexating ligands-synthesis, characterization and use in high-performance ligand-exchange chromatography (hplec). Chromatographia 1982;16:117–25.
13. Geibel C, Theiner J, Wolter M, Kramer M, Lindner W, Lämmerhofer M. Controllable organosilane monolayer density of surface bonding using silatranes for thiol functionalization of silica particles for liquid chromatography and validation of microanalytical method for elemental composition determination. J Chromatogr A. 2021;1653:462418.
14. Chu ZY, Zhang LY, Zhang WB. Preparation and evaluation of maltose modified polymer-silica composite based on cross-linked poly glycidyl methacrylate as high performance liquid chromatography stationary phase. Anal Chim Acta. 2018;1036:179–86.
15. Sun M, Qiu HD, Wang LC, Liu X, Jiang SX. Poly(1-allylimidazole)-grafted silica, a new specific stationary phase for reversed-phase and anion-exchange liquid chromatography. J Chromatogr A. 2009;1216:3904–9.
16. Wolter M, Chen X, Woiwode U, Geibel C, Lämmerhofer M. Preparation and characterization of poly(3-mercaptopropyl)methylsiloxane functionalized silica particles and their further modification for silver ion chromatography and enantioselective high-performance liquid chromatography. J Chromatogr A. 2021;1643:462069.
17. Zimmermann A, Horak J, Sievers-Engler A, Sanwald C, Lindner W, Kramer M, Lämmerhofer M. Surface-cross-linked poly(3-mercaptopropyl)methylsiloxane-coatings on silica as new platform for low-bleed mass spectrometry-compatible functionalized stationary phases synthesized via thiol-ene click reaction. J Chromatogr A. 2016;1436:73–83.
18. Geibel C, Dittrich K, Wolter M, Lämmerhofer M. Thiol-ene photo-click immobilization of a chiral chromatographic ligand on silica particles. J Chromatogr A. 2020;1622:461133.
19. Lawson TG, Regnier FE, Weith HL. Separation of synthetic oligonucleotides on columns of microparticulate silica coated with cross-linked polyethylene imine. Anal Biochem. 1983;133:85–93.
20. Alpert AJ, Regnier FE. Preparation of a porous microparticulate anion-exchange chromatography support for proteins. J Chromatogr. 1979;185:375–92.

21. Kopaciewicz W, Rounds MA, Regnier FE. Stationary phase contributions to retention in high-performance anion-exchange protein chromatography-ligand density and mixed-mode effects. J Chromatogr. 1985;318:157–72.
22. Cai TP, Zhang HJ, Chen J, Li Z, Qiu HD. Polyethyleneimine-functionalized carbon dots and their precursor co-immobilized on silica for hydrophilic interaction chromatography. J Chromatogr A. 2019;1597:142–8.
23. Luda AAG, Shlyakhtenko S, Lyubchenko YL. Mica functionalization for imaging of DNA and protein-DNA complexes with atomic force microscopy. Methods Mol Biol. 2012;931:195-312.
24. Kallury KMR, Macdonald PM, Thompson M. Effect of surface-water and base catalysis on the silanization of silica by (aminopropyl)alkoxysilanes studied by X-ray photoelectron-spectroscopy and C-13 cross-polarization magic-angle-spinning nuclear-magnetic-resonance. Langmuir 1994;10:492-499.
25. Blitz JP, Murthy RSS, Leyden DE. The role of amine structure on catalytic activity for silylation reactions with Cab-O-Sil. J Colloid Interf Sci. 1988;126:387–92.
26. Lee SH, Kang JS, Kim D. A mini review: recent advances in surface modification of porous silicon. Materials 2018;11:2557.
27. Locke DC. Chemically bonded stationary phases for liquid chromatography. J Chromatogr Sci. 1973;11:120–8.
28. Vrancken KC, Van Der Voort P, Gillis-D'Hamers I, Vansant EF, Grobet P. Influence of water in the reaction of gamma-aminopropyltriethoxysilane with silica-gel - a fourier-transform infrared and cross-polarization magic-angle-spinning nuclear-magnetic-resonance study. J Chem Soc Faraday T. 1992;88:3197–200.
29. Goerl U, Hunsche A, Mueller A, Koban HG. Investigations into the silica/silane reaction system. Rubber Chem Technol. 1997;70:608–23.
30. Hellriegel C, Skogsberg U, Albert K, Lämmerhofer M, Maier NM, Lindner W. Characterization of a chiral stationary phase by HR/MAS NMR spectroscopy and investigation of enantioselective interaction with chiral ligates by transferred NOE. J Am Chem Soc. 2004;126:3809–16.
31. Jackowska M, Bocian S, Buszewski B. Dendrimer modified silica gel for anion exchange chromatography: synthesis, characterization and application. Analyst 2012;137:4610-4617.
32. Choi S, Janisse AP, Liu CH, Douglas EP.Effect of water addition on the cure kinetics of an epoxy-amine thermoset. J Polym Sci Pol Chem. 2011;49:4650–9.
33. Mora AS, Tayouo R, Boutevin B, David G, Caillol S. A perspective approach on the amine reactivity and the hydrogen bonds effect on epoxy-amine systems. Eur Polym J. 2020;123:109460.
34. Azizi N, Saidi MR. Highly chemoselective addition of amines to epoxides in water. Org Lett. 2005;7:3649–51.
35. Ehlers JE, Rondan NG, Huynh LK, Pham H, Marks M, Truong TN. Theoretical study on mechanisms of the epoxy - amine curing reaction. Macromolecules 2007;40:4370–7.
36. Vyazovkin S, Sbirrazzuoli N. Mechanism and kinetics of epoxy-amine cure studied by differential scanning calorimetry. Macromolecules 1996;29:1867–73.
37. Pohl CA, Srinivasan K. Electrostatically attached highly branched anion-exchange phases derived from diamines and diepoxides. Talanta 2018;184:338–46.
38. Zuvela P, Skoczylas M, Liu JJ, Baczek T, Kaliszan R, Wong MW, Buszewski B. Column characterization and selection systems in reversed-phase high-performance liquid chromatography. Chem Rev. 2019;119:3674–729.
39. Jandera P. Advances in hydrophilic interaction liquid chromatography: handbook of advanced chromatography/mass spectrometry techniques. 1st ed. Amsterdam: Elsevier; 2017.
40. Jandera P. Stationary and mobile phases in hydrophilic interaction chromatography: a review. Anal Chim Acta. 2011;692:1-25.
41. Ikegami T, Taniguchi T, Okada T, Horie K, Arase S, Ikegami Y. Functionalization using polymer or silane? A practical test method to characterize hydrophilic interaction chromatography phases in terms of their functionalization method. J Chromatogr A. 2021;1638:461850.
42. Bäurer S, Polnick S, Sanchez-Munoz OL, Kramer M, Lämmerhofer M. *N*-Propyl-*N*'-2-pyridylurea-modified silica as mixed-mode stationary phase with moderate weak anion exchange capacity and pH-dependent surface charge reversal. J Chromatogr A. 2018;1560:45–54.
43. Stahlberg J. Retention models for ions in chromatography. J Chromatogr A. 1999;855:3–55.
44. Taniguchi A, Ikegami T. Comparison of the steric selectivity on hydrophilic interaction chromatography columns modified with poly(acrylamide) possessing different morphology. J Chromatogr A. 2021;1650:462207.
45. Fu X, Cebo M, Ikegami T, Lämmerhofer M. Retention characteristics of poly(N-(1H-tetrazole-5-yl)-methacrylamide)-bonded stationary phase in hydrophilic interaction chromatography. J Chromatogr A. 2020;1609:460500.
46. Buckenmaier SMC, McCalley DV, Euerby MR. Rationalisation of unusual changes in efficiency and retention with temperature shown for bases in reversed-phase high-performance liquid chromatography at intermediate pH. J Chromatogr A. 2004;1060:117–26.
47. Albert K, Brindle R, Schmid J, Buszewski B, Bayer E. CP/MAS NMR investigations of silica-gel surfaces modified with aminopropylsilane. Chromatographia 1994;38:283–90.
48. Caravajal GS, Leyden DE, Quinting GR, Maciel GE. Structural characterization of (3-aminopropyl)triethoxysilane-modified silicas by Si-29 and C-13 nuclear magnetic-resonance. Anal Chem. 1988;60:1776–86.
49. Zhmud BV, Sonnefeld J. Aminopolysiloxane gels: production and properties. J Non-Cryst Solids. 1996;195:16–27.

## SUPPORTING INFORMATION

Additional supporting information can be found online in the Supporting Information section at the end of this article.

**How to cite this article:** Wolter M, Geibel C, Olfert M, Su M, Bicker W, Kramer M, Lindner W, Lämmerhofer M. Development and chromatographic exploration of stable-bonded cross-linked amino silica against classical amino phases. J Sep Sci 2022;45:3286–3300. https://doi.org/10.1002/jssc.202200268

## X.2 Publication V – Supplementary Material

# Development and chromatographic exploration of stable-bonded cross-linked amino silica against classical amino phases

**Marc Wolter** [a], Christian Geibel [a], Matthias Olfert [a], Min Su [a], Wolfgang Bicker [a, b], Markus Kramer [c], Wolfgang Lindner [b], Michael Lämmerhofer [a,*]

[a] Institute of Pharmaceutical Sciences, Pharmaceutical (Bio-)Analysis, University of Tübingen, Auf der Morgenstelle 8, 72076 Tübingen, Germany

[b] Institute of Analytical Chemistry, University of Vienna, Währinger Straße 38, 1090 Vienna, Austria

[c] FTC – Forensic-Toxicological Laboratory, Gaudenzdorfer Gürtel 43-45, 1120 Vienna, Austria

[d] Institute of Organic Chemistry, University of Tübingen, Auf der Morgenstelle 18, 72076 Tübingen, Germany

* corresponding author

# Table of contents

**PART VI: Exploration of the ion-exchange characteristics**

- Figure S17 Chromatograms obtained for crosslinked amino phase from ion-exchange chromatography test.
- Figure S18 Analytes applied for ion-exchange chromatography test.
- Table S3 Chromatographic parameters obtained from ion-exchange chromatography test.

**PART VII: Stationary phase classification**

- Table S4 Elemental compositions and surface areas of commercial columns used for PCA.
- Figure S19 Surface chemistries of commercial columns classified by PCA.
- Table S5 Retention factors obtained from RPC and HILIC test.
- Figure S20 Surface chemistries of classical APS and polymeric APS.
- Figure S21 Loading scatter plot of PCA.

**PART VIII: Carbohydrate analysis**

- Figure S22 Results form HILIC of carbohydrates on crosslinked amino phase.
- Figure S23 Carbohydrates investigated under HILIC conditions.
- Table S6 Chromatographic parameters obtained from carbohydrate analysis.
- Table S7 Mass spectrometry parameters used for carbohydrate analysis.

**PART IX: Sulfonamide analysis**

- Figure S24 Separation of sulfonamides on crosslinked amino phase.
- Figure S25 Structure of sulfonamides investigated.
- Table S8 Chromatographic parameters obtained from sulfonamide analysis.

**PART X: References**

## PART I: Synthesis of (3-aminopropyl)silatrane

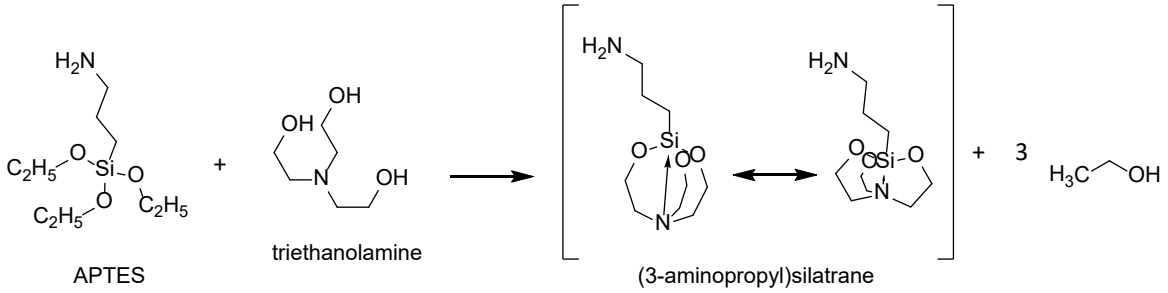


**Fig. S1.** Reaction scheme for condensation reaction between APTES and triethanolamine resulting in the formation of (3-aminopropyl)silatrane. Synthesis procedure: 0.1 mol APTES, 0.1 mol triethanolamine and 4 mg sodium hydroxide were dispersed initially in 20 mL methanol within a 250 mL round bottom flask. Thereafter, methanol was slowly evaporated using a rotary evaporator equipped with a water bath kept at 25 °C. When the solvent was fully evaporated, the water bath temperature was adjusted to 60 °C and ethanol formed in the condensation reaction between APTES and triethanolamine was constantly removed by evaporation. After precipitation of the reaction product evaporation was proceeded for additional 30 min. Subsequently, the reaction product was dissolved in 15 mL methanol and recrystallized from 150 mL toluene for 12 h. Hereafter, the reaction product was collected and carefully washed 3 times with 25 mL cold toluene using a glass funnel of porosity 5 and dried under permanent vacuum at 40 °C for 24 h. Finally, (3-aminopropyl)silatrane was stored under vacuum at 8 °C until it was used for silica modification. Synthesis control was carried out by NMR. The corresponding NMR spectra are depicted in Fig. S2-S3.

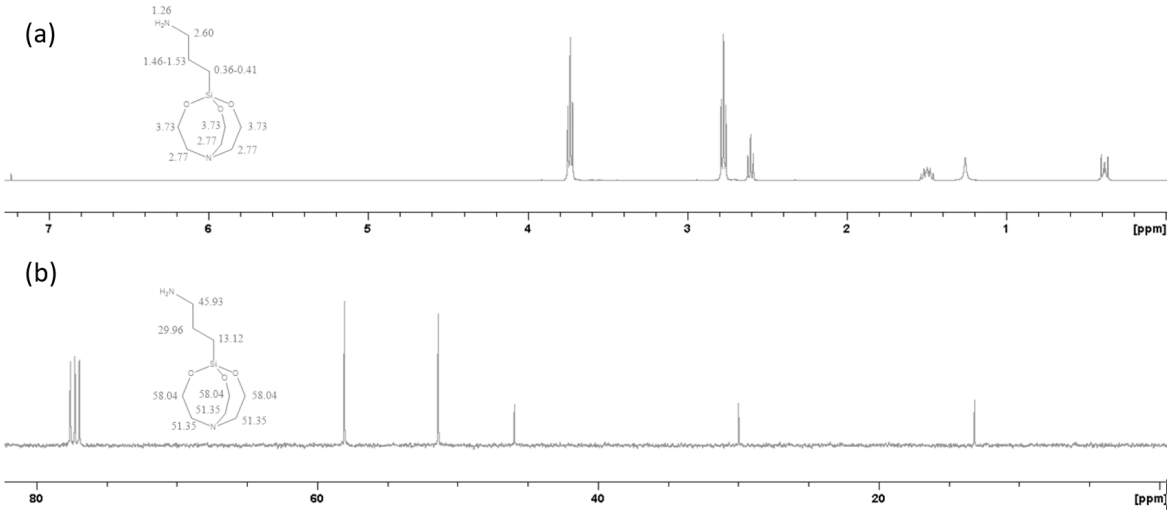


**Fig. S2.** NMR spectra of (3-aminopropyl)silatrane: (a) $^{1}$H NMR spectrum (($J_t$ [Hz]), $CDCl_3$, 400 MHz): δ 0.36-0.41 ppm (m, 2H), 1.26 ppm (br s, 2H), 1.46-1.53 ppm (m, 2H), 2.60 ppm (t, $J_t$ = 6.92, 2H), 2.77 ppm (t, $J_t$ = 5.82, 6H), 3.73 ppm (t, $J_t$ = 5.82, 6H); (b) $^{13}$C NMR ($CDCl_3$, 400 MHz): δ 13.12 ppm (1C), 29.96 ppm (1C), 45.93 ppm (1C), 51.35 ppm (3C), 58.04 ppm (3C). NMR spectra were calibrated to the solvent peaks with δ(1H) = 7.24 ppm and δ(13C) = 77.23 ppm [1].

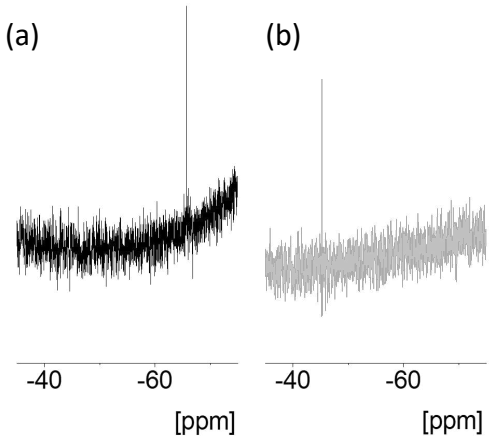


**Fig. S3.** Comparison of $^{29}$Si NMR spectra ($CDCl_3$, 400 MHz) of (a) (3-aminopropyl)silatrane and (b) (3-aminopropyl)triethoxysilane (APTES). Here, the increased electron density on the silatrane´s silicon due to the transannular donor-acceptor N→Si bond provokes the high-field shift from ~ 45 ppm to ~ 65 ppm.

## PART II: Synthesis of amino phases

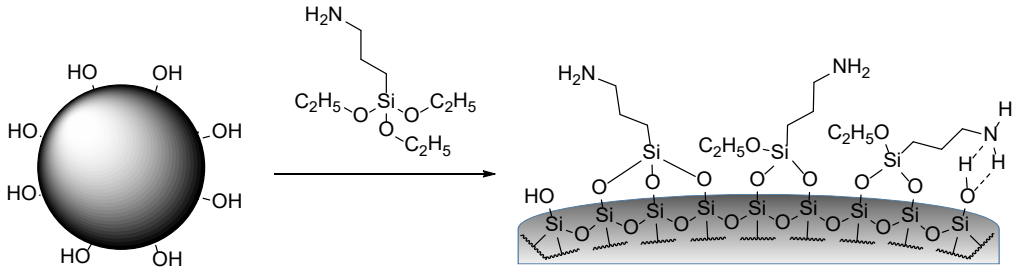

**Fig. S4.** Preparation of APTES-SP. Synthesis procedure: Bare silica particles (5 g; 100 Å, 5 µm, 320 $m^2$/g) were suspended in 25 mL anhydrous toluene within a 100 mL triple neck flask equipped with a mechanical stirrer and a reflux condenser with a nitrogen supply. Then, (3-aminopropyl)triethoxysilane (8 µmol/$m^2$) and 4-dimethylaminopyridine (5 % n/n of APTES) were added to the suspension and the reaction vessel was heated up to reflux. Subsequently, the reaction was allowed to proceed for 3 h under nitrogen atmosphere. Afterwards, the silica was washed 3 times with boiling methanol and boiling toluene each using a glass funnel of porosity 4. Finally, the silica was dried in a vacuum chamber at 60 °C for 24 h.

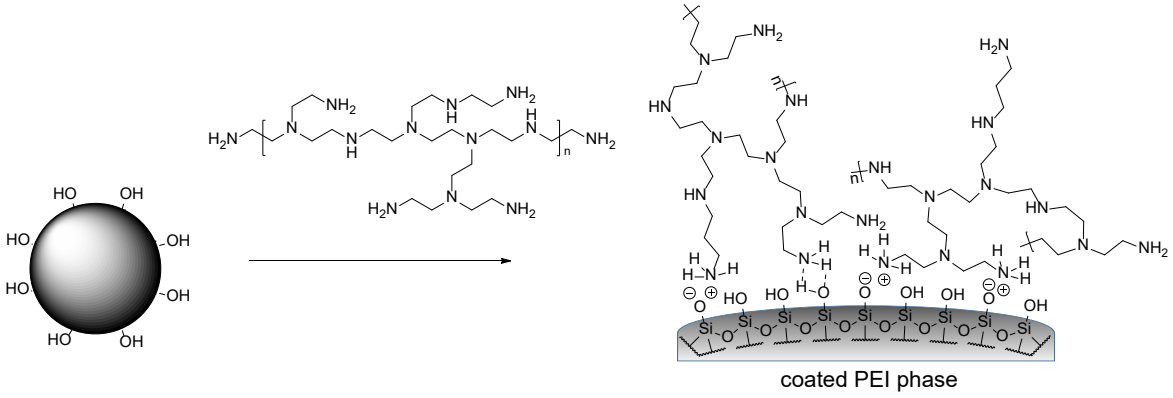


**Fig. S5.** Preparation of coated PEI phase by adsorption of PEI onto bare silica particles. Synthesis procedure: 0.5 g bare silica was weighed into a 100 mL round bottom flask and suspended in 25 mL chloroform. Subsequently, branched polyethylenimine (8 µmol N/$m^2$; assuming 1 mol N per 43.07 g PEI) was added and the suspension carefully mixed. Then, the flask was attached to a rotary evaporator equipped with a water bath kept at 25 °C and the solvent was evaporated generating a thin silica film on the inner wall of the flask. Thereafter, the flask was

flushed with nitrogen for 10 min and placed in a heating chamber tempered at 100 °C for 6 h. Finally, the silica was washed with boiling methylene chloride, a mixture of boiling methanol and water (80/20; v/v), boiling methanol and boiling toluene three times each and dried in a vacuum chamber at 60 °C for 24 h.

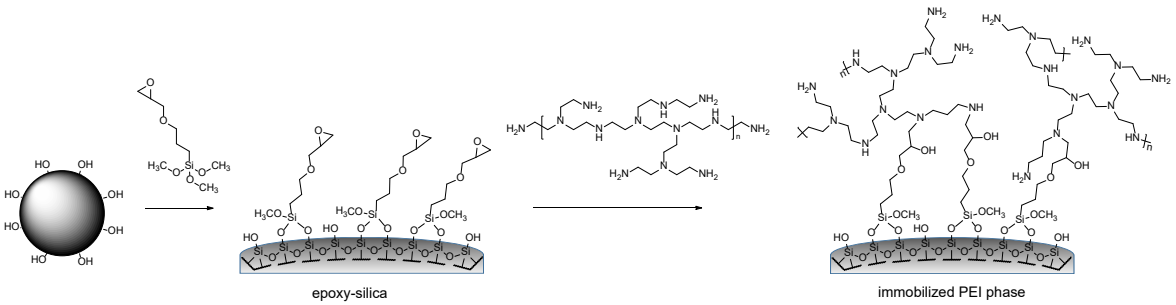


**Fig. S6.** Preparation of epoxy-silica and immobilized PEI phase. Synthesis procedure for epoxy-silica: Bare silica particles (1.0 g; 100 Å, 5 µm, 320 $m^2$/g) were suspended in 25 mL anhydrous toluene within a 100 mL triple neck flask equipped with a mechanical stirrer and a reflux condenser with a nitrogen supply. After adding (3-glycidyloxypropyl)trimethoxysilane (8 µmol/$m^2$) to the suspension the reaction vessel was heated up to 80 °C and the reaction was allowed to proceed for 24 h. Thereafter, the silica was washed with boiling toluene and boiling methylene chloride three times each using a glass funnel of porosity 4 and dried in a vacuum chamber at 60 °C for 2 h. Synthesis procedure for immobilized PEI phase: 0.5 g of epoxy-silica was transferred to a 100 mL round bottom flask and suspended in 25 mL chloroform. Subsequent to the adding of branched polyethylenimine (8 µmol N/$m^2$; assuming 1 mol N per 43.07 g PEI) the flask was attached to a rotary evaporator equipped with a water bath tempered at 25 °C and the solvent was evaporated generating a thin silica film on the inner wall of the flask. Hereafter, the flask was flushed with nitrogen for 10 min and placed in a heating chamber tempered at 100 °C for 6 h. Lastly, the silica was washed with boiling methylene chloride, a mixture of boiling methanol and water (80/20; v/v), boiling methanol and boiling toluene three times each and dried in a vacuum chamber at 60 °C for 24 h.

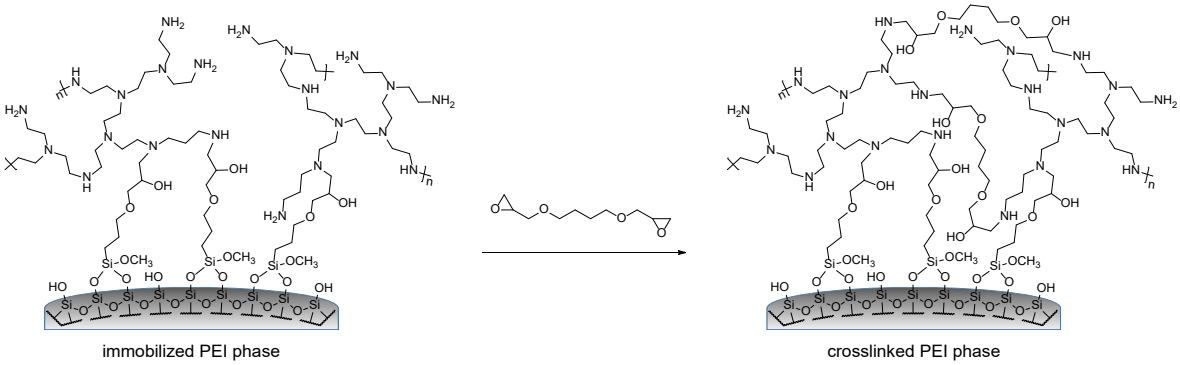


**Fig. S7.** Preparation of crosslinked PEI phase. Synthesis procedure: 0.25 g of immobilized PEI phase were suspended in 10 mL of a solution of 1,4-butanediol diglycidyl ether and 1,4-dioxane (5/95; v/v) within a 100 mL round bottom flask under nitrogen atmosphere. After 2 h the flask was equipped with a reflux condenser and the suspension was heated up to 100 °C for 45 min under nitrogen atmosphere. Finally, the resulting silica (crosslinked PEI phase) was washed with boiling methanol and boiling toluene three times each and dried in a heating chamber at 60 °C under vacuum.

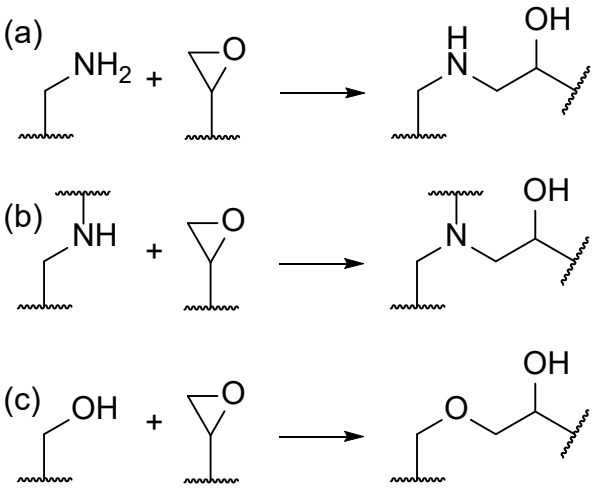


**Fig. S8.** Scheme of amine-epoxy reactions for (a) primary amines, (b) secondary amines and (c) hydroxy-epoxy addition reaction.

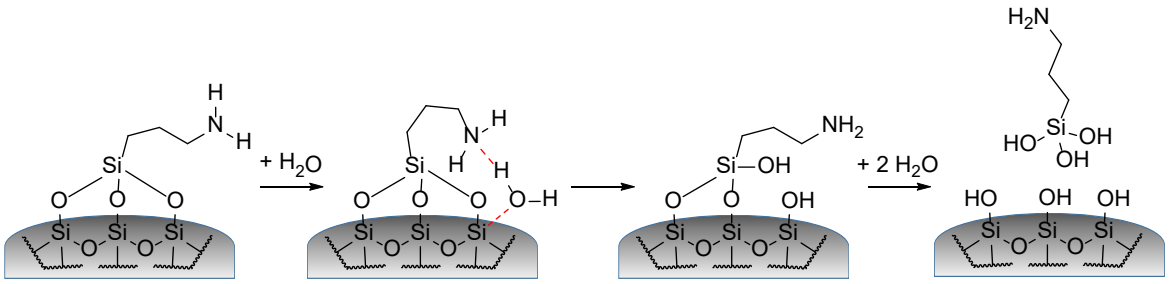


**Fig. S9.** Proposed reaction process for the detachment of functional aminopropyl moiety via hydrolysis under aqueous conditions due to the catalytic effect of the amino group based on [2] and [3].

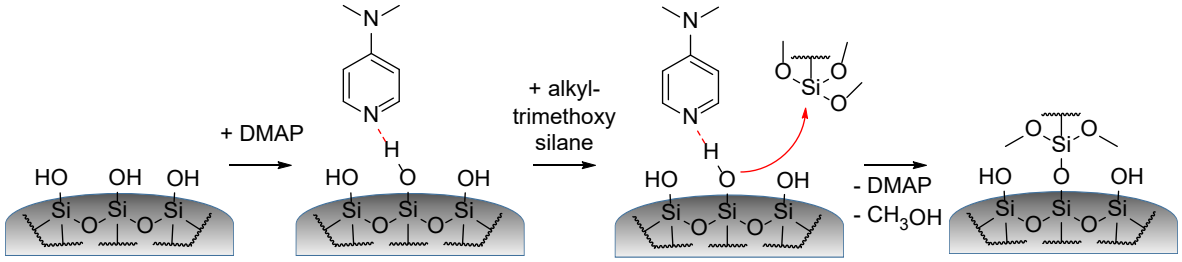


**Fig. S10.** Proposed mechanism of silanization reaction using 4-dimethylaminopyridine (DMAP) as catalyst based on [4] and [5]. Firstly, DMAP adsorbs to the silica surface and forms a hydrogen bond to a surface silanol. The accompanying increased nucleophilicity of the silanol´s oxygen provokes finally the nucleophilic attack on the silanization agent´s silicon. Likewise, the deprotonation of the surface silanol by DMAP is conceivable in a first step leading to the nucleophilic silanolate anion.

**Table S1.** Deconvolution of $^{29}Si$ CP/MAS NMR signals of APTES-SP and APS-SP1-8: Proportion of T1, T2 and T3. Deconvolution was carried out using Topspin 4.0.8 software from Bruker by applying Gaussian curves over the signals.

| SP | T1[1] [%] | T2[2] [%] | T3[3] [%] |
|---|---|---|---|
| APTES-SP | 16.3 | 50.6 | 33.1 |
| APS-SP1 | 7.9 | 42.9 | 49.2 |
| APS-SP2 | 6.3 | 45.5 | 48.2 |
| APS-SP3 | 10.3 | 41.0 | 48.7 |
| APS-SP4 | 3.7 | 45.2 | 51.1 |
| APS-SP5 | 5.5 | 41.2 | 53.3 |
| APS-SP6 | 6.3 | 31.4 | 62.3 |
| APS-SP7 | 5.5 | 29.5 | 65.0 |
| APS-SP8 | 0.9 | 29.0 | 70.1 |

[1] corresponding to monofunctional attached ligand

[2] corresponding to difunctional attached ligand

[3] corresponding to trifunctional attached ligand

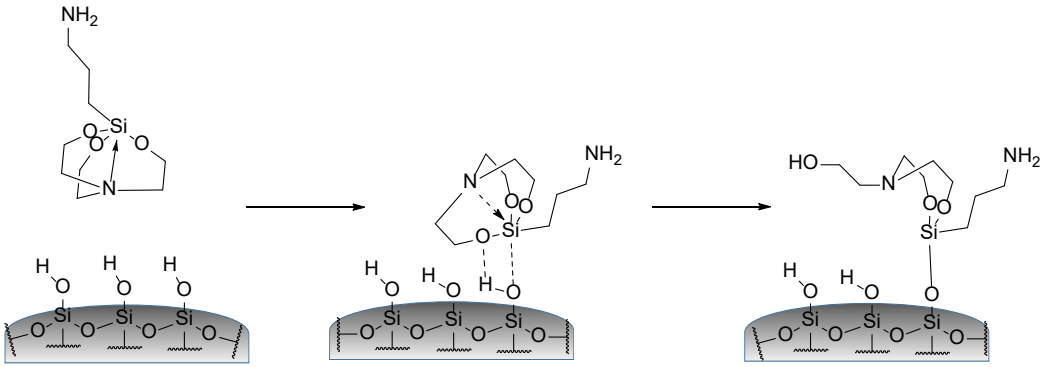


**Fig. S11.** Initial mechanism of acid-catalyzed silica surface modification using (3-aminopropyl)silatrane. Due to the transannular donor-acceptor N→Si bond of the silatrane, the silatrane´s silicon atom is not prone to nucleophilic attacks, since it remains less polarized [6]. Nevertheless, the reactivity of the silatrane bumps up in acidic environments (as silica surfaces) due to its oxygen atoms´ proton affinity (which is higher than for its nitrogen atom due to kinetic reasons [7]). By this means the formation of polarized hydrogen-bond complexes between the reactive acidic silanol groups on the silica surface and the Si-O bond of the silatrane becomes feasible making its linking to the surface in a concerted nucleophilic substitution reaction subsequently happen. Withal these reaction protonation of the oxygen can occur first alike making the silatrane´s silicon atom susceptible to the ensuing nucleophilic attack of the silanol groups as well. However, both processes lead to the same outcome [8].

## PART III: van Deemter analysis

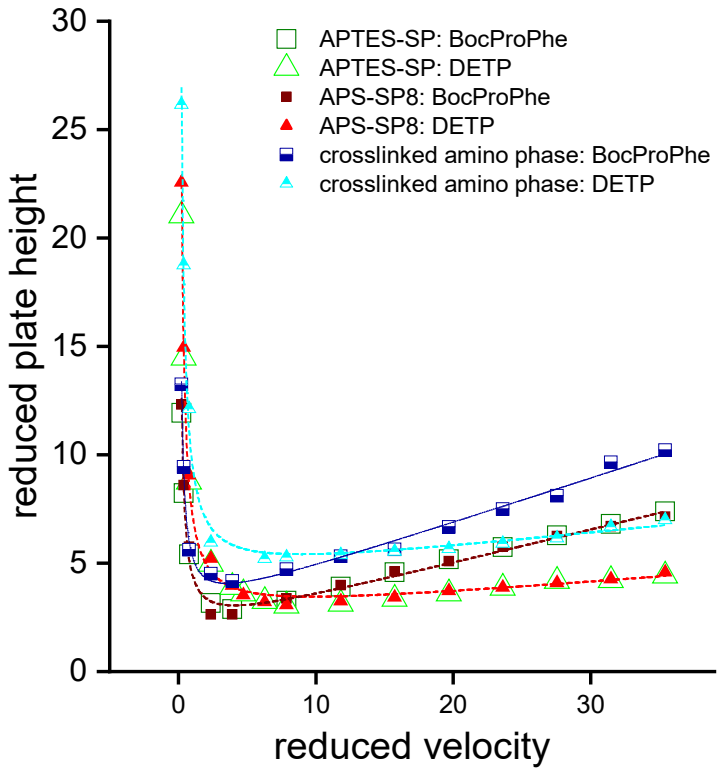


**Fig. S12**. H/u curves recorded for APTES-SP, APS-SP8 and crosslinked amino phase using BocProPhe and DETP. H/u-curves were recorded under isoeluotropic conditions. A mixture of acetonitrile, water and acetic acid (30/70/0.1; v/v/v, pH adjusted to 5 with ammonia) was used as mobile phase and measurements were performed at 25 °C. Isoelutropic conditions were achieved by adding acetonitrile to the mobile phase. The injection volume was amounted to 2 µL and detection was carried out at 220 nm. Acetone served as void volume marker. Van Deemter analysis was conducted according to [9] and delivered the following results: for APTES-SP: a-term = 2.53 ± 0.18 (DETP), 1.89 ± 0.11 (BocProPhe); b-term = 4.48 ± 0.09 (DETP), 2.40 ± 0.05 (BocProPhe); c-term = 0.05 ± 0.01 (DETP), 0.16 ± 0.05 (BocProPhe); APS-SP8: a-term = 2.47 ± 0.16 (DETP), 1.79 ± 0.21 (BocProPhe); b-term = 4.81 ± 0.08 (DETP), 2.54 ± 0.10 (BocProPhe); c-term = 0.05 ± 0.01 (DETP), 0.16 ± 0.05 (BocProPhe); crosslinked amino phase: a-term = 4.21 ± 0.35 (DETP), 2.62 ± 0.178 (BocProPhe); b-term = 5.36 ± 0.16 (DETP), 2.52 ± 0.08 (BocProPhe); c-term = 0.06 ± 0.02 (DETP), 0.20 ± 0.01 (BocProPhe). The similar c-terms found

for APTES-SP and APS-SP8 may indicate similar ligand film thickness on the silica surface. Although silatranes were reported to produce thinner and more homogenous films [10], here silatrane modification was apparently not superior to APTES modification in this regard. This might be explained by the fast physisorption of APTES to the supports surface by hydrogen-bonding and electrostatic interaction between its basic amino moiety and the acidic silica silanols which might lead as well to a favored reaction directly on the silica surface, as it is assumed for silatranes. Remarkably, the crosslinking of the aminopropyl brushes in the amido-amino network silica phase did not have a significant effect on the c-term but the a-term was a bit compromised. It may be possible that the packing procedure needs re-optimization to reduce the packing factor of the a-term. Since the c-term was not significantly affected, it can be concluded that the bonding chemistry with the network structure on the surface is a viable approach useful for synthesis of a stable stationary amino phase.

## PART IV: Stress test

**Table S2.** Chromatographic parameters of the investigated in-house prepared stationary phases during the stress test.

| BocProPhe | | | | |
|---|---|---|---|---|
| | 0 h<br>K | 7 h<br>k | 20 h<br>k | 50 h<br>k |
| APTES-SP | 12.89 | 5.55 | 1.87 | 0.37 |
| APS-SP8 | 13.72 | 10.39 | 5.50 | 1.61 |
| crosslinked amino phase | 11.16 | 9.42 | 9.26 | 9.28 |
| immobilized PEI phase | 20.61 | 15.48 | 13.47 | 11.66 |
| crosslinked PEI phase | 18.80 | 17.53 | 17.32 | 16.59 |

| DETP | | | | |
|---|---|---|---|---|
| | 0 h<br>K | 7 h<br>k | 20 h<br>k | 50 h<br>k |
| APTES-SP | 26.35 | 4.45 | 1.57 | 0.24 |
| APS-SP8 | 28.38 | 12.35 | 5.32 | 1.40 |
| crosslinked amino phase | 13.54 | 11.61 | 12.06 | 12.64 |
| immobilized PEI phase | 36.84 | 24.42 | 19.73 | 16.40 |
| crosslinked PEI phase | 29.44 | 25.80 | 24.64 | 22.97 |

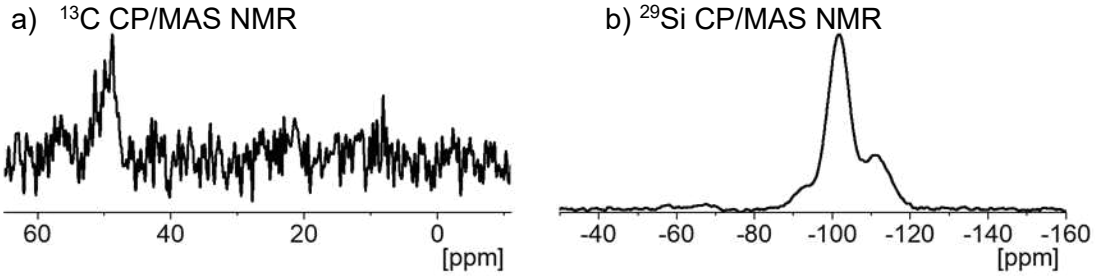


**Fig. S13.** Solid-state CP/MAS NMR spectra of APTES-SP after exposure to stress test conditions. The small carbon signal at ~ 50 ppm can be assigned to the carbons of methoxy groups generated on the silica surface during the flushing with methanolic solvent. For CP/MAS NMR measurements magic angle spinning was carried out using 7 mm double bearing zirconia rotors and spinning rates of 8000 Hz for $^{13}$C NMR and 4000 Hz for $^{29}$Si NMR measurements. For $^{13}$C NMR measurements the 90 ° proton pulse length was 2.5 µs, the contact relaxation delay times 2 µs and the pulse interval 2 ms. For $^{29}$Si CP/MAS NMR the 90 ° proton pulse length was 3.3 µs, the contact relaxation delay times 2 ms and the pulse interval 5 ms.

## PART V: Characterization under RPLC and HILIC conditions

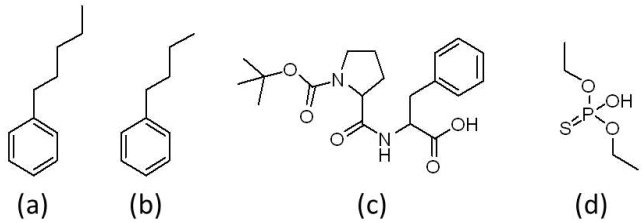


**Fig. S14.** The chromatographic performance under RPC conditions (cf Fig. 6A) was investigated by the separation of the four analytes PeB (1; logD(pH 6) ~ 4.26[1]), BuB (2; logD(pH 6) ~ 3.82[1]), BocProPhe (3; $pK_a$ ~ 3.6[1], logD(pH 6) ~ -0.06[1]) and DETP ($pK_a$ ~ 3.6[1], logD(pH 6) ~ -0.97[1]). Here, a mixture of ACN and water (40:60, v/v) containing 50 mM acetic acid was used as mobile phase and the pH of the mobile phase was adjusted to 6 with ammonia. The linear flow velocity was set to 1.7 mm/s and detection was carried out at 220 nm. The injection volume was amounted to 2 µL and the temperature set to 25 °C. The analytes were all dissolved in the mobile phase reaching a concentration of 0.8 mg/mL. Uracil was used as void volume marker.[1]calculated using MarvinSketch 20.19 software (ChemAxon, www.chemaxon.de).

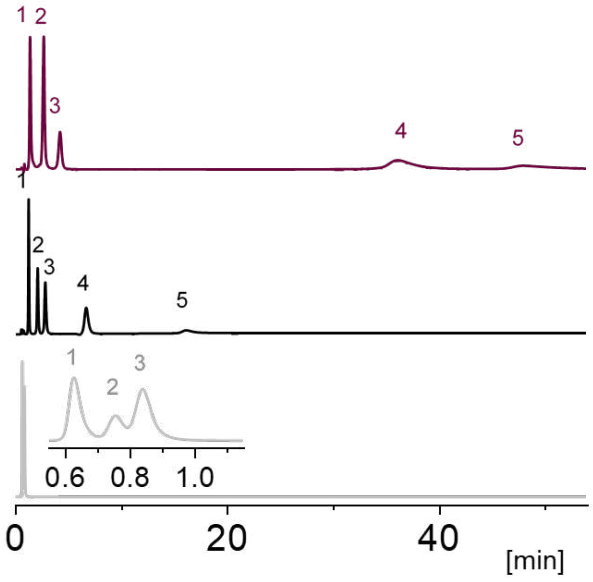


**Fig. S15.** Chromatograms obtained from investigation of crosslinked amino phase under HILIC conditions. For the characterization under HILIC conditions three sets of analytes were investigated. The first set consisted of xanthines (grey: 1-caffeine, 2-theobromine, 3-theophylline), the second one of vitamins (black: 1-thiamine, 2-

pyriodxine, 3-riboflavine, 4-nicotinic acid, 5-ascorbic acid) and the third one of nucleosides (red: 1-thymidine, 2-uridine, 3-adenosine, 4-cytidine, 5-guanosine). For the investigation of xanthines a mobile phase consisting of ACN and water (90:10, v/v) containing 5 mM ammonium acetate was utilized, for the investigation of vitamins and nucleosides a mobile phase consisting of ACN and water (95:5, v/v) containing 5 mM ammonium acetate. The flow rate was calculated to the corresponding linear velocity of 1.7 mm/s. The injection volume was set to 2 µL, the temperature to 25 °C and detection was carried out at 254 nm. The void volume was determined by toluene. All analytes were dissolved in the mobile phase reaching a concentration of 1 mg/mL.

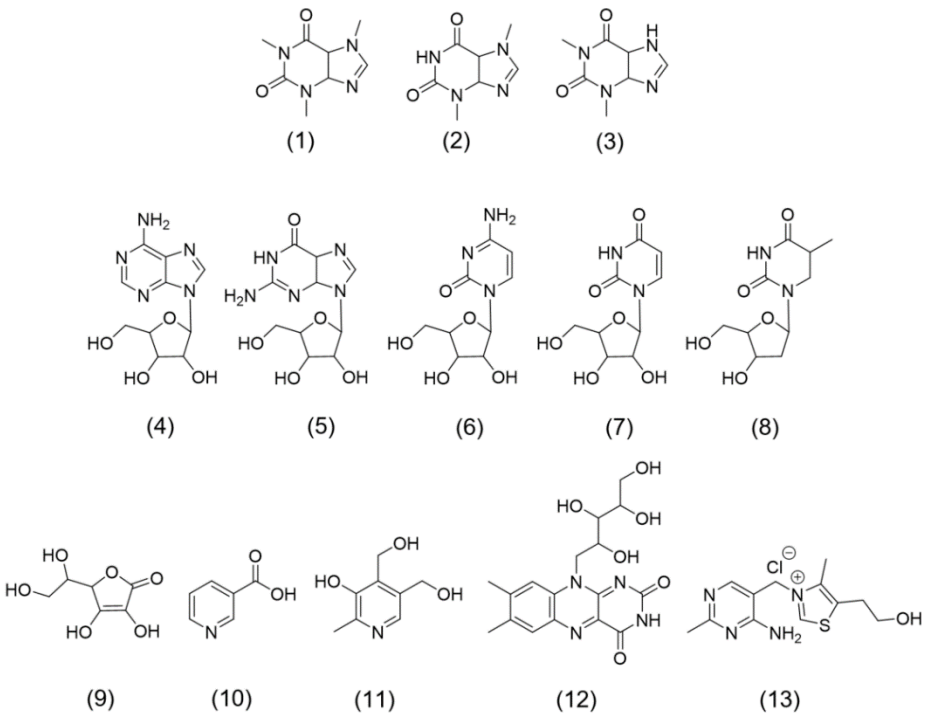


**Fig. S16.** Xanthines, nucleosides and vitamins submitted to HILIC test as test analytes: (1) caffeine (logD(pH 8) ~ -1.06[1]), (2) theobromine (logD(pH 8) ~ -1.28[1]), (3) theophylline (logD(pH 8) ~ -1.32[1]), (4) adenosine (logD(pH 8) ~ -2.09[1]), (5) guanosine (logD(pH 8) ~ -3.22[1]), (6) cytidine (logD(pH 8) ~ -2.80[1]), (7) uridine (logD(pH 8) ~ -2.42[1]), (8) thymidine (logD(pH 8) ~ -1.33[1]), (9) ascorbic acid ($pK_a$ ~ 4.2[1], logD(pH 8) ~ -5.27[1]), (10) nicotinic acid ($pK_a$ ~ 2.8[1], logD(pH 8) ~ -3.04[1]), (11) pyridoxine (logD(pH 8) ~ -0.97[1]), (12) riboflavin ($pK_a$ ~ 6.0[1], logD(pH 8) ~ -2.60[1]), (13) thiamine hydrochloride (logD(pH 8) ~ -3.10[1]). [1]calculated using MarvinSketch 20.19 software (ChemAxon, www.chemaxon.de)

## PART VI: Exploration of the ion-exchange characteristics

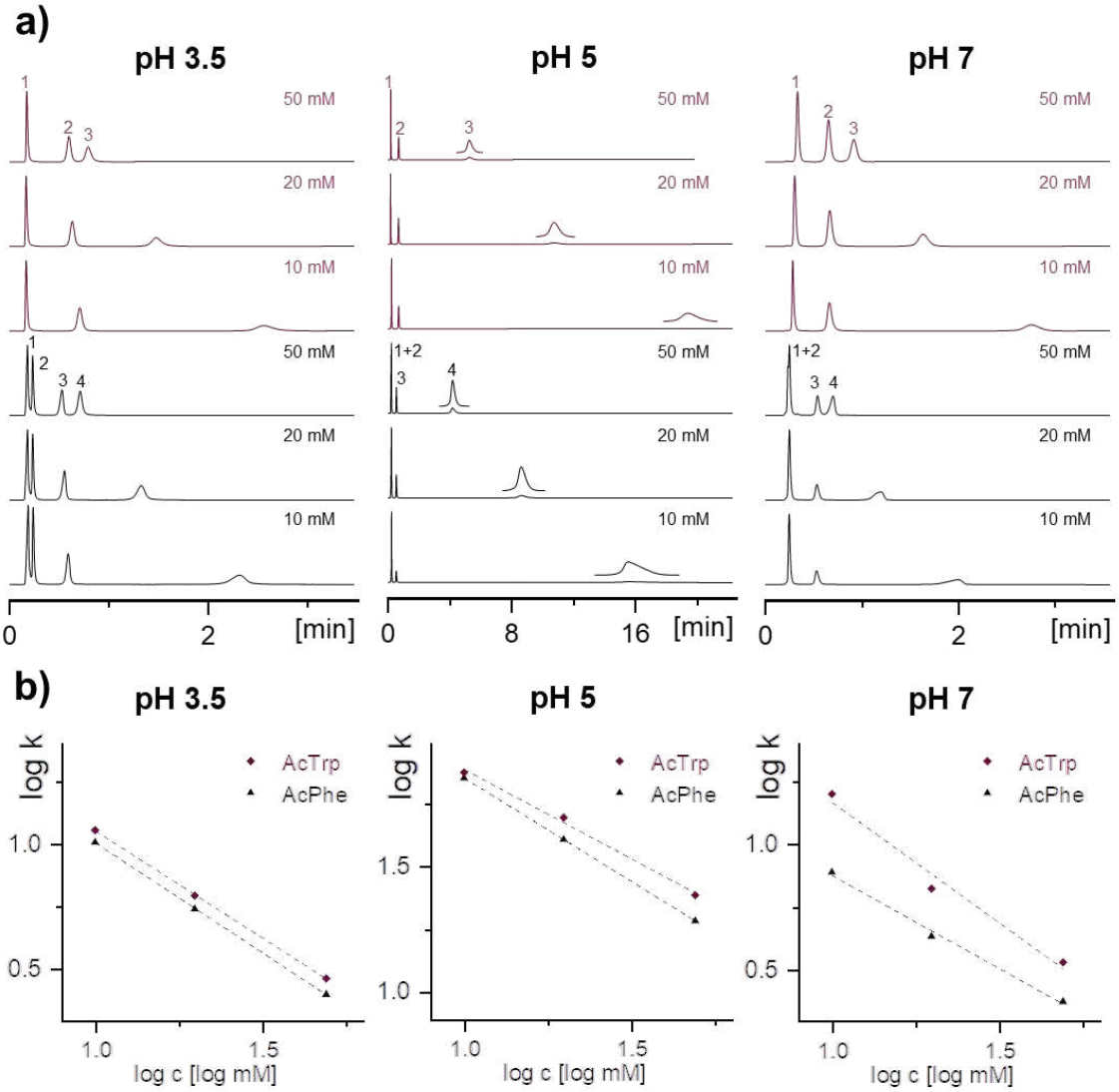


**Fig. S17.** Exploration of the ion exchange characteristics of the crosslinked amino phase at different pH values and ionic strengths of the mobile phase. For the evaluation of the ion exchange retention mechanism of the prepared stationary phase the separation of phenylalanine (coloured black) and tryptophan (coloured red) derivatives (black: 1-PheOMe, 2-AcPheOEt, 3-Phe, 4-AcPhe; red: 1-TrpAmide, 2-Trp, 3-AcTrp) was investigated under mobile phase conditions with varying ionic strength and pH. The obtained chromatograms are depicted in a). The log k vs. log c (buffer) plots (according to the stoichiometric displacement model) are presented in b). In this study, a mobile phase consisting of ACN and water (80:20, v/v) adjusted to pH 3.5, 5 or 7 and containing 10 mM, 20 mM or 50 mM of formic acid (for pH 3.5)

or acetic acid (for pH 5 and 7) was used. The pH was adjusted with ammonia. The flow rate was set to 1 mL/min, the temperature to 25 °C, the injection volume to 2 µL and detection was carried out at 258 nm (for the phenylalanine derivatives) and 280 nm (for the tryptophan derivatives), respectively. The analytes were dissolved in ACN/$H_2O$ (80/20, v/v) reaching a concentration of 0.5 mg/mL. Toluene was used as void volume marker.

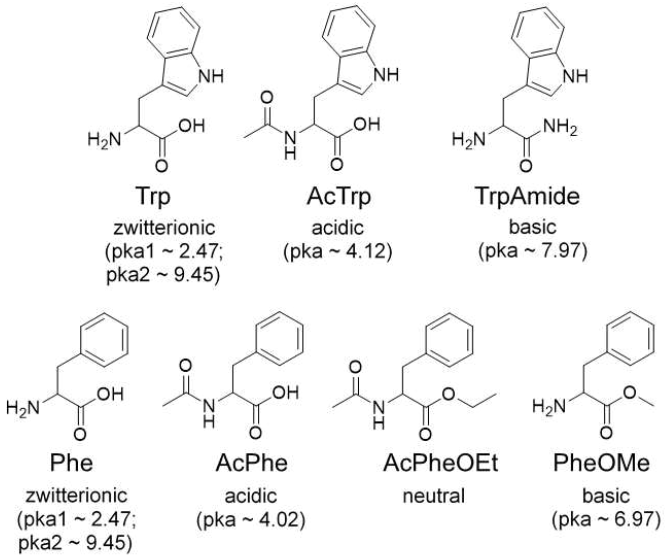


**Fig. S18.** Phenylalanine and tryptophan derivatives employed for the exploration of the ion-exchange characteristics of crosslinked amino phase; $pK_a$ values were calculated using MarvinSketch 20.19 software (ChemAxon, www.chemaxon.de).

**Table S3.** Chromatographic parameters obtained from analysis of amino acid derivatives on crosslinked amino phase.

| | **pH 3.5** | | | **pH 5** | | | pH 7 | | |
|---|---|---|---|---|---|---|---|---|---|
| | 10 mM | 20 mM | 50 mM | 10 mM | 20 mM | 50 mM | 10 mM | 20 mM | 50 mM |
| | K | K | k | k | k | K | k | k | k |
| Phe | 1.82 | 1.69 | 1.58 | 1.54 | 1.61 | 1.66 | 1.49 | 1.51 | 0.19 |
| AcPhe | 10.11 | 5.44 | 2.47 | 71.31 | 40.4 | 18.96 | 7.68 | 4.25 | 2.32 |
| PheOMe | with $t_0$ | with $t_0$ | with $t_0$ | 0.01 | with $t_0$ | 0.06 | 0.14 | 0.16 | 0.12 |
| AcPheOEt | 0.13 | 0.14 | 0.14 | 0.12 | 0.13 | 0.14 | 0.14 | 0.16 | 0.12 |
| Trp | 2.40 | 2.07 | 1.92 | 1.55 | 2.24 | 2.34 | 2.08 | 2.11 | 2.11 |
| AcTrp | 11.30 | 6.16 | 2.86 | 75.22 | 49.4 | 24.12 | 11.75 | 6.60 | 3.34 |
| TrpAmide | with $t_0$ | with $t_0$ | with $t_0$ | 0.14 | with $t_0$ | with $t_0$ | 0.32 | 0.42 | 0.59 |

## PART VII: Stationary phase classification

**Table S4.** Elemental composition and surface areas of commercial columns used for PCA. Data were taken from [11].

| | C [w-%] | H [w-%] | N [w-%] | surface area [$m^2/g$] | selector coverage [mmol/g] |
|---|---|---|---|---|---|
| Acclaim Mixed Mode WAX-1 | 12.70 | 2.50 | 1.46 | 300 | 0.52 |
| Uptisphere 5 MM3 | 8.14 | 1.79 | 0.19 | 320 | 0.14 |
| Primesep B2 | 8.38 | 1.83 | 0.65 | n/a | 0.46 |
| Obelisc R | 8.93 | 1.92 | 0.66 | n/a | 0.47 |
| Obelisc N | 4.59 | 1.21 | 0.30 | n/a | 0.21 |
| Chiralpak QN-AX | 15.14 | 2.38 | 1.59 | 300 | 0.38 |
| BioBasic AX | 3.7 | 0.77 | 0.58 | 100 | 0.22 |
| Synergi Fusion-RP | 12.00 | n/a | - | 475 | n/a |
| TSKGel Amide-80 | 11.06 | 1.99 | 2.46 | n/a | 1.76 |
| Polysulfoethyl A | 9.95 | 1.74 | 3.47 | 100 | 0.55 |
| ZIC-HILIC | 8.74 | 1.77 | 1.02 | 140 | 0.59 |
| Chromolith Performance Si | - | - | - | 300 | - |

n/a = not available

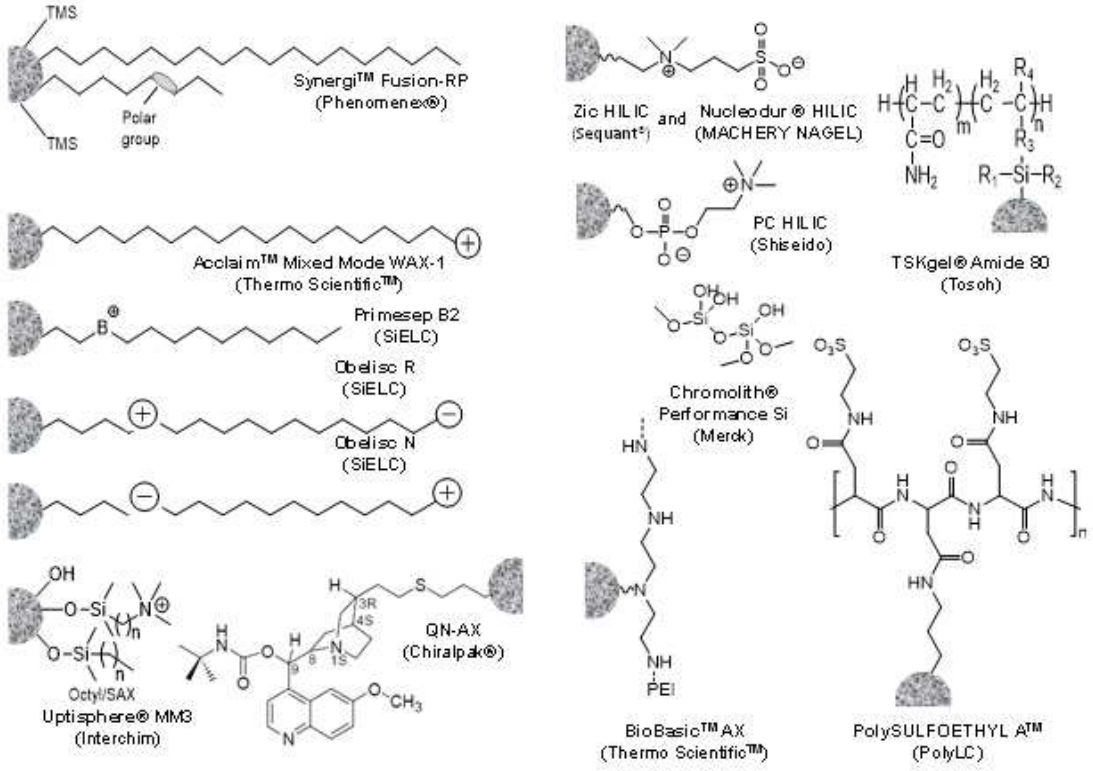


**Fig. S19.** Surface chemistries of commercial columns classified by PCA.

**Table S5.** Retention factors obtained from RPC and HILIC test for in-house prepared and commercial columns used for PCA. Data of commercial columns were partially taken from [12].

| | $k_{BuB}$ | $k_{PeB}$ | $k_{DETP}$ | $k_{BocProPhe}$ |
|---|---|---|---|---|
| Acclaim Mixed Mode WAX-1 | 5.52 | 8.47 | 14.45 | 34.75 |
| Uptisphere 5 MM3 | 27.73 | 48.89 | 0.19 | 0.28 |
| Primesep B2 | 9.97 | 15.59 | 1.97 | 5.36 |
| Obelisc R | 6.22 | 9.47 | 3.59 | 10.97 |
| Obelisc N | 1.00 | 1.35 | 4.00 | 3.64 |
| Chiralpak QN-AX | 4.11 | 5.76 | 5.76 | 7.69 |
| BioBasic AX | with $t_0$ | with $t_0$ | 1.05 | 0.53 |
| Synergi Fusion-RP | 24.17 | 43.28 | with $t_0$ | 0.06 |
| TSKGel Amide-80 | with $t_0$ | with $t_0$ | with $t_0$ | with $t_0$ |
| PolysulfoethylA | with $t_0$ | with $t_0$ | with $t_0$ | with $t_0$ |
| ZIC-HILIC | with $t_0$ | with $t_0$ | 0.14 | with $t_0$ |
| Nucleodur HILIC | with $t_0$ | with $t_0$ | with $t_0$ | with $t_0$ |
| Chromolith Performance Si | with $t_0$ | with $t_0$ | with $t_0$ | with $t_0$ |
| PC-HILIC | with $t_0$ | with $t_0$ | with $t_0$ | with $t_0$ |
| classical APS | 0.10 | 0.19 | 0.78 | 0.89 |
| polymeric APS | with $t_0$ | with $t_0$ | 4.39 | 1.76 |
| APS-SP8 | with $t_0$ | with $t_0$ | 3.51 | 2.18 |
| crosslinked amino phase | with $t_0$ | with $t_0$ | 2.07 | 1.41 |

| | $k_{thiamine}$ | $k_{pyridoxine}$ | $k_{riboflavine}$ | $k_{ascorbic\ acid}$ | $k_{nicotinic\ acid}$ |
|---|---|---|---|---|---|
| Acclaim Mixed Mode WAX-1 | 0.17 | 1.11 | 1.66 | n.d. | 31.14 |
| Uptisphere 5 MM3 | 0.60 | 0.13 | 0.13 | 5.27 | 3.03 |
| Primesep B2 | 3.92 | 0.36 | 0.04 | 0.04 | 0.73 |
| Obelisc R | 10.11 | 0.78 | 0.78 | 2.73 | 10.11 |
| Obelisc N | n.d. | 6.65 | 1.15 | 1.15 | 0.66 |
| Chiralpak QN-AX | 1.17 | 0.41 | 0.32 | n.d. | 3.52 |
| BioBasic AX | 0.43 | 0.43 | 0.89 | n.d. | 10.88 |
| Synergi Fusion-RP | 14.94 | 0.11 | with $t_0$ | with $t_0$ | 0.44 |
| TSKGel Amide-80 | 43.54 | 1.49 | 4.77 | 20.70 | 5.49 |
| PolysulfoethylA | 26.81 | 2.73 | 3.10 | n.d. | 2.73 |
| ZIC-HILIC | 29.30 | 1.20 | 2.20 | 35.13 | 4.89 |
| Nucleodur HILIC | 99.31 | 1.73 | 1.78 | 6.26 | 1.78 |
| Chromolith Performance Si | 28.20 | 0.65 | 0.65 | 1.41 | 1.85 |
| PC-HILIC | 95.49 | 1.91 | 2.66 | 6.65 | 2.05 |
| classical APS | 0.44 | 2.48 | 6.40 | 134.63 | 30.59 |
| polymeric APS | 0.95 | 2.64 | 3.10 | 28.74 | 24.90 |
| APS-SP8 | 4.50 | 20.68 | 22.71 | n.d. | 112.87 |
| crosslinked amino phase | 2.24 | 3.39 | 7.07 | 92.12 | 70.22 |

| | $k_{thymidine}$ | $k_{adenosine}$ | $k_{uridine}$ | $k_{cytidine}$ | $k_{guanosine}$ | $k_{caffeine}$ | $k_{theobromine}$ | $k_{theophylline}$ |
|---|---|---|---|---|---|---|---|---|
| Acclaim Mixed Mode WAX-1 | 0.88 | 1.67 | 1.90 | 4.18 | 7.15 | 0.10 | 0.26 | 0.84 |
| Uptisphere 5 MM3 | with $t_0$ | 0.15 | 0.15 | 0.81 | 1.05 | with $t_0$ | with $t_0$ | with $t_0$ |
| Primesep B2 | with $t_0$ | 0.10 | with $t_0$ | 0.22 | 0.22 | 0.02 | 0.02 | 0.11 |
| Obelisc R | 0.09 | 0.48 | 0.48 | 2.15 | 2.69 | 0.06 | 0.14 | 0.26 |
| Obelisc N | 0.23 | 0.59 | 0.48 | 2.75 | 1.61 | 0.15 | 0.22 | 0.22 |
| Chiralpak QN-AX | 0.15 | 0.15 | 0.15 | 0.29 | 0.29 | 0.10 | 0.24 | 0.44 |
| BioBasic AX | 0.35 | 0.84 | 0.75 | 2.18 | 3.42 | 0.08 | 0.18 | 0.18 |
| Synergi Fusion-RP | with $t_0$ | 0.04 | with $t_0$ | 0.16 | 0.04 | with $t_0$ | with $t_0$ | with $t_0$ |
| TSKGel Amide-80 | 1.27 | 3.12 | 3.45 | 10.20 | 12.8 | 0.40 | 0.76 | 1.16 |
| PolysulfoethylA | 0.77 | 2.08 | 3.14 | 15.02 | 16.69 | 0.20 | 0.45 | 0.51 |
| ZIC-HILIC | 0.89 | 2.09 | 3.24 | 9.54 | 12.63 | 0.28 | 0.63 | 0.63 |
| Nucleodur HILIC | 0.91 | 1.64 | 2.08 | 5.05 | 6.53 | 0.36 | 0.67 | 0.67 |
| Chromolith Performance Si | 0.29 | 0.76 | 0.61 | 2.26 | 2.04 | 0.19 | 0.19 | 0.19 |
| PC-HILIC | 1.00 | 2.29 | 1.66 | 4.70 | 5.21 | 0.60 | 1.03 | 1.03 |
| classical APS | 0.97 | 2.90 | 1.89 | 10.61 | 12.86 | 0.22 | 0.35 | 0.44 |
| polymeric APS | 1.21 | 3.80 | 3.80 | 11.99 | 19.18 | 0.31 | 0.67 | 3.19 |
| APS-SP8 | 2.68 | 6.32 | 6.46 | 28.87 | 53.16 | 0.51 | 0.83 | 0.97 |
| crosslinked amino phase | 1.38 | 4.42 | 3.03 | 11.93 | 30.32 | 0.22 | 0.46 | 0.62 |

n.d. = not detected


**Fig. S20.** Surface chemistries of (a) classical APS and (b) polymeric APS according to manufacturers.

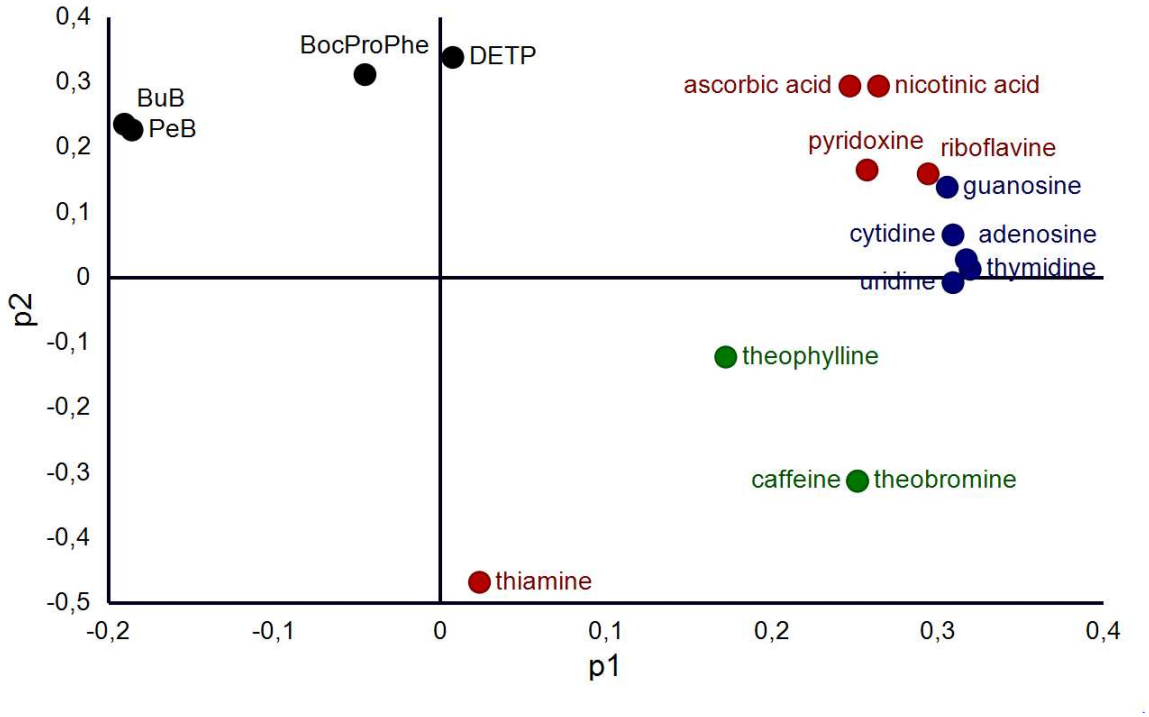


**Fig. S21**. Loadings scatter plot: p1 vs. p2. p1 is the loading in the first component and p2 the loading in the second component. The loadings express the dominating correlation structure of the X matrix. Hence, p1 vs. p2 displays how the X-variables correlate to each other. The plot shows how the X-variables vary in relation to each other, which ones provide similar information, which ones are negatively correlated, or not related to each other, and which ones are not well explained by the model (p1 and p2 close to 0).

## PART VIII: Carbohydrate analysis

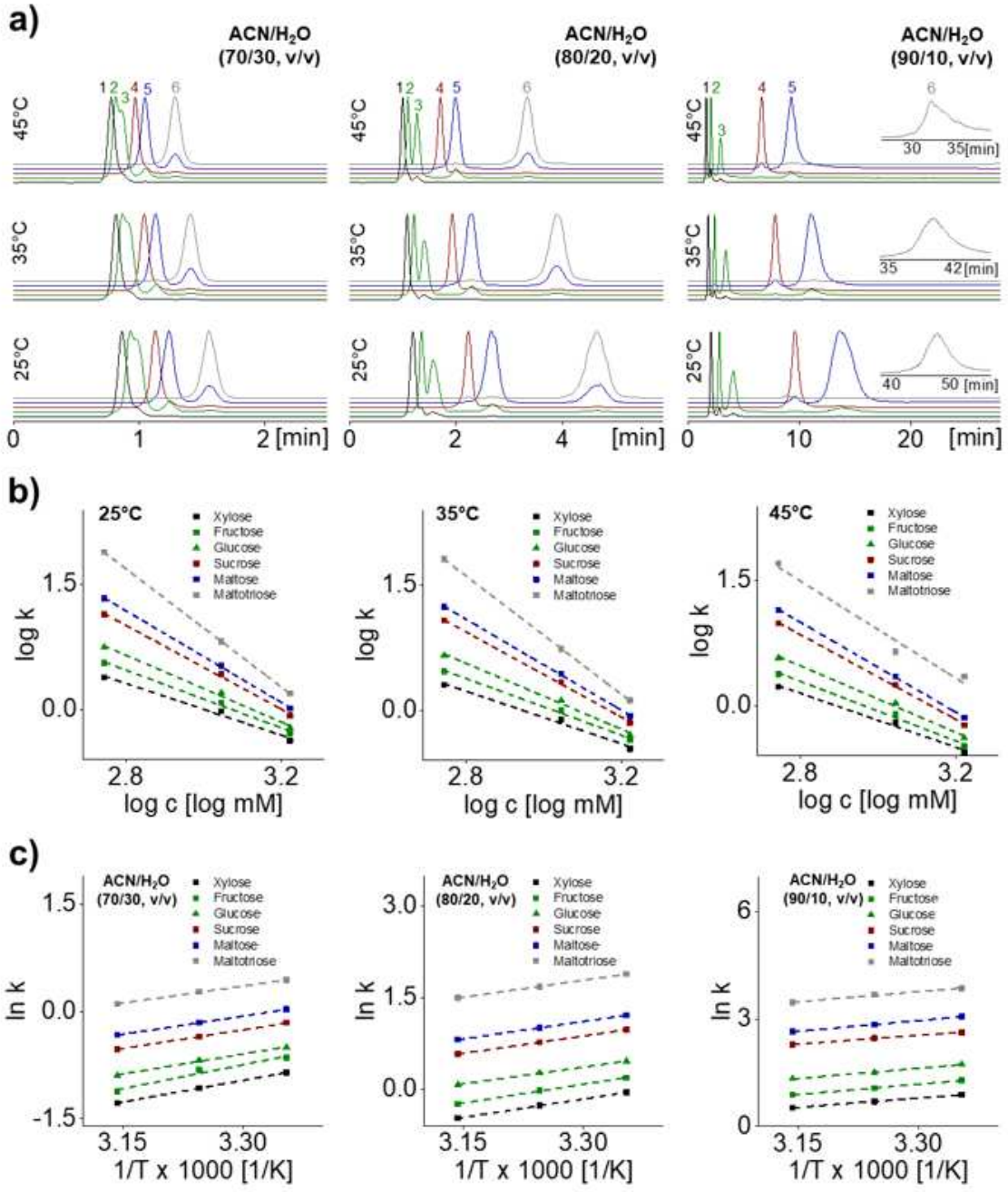


**Fig. S22.** Analysis of carbohydrates under HILIC conditions at different temperatures and varying ACN/$H_2O$ ratios using the crosslinked amino phase: a) LC-MS/MS chromatograms of six carbohydrates (1: xylose, 2: fructose, 3: glucose, 4: sucrose, 5: maltose, 6: maltotriose); b) stoichiometric displacement model illustrating the effect of $H_2O$ concentration *c* on the retention factor *k* of the analytes; c) van´t Hoff plots illustrating the effect of temperature T on the retention factors *k*

of the analytes. The mobile phase consisted of varying ACN/$H_2O$ ratios and experiments were performed at different temperatures. The flow rate was set at 0.5 mL/min and the injection volume amounted to 5 µL. The analytes were dissolved in a mixture of ACN/$H_2O$ (80/20, v/v) at a concentration of 1 µg/mL. The mass spectrometric detection was operated in negative mode and multiple reaction monitoring (MRM) was utilized for detection of analytes. MRM transitions, declustering potentials and collision energies for the single analytes as well as collision cell exit potentials are specified in the Table S7. The entrance potential was set to -10 V. Ion source parameters were constant for all analytes. The capillary voltage was set to 4500 V and the source temperature to 500 °C. Nebulizing gas, curtain gas and drying gas were all adjusted to 30 psi.

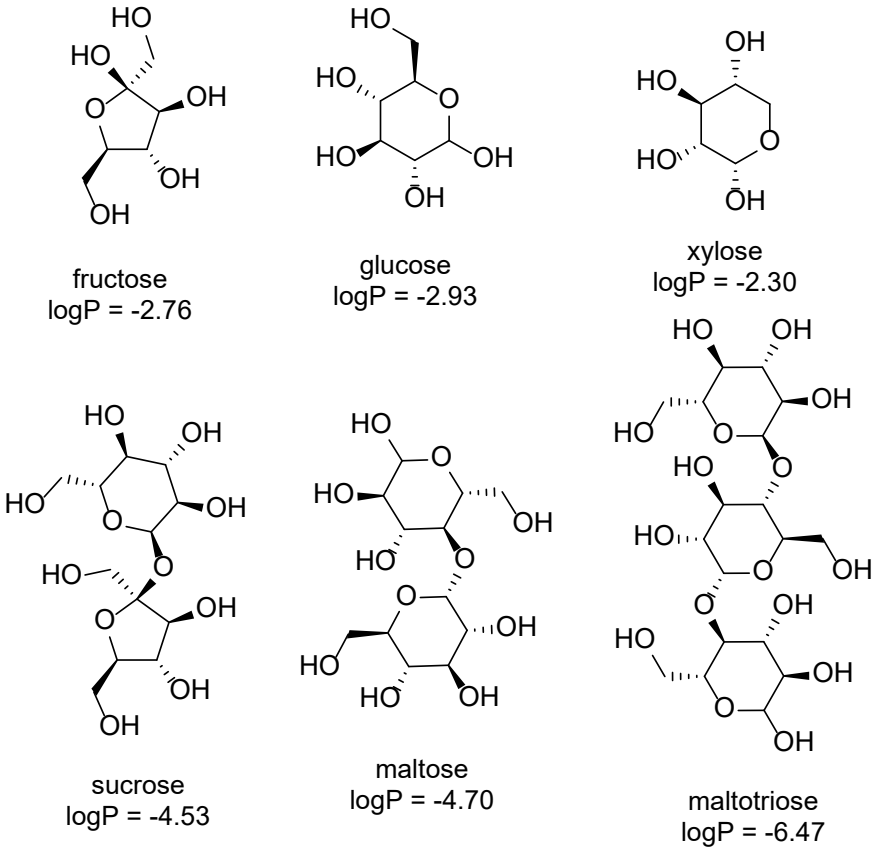


**Fig. S23.** Chemical structure of carbohydrates and their respective logP values; logP values were calculated using MarvinSketch 20.19.(ChemAxon, www.chemaxon.de).

**Table S6.** Chromatographic parameters obtained from carbohydrate analysis on crosslinked amino phase. Mass spectrometry parameters can be found in Table S7.

| | ACN/$H_2O$ (70/30, v/v) | | | ACN/$H_2O$ (80/20, v/v) | | | ACN/$H_2O$ (90/10, v/v) | | |
|---|---|---|---|---|---|---|---|---|---|
| | 25°C | 35°C | 45°C | 25°C | 35°C | 45°C | 25°C | 35°C | 45°C |
| | k | k | k | k | k | K | k | k | K |
| Xylose | 0.43 | 0.34 | 0.28 | 0.95 | 0.77 | 0.62 | 2.43 | 2.00 | 1.69 |
| Fructose | 0.52 | 0.44 | 0.33 | 1.21 | 0.98 | 0.79 | 3.62 | 2.92 | 2.41 |
| Glucose | 0.61 | 0.51 | 0.41 | 1.59 | 1.31 | 1.08 | 5.64 | 4.56 | 3.79 |
| Galactose | 0.61 | 0.51 | 0.41 | 1.59 | 1.31 | 1.08 | 5.64 | 4.56 | 3.79 |
| Sucrose | 0.85 | 0.70 | 0.59 | 2.66 | 2.16 | 1.79 | 13.85 | 11.82 | 9.82 |
| Maltose | 1.03 | 0.85 | 0.72 | 3.38 | 2.74 | 2.26 | 21.62 | 17.23 | 14.18 |
| Lactose | 1.03 | 0.85 | 0.72 | 3.38 | 2.74 | 2.26 | 21.62 | 17.23 | 14.18 |
| Maltotriose | 1.56 | 1.31 | 1.11 | 6.61 | 5.39 | 4.48 | 77.31 | 64.26 | 51.62 |

**Table S7.** Mass spectrometry parameters used for carbohydrate analysis.

| | precursor ion | product ion | declustering potential | collision energy | collision cell exit potential |
|---|---|---|---|---|---|
| | [m/z] | [m/z] | [V] | [v] | [v] |
| Xylose | 148.9 | 88.9 | -52 | -9 | -15 |
| Fructose | 178.8 | 88.7 | -21 | -12 | -9 |
| Glucose | 178.8 | 88.7 | -21 | -12 | -9 |
| Sucrose | 341.1 | 88.8 | -85 | -32 | -15 |
| Maltose | 341.0 | 160.8 | -30 | -11 | -15 |
| Maltotriose | 503.1 | 161.1 | -65 | -19.6 | -15 |

## PART IX: Sulfonamide analysis

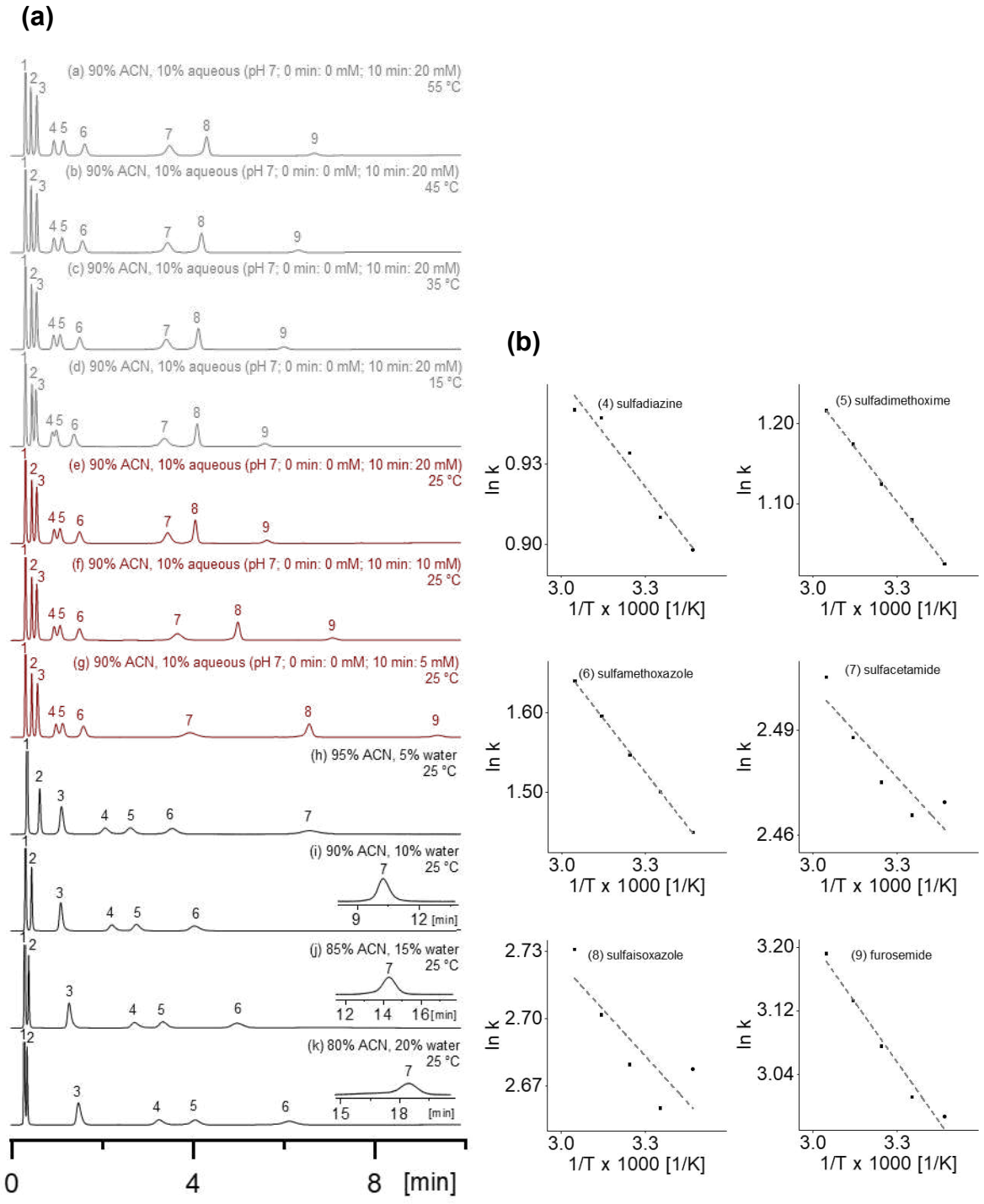


**Fig. S24.** Separation of sulfonamides on crosslinked amino phase (1: sulfanilamide, 2: sulfaguanidine, 3: sulfamerazine, 4: sulfadiazine, 5: sulfadimethoxime, 6: sulfamethoxazole, 7: sulfacetamide, 8: sulfaisoxazole, 9: furosemide): a) chromatograms obtained from experiments in isocratic HILIC (h-k) and HILIC-WAX

gradient elution (a-g) modes. The effect of varying water content in the mobile phase was investigated under isocratic conditions, whereas the influence of temperature and ammonium acetate concentration was investigated under gradient elution conditions. The specified conditions are given on top of the respective chromatograms. The flow rate was set to 1 mL/min and the injection volume to 2 µL. UV-detection was carried out at 230 nm. b) van´t Hoff plots illustrating the effect of temperature T on the obtained retention factors k.

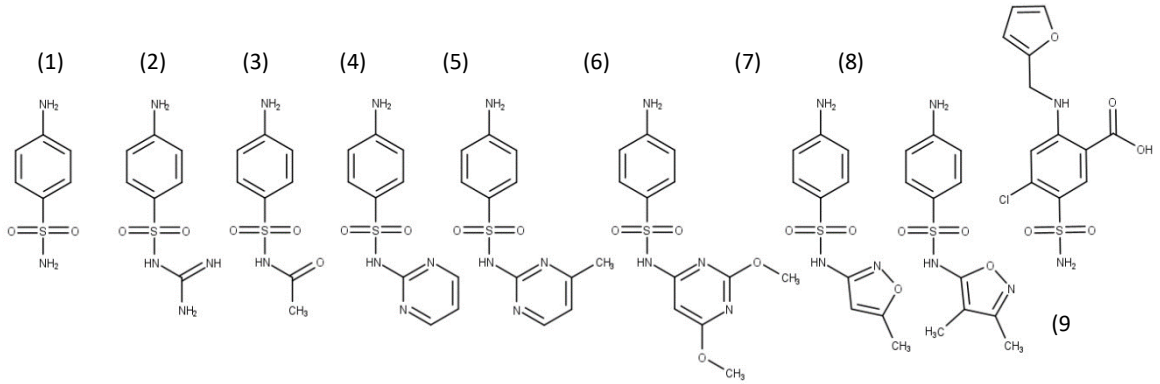


**Fig. S25.** Sulfonamides separated on crosslinked amino phase: (1) sulfanilamide ($pK_{a1}$ = 2.27[1], $pK_{a2}$ = 10.99[1]), (2) sulfaguanidine ($pK_{a1}$ = 2.11[1], $pK_{a2}$ = 7.72[1], $pK_{a3}$ = 10.53[1]), (3) sulfacetamide ($pK_{a1}$ = 2.14[1], $pK_{a2}$ = 4.30[1]), (4) sulfamerazine ($pK_{a1}$ = 2.01[1], $pK_{a2}$ = 6.99[1]), (5) sulfadiazine ($pK_{a1}$ = 2.00[1], $pK_{a2}$ = 6.99[1]), (6) sulfadimethoxime ($pK_{a1}$ = 1.95[1], $pK_{a2}$ = 6.91[1]), (7) sulfamethoxazole ($pK_{a1}$ = 0.25[1], $pK_{a2}$ = 1.97[1], $pK_{a3}$ = 6.16[1]), (8) sulfaisoxazole ($pK_{a1}$ = 1.42[1], $pK_{a2}$ = 2.17[1], $pK_{a3}$ = 5.80[1]), (9) furosemide ($pK_{a1}$ = 4.25[1], $pK_{a2}$ = 9.83[1], $pK_{a3}$ = 16.96[1]); [1]$pK_a$ values were calculated using MarvinSketch 20.19 software (ChemAxon, www.chemaxon.de).

**Table S8.** Chromatographic parameters obtained from analysis of sulfonamides on crosslinked amino phase. Chromatographic conditions for the experiments RUN a-k can be found in Fig. S24.

| | sulfanilamide | sulfaguanidine | sulfamerazine | sulfadiazine | sulfadimethoxime |
|---|---|---|---|---|---|
| RUN | K | K | k | K | k |
| a | 0.19 | 0.66 | 1.16 | 2.59 | 3.38 |
| b | 0.20 | 0.69 | 1.15 | 2.58 | 3.24 |
| c | 0.20 | 0.72 | 1.13 | 2.55 | 3.08 |
| d | 0.20 | 0.76 | 1.08 | 2.45 | 2.79 |
| e | 0.20 | 0.72 | 1.09 | 2.48 | 2.94 |
| f | 0.20 | 0.74 | 1.15 | 2.60 | 3.10 |
| g | 0.20 | 0.73 | 1.22 | 2.76 | 3.32 |
| h | 0.33 | 1.40 | 3.22 | 6.87 | 8.95 |
| i | 0.20 | 0.73 | 3.16 | 7.42 | 9.47 |
| j | 0.13 | 0.48 | 3.85 | 9.31 | 11.68 |
| k | 0.09 | 0.35 | 4.63 | 11.38 | 14.38 |

| | sulfamethoxazole | sulfacetamide | sulfaisoxazole | furosemide |
|---|---|---|---|---|
| RUN | K | K | k | K |
| a | 5.15 | 12.25 | 15.35 | 24.34 |
| b | 4.93 | 12.04 | 14.91 | 22.93 |
| c | 4.70 | 11.88 | 14.58 | 21.66 |
| d | 4.26 | 11.82 | 14.55 | 19.83 |
| e | 4.48 | 11.77 | 14.30 | 20.32 |
| f | 4.71 | 12.91 | 17.96 | 25.89 |
| g | 5.05 | 13.95 | 23.92 | 34.68 |
| h | 12.47 | 23.99 | - | - |
| i | 14.32 | 37.89 | - | - |
| j | 17.88 | 53.25 | - | - |
| k | 22.27 | 68.95 | - | - |

## PART X: References

[1] Montes L.F., Oliveira E.C.S., Neto A.C., Menezes S.M.C., Castro E.R.V., Barbosa L.L., Low-field nmr: a new alternative to determine the aromatic content of petroleum distillates, Fuel, 2019;239:413-420.

[2] Etienne M., Walcarius A., Analytical investigation of the chemical reactivity and stability of aminopropyl-grafted silica in aqueous medium, Talanta, 2003;59:1173-1188.

[3] Meier L., Monteiro G.C., Baldissera R.A.M., Sa M.M., Simple method for fast deprotection of nucleosides by triethylamine-catalyzed methanolysis of acetates in aqueous medium, J. Brazil. Chem. Soc., 2010;21:859-866.

[4] Blitz J.P., Murthy R.S.S., Leyden D.E., The role of amine structure on catalytic activity for silylation reactions with Cab-O-Sil, J. Colloid. Interf. Sci., 1988;126:387-392.

[5] Tripp C.P., Hair M.L., Chemical attachment of chlorosilanes to silica - a 2-step amine-promoted reaction, J. Phys. Chem.-Us, 1993:97:5693-5698.

[6] Puri J.K., Singh R., Chahal V.K., Silatranes: a review on their synthesis, structure, reactivity and applications, Chem. Soc. Rev., 2011;40:1791-1840.

[7] Sok S., Gordon M.S., A dash of protons: a theoretical study on the hydrolysis mechanism of 1-substituted silatranes and their protonated analogs, Comput. Theor. Chem., 2012; 987:2-15.

[8] Shlyakhtenko L.S., Gall A.A., Filonov A., Cerovac, Z. Lushnikov A., Lyubchenko Y.L., Silatrane-based surface chemistry for immobilization of DNA, protein-DNA complexes and other biological materials, Ultramicroscopy, 2003;97:279-287.

[9] Geibel C., Dittrich K., Woiwode U., Kohout M., Zhang T., Lindner W., Lämmerhofer M., Evaluation of superficially porous particle based zwitterionic chiral ion exchangers against fully porous particle benchmarks for enantioselective ultra-high performance liquid chromatography, J. Chromatogr. A, 2019;1603:130-140.

[10] Geibel C., Theiner J., Wolter M., Kramer M., Lindner W., Lämmerhofer M., Controllable organosilane monolayer density of surface bonding using silatranes for thiol functionalization of silica particles for liquid chromatography and validation of microanalytical method for elemental composition determination, J. Chromatogr. A, 2021;1653.

[11] Lämmerhofer M., Richter M., Wu J.Y., Nogueira R., Bicker W., Lindner W., Mixed-mode ion-exchangers and their comparative chromatographic characterization in reversed-phase and hydrophilic interaction chromatography elution modes, J. Sep. Sci., 2008;31:2572-2588.

[12] Zimmermann A., Horak J., Sanchez-Munoz O.L., Lämmerhofer M., Surface charge fine tuning of reversed-phase/weak anion-exchange type mixed-mode stationary phases for milder elution conditions, J. Chromatogr. A, 2015;1409:189-200.

# XI. CHAPTER SEVEN

## Wide pore fully porous mixed-mode octyl/pyridyl-bonded silica material with pH-dependent surface charge reversal for high-performance hydrophobic charge-induction chromatography of proteins

## XI.1 Publication VI – Main Document

Journal of Chromatography A 1737 (2024) 465429

Contents lists available at ScienceDirect

Journal of Chromatography A

journal homepage: www.elsevier.com/locate/chroma

# Wide-pore fully porous mixed-mode octyl/pyridyl-bonded silica material with pH-dependent surface charge reversal for high-performance hydrophobic charge-induction chromatography of proteins

Marc Wolter [a], Christoph Barth [a], Mirna Maalouf [a], Markus Kramer [b], Adrian Sievers-Engler [a], Michael Lämmerhofer [a,*]

[a] Institute of Pharmaceutical Sciences, Pharmaceutical (Bio-)Analysis, University of Tübingen, Auf der Morgenstelle 8, Tübingen 72076, Germany
[b] Institute of Organic Chemistry, University of Tübingen, Auf der Morgenstelle 18, Tübingen 72076, Germany

ARTICLE INFO

*Keywords:*
Stationary phase
Mixed-mode chromatography
Hydrophobic charge-induction chromatography
Protein analysis
Silatranes

ABSTRACT

In an attempt to overcome silanophilic interactions like observed on popular reversed-phase butyl-bonded silica stationary phases in protein HPLC, a mixed-mode stationary phase based on wide pore silica (3 μm, 300 Å) was prepared by co-immobilization of octyl and 2-pyridylethyl ligands. The surface modification was performed by a new approach using synthesized functional silatranes of the above ligands and prewetted silica. It allowed to generate a dense polymeric siloxane layer on the silica surface. Butyl-bonded silica and octyl/3-aminopropyl-bonded mixed-mode silica phases were prepared for comparison. The modified silicas were subsequently characterized by elemental analysis regarding ligand densities, by solid-state $^{29}$Si and $^{13}$C cross polarization/magic angle spinning nuclear magnetic resonance spectroscopy for confirming the surface-bonded structure, and by pH-dependent ζ-potential measurements via electrophoretic light scattering providing net surface charge information at distinct pH values. While the classical butyl-bonded stationary phase revealed negative ζ-potential over the entire pH range investigated (pH 3.5–9.5) due to residual silanols and the mixed-mode octyl/3-aminopropyl-bonded silica positive ζ-potential over the entire pH range, pH-dependent charge reversal was observed at approximately pH 5.5 for the octyl/pyridyl-bonded stationary phase. Then, a test set of proteins differing in hydrophobicities and isoelectric points was employed to evaluate the retention characteristics of all three synthesized stationary phases over the pH range of 3 to 7.5 by acetonitrile-gradient elution reversed-phase HPLC. Under acidic conditions (pH 3) the mixed-mode phases octyl/pyridyl-silica and octyl/aminopropyl-silica showed reduced retention and improved peak shapes due to repulsive interactions preventing silanophilic interactions, while protein separations by their hydrophobicities were achieved (repulsive charge-assisted protein RPLC). Finally, the prepared novel mixed-mode octyl/pyridyl-bonded stationary phase was evaluated in hydrophobic charge induction chromatography mode for protein separation of the same test set. Instead of an organic modifier gradient, elution was enforced by a pH gradient from almost neutral to acidic pH at constant organic modifier content of 10 %. This chromatographic mode showed orthogonal retention characteristics and reversed elution order compared to above organic gradient RP-HPLC. In addition, significantly less organic solvent was used under these conditions, classifying it as a green protein LC technology.

## 1. Introduction

Therapeutic proteins are an indispensable group of drugs and the number of protein-based drugs increases rapidly. Consequently, protein analysis has become an extremely important field within pharmaceutical analysis. An array of techniques, such as nuclear magnetic resonance spectroscopy (NMR), mass spectrometry (MS), gel and capillary electrophoresis and high-pressure liquid chromatography (HPLC), is commonly applied to fully characterize therapeutic proteins, their macro- and microheterogeneity as well as degradation products [1]. Amongst the array of analytical techniques, reversed phase (RP), ion-exchange (IEX), mixed-mode (MMC), size-exclusion (SEC), hydrophobic (HIC) and hydrophilic interaction chromatography (HILIC) are routinely carried out in pharmaceutical quality control laboratories for

* Corresponding author.
*E-mail address:* michael.laemmerhofer@uni-tuebingen.de (M. Lämmerhofer).

https://doi.org/10.1016/j.chroma.2024.465429
Received 31 August 2024; Received in revised form 5 October 2024; Accepted 7 October 2024
Available online 9 October 2024

characterization of proteins in terms of hydrophobicity, charge, hydrodynamic radius and glycosylation patterns due to their particular specificities, accuracy and robustness [2–8]. For preparative scale LC purification, also other chromatographic modes are widely applied. Affinity chromatography (with protein A resins) has become the gold standard for monoclonal antibody purification [9,10]. Mixed-mode chromatography was frequently evaluated to replace protein A chromatography [11]. As a specific chromatographic mode, hydrophobic charge induction chromatography (HCIC) was reported to be a promising alternative technique for purification of proteins and other biomolecules, since mild elution conditions can be applied and costs are significantly lower compared to the expensive affinity chromatography [12,13]. HCIC represents a type of mixed-mode chromatography, since both hydrophobic and electrostatic interactions are combined. Firstly, the analytes are adsorbed on the stationary phase due to hydrophobic interactions at usually neutral pH and then eluted from the column due to electrostatic repulsion. This repulsion is usually enforced by changing the mobile phase pH to acidic conditions which leads to protonation of weakly basic ligands (such as pyridine) and simultaneously shifts the net charge of the proteins to positive values (< pI). This chromatographic principle has been introduced for protein purification [13–22], but has not been established for high-performance LC protein separations.

In this study, a mixed-mode chromatography (MMC) phase for HCIC was developed by simultaneous immobilization of octyl and pyridine moieties onto a fully porous silica support (3 μm, 300 Å). Thus, mixed-ligands particles were generated offering especially hydrophobic and pH-dependent electrostatic interaction sites suitable for HCIC. The idea was to facilitate protein desorption from siliceous material by repulsive interactions, tentatively also changing the retention mechanism compared to standard reversed-phase separation on butyl-modified silica. Altered mechanisms may lead to orthogonal selectivity which should be valuable for protein macro- and microcomponent separations and full characterization of therapeutic proteins. A further aim of this study was the evaluation of a new bonding chemistry. Silica modification is typically carried out by utilizing alkoxysilanes or chlorosilanes. Disadvantageously, such reagents were reported to undergo easily hydrolysis and polymerization in the reaction solution prior to the immobilization process leading to unfavorable inhomogeneous and thick ligand films on the silica surface [23]. Consequently, in this study, respective silatranes were firstly synthesized from the alkoxysilane derivatives and then used for silica surface modification. Silatranes have beneficial properties in terms of surface functionalization. Especially, silatranes are not prone to hydrolysis under neutral aqueous conditions and were reported to form thinner and more homogenous ligand films on the surface accompanied by higher ligand densities on the support surface [23,24]. This could better shield proteins from siliceous interactions and also lead to increased column life time due to less ligand bleeding.

## 2. Experimental

### 2.1. Materials

Spherical silica particles (Daisogel, 3 μm, 300 Å, 100 $m^2/g$) were received from DaisoFine Chem GmbH (Düsseldorf, Germany). Empty stainless-steel columns (50 mm x 3 mm) were purchased from Bischoff Chromatography (Leonberg, Germany). 2-(2-Pyridylethyl)trimethoxysilane and n-octyltrimethoxysilane were obtained from Gelest Inc. (Morrisville, PA, USA) and n-butyltrimethoxysilane from ABCR Chemicals (Karlsruhe, Germany). Acetonitrile (HPLC grade), acetic acid (analytical grade), formic acid (FA, analytical grade), ammonium acetate, 4-dimethylaminopyridine (DMAP), sodium hydroxide, deuterated chloroform, triethanolamine, butylbenzene (BuB), pentylbenzene (PeB), adenosine, guanosine, cytidine, thymidine, uridine, nicotinic acid, pyridoxine hydrochloride, ascorbic acid, riboflavin, thiamine hydrochloride, caffeine, theophylline, theobromine, *O,O*-diethylchlorothiophosphate (DECTP), triethylamine, *N-tert*-butoxycarbonyl-prolyl-phenylalanine (BocProPhe), L-phenylalanine (Phe), *N*-acetyl-L-phenylalanine (AcPhe), L-tryptophan (Trp), *N*-acetyl-L-tryptophan (AcTrp), ribonuclease A, cytochrome C, myoglobin and β-lactoglobulin were supplied from Sigma Aldrich (Munich, Germany). *O,O*-Diethylthiophosphate (DETP) was generated from hydrolysis of DECTP in presence of trimethylamine. L-Phenylalanine methyl ester (PheOMe), L-tryptophan-amide hydrochloride ($TrpNH_2$) and *N*-acetyl phenylalanine ethyl ester (AcPheOEt) were purchased from ABCR Chemicals (Karlsruhe, Germany). (3-Aminopropyl) silatrane was synthesized according to [24]. The synthesis of octyl silatrane and 2-(2-pyridylethyl) silatrane is described in chapters 2.3.1 and 2.3.2. Reaction schemes and NMR data are given in Figs. S1–S4. The solvents toluene, methanol and methylene chloride were of technical grade or HPLC grade and purchased from Brenntag (Essen, Germany) or Sigma Aldrich (Munich, Germany). MilliQ water was prepared by using an Elga PureLab Ultra Purification System (Celle, Germany).

### 2.2. Instrumentation and software

Elemental analysis was performed utilizing an EA 3000 CHNS-O elemental analyser from EuroVector SpA (Milan, Italy) as described in [23]. ζ-Potentials were measured in accordance to [25] by electrophoretic light scattering using a Zetasizer NanoZS particle analyzer from Malvern Instruments (Herrenberg, Germany). $pK_a$ values were calculated by utilizing MarvinSketch 20.19 software (ChemAxon, www.chemaxon.de). Liquid-state nuclear magnetic resonance spectroscopy (NMR) experiments were carried out on a Bruker Avance 400 MHz spectrometer (Bruker, Rheinstetten, Germany), solid-state nuclear magnetic resonance spectroscopy (solid-state NMR) experiments were performed on a Bruker Avance III HD 300 XWB spectrometer. The applied parameters can be found in [23]. NMR data processing was carried out using Topspin 4.0.8 software from Bruker. HPLC experiments were all performed on HPLC systems from Agilent Technologies (Waldbronn, Germany). Thereby, measurements were usually performed using an Agilent 1260 series HPLC system featured with a degasser, flexible pump, autosampler, column compartment (TCC) and a diode array detector (DAD) or an Agilent 1100 series HPLC equipped with a degasser, quaternary pump, autosampler, column compartment (TCC) and variable wavelength detector (VWD). OpenLab CDS ChemStation Online Software (Rev. C.01.03 (37), 2011) and ChemStation Offline Software (Rev. B.04.03 (16), 2010) from Agilent Technologies were used for data acquisition and analysis. A Smartline Pneumatic Pump 1950 from Knauer (Berlin, Germany) was utilized for slurry packing of silica particles into stainless steel columns (50 mm x 3 mm). OriginPro 2019 (OriginLab, Northampton, Massachusetts, USA) was utilized for data visualization. More detailed information is given in respective figure captions or subchapters.

### 2.3. Preparation of stationary phases

#### 2.3.1. Synthesis of 2-(2-pyridylethyl) silatrane

2-(2-Pyridylethyl) silatrane was synthesized from a mixture of 0.01 mol 2-(2-pyridylethyl)trimethoxysilane, 0.01 mol triethanolamine, 5 mL methanol and 1 mL of methanolic sodium hydroxide solution (2 %, m/v) within a round bottom flask. Thereafter, the flask was attached to a reflux condenser equipped with a nitrogen supply and the reaction mixture was heated up to 80 °C using an oil bath. Then, the reaction was allowed to proceed for 96 h under continuous gentle nitrogen rinsing and magnetic stirring. Thereafter, the reaction mixture was cooled down to room temperature and the round bottom flask was attached to a rotary evaporator. Subsequently, methanol was evaporated provoking the precipitation of pale brownish crystals. Lastly, the reaction product was recrystallized from methylene chloride leading to 2-(2-pyridylethyl) silatrane.

*2.3.2. Synthesis of octyl silatrane*

Octyl silatrane was synthesized from a mixture of 0.1 mol n-octyltrimethoxysilane, 0.1 mol triethanolamine, 10 mL toluene and 4 mL of methanolic sodium hydroxide solution (2 %, m/v) within a round bottom flask. The flask was attached to a reflux condenser equipped with a nitrogen supply and heated up to 110 °C using an oil bath. The reaction was allowed to proceed for 96 h under continuous magnetic stirring and gentle nitrogen rinsing. Thereafter, the reaction mixture was cooled down to ambient temperature and a hard, white to slightly yellowish reaction product precipitated. Finally, the reaction product was recrystallized from methylene chloride to result in n-octyl silatrane.

*2.3.3. Preparation of C4-SP: immobilization of n-butyl trimethoxysilane onto silica*

Initially, 0.5 g bare silica particles, n-butyltrimethoxysilane (6 µmol/m$^2$) and DMAP (5 % n/n related to n-butyltrimethoxysilane) were dispersed in 20 mL anhydrous toluene within a triple neck flask equipped with a reflux condenser, a mechanical stirrer and a nitrogen supply. Then, the suspension was heated up to reflux and the reaction was allowed to proceed for 17 h under continuous nitrogen rinsing and stirring. Thereafter, the silica was washed three times with boiling methanol and boiling toluene each using a glass funnel of porosity 5 and dried in a vacuum chamber at 60 °C for 12 h. The dried modified silica was subjected to elemental analysis. The results can be found in Table S1.

*2.3.4. Preparation of C8Pyr-SP and C8APS-SP: co-immobilization of octyl silatrane and (3-aminopropyl) silatrane or 2-(2-pyridylethyl) silatrane, respectively, onto silica*

In the first step, 2 g bare silica particles were dispersed in 20 mL MilliQ water and sonicated for 5 min within a glass flask. Thereafter, the suspension was transferred to a glass funnel of porosity 5 and the water removed by applying a slight vacuum for 16 h. Afterwards, 1.2 g of the humidified silica was dispersed in 16 mL anhydrous toluene and 4 mL anhydrous methanol within a triple neck flask equipped with a mechanical stirrer, a nitrogen supply and a reflux condenser. Then, octyl silatrane (6 µmol/m$^2$), 2-(2-pyridylethyl) silatrane (2 µmol/m$^2$, for C8Pyr-SP) or (3-aminopropyl) silatrane (2 µmol/m$^2$, for C8APS-SP), respectively, and DMAP (0.4 µmol/m$^2$) were added to the suspension and the mixture was heated to reflux for 7 h. In the next step, the silica was washed three times with boiling methanol and toluene each using a glass funnel with porosity 5. Thereafter the modified silica particles were dried in a vacuum chamber at 60 °C for 12 h. The amount of adsorbed water on the silica surface at the beginning of the bonding procedure was determined in accordance to the European Pharmacopeia. Thus, the humidified silica was dried in a drying chamber at 110 °C for 96 h and the drying loss determined by weighing the silica before and after the drying process. Elemental analysis results for the modified silicas can be found in Table S1.

## 3. Results and discussion

*3.1. Synthesis of octyl/pyridyl-, octyl/aminopropyl-, and butyl-bonded silica stationary phases*

In this study, a wide-pore mixed-ligand octyl/pyridyl-MMC silica-based material (C8Pyr-SP) was designed and synthesized for HCIC. Additionally, for comparison purposes, two other stationary phases were prepared on the same supporting silica, namely an octyl/3-aminopropyl-bonded silica (C8APS-SP) and a butyl-bonded silica (C4-SP) (Fig. 1). All of these phases offer hydrophobic interaction sites, but different charge characteristics. Wide-pore silica of 300 Å pore size and 3 µm particle diameter was selected as support for all 3 stationary phases. A pore size of 300 Å was considered a good compromise between effective pore

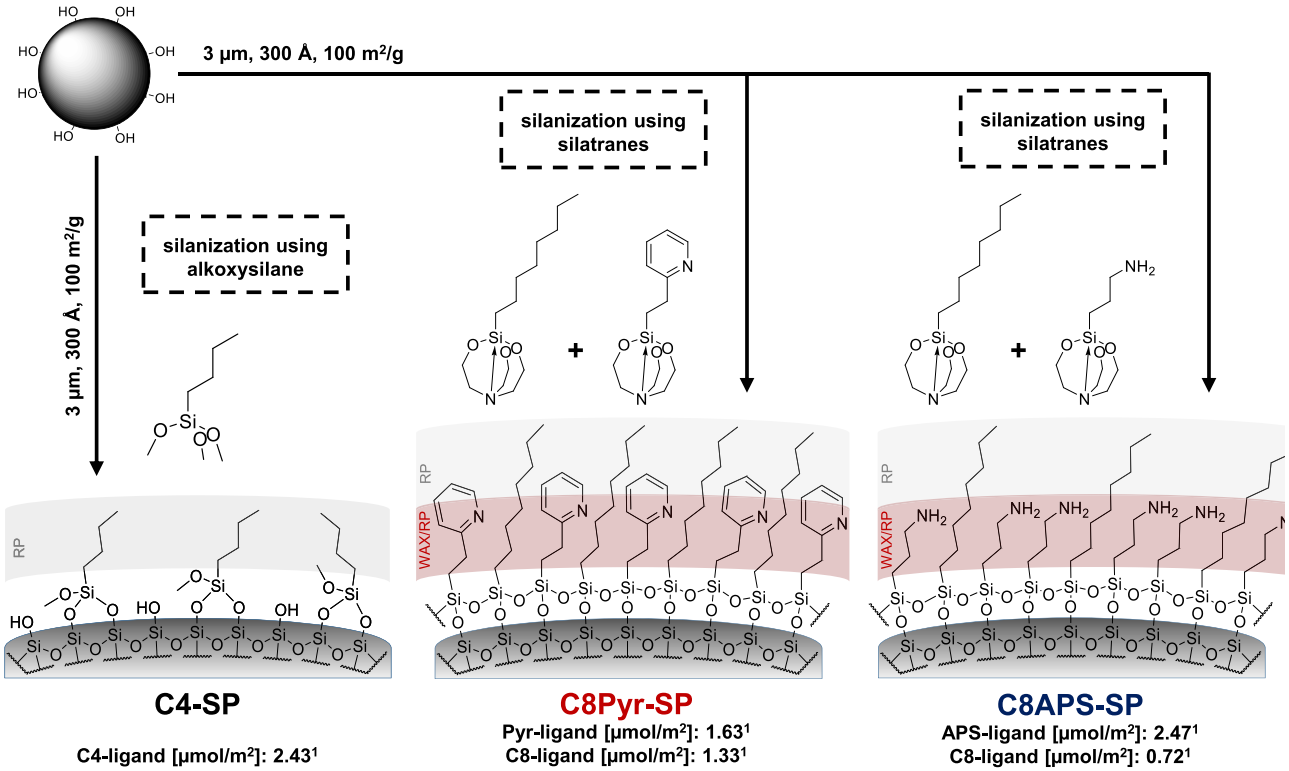


**Fig. 1.** Scheme for the preparation of stationary phases C4-SP, C8Pyr-SP, C8APS-SP and obtained ligand densities. C4-SP was prepared utilizing alkoxysilane chemistry, whereas C8Pyr-SP and C8APS-SP were synthesized using silatrane chemistry. The WAX sites of C8Pyr-SP and C8APS-SP were partially shielded by the long octadecyl-ligands. Since C8APS-SP contained a factor 2 lower C8-ligand density, the WAX sites were less strongly shielded than those of the C8Pyr-SP. Bare silica particles of 300 Å (100 m$^2$/g) were used as starting material. [1] calculated on basis of elemental analysis results (see Table S1).

diffusion and large enough adsorption surface for proteins [26,27].

The design considerations were the following. C4-bonded silica has become a popular stationary phase for protein separations [28]. Such stationary phases have commonly a high density of C4 ligands and are fully endcapped to shield the surface from silanophilic interactions with proteins. However, residual silanols may still be available and interact with proteins. Such secondary silanophilic interactions are disadvantageous and lead to poor peak shapes. For this reason, a pyridyl co-ligand was considered to be embedded in the alkyl surface coating. The pyridyl nitrogen points towards the silica surface which is thus somehow shielded from short-range interactions with proteins (Fig. 1). To favor hydrophobic interactions with the alkyl strands, the chain length was extended to octyl as compared to C4-SP. Under acidic mobile phase conditions, the pyridyl ring is protonated like the proteins to be separated. As a result, the proteins are electrostatically repelled from the silica surface. Thus, hydrophobic interactions can take place without secondary silanophilic interactions. On the other hand, at an eluent pH above the $pK_a$ of the pyridine ring, proteins can interact with both octyl and pyridyl ring by hydrophobic, π-π- (in particular with MeOH as organic modifier) and possibly H-bond interactions. Using a mixed pH/organic modifier gradient from neutral to acidic, repulsive electrostatic interactions are induced at pH-values below the $pK_a$ of the pyridine and the pI of the proteins, and the proteins can be efficiently desorbed. The corresponding C8APS-SP does not have the possibility of charge switching and carries a positive surface charge over the entire pH range commonly used with silica-based SPs. Therefore, comparison with this phase should lead to useful mechanistic information.

Both, C8Pyr-SP and C8APS-SP offer weak anion exchange (WAX)

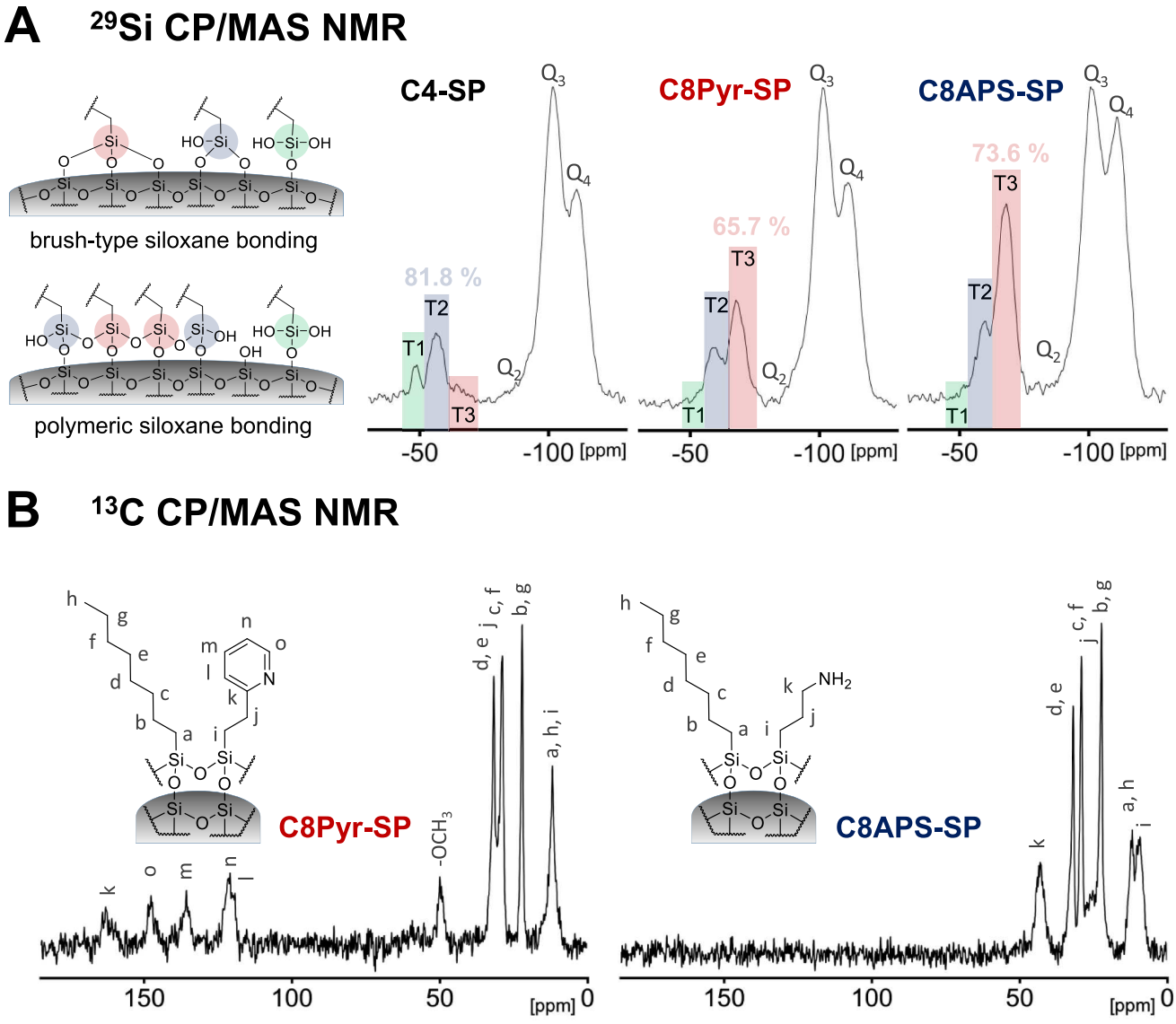


**Fig. 2.** Solid-state $^{29}Si$ and $^{13}C$ CP/MAS NMR spectra of C4-SP, C8Pyr-SP and C8APS-SP. A: $^{29}Si$ CP/MAS NMR spectra: In addition to the three typical signals for silica (Q2: geminal silanol groups, Q3: free single and vicinal silanol groups, Q4: siloxane groups), signals were found in the range between - 50 ppm and - 80 ppm (T1, T2, and T3). T1, T2 and T3 represent mono-, di- and trifunctional bonded siloxane atoms [23,24,31]. A large amount of trifunctional siloxane bonded ligands resulted from the innovative silatrane grafting process, whereas mostly bifunctional siloxane bonded ligands were found for C4-SP, which was prepared by classic silanization using a trialkoxysilane. B: $^{13}C$ CP/MAS NMR spectra: Signals were assigned to the carbon atoms of the respective ligands proving the successful incorporation. Furthermore, no signals could be found for residual triethanolamine moieties at approximately 60 ppm (cf. Fig. S5), which indicated the efficient hydrolytic cleavage of these undesired residues [23,24]. However, interestingly, the spectrum of C8Pyr-SP exhibited a signal at approximately 50 ppm, which is typical for methoxy groups. These might most probably be generated due to reaction with the methanolic solvent. The spectrum of C8APS-SP lacked the signal for such generated methoxy groups. This is in agreement with observations from previous studies and most probably caused by the catalytic effect of aminopropyl moieties in terms of hydrolysis [24,43].

properties, the latter over a wider pH range and the former only at low pH. C4-SP offers no ionic or only weak anionic interaction sites (due to the residual silanols on the surface).

The C4-SP was synthesized by silanization of the wide pore silica with n-butyltrimethoxysilane (Fig. 1) [29]. As expected, mainly bifunctional siloxane bonding was detected by solid-state $^{29}$Si CP-MAS NMR (indicated by T2 signal in the spectrum, see Fig. 2A). C8Pyr-SP and C8APS-SP were synthesized by means of an innovative silatrane functionalization strategy. The corresponding silatranes, 2-(2-pyridylethyl) silatrane, octyl silatrane and (3-aminopropyl) silatrane were synthesized in-house by a classical condensation reaction of the respective alkoxysilanes with triethanolamine (for reaction schemes and $^{1}$H- and $^{13}$C NMR spectra see Fig. S1–4) [23,24]. Subsequently, the co-immobilization of octyl silatrane with 2-(2-pyridylethyl) silatrane or (3-aminopropyl) silatrane onto the silica surface was carried out simultaneously by charging the reaction mixture with the two silatranes at a ratio of 6:2 μmol/m$^2$. Initially, a 2-step synthesis approach as reported previously for a chiral stationary phase was evaluated [23,24]. Thus, the silanization reaction was carried out with dried silica in anhydrous toluene resulting in a surface bonding where the triethanolamine residue remained attached to the immobilized silane (for structural details see Fig. S5). Therefore, a subsequent acidic hydrolysis step was required to remove the surface-bound triethanolamine residues. Significant amounts of bi- and trifunctional siloxane bonds (T2 and T3) were observed in the $^{29}$Si CP/MAS NMR spectra (see Fig. S5).

Since this 2-step approach is inefficient, a 1-step procedure was developed for surface functionalization with silatranes. It is based on the use of humidified silica for silanization reaction with the silatranes. The water content of the humidified silica was determined to be 51 % (w/w). The water adsorbed to the silica surface facilitates the full cleavage of the triethanolamine residues of the silatranes after binding to the silica surface. This procedure allows the coating process to be completed in a single step. Solid-state $^{29}$Si CP/MAS NMR analysis revealed the large amount of trifunctional bonded ligands (T3) for the silatrane-derived materials. Such trifunctional bonding provides better hydrolytic stability and dense silanol coverage (Fig. 2). In accordance to the literature, it is assumed that a polymeric siloxane bonding is obtained (Fig. S6) [30,31]. Unlike alkoxysilanes, silatranes are not prone to hydrolysis under aqueous conditions and do not form oligomeric structures in solution (Fig. S7), since the cage-like structure and the transannular N→Si bond usually impede nucleophilic reactions at the silicon atom. Advantageously, however, silanols at the silica surface can act as catalysts enabling the condensation reaction of the silatranes with the silica surface (Fig. S6). Thus, reactivity increases only in close proximity to the silica surface and ring-opening of the silatrane takes only place directly at the support surface and not in solution [32,33]. This leads to more homogenous, thinner ligand layers and accompanying better chromatographic performance of the separation material due to reduced mass transfer resistance [23,34]. On contrary, alkoxysilanes (as used herein for C4-SP) can easily form oligomeric structures in solution which are then attached to the silica surface in a random, disordered thicker surface layer with suboptimal coverage and impaired chromatographic performance (see Fig. S7).

In order to determine the obtained ligand densities, all modified silica gels were submitted to elemental analysis. Total ligand densities of 2.43 μmol/m$^2$, 2.96 μmol/m$^2$ and 3.19 μmol/m$^2$ were calculated for the three stationary phases, C4-SP, C8Pyr-SP and C8APS-SP, respectively (see Fig. 1). Interestingly, ligand densities of the silatrane-derived materials were significantly higher than the one achieved via the classical alkoxysilane functionalization approach in spite of their sterically more demanding substituents. This is consistent with observations from previous studies and might be caused by higher reaction kinetics of the silatrane chemistry, formation of a dense polysiloxane layer and less clogged pores [23,24]. The prevention of polymer formation in solution due to the usage of hydrolytically stable silatranes may result in higher amounts of accessible pores and consequently to higher ligand loadings. Furthermore, estimation of the ligand ratio of the mixed-ligand phases was possible on basis of the elemental analysis results. A C8 to APS molar ratio of approximately 1 to 3.4 was calculated for C8APS-SP. The molar ratio of C8 to Pyr for C8Pyr-SP was determined to be 1 to 1.2. While the ratio of octyl and pyridyl ligand was almost equimolar for C8Pyr-SP, the significantly higher coverage with 3-aminopropyl compared to octyl ligand may be explained by the basicity of the primary amine of (3-aminopropyl) silatrane, which most probably leads to an enrichment of the reagent on the silica surface due to electrostatic interactions with the acidic silanols at the beginning of the immobilization process [24,29]. Larger steric hindrance of the pyridyl ligand may contribute to its lower density as well. Consequently, C8Pyr-SP offered a lower number of WAX interaction sites, which were also more efficiently shielded by the larger number of C8-ligands than in the C8APS-SP. This should therefore lead to a lower WAX activity of C8Pyr-SP compared to C8APS-SP under acidic conditions.

### 3.2. Investigation of pH-dependent surface charge

In addition to the alkyl ligand densities and hydrophobicities, the surface charge of the stationary phases is of prime importance for their chromatographic behaviour and retention characteristics of charged molecules like proteins. While the charge of C4-SP is completely determined by the residual silanols available after bonding of butyl ligands, the surface charge characteristics of C8Pyr-SP and C8APS-SP is more complex. In addition to residual silanols, both offer, depending on the eluent pH, cationic moieties and anion-exchange sites, respectively.

Based on the theoretical p$K_a$ value of the 2-(2-pyridyl)ethyl moiety (calculated as 5.5) the pyridyl-group should be fully positively charged at pH values below 4 and fully non-ionic at pH above 7 (see Fig. S8). In contrast, the 3-aminopropyl group (with calculated p$K_a$ of 10.1) should be fully ionized up to pH 9. However, residual silanols may actually modulate such theoretical charge states calculated by the ligand moieties only.

For this reason, the surface charge was experimentally determined by ζ-potential measurements under fully aqueous conditions (1 mM buffer in 10 mM KCl). Fig. 3 illustrates the ζ-potentials in dependence of the pH determined by electrophoretic light scattering for the synthesized phases and bare silica gel (SiOH-SP) [35]. As expected, unmodified silica had a negative ζ-potential over the entire pH range which gradually increased from around −15 mV at pH 3.5 to over −50 mV at pH above 7.5 due to increasing dissociation of silanols (Fig. 3). C4-SP revealed also negative surface charge over the entire pH range, yet with around 10 mV offset due to modification and shielding of some silanols by the butyl-silyl surface modification. In sharp contrast, C8APS-SP showed consistently positive surface charge over the entire pH range. Between pH 3.5 and 7.5 the net positive ζ-potential only slightly declined, and then dropped significantly as the amino groups got more and more deprotonated [24]. Evidently, the silanol groups on the modified silica surface slightly modulate the charge characteristics discussed in Fig. S8 for the ligand alone without silica. On the contrary, C8Pyr-SP exhibited a pH-dependent charge reversal at approximately pH 5.5. At low pH values, protonation of the pyridine group leads to a net positive charge. The proportion of protonated species decreases with increasing pH above pH 4 due to the weak basicity of the pyridine (see Fig. S8) [36,37]. Above pH 5.5, dissociated residual silanols dominate the surface charge which leads to a net negative surface charge and ζ-potential, respectively [38]. Accordingly, the C8Pyr-SP should exhibit WAX properties at low pH values of the mobile phase, whereas at high pH values above pH 5.5 it is supposed to lose its WAX properties. In view of protein separations, repulsive electrostatic interactions between protonated C8Pyr-SP and proteins below their isoelectric point (pI) should dominate in the acidic range. Above pH 5.5, proteins above their pI should also exhibit electrostatic repulsion, however, amino groups are still positively charged in the common pH range in which silica-based materials can be used. Hence, a mixture of electrostatic attraction and repulsion

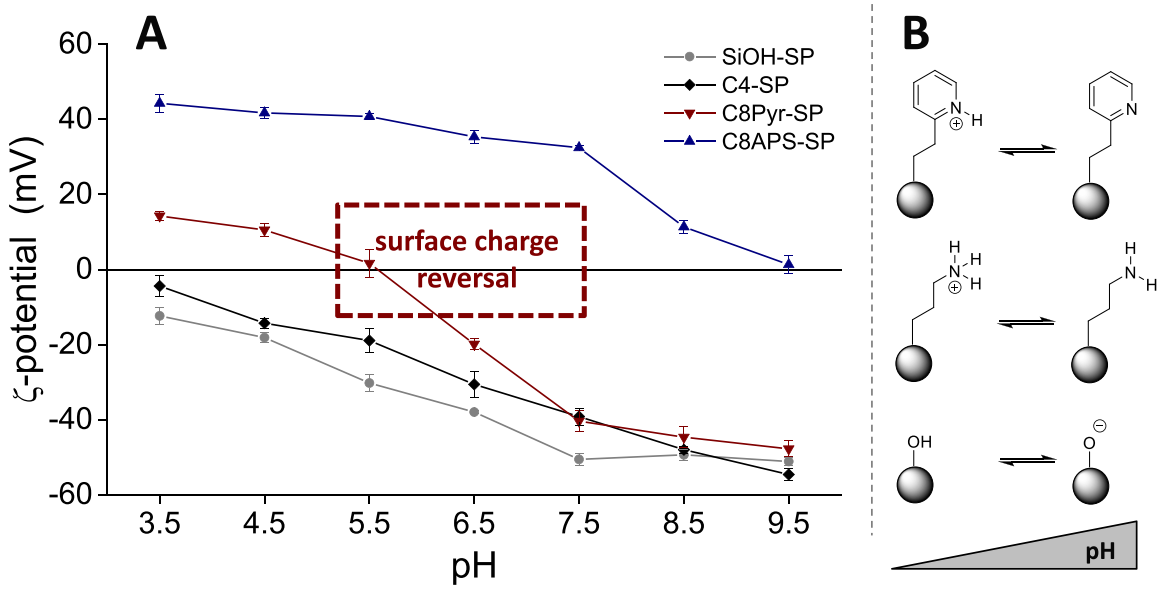


**Fig. 3.** A: ζ-potentials determined for unmodified silica (SiOH-SP), C4-SP, C8Pyr-SP and C8APS-SP at different pH values. ζ-potentials represent the net charge of the particles at the shear surface and were determined over the pH range from 3.5 to 9.5 at constant ionic strength (1 mM buffer in 10 mM KCl) [35,44,45]. Remarkably, C8Pyr-SP exhibits a surface charge reversal at approximately pH 5.5 due to the weak basicity of the pyridine-ligand and the acidity of residual silanol groups on the silica surface. B: depicts possible protonation and charge states of the bonded ligands and the silanol groups of the support. The C4- and the C8-ligands are not illustrated, since they are neutral and do not contribute to surface charge.

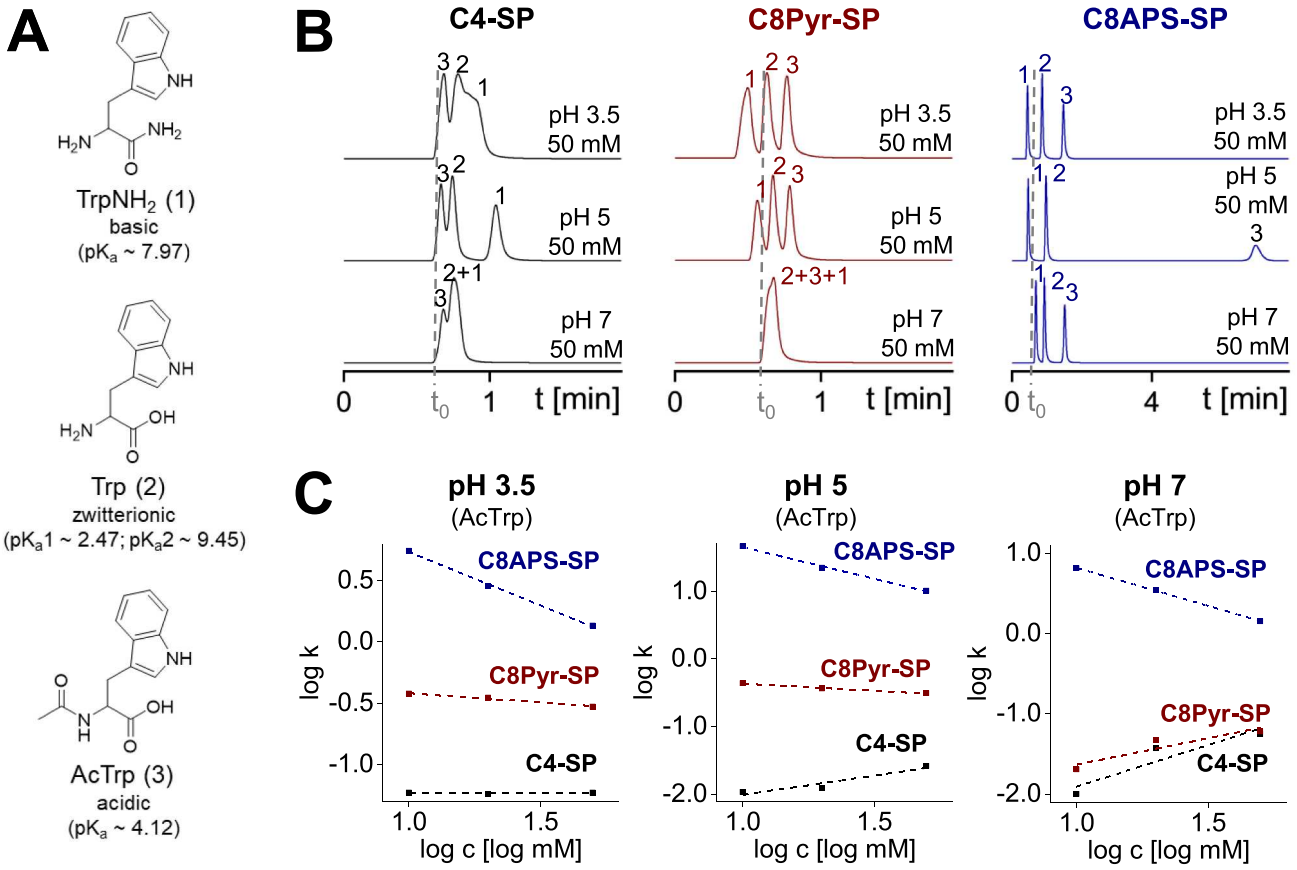


**Fig. 4.** Chromatographic evaluation of retention characteristics using tryptophan derivatives as low molecular probes for the investigation of the surface charge and ion-exchange capacity of C4-SP, C8Pyr-SP and C8APS-SP at different pH values. A depicts the structure of the applied tryptophan derivatives as well as their $pK_a$ values. B and C illustrate the obtained chromatograms (buffer concentration: 50 mM) as well as the resultant log *c*/log *k* plots for AcTrp. The mobile phase consisted of ACN and water (80:20, v/v) containing 10, 20 or 50 mM of the corresponding acid (formic acid: pH 3.5, acetic acid: pH 5 and 7), respectively. The pH was adjusted with ammonia. The flow rate was 1 mL/min, the temperature was set to 25 °C, the injection volume to 2 µL and detection was carried out at 280 nm. Additional experimental data can be found in Fig. S11–13 and Table S3.

(superimposed over hydrophobic interactions) may exist and it is hard to predict which of the two prevails.

### 3.3. Chromatographic study of surface charge and ion exchange capacity

Above ζ-potential measurements can only describe the total net charge in dependence on pH and constant ionic strength under fully aqueous conditions. However, they do not reflect realistic chromatographic conditions and do not provide information on the accessibility of the ionic interaction sites at the surface during the chromatographic process. It was of interest to what extent the residual silanol groups influence the chromatographic process due to their partial shielding by the embedded ligands. However, the influence of silanols can only be eliminated to a limited extent by steric shielding, as electrostatic interactions are considered to be long range interactions [39]. For this reason, a set of small molecule probes (instead of proteins which are more complex making the interpretation complicated) were first used to design a chromatographic test which allows screening of the charge state of the bonded SPs and derive information on actual ion-exchange capacities under various conditions.

Hence, a set of basic, acidic, zwitterionic tryptophan derivatives were injected to all three prepared columns at different pH values (pH 3.5, 5, and 7) and ionic strengths (10, 20 and 50 mM) of the mobile phase. The respective results are depicted in Fig. 4. On the C4-SP, there seems to be a dominating effect of the residual silanols. The basic analyte ($TrpNH_2$) always eluted last due to interactions with silanols, while the acidic analyte eluted first due to electrostatic repulsion. In contrast, on C8Pyr-SP the elution order was reversed at pH 3.5 and 5. No separation was observed at pH 7. Basic $TrpNH_2$ showed slightly enhanced retention as the pH was increased (indicating stronger silanol interactions). AcTrp was no longer sufficiently retained at pH 7, since the pyridine moiety was present as free base at this pH and repulsive electrostatic interactions with dissociated silanols existed. On C8APS-SP, the same elution order was observed as on C8Pyr-SP, but it showed stronger retention and better selectivity, especially for the zwitterionic (Trp) and acidic (AcTrp) analytes over all mobile phase pH values. This documents a stronger WAX characteristics of C8APS-SP due to a higher surface density of amino groups.

Interestingly, AcTrp exhibited the strongest retention on C8APS-SP at pH 5 which is typical for silica-based WAX-type SPs. At low pH, e.g. pH 3.5, reduced dissociation of the carboxylic group leads to lower retention and at high pH, e.g. pH 7, increasing dissociation of silanols leads to repulsive interactions and reduced dissociation of the amino groups which reduces the actual WAX-capacity.

To monitor the effective charges that are involved in analyte-sorbent interactions, the effect of the retention factors on the salt concentration in the mobile phase was investigated. In double logarithmic plots, a negative slope of the linear trend line indicates attractive ionic interactions (ion-exchange process), a positive slope repulsive electrostatic interactions, and a flat horizontal line parallel to the x-axis no significant ionic interactions [40]. AcTrp was selected as probe for this purpose. As can be seen in Fig. 4C, at pH 3.5 ionic interactions are negligible on the C4-SP. In contrast, the C8Pyr-SP shows a slight attractive ionic interaction (corresponding to a slight weak anion-exchange process superimposed upon hydrophobic interactions), and the C8APS-SP a much larger extent of attractive electrostatic interactions (WAX process). At pH 5, slight repulsive electrostatic interactions are observed for the C4-SP, while the trends for C8Pyr-SP and C8APS-SP are largely the same. At pH 7, both C4-SP and C8Pyr-SP display repulsive ionic interactions, while the C8APS-SP still features a WAX process. These findings are supported by the ζ-potential measurements (Fig. 3) and further chromatographic tests (see suppl. Fig. S9 and Table S2 for the simple benzylamine/phenol/*p*-toluene sulfonic acid test mix, and Figs. S10–13 and Table S3 for the phenylalanine derivatives).

Overall, the chromatographic observations showed that C8Pyr-SP offered weaker attractive electrostatic interactions than C8APS-SP under weakly acidic mobile phase conditions and allowed pH-dependent charge switching at neutral pH of the mobile phase. Further chromatographic characterization of C8Pyr-SP, especially under RP and HILIC conditions, can be found in the supplementary material (see Figs. S14–19 and Table S4).

### 3.4. Protein analysis in gradient reversed-phase chromatography mode

Protein analysis by HPLC is nowadays often based on C4-bonded silica columns [28]. A butyl-ligand provides usually sufficient retention and selectivity while C8 and C18 are often too hydrophobic imposing too strong retention, even on wide pore stationary phases with lower total surface area. A C4-SP synthesized in-house was therefore employed as a kind of benchmark for comparison. In reversed-phase chromatography of proteins, gradient elution is usually applied in order to overcome the strong adsorption of proteins due to their multipoint attachment as reflected by steep adsorption isotherms. It makes use of short columns possible or even advisable [41]. Here, 5 cm columns were used as a compromise. Acetonitrile was applied as organic modifier which supresses π-π-interactions between the analytes and the pyridine ligand of C8Pyr-SP [42]. Gradient elution RPLC of proteins makes typically use of acidic mobile phases, e.g. 0.1 % TFA, leading to denaturing of proteins. Moreover, elevated column temperatures (80–90 °C) are beneficial, since diffusion rates and (stationary phase) mass transfer are accelerated. Also secondary (silanophilic) interactions are diminished and consequently peak widths and tailing can be reduced. This could be confirmed in a preliminary test also for C8Pyr-SP varying column temperatures between 30 and 50 °C (see Fig. S20A). Therefore, in this work a temperature of 50 °C was selected as a compromise since column stability above 50 °C was still uncertain at the beginning of the study and it was desirable to perform a reasonable number of experiments without stationary phase degrading. In retrospect, however, both novel mixed-mode columns showed high chemical stability. No significant drop in performance was observed even after exposing the columns to highly aqueous mobile phase conditions (with varying pH values between 3 and 8 and water content up to 100 %) at elevated temperatures (up to 50 °C) for hundreds of experimental runs. Such good stability of current mixed-mode SPs stands in sharp contrast to classical aminopropyl-phases which are typically extremely susceptible to hydrolysis and suffer from short column lifetimes when applied to highly aqueous conditions [24,43]. More detailed studies on the hydrolytic stability of the current mixed-mode columns will be performed in future work to confirm this first impression.

A test mixture composed of 4 proteins (ribonuclease A, cytochrome C, myoglobin, and β-lactoglobulin) differing in hydrophobicity (as measured by the GRAVY scale) and isoelectric point (pI) was selected to study the retention characteristics of the C8Pyr-SP in comparison to C4-SP and C8APS-SP (Fig. 5). A total buffer concentration in the mobile phase of 20 mM ammonium formate was selected, as it showed better efficiency than lower concentrations (see Fig. S20B). As can be seen from Fig. 5A, at pH 3 the C4-SP shows a decent separation of the 4 proteins, yet poor peak shapes (especially for cyctochrome C; see also Fig. S21 and Table S5 for comparison with commercial C4 columns). Amongst the three tested SPs the C4-SP exhibited the strongest retention. It can be assumed that secondary interactions with silanols contribute to the stronger retention (since according to Fig. 3, the C4-SP has still slight net negative surface charge at low pH). At pH 3, at which all proteins were below their pI and hence net positively charged, the retention order follows largely their hydrophobicities on all three SPs (Fig. 5A). Thus, the more hydrophilic proteins ribonuclease A and cytochrome C eluted first on all columns at pH 3, whereas the less hydrophilic β-lactoglobulin eluted last. The C8Pyr-SP was designed to enforce electrostatic repulsion at low pH overcoming silanophilic interactions of proteins (repulsive charge-assisted RPLC). The chromatogram in Fig. 5A, pH 3, indeed allows to assume that this could be achieved. Retention is shorter, in spite

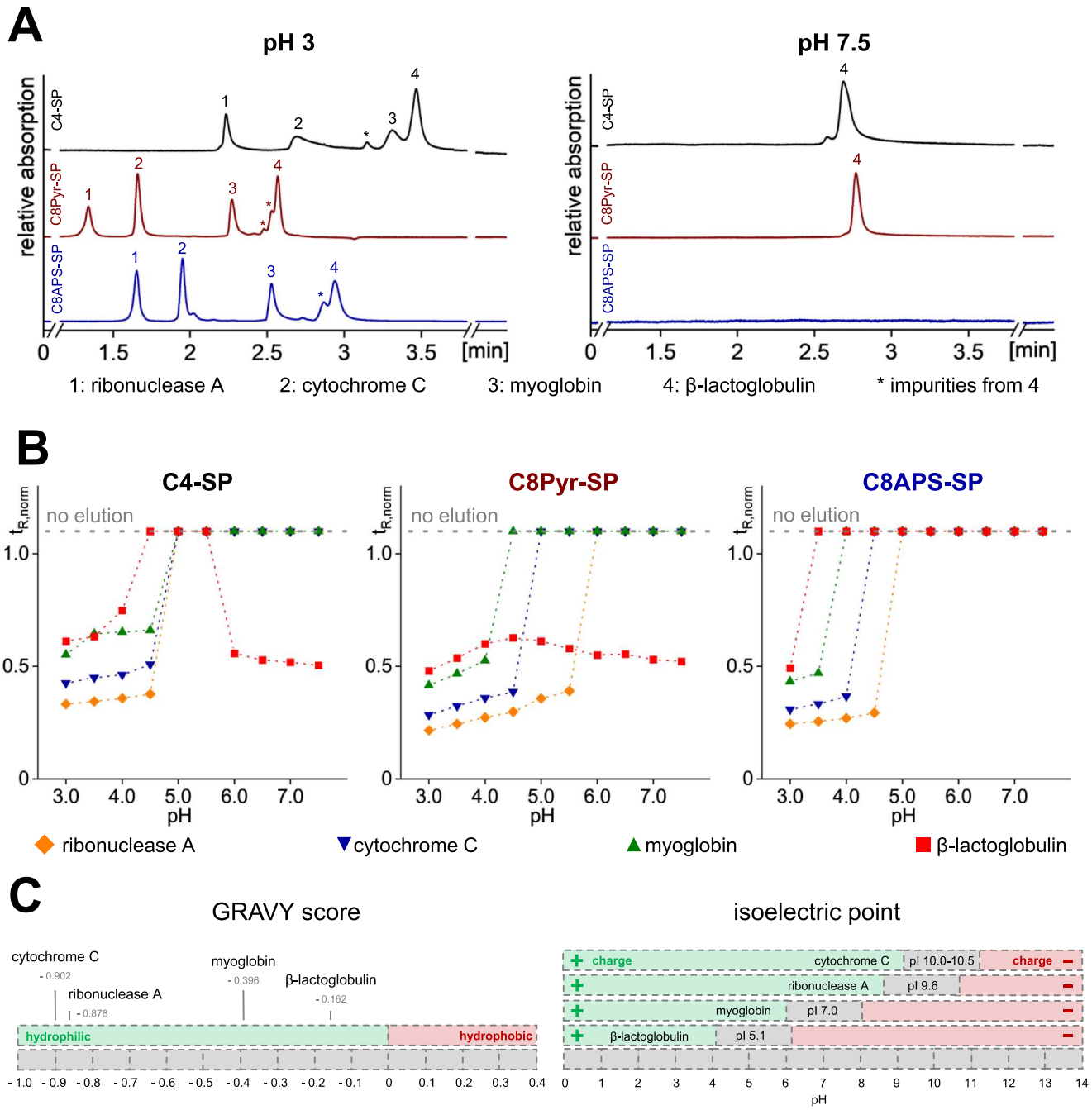


**Fig. 5.** Analysis of the protein mixture on C4-SP, C8Pyr-SP and C8APS-SP under acetonitrile-gradient elution reversed-phase HPLC conditions at different mobile phase pH values. Chromatographic conditions: mobile phase A (ACN/aqueous ammonium formate buffer with pH adjusted in the aqueous phase (10/90, v/v), total concentration $C_{tot}$ in the mixture 20 mM), mobile phase B (ACN/aqueous ammonium formate buffer with pH adjusted in the aqueous phase (90/10, v/v), $C_{tot}$= 20 mM), flow rate: 1 mL/min, temperature: 50 °C, gradient: 0 to 5 min: 0 % B to 100 % B. In A, chromatograms are illustrated for the analysis at constant pH 3 and constant pH 7.5. In B, gradient-time-normalized retention times ($t_{R,norm}$) for the different proteins were plotted against the mobile phase pH. In C, gravy scores and isoelectric points of the applied proteins are depicted [46].

of a higher carbon content and total ligand density, and peak shapes are significantly improved (in particular also for cytochrome C). On the other hand, at pH 3 retention was increased on C8APS-SP compared to C8Pyr-SP despite a lower C8 and a higher APS ligand density which would suggest the opposite trend (less hydrophobic retention, stronger repulsive interactions). In general, the C8APS-SP shows also quite good selectivity and improved peak shape compared to the C4-SP (Fig. 5A). Given these experimental results, it can be hypothesized that the APS ligands may be amenable to interactions with carboxylate groups on the proteins, even if the proteins are net positively charged (e.g. due to charge asymmetry [39]). Overall, it is striking that the retention was lowest on C8Pyr-SP, even though it has the highest carbon loading. Since hydrophobicity should increase with carbon loading, retention on C8Pyr-SP (2.7 wt% C) was expected to be stronger than on C8APS-SP (1.6 wt% C) or C4-SP (1.5 wt% C) (see Table S1). However, the pyridine moiety seems to be difficult to access for large molecules such as proteins due to shielding by the (relatively densely) embedded C8 ligands (compared to C8APS-SP) and may therefore be less available for hydrophobic interactions. As hydrophobic interactions can only occur in close proximity of hydrophobic moieties with alkyl ligands, protein

retention is consequently decreased.

In contrast, at pH 7.5, the retention behaviour of the analytes on the distinct SPs cannot be simply explained by stationary phase hydrophobicity. Only β-lactoglobulin, which was significantly above its pI by around 2 pH units, was eluted from C8Pyr-SP and C4-SP (both net negative surface charge according to Fig. 3), presumably driven by electrostatic repulsion. The other proteins had higher isoelectric points than β-lactoglobulin and were consequently overall positively charged (cytochrome C, ribonuclease A) or overall neutral (myoglobin) at pH 7.5, which caused irreversible adsorption by strong ionic and hydrophobic interactions simultaneously. From C8APS-SP there was no elution of any analyte observed at pH 7.5, although electrostatic repulsion was anticipated for cytrochrome C and ribonuclease A on the C8APS-SP at this pH.

In order to gain a more thorough understanding of pH effects, the retention behaviour of the proteins was also investigated at the pH values between pH 3 and 7.5 in steps of 0.5 pH units (Figs. 5B and S21). It becomes evident that the retention for all proteins on all columns increased steadily with pH until no elution was observed anymore. The single exception was β-lactoglobulin which ran through a maximum on C4-SP and C8Pyr-SP at around pH 4.5–5.0 followed by a slight decline in retention. It can be concluded that the new C8Pyr-SP, like the classical C4-SP, shows chromatographic utility for gradient RPLC protein separations in the acidic pH range. The repulsive interactions from the positively charged pyridine ring indeed could lead to a favourable peak shape due to electrostatic repulsions of net positive proteins (below their pI) and reduced silanol interactions (repulsive charge-assisted RPLC).

### *3.5. Protein analysis under hydrophobic charge-induction chromatography conditions*

It was anticipated that the C8Pyr-SP could be suited for HCIC due to the combination of its hydrophobic properties and the observed surface charge reversal at approximately pH 5.5. The question was whether this different chromatographic mode provides orthogonality in retention and selectivity, respectively, to above mentioned gradient RPLC. In HCIC, the analytes are usually adsorbed to the stationary phase by hydrophobic interactions in a first step. In a second step, the analytes are eluted from the stationary phase by electrostatic repulsion provoked by the change of the mobile phase pH.

The suitability of the C8Pyr-SP for this chromatographic mode was assessed by applying the same set of distinct proteins under HCIC elution conditions (see Fig. 6). Instead of an acetonitrile-gradient at constant pH, a pH gradient was run and the proportion of organic modifier kept constant (only 10 % acetonitrile). The organic modifier was added because initial experiments under purely aqueous conditions showed only elution for ribonuclease A. Surprisingly, the other proteins eluted earlier than ribonuclease A after adding the organic modifier. Starting from pH 7.5, the pyridine moieties of the stationary phase surface were initially not protonated and the proteins firstly adsorbed by hydrophobic interactions or electrostatic interactions with the ionized surface silanols, or both. Then, the pH was shifted to lower values, as the percentage of mobile phase B, which contained 0.1 % formic acid, was increased. As a result, the surface charge of the stationary phase as well as the net charge of the proteins gradually adopted positive values. Consequently, the proteins were eluted by electrostatic repulsion at lower pH values depending on their pI. Interestingly, the elution order was reversed compared to (repulsive charge-assisted) gradient reversed-phase LC conditions at low pH (shown in Fig. 5). Here, the elution order derived from complex interactions of the different charge states of the proteins and the stationary phase. These charge states changed constantly during the chromatographic run depending on the pH value of the actual mobile phase. β-Lactoglobulin had the lowest isoelectric point (pI = 5.1) of the four test proteins. It is similar to the pI of the C8Pyr-SP surface and corresponds closely to the pH (5.5) at which polarity reversal was observed in Fig. 3. Therefore, this protein experienced electrostatic repulsion first amongst all 4 test proteins during the chromatographic run and eluted consequently first. This repulsion was initially probably provoked by negative charges of the protein (at pH 7.5) and the ionized silanols and afterwards caused by positive charges of the protein and the pyridine moieties. Myoglobin, in contrast, had an isoelectric point of approximately 7 and was close to its pI at the beginning of the gradient. Therefore, it did not experience electrostatic repulsion at the beginning of the gradient elution unlike β-lactoglobulin and eluted second.

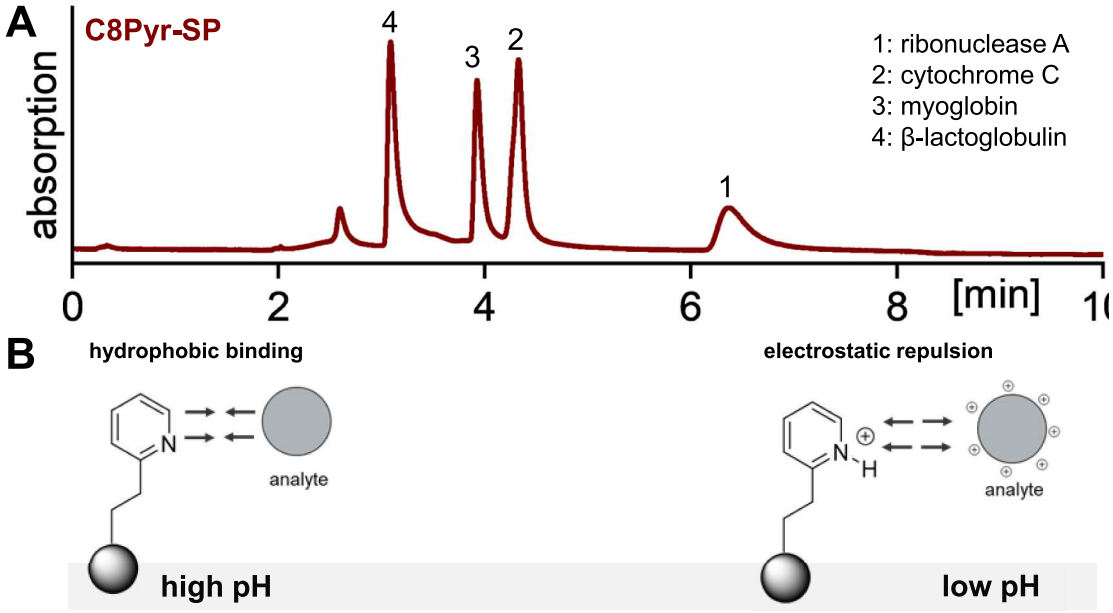


**Fig. 6.** Protein analysis under HCIC conditions on C8Pyr-SP. In A, the obtained chromatogram of protein-HCIC is illustrated. The chromatographic conditions were the following: mobile phase A (ACN/aqueous ammonium formate buffer (10/90, v/v) with pH adjusted to 7.5 in the aqueous phase, $C_{tot}$ = 20 mM), mobile phase B (ACN/water/formic acid (10/90/0.1, v/v/v)), flow rate: 1 mL/min, temperature: 50 °C, gradient: 0 to 5 min, 0 % B to 100 % B, and 5 to 10 min, 100 % B. In B, the principle of HCIC is illustrated. Initially, the analytes adsorb to the stationary phase and were subsequently repelled from the stationary phase by electrostatic repulsion generated by pH switch of the mobile phase.

However, cytochrome C and ribonuclease A were already overall positively charged initially and were adsorbed to the stationary phase by hydrophobic and electrostatic interactions. The elution of these proteins therefore only took place after the stationary phase changed its charge state to positive values. Hence, these proteins eluted last but not simultaneously. The differences in the retention times of these two proteins might originate from slight differences in hydrophobicity or pI or by spatial effects causing distinct accessibility of these interaction sites.

Conclusively, all four proteins were successfully separated under HCIC conditions proving the suitability of the novel C8Pyr-SP for such HCIC-type protein separations with strongly orthogonal retention and selectivity as documented by a reversed elution order. As this chromatographic mode does not elute with an organic modifier gradient but a pH switch, it requires less organic solvent and can therefore be considered a greener technology of protein HPLC. Hence, the HCIC experiments (Figs. 6 and S23) used 5 times less organic modifier per minute run time than the experiments with organic modifier gradient (Fig. 5).

## 4. Conclusions

In this study, a novel mixed-mode-SP with pH-dependent surface charge reversal for hydrophobic charge induction chromatography was developed. It is based on a mixed-ligand approach of which one is an octyl and the other one a 2-pyridylethyl ligand. As a result, the developed phase can change its ionization state at around pH 5.5 from positive surface charge, due to protonated pyridyl groups at lower pH, to negative net charge at higher pH, due to deprotonation of pyridyl groups and ionization of residual silanols. Besides, two other stationary phases were synthesized for comparison. Thus, a classical butyl-bonded RP-SP and another mixed-mode octyl/3-aminopropyl-bonded RP/WAX-SP with positively charged surface over the entire pH-range available for silica-based phases were prepared. Both mixed-mode stationary phases were synthesized by a new approach utilizing silatranes and prewetted silica for surface functionalization providing denser surface coverage due to a polymeric siloxane bonding on the silica surface. In contrast, the reversed-phase C4-SP column was prepared by a conventional approach using a trialkoxysilane as silica functionalization agent. As a result, the silatrane-derived stationary phases exhibited a higher percentage of trifunctional bonded ligands than the RP-C4-SP, as proven by $^{29}$Si CP/MAS NMR experiments. The mixed-mode-SPs differed especially in acido-basic characteristics due to dissimilar basicities of the embedded WAX-type ligands, due to unequal ligand densities and different amount of residual silanols. On all three phases, a set of proteins differing in hydrophobicities and isoelectric points was successfully separated by denaturing organic modifier-gradient reversed-phase chromatography mode (repulsive charge-assisted RPLC). Finally, the suitability of the octyl/pyridyl-bonded SP with pH-dependent surface charge reversal for hydrophobic charge induction chromatography was examined. The test set of proteins could be successfully separated under HCIC conditions with orthogonal retention profile and reversed elution order compared to gradient RP-HPLC. Since employed HCIC conditions only required 10 % acetonitrile and elution was not depending on increase of organic solvent but by pH-switch, it represents a green methodology of protein HPLC. The method performance was reasonable, although no endcapping has been performed, no bioinert column hardware was employed and column temperatures were far from the optimum. Future work will focus on use of core-shell particle technology, stability at high temperature (80–90 °C), optimization of co-ligand ratio and alkyl chain length and further exploration of the HCIC mode for protein separations.

## CRediT authorship contribution statement

**Marc Wolter:** Writing – review & editing, Writing – original draft, Visualization, Supervision, Methodology, Investigation, Formal analysis, Data curation, Conceptualization. **Christoph Barth:** Investigation. **Mirna Maalouf:** Investigation. **Markus Kramer:** Writing – review & editing, Methodology, Investigation. **Adrian Sievers-Engler:** Writing – review & editing, Supervision. **Michael Lämmerhofer:** Writing – review & editing, Supervision, Resources, Project administration, Methodology, Conceptualization.

## Declaration of competing interest

The authors declare that they have no known competing financial interests or personal relationships that could have appeared to influence the work reported in this paper.

The author is an Editorial Board Member for *Journal of Chromatogr A* and was not involved in the editorial review or the decision to publish this article.

## Supplementary materials

Supplementary material associated with this article can be found, in the online version, at doi:10.1016/j.chroma.2024.465429.

## Data availability

Data will be made available on request.

## References

[1] A. Beck, E. Wagner-Rousset, D. Ayoub, A. Van Dorsselaer, S. Sanglier-Cianférani, Characterization of therapeutic antibodies and related products, Anal. Chem. 85 (2013) 715–736.
[2] S.X. Liu, Z.H. Li, B. Yu, S. Wang, Y.Q. Shen, H.L. Cong, Recent advances on protein separation and purification methods, Adv. Colloid Interfaces 284 (2020).
[3] J.Z. Wang, J.S. Wang, X.H. Ning, J.W. Liu, H.J. Xia, G.P. Wan, Q. Bai, pH-dependent selective separation of acidic and basic proteins using quaternary ammoniation functionalized cysteine-zwitterionic stationary phase with RPLC/IEC mixed-mode chromatography, Talanta 225 (2021).
[4] Q. Bai, Y.N. Liu, Y.X. Wang, K.L. Zhao, F. Yang, J.W. Liu, J.W. Shen, Q.Y. Zhao, Protein separation using a novel silica-based RPLC/IEC mixed-mode stationary phase modified with N-methylimidazolium ionic liquid, Talanta 185 (2018) 89–97.
[5] Y. Yang, X.D. Geng, Mixed-mode chromatography and its applications to biopolymers, J. Chromatogr. A 1218 (2011) 8813–8825.
[6] K.L. Zhao, F. Yang, H.J. Xia, F. Wang, Q.G. Song, Q. Bai, Preparation of a weak anion exchange/hydrophobic interaction dual-function mixed-mode chromatography stationary phase for protein separation using click chemistry, J. Sep. Sci. 38 (2015) 703–710.
[7] S. Tengattini, G. Massolini, F. Rinaldi, E. Calleri, C. Temporini, Hydrophilic interaction liquid chromatography (HILIC) for the analysis of intact proteins and glycoproteins, Trac-Trend Anal. Chem. 174 (2024).
[8] S. Fekete, D. Guillarme, Ultra-high-performance liquid chromatography for the characterization of therapeutic proteins, Trac-Trend Anal. Chem. 63 (2014) 76–84.
[9] A.M. Ramos-de-la-Peña, J. González-Valdez, O. Aguilar, Protein A chromatography: challenges and progress in the purification of monoclonal antibodies, J. Sep. Sci. 42 (2019) 1816–1827.
[10] V. Amritkar, S. Adat, V. Tejwani, A. Rathore, R. Bhambure, Engineering protein A for high-throughput affinity purification of monoclonal antibodies, Biotechnol. Adv. 44 (2020).
[11] J.J. Milne, Mixed-mode chromatography and its role in monoclonal antibody purification, in: S.T. Loughran, J.J. Milne (Eds.), Protein Chromatography: Methods and Protocols, Springer US, New York, NY, 2023, pp. 15–29.
[12] G.F. Zhao, X.Y. Dong, Y. Sun, Ligands for mixed-mode protein chromatography: principles, characteristics and design, J. Biotechnol. 144 (2009) 3–11.
[13] M.T. Li, Q.L. Zhang, D.Q. Lin, S.J. Yao, Development and application of hydrophobic charge-induction chromatography for bioseparation, J. Chromatogr. B 1134 (2019).
[14] H. Bak, O.R.T. Thomas, Hydrophobic charge induction chromatography for the purification of polyclonal antibodies from clarified rabbit antisera, J. Biotechnol. 131 (2007) S130–S131.
[15] E. Boschetti, D. Judd, W.E. Schwartz, P. Tunon, Hydrophobic charge-induction chromatography - method has some advantages over traditional antibody production methods, Genet. Eng. News 20 (2000) 34. -+.
[16] E. Boschetti, Antibody separation by hydrophobic charge induction chromatography, Trends Biotechnol. 20 (2002) 333–337.
[17] S. Ghose, B. Hubbard, S.M. Cramer, Protein interactions in hydrophobic charge induction chromatography (HCIC), Biotechnol. Prog. 21 (2005) 498–508.
[18] W. Schwartz, D. Judd, M. Wysocki, L. Guerrier, E. Birck-Wilson, E. Boschetti, Comparison of hydrophobic charge induction chromatography with affinity chromatography on protein A for harvest and purification of antibodies, J. Chromatogr. A 908 (2001) 251–263.

[19] J.L. Ye, Y.F. Zhang, J.Q. Meng, Protein-Ligand interactions for hydrophobic charge-induction chromatography: a QCM-D study, Appl. Surf. Sci. 572 (2022).
[20] G.F. Zhao, F.Q. Li, G.Y. Peng, Q.H. Shi, Y. Sun, A new ligand for hydrophobic charge induction chromatography, J. Biotechnol. 136 (2008). S29-S29.
[21] W. Shi, S.Q. Zhang, K.B. Li, X.B. Zhang, C.Y. Fang, T.Y. Zhang, D.M. Han, Enhancing the performance limits of hydrophobic charge-induction chromatography with the introduction of a second ligand, Biochem. Eng. J. 209 (2024).
[22] W. Shi, T.Y. Zhang, C.Y. Fang, S.Q. Zhang, K.B. Li, X.B. Zhang, D.M. Han, Transforming waste into valuables: preparation and evaluation of dual-ligand hydrophobic charge-induction chromatography using two poor performing ligands, J. Chromatogr. A 1726 (2024).
[23] C. Geibel, J. Theiner, M. Wolter, M. Kramer, W. Lindner, M. Lämmerhofer, Controllable organosilane monolayer density of surface bonding using silatranes for thiol functionalization of silica particles for liquid chromatography and validation of microanalytical method for elemental composition determination, J. Chromatogr. A 1653 (2021).
[24] M. Wolter, C. Geibel, M. Olfert, M. Su, W. Bicker, M. Kramer, W. Lindner, M. Lämmerhofer, Development and chromatographic exploration of stable-bonded cross-linked amino silica against classical amino phases, J. Sep. Sci. 45 (2022) 3286–3300.
[25] M. Wolter, X.Y. Chen, U. Woiwode, C. Geibel, M. Lämmerhofer, Preparation and characterization of poly(3-mercaptopropyl)methylsiloxane functionalized silica particles and their further modification for silver ion chromatography and enantioselective high-performance liquid chromatography, J. Chromatogr. A 1643 (2021).
[26] S.A. Schuster, B.M. Wagner, B.E. Boyes, J.J. Kirkland, Optimized superficially porous particles for protein separations, J. Chromatogr. A 1315 (2013) 118–126.
[27] W. Chen, K.Q. Jiang, A. Mack, B. Sachok, X. Zhu, W.E. Barber, X.L. Wang, Synthesis and optimization of wide pore superficially porous particles by a one-step coating process for separation of proteins and monoclonal antibodies, J. Chromatogr. A 1414 (2015) 147–157.
[28] S. Jaag, C.M. Wen, B. Peters, M. Lammerhofer, Kinetic performance comparison of superficially porous, fully porous and monolithic reversed-phase columns by gradient kinetic plots for the separation of protein biopharmaceuticals, J. Chromatogr. A 1676 (2022).
[29] P. VanDerVoort, E.F. Vansant, Silylation of the silica surface a review, J. Liq. Chromatogr. Relat. Technol. 19 (1996) 2723–2752.
[30] K. Albert, E. Bayer, Characterization of bonded phases by solid-state Nmr-spectroscopy, J. Chromatogr. 544 (1991) 345–370.
[31] C. Hellriegel, U. Skogsberg, K. Albert, M. Lämmerhofer, N.M. Maier, W. Lindner, Characterization of a chiral stationary phase by HR/MAS NMR spectroscopy and investigation of enantioselective interaction with chiral ligates by transferred NOE, J. Am. Chem. Soc. 126 (2004) 3809–3816.
[32] S. Sok, M.S. Gordon, A of protons: a theoretical study on the hydrolysis mechanism of 1-substituted silatranes and their protonated analogs, Comput. Theor. Chem. 987 (2012) 2–15.
[33] L.S. Shlyakhtenko, A.A. Gall, A. Filonov, Z. Cerovac, A. Lushnikov, Y. L. Lyubchenko, Silatrane-based surface chemistry for immobilization of DNA, protein-DNA complexes and other biological materials, Ultramicroscopy 97 (2003) 279–287.
[34] C. Geibel, M. Kramer, M. Laemmerhofer, Study of microheterogeneity of silatrane-based silica surface bonding chemistry and its optimization for the synthesis of chiral stationary phases for enantioselective liquid chromatography, J. Chromatogr. A 1674 (2022).
[35] O.L.S. Muñoz, E.P. Hernández, M. Lämmerhofer, W. Lindner, E. Kenndler, Estimation and comparison of ζ-potentials of silica-based anion-exchange type porous particles for capillary electrochromatography from electrophoretic and electroosmotic mobility, Electrophoresis 24 (2003) 390–398.
[36] S. Bäurer, S. Polnick, O.L. Sánchez-Muñoz, M. Kramer, M. Lämmerhofer, N-Propyl-N'-2-pyridylurea-modified silica as mixed-mode stationary phase with moderate weak anion exchange capacity and pH-dependent surface charge reversal, J. Chromatogr. A 1560 (2018) 45–54.
[37] A. Habibi-Yangjeh, E. Pourbasheer, M. Danandeh-Jenagharad, Prediction of basicity constants of various pyridines in aqueous solution using a principal component-genetic algorithm-artificial neural network, Monatsh. Chem. 139 (2008) 1423–1431.
[38] S. Bocian, B. Buszewski, Residual silanols at reversed-phase silica in HPLC - a contribution for a better understanding, J. Sep. Sci. 35 (2012) 1191. --+.
[39] W. Kopaciewicz, M.A. Rounds, J. Fausnaugh, F.E. Regnier, Retention model for high-performance ion-exchange chromatography, J. Chromatogr. 266 (1983) 3–21.
[40] R.R. Drager, F.E. Regnier, Application of the stoichiometric displacement model of retention to anion-exchange chromatography of nucleic-acids, J. Chromatogr. 359 (1986) 147–155.
[41] S. Fekete, B. Bobály, J.M. Nguyen, A. Beck, J.L. Veuthey, K. Wyndham, M. A. Lauber, D. Guillarme, Use of ultrashort columns for therapeutic protein separations. part 1: theoretical considerations and proof of concept, Anal. Chem. 93 (2021) 1277–1284.
[42] M. Yang, S. Fazio, D. Munch, P. Drumm, Impact of methanol and acetonitrile on separations based on π-π interactions with a reversed-phase phenyl column, J. Chromatogr. A 1097 (2005) 124–129.
[43] M. Etienne, A. Walcarius, Analytical investigation of the chemical reactivity and stability of aminopropyl-grafted silica in aqueous medium, Talanta 59 (2003) 1173–1188.
[44] B. Buszewski, M. Jackowska, S. Bocian, E. Dziubakiewicz, Application of the zeta potential for stationary phase characterization in ion chromatography, J. Sep. Sci. 36 (2013) 156–163.
[45] C. Kulsing, Y.Z. Yang, C. Munera, C. Tse, M.T. Matyska, J.J. Pesek, R.I. Boysen, M. T.W. Hearn, Correlations between the zeta potentials of silica hydride-based stationary phases, analyte retention behaviour and their ionic interaction descriptors, Anal. Chim. Acta 817 (2014) 48–60.
[46] S. Jaag, M. Shirokikh, M. Lämmerhofer, Charge variant analysis of protein-based biopharmaceuticals using two-dimensional liquid chromatography hyphenated to mass spectrometry, J. Chromatogr. A 1636 (2021).

## XI.2 Publication VI – Supplementary Material

# Wide-pore fully porous mixed-mode octyl/pyridyl-bonded silica material with pH-dependent surface charge reversal for high-performance hydrophobic charge-induction chromatography of proteins

**Marc Wolter** [1], Christoph Barth [1], Mirna Maalouf [1], Markus Kramer [2], Adrian Sievers-Engler [1], Michael Lämmerhofer [1, *]

[1] Institute of Pharmaceutical Sciences, Pharmaceutical (Bio-)Analysis, University of Tübingen, Auf der Morgenstelle 8, 72076 Tübingen, Germany
[2] Institute of Organic Chemistry, University of Tübingen, Auf der Morgenstelle 18, 72076 Tübingen, Germany
* corresponding author

# Table of contents

- Figure S13 Exploration of the surface charge and ion exchange characteristics of C8APS-SP at different pH values and ionic strengths of the mobile phase.
- Table S3 Chromatographic parameters obtained from analysis of amino acid derivatives.

**PART V: Stationary phase classification by multivariate data analysis**

- Figure S14 Score plot for stationary phase classification.
- Figure S15 Loadings scatter plot of PCA.
- Figure S16 Surface chemistries of commercial and in-house prepared columns used for stationary phase classification by PCA.
- Figure S17 Analytes applied for RPLC test.
- Figure S18 Analytes applied for HILIC test.
- Figure S19 Chromatograms obtained from RPLC and HILIC test.
- Table S4 Retention factors obtained from RPLC and HILIC test for in-house prepared and commercial columns used for PCA.

**PART VI: High-performance liquid chromatography of proteins**

- Figure S20 Influence of temperature and buffer concentration on retention of proteins on C8Pyr-SP under gradient reversed phase chromatography conditions.
- Figure S21 Comparison of C4-SP and commercial Acquity BEH C4 and Solas C4.
- Table S5 Gradient-time-normalized retention times for the four test proteins under gradient reversed phase conditions.
- Figure S22 Analysis of a protein mixture on C4-SP, C8Pyr-SP and C8APS-SP under gradient reversed phase chromatography conditions at different mobile phase pH values.
- Figure S23 Protein analysis under HCIC conditions on C8Pyr-SP at different starting pH values of the mobile phase.

**PART VII: References**

## PART I: Synthesis of silatranes

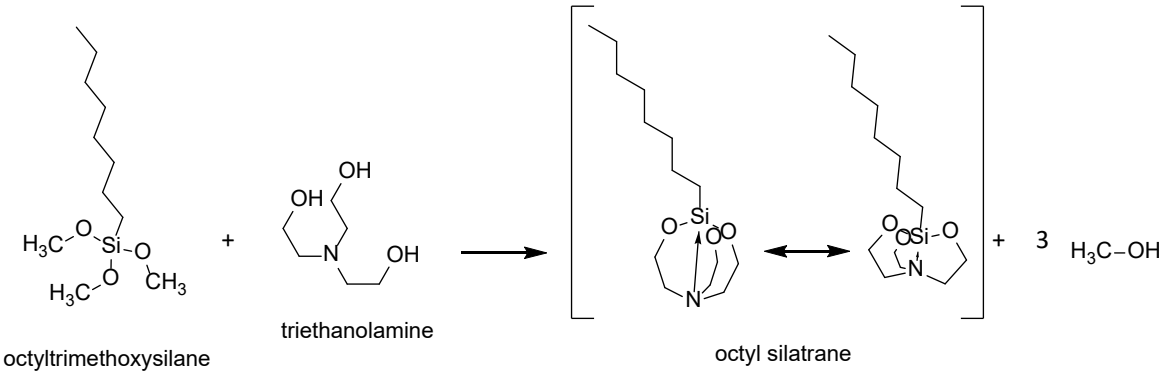


**Fig. S1.** Reaction scheme for synthesis of octyl silatrane. The condensation reaction between octyltrimethoxysilane and triethanolamine results in the formation of octyl silatrane. The synthesis procedure is described in the main document. The yield was 82 % and synthesis control was carried out by nuclear magnetic resonance (NMR) analysis revealing a product purity of 98 % according to $^{1}$H-NMR data. The corresponding NMR spectra are depicted in Fig. S3.

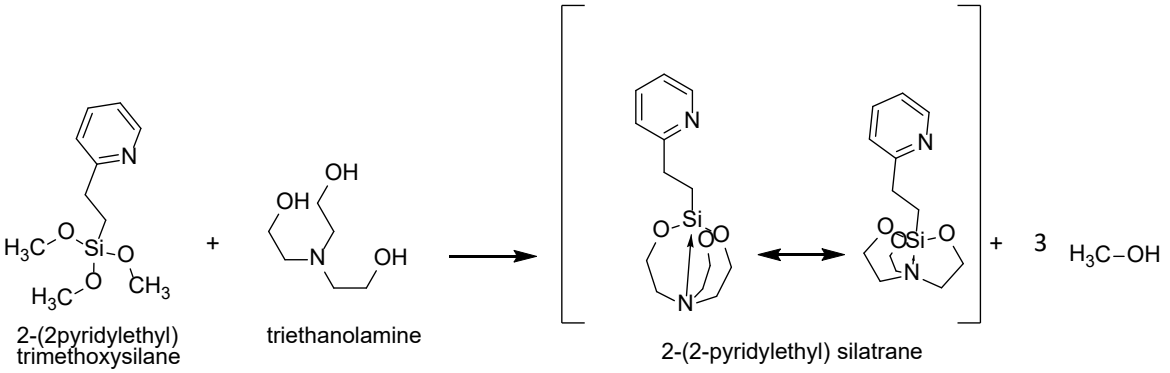


**Fig. S2.** Reaction scheme for synthesis of 2-(2-pyridylethyl) silatrane. The condensation reaction between 2-(2-pyridylethyl)trimethoxysilane and triethanolamine results in the formation of 2-(2-pyridylethyl) silatrane. The synthesis procedure is described in the main document. According to $^{1}$H-NMR analysis the purity was 99 %. The yield was 47 % of the theoretical yield and synthesis control was carried out by $^{1}$H- and $^{13}$C-NMR analysis. The corresponding NMR spectra are depicted in Fig. S4.

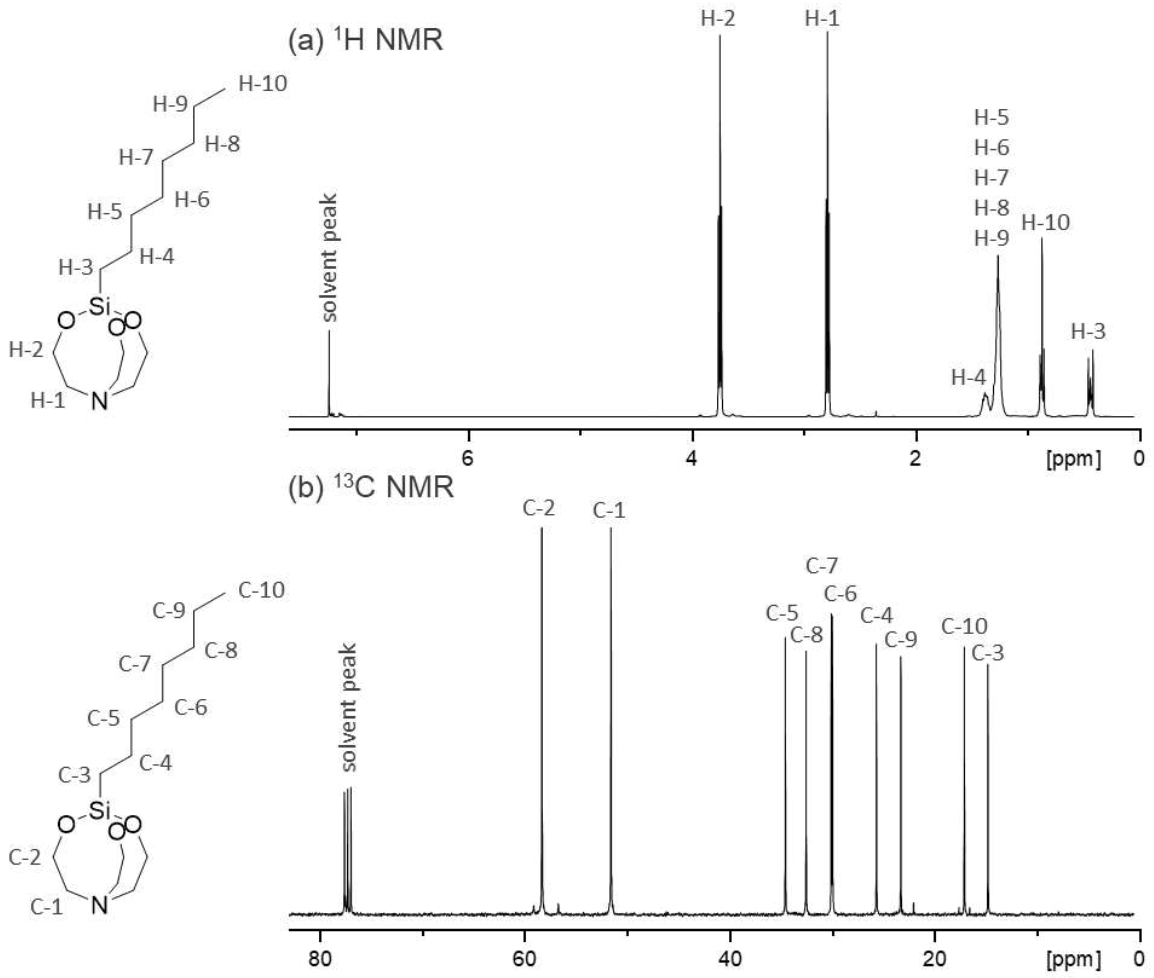


**Fig. S3.** NMR spectra of octyl silatrane. (a) $^{1}H$ NMR spectrum (($J_t$ [Hz]), $CDCl_3$, 400 MHz): δ 0.38-0.42 ppm (m, 2H), 0.81-0.85 ppm (m, 3H), 1.17-1.29 ppm (m, 10H), 1.29-1.39 ppm (m, 2H), 2.77 ppm (t, Jt = 5.82, 6H), 3.73 ppm (t, Jt = 5.82, 6H); (b) $^{13}C$ NMR ($CDCl_3$, 100.6 MHz): δ 14.34ppm (1C), 16.64 ppm (1C), 22.91 ppm (1C), 25.73 ppm (1C), 29.61 ppm (1C), 29.74 ppm (1C), 32.21 ppm (1C), 34.24 ppm (1C), 51.41 ppm (3C), 58.18 ppm (3C). NMR spectra were calibrated to the solvent peaks with δ($^{1}H$) = 7.24 ppm and δ($^{13}C$) = 77.23 ppm [1].

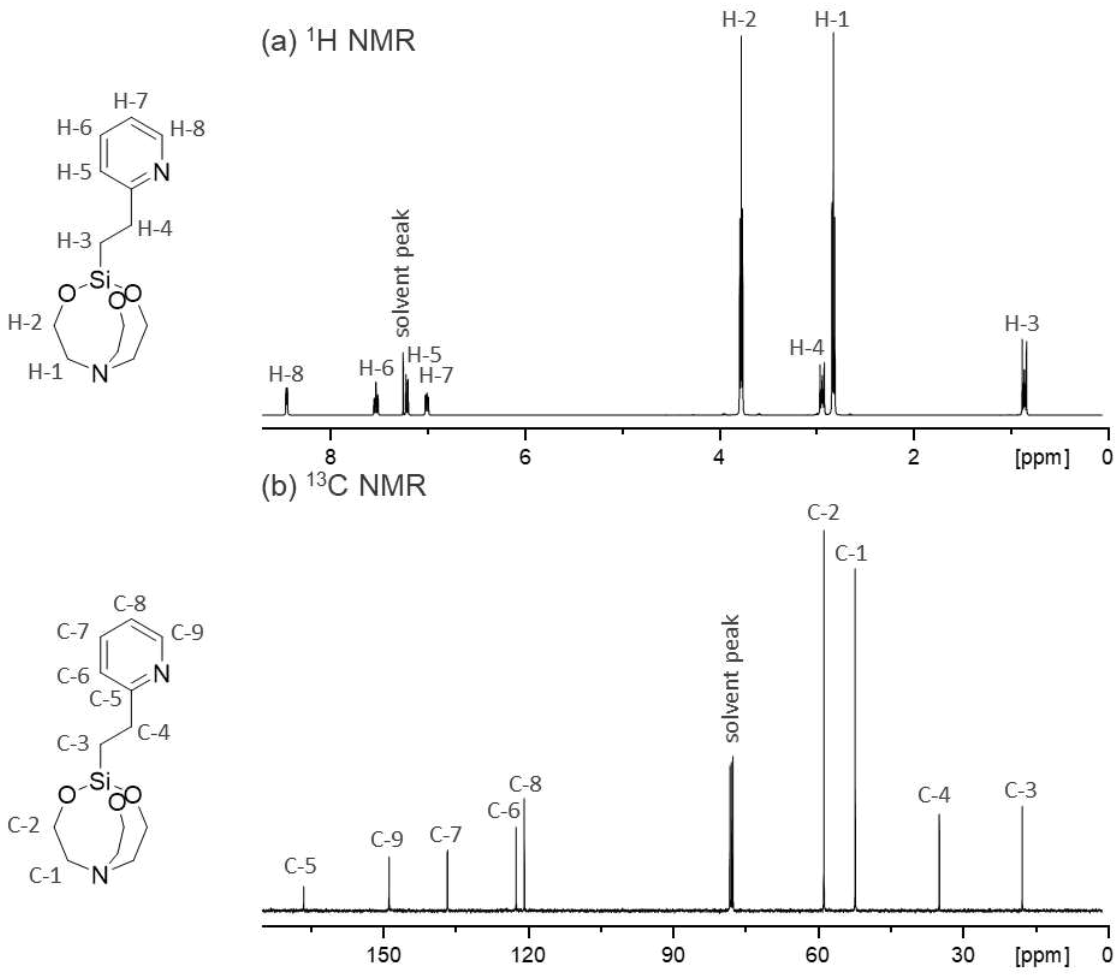


**Fig. S4.** NMR spectra of 2-(2-pyridylethyl) silatrane. (a) $^{1}$H NMR spectrum (($J_t$ [Hz]), $CDCl_3$, 400 MHz): δ 0.78-0.83 ppm (m, 2H), 2.77 ppm (t, Jt = 5.82, 6H), 2.87-2.92 ppm (m, 2H), 3.73 ppm (t, Jt = 5.82, 6H), 6.97-7.01 ppm (m, 1H), 7.18-7.21 ppm (m, 1H), 7.49-7.54 ppm (m, 1H), 8.43-8.46 ppm (m, 1H); (b) $^{13}$C NMR ($CDCl_3$, 100.6 MHz): δ 16.61 ppm (1C), 33.89 ppm (1C), 51.43 ppm (3C), 57.96 ppm (3C), 120.36 ppm (1C), 122.11 ppm (1C), 136.42 ppm (1C), 148.59 ppm (1C), 166.36 ppm (1C). NMR spectra were calibrated to the solvent peaks with δ($^{1}$H) = 7.24 ppm and δ($^{13}$C) = 77.23 ppm [1].

## PART II: Characterization of modified silica particles via EA and NMR

**Table S1.** Elemental analysis results and calculated ligand densities for C4-SP, C8Pyr-SP and C8APS-SP.

**Elemental analysis results**

| SP | C[1] [w-%] | H[1] [w-%] | N[1] [w-%] | S[1] [w-%] |
|---|---|---|---|---|
| C4-SP | 1.462 ± 0.040 | 0.449 ± 0.010 | < 0.03 | < 0.02 |
| C8Pyr-SP | 2.650 ± 0.020 | 0.556 ± 0.019 | 0.229 ± 0.005 | < 0.02 |
| C8APS-SP | 1.580 ± 0.020 | 0.479 ± 0.009 | 0.346 ± 0.009 | < 0.02 |

**Calculated ligand densities**

| SP | N[2] [µmol/m$^2$] | C[2] [µmol/m$^2$] | N-ligand[2] [µmol/m$^2$] | $C_8$-ligand[2] [µmol/m$^2$] | $C_4$-ligand[2,3] [µmol/m$^2$] | total ligand coverage[2] [µmol/m$^2$] |
|---|---|---|---|---|---|---|
| C4-SP | - | 9.72 | - | - | 2.43 | 2.43 |
| C8Pyr-SP | 1.63 | 22.06 | 1.63 | 1.33 | - | 2.96 |
| C8APS-SP | 2.47 | 13.15 | 2.47 | 0.72 | - | 3.19 |

[1] determined by elemental analysis
[2] calculated based on elemental analysis data
[3] assuming bifunctional bonding

## PART III: Silanization using silatranes

### Synthesis overview

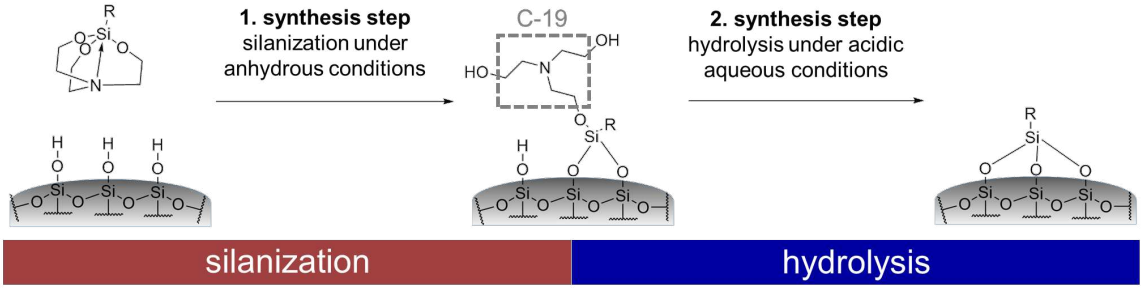


### Elemental analysis

| after silanization | | after hydrolysis | |
|---|---|---|---|
| **2step-C8Pyr-SP** | **2step-C8APS-SP:** | **2step-C8Pyr-SP** | **2step-C8APS-SP:** |
| C [w-%]: 2.650 ± 0.020 | C [w-%]: 1.340 ± 0.003 | C [w-%]: 2.017 ± 0.006 | C [w-%]: 1.258 ± 0.005 |
| H [w-%]: 0.556 ± 0.019 | H [w-%]: 0.402 ± 0.016 | H [w-%]: 0.426 ± 0.010 | H [w-%]: 0.376 ± 0.005 |
| N [w-%]: 0.260 ± 0.003 | N [w-%]: 0.358 ± 0.008 | N [w-%]: 0.229 ± 0.005 | N [w-%]: 0.322 ± 0.006 |

### $^{13}$C CP/MAS NMR

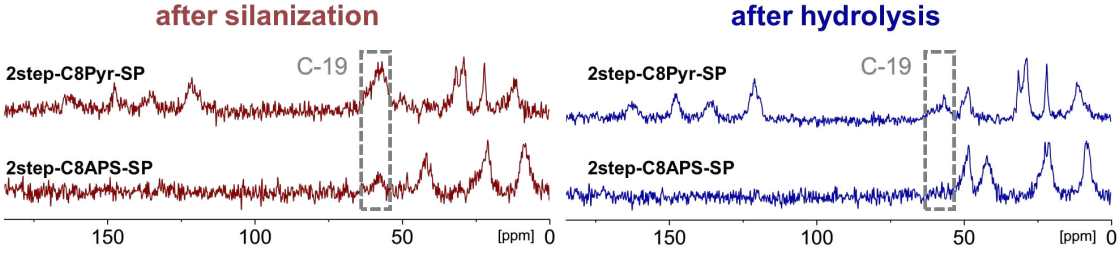


### $^{29}$Si CP/MAS NMR

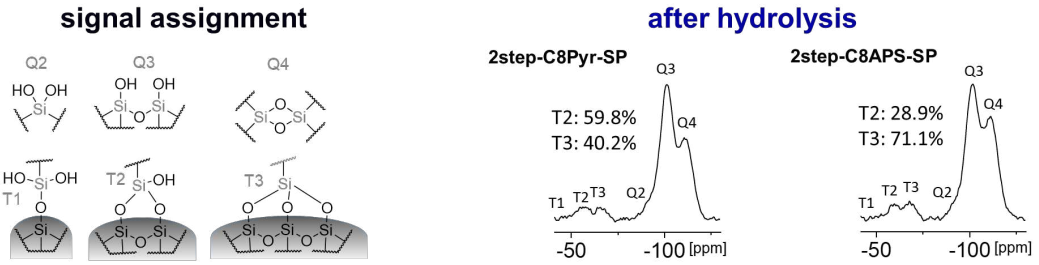


**Fig. S5.** Two-step synthesis approach for silatrane-modified silica. Prior to preparation of C8Pyr-SP and C8APS-SP according to the procedure described in the main document, synthesis of both stationary phases was performed by a two-step synthesis approach resulting in 2step-C8Pyr-SP and 2step-C8APS-SP [1, 2]. In this approach, the silanization reaction was conducted in anhydrous toluene, leading to a surface bonding in which the triethanolamine residue remained

attached to the immobilized silane in the first step. Therefore, an acidic hydrolysis step was required to remove the surface-bound triethanolamine moiety in a second step. The synthesis procedure was the following: 1 g bare silica particles were suspended in 20 mL anhydrous toluene within a 100 mL triple neck flask. After adding (3-aminopropyl) silatrane or 2-(2-pyriylethyl) silatrane (2 µmol per $m^2$) and octyl silatrane (6 µmol per $m^2$) and 4-dimethylaminopyridine (10 mol % related to silatrane content) a reflux condenser equipped with a nitrogen supply and a mechanical stirrer were attached to the flask and the system was flushed with nitrogen for 10 min. Afterwards, the reaction vessel was heated up to reflux and the reaction was allowed to proceed for 3 h under nitrogen atmosphere. Hereafter, the reaction product was transferred to a glass funnel of porosity 5, washed with boiling methanol and boiling toluene three times each and dried in a vacuum chamber for 12 h at 60 °C. Then, the modified silica particles were treated with a mixture of methanol, water and formic acid (20/80/0.1; v/v/v; 50 mL) under reflux for 2 h. Thereafter, the silica was washed again with hot methanol and hot toluene three times each and dried in a vacuum chamber at 60 °C.

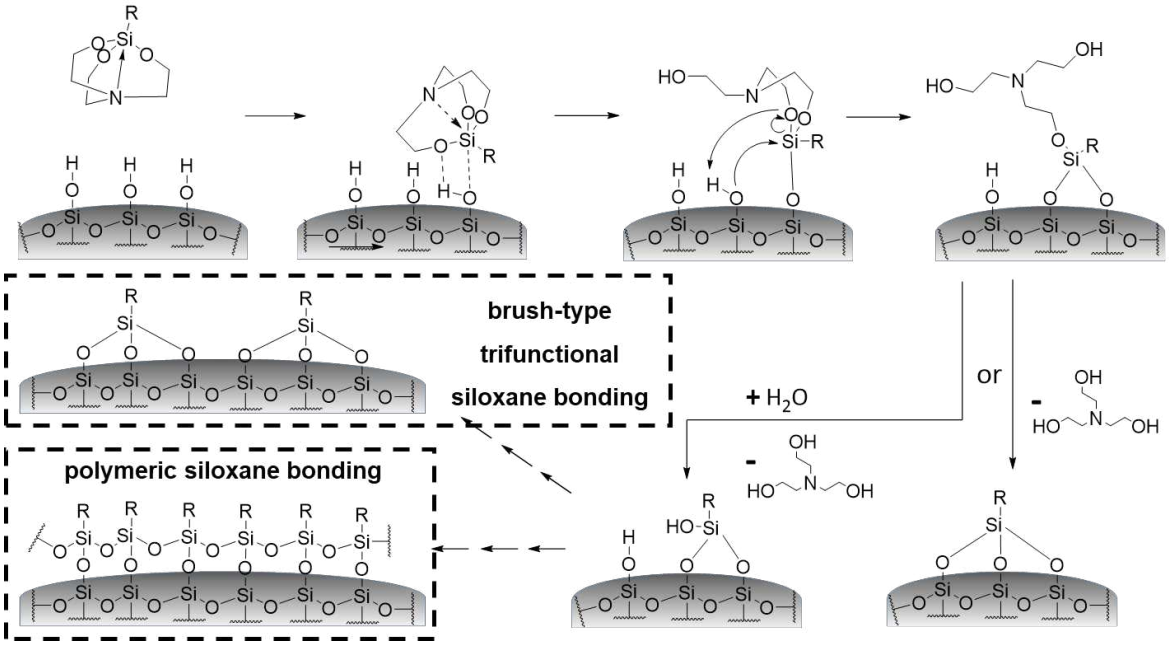


**Fig. S6.** Proposed mechanism of acid-catalyzed silica surface functionalization by silatranes on humidified silica. The silanols on the surface act as catalyst facilitating nucleophilic substitution reaction at the silicon [3]. Typically, silatranes are not prone

to nucleophilic attacks, since the transannular donor-acceptor N→Si bond increases the electron density at the silicon. However, next to acidic environments the reactivity of silatranes increases significantly due to the oxygen atoms´ proton affinity [4]. By this means the formation of a polarized hydrogen-bond complex between the silanol and the Si-O bond of the silatrane becomes feasible making its linking to the surface in a concerted nucleophilic substitution reaction subsequently happen. With this reaction, protonation of the oxygen can occur first alike making the silatrane´s silicon atom susceptible to the ensuing nucleophilic attack of the silanol groups as well. Both processes lead to the same outcome [5]. Although the proposed mechanism would allow the complete cleavage of the triethanolamine group without water, it has been found that water is usually required for full cleavage [1,2]. Two possibilities are conceivable for the linkage of the silanization agents on the silica surface: i) a brush-type trifunctional siloxane bonding, and ii) a polymeric siloxane bonding.

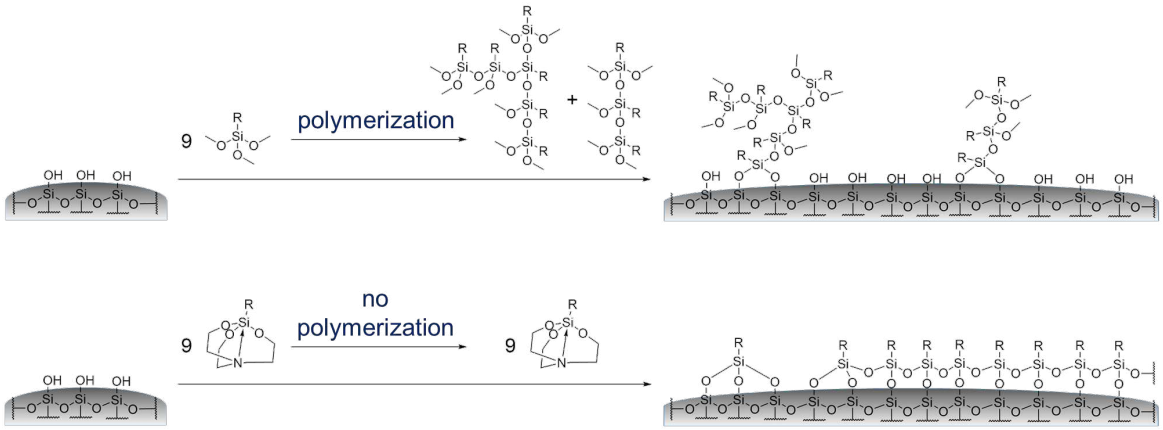


**Fig. S7.** Silanization: Alkoxysilanes vs. silatranes. Silanization using alkoxysilanes or silatranes leads to distinct properties of the ligand films created on the silica surface. During silanization with alkoxysilanes, polymerization of alkoxysilanes in solution takes place in presence of water leading to the formation of a disordered functional layer on the silica surface. In contrast, silatranes are not prone to polymerization in solution which leads to a thin, homogenous polysiloxane layer of ligands on the silica surface [1].

## PART IV: Surface charge of modified silica particles

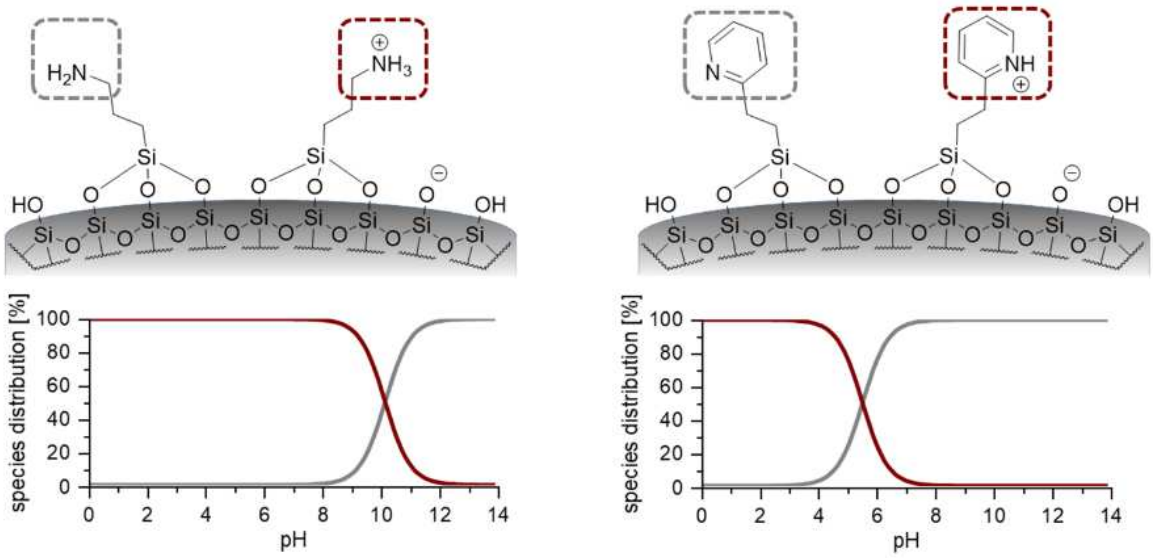


**Fig. S8.** pH-Dependent distribution of charged and uncharged species of amino groups and pyridine moieties. Calculation was performed using MarvinSketch 20.19 (ChemAxon, www.chemaxon.de).

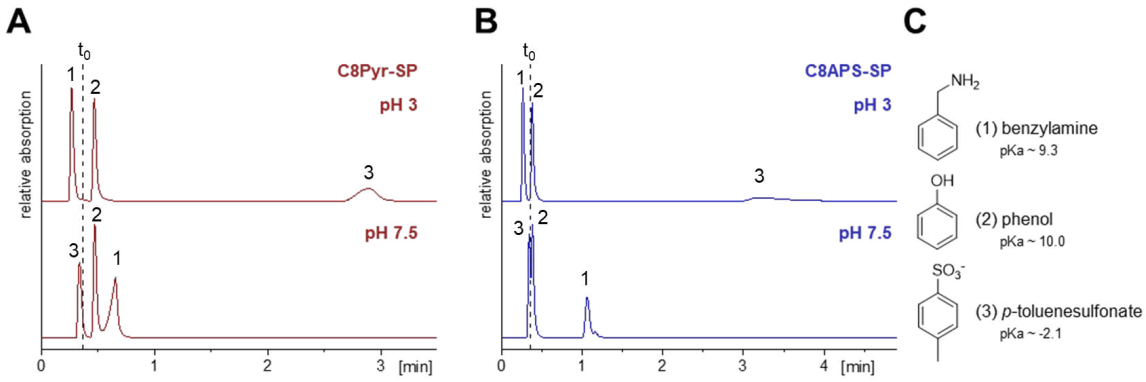


**Fig. S9.** Evaluation of surface charge and ion exchange characteristics of C8Pyr-SP (A) and C8APS-SP (B) at pH 3 and pH 7.5. The chemical structures of the analytes applied are depicted in C; $pK_a$ values were calculated using MarvinSketch 20.19 software (ChemAxon, www.chemaxon.de). Chromatographic conditions: Mobile phase consisted of MeOH/aqueous ammonium phosphate buffer (20 mM, adjusted to pH 3 or pH 7.5) (30/70, v/v), flow rate: 1 mL/min, temperature: 25 °C, injection volume: 5 µL. Additional experimental data can be found in Table S3.

**Table S2.** Chromatographic data obtained from the separation of benzylamine, phenol and p-toluenesulfonic acid on C8Pyr-SP and C8APS-SP. Chromatograms are depicted in Fig. S9.

| | retention factor k | | | | | |
|---|---|---|---|---|---|---|
| | benzylamine | | phenol | | p-toluensulfonate | |
| | pH 3 | pH 7.5 | pH 3 | pH 7.5 | pH 3 | pH 7.5 |
| C8Pyr-SP | before $t_0$ | 0.80 | 0.29 | 0.30 | 6.95 | before $t_0$ |
| C8APS-SP | before $t_0$ | 1.92 | 0.05 | 0.06 | 7.82 | before $t_0$ |

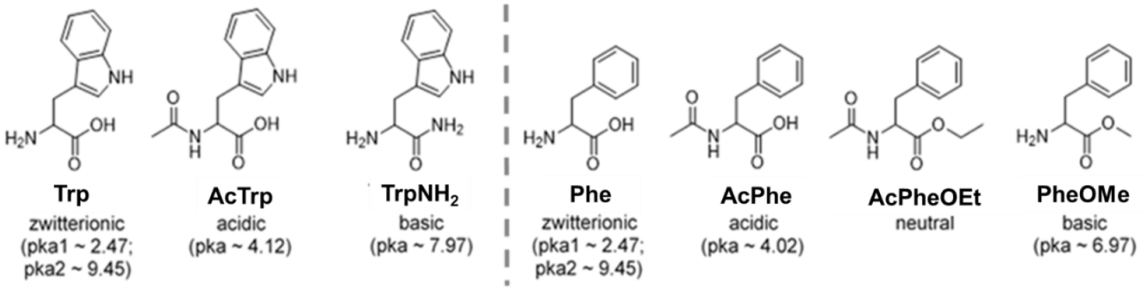


**Fig. S10.** Phenylalanine and tryptophan derivatives employed for the exploration of the surface charge and ion-exchange characteristics, respectvely. $pK_a$ values were calculated using MarvinSketch 20.19 software (ChemAxon, www.chemaxon.de).

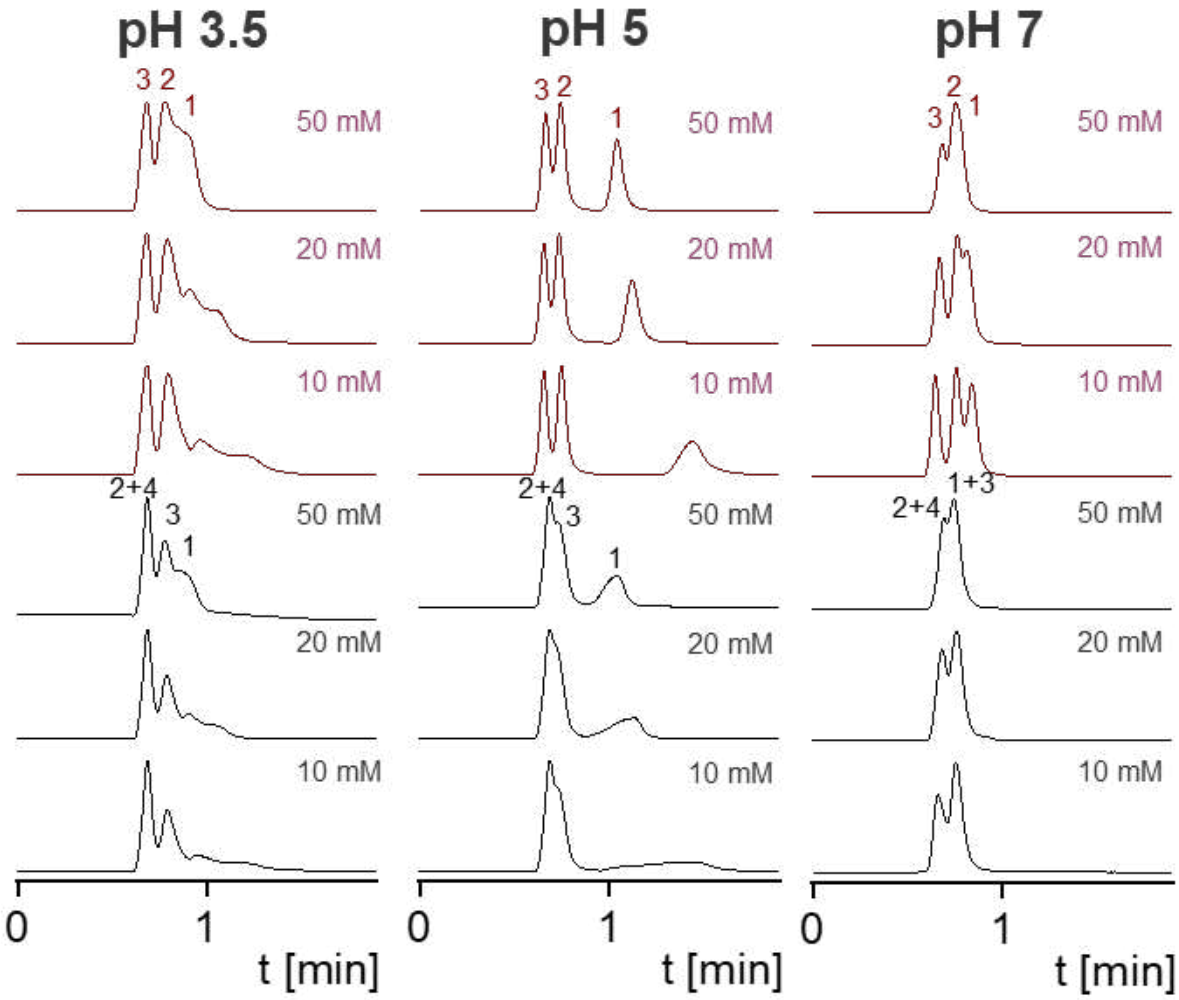


**Fig. S11.** Exploration of the surface charge and ion exchange characteristics, respectively, of C4-SP at different pH values and ionic strengths of the mobile phase. For the evaluation of the ion exchange retention mechanism of the prepared stationary phase the separation of phenylalanine (coloured black) and tryptophan (coloured red) derivatives (black: 1-PheOMe, 2-AcPheOEt, 3-Phe, 4-AcPhe; red: 1-Trp$NH_2$, 2-Trp, 3-AcTrp) was investigated under mobile phase conditions with varying ionic strength and pH. The mobile phase consisted of ACN and water (80:20, v/v) containing 10, 20 or 50 mM of the corresponding acid (formic acid: pH 3.5, acetic acid: pH 5 and 7), respectively. The pH was adjusted with ammonia. The flow rate was 1 mL/min, the temperature was set to 25 °C, the injection volume to 2 µL and detection was carried out at 280 nm.

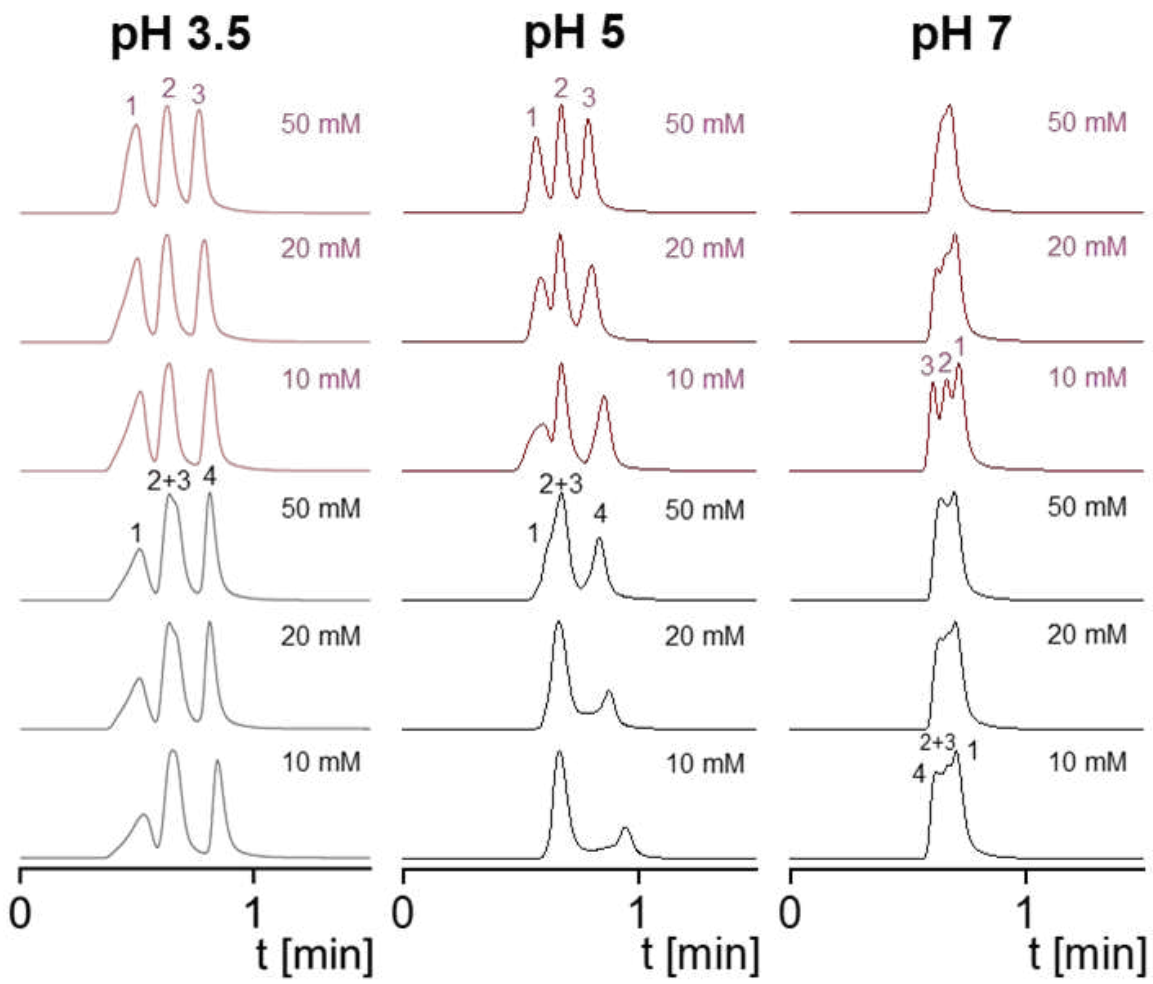


**Fig. S12.** Exploration of the surface charge and ion exchange characteristics, respectively, of C8Pyr-SP at different pH values and ionic strengths of the mobile phase. For the evaluation of the ion exchange retention mechanism of the prepared stationary phase the separation of phenylalanine (coloured black) and tryptophan (coloured red) derivatives (black: 1-PheOMe, 2-AcPheOEt, 3-Phe, 4-AcPhe; red: 1-Trp$NH_2$, 2-Trp, 3-AcTrp) was investigated under mobile phase conditions with varying ionic strength and pH. The mobile phase consisted of ACN and water (80:20, v/v) containing 10, 20 or 50 mM of the corresponding acid (formic acid: pH 3.5, acetic acid: pH 5 and 7), respectively. The pH was adjusted with ammonia. The flow rate was 1 mL/min, the temperature was set to 25 °C, the injection volume to 2 µL and detection was carried out at 280 nm.

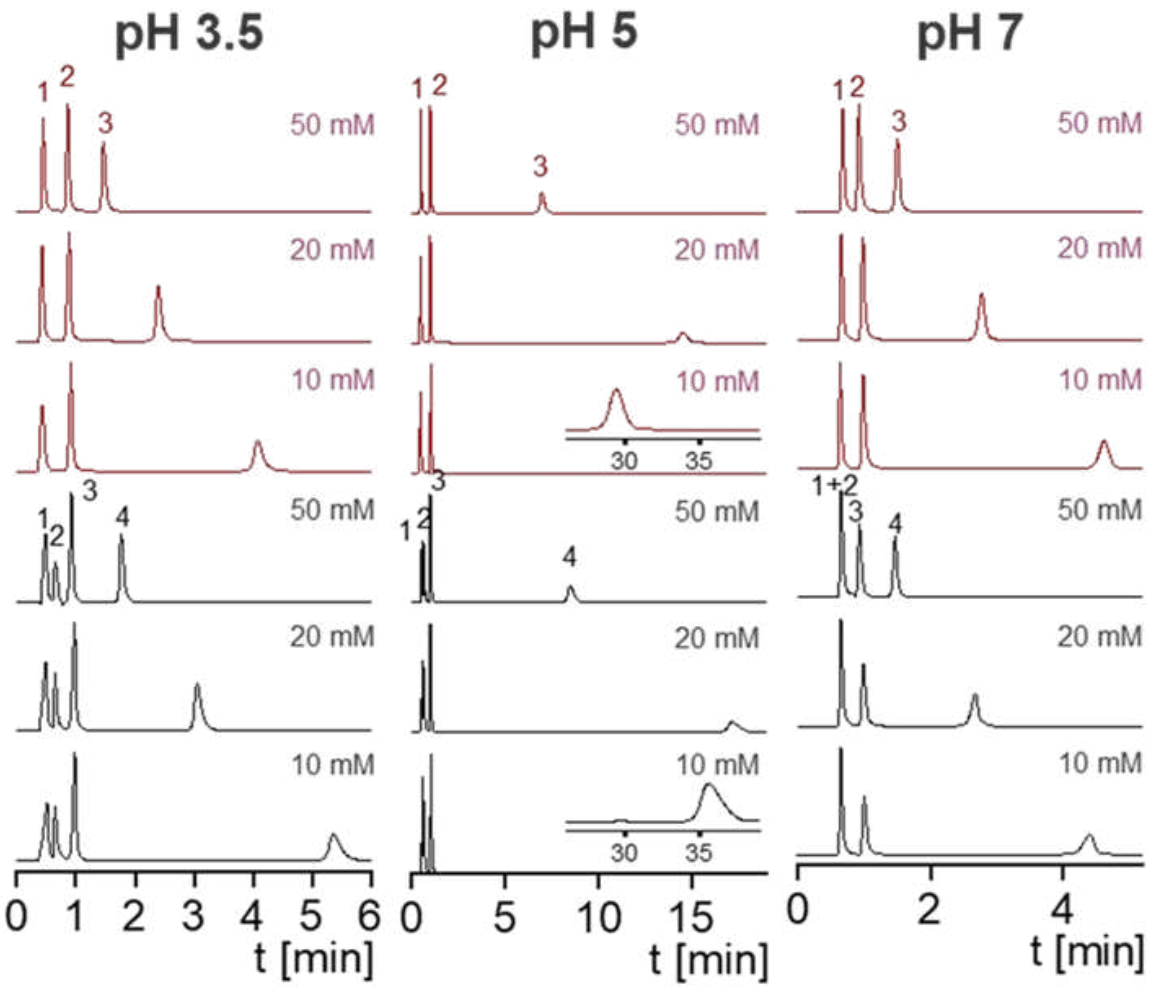


**Fig. S13.** Exploration of the surface charge and ion exchange characteristics, respectively, of C8APS-SP at different pH values and ionic strengths of the mobile phase. For the evaluation of the ion exchange retention mechanism of the prepared stationary phase the separation of phenylalanine (coloured black) and tryptophan (coloured red) derivatives (black: 1-PheOMe, 2-AcPheOEt, 3-Phe, 4-AcPhe; red: 1-$TrpNH_2$, 2-Trp, 3-AcTrp) was investigated under mobile phase conditions with varying ionic strength and pH. The mobile phase consisted of ACN and water (80:20, v/v) containing 10, 20 or 50 mM of the corresponding acid (formic acid: pH 3.5, acetic acid: pH 5 and 7), respectively. The pH was adjusted with ammonia. The flow rate was 1 mL/min, the temperature was set to 25 °C, the injection volume to 2 µL and detection was carried out at 280 nm.

**Table S3.** Chromatographic parameters obtained from analysis of amino acid derivatives. Chromatographic conditions are given in Fig. S12-14.

| **C4-SP** | pH 3.5 k | | | pH 5 k | | | pH 7 k | | |
|---|---|---|---|---|---|---|---|---|---|
| | 10 | 20 | 50 | 10 | 20 | 50 | 10 | 20 | 50 |
| Phe | 0.22 | 0.22 | 0.21 | 0.15 | 0.13 | 0.15 | 0.18 | 0.19 | 0.16 |
| AcPhe | 0.05 | 0.06 | 0.06 | 0.04 | 0.04 | 0.04 | 0.02 | 0.05 | 0.06 |
| PheOMe | 0.47 | 0.40 | 0.33 | 1.22 | 0.71 | 0.58 | 0.13 | 0.15 | 0.14 |
| AcPheOEt | 0.07 | 0.06 | 0.06 | 0.07 | 0.07 | 0.07 | 0.07 | 0.07 | 0.07 |
| Trp | 0.23 | 0.23 | 0.21 | 0.15 | 0.14 | 0.15 | 0.17 | 0.17 | 0.15 |
| AcTrp | 0.06 | 0.06 | 0.06 | 0.01 | 0.01 | 0.03 | 0.01 | 0.04 | 0.06 |
| $TrpNH_2$ | 0.49 | 0.40 | 0.32 | 1.20 | 0.72 | 0.59 | 0.30 | 0.27 | 0.20 |

| **C8Pyr-SP** | pH 3.5 k | | | pH 5 k | | | pH 7 k | | |
|---|---|---|---|---|---|---|---|---|---|
| | 10 | 20 | 50 | 10 | 20 | 50 | 10 | 20 | 50 |
| Phe | 0.08 | 0.06 | 0.06 | 0.12 | 0.11 | 0.12 | 0.11 | 0.11 | 0.10 |
| AcPhe | 0.43 | 0.33 | 0.31 | 0.59 | 0.49 | 0.42 | 0.03 | 0.05 | 0.06 |
| PheOMe | ≤ $t_0$ | ≤ $t_0$ | ≤ $t_0$ | 0.10 | 0.09 | 0.03 | 0.21 | 0.20 | 0.19 |
| AcPheOEt | 0.14 | 0.14 | 0.14 | 0.14 | 0.14 | 0.14 | 0.15 | 0.14 | 0.14 |
| Trp | 0.07 | 0.06 | 0.06 | 0.13 | 0.12 | 0.13 | 0.12 | 0.12 | 0.10 |
| AcTrp | 0.38 | 0.35 | 0.30 | 0.44 | 0.36 | 0.31 | 0.02 | 0.05 | 0.06 |
| $TrpNH_2$ | ≤ $t_0$ | ≤ $t_0$ | ≤ $t_0$ | ≤ $t_0$ | ≤ $t_0$ | ≤ $t_0$ | 0.21 | 0.19 | 0.15 |

| **C8APS-SP** | pH 3.5 k | | | pH 5 k | | | pH 7 k | | |
|---|---|---|---|---|---|---|---|---|---|
| | 10 | 20 | 50 | 10 | 20 | 50 | 10 | 20 | 50 |
| Phe | 0.58 | 0.57 | 0.50 | 0.62 | 0.57 | 0.56 | 0.60 | 0.59 | 0.50 |
| AcPhe | 7.63 | 3.91 | 1.86 | 56.09 | 26.57 | 12.60 | 6.08 | 3.29 | 1.36 |
| PheOMe | ≤ $t_0$ | ≤ $t_0$ | ≤ $t_0$ | ≤ $t_0$ | ≤ $t_0$ | ≤ $t_0$ | 0.05 | 0.05 | 0.06 |
| AcPheOEt | 0.04 | 0.04 | 0.04 | 0.04 | 0.04 | 0.04 | 0.05 | 0.05 | 0.05 |
| Trp | 0.53 | 0.43 | 0.39 | 0.61 | 0.56 | 0.56 | 0.58 | 0.58 | 0.58 |
| AcTrp | 5.56 | 2.85 | 1.36 | 46.14 | 22.32 | 10.18 | 6.46 | 3.46 | 1.42 |
| $TrpNH_2$ | ≤ $t_0$ | ≤ $t_0$ | ≤ $t_0$ | ≤ $t_0$ | ≤ $t_0$ | ≤ $t_0$ | 0.03 | 0.06 | 0.06 |

## PART V: Stationary phase classification by multivariate data analysis

In order to assess the chromatographic properties of the novel stationary phase C8Pyr-SP in comparison to a set of commercially available columns, two other in-house prepared pyridine-modified stationary phases (see Fig. S16) and the C8APS-SP as well as C4-SP, HILIC and RP tests were carried out with diverse low molecular probes differing in charge and hydrophobicity/hydrophilicity. The experimental details and columns can be found in Fig. S17-19 and Table S4. For this purpose, the resultant retention factors were subjected to principal component analysis (PCA). The score plot is shown in Fig. S14 and the corresponding loading scatter plot in Fig. S15. Stationary phases with highly similar chromatographic properties cluster in close proximity, whereas phases with distinct characteristics are located in the score plot far distant from each other indicating chromatographic orthogonality. The PC1 axis reflects the hydrophobicity and the PC2 axis the surface charge of the chromatographic materials. More precisely, hydrophobicity of the phases decreases from low to high PC1 values, whereas surface net charge alters from positive to negative values from low to high PC2 values. C8Pyr-SP and C4-SP have similar PC2 values (paramount to similar charge under employed mobile phase conditions, i.e. at about neutral pH with unadjusted ammonium acetate), like the 2-pyridylpropylurea-SP and the ZIC-HILIC column. Consequently, the uncharged state of the pyridine functionality under the applied conditions became apparent. The overall negative charge, however, resulted from the residual silanol activity. On the other hand, C8APS-SP was found in the score plot far away from C8Pyr-SP at the same PC2 level as Chiralpak QN-AX, Luna NH2 and QNPyr-SP. This clearly illustrated the positive surface charge characteristics of C8APS-SP and consequently the pH-dependent differences in charge characteristics between C8Pyr-SP and C8APS-SP. The amino column Lichrospher NH2, with APS but no C8 co-ligand, was found at a lower PC2 value than C8APS-SP due to its low ligand density and its accompanying high silanol activity. In terms of hydrophobicity, C8Pyr-SP offered the highest of the three phases prepared in this study and was located at a similar PC1 level as the mixed-mode column Primesep B2. In contrast, C4-SP provided less hydrophobicity than C8Pyr-SP due to the shorter alkyl ligand,

the lower ligand density and the lower shielding of the silanol groups and was consequently found at a higher PC1 value. C8APS-SP showed the lowest hydrophobicity and was grouped together with mixed-mode columns such as Obelisc N, Obelisc R and the anion-exchange column BioBasic AX. However, C8APS-SP still provided more hydrophobicity than classical amino phases such as Lichrospher NH2 and Phenomenex Luna NH2 which were located on the PC1 axis at the upper end of the hydrophilicity scale. Overall, there seems to be a significant physicochemical and chromatographic difference between the two novel prepared mixed-mode phases C8Pyr-SP and C8APS-SP and the applied methodology of column classification allowed to gain some insight on the general characteristics in relation to other stationary phases, even if the analytes were not proteins for which the phases have been ultimately prepared.

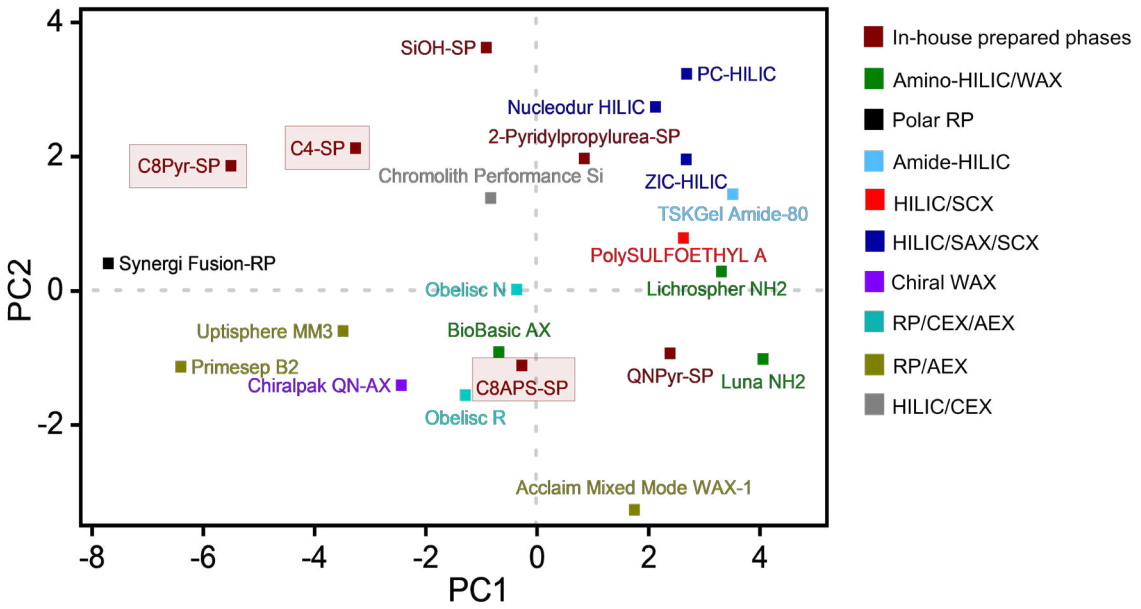


**Fig. S14.** Score plot for stationary phase classification. Classification was done by principal component analysis based on retention factors as variables obtained from characterization under RP and HILIC conditions (see Fig.S17-19 and Table S4) via multivariate data analysis software SIMCA (17.0.2) from Sartorius Stedim Data Analytics AB (Umeå, Sweden). PC1 reflects the hydrophobicity and PC2 the surface net charge of the investigated stationary phases. Hydrophobicity decreases from low to high PC1 values. The surface net charge alters from positive to negative values from low to high PC2 values. The surface chemistries of the various stationary phases are depicted in Fig. S16.

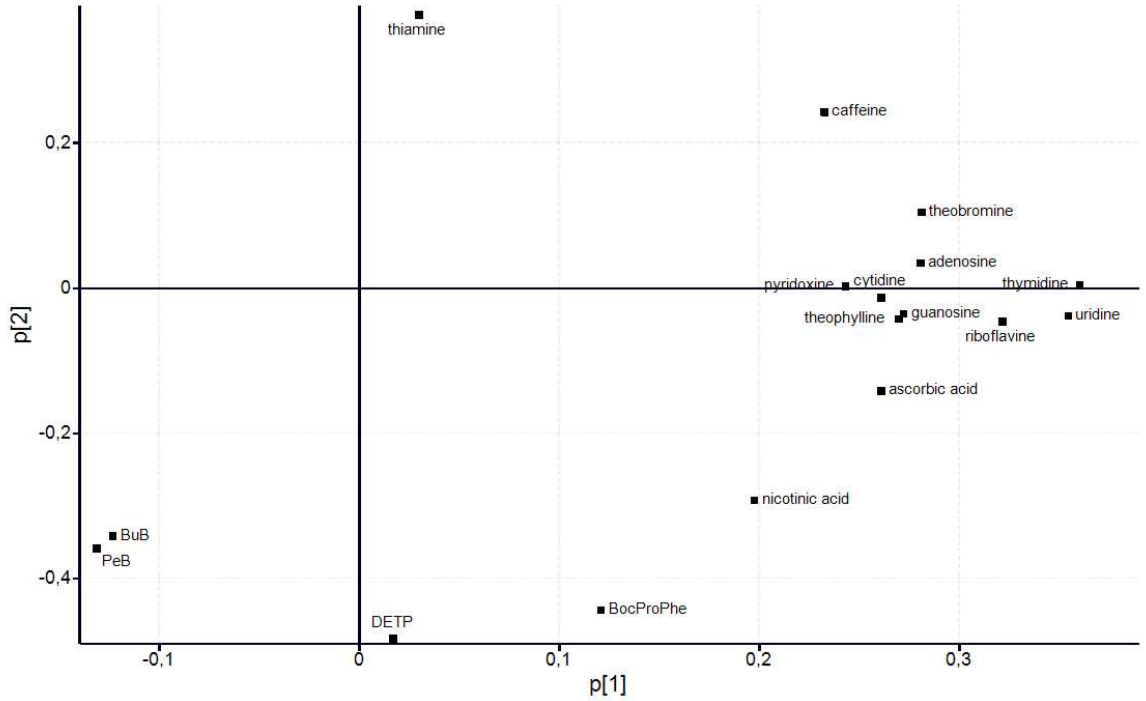


**Fig. S15.** Loadings scatter plot of PCA. p1 vs. p2. p1 is the loading in the first component and p2 the loading in the second component. Loadings express the dominating correlation structure of the X matrix.

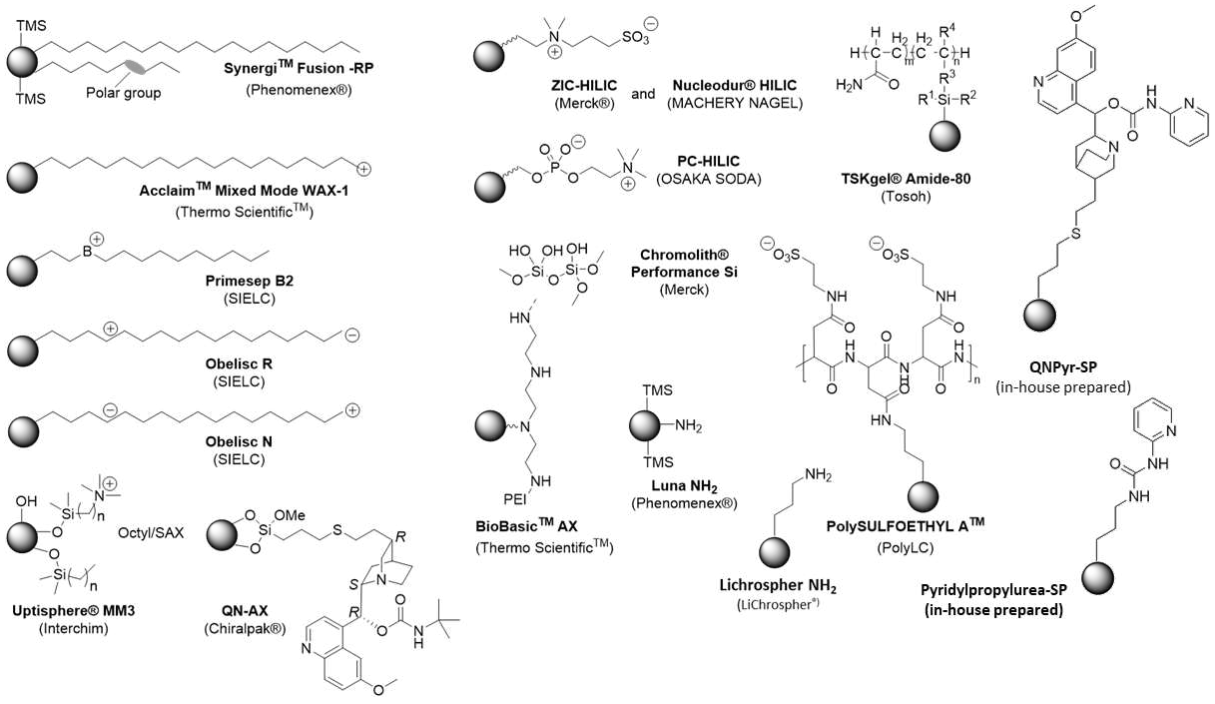


**Fig. S16.** Surface chemistries of commercial and in-house prepared columns used for stationary phase classification by PCA.

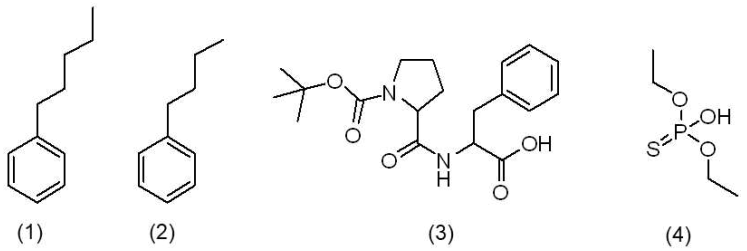


**Fig. S17.** Analytes applied for RPLC test. The chromatographic performance under RPLC conditions was investigated by the separation of the four analytes PeB (1; logD(pH 6) ~ 4.26[1]), BuB (2; logD(pH 6) ~ 3.82[1]), BocProPhe (3; $pK_a$ ~ 3.6[1], logD(pH 6) ~ -0.06[1]) and DETP ($pK_a$ ~ 3.6[1], logD(pH 6) ~ -0.97[1]). The chromatographic conditions, the obtained chromatograms and the chromatographic data can be found in Fig. S19 and Table S4. [1]calculated using MarvinSketch 20.19 software (ChemAxon, www.chemaxon.de).

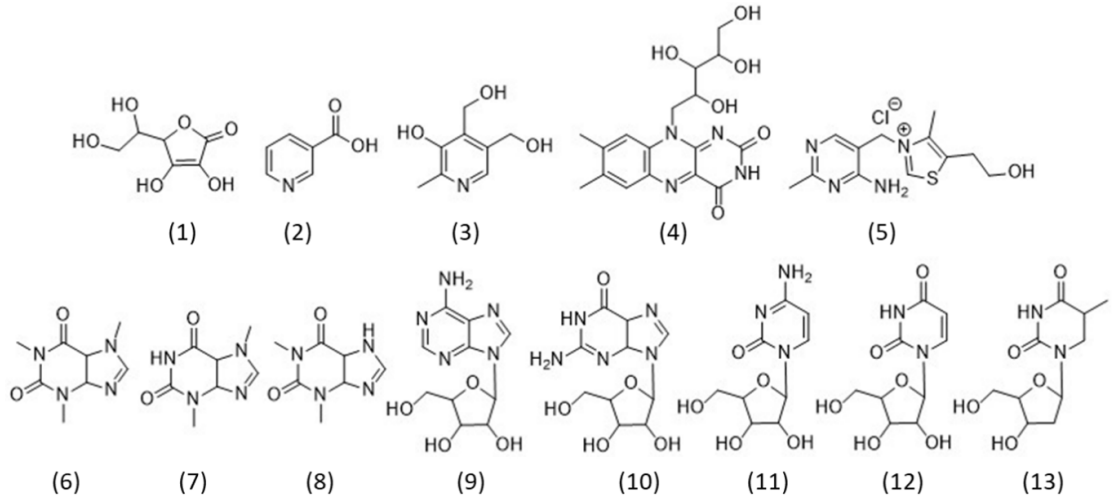


**Fig. S18.** Analytes applied for HILIC test. The chromatographic performance under HILIC conditions was investigated by the separation of xanthines, nucleosides and vitamins. The following analytes were submitted to HILIC test: (1) ascorbic acid ($pK_a$ ~ 4.2[1], logD(pH 8) ~ -5.27[1]), (2) nicotinic acid ($pK_a$ ~ 2.8[1], logD(pH 8) ~ -3.04[1]), (3) pyridoxine (logD(pH 8) ~ -0.97[1]), (4) riboflavin ($pK_a$ ~ 6.0[1], logD(pH 8) ~ -2.60[1]), (5) thiamine hydrochloride (logD(pH 8) ~ -3.10[1]), (6) caffeine (logD(pH 8) ~ -1.06[1]), (7) theobromine (logD(pH 8) ~ -1.28[1]), (8) theophylline (logD(pH 8) ~ -1.32[1]), (9) adenosine (logD(pH 8) ~ -2.09[1]), (10) guanosine (logD(pH 8) ~ -3.22[1]), (11) cytidine (logD(pH 8) ~ -2.80[1]), (12) uridine (logD(pH 8) ~ -2.42[1]), (13) thymidine (logD(pH 8) ~ -1.33[1]). The chromatographic conditions, the obtained chromatograms and the chromatographic data can be found in Fig. S19 and Table S4 [1]calculated using MarvinSketch 20.19 software (ChemAxon, www.chemaxon.de)

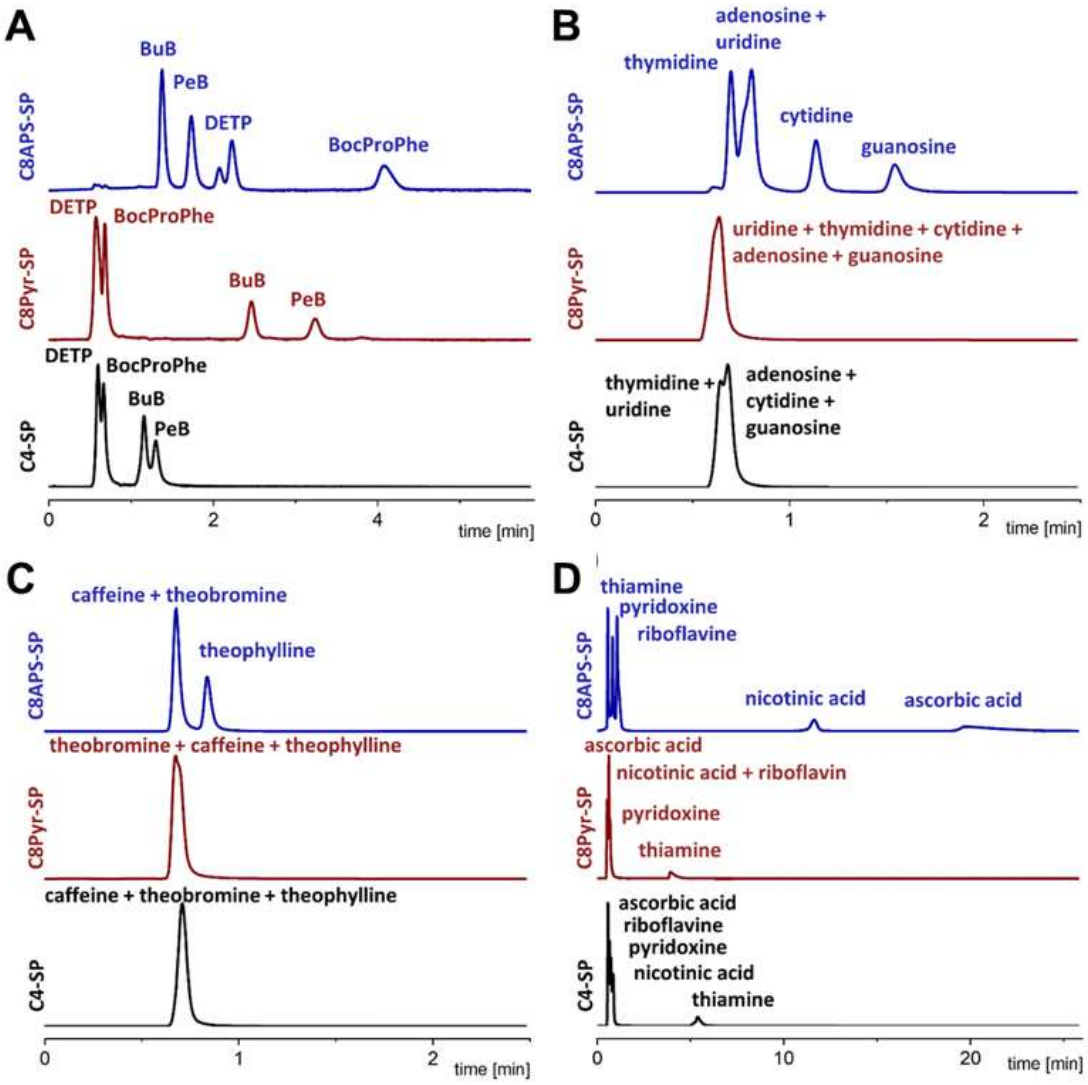


**Fig. S19.** Chromatograms obtained from RPLC and HILIC test. Investigation of the three prepared stationary phases was carried out under RPLC (A) and HILIC (B-D) conditions applying different sets of analytes. RP chromatography was performed using a mixture of ACN and water (40/60, v/v) containing 50 mM acetic acid as mobile phase. The mobile phase pH was adjusted to pH 6 with ammonia. The linear flow velocity was set to 1.7 mm/s and detection was carried out at 220 nm. The injection volume was 2 µL and the temperature 25°C. For the investigation of xanthines under HILIC conditions a mobile phase consisting of ACN and water (90:10, v/v) containing 5 mM ammonium acetate was utilized, for the investigation of vitamins and nucleosides a mobile phase consisting of ACN and water (95:5, v/v) containing 5 mM ammonium acetate. The flow rate was calculated to the corresponding linear velocity of 1.7 mm/s. The injection volume was set to 2 µL, the temperature to 25 °C and detection was carried out at 254 nm.

**Table S4.** Retention factors obtained from RPLC and HILIC test for in-house prepared and commercial columns used for PCA. Data of commercial columns were partially taken from [2] and [6]. Chromatographic conditions can be found in Fig. S20.

| | k | | | | | | | | | | | | | | | | | | |
|---|---|---|---|---|---|---|---|---|---|---|---|---|---|---|---|---|---|---|---|
| | thymidine | adenosine | uridine | cytidine | guanosine | caffeine | theobromine | theophylline | thiamine | pyridoxine | riboflavine | ascorbic acid | nicotinic acid | BuB | PeB | DETP | BocProPhe |
| Acclaim Mixed Mode WAX-1 | 0.88 | 1.67 | 1.90 | 4.18 | 7.15 | 0.10 | 0.26 | 0.84 | 0.17 | 1.11 | 1.66 | n.d. | 31.14 | 5.52 | 8.47 | 14.45 | 34.75 |
| Uptisphere 5 MM3 | with $t_0$ | 0.15 | 0.15 | 0.81 | 1.05 | with $t_0$ | with $t_0$ | with $t_0$ | 0.60 | 0.13 | 0.13 | 5.27 | 3.03 | 27.73 | 48.89 | 0.19 | 0.28 |
| Primesep B2 | with $t_0$ | 0.10 | with $t_0$ | 0.22 | 0.22 | 0.02 | 0.02 | 0.11 | 3.92 | 0.36 | 0.04 | 0.04 | 0.73 | 9.97 | 15.59 | 1.97 | 5.36 |
| Obelisc R | 0.09 | 0.48 | 0.48 | 2.15 | 2.69 | 0.06 | 0.14 | 0.26 | 10.11 | 0.78 | 0.78 | 2.73 | 10.11 | 6.22 | 9.47 | 3.59 | 10.97 |
| Obelisc N | 0.23 | 0.59 | 0.48 | 2.75 | 1.61 | 0.15 | 0.22 | 0.22 | n.d | 6.65 | 1.15 | 1.15 | 0.66 | 1.00 | 1.35 | 4.00 | 3.64 |
| Chiralpak QN-AX | 0.15 | 0.15 | 0.15 | 0.29 | 0.29 | 0.10 | 0.24 | 0.44 | 1.17 | 0.41 | 0.32 | n.d. | 3.52 | 4.11 | 5.76 | 5.76 | 7.69 |
| Luna NH2 | 1.21 | 3.80 | 3.80 | 11.99 | 19.18 | 0.31 | 0.67 | 3.19 | 0.95 | 2.64 | 3.10 | 28.74 | 24.90 | with $t_0$ | with $t_0$ | 4.39 | 1.76 |
| Lichrospher NH2 | 0.97 | 2.90 | 1.89 | 10.61 | 12.86 | 0.22 | 0.35 | 0.44 | 0.44 | 2.48 | 6.40 | 134.63 | 30.59 | 0.10 | 0.19 | 0.78 | 0.89 |
| BioBasic AX | 0.35 | 0.84 | 0.75 | 2.18 | 3.42 | 0.08 | 0.18 | 0.18 | 0.43 | 0.43 | 0.89 | n.d. | 10.88 | with $t_0$ | with $t_0$ | 1.05 | 0.53 |
| Synergi Fusion-RP | with $t_0$ | 0.04 | with $t_0$ | 0.16 | 0.04 | with $t_0$ | with $t_0$ | with $t_0$ | 14.94 | 0.11 | with $t_0$ | with $t_0$ | 0.44 | 24.17 | 43.28 | with $t_0$ | 0.06 |
| TSKGel Amide-80 | 1.27 | 3.12 | 3.45 | 10.20 | 12.80 | 0.40 | 0.76 | 1.16 | 43.54 | 1.49 | 4.77 | 20.70 | 5.49 | with $t_0$ | with $t_0$ | with $t_0$ | with $t_0$ |
| PolysulfoethylA | 0.77 | 2.08 | 3.14 | 15.02 | 16.69 | 0.20 | 0.45 | 0.51 | 26.81 | 2.73 | 3.10 | n.d. | 2.73 | with $t_0$ | with $t_0$ | with $t_0$ | with $t_0$ |
| ZIC-HILIC | 0.89 | 2.09 | 3.24 | 9.54 | 12.63 | 0.28 | 0.63 | 0.63 | 29.30 | 1.20 | 2.20 | 35.13 | 4.89 | with $t_0$ | with $t_0$ | 0.14 | with $t_0$ |
| Nucleodur HILIC | 0.91 | 1.64 | 2.08 | 5.05 | 6.53 | 0.36 | 0.67 | 0.67 | 99.31 | 1.73 | 1.78 | 6.26 | 1.78 | with $t_0$ | with $t_0$ | with $t_0$ | with $t_0$ |
| Chromolith Performance Si | 0.29 | 0.76 | 0.61 | 2.26 | 2.04 | 0.19 | 0.19 | 0.19 | 28.20 | 0.65 | 0.65 | 1.41 | 1.85 | with $t_0$ | with $t_0$ | with $t_0$ | with $t_0$ |
| PC-HILIC | 1.00 | 2.29 | 1.66 | 4.70 | 5.21 | 0.60 | 1.03 | 1.03 | 95.49 | 1.91 | 2.66 | 6.65 | 2.05 | with $t_0$ | with $t_0$ | with $t_0$ | with $t_0$ |
| SiOH-SP | 0.23 | with $t_0$ | 0.34 | 1.28 | with $t_0$ | 0.19 | 0.17 | 0.34 | 36.19 | 0.58 | 0.18 | 1.62 | 1.97 | 0.04 | 0.06 | with $t_0$ | with $t_0$ |
| C4-SP | 0.11 | 0.17 | 0.11 | 0.19 | 0.27 | 0.21 | 0.22 | 0.26 | 8.30 | 0.28 | 0.16 | with $t_0$ | 0.50 | 0.94 | 1.18 | with $t_0$ | 0.12 |
| C8Pyr-SP | 0.04 | 0.10 | 0.03 | 0.08 | 0.14 | 0.15 | 0.13 | 0.19 | 5.96 | 0.18 | 0.08 | with $t_0$ | 0.07 | 3.11 | 4.40 | with $t_0$ | 0.14 |
| C8APS-SP | 0.23 | 0.35 | 0.42 | 1.00 | 1.71 | 0.11 | 0.19 | 0.47 | with $t_0$ | 0.45 | 0.88 | 33.71 | 19.47 | 1.35 | 1.95 | 2.79 | 5.94 |
| 2-Pyridylpropylurea-SP | 0.49 | 1.04 | 0.59 | 1.35 | 1.64 | 0.52 | 0.81 | 0.88 | 12.22 | 0.91 | 1.87 | 1.19 | 1.87 | 0.95 | 1.12 | 0.19 | 0.59 |
| QNPyr-SP | 0.70 | 0.86 | 0.93 | 1.06 | 2.19 | 0.63 | 1.49 | 1.75 | 9.49 | 1.41 | 2.80 | n.d. | 15.30 | 2.90 | 3.86 | 7.65 | 13.79 |

n.d. = not detected

## PART VI: High-performance liquid chromatography of proteins

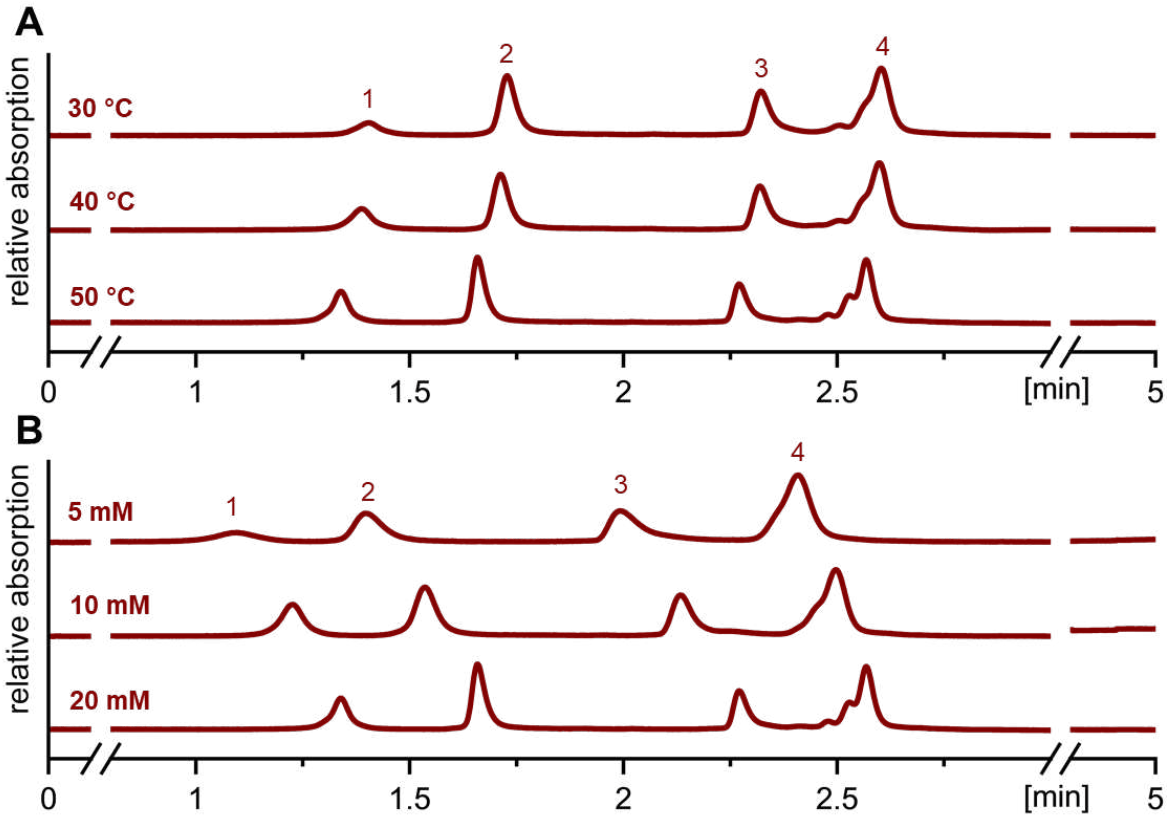


**Fig. S20.** Influence of temperature (A) and buffer concentration (B) on retention of proteins on C8Pyr-SP under gradient reversed phase chromatography conditions. Elevated temperatures and increasing buffer concentrations lead to better peak shapes in both cases. In A, the buffer concentration was set to 20 mM and the temperature varied. In B, the temperature was set to 50°C and the buffer concentration varied. In both cases, the mobile phase A consisted of acetonitrile and an aqueous ammonium formate buffer (10/90, v/v). Mobile phase B consisted of acetonitrile and an aqueous ammonium formate buffer (90/10, v/v). The pH value of the mobile phases was adjusted to pH 3 in the aqueous phase. The flow rate was set to 1 mL/min and the gradient from 0 to 5 min from 0% B to 100% B.

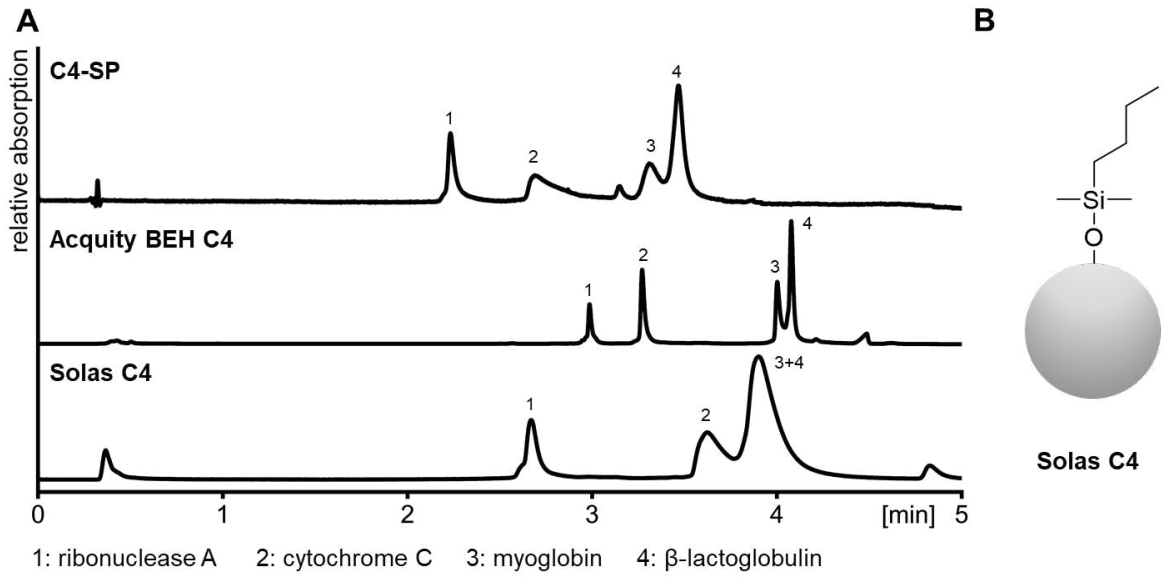


**Fig. S21.** Comparison of C4-SP (50 x 3 mm, 3 µm, 300 Å) and commercial Acquity Protein BEH C4 column (50 x 2.1 mm, 1.7 µm, 300 Å; from Waters Corperation, Milford, MA, USA) and Solas C4 column (50 x 2.1 mm, 1.7 µm, 400 Å; from Glantreo, Cork, Ireland). In A, the chromatographic results for both columns under gradient reversed phase conditions at pH 3 are depicted (for further chromatographic conditions see Fig. S21, flow rates were adjusted to the same linear velocity). In B, the surface chemistry of commercial Solas C4 is illustrated. A detailed description of the surface chemistry of Acquity BEH C4 was not available.

**Table S5.** Gradient-time-normalized retention times ($t_{R,norm}$) for the four test proteins under gradient reversed phase conditions (see Fig. S21 and Fig. S22) at mobile phase pH 3 ($t_{R,norm} = (t_R-t_0)/(t_G-t_0)$).

| | $t_{R,norm}$ | | | |
|---|---|---|---|---|
| | ribonuclease A | cytochrome C | myoglobin | beta-lactoglobulin |
| Solas C4 | 0.50 | 0.70 | 0.76 | 0.76 |
| Acquity BEH C4 | 0.56 | 0.63 | 0.78 | 0.80 |
| C4-SP | 0.33 | 0.43 | 0.55 | 0.61 |
| C8Pyr-SP | 0.22 | 0.28 | 0.42 | 0.48 |
| C8APS-SP | 0.24 | 0.31 | 0.43 | 0.49 |

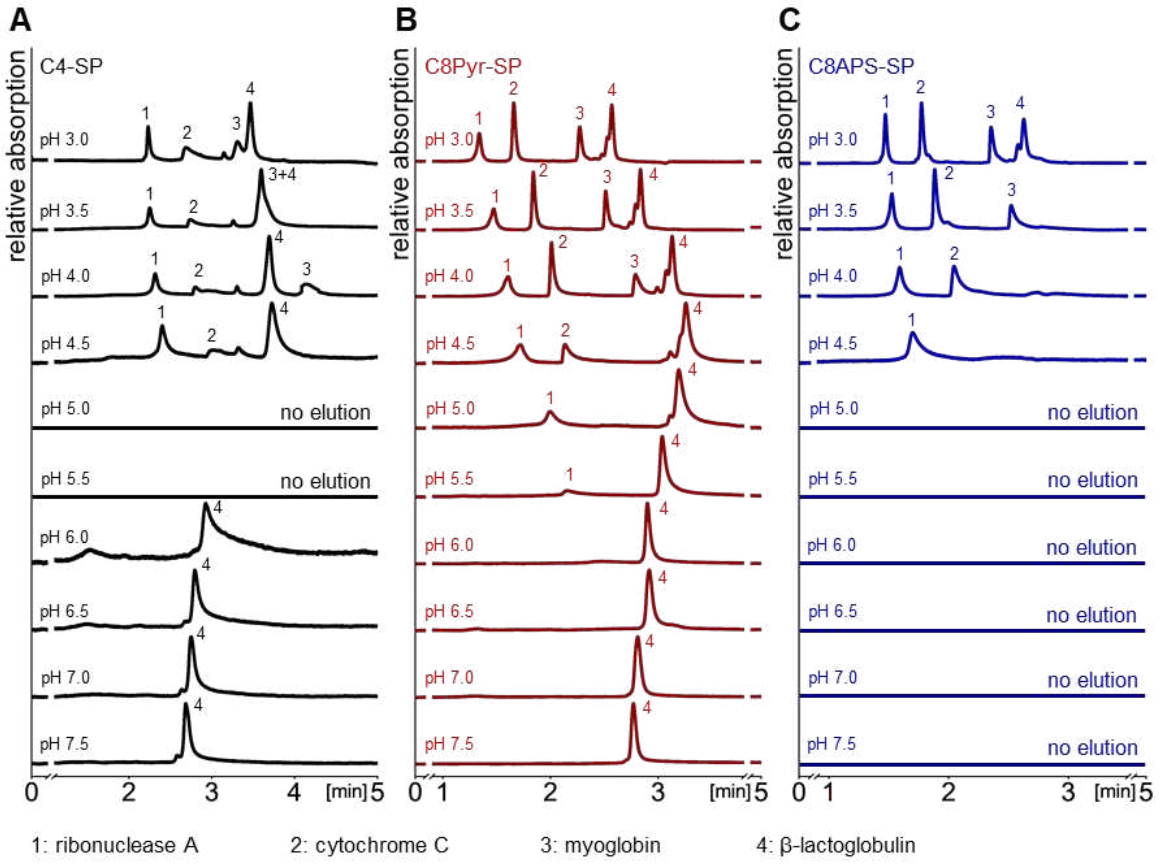


**Fig. S22.** Analysis of a protein mixture on C4-SP (A), C8Pyr-SP (B) and C8APS-SP (C) under gradient reversed phase chromatography conditions at different mobile phase pH values. Chromatographic conditions: mobile phase A (ACN/aqueous ammonium formate buffer with respectively adjusted pH in the aqeous phase, $C_{tot}$ = 20 mM (10/90, v/v)), mobile phase B (ACN/aqueous ammonium formate buffer with respectively adjusted pH in the aqeous phase, $C_{tot}$ = 20 mM (90/10, v/v)), flow rate: 1 mL/min, temperature: 50 °C, gradient: 0 to 5 min: 0% B to 100% B.

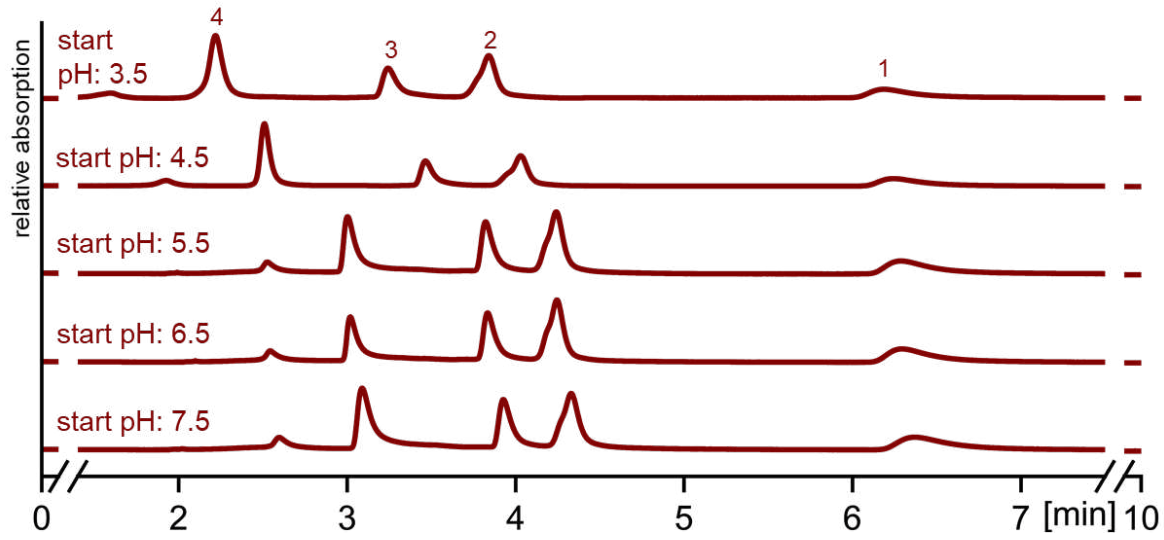


**Fig. S23.** Protein analysis under HCIC conditions on C8Pyr-SP at different starting pH values of the mobile phase (1: ribonuclease A, 2: cytochrome C, 3: myoglobin, 4: β-lactoglobulin). Chromatograpic conditions: mobile phase A (ACN/aqueous ammonium formate buffer with varying pH (adjusted in the aqueous phase), $C_{tot}$ = 20 mM (10/90, v/v)), mobile phase B (ACN/water/formic acid (10/90/0.1, v/v/v)), flow rate: 1 mL/min, temperature: 50 °C, gradient: 0 to 5 min: 0% B to 100% B, 5 to 10 min: 100% B.

## PART VII: References

[1] Geibel C., Theiner J., Wolter M., Kramer M., Lindner W., Laemmerhofer M., Controllable organosilane monolayer density of surface bonding using silatranes for thiol functionalization of silica particles for liquid chromatography and validation of microanalytical method for elemental composition determination, J. Chromatogr. A, 2011;1653:462418.

[2] Wolter M., Geibel C., Olfert M., Su M., Bicker W., Laemmerhofer M., Development and chromatographic exploration of stable-bonded cross-linked amino silica against classical amino phases, J. Sep. Sci., 2022;1-15.

[3] Puri J.K., Singh R., Chahal V.K., Silatranes: a review on their synthesis, structure, reactivity and applications, Chem. Soc. Rev., 2011;40:1791-1840.

[4] Sok S., Gordon M.S., A dash of protons: a theoretical study on the hydrolysis mechanism of 1-substituted silatranes and their protonated analogs, Comput. Theor. Chem., 2012;987:2-15.

[5] Shlyakhtenko L.S., Gall A.A., Filonov A., Cerovac, Z. Lushnikov A., Lyubchenko Y.L., Silatrane-based surface chemistry for immobilization of DNA, protein-DNA complexes and other biological materials, Ultramicroscopy, 2003;97:279-287.

[6] Zimmermann A., Horak J., Sanchez-Munoz O.L., Laemmerhofer M., Surface charge fine tuning of reversed-phase/weak anion-exchange type mixed-mode stationary phases for milder elution conditions, J. Chromatogr. A, 2015;1409:189-200.

# XII. CHAPTER EIGHT

# Triphenyl-modified mixed-mode stationary phases with and without embedded ion-exchange sites for high performance liquid chromatography

## XII.1 Publication VII – Main Document

*Journal of Separation Science*

WILEY-VCH

JOURNAL OF SEPARATION SCIENCE

ORIGINAL ARTICLE OPEN ACCESS

# Triphenyl-Modified Mixed-Mode Stationary Phases With and Without Embedded Ion-Exchange Sites for High-Performance Liquid Chromatography

Marc Wolter[1] | Mirna Maalouf[1] | Mateusz Janek[1] | Cornelius Knappe[1] | Markus Kramer[2] | Michael Lämmerhofer[1]

[1]Institute of Pharmaceutical Sciences, Pharmaceutical (Bio-)Analysis, University of Tübingen, Tübingen, Germany | [2]Institute of Organic Chemistry, University of Tübingen, Tübingen, Germany

**Correspondence:** Michael Lämmerhofer (michael.laemmerhofer@uni-tuebingen.de)

**Received:** 28 September 2024 | **Revised:** 2 December 2024 | **Accepted:** 6 December 2024

**Keywords:** mixed-mode chromatography | oligonucleotide | silatrane | stationary phase | thiol-yne/ene click reaction

## ABSTRACT

The present work reports on the preparation, characterization, and evaluation of a set of novel triphenyl-modified silica-based stationary phases without and with embedded ion-exchange sites for mixed-mode liquid chromatography. The three synthesized triphenyl phases differed in additionally incorporated ion-exchange sites. In one embodiment, allyltriphenylsilane was bonded to thiol-modified silica by thiol-ene click reaction, leading to particles with no ion-exchange sites. A second stationary phase was obtained by thiol-yne click reaction of thiol silica with 2-propinyl-triphenylphosphonium bromide, yielding a strong anion-exchanger (SAX). A third stationary phase was obtained from this SAX phase by the oxidation of residual thiols to sulfonic acid moieties, leading to a zwitterionic surface. All synthesized materials were subjected to elemental analysis, $^{13}C$ and $^{29}Si$ solid-state cross-polarization/magic angle spinning nuclear magnetic resonance (CP/MAS NMR) spectroscopy analysis, and pH-dependent $\zeta$-potential determinations via electrophoretic light scattering. The prepared stationary phases were chromatographically evaluated under classical reversed-phase, ion-exchange, and hydrophilic interaction chromatography conditions and classified within a set of commercially available columns by principal component analysis of retention factors. Finally, the obtained stationary phases were applied for biomolecule separations (e.g., teicoplanin and siRNA patisiran). These LC tests proved the orthogonality of the three prepared stationary phases and indicated possible fields of application.

## 1 | Introduction

Nowadays, in biochemical and pharmaceutical analysis, a variety of diverse liquid chromatography modes are applied. Besides the most common reversed-phase (RP) and hydrophilic interaction chromatography (HILIC) modes, mixed-mode chromatography (MMC) is constantly getting more popular. Such MMC stationary phases offer two or more different types of interactions with the analyte and hence orthogonal retention mechanisms. Due to the complementarity of the interactions, distinct selectivities, more flexibility for optimization of separation conditions, and extended fields of applicability can usually be achieved than would be feasible with single-mode chromatography. Therefore, hydrophobic, hydrophilic, and ionic interaction sites are most frequently combined with each other within one analytical column [1–3]. To this end, mixed beads, mixed ligands, or single multifunctional ligands strategies have been used to create the MMC character of the stationary phase [4]. The hydrophobic properties are typically

**Abbreviations:** CP/MAS, cross-polarization/magic angle spinning; MMC, mixed-mode chromatography; siRNA, small interfering ribonucleic acid; SP, stationary phase; ZWIX, zwitterionic ion exchanger.

This paper is included in the Special Collection 'Stationary Phase and Column Technologies' edited by Michael Laemmerhofer.

incorporated by the implementation of alkyl moieties on the surface of the support, the hydrophilic character by embedding polar functional groups such as amide, urea, carbamate, ether or thioether moieties (as hydrogen acceptor or donor sites), whereas ionic interaction sites are usually introduced by the incorporation of permanently or pH-dependent charged functional groups [2, 4–6]. Interestingly, aromatic groups, as for instance phenyl-moieties, are rarely reported to be applied as the hydrophobic part of mixed-mode phases [7, 8]. Some selected examples are typical ionic liquid phases that have immobilized, for example, imidazole-type ionic liquids [9–11]. On the other hand, classical phenyl phases, including phenyl-, biphenyl-, phenylhexyl-, and polyphenyl-modified silica, reached attractiveness as alternative RP-type stationary phases with complementary retention profiles when used with methanolic mobile phases that do not disrupt $\pi$-$\pi$-interactions like acetonitrile [12–16].

Phenyl groups alone have numerous other interaction options in addition to the hydrophobic ones, which makes them promising candidates for MMC phases. Thus, $\pi$—$\pi$-, cation—$\pi$-, anion—$\pi$-, dipole—dipole-, hydrogen-bonding and weak electrostatic interactions are possible. In addition, the anchoring of such bulky phenyl groups to the silica surface can effectively shield free silanols and prevent detrimental analyte–silanol interactions. In particular, in the analysis of biopolymers, free and accessible silanol groups have been reported to be responsible for poor recoveries, badly shaped peaks, and low efficiencies. However, this phenomenon is usually largely solved by end capping strategies or the use of polymer-based non-silica supports [17–20].

Against this backdrop, stationary phases with implemented bulky triphenyl residues imparting, on the one hand, RP chromatography properties and with embedded ionic moieties conferring, on the other hand, ion-exchange properties were synthesized to create new RP/IEX MMC stationary phases. The latter was obtained by incorporation of permanently positively charged phosphonium groups and negatively charged sulfonic acid moieties on the surface. In contrast to sulfonic acid groups, only a few phosphonium-type silica phases have been reported in liquid chromatography yet. A few permanently positively charged phosphonium-functionalized stationary phases for HILIC of, for instance, phospholipids were reported, as well as stationary phases suitable for the analysis of inter alia lignin degradation products [21–23]. Phosphonium-based ionic liquid stationary phases were mainly investigated in gas chromatography [24–26]. Furthermore, zwitterionic phases, including combined phosphonium, and sulfonic acid functionalities, were fabricated by Qui et al. and successfully applied for HILIC of inter alia nucleic acids, nucleosides, and water-soluble vitamins [27]. In this study, the synthesis, characterization, and applicability of neutral, SAX-type, and zwitterionic-type triphenyl-stationary phases with distinct surface charge will be briefly addressed.

## 2 | Experimental

### 2.1 | Materials

Spherical silica particles (Daisogel, 3 µm, 300 Å, 100 $m^2/g$) were purchased from Daiso Fine Chem GmbH (Düsseldorf, Germany), and empty stainless-steel columns (50 mm × 3 mm) were purchased from Bischoff Chromatography (Leonberg, Germany). Allyltriphenylsilane, *n*-octadecyltrimethoxysilane, and *n*-butyltrimethoxysilane were supplied from ABCR Chemicals (Karlsruhe, Germany). (3-Mercaptopropyl)trimethoxysilane, 2-propinyl-triphenylphosphonium bromide, azobis (isobutyronitrile) (AIBN), 2,2′-dipyridyl disulfide (DPDS), acetic acid (analytical grade), formic acid (FA, analytical grade), ammonium acetate, 4-dimethylaminopyridine (DMAP), sodium hydroxide, deuterated chloroform, triethanolamine, butylbenzene (BuB), pentylbenzene (PeB), triphenylene, *o*-terphenyl, pyridine, phenol, benzylamine, sodium *p*-toluenesulfonate, adenosine, guanosine, cytidine, thymidine, uridine, nicotinic acid, pyridoxine hydrochloride, ascorbic acid, riboflavin, thiamine hydrochloride, caffeine, theophylline, theobromine, *O*,*O*-diethylchlorothiophosphate (DECTP), triethylamine were received from Sigma-Aldrich (Munich, Germany). *O*,*O*-Diethylthiophosphate (DETP) was obtained from the hydrolysis of DECTP in the presence of triethylamine. (3-Mercaptopropyl)silatrane (MPS) was synthesized as described in the Supporting Information (see Figures S1 and S2). The solvents toluene, methanol, and methylene chloride were of technical grade or HPLC grade and purchased from Brenntag (Essen, Germany) or Sigma-Aldrich (Munich, Germany). MilliQ water was prepared by using an Elga PureLab Ultra Purification System (Celle, Germany).

### 2.2 | Instrumentation and Software

Elemental analysis was conducted using an EA 3000 CHNS-O elemental analyzer from EuroVector SpA (Milan, Italy) as described in [28, 29]. Determination of free and reactive sulfhydryl groups by a thiol-disulfide exchange reaction using DPDS assay was carried out according to [29]. $\zeta$-Potentials were determined in accordance with [30] by electrophoretic light scattering measurements using a Zetasizer NanoZS particle analyzer from Malvern Instruments (Herrenberg, Germany). MarvinSketch 20.19 software (ChemAxon, www.chemaxon.de) was used to calculate $pK_a$ values. Liquid-state nuclear magnetic resonance (NMR) spectroscopy experiments were carried out using a Bruker Avance 400 MHz spectrometer (Bruker, Rheinstetten, Germany), whereas solid-state NMR spectroscopy experiments were performed using a Bruker Avance III HD XWB 300 spectrometer (applied parameters can be found in [28]). NMR data were processed by Topspin 4.0.8 software from Bruker. HPLC experiments were all performed on HPLC systems from Agilent Technologies (Waldbronn, Germany). Thereby, measurements were usually performed using an Agilent 1260 series HPLC system featuring a degasser, flexible pump, autosampler, temperature-controlled column compartment (TCC), and a diode array detector (DAD), or an Agilent 1100 series HPLC equipped with a degasser, quaternary pump, autosampler, TCC, and variable wavelength detector (VWD). OpenLab CDS ChemStation Online Software (Rev. C.01.03 (37), 2011) and ChemStation Offline Software (Rev. B.04.03 (16), 2010) from Agilent Technologies were used for data acquisition and analysis. Stationary phases were slurry packed into stainless steel columns using a Smartline Pneumatic Pump 1950 from Knauer (Berlin, Germany) and a packing apparatus obtained from Dr. Maisch HPLC GmbH (Ammerbuch, Germany) (see Figure S7). Principal component

analysis (PCA) was carried out by using the multivariate data analysis software SIMCA (17.0.2) from Sartorius Stedim Data Analytics AB (Umeå, Sweden). Data visualization was carried out using OriginPro 2022 (OriginLab, Northampton, MA, USA). More detailed information is given in respective figure captions or subchapters.

## 2.3 | Preparation of Modified Silica Particles

### 2.3.1 | Preparation of Thiol Silica by Functionalization with Silatrane

In the first step, 2 g bare silica particles (3 µm, 300 Å, 100 $m^2/g$) were dispersed in 20 mL of MilliQ water and sonicated for 5 min within a glass flask. Thereafter, the suspension was transferred to a glass funnel of porosity 5, and the water was removed by applying a slight vacuum for 16 h. Afterward, 3.5 g of the humidified silica was dispersed in 16 mL toluene and 4 mL methanol within a triple neck flask equipped with a mechanical stirrer, a nitrogen supply, and a reflux condenser. Then, 3-meracptopropylsilatrane (8 µmol/$m^2$) and DMAP (0.4 µmol/$m^2$), both referring to dry silica, were added to the suspension, and the mixture was heated to reflux for 7 h. In the next step, the silica was washed three times with boiling methanol and toluene, each using a glass funnel with porosity 5. Thereafter, the modified silica particles were dried in a vacuum chamber at 60°C for 12 h. The amount of adsorbed water on the silica surface at the beginning of the grafting procedure was determined in accordance with the European Pharmacopeia. Thus, the humidified silica was dried in a heating chamber at 110°C for 96 h, and the drying loss was determined by weighing the silica before and after the drying process. Elemental analysis results for the modified silica can be found in Table 1.

### 2.3.2 | Preparation of Triphenyl-Stationary Phase by Thiol-Ene Click Reaction

Around 0.5 g dry thiol-modified silica particles (SH-SP) were suspended in 20 mL anhydrous toluene within a triple neck flask equipped with a mechanical stirrer, a reflux condenser, and a nitrogen supply. After adding allyltriphenylsilane (6 µmol/$m^2$) and AIBN (5 mol% related to the quantity of ene-groups) to the suspension, the reaction mixture was heated up to reflux, and the reaction was allowed to proceed for 7 h under continuous stirring and nitrogen rinsing. Thereafter, the modified silica particles were washed with boiling toluene and boiling methanol three times each using a glass funnel of porosity 5 and subsequently dried in a vacuum oven at 60°C for 24 h. Elemental analysis results for the modified silica can be found in Table 1.

### 2.3.3 | Preparation of Triphenyl-SAX Stationary Phase by Thiol-Yne Click Reaction

One gram dried thiol-modified silica particles were suspended in 20 mL anhydrous methanol within a triple neck flask equipped with a mechanical stirrer, a reflux condenser, and a nitrogen supply. After adding 2-propinyl-triphenylphosphonium bromide (6 µmol/$m^2$) and AIBN (10 mol% related to the quantity of yne-groups) to the suspension, the reaction mixture was heated up to reflux, and the reaction was allowed to proceed for 7 h under continuous stirring and nitrogen rinsing. Thereafter, the modified silica particles were washed with boiling methanol and boiling toluene three times each using a glass funnel of porosity 5 and subsequently dried in a vacuum oven at 60°C for 24 h. Elemental analysis results for the modified silica can be found in Table 1.

### 2.3.4 | Preparation of Triphenyl-ZWIX Stationary Phase by Oxidation of Triphenyl-SAX

Around 0.5 g triphenylphosphonium-modified silica particles were dispersed in a mixture of 40 mL methanol and 2.1 mL formic acid. Subsequently, a mixture of 0.5 mL hydrogen peroxide (30%, v/v) and 9.5 mL formic acid was added dropwise to the suspension. Thereafter, the reaction was allowed to proceed for 4 h under ice bath cooling and permanent mechanical stirring. Finally, the silica was washed three times with boiling methanol using a glass funnel of porosity 5 and dried in a vacuum oven at 60°C for 24 h. Elemental analysis results for the modified silica can be found in Table 1.

## 3 | Results and Discussion

### 3.1 | Trifunctional Bonded Platform Thiol-Silica by Silatrane Immobilization

Thiolated brush-type silica (Figure 1) is a frequently used carrier for the preparation of further functionalized silica by efficient and straightforward thiol-ene or thiol-yne click reactions (Figure 2). Usually, such thiol silicas are prepared by classical silylation reactions through condensation using functional trialkoxysilanes. Such a reaction leads mainly to immobilization by bifunctional siloxane bonding (vide infra). C4-SP and C18-SP, which were synthesized for comparison, were prepared conventionally utilizing the respective trialkoxysilanes (see Figure S3). In this study, (3-mercaptopropyl)silatrane was employed for the preparation of the triphenyl phases (see Figure S4). The beneficial properties of silatranes over traditionally used alkoxysilanes for the bonding of chromatographic ligands to the silica surface were recently demonstrated [28]. Due to their cage-like structure and the transannular N→Si bond, silatranes are not prone to hydrolysis under aqueous conditions and thus do not form oligomeric/polymeric structures in the reaction solution. However, silatranes can undergo condensation reactions with the silanols located on the silica surface due to acid catalysis of silica (Figure S5) [31–33]. Consequently, the formation of thin self-assembling sulfhydryl layers takes place on the surface. In the previous study (see [28]), a two-step synthesis approach was necessary to form the favorable self-assembled polysiloxane surface layer. Under nonaqueous conditions, in the first step, the triethanolamine moiety remains attached to the silica surface (see Figure S5). It needs to be removed by a second hydrolysis step. In order to simplify the synthesis and reduce overall reaction time, a single-step synthesis approach was developed in this study. The key to making a single-step silanization with silatranes possible is the humidification of the silica prior to the silanization

**TABLE 1** | Elemental analysis results and calculated ligand densities.

| SP | C[a] [w-%] | H[a] [w-%] | N[a] [w-%] | S[a] [w-%] | C[b] [µmol/m²] | Residual SH-ligand[b] [µmol/m²] | Residual SH-ligand[c] [µmol/m²] | C18-ligand[d] [µmol/m²] | C4-ligand[d] [µmol/m²] | Triphenyl-ligand[e] [µmol/m²] | $SO_3H$-ligand[f] [µmol/m²] |
|---|---|---|---|---|---|---|---|---|---|---|---|
| C4-SP | 1.46 ± 0.04 | 0.45 ± 0.01 | < 0.03 | < 0.02 | 9.72 | — | | — | 2.43 | — | — |
| C18-SP | 2.74 ± 0.05 | 0.64 ± 0.01 | < 0.03 | < 0.02 | 22.81 | — | | 1.20 | — | — | — |
| SH-SP | 1.88 ± 0.01 | 0.43 ± 0.00 | < 0.03 | 1.32 ± 0.02 | 15.65 | 4.12 | 3.79 | — | — | — | — |
| Triphenyl-SP | 6.82 ± 0.02 | 0.88 ± 0.01 | < 0.03 | 1.29 ± 0.02 | 56.78 | 2.06 | 1.74 | — | — | 1.96 | — |
| Triphenyl-SAX-SP | 4.22 ± 0.01 | 0.68 ± 0.01 | < 0.03 | 1.24 ± 0.00 | 35.13 | 2.01 | 1.49 | — | — | 0.93 | — |
| Triphenyl-ZWIX-SP | 3.94 ± 0.04 | 0.65 ± 0.01 | < 0.03 | 1.20 ± 0.02 | 32.80 | — | < 0.1 | — | — | 0.82 | 2.10 |

[a]Determined by elemental analysis.
[b]Calculated based on sulfur content (EA) and quantity of attached ligand assuming complete reaction (note, surface area of non-modified silica was used for all calculations of surface coverages).
[c]Determined by DPDS assay for determination of reactive sulfhydryls.
[d]Calculated based in elemental analysis data assuming bifunctional bonding.
[e]Calculated based on elemental analysis data of SH-SP and the respective SPs.
[f]Calculated assuming full oxidation.

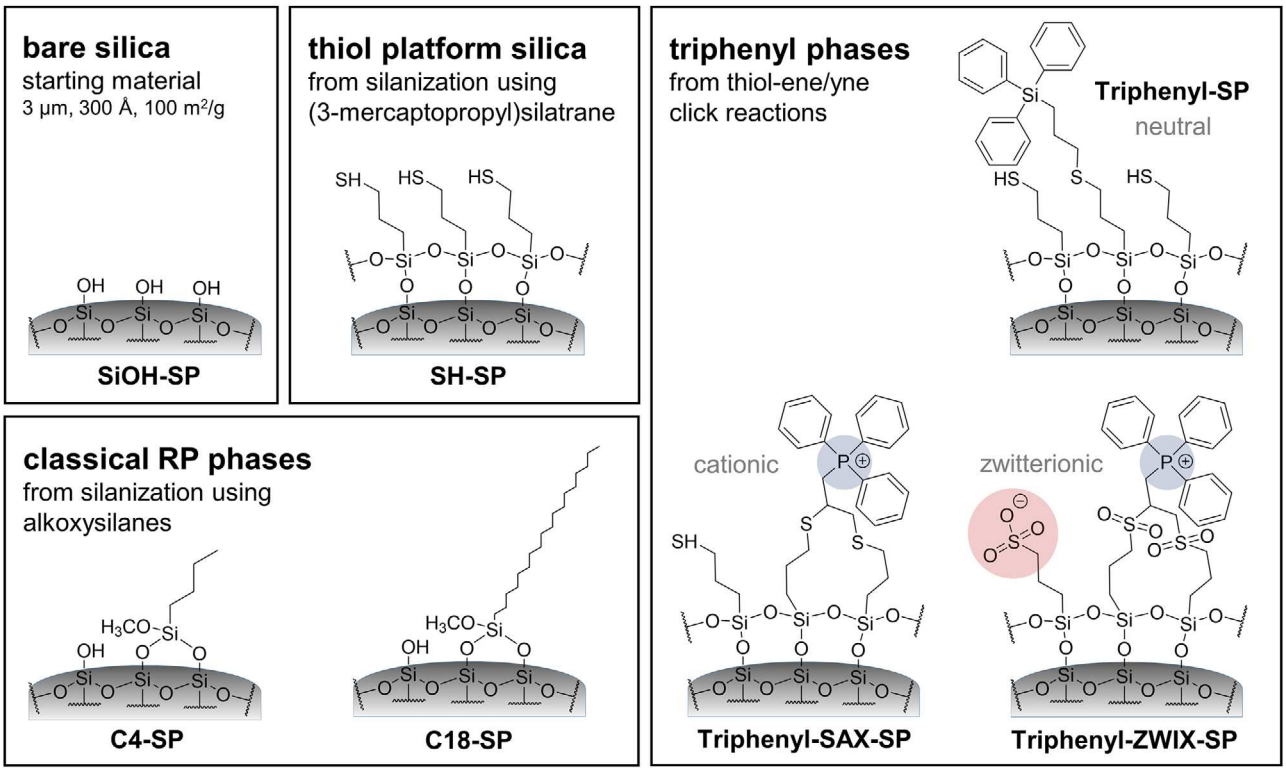


**FIGURE 1** | Surface chemistries of the prepared stationary phases. Synthesis procedures for C4-SP and C18-SP are described in the supplementary material (see Figure S3). All stationary phases were manufactured starting from the same spherical silica (3 µm, 300 Å, 100 $m^2$/g).

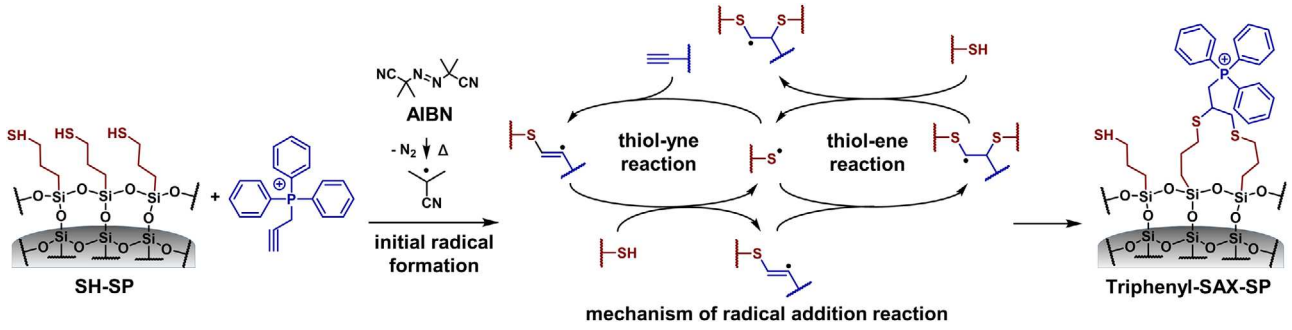


**FIGURE 2** | Synthesis scheme for the preparation of the triphenyl-SAX-SP by thiol-yne/ene click reaction. After thermally initiated radical formation, the radical is transferred from the decomposition product of the initiator to the thiol groups. The thiyl radical generated causes a hydrothiolation reaction on the double or triple bonds of the reaction partners. As a result, the formation of a thioether takes place subsequently. In this process, a carbon-centered radical is formed intermediately, which provokes a prolonged reaction by transferring the radical to the next thiol group. Therefore, double bonds can react once with one thiol group, whereas triple bonds can react with up to two thiol groups.

reaction to ensure that all triethanolamine moieties are cleaved off in the course of the reaction. Herein, the water content of the humidified silica was determined to be 48% (w/w). Subsequently, the resultant thiol silica was analyzed by elemental analysis (see Table 1) and solid-state $^{13}C$ and $^{29}Si$ CP/MAS NMR spectroscopy (see Figure 3). It showed similar results in agreement with the two-step silanization approach using silatrane in the previous study [28]. It can be seen from Table 1 that a very high density of incorporated sulfhydryl groups (4.12 µmol/$m^2$) was obtained by the single-step silanization reaction with silatrane. It indicates a polysiloxane layer on the silica surface rather than a trifunctional brush-type immobilization, which does not reach such high surface coverage (see Figure S6). The $^{29}Si$ CP/MAS NMR spectrum (Figure 3A) reveals that the thiol ligands are mainly attached by trifunctional siloxane bonding to the support (T3: 67.8%) with less bifunctional bonding (T2: 28.3%). There are very few monofunctional siloxane-bonded ligands (T1: 3.9%). In contrast to the findings of the previous two-step study, however, more than 90% of the thiol groups calculated by elemental analysis could also be detected by means of a thiol-disulfide exchange reaction, indicating the accessibility and reactivity of the sulfhydryl moieties incorporated by this single-step approach. It can be concluded that the present single-step surface functionalization leads to less oxidation than the previous two-step approach. It is favorable as a higher concentration of reactive surface sulfhydryls is available for ligand attachment. These findings indicate the superiority of

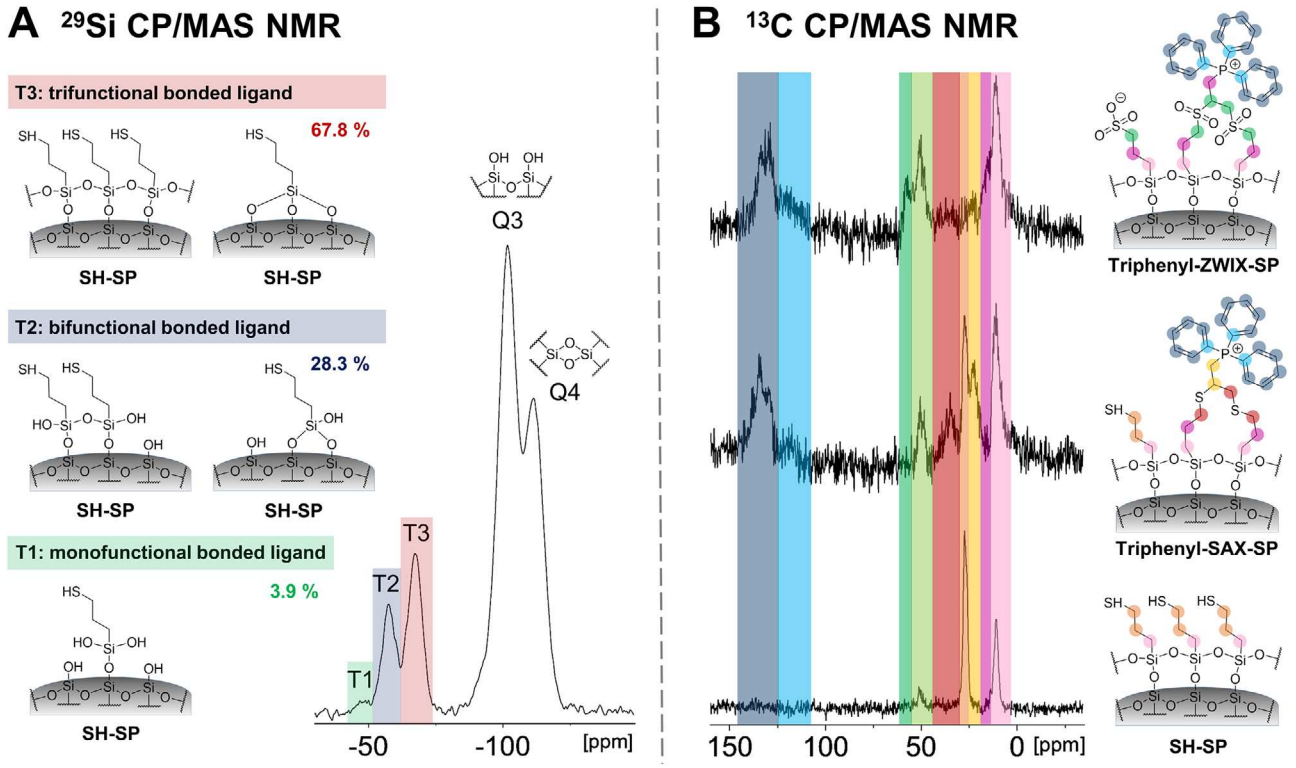


**FIGURE 3** | (A) $^{29}$Si CP/MAS NMR analysis of SH-SP and (B) $^{13}$C CP/MAS NMR spectra for SH-SP, triphenyl-SAX-SP and triphenyl-ZWIX-SP. (A) The $^{29}$Si NMR spectrum of SH-SP exhibits the three characteristic signals for modified silica (T1, T2, and T3) beside the typical signals for the silica support (Q3: free single and vicinal silanol groups, Q4: siloxane groups). T1, T2, and T3 can be assigned to the silicon atoms of the diverse 3-mercaptopropyl siloxane bonds immobilized on the silica surface, giving information about the proportion of mono-, di-, and trifunctional siloxane-linked moieties. (B) $^{13}$C NMR spectra illustrate the successful synthesis of SH-SP, triphenyl-SAX-SP, and triphenyl-ZWIX-SP. Thus, the successful immobilization of the phenyl ligands is proven as well as the accomplished oxidation of the residual sulfhydryl groups. The signal at approximately 50 ppm (bright green) can be attributed to methoxy groups generated on the silica surface due to the methanolic solvent used in the synthesis.

the new single-step grafting approach and make it a viable way to overcome the accessibility problems of the sulfhydryl groups that occurred by earlier synthesis approaches.

### 3.2 | Immobilization of Triphenyl Ligands by Thiol-Yne/Ene Click Reaction

A set of diverse triphenyl-modified stationary phases was prepared by further decoration of the thiol platform silica by efficient immobilization through thiol-ene/yne click reactions. These radical addition reactions are simple, generally highly efficient, proceed with high yields, and are characterized by fast reaction kinetics, high selectivities, and mild reaction conditions. They are therefore a powerful chemical strategy for surface modification of silica involving the reaction between a thiol and an ene- or yne-group-bearing component. As a result, the formation of one or two new carbon-sulfur bonds occurs, respectively [29, 34, 35]. For the preparation of uncharged triphenyl-SP, allyltriphenylsilane was used as the ene component, and thermal initiation with AIBN as radical initiator was applied (see Figure S4). Elemental analysis results revealed that about 50% of the determined sulfhydryl groups reacted with the triphenyl-ligand providing a calculated ligand coverage of 1.96 µmol/m$^2$ for the triphenyl-SP (see Table 1). This was significantly higher compared with the quantity of immobilized *tert*-butyl quinine (0.25 µmol/m$^2$) reported in the previous study (see [28]) for the thiol-ene reaction on thiol-silica from a two-step synthesis approach. This stationary phase still contained around 1.74 µmol/m$^2$ reactive sulfhydryls after ligand immobilization.

The permanently positively charged triphenyl-SAX-SP was prepared with 2-propinyl-triphenylphosphonium bromide as the yne component (see Figure S4). The reaction mechanism is schematically illustrated in Figure 2. While ene components can only react with a single sulfhydryl group on the silica surface, leading to the anti-Markovnikov product, yne components can react with two sulfhydryl moieties (Figure 2). This might be beneficial since it leads to doubly tethered linkages to the surface resulting in higher chemical stability of the surface chemistry and lower ligand bleeding, respectively. From elemental analysis data, a surface coverage of 0.93 µmol/m$^2$ was calculated for the triphenyl-SAX-SP (see Table 1). A relative ligand density ratio between triphenyl-SP (thiol-ene, 1 thiol per ene) and triphenyl-SAX-SP (thiol-yne, two thiols per yne) of 2.1:1.0 was calculated from EA, which corresponds almost exactly to the ratio of reactions with thiol groups possible per immobilized ligand (2:1, yne-/ene-component). The $^{13}$C CP/MAS NMR spectrum of the triphenyl-SAX-SP shows additional signals from the thioether-bonded alkyne group between 30 and 40 ppm and the phenyl residues at around 120–140 ppm confirming the successful immobilization of the ligand (see Figure 3). In contrast to the

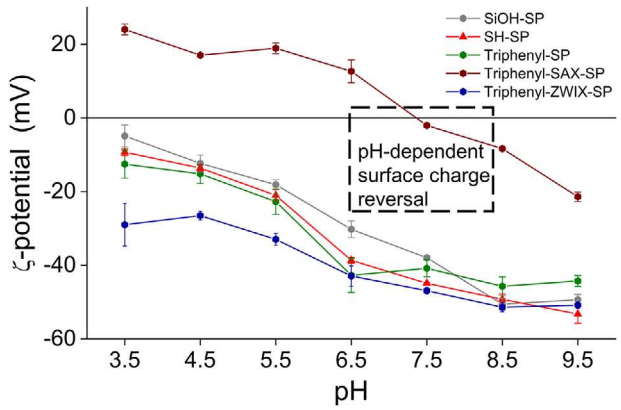


**FIGURE 4** | ζ Potentials of the modified silica particles determined by electrophoretic light scattering at different pH values (10 mM KCl in 1 mM buffer).

triphenyl-SP, the triphenyl-SAX-SP offers an additional anion exchange site due to the central phosphonium group, which is surrounded by three bulky phenyl groups. Such bulky moieties were assumed to shield the charged site from short-range ionic interactions with counterionic analytes and diminish silanol interactions of the analytes by electrostatic shielding or steric hindrance.

### 3.3 | Generation of Zwitterionic Surface by Oxidation of Residual Thiols

Zwitterionic surfaces have shown interesting and promising properties in LC, in particular in HILIC and ion chromatography. In order to insert additional strong cation-exchange sites and enable attractive and repulsive electrostatic interactions simultaneously, triphenyl-SAX-SP was oxidized using performic acid. Performic acid is an efficient oxidizing agent that can be used under mild conditions at which silica and siloxane bonds are stable. Hereby, unreacted residual sulfhydryl groups were oxidized to sulfonic acid moieties, and consequently a zwitterionic surface was created [36]. Contrary to classical sulfobetaine phases widely used in HILIC, opposite charges were on distinct ligands and farther apart from each other, probably leading to imperfect charge compensation.

The successful oxidation was proven by determination of sulfhydryl groups via a thiol-disulfide exchange reaction using DPDS, $^{13}$C CP/MAS NMR analysis, and pH-dependent ζ-potential measurements (vide infra). After the oxidation procedure, no remaining residual thiol groups could be detected by the DPDS assay (see Table 1). According to elemental analysis, there is a 2-fold excess of sulfonic acid moieties compared to phosphonium groups, which may lead to the assumption that the surface is net negatively charged (see ζ-potential measurements in Figure 4). In the $^{13}$C NMR spectrum, typical signals for the mercaptopropyl moiety at around 20–30 ppm disappeared or were shifted, being indicative of a successful oxidation of both sulfhydryls and thioethers of triphenyl-SAX-SP (see Figure 3). Sulfhydryls are oxidized to sulfonic acids while thioethers get oxidized to sulfone groups.

### 3.4 | Surface Charge Characterization by ζ-Potential Measurements

ζ-Potentials have been determined by electrophoretic light scattering with suspensions of the (modified) silica particles in a solution of 10 mM KCl in 1 mM buffer [37]. It allows one to indicate changes in the surface chemistry and gives an orientation of the charge state under distinct chromatographic conditions. Thus, ζ-potentials were recorded for all materials, including the bare silica support (SiOH-SP), at different pH values in the range between pH 3.5 and 9.5. It can be seen in Figure 4 that bare silica shows negative ζ-potentials over the entire pH range. With increasing pH, the surface charge increases as more and more silanols get dissociated, and hence the negative ζ-potentials increase from −5 mV at pH 3.5 (silanols mostly non-dissociated) to −50 mV (silanols fully dissociated). There is a slight change in the ζ-potentials of the thiol-modified particles and the triphenyl-SP with a neutral surface bonding structure to more negative values, which appears unexpected at first instance as some silanols are modified and hence less residual silanols are expected to be available. However, the aqueous treatment of the bare silica prior to thiol modification (prewetting step) can lead to the hydrolytic cleavage of siloxane bonds and consequently to the formation of new silanol groups. Thus, the net charge of SH-SP and triphenyl-SP was found to be more negative than for precursor SiOH-SP. In sharp contrast, modification of the SH-SP particles with triphenylphosphonium moieties in triphenyl-SAX-SP shifted its ζ-potential to positive values in the low pH range, being indicative of a net positive surface charge. However, charge reversal (umpolung) occurs for this material at approximately pH 7.5, leading to negative surface charges above this pH value due to the increasing deprotonation of the silanols. Furthermore, ζ-potentials of the triphenyl-ZWIX-SP particles dropped significantly after oxidation by −30 mV (high pH) to −50 mV (low pH) due to the embedded, permanently negatively charged sulfonate groups which confirms the successful oxidation of the residual thiols as derived from the DPDS assay and elemental analysis. It also indicates the excess of sulfonate groups, over phosphonium moieties (see Figure 4).

### 3.5 | Chromatographic Evaluation

As the first chromatographic test to characterize primarily the RP-type triphenyl-SP with neutral surface bonding in comparison to C4- and C18-SP as benchmarks, a Tanaka test was performed on all columns [38–40]. The different properties tested and analytes used as probes to do so, as well as corresponding calculations of characteristic values (typically obtained as separation factors of the ratio of the retention factors of two specific analytes), are briefly summarized in Table S1. The results of the Tanaka test achieved for the various SPs are depicted in suppl. Table S2, and a graphical representation by a spider plot is given in Figure 5. The Tanaka test is designed to compare RP-type phases, and therefore the results are particularly meaningful for RP-type phases. The results for ionic mixed-mode phases (see Figure S8) must be interpreted with caution, taking into account the effects of ion-exchange sites, which are not present in classical RP-type phases (with the exception of pH-dependent ionized residual silanols).

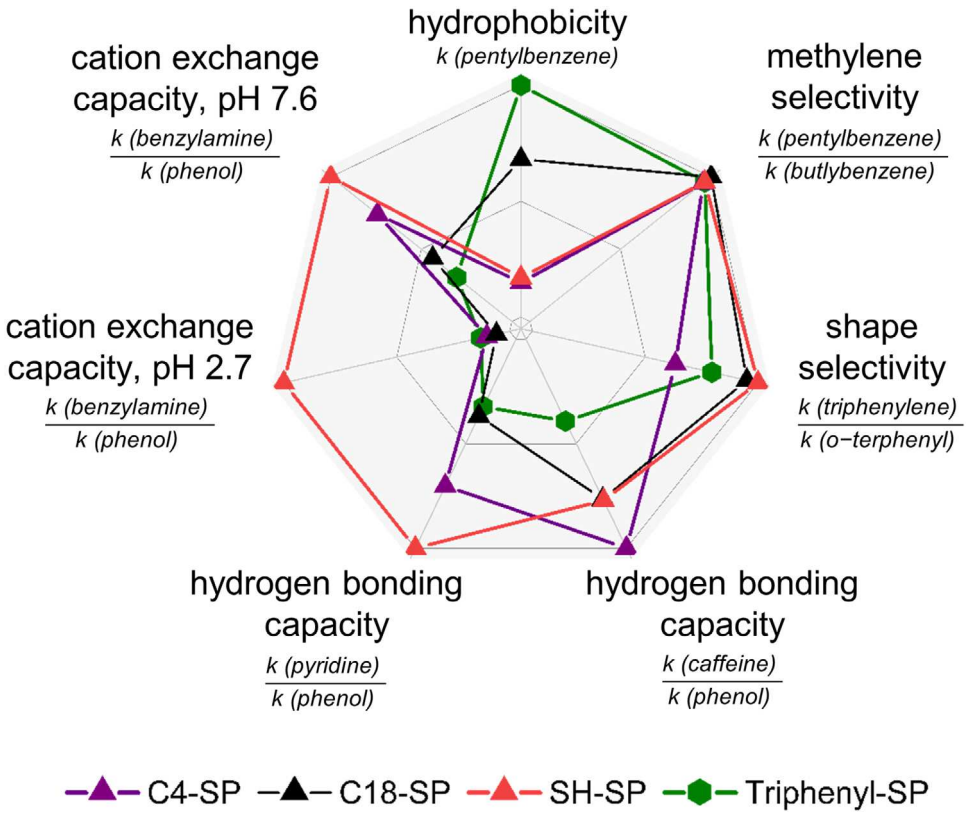


**FIGURE 5** | Normalized radar plot based on chromatographic investigation under Tanaka test conditions for RP-type phases. Further information concerning chromatographic conditions and parameters can be found in Figures S8 and S9 and Tables S1 and S2.

Since all stationary phases were based on 300 Å pore size silica, the hydrophobicity of the SPs and hydrophobic retention (as measured by *k* of pentylbenzene), respectively, are relatively small as compared to standard 100 Å RP18 stationary phases. It declined in the order of triphenyl-SP > C18-SP > C4 ~ SH-SP, roughly in the order of the carbon content determined by elemental analysis (see Figure 5) (note, mixed-mode phases will be discussed separately below). Accordingly, also the hydrophobic selectivity was smaller herein than on 100 Å RP18 stationary phases (C18-SP > triphenyl-SP ~ SH-SP > C4-SP). The shape selectivity was the highest for the SH-SP, as the 3-mercaptopropyl ligands were most densely packed, followed by the C18-SP > triphenyl-SP > C4-SP (Figure 5). The separation factors between caffeine and phenol, as well as pyridine and phenol, represent the hydrogen acceptor and hydrogen donor capacities of the SPs, respectively (collectively hydrogen bonding capacities). The radar plot in Figure 5 reveals that the triphenyl-SP exhibits the lowest hydrogen bonding capacities of these four RP-type phases, both regarding H-acceptor and H-donor capacities. Since it depends on the available silanol moieties, it can be concluded that the triphenyl-phase has fewer silanol interactions than the other three RP-type phases tested. In contrast to C4- and C18-SP, the triphenyl-SP exhibits therefore also less cation exchange properties at pH 2.6 and pH 7.6, which indicates a better shielding of the analytes from the surface silanols as well. Furthermore, the high value for silanol activity of the precursor SH-SP may be partly explained by the weakly acidic sulfhydryls, which may contribute to this parameter.

Table S2 and Figure S8 also show the corresponding results of the mixed-mode ion-exchange phases triphenyl-SAX-SP and triphenyl-ZWIX-SP (for structures of the analytes employed for the Tanaka test, see Figure S9). Both mixed-mode ion-exchange phases have lower hydrophobicity due to the charged phosphonium moiety and sulfonic acid residues, respectively, and lose their methylene selectivity. On the other hand, both mixed-mode ion-exchange phases show surprisingly high shape selectivity, which is significantly higher than the one of triphenyl-SP (Table S2). It is striking that this is an incident with the type of immobilization by thiol-yne click reaction, which leads to doubly tethered chromatographic ligands imposing rigidity to the pendant triphenyl phosphonium selector. The H-bond acceptor properties of the triphenyl-SAX-SP are comparable to those of the triphenyl-SP (since it depends on the residual silanol surface, which is similar in the two phases). On the triphenyl-ZWIX-SP, the H-acceptor properties are significantly enhanced due to sulfone and sulfonate moieties. The test for the H-donor properties ($k_{pyridine}/k_{phenol}$) of the triphenyl-SAX-SP is affected by superimposed repulsive electrostatic interactions between the phosphonium moiety and the pyridine probe, perturbing the assessment of the H-donor properties of the SP. On the contrary, on triphenyl-ZWIX-SP, a cation-exchange process is superimposed so that the H-donor test is actually additively composed of the sum of retention increments from H-donor interactions and cation-exchange. The cation exchange test at pH 2.7 shows strong repulsive interactions between the phosphonium moiety and benzylammonium probe of the Tanaka test on the

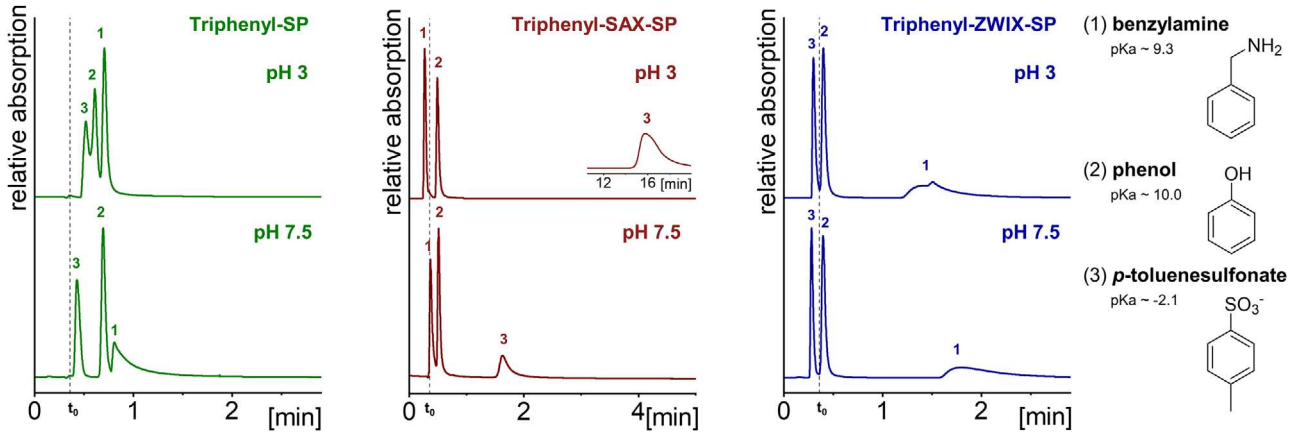


**FIGURE 6** | Evaluation of the ion exchange characteristics of the triphenyl-SP, triphenyl-SAX-SP and triphenyl-ZWIX-SP at pH 3 and pH 7.5. Chromatographic conditions: The mobile phase consisted of MeOH/aqueous ammonium phosphate buffer (20 mM, adjusted to pH 3 or pH 7.5) (30/70, v/v), flow rate: 1 mL/min, temperature: 25°C, injection volume: 5 µL.

triphenyl-SAX-SP, while a strong cation-exchange retention mechanism is imposed on the triphenyl-ZWIX-SP due to sulfonic acid moieties. At pH 7.6, the triphenyl-SAX-SP is close to its pI (near the neutral net surface), and hence repulsive electrostatic interactions as well as, cation-exchange (with dissociated silanols), become negligible. In contrast, on the triphenyl-ZWIX-SP a strong cation exchange process gets activated at pH 7.6 for benzylammonium as expected from the sulfonic acid groups.

In addition, the surface charge characteristics were investigated chromatographically by another test mixture consisting of a set of three different analytes with varying $pK_a$ values (acidic, neutral, basic) that were applied at different mobile phase pH values (pH 3 and 7.5). The results are illustrated in Figure 6 and Table S3. Here, both triphenyl-SP (due to residual silanols) and triphenyl-ZWIX-SP (due to sulfonic acid moieties) demonstrated cation-exchange characteristics at both pH values. Thus, benzylamine eluted last on both columns. The negatively charged analyte *p*-toluenesulfonate eluted first on these two SPs due to repulsive electrostatic interactions and interestingly prior to the dead volume marker on the triphenyl-ZWIX-SP due to (partial) ion-exclusion from the pores. In contrast, there was still retention observed for the analyte on triphenyl-SP, most probably due to the higher proportion of hydrophobic interactions (cf. ligand densities; Table 1) and less accessible anionic interaction sites. The triphenyl-SAX-SP, on the other hand, showed a different behavior and exhibited anion-exchange properties, as expected. Consequently, the elution order was reversed in comparison to the two other triphenyl-modified SPs, and the anionic analyte eluted last. However, its retention was dramatically reduced by switching the pH from 3 to 7.5, which is quite common for silica-based anion exchangers, indicating the immense influence of the deprotonated silanols on the surface charge. According to the determined ζ-potentials, even a reversal of the elution order could be expected above pH 7.5. In this case, however, the net charge does probably not correspond exactly to the chromatographically accessible charged interaction sites at the surface, as the bulky triphenyl groups might impede the penetration of the analytes to the unmodified silica surface and therefore suppress direct interactions with the deprotonated silanol groups. Instead, the benzylammonium analyte is repelled from the surface by the phosphonium moiety and elutes therefore before $t_0$ with a slight ion-exclusion effect.

### 3.6 | Stationary Phase Classification via PCA

In order to classify the novel stationary phases within a set of commercially available columns, standard HILIC and RPLC tests were performed, and the resultant retention factors subjected to PCA. Chromatographic conditions, data obtained, and the surface chemistries of commercial columns are illustrated and summarized in Figures S10–S13 and Table S4. The score plot is depicted in Figure 7. Here, apparently, the latent variable PC1 encodes mostly for the hydrophobicity of the stationary phases (which decreases from low to high PC1), whereas PC2 reflects primarily the surface charge (net charge positive at low PC2 values and negative at high PC2).

As expected, amongst the new triphenyl phases, triphenyl-SP was found to be the phase with the most pronounced hydrophobic properties, which is underpinned by its close clustering to Synergi Fusion-RP (which is a polar embedded C18 phase that offers balanced polar and hydrophobic selectivity). This hydrophobic character was reduced by the introduction of the ionic interaction sites in triphenyl-SAX-SP and triphenyl-ZWIX-SP, which are located on the PC1 scale between the classic alkyl phases (C4- and C8-SP), which are more hydrophobic, and pure silica (SiOH-SP), which is less hydrophobic. In terms of hydrophobicities, these two mixed-mode phases are similar to those of Uptisphere MM3 (RP phase with cationic endcapping; octyl/strong anion exchanger) and Chiralpak QN-AX (chiral stationary phase with properties resembling achiral RP/WAX columns). The zwitterionic mixed-mode phase Obelisc R is a bit less hydrophobic. In terms of surface charge, triphenyl-SP is located closely to C18-SP, which illustrates the shielding effect of the bulky phenyl moieties similar to the long octadecyl moieties. Due to the shielding, silanols are less accessible for chromatographic interactions with the analytes than it is the case for phases containing smaller ligands, which cannot shield the silanols (cf. C4-SP). On the contrary, triphenyl-SAX-SP and triphenyl-ZWIX-SP exhibited more distinctive surface charge characteristics. Thus, triphenyl-SAX-SP

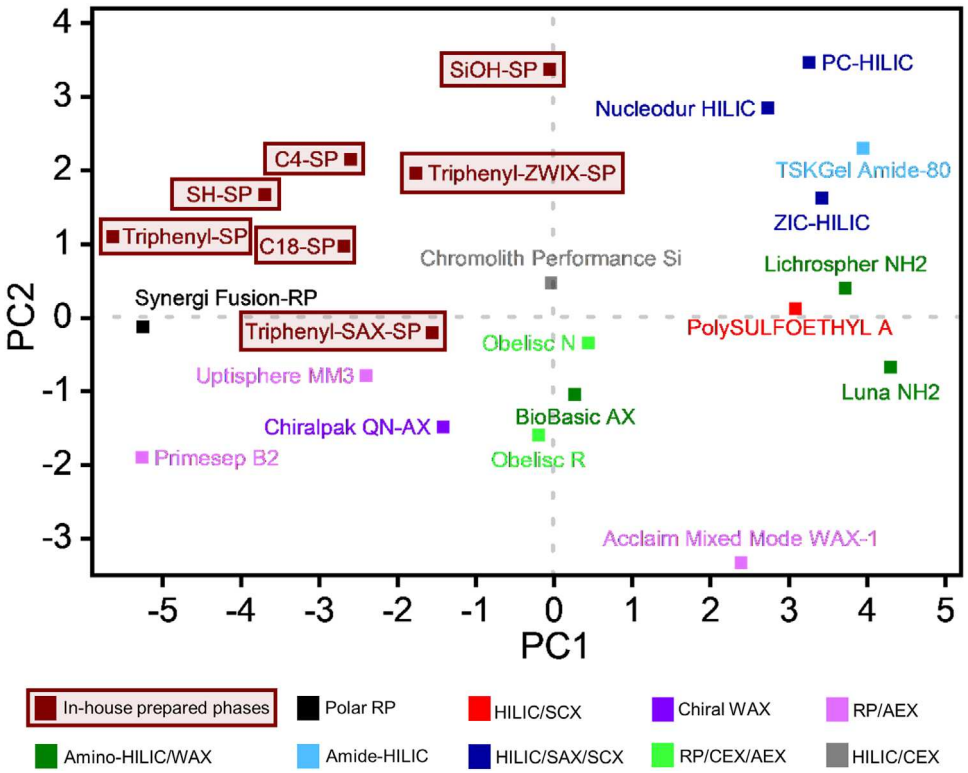


**FIGURE 7** | Score plot of principal component analysis (PCA) for column classification. The corresponding loading plot can be found in Figure S13.

showed a slightly positive surface charge, according to the PCA score plot, similar to the zwitterionic mixed-mode phase Obelisc N with a terminal positively charged group and an interior negatively charged functional group embedded in the alkyl ligand strand (see Figure S12) and the amino phase Uptisphere MM3 (octyl-SP with SAX endcapping). The zwitterionic mixed-mode phase triphenyl-ZWIX-SP, on the other hand, is located between the two sulfobetaine-type zwitterionic columns ZIC-HILIC and Nucleodur HILIC in terms of PC2 (indicative of its negative surface charge). In conclusion, the three prepared phenyl-phases cover a broad range of hydrophobicity and surface charge, leading to orthogonality of retention characteristics. This might make the set of triphenyl-modified SPs a useful tool for a variety of analytical separations.

### 3.7 | Analysis of Glycopeptide Teicoplanin Utilizing Triphenyl-Modified Stationary Phases

Teicoplanin is a multicomponent antibiotic drug and consists of several glycopeptides varying in the attached fatty acid residue (see Figure S14). Thus, they differ mainly in hydrophobicity. Consequently, these different species are typically resolved by reversed-phase chromatography [41, 42]. Accordingly, the two synthesized classical RP phases (C4-SP and C18-SP) were utilized as benchmarks for comparison. As it can be seen in Figure 8A, all columns were able to resolve at least three peaks. In this particular application, it seems that the SPs with neutral hydrophobic surface bonding (triphenyl-SP and C18-SP) are beneficial, as the glycopeptide variants differ in the lipophilicity of the fatty acyl side chains. The triphenyl-SP shows stronger retention than the C18-SP and some minor differences in the selectivity profile. The C4-SP does not have enough hydrophobicity to sufficiently separate the different forms differing in fatty acyl hydrophobicity and branching. In contrast, the other two triphenyl mixed-mode SPs offer additional electrostatic interactions. Obviously, these additional interactions caused peak broadening and an accompanying loss of resolution due to slow adsorption–desorption–kinetics of ion-exchange processes. Since teicoplanin offers an excess of negatively charged sites due to the carboxylic acid function and the phenolic hydroxyl groups, repulsion on the net negatively charged triphenyl-ZWIX-SP leads to faster elution of the analytes than observed on the triphenyl-SP. In contrast, the triphenyl-SAX-SP showed increased retention for the analytes due to the embedded positively charged phosphonium moieties leading to a superimposed anion exchange process. However, this is not of benefit for the present application, as the macro- and micro-variants do not differ in charge nor hydrophilicity. Consequently, for this specific application, the triphenyl-SP has a clear advantage over the triphenyl mixed-mode SPs (triphenyl-SAX-SP, triphenyl-ZWIX-SP).

### 3.8 | Analysis of Small Interfering Ribonucleic Acid Patisiran Utilizing Triphenyl-Modified Stationary Phases

Patisiran is a small interfering ribonucleic acid (siRNA) that is utilized for the medical treatment of hereditary transthyretin-mediated amyloidosis. It consists of two partially complementary single strands. The sense and the antisense strand are composed of 21 nucleotides that are linked via phosphodiester bonds; some of the 2′-hydroxyls are methylated (indicated with m, see Figure S15). The two-nucleotide overhang consists of

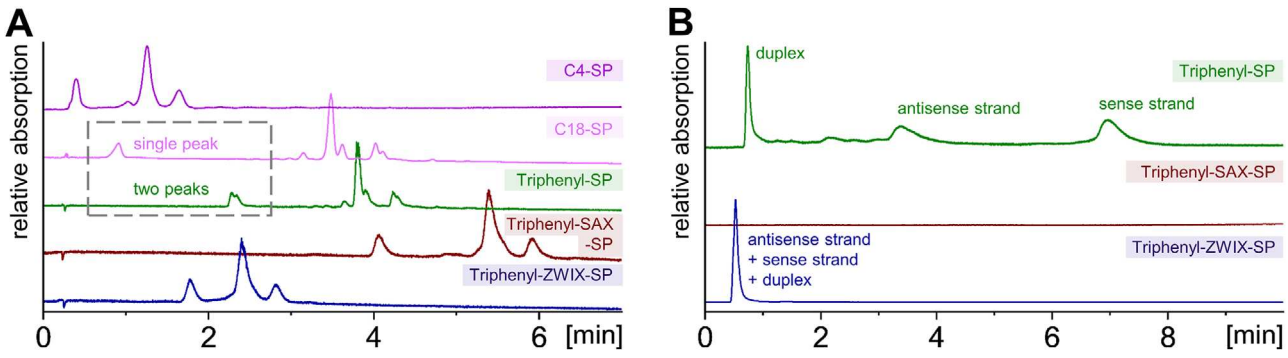


**FIGURE 8** | (A) Analysis of the biomolecules teicoplanin and (B) patisiran. The chemical structure of the biomolecules can be found in Figures S14 and S15. (A) Analysis of teicoplanin subspecies utilizing the set of triphenyl-modified SPs and comparative RP-SPs. Chromatographic conditions: Mobile Phase A consisted of water containing 10 mM ammonium acetate (pH adjusted to pH 5.4), mobile Phase B consisted of mobile Phase A and acetonitrile (5/95, v/v), flow rate: 1.0 mL/min, gradient time: 20 min (10% B to 100% B) temperature: 30°C, injection volume: 3 µL, detection: 210 nm. (B) Comparison of patisiran sense and antisense strand analysis on the three triphenyl-modified SPs. Chromatographic conditions: Mobile Phase A consisted of water containing 20 mM ammonium acetate, mobile Phase B consisted of mobile Phase A and methanol (90/10, v/v), flow rate: 0.6 mL/min, gradient time: 10 min (5% B to 20% B), temperature: 40°C, injection volume: 5 µL, detection: 254 nm.

desoxyribose residues. For liquid chromatography of oligonucleotides, ion-pairing reversed-phase liquid chromatography is usually the technique of choice. However, there is a quest for ion-pair-free RP or HILIC methods that prevent contamination of the LC-MS system with ion-pairing agents [43–48].

In this study, ion-pair reagent-free reversed-phase chromatography was carried out using 20 mM ammonium acetate buffer and a methanol gradient for elution. As it is shown in Figure 8B, the sense and antisense strands were well resolved on the triphenyl-SP under these conditions. As can be seen from Figure S16, the selectivity between sense and antisense strands is significantly larger than in ion-pair RPLC with BEH C18. It can be assumed that both hydrophobic and $\pi$–$\pi$-interactions contribute to the separation of the two strands on the triphenyl-SP. In this context, it should be mentioned that the separation was performed at a column temperature (40°C) close to the melting temperature of patisiran ($T_{m,calc}$ = 46.9°C). Hence, both duplex and single strands are visible. At temperatures significantly above $T_m$, the duplex peak should disappear. The duplex species eluted earlier, close to $t_0$, since the nucleobases are mutually saturated by intermolecular hydrogen bonding and base stacking and thus shielded from interaction with the triphenyl-SP. Since there are multiple negatively charged phosphate groups freely available in the duplex siRNA, elution close to $t_0$ might be driven by repulsive electrostatic interactions with dissociated silanols. In sharp contrast, ionic interactions play a decisive role in the retention and elution of patisiran on the other two triphenyl-modified phases. Since the sugar-phosphate backbones of the siRNA strands offer negatively charged interaction sites, strong retention occurred on the positively charged triphenyl-SAX-SP in accordance with an anion-exchange process, and no elution was observed with typical RP conditions due to the multiply negatively charged analyte and a weak elution strength of the mobile phase (low ionic strength of 20 mM ammonium acetate). However, in anion-exchange mode with gradient elution using 1 M NaCl, the patisiran single and duplex strands (injected as single component standards) could be eluted and were well separated (Figure S17A). In contrast, there was no retention observed on the zwitterionic triphenyl-ZWIX-SP, which possesses an overall negative net charge due to the excess of negatively charged sulfonate groups, and hence electrostatic repulsion leads to fast elution, even faster than the elution of the duplex species on triphenyl-SP. These results suggest that a fine-tuning of the mobile phase or of the proportion of negatively and positively charged sites on the triphenyl-SPs can lead to a very useful stationary phase for charged analytes with combined adsorptive and repulsive interaction sites offering complementary selectivities.

## 4 | Concluding Remarks

In this work, the preparation of a new set of triphenyl-modified stationary phases, partially embedded with ion-exchange properties leading to mixed-mode RP/ion-exchange phases, for high-performance liquid chromatography was reported. For this purpose, thiol-silica was utilized as a carrier and further decorated with triphenyl-ligands by thiol-ene/yne click immobilization reaction. Herein, also an innovative strategy utilizing silatrane chemistry for the synthesis of the thiol-silica was applied. Thus, thiol-silica with a great amount of trifunctional siloxane-bonded ligands was obtained, and the accessibility of the sulfhydryl groups was preserved. Chromatographic tests indicated the increased shielding of silanols due to the introduction of a dense polysiloxane layer and bulky triphenyl moieties. The PCA illustrated the similarities and orthogonality to commercially available columns. Additionally, $\zeta$-potential determinations exhibited the differences in pH-dependent surface charges of the prepared phases. Finally, the prepared columns were applied for liquid chromatography analysis of the biomolecules teicoplanin and patisiran. These analyses showed that there is still fine-tuning of chromatographic conditions and charge properties of the phases needed. However, the concept seems to be promising, and further investigation will be part of future studies.

### Author Contributions

**Marc Wolter**: investigation, conceptualization, methodology, formal analysis, data curation, visualization, supervision, writing–original draft,

writing–review and editing. **Mirna Maalouf**: investigation. **Mateusz Janek**: investigation. **Cornelius Knappe**: supervision. **Markus Kramer**: investigation. **Michael Lämmerhofer**: conceptualization, methodology, supervision, writing–review and editing, resources.

**Acknowledgments**

Open access funding enabled and organized by Projekt DEAL.

**Conflicts of Interest**

The authors declare no conflicts of interest.

**Data Availability Statement**

The data that supports the findings of this study are available in the Supporting Information Material of this article.

**References**

1. D. Sykora, P. Rezanka, K. Záruba, and V. Král, "Recent Advances in Mixed-Mode Chromatographic Stationary Phases," *Journal of Separation Science* 42 (2019): 89–129.

2. L. J. Wang, W. L. Wei, Z. N. Xia, X. Jie, and Z. Z. L. Xia, "Recent Advances in Materials for Stationary Phases of Mixed-Mode High-Performance Liquid Chromatography," *TRAC-Trends in Analytical Chemistry* 80 (2016): 495–506.

3. L. Zhang, Q. Dai, X. Q. Qiao, C. Y. Yu, X. Y. Qin, and H. Y. Yan, "Mixed-Mode Chromatographic Stationary Phases: Recent Advancements and Its Applications for High-Performance Liquid Chromatography," *TRAC-Trends in Analytical Chemistry* 82 (2016): 143–163.

4. K. Zhang and X. D. Liu, "Mixed-Mode Chromatography in Pharmaceutical and Biopharmaceutical Applications," *Journal of Pharmaceutical and Biomedica* 128 (2016): 73–88.

5. M. Laemmerhofer, M. Richter, J. Y. Wu, R. Nogueira, W. Bicker, and W. Lindner, "Mixed-Mode Ion-Exchangers and Their Comparative Chromatographic Characterization in Reversed-Phase and Hydrophilic Interaction Chromatography Elution Modes," *Journal of Separation Science* 31 (2008): 2572–2588.

6. J. L. Dores-Sousa, J. De Vos, W. T. Kok, and S. Eeltink, "Probing Selectivity of Mixed-Mode Reversed-Phase/Weak-Anion-Exchange Liquid Chromatography to Advance Method Development," *Journal of Chromatography A* 1570 (2018): 75–81.

7. X. J. Ren, C. X. Hu, D. Gao, et al., "Preparation of a Poly(Ethyleneimine) Embedded Phenyl Stationary Phase for Mixed-Mode Liquid Chromatography," *Analytica Chimica Acta* 1042 (2018): 165–173.

8. J. Q. Zhou, M. J. Wan, X. M. Dai, et al., "Polar-Embedded Phenyl Dendritic Stationary Phase for Multi-Mode Chromatographic Separation," *Microchemical Journal* 185 (2023): 108303.

9. B. B. Yang, H. M. Liu, J. Chen, M. Guan, and H. D. Qiu, "Preparation and Evaluation of 2-Methylimidazolium-Functionalized Silica as a Mixed-Mode Stationary Phase for Hydrophilic Interaction and Anion-Exchange Chromatography," *Journal of Chromatography A* 1468 (2016): 79–85.

10. Y. L. Yang, J. Chen, X. J. Liang, et al., "Adjustable Chromatographic Performance of Silica-Based Mixed-Mode Stationary Phase Through the Control of Co-Grafting Amounts of Imidazole and C18 Chain," *Journal of Chromatography A* 1722 (2024): 464889.

11. M. X. Sun, J. J. Feng, Y. Feng, X. B. Xin, Y. L. Ding, and M. Sun, "Ionic Liquid-Functionalized Dendrimer Grafted Silica for Mixed-Mode Chromatographic Separation and Online Solid-Phase Extraction," *Separation and Purification Technology* 311 (2023): 123266.

12. I. Jardim, L. Maldaner, J. Lourenço, L. M. A. Fioravanti, and C. H. Collins, "Some New Selective Stationary Phases for RP-HPLC," *Journal of Separation Science* 33 (2010): 2917–2929.

13. K. Nakamura, S. Saito, and M. Shibukawa, "Intrinsic Difference Between Phenyl Hexyl- and Octadecyl-Bonded Silicas in the Solute Retention Selectivity in Reversed-Phase Liquid Chromatography With Aqueous Mobile Phase," *Journal of Chromatography A* 1628 (2020): 461450.

14. S. Bocian and B. Buszewski, "Phenyl-Bonded Stationary Phases—The Influence of Polar Functional Groups on Retention and Selectivity in Reversed-Phase Liquid Chromatography," *Journal of Separation Science* 37 (2014): 3435–3442.

15. Y. Sun, Z. A. Sun, C. Z. Wang, and Y. M. Wei, "Effect of Phenyl Numbers in Polyphenyl Ligand on Retention Properties of Aromatic Stationary Phases," *Journal of Chromatography A* 1674 (2022): 463152.

16. K. Croes, A. Steffens, D. H. Marchand, and L. R. Snyder, "Relevance of $\pi$—$\pi$ and Dipole—Dipole Interactions for Retention on Cyano and Phenyl Columns in Reversed-Phase Liquid Chromatography," *Journal of Chromatography A* 1098 (2005): 123–130.

17. Z. Kadlecová, P. Kozlík, E. Tesarová, M. Gilar, and K. Kalíková, "Characterization and Comparison of Mixed-Mode and Reversed-Phase Columns; Interaction Abilities and Applicability for Peptide Separation," *Journal of Chromatography A* 1648 (2021): 462182.

18. D. V. McCalley, "Understanding and Managing Peak Shape for Basic Solutes in Reversed-Phase High Performance Liquid Chromatography," *Chemical Communications* 59 (2023): 7887–7899.

19. V. D'Atri, A. Murisier, S. Fekete, J. L. Veuthey, and D. Guillarme, "Current and Future Trends in Reversed-Phase Liquid Chromatography-Mass Spectrometry of Therapeutic Proteins," *TRAC-Trends in Analytical Chemistry* 130 (2020): 115962.

20. S. Bocian and B. Buszewski, "Residual Silanols at Reversed-Phase Silica in HPLC—A Contribution for a Better Understanding," *Journal of Separation Science* 35 (2012): 1191–1200.

21. T. K. F. Dier, D. Rauber, J. Jauch, R. Hempelmann, and D. A. Volmer, "Novel Mixed-Mode Stationary Phases for Chromatographic Separation of Complex Mixtures of Decomposed Lignin," *ChemistrySelect* 2 (2017): 779–786.

22. D. L. Liu, H. Y. Wang, M. Y. Liang, et al., "Polymerized Phosphonium Ionic Liquid Functionalized Silica Microspheres as Mixed-Mode Stationary Phase for Liquid Chromatographic Separation of Phospholipids," *Journal of Chromatography A* 1660 (2021): 462676.

23. D. Moravcová, J. Planeta, A. W. T. King, and S. K. Wiedmer, "Immobilization of a Phosphonium Ionic Liquid on a Silica Monolith for Hydrophilic Interaction Chromatography," *Journal of Chromatography A* 1552 (2018): 53–59.

24. Z. S. Breitbach and D. W. Armstrong, "Characterization of Phosphonium Ionic Liquids Through a Linear Solvation Energy Relationship and Their Use as GLC Stationary Phases," *Analytical and Bioanalytical Chemistry* 390 (2008): 1605–1617.

25. R. A. Patil, M. Talebi, L. M. Sidisky, A. Berthod, and D. W. Armstrong, "Gas Chromatography Selectivity of New Phosphonium-Based Dicationic Ionic Liquid Stationary Phases," *Journal of Separation Science* 41 (2018): 4142–4148.

26. J. V. Seeley, S. K. Seeley, E. K. Libby, Z. S. Breitbach, and D. W. Armstrong, "Comprehensive Two-Dimensional Gas Chromatography Using a High-Temperature Phosphonium Ionic Liquid Column," *Analytical and Bioanalytical Chemistry* 390 (2008): 323–332.

27. H. X. Qiu, E. Wanigasekara, Y. Zhang, T. Tran, and D. W. Armstrong, "Development and Evaluation of New Zwitterionic Hydrophilic Interaction Liquid Chromatography Stationary Phases Based on 3-P,P-Diphenylphosphonium-Propylsulfonate," *Journal of Chromatography A* 1218 (2011): 8075–8082.

28. C. Geibel, J. Theiner, M. Wolter, M. Kramer, W. Lindner, and M. Laemmerhofer, "Controllable Organosilane Monolayer Density of Surface Bonding Using Silatranes for Thiol Functionalization of Silica Particles for Liquid Chromatography and Validation of Microanalyt-

ical Method for Elemental Composition Determination," *Journal of Chromatography A* 1653 (2021): 462418.

29. M. Wolter, X. Y. Chen, U. Woiwode, C. Geibel, and M. Laemmerhofer, "Preparation and Characterization of Poly(3-Mercaptopropyl)Methylsiloxane Functionalized Silica Particles and Their Further Modification for Silver Ion Chromatography and Enantioselective High-Performance Liquid Chromatography," *Journal of Chromatography A* 1643 (2021): 462069.

30. M. Ferri, S. Baeurer, A. Carotti, et al., "Fragment-Based Design of Zwitterionic, Strong Cation- and Weak Anion-Exchange Type Mixed-Mode Liquid Chromatography Ligands and Their Chromatographic Exploration," *Journal of Chromatography A* 1621 (2020): 461075.

31. J. K. Puri, R. Singh, and V. K. Chahal, "Silatranes: A Review on Their Synthesis, Structure, Reactivity and Applications," *Chemical Society Reviews* 40 (2011): 1791–1840.

32. L. S. Shlyakhtenko, A. A. Gall, A. Filonov, Z. Cerovac, A. Lushnikov, and Y. L. Lyubchenko, "Silatrane-Based Surface Chemistry for Immobilization of DNA, Protein-DNA Complexes and Other Biological Materials," *Ultramicroscopy* 97 (2003): 279–287.

33. S. Sok and M. S. Gordon, "A Dash of Protons: A Theoretical Study on the Hydrolysis Mechanism of 1-Substituted Silatranes and Their Protonated Analogs," *Computational & Theoretical Chemistry* 987 (2012): 2–15.

34. C. E. Hoyle and C. N. Bowman, "Thiol-Ene Click Chemistry," *Angewandte Chemie International Edition* 49 (2010): 1540–1573.

35. C. Geibel, K. Dittrich, M. Wolter, and M. Laemmerhofer, "Thiol-ene Photo-Click Immobilization of a Chiral Chromatographic Ligand on Silica Particles," *Journal of Chromatography A* 1622 (2020): 461133.

36. U. Woiwode, A. Sievers-Engler, A. Zimmermann, W. Lindner, O. L. Sánchez-Muñoz, and M. Laemmerhofer, "Surface-Anchored Counterions on Weak Chiral Anion-Exchangers Accelerate Separations and Improve Their Compatibility for Mass-Spectrometry-Hyphenation," *Journal of Chromatography A* 1503 (2017): 21–31.

37. O. L. Sanchez-Muñoz, E. P. Hernández, M. Laemmerhofer, W. Lindner, and E. Kenndler, "Estimation and Comparison of $\zeta$-Potentials of Silica-Based Anion-Exchange Type Porous Particles for Capillary Electrochromatography From Electrophoretic and Electroosmotic Mobility," *Electrophoresis* 24 (2003): 390–398.

38. C. McHale, A. Soliven, and S. Schuster, "A Simple Approach for Reversed Phase Column Comparisons via the Tanaka Test," *Microchemical Journal* 162 (2021): 105793.

39. K. Kimata, S. Onishi, K. Jinno, et al., "Chromatographic Characterization of Silica C18 Packing Materials. Correlation Between a Preparation Method and Retention Behavior of Stationary Phase," *Journal of Chromatographic Science* 27 (1989): 721–728.

40. M. Euerby and P. Petersson, "Chromatographic Classification and Comparison of Commercially Available Reversed-Phase Liquid Chromatographic Columns Using Principal Component Analysis," *Journal of Chromatography A* 994 (2003): 13–36.

41. Teicoplanin monograph. in: European Pharmacopoeia. 11.0, 2358 (2022): 4143–4146.

42. E. Riva, N. Ferry, A. Cometti, G. Cuisinaud, G. G. Gallo, and J. Sassard, "Determination of Teicoplanin in Human-Plasma and Urine by Affinity and Reversed-Phase High-Performance Liquid-Chromatography," *Journal of Chromatography B* 421 (1987): 99–110.

43. X. P. Zhang, V. Goel, and G. J. Robbie, "Pharmacokinetics of Patisiran, the First Approved RNA Interference Therapy in Patients With Hereditary Transthyretin-Mediated Amyloidosis," *Journal of Clinical Pharmacology* 60 (2020): 573–585.

44. A. Goyon, P. Yehl, and K. Zhang, "Characterization of Therapeutic Oligonucleotides by Liquid Chromatography," *Journal of Pharmaceutical and Biomedica* 182 (2020): 113105.

45. F. Hannauer, R. Black, A. D. Ray, E. Stulz, G. J. Langley, and S. W. Holman, "Advancements in the Characterisation of Oligonucleotides by High Performance Liquid Chromatography-Mass Spectrometry in 2021: A Short Review," *Analytical Science Advances* 3 (2022): 90–102.

46. M. Huang, X. B. Xu, H. B. Qiu, and N. Li, "Analytical Characterization of DNA and RNA Oligonucleotides by Hydrophilic Interaction Liquid Chromatography-Tandem Mass Spectrometry," *Journal of Chromatography A* 1648 (2021): 462184.

47. H. Lardeux, V. D'Atri, and D. Guillarme, "Recent Advances and Current Challenges in Hydrophilic Interaction Chromatography for the Analysis of Therapeutic Oligonucleotides," *TRAC-Trends in Analytical Chemistry* 176 (2024): 117758.

48. F. Y. Li, S. K. Chen, S. Studzinska, and M. Laemmerhofer, "Polybutylene Terephthalate-based Stationary Phase for Ion-Pair-Free Reversed-Phase Liquid Chromatography of Small Interfering RNA. Part 2: Use for Selective Comprehensive Two-Dimensional Liquid Chromatography," *Journal of Chromatography A* 1701 (2023): 464069.

**Supporting Information**

Additional supporting information can be found online in the Supporting Information section.

## XII.2 Publication VII – Supplementary Material

# Triphenyl-modified mixed-mode stationary phases with and without embedded ion-exchange sites for high performance liquid chromatography

**Marc Wolter** [1], Mirna Maalouf [1], Mateusz Janek [1], Cornelius Knappe [1], Markus Kramer [2], Michael Lämmerhofer [1, *]

[1] Institute of Pharmaceutical Sciences, Pharmaceutical (Bio-)Analysis, University of Tübingen, Auf der Morgenstelle 8, 72076 Tübingen, Germany

[2] Institute of Organic Chemistry, University of Tübingen, Auf der Morgenstelle 18, 72076 Tübingen, Germany

* corresponding author

# Table of contents

## PART I: Synthesis of (3-mercaptopropyl)silatrane

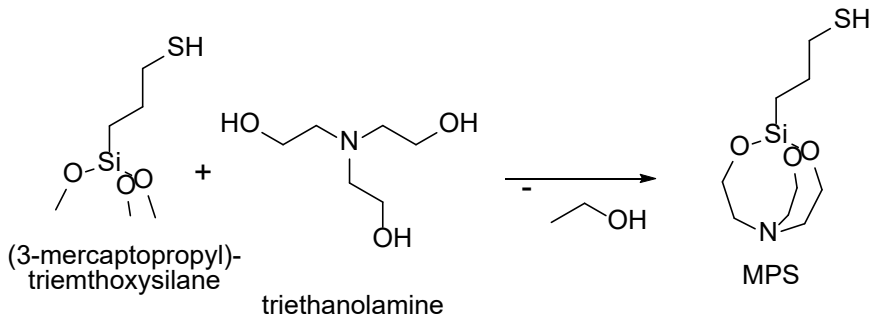


**Fig. S1.** Synthesis of (3-mercaptopropyl)silatrane. The condensation reaction between (3-mercaptopropyl)trimethoxysilane and triethanolamine results in the formation of (3-mercaptopropyl)silatrane. Synthesis procedure: Initially, 0.1 mol (3-mercaptopropyl)trimethoxysilane and 0.1 mol triethanolamine were carefully weighed into a round bottom flask (250 mL). After adding 20 mL methanol and 2 mL methanolic sodium hydroxide solution (2 mg/mL) to the solution the flask was attached to a rotary evaporator and the solvent was slowly evaporated at 40 °C. Thereafter, the reaction was heated up to 60 °C and allowed to react for 12 h. Meanwhile, the methanol formed in the condensation reaction was steadily evaporated. Lastly, the obtained white product was recrystallized from hexane in order to give pure (3-mercaptopropyl)silatrane (MPS). The yield was 91 % and synthesis control was carried out by nuclear magnetic resonance (NMR) analysis revealing a product purity of 99 % according to $^{1}$H-NMR data. The corresponding NMR spectra are depicted in Fig. S2.

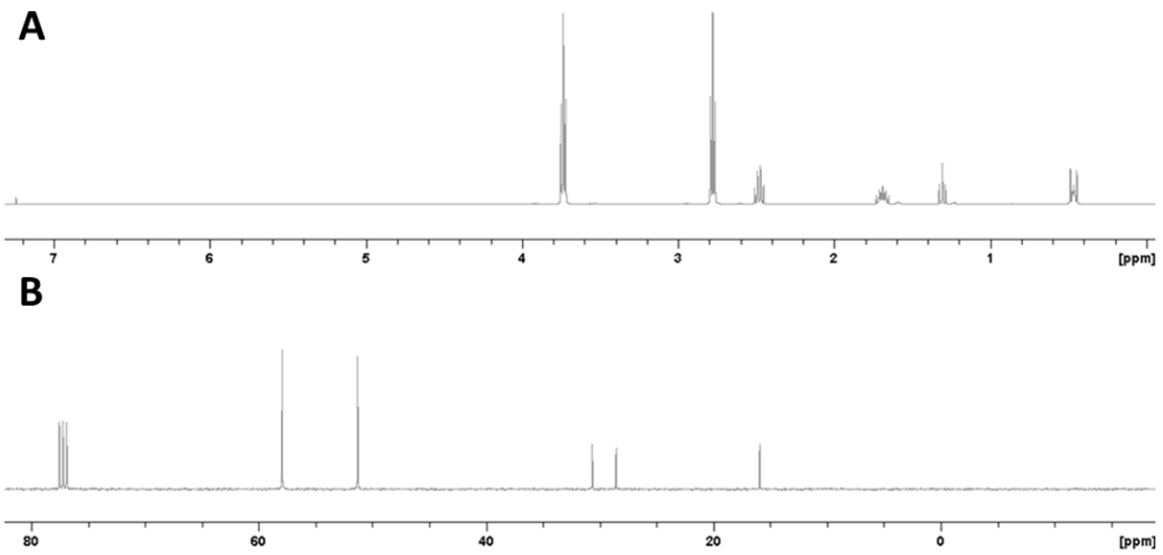


**Fig. S2.** NMR spectra of (3-mercaptopropyl)silatrane. A: 1H NMR spectrum ((Jt [Hz]), CDCl3, 400 MHz): δ 0.44-0.48 ppm (m, 2H), 1.31 ppm (t, Jt = 7.90 Hz, 1H), 1.69 ppm (quintet, Jt = 7.88 Hz, 2H), 2.78 ppm (t, Jt = 5.82 Hz, 6H) , 3.74 ppm (t, Jt = 5.82 Hz, 6H); B: 13C NMR (CDCl3, 100.6 MHz): δ 15.95 ppm (1 C), 28.58 ppm (1 C), 30.68 ppm (1 C), 51.32 ppm (3 C), 57.95 ppm (3 C). NMR spectra were calibrated to the solvent peaks with δ(1H) = 7.24 ppm and δ(13C) = 77.23 ppm.

## PART II: Synthesis of modified silica particles and column packing

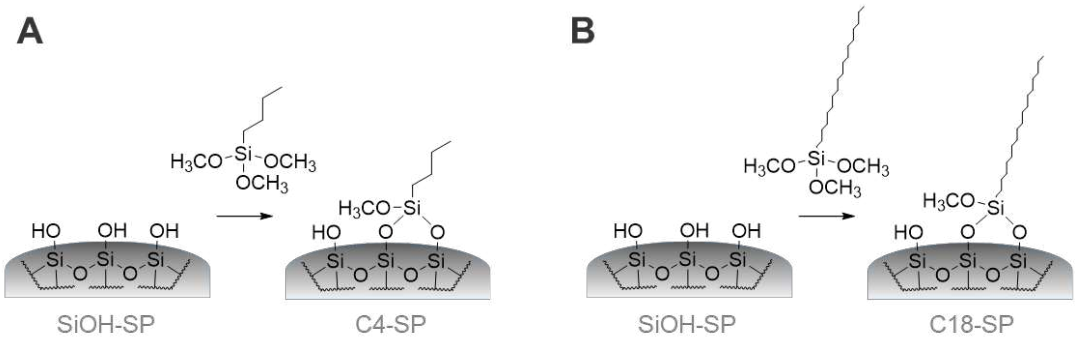


**Fig. S3.** Reaction scheme for the preparation of C4-SP (A) and C18-SP (B). Synthesis procedure: Initially, 0.5 g bare silica particles, n-butyltrimethoxysilane (6 µmol/m$^2$) or n-octadecyltrimethoxysilane (6 µmol/m$^2$), respectively, and DMAP (0.3 µmol/m$^2$) were dispersed in 20 mL anhydrous toluene within a triple neck flask equipped with a reflux condenser, a mechanical stirrer and a nitrogen supply. Then, the suspension was heated up to reflux and the reaction was allowed to proceed for 17 h under continuous nitrogen rinsing and stirring. Thereafter, the silica was washed three times with boiling methanol and boiling toluene each using a glass funnel of porosity 5 and dried in a vacuum chamber at 60 °C for 12 h.

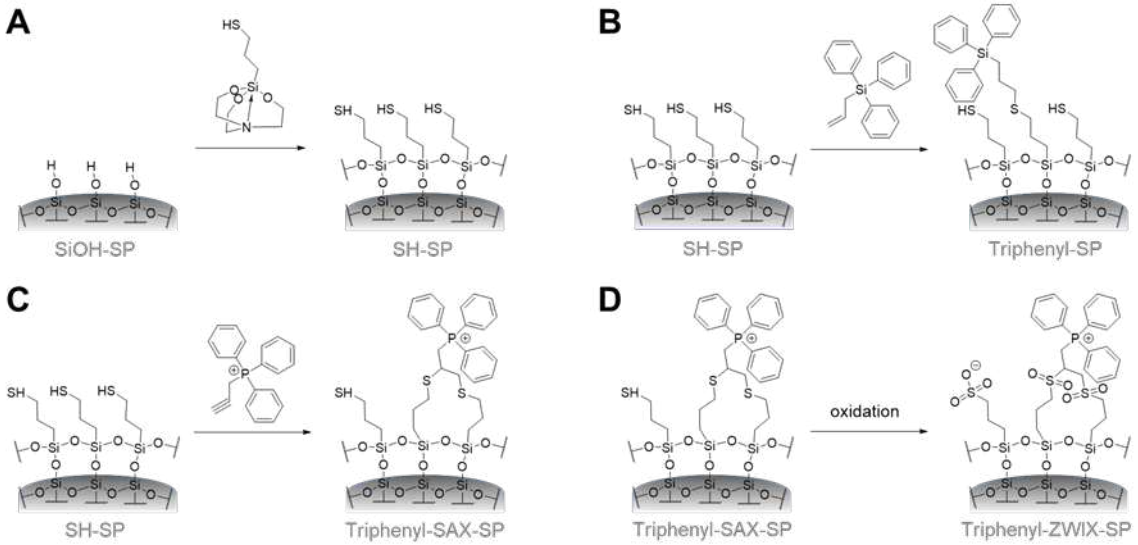


**Fig. S4.** Reaction schemes for the preparation of SH-SP (A), Triphenyl-SP (B), Triphenyl-SAX-SP (C) and Triphenl-ZWIX-SP (D). Synthesis procedures can be found in the main document.

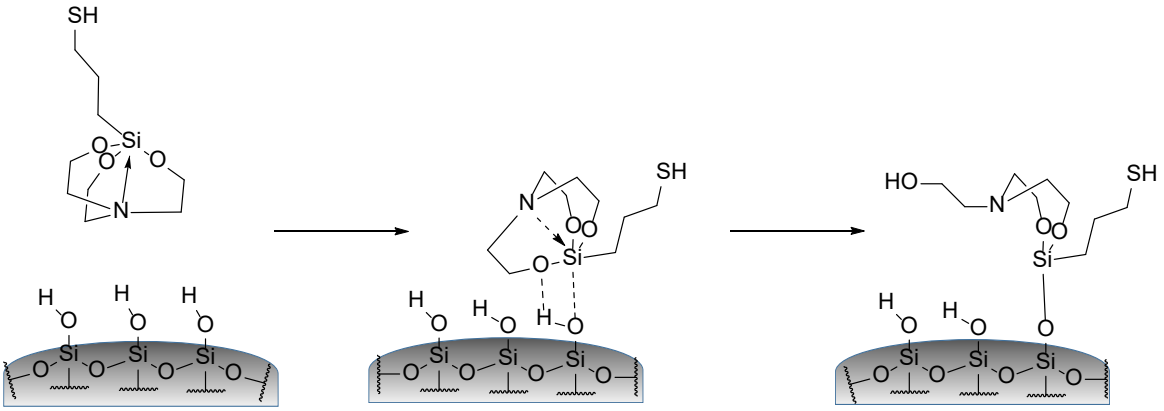


**Fig. S5.** Initial mechanism of silanol-catalyzed silica surface modification using (3-mercaptopropyl)silatrane. Due to the transannular donor-acceptor N→Si bond of the silatrane, the silatrane´s silicon atom is not prone to nucleophilic attacks, since it remains less polarized [1]. Nevertheless, the reactivity of the silatrane bumps up in acidic environments (such as silica surfaces) due to its oxygen atoms´ proton affinity (which is higher than for its nitrogen atom due to kinetic reasons [2]). By this means the formation of polarized hydrogen-bond complexes between the reactive acidic silanol groups on the silica surface and the Si-O bond of the silatrane becomes feasible making its linking to the surface in a concerted nucleophilic substitution reaction subsequently happen. During this reaction, the oxygen of the silatrane can also become protonated, making the silicon atom of the silatrane also susceptible to the subsequent nucleophilic attack of the silanol groups. However, both processes lead to the same outcome [3].

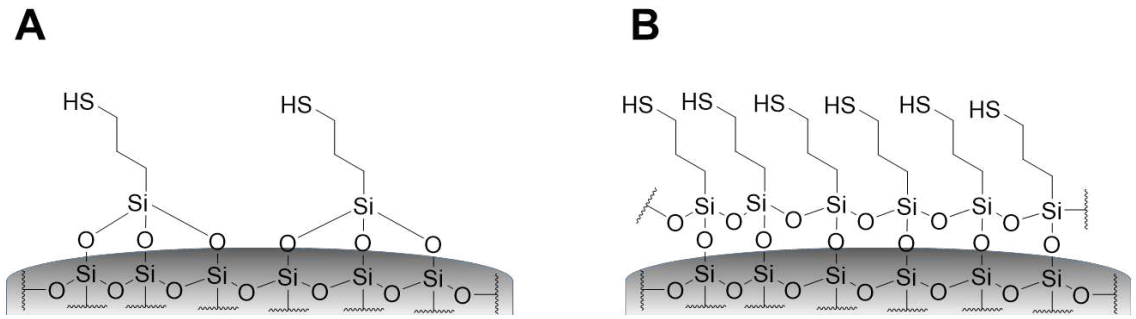


**Fig. S6.** Surface chemistries of silatrane-modified silica. There are two possibilities conceivable for the linkage of the silanization agents on the silica surface: brush-type trifunctional siloxane bonding (A) and polymeric siloxane bonding (B).

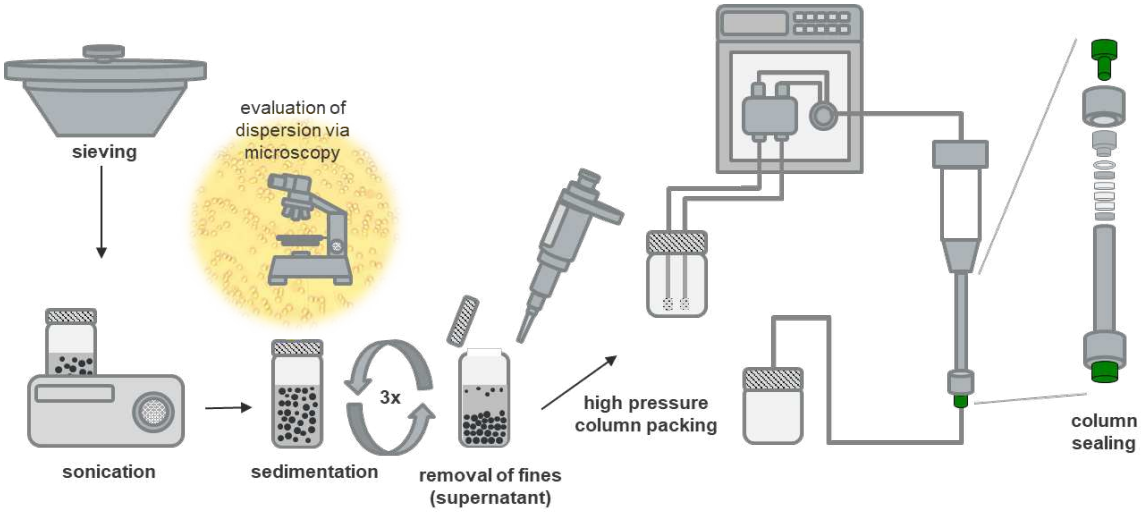


**Fig. S7.** General scheme of the in-house performed column packing procedure. The column packing procedure for analytical HPLC columns is a critical step in the preparation of analytical stationary phases. For the presented study, the prepared stationary phases were slurry packed into empty stainless-steel columns (50 mm x 3 mm) applying a pressure of 500 bar for 1 h. Beforehand, the slurry was prepared by suspending 250 mg silica in 5 mL 2-propanol. Methanol was used as pushing solvent. In the end, the column was rinsed for 24 h with methanol at a flow rate of 0.2 mL/min.

## PART III: Chromatographic tests and stationary phase classification

**Table S1.** Chromatographic conditions of the Tanaka test for RP phases [4]. The hydrophobicity (test A) depends on the carbon load and surface area. It reflects the hydrophobic retention and surface area of the column. The methylene selectivity (test B) describes the ability of the stationary phase to discriminate analytes that differ in one methyl unit. The shape selectivity (test C) accounts for the capacity of a stationary phase to discriminate compounds of identical elemental composition but different three dimensional structure. Hydrogen bonding capacity (test D and E) depends on the amount of available silanol groups present on the phase and reflects the H-bonding capacity of a column. Ion exchange capacity at pH >7 (test F) reflects electrostatic attraction on the column, since at this pH most silanols possess a negative charge while benzylamine is positively charged. Ion exchange capacity at pH <3 (test G) reflects the number of acidic silanol groups on the column, since at this pH silanols are predominantly uncharged while benzylamine is protonated.

| test | property tested | associated stationary phase characteristics | isocratic mobile phase | flow rate, temperature | chromatographic measurements |
|---|---|---|---|---|---|
| A | hydrophobicity | surface area, surface coverage, amount of alkyl chains | methanol/water (80/20, v/v) | 0.5 mL/min, 30 °C | *k (pentylbenzene)* |
| B | hydrophobic selectivity (methylene selectivity) | surface coverage, hydrophobicity of surface chemistry | methanol/water (80/20, v/v) | 0.5 mL/min, 30 °C | $\frac{k\,(pentylbenzene)}{k\,(butylbenzene)}$ |
| C | shape/steric selectivity | functionalization type, surface coverage | methanol/water (80/20, v/v) | 0.5 mL/min, 30 °C | $\frac{k\,(triphenylene)}{k\,(o-terphenyl)}$ |
| D | hydrogen bonding capacity | quantity of silanols, endcapping, surface coverage | methanol/water (30/70, v/v) | 0.5 mL/min, 30 °C | $\frac{k\,(caffeine)}{k\,(phenol)}$ |
| E | hydrogen bonding capacity | quantity of silanols, endcapping, surface coverage | methanol/water (30/70, v/v) | 0.5 mL/min, 30 °C | $\frac{k\,(pyridine)}{k\,(phenol)}$ |
| F | ion exchange capacitiy (pH>7) | quantity of silanols, ion exchange sites | methanol/aqueous phosphate buffer pH 7.6 | 0.5 mL/min, 30 °C | $\frac{k\,(benzylamine)}{k\,(phenol)}$ |
| G | ion exchange capacity (pH<3) | quantity of silanols, ion exchange sites | methanol/aqueous phosphate buffer pH 2.7 | 0.5 mL/min, 30 °C | $\frac{k\,(benzylamine)}{k\,(phenol)}$ |

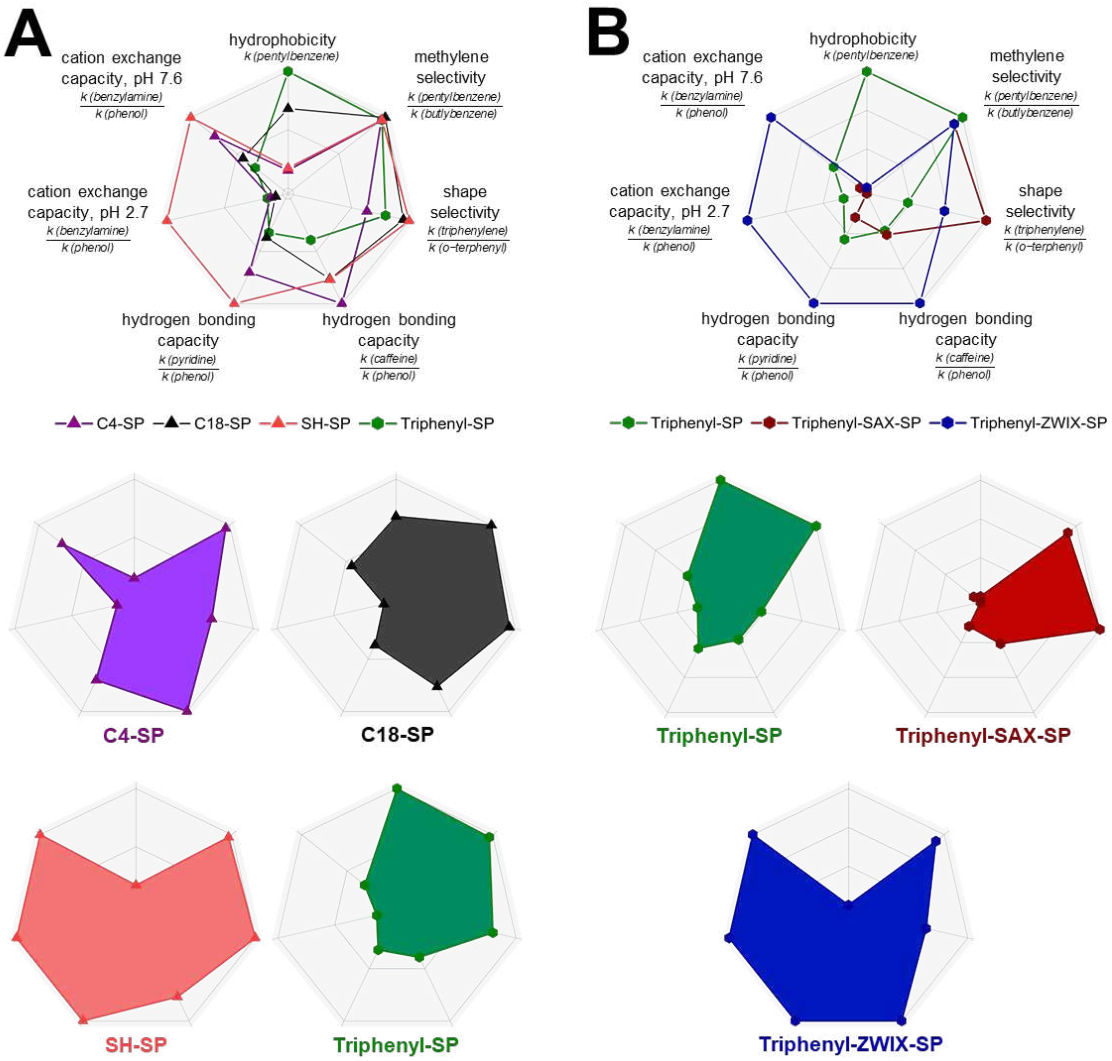


**Fig. S8.** Normalized radar plots obtained from Tanaka test. A: Comparison of the non-polar SPs (RP-type) C4-SP, C18-SP, SH-SP and Triphenyl-SP. B: Comparison of the three triphenyl-modified SPs Triphenyl-SP, Triphenyl-SAX-SP and Triphenyl-ZWIX-SP. In contrast to SH-, C4- and C18-SP, Triphenyl-SP exhibits less cation exchange properties at pH 7.6. This might indicate the efficient shielding of free silanol groups on the silica surface due to bulky phenyl groups diminishing the interaction between the silanols and the analytes.

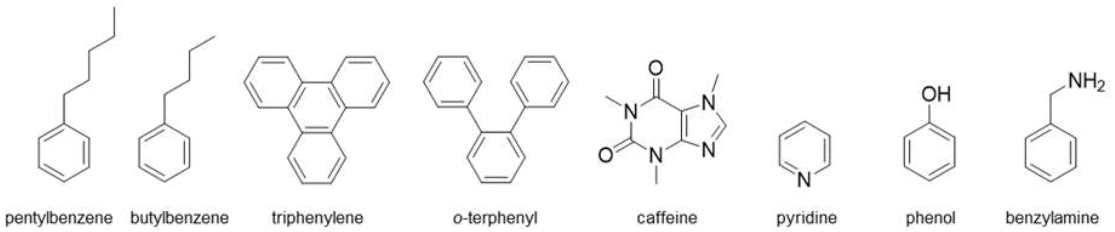


**Fig. S9.** Analytes applied in Tanaka test.

**Table S2.** Results of Tanka test.

| Analyte | C4-SP | C18-SP | SH-SP | Triphenyl-SP | Triphenyl-SAX-SP | Triphenyl-ZWIX-SP |
|---|---|---|---|---|---|---|
| *k (pentylbenzene)* | 0.09 | 0.32 | 0.10 | 0.47 | with $t_0$ | with $t_0$ |
| $\frac{k\text{ (pentylbenzene)}}{k\text{ (butylbenzene)}}$ | 1.09 | 1.14 | 1.10 | 1.10 | 1.00 | 1.00 |
| $\frac{k\text{ (triphenylene)}}{k\text{ (o-terphenyl)}}$ | 0.90 | 1.35 | 1.42 | 1.13 | 3.63 | 2.30 |
| $\frac{k\text{ (caffeine)}}{k\text{ (phenol)}}$ | 1.45 | 1.11 | 1.12 | 0.57 | 0.64 | 1.85 |
| $\frac{k\text{ (pyridine)}}{k\text{ (phenol)}}$ | 2.78 | 1.46 | 3.96 | 1.28 | 0.59 | 3.28 |
| $\frac{k_{pH\ 2.7}\text{ (benzylamine)}}{k_{pH\ 2.7}\text{ (phenol)}}$ | 0.40 | 0.23 | 3.97 | 0.51 | -0.95[1] | 3.32 |
| $\frac{k_{pH\ 7.6}\text{ (benzylamine)}}{k_{pH\ 7.6}\text{ (phenol)}}$ | 3.14 | 1.85 | 4.23 | 1.29 | 0.10 | 4.11 |

[1] elution of benzylamine was observed prior to $t_0$

**Table S3.** Chromatographic data obtained from ion-exchange test. The separation of benzylamine, phenol and p-toluenesulfonic acid on Triphenyl-SP, Triphenyl-SAX-SP and Triphenyl-ZWIX-SP was investigated. Chromatographic conditions: Mobile phase consisted of MeOH/aqueous ammonium phosphate buffer (20 mM, adjusted to pH 3 or pH 7.5) (30/70, v/v), flow rate: 1 mL/min, temperature: 25 °C, injection volume: 5 µL.

| | k(benzylamine) | | k(phenol) | | k(p-toluenesulfonate) | |
|---|---|---|---|---|---|---|
| | pH 3 | pH 7.5 | pH 3 | pH 7.5 | pH 3 | pH 7.5 |
| Triphenyl-SP | 0.97 | 1.25 | 0.70 | 0.93 | 0.45 | 0.19 |
| Triphenyl-SAX-SP | before $t_0$ | 0.03 | 0.37 | 0.43 | 42.92 | 3.53 |
| Triphenyl-ZWIX-SP | 3.08 | 3.87 | 0.08 | 0.08 | before $t_0$ | before $t_0$ |

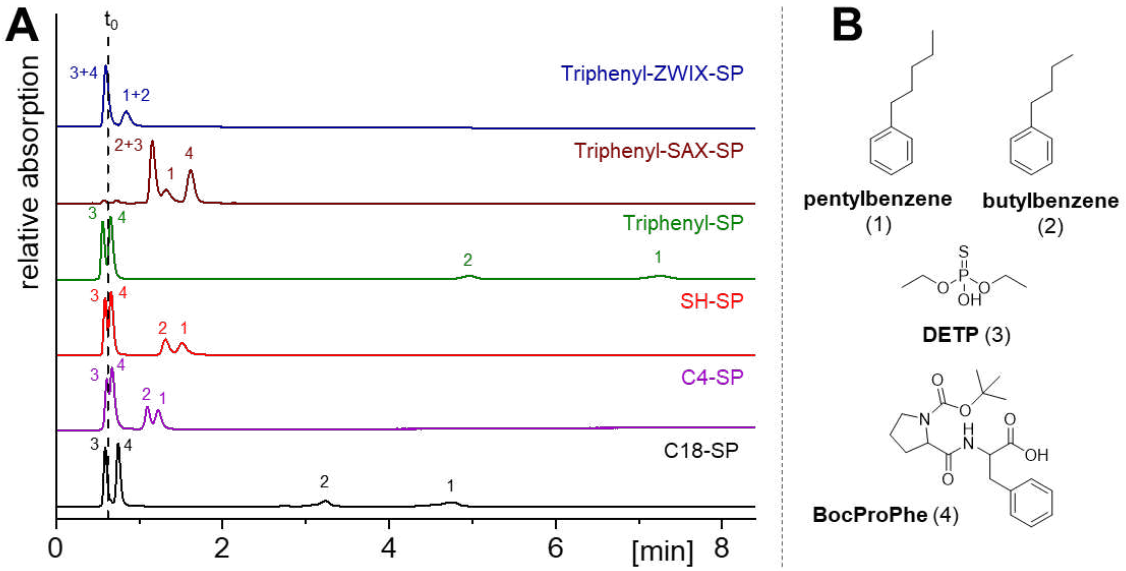


**Fig. S10.** Chromatograms obtained from RP test (A) and analytes applied (B). A mixture of ACN and water (40:60, v/v) containing 50 mM acetic acid was used as mobile phase. The pH of the mobile phase was adjusted to 6 utilizing ammonia. The linear flow velocity was set to 1.7 mm/s and detection was carried out at 220 nm. The injection volume was amounted to 2 µL and the temperature set to 25 °C. The analytes were all dissolved in the mobile phase reaching a concentration of 0.8 mg/mL. Uracil was used as void volume marker.

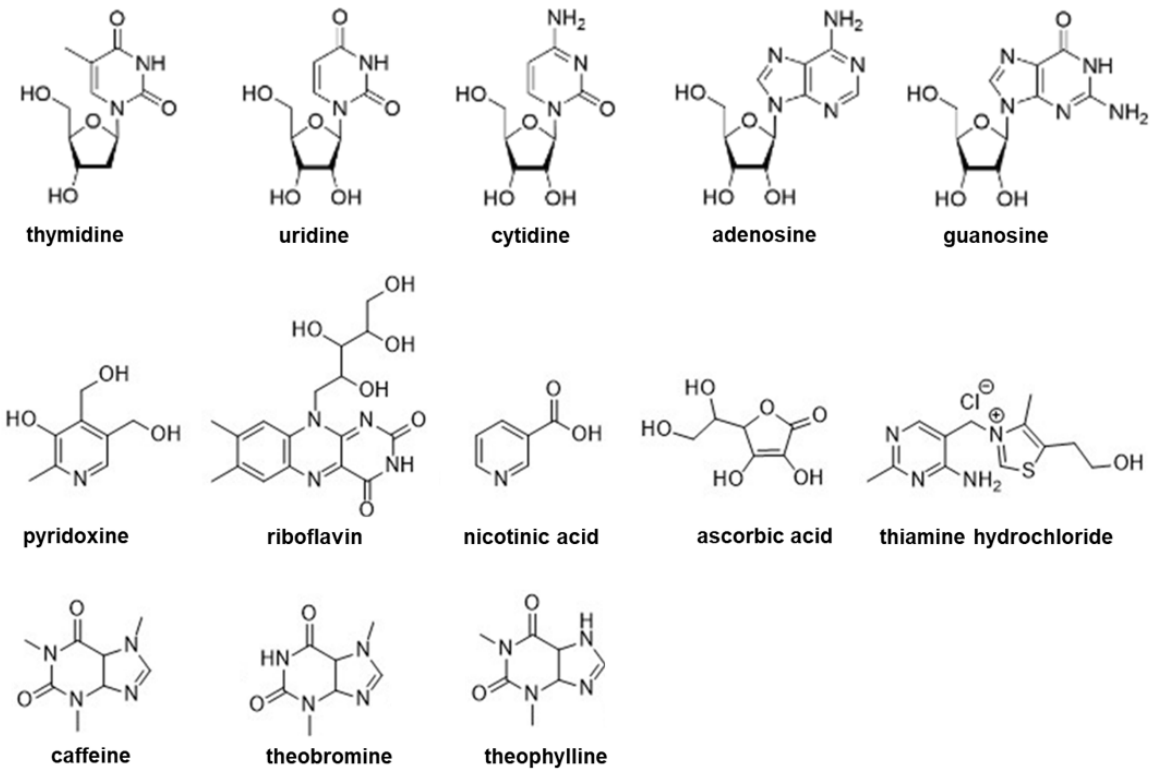


**Fig. S11.** Analytes applied for the HILIC tests. The chromatographic performance under HILIC conditions was investigated by the separation of xanthines (caffeine, theobromine, theophylline), nucleosides (adenosine, cytidine, guanosine, thymidine, uridine) and vitamins (nicotinic acid, pyridoxine, riboflavin, thiamine, ascorbic acid). The mobile phases consisted of ACN and water. The mixing ratio was 95:5 (v/v) for the xanthines and 90:10 (v/v) for the vitamins and nucleosides. Both mobile phases contained 5 mM ammonium acetate and showed an unadjusted apparent pH of 8 (measured in the hydro-organic mixture). The flow rate was calculated to the corresponding linear velocity of 1.7 mm/s. The void volume was determined by toluene.

**Table S4.** Retention factors obtained from RPLC and HILIC test. The retention factors listed for in-house prepared and commercial columns were used for PCA. Data of commercial columns were partially taken from [5] and [6].

| | | | | | k | | | |
|---|---|---|---|---|---|---|---|---|
| SP | thymidine | adenosine | uridine | cytidine | guanosine | caffeine | theobromine | theophylline |
| Acclaim Mixed Mode WAX-1 | 0.88 | 1.67 | 1.90 | 4.18 | 7.15 | 0.10 | 0.26 | 0.84 |
| Uptisphere 5 MM3 | with $t_0$ | 0.15 | 0.15 | 0.81 | 1.05 | with $t_0$ | with $t_0$ | with $t_0$ |
| Primesep B2 | with $t_0$ | 0.10 | with $t_0$ | 0.22 | 0.22 | 0.02 | 0.02 | 0.11 |
| Obelisc R | 0.09 | 0.48 | 0.48 | 2.15 | 2.69 | 0.06 | 0.14 | 0.26 |
| Obelisc N | 0.23 | 0.59 | 0.48 | 2.75 | 1.61 | 0.15 | 0.22 | 0.22 |
| Chiralpak QN-AX | 0.15 | 0.15 | 0.15 | 0.29 | 0.29 | 0.10 | 0.24 | 0.44 |
| Luna NH2 | 1.21 | 3.80 | 3.80 | 11.99 | 19.18 | 0.31 | 0.67 | 3.19 |
| Lichrospher NH2 | 0.97 | 2.90 | 1.89 | 10.61 | 12.86 | 0.22 | 0.35 | 0.44 |
| BioBasic AX | 0.35 | 0.84 | 0.75 | 2.18 | 3.42 | 0.08 | 0.18 | 0.18 |
| Synergi Fusion-RP | with $t_0$ | 0.04 | with $t_0$ | 0.16 | 0.04 | with $t_0$ | with $t_0$ | with $t_0$ |
| TSKGel Amide-80 | 1.27 | 3.12 | 3.45 | 10.20 | 12.80 | 0.40 | 0.76 | 1.16 |
| PolysulfoethylA | 0.77 | 2.08 | 3.14 | 15.02 | 16.69 | 0.20 | 0.45 | 0.51 |
| ZIC-HILIC | 0.89 | 2.09 | 3.24 | 9.54 | 12.63 | 0.28 | 0.63 | 0.63 |
| Nucleodur HILIC | 0.91 | 1.64 | 2.08 | 5.05 | 6.53 | 0.36 | 0.67 | 0.67 |
| Chromolith Performance Si | 0.29 | 0.76 | 0.61 | 2.26 | 2.04 | 0.19 | 0.19 | 0.19 |
| PC-HILIC | 1.00 | 2.29 | 1.66 | 4.70 | 5.21 | 0.60 | 1.03 | 1.03 |
| SiOH-SP | 0.23 | with $t_0$ | 0.34 | 1.28 | with $t_0$ | 0.19 | 0.17 | 0.34 |
| C4-SP | 0.11 | 0.17 | 0.11 | 0.19 | 0.27 | 0.21 | 0.22 | 0.26 |
| C18-SP | 0.1 | 0.1 | 0.11 | 0.46 | 0.09 | 0.23 | 0.11 | 0.29 |
| SH-SP | 0.05 | 0.08 | 0.05 | 0.22 | with $t_0$ | 0.13 | 0.08 | 0.18 |
| Triphenyl-SP | 0.03 | 0.09 | 0.02 | 0.06 | 0.01 | 0.15 | 0.13 | 0.14 |
| Triphenyl-SAX-SP | 0.13 | 0.15 | 0.21 | 0.39 | 0 | 0.08 | 0.11 | 0.43 |
| Triphenyl-ZWIX-SP | 0.15 | 0.11 | 0.23 | 0.73 | with $t_0$ | 0.08 | 0.17 | 0.23 |

| | | | | | k | | | | |
|---|---|---|---|---|---|---|---|---|---|
| SP | thiamine | pyridoxine | riboflavine | ascorbic acid | nicotinic acid | BuB | PeB | DETP | BocProPhe |
| Acclaim Mixed Mode WAX-1 | 0.17 | 1.11 | 1.66 | n.d. | 31.14 | 5.52 | 8.47 | 14.45 | 34.75 |
| Uptisphere 5 MM3 | 0.60 | 0.13 | 0.13 | 5.27 | 3.03 | 27.73 | 48.89 | 0.19 | 0.28 |
| Primesep B2 | 3.92 | 0.36 | 0.04 | 0.04 | 0.73 | 9.97 | 15.59 | 1.97 | 5.36 |
| Obelisc R | 10.11 | 0.78 | 0.78 | 2.73 | 10.11 | 6.22 | 9.47 | 3.59 | 10.97 |
| Obelisc N | n.d | 6.65 | 1.15 | 1.15 | 0.66 | 1.00 | 1.35 | 4.00 | 3.64 |
| Chiralpak QN-AX | 1.17 | 0.41 | 0.32 | n.d. | 3.52 | 4.11 | 5.76 | 5.76 | 7.69 |
| Luna NH2 | 0.95 | 2.64 | 3.10 | 28.74 | 24.90 | with $t_0$ | with $t_0$ | 4.39 | 1.76 |
| Lichrospher NH2 | 0.44 | 2.48 | 6.40 | 134.63 | 30.59 | 0.10 | 0.19 | 0.78 | 0.89 |
| BioBasic AX | 0.43 | 0.43 | 0.89 | n.d. | 10.88 | with $t_0$ | with $t_0$ | 1.05 | 0.53 |
| Synergi Fusion-RP | 14.94 | 0.11 | with $t_0$ | with $t_0$ | 0.44 | 24.17 | 43.28 | with $t_0$ | 0.06 |
| TSKGel Amide-80 | 43.54 | 1.49 | 4.77 | 20.70 | 5.49 | with $t_0$ | with $t_0$ | with $t_0$ | with $t_0$ |
| PolysulfoethylA | 26.81 | 2.73 | 3.10 | n.d. | 2.73 | with $t_0$ | with $t_0$ | with $t_0$ | with $t_0$ |
| ZIC-HILIC | 29.30 | 1.20 | 2.20 | 35.13 | 4.89 | with $t_0$ | with $t_0$ | 0.14 | with $t_0$ |
| Nucleodur HILIC | 99.31 | 1.73 | 1.78 | 6.26 | 1.78 | with $t_0$ | with $t_0$ | with $t_0$ | with $t_0$ |
| Chromolith Performance Si | 28.20 | 0.65 | 0.65 | 1.41 | 1.85 | with $t_0$ | with $t_0$ | with $t_0$ | with $t_0$ |
| PC-HILIC | 95.49 | 1.91 | 2.66 | 6.65 | 2.05 | with $t_0$ | with $t_0$ | with $t_0$ | with $t_0$ |
| SiOH-SP | 36.19 | 0.58 | 0.18 | 1.62 | 1.97 | 0.04 | 0.06 | with $t_0$ | with $t_0$ |
| C4-SP | 8.30 | 0.28 | 0.16 | with $t_0$ | 0.50 | 0.94 | 1.18 | with $t_0$ | 0.12 |
| C18-SP | 23.25 | 0.37 | 0.08 | with $t_0$ | 1.03 | 4.29 | 6.78 | with $t_0$ | 0.21 |
| SH-SP | 11.83 | 0.24 | 0.05 | with $t_0$ | 0.42 | 1.14 | 1.47 | with $t_0$ | with $t_0$ |
| Triphenyl-SP | 4.75 | 0.11 | 0.02 | with $t_0$ | 0.09 | 7.58 | 11.55 | with $t_0$ | 0.13 |
| Triphenyl-SAX-SP | 1.09 | 0.44 | 0.09 | 3.02 | 5.03 | 0.88 | 1.13 | 0.84 | 1.56 |
| Triphenyl-ZWIX-SP | 13.50 | 0.35 | 0.14 | with $t_0$ | 0.57 | 0.30 | 0.37 | with $t_0$ | with $t_0$ |

n.d. = not detected

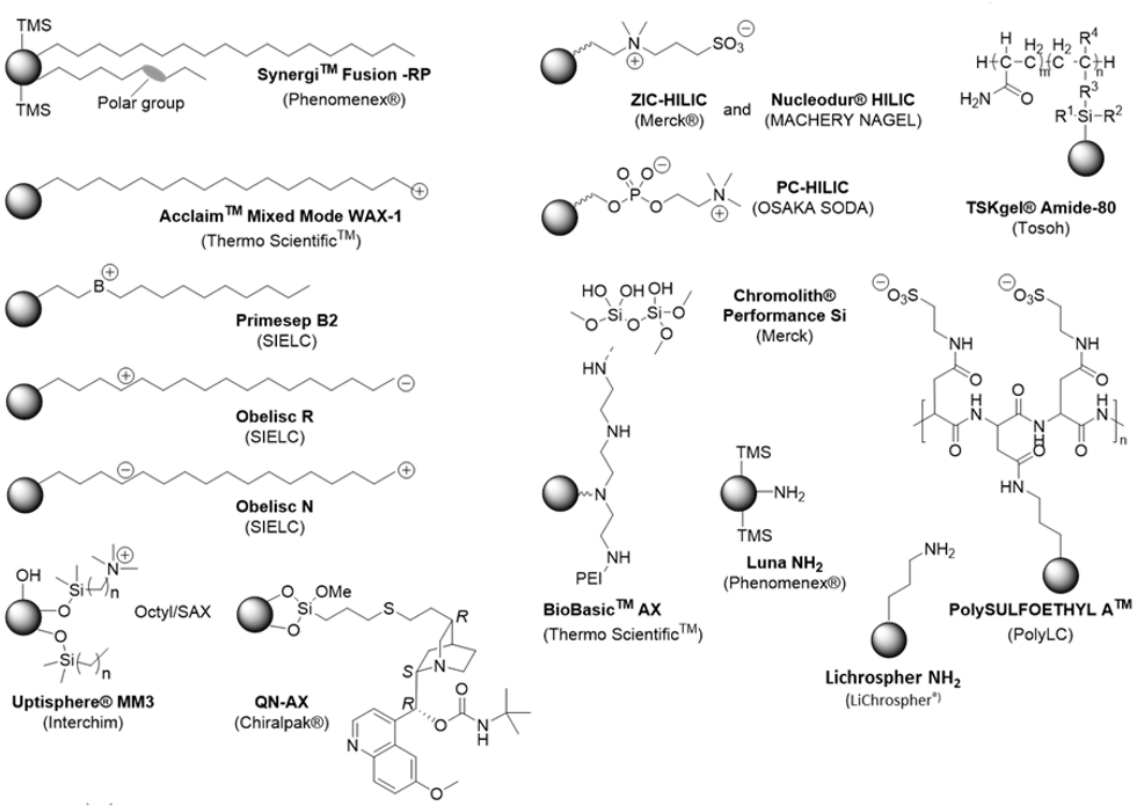


**Fig. S12.** Surface chemistries of commercial columns. In-house prepared columns C4-SP, C18-SP, SH-SP, Triphenyl-SP, Triphenyl-SAX-SP, Triphenyl-ZWIX-SP were compared to commercial columns based on the results from standard RP and HILIC tests via principal component analysis.

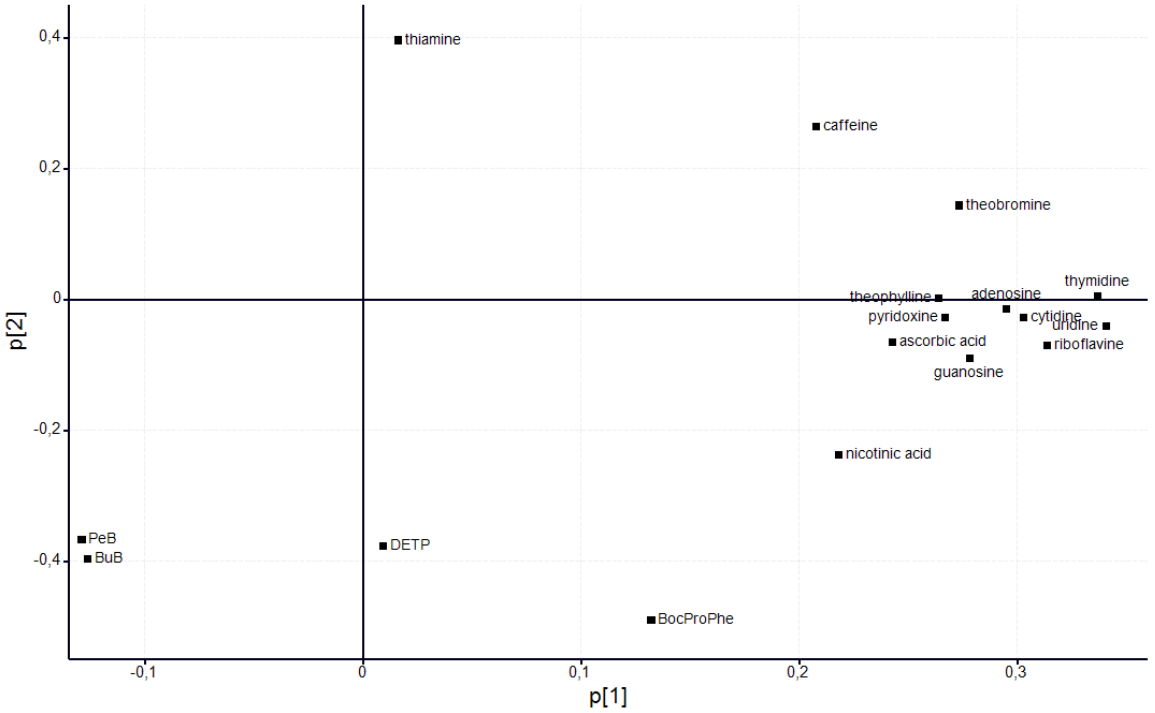


**Fig. S13.** Loadings scatter plot of principal component analysis: p1 vs. p2. p1 is the loading in the first component and p2 the loading in the second component. The loadings express the dominating correlation structure of the X matrix. Hence, p1 vs. p2 displays how the X-variables correlate to each other. The plot shows how the X-variables vary in relation to each other, which ones provide similar information, which ones are negatively correlated, or not related to each other, and which ones are not well explained by the model (p1 and p2 close to 0).

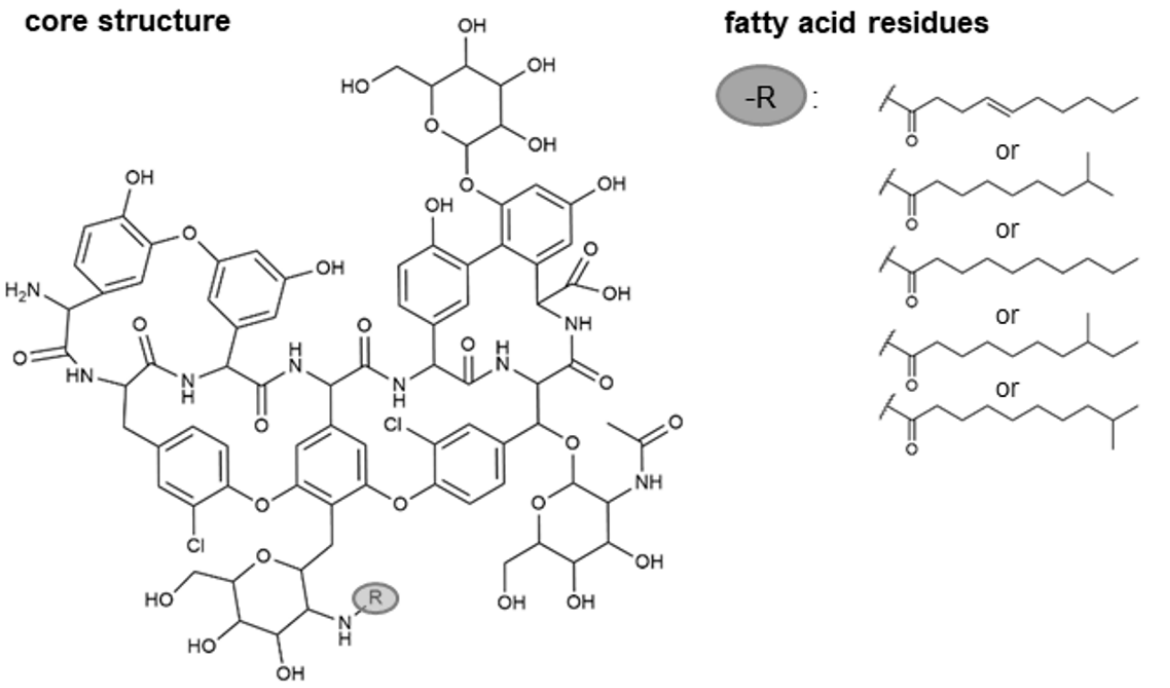


**Fig. S14.** Chemical structure of teicoplanin. Teicoplanin is a multicomponent antibiotic drug and consists of several glycopeptides varying in the attached fatty acid residue. [7]

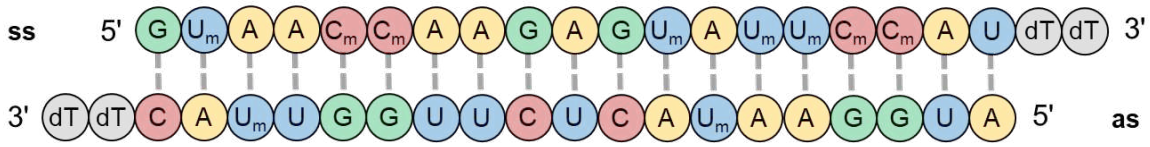


**Fig. S15.** Chemical structure of patisiran (ss: sense strand, antisense strand, dT: deoxythymidine, G: guanosine, C: cytidine, U: uridine, A, m: methylated). [8]

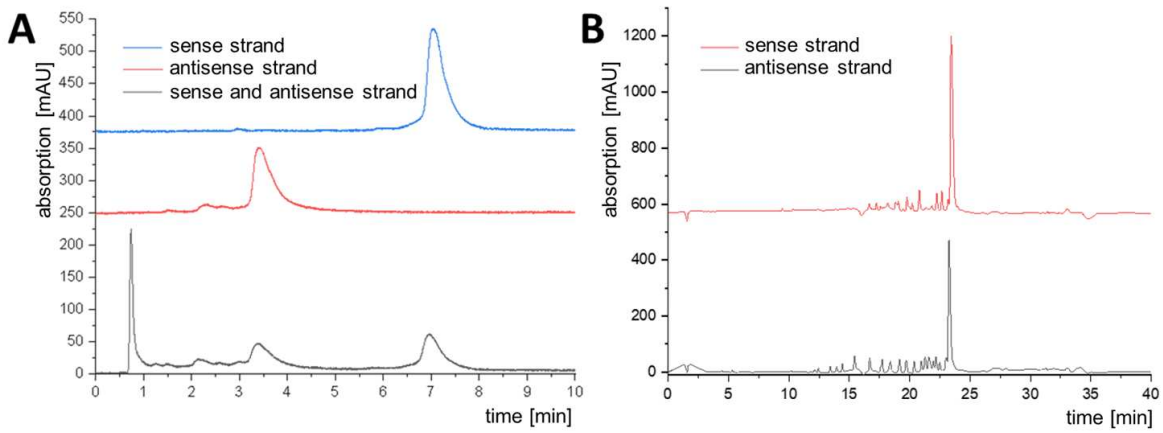


**Fig. S16.** Analysis of Patisiran (siRNA) strand and antisense strand. A: Analysis using in-house prepared Triphenyl-SP (50 x 3.0 mm, 3 µm, 300 Å). Chromatographic conditions: mobile phase A: aqueous 20 mM ammonium acetate, pH 6.8, mobile phase B: MeOH/water (9:1; v/v), containing 20 mM ammonium acetate, pH 6.8, gradient: 5% to 20% B in 10 min, temperature: 40 °C flow rate: 0.6 mL/min. B: Analysis using commercial BEH C18 column (50 x 2.1 mm, 1.7 µm, 130 Å,). Chromatographic conditions: mobile phase A: aqueous 100 mM tripropylammonium acetate, pH 7, mobile phase B: ACN/water (9:1; v/v), containing 100 mM tripropylammonium acetate , pH 7, gradient: 10 to 55% B in 32.5 min, temperature: 30 °C, flow rate: 0.3 mL/min.

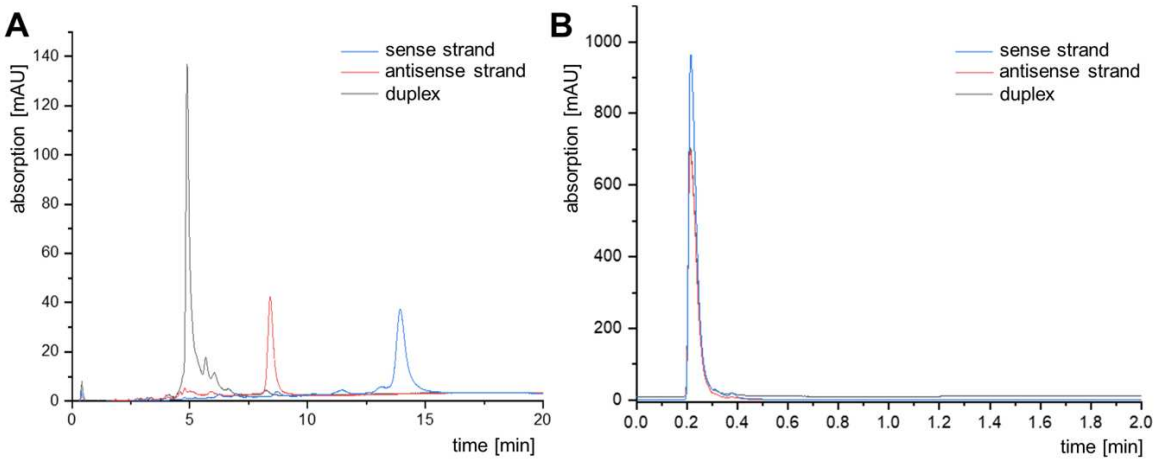


**Fig. S17.** Analysis of Patisiran (sense strand, antisense strand and duplex). A: Analysis using in-house prepared Triphenyl-SAX-SP (50 x 3.0 mm, 3 µm, 300 Å). Chromatographic conditions: mobile phase A: ACN/water (1:9; v/v), containing 20 mM phosphate buffer, pH 7, mobile phase B: ACN/water (1:9; v/v), containing 20 mM phosphate buffer and 1 M NaCl, pH 8; gradient: 0% to 50% B in 5 min; 50% to 100% B in 10 min, 100% B for 3 min, 0% B for 8 min, temperature: 50° C, flow rate: 1 mL/min. B: Analysis using in-house prepred Triphenyl-ZWIX-SP (50 x 3.0 mm, 3 µm, 300 Å). Chromatographic conditions: same as in A.

## PART IV: References

[1] Puri J.K., Singh R., Chahal V.K., Silatranes: a review on their synthesis, structure, reactivity and applications, Chem. Soc. Rev., 2011;40:1791-1840.

[2] Sok S., Gordon M.S., A dash of protons: a theoretical study on the hydrolysis mechanism of 1-substituted silatranes and their protonated analogs, Comput. Theor. Chem., 2012; 987:2-15.

[3] Shlyakhtenko L.S., Gall A.A., Filonov A., Cerovac, Z. Lushnikov A., Lyubchenko Y.L., Silatrane-based surface chemistry for immobilization of DNA, protein-DNA complexes and other biological materials, Ultramicroscopy, 2003;97:279-287.

[4] Kimata K., Iwaguchi K., Onishi S., Jinno K., Eksteen R., Hosoya K., Araki M., Tanaka N., Chromatographic characterization of silica C18 packing materials. Correlation between a preparation method and retention behavior of stationary phase, J. of Chrom. Sci., 1989; 27:721-728.

[5] Wolter M., Geibel C., Olfert M., Su M., Bicker W., Laemmerhofer M., Development and chromatographic exploration of stable-bonded cross-linked amino silica against classical amino phases, J. Sep. Sci., 2022;1-15.

[6] Zimmermann A., Horak J., Sanchez-Munoz O.L., Laemmerhofer M., Surface charge fine tuning of reversed-phase/weak anion-exchange type mixed-mode stationary phases for milder elution conditions, J. Chromatogr. A, 2015;1409:189-200.

[7] Geibel C., Olfert M., Knappe C., Serafimov K., Laemmerhofer M., Banched medium-chain fatty acid profiling and enantiomer separation of anteiso-forms of teicoplanin fatty acyl side chain RS3 using UHPLC-MS/MS with polysaccharide columns, J. Pharm. Biomed. Anal., 2023, 115162.

[8] Li F., Chen S., Studzinska S, Laemmerhofer M., Polybutylene terephtalate-based stationary phase for ion-pair-free reversed-phase liquid chromatography of small interfering RNA. Part 2: Use for selective comprehensive two-dimensional liquid chromatography, J. Chromatogr. A, 2023, 464069.

# VII. Concluding remarks

This thesis reported on the design, preparation and characterization of novel stationary phases based on the modification of silica particles and their application in high-performance liquid chromatography. Although other innovative alternatives such as three-dimensional printing of columns are being investigated nowadays, silica particles remain the most important and widely used stationary phase support. This is mainly due to their high mechanical strength, broad solvent compatibility, availability of distinct and customizable morphologies, and ease of modification. These advantages outweigh some disadvantages in terms of chemical stability of silica and limitations in kinetic performance of particle-packed columns. Also, some developments in particle design and the introduction of hybrid-materials have reduced these disadvantages to an acceptable level. In this thesis, stationary phases were prepared by classical silanization reactions using alkoxysilanes, by innovative silanization reactions with silatranes, and by modification reactions employing polymer coating strategies. The modification with silatranes was found to be clearly superior to the classical procedure with alkoxysilanes. The immobilization of polymers has resulted in highly stable platform silica for further modifications. Thermal or photo-initiated radical addition reactions, amine-epoxy reactions and oxidation reactions were applied for further modification of functionalized silica particles. As a result, stationary phases with improved chemical stability, novel surface chemistries and selectivities have been synthesized that are applicable to a variety of chromatographic modes and analytical issues. The stationary phases have been intensively characterized using various techniques such as elemental analysis, cross-polarization / magic angle nuclear magnetic resonance spectroscopy and ζ-potential measurements. In addition, the stationary phases were investigated under different chromatographic conditions and compared with commercial columns employing principal component analysis. This revealed similarities and orthogonalities among the stationary phases. Overall, the usefulness of silica particles as stationary phase support, the scope for improvement in synthesis procedures, and the opportunities associated with the design of surface chemistries were demonstrated.

*Thanks to Michael and all my colleagues who accompanied me on this journey for the last few years. I am very grateful for your help, support, all the fruitful discussions we had and the memories we share.*